Yi Li
Daniel Lu
C.P. Wong

Electrical Conductive Adhesives with Nanotechnologies

Springer

Electrical Conductive Adhesives with Nanotechnologies

Yi Li · Daniel Lu · C.P. Wong

Electrical Conductive Adhesives with Nanotechnologies

Yi Li
School of Materials Science
and Engineering
Georgia Institute of Technology
771 Ferst Drive
Atlanta, GA 30332-0245
USA
yi.li@intel.com

C.P. Wong
School of Materials Science
and Engineering
Georgia Institute of Technology
771 Ferst Drive
Atlanta, GA 30332-0245
USA
cp.wong@mse.gatech.edu

Daniel Lu
Henkel Loctite (China) Co. Ltd.
5000 W. Chandler Blvd.
264006 Chandler
People's Republic of China
daniel.lu@cn.henkel.com

ISBN 978-0-387-88782-1 e-ISBN 978-0-387-88783-8
DOI 10.1007/978-0-387-88783-8
Springer New York Dordrecht Heidelberg London

Library of Congress Control Number: 2009933981

Preface

With the phasing out of lead-bearing solders, electrically conductive adhesives (ECAs) have been identified as one of the environmentally friendly alternatives to tin/lead (Sn/Pb) solders in electronics packaging applications. In particular, with the requirements for fine-pitch and high-performance interconnects in advanced packaging, ECAs with nano-materials or other nano-technology are becoming more and more important due to the special electrical, mechanical, optical, magnetic, and chemical properties that nano-sized materials can possess. There has been extensive research for the last few years on materials and process improvement of ECAs, as well as on the advances of nanoconductive adhesives that contain nano-filler, such as nano-particles, nanowires, or carbon nanotubes and nano monolayer graphenes.

The objective of this book is to review the most recent advances of various types of electrically conductive adhesives with the particular emphasis on the emerging nanotechnology, including materials development and characterizations, processing optimization, reliability improvement, and future challenges/opportunities identification.

This book consists of nine Chapters, each representing a specific field of interest. Chapter 1 discusses an overview of electronic packaging and the evolvement of different types of conductive adhesives. Chapter 2 describes the latest development of nano-materials, nanotechnology and their applications in microelectronics packaging. Chapter 3 reviews the key polymeric materials used in conductive adhesives and the analytic approaches for ECA characterizations. Chapter 4 deals with the recent advances in materials, processes, and applications of isotropically conductive adhesives (ICAs), particularly focusing on the fundamental understanding and improvement of materials properties for ICAs and nano-ICAs. Chapter 5 discusses the recent development and applications of anisotropically conductive adhesives (ACA) with the emphasis on the nano-materials implementation for improved performance. Chapter 6 describes the latest materials and processing development of non-conductive adhesives (NCA). Chapter 7 discusses the details of conductive nano-inks and their applications in transparent electrodes, printed electronics, and other packaging areas. Chapter 8 focuses on the recent research and development of materials and applications of intrinsically conducting polymers. And finally, Chapter 9 summarizes the recent advances of conductive adhesives with nanotechnology and discusses the challenges and opportunities for continuing the work on nanoconductive adhesives.

The field of electrically conductive adhesives and nanotechnology is quite broad and their development is dynamic, so it is impossible to cover every aspect of them. We have attempted to include most major areas with the latest references which should be useful to our audience who work in this vast growing discipline. With the advances of microelectronics packaging and nanotechnology, there is always a constant need of improved materials and technology. This is a challenge that requires the continuous and active collaborative efforts between materials scientists, chemists, physicists, device and package design engineers.

We express our gratitude to many of our colleagues and friends in the field of microelectronics packaging, conductive adhesives and nanoscience and nanotechnology. Many of their published works have been cited in this book, including work published by many other experts in the fields. We would also like to thank Owen Hildreth and Angela Duan for proofreading some chapters and Steven Elliot and Andrew Leigh for editorial suggestions.

Chandler, AZ — Yi Li
Yantai, China — Daniel Lu
Atlanta, GA — C.P. Wong

Contents

Chapter 1
Introduction

1.1 Electronics Packaging and Interconnect

Integrated circuits (ICs) form the bases of all modern electronic products. However, an IC alone does not form a complete system and it must be integrated with other components into a system-level board. "Electronic Packaging" is defined as the bridge that interconnects the integrated circuits (ICs) and other components into a system-level board to form electronic products [1]. The packaging has four main functions: (1) signal distribution, mainly involving topological and electromagnetic considerations; (2) power distribution, involving electromagnetic, structural, and material aspects; (3) heat dissipation (thermal management), involving structural and material considerations; (4) and protection (mechanical, chemical, electromagnetic) of components and interconnections. Furthermore, design for x (where x stands for performance, environment, manufacturability, and reliability) at the front end and system test at the final stage prior to the system shipment are also important functions for electronic packaging. The challenge for the package is to provide all crucial functions required by the microelectronic system without limiting the performance of the individual part.

From the bare chip fabricated from the silicon wafer to the final product ready for use, the whole system can be divided into various levels of the packaging. The first-level packaging provides the interconnection between an IC and the package. At this level, the packaging acts as an IC "carrier." The IC carrier allows IC to be shipped after "burn-in" (an accelerated test with high bias, temperature, and other accelerated factors designed to wipe out those inferior components to reduce the infant mortality of the IC) and electrical test to be ready for assembly onto a system-level board by end product or contract manufacturers.

Due to the complexity of modern electronics packaging, there are many levels of interconnects with first-level interconnects defined as the connections between the IC and the IC carrier. Currently, two types of first-level interconnection dominate the industry: (1) wire bonding and (2) flip chip attachment.

Y. Li et al., *Electrical Conductive Adhesives with Nanotechnologies*,
DOI 10.1007/978-0-387-88783-8_1, © Springer Science+Business Media, LLC 2010

Many other interconnection methods exist to meet special needs or performance requirements. These range from tape automated bonding (TAB) which, at times, has seen significant usage within certain product lines to novel interconnection schemes, involving deposited thin films [2], compliant G-shaped springs [3], laser-deposited (written) conductors [4–6], copper pillar with solder cap [7–9], pure copper interconnect [10], and carbon nanotube (CNT)-based interconnect [11]. Pressure contacts using de-formable conducting polymers or elastomers have been used where the need to easily remove and replace the IC is a primary concern.

Wire bonding is the process of providing electrical connection between the silicon chip and the external leads of the semiconductor device using very fine bonding wires. The wire used in wire bonding is usually made either of gold (Au) or aluminum (Al). However, copper (Cu) wire bonding is starting to gain a foothold in the semiconductor manufacturing industry because Cu wire has a cost saving of more than 80% as compared to Au wire, higher thermal and electrical conductivity with lower power loss, and higher current flow as compared to Au wire which are important for enhanced device performance and reliability. There are two common wire bonding processes: Au ball bonding (Fig.1.1) and Al wedge bonding (Fig. 1.2) [12].

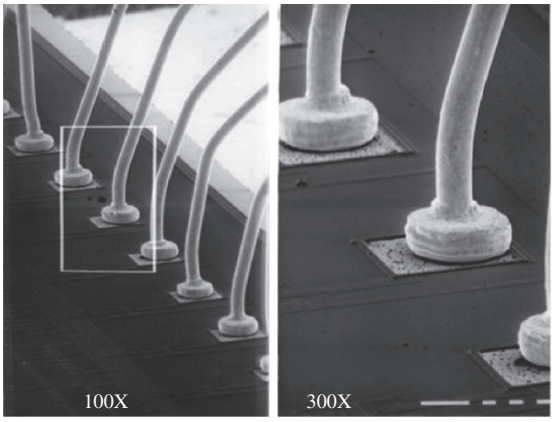

(a)

Fig. 1.1. Ball bonds (thermo-compression or thermosonic). (**a**) Scanning electron microscope photo micrograph of typical ball bonds and (**b**) schematic representation of ball bonds with important parameters indicated

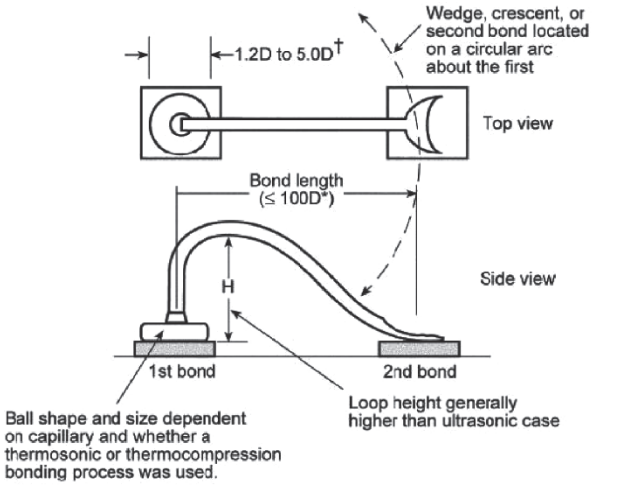

(b)

Fig. 1.1. (Continued)

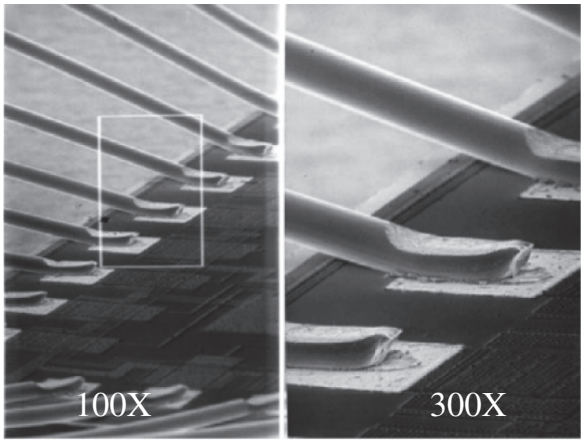

(a)

Fig. 1.2. Ultrasonic bonds (wedge bonds). (**a**) Scanning electron microscope photo micrographs of typical ultrasonic wedge bonds and (**b**) schematic representation of ultrasonic bonds with important parameters indicated

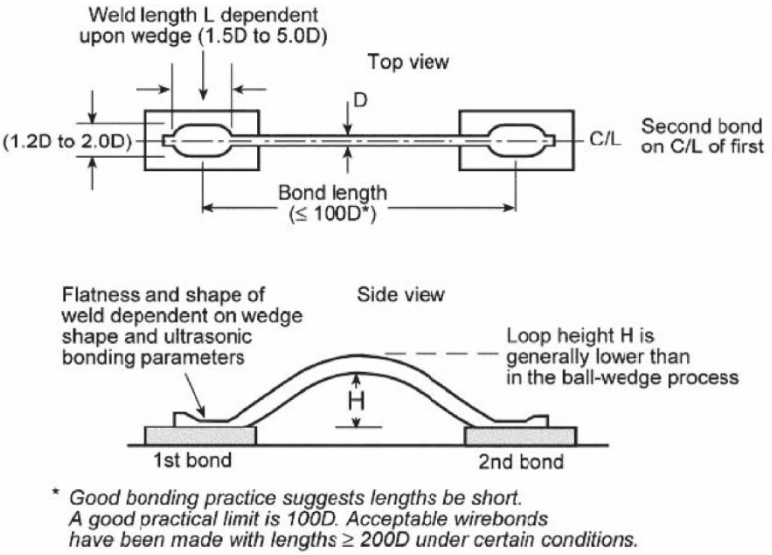

(b)

Fig. 1.2. (Continued)

Gold ball bonding starts when a gold wire is fed through what is called a capillary. The capillary holds the gold wire as an electronic flame-off (EFO) is used to melt the end of the wire, forming a gold ball with a free-air ball diameter ranging from 1.5 to 2.5 times the wire diameter, with a typical wire diameter ~25–30 µm. Free air ball size consistency, controlled by the EFO and the tail length, is critical in good bonding. The free- air ball is then brought into contact with the bond pad. Adequate amounts of pressure, heat, and ultrasonic forces are then applied to the ball for a specific amount of time, forming the initial metallurgical weld between the ball and the bond pad as well as deforming the ball bond itself into its final shape. The wire is then run to the corresponding finger of the leadframe, forming a gradual arc or "loop" between the bond pad and the leadfinger. Pressure and ultrasonic forces are applied to the wire to form the second bond (known as a wedge bond, stitch bond, or fishtail bond), with the leadfinger. The wire bonding machine or wire bonder breaks the wire in preparation for the next wire bond cycle by clamping the wire and raising the capillary.

During aluminum wedge bonding, a clamped aluminum wire is brought in contact with the aluminum bond pad. Ultrasonic energy is then applied

to the wire for a specific duration while being held down by a specific amount of force, forming the first wedge bond between the wire and the bond pad. The wire is then run to the corresponding lead finger, against which it is again pressed, and a second bond formed by applying ultrasonic energy to the wire. The wire is then broken off by clamping and movement of the wire.

The gold ball bonding is non-directional and, as a result, is much faster than aluminum wedge bonding, which is why it is extensively used in plastic packaging. Unfortunately, gold ball bonding on Al bond pads cannot be used in hermetic packages, primarily because the high sealing temperatures (400–450^{o} C) used for these packages tremendously accelerate the formation of Au–Al intermetallics, which can lead to early life failures. Gold ball bonding on gold bond pads, however, may be employed in hermetic packages.

Unlike Al–Al ultrasonic wedge bonding, Au–Al thermosonic ball bonding requires heat to facilitate the bonding process. The Al bond pad is harder than the Au ball bond, and it is impossible to make good bonding between them through purely ultrasonic without causing wire, bond pad, or silicon substrate damage. The application of thermal energy to the Al bond pads "softens" them, promoting the inter-diffusion of Au and Al atoms that ultimately form the Au–Al bond. Heat application also improves bonding by removing organic contaminants on the bond pad surface.

The tape automated bonding (TAB) technology is a usual microelectronic industrial process. TAB involves bonding a gold-bumped die to a leadframe circuit built on a flexible tape material, such as polyimide or polyester (Fig. 1.3). The TAB is used primarily in the flat panel display industry to mount driver chips between the glass of the display and the input circuitry behind the display, because of its low dimension interconnection. The flexible circuit using in TAB allows the package to be bent upward of 180°, allowing the circuit to be routed within the small confines of a flat panel display. It is also used in optical applications such as the sensors of stepper motors.

TAB is also utilized as a package format for Multi Chip Modules (MCM). In this format, the die and some of the leads are punched from the tape, the leads are formed, and then the package is mounted in a method similar to a J-Lead package. In some cases, the leads are not formed, but are soldered directly to the board.

TAB is typically a single-sided polyimide-based circuit, although a more expensive two-metal or four-metal tape is available. A copper metallization layer is bonded to the polyimide in one of two ways, either the copper is electrodeposited to the tape or an adhesive is used to bond rolled copper to the tape. Once the copper has been bonded to the polyimide the circuitry is imaged using a photolithography process, which allows for a

tight line pitch of up to 45 μm with a 22.5 μm lines and space widths. The tight pitch of TAB is very advantageous and allows for high-density circuits for high pin count devices.

There are two methods to achieve the connection between the die and the circuit. The first one is a single-point thermosonic bond. Single-point bonding requires each bond pad position to be individually bonded using heat, time, pressure, and ultrasonic applied to the TAB lead which is directly over its unique gold-bumped bond pad. This process does not require specific tools but on the other hand, it takes several times. The second one, the "Gang bonding," uses thermo-compression bonding to create a diffusion bond between all leads and bumps at the same time, all interconnections are performed in a one-step process-gang bonding. A specially designed tool bonds all the leads to the die using force, temperature, and time. It has the highest throughput. Then, the devices can be encapsulated, delivered in a reel-to-reel or singular format. Another advantage of this process is the minimized size of the circuits: the resulting height is the sum thickness of the die, the bumps, and the copper track.

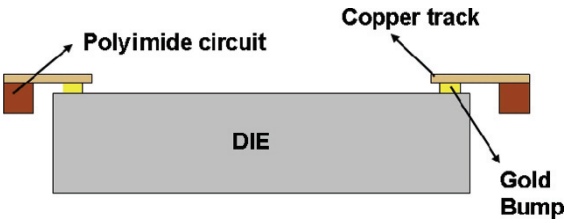

Fig. 1.3. A schematic of TAB interconnect

In contrast to wire bonding, in which the active silicon is "face-up," flip chip microelectronics assembly utilizes a different assembly method in which active silicon is flipped "face-down." With the active silicon face-down, electrical connections between the silicon and the substrate, circuit board, or carrier are made using conducive bumps on chip bond pads (Fig. 1.4) [12]. In contrast, wire bonding uses face-up chips with a wire connection to each pad. A comparison of wire bonding and flip chip is shown in Table 1.1. Flip chip components are predominantly semiconductor devices; however, components such as passive filters, detector arrays, and microelectromechanical system (MEMs) devices are also beginning to use flip chip bonding technologies.

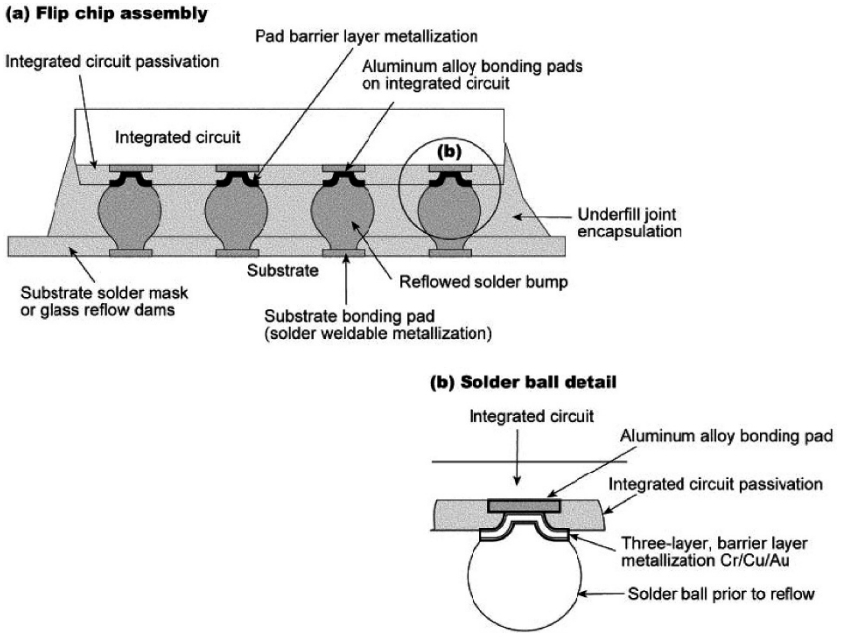

Fig. 1.4. Schematic representation of the flip chip bonding process. (**a**) Cross-section of a flip chip assembly and (**b**) detail of the solder ball and barrier layer metallization prior to reflow

Flip chip packaging has been widely adopted by the industry due to the technology's advantages in size, performance, flexibility, reliability, and cost over other packaging methods:

- *Smallest size* Eliminating packages and bond wires reduces the required board area by up to 95% and requires far less weight. Weight can be less than 5% of packaged device weight. Flip chip is the simplest minimal package, smaller than chip-scale packages (CSP) because of its chip size.
- *Highest performance* Flip chip offers the highest speed electrical performance of any assembly method. Eliminating bond wires reduces the delaying inductance and capacitance of the connection by a factor of 10 and shortens the path by a factor of 25–100. The result is high-speed off-chip interconnection.
- *Greatest I/O flexibility* Flip chip has the highest input/output connection flexibility of any interconnect technology. Wire bond connections are limited to the perimeter of the die, driving die sizes up as the number of connections increases, while flip chip connections can use the whole area of the die, accommodating many more connections on a smaller die. Area

connections also allow 3-D stacking of dies (via through silicon via [TSV], wire bonding, anisotropic conductive adhesive film (ACF) as well as flip chip interconnections) and other components.

- *Lowest cost* Flip chip can be the lowest cost interconnection for high-volume automated production as it can provide thousands of interconnection at once via a solder reflow process as such, costs below $0.01 per I/O connection. This explains flip chip's longevity in the cost-conscious automotive world, pervasiveness in low-cost consumer watches, and growing popularity in smart cards, RF-ID cards, cellular telephones, and other cost-dominated applications.

Early flip chip technologies used solder balls, or "bumps," to electrically connect the chip to the substrate. Even though materials other than solder balls have been developed, the term bump is still widely used by the industry; however, the primary functions of bumps remain the same. First, the bump provides the conductive path from chip to substrate. The bump also provides a thermally conductive path to carry heat from the chip to the substrate. In addition, the bump provides part of the mechanical mounting of the die to the substrate. Finally, the bump provides a spacer, preventing electrical contact between the chip and the substrate conductors, and acting as a short lead to relieve mechanical strain between board and substrate.

Flip chip packages can be classified into the following categories based on the processes for forming the bump and the interconnection between the die and the chip carrier:

- *Solder bump flip chip* The solder bumping process requires that an under-bump metallization (UBM) be placed on the chip bond pads by sputtering, plating, or other means. This UBM layer replaces the insulating aluminum oxide layer and also defines and limits the solder-wetted area. Solder is deposited over the UBM by evaporation, electroplating, screen printing solder paste, or needle depositing. After solder bumping, the wafer is sawn into individual chips called "bumped die." The bumped die is placed on the substrate pads, and the assembly is heated to make a solder connection.
- *Plated bump flip chip* Plated bump flip chip uses wet chemical processes to remove the aluminum oxide and plate conductive metal bumps onto the wafer bond pads. Plated nickel-gold bumps are formed on the semiconductor wafer by electroless nickel plating of the aluminum bond pads of the chips. After plating with the desired thickness of nickel, an immersion gold layer is added for protection, and the wafer is diced into bumped die. Plating copper bumps (posts) on wafers have also been demonstrated [13].

Attachment generally is by solder or adhesive, which may be applied to the bumps or the substrate bond pads by various techniques.

- *Stud bump flip chip* The gold stud bump flip chip process bumps die by a modified standard wire bonding technique. This technique makes a gold ball for wire bonding by melting the end of a gold wire to form a sphere. The gold ball is attached to the chip bond pad as the first part of a wire bond. To form gold bumps instead of wire bonds, wire bonders are modified to break off the wire after attaching the ball to the chip bond pad. The gold ball, or "stud bump" remaining on the bond pad, provides a permanent connection through the aluminum oxide to the underlying metal. The gold stud bump process is unique in being readily applied to individual single die or to wafers. Gold stud bump flip chips may be attached to the substrate bond pads with adhesive [14] or by thermosonic gold-to-gold connection. Die bumping and assembly services are available from several suppliers such as PacTech in Germany, Flip Chip International in USA.

- *Polymer bump flip chip* This adhesive bump flip chip process stencils a conductive adhesive to form bumps onto an under-bump metal [15–18]. Once cured, the adhesive acts as bumps and an additional attachment of conductive adhesive bonds the bumps to the mating chip or substrate. There are three stages in making flip chip assemblies: bumping the die or wafer, attaching the bumped die to the board or substrate, and, in most cases, filling the remaining space under the die with an electrically non-conductive "underfill" material.

Table 1.1. Comparison of wire bonding and flip chip interconnection factors [12]

Factor	Wire bond	Flip chip
Area	Requires space outside of chip perimeter for second bond	Within chip perimeter
Number I/O	Limited: 1–4 perimeter rows (100s–1,000s possible)	Full area array. Outperforms wire bonding even with a larger pitch (1,000s–10,000s possible)
Flexibility	Very flexible. Ability to shift I/O. Accommodate different die orientations, die sizes, package layout, etc. (within reason, of course)	None. Substrate pattern must match I/O pattern on chip. (Some self-aligning force.)
Electrical performance	Long round wires limits low loss frequency response to between 5 and10 GHz	Short , fat solder joint pillars allow low loss frequency response above 100 GHz
Cost	Typically \$0.0005–\$0.001 per interconnect with full automation	Ranges from \$0.01 to \$0.05 per interconnect [a]
Bonding time	Sequential (10–20 bonds/second)	Gang (all bonding at one reflow)
Bond type	Weld: Au–Al, Au–Au, Al–Al, Au–Cu,Cu–Cu	Solder : Sn63, Sn5, Sn10, Lead free (SnAg, SnAgCu,…)

Reliability	Monometallic systems, extremely reliable, flexible lead, eliminates or reduces any CTE issues. Bimetallic system could be susceptible to intermetallic growth and voiding	Solder fatigue a concern due to CTE mismatches. Typically requires underfill. Intermetallic growth and voiding problems with Sn and Cu
Environmental	Au, Al, environmentally friendly	Pb an environmental concern, hence lead-free alloys are used

[a] Includes extra cost for custom under-bump metallurgy and a penalty for substrate repatterning if the die shrink or pin out changes could be accommodated by the wire bond technology without changing the substrate pattern

Second-level packaging provides the interconnection between the interposer and substrate to either a printed wiring board (PWB) or a card. This interconnection can be realized by through-hole (TH) technology, surface mount technology (SMT) including dual-in-line, quad-in-line, ball grid array (BGA), and chip-scale package (CSP). Traditional through-hole dual in-line package (DIP) assemblies reached their limits in terms of improvements in cost, weight, volume, and reliability at approximately 68 leads. SMT allows production of more reliable assemblies with higher I/O, increased board density, and reduced weight, volume, and cost.

Third-level packaging mainly is the process to put second-level packages (i.e., FR 4 motherboard) onto a backplane. With the requirements toward low cost, miniaturization, and high performance for the current semiconductor devices, the bare IC chips can also be connected to the integrated board using flip chip technology directly [19], which is called flip chip on board (FCOB) or direct chip attach (DCA). The advantage is to eliminate the first-level package (chip to package), reduce assembly cost, and enhance performance.

The packaging concepts and technologies at all packaging levels are under quick evolution because of the dramatic changes in the computer, telecommunications, automotive, and consumer electronics industries to low cost, portability, high performance, diverse functions, and environment- and user-friendliness. Figure 1.5 illustrates the historical evolution of packaging [20]. Packages have evolved from traditional DIP (dual-in-line packages), quad flat packages (QFP) to area array flip chip, and BGA (ball grid array) packages. The silicon efficiency in the package has increased to almost 100% with the following CSP (chip-scale packages) and now in excess of 100% silicon efficiency by stacking those thin dies in three-dimensional stacked packages. In order to increase the efficiency of packaging, there is a paradigm shift to wafer level packaging (WLP) and through silicon vias (TSVs). WLP is a packaging technology where most or all of the IC packaging process steps are carried out at the wafer level. TSV technology enables the chips (or wafers) to be stacked vertically, thus reducing the wiring length to the thickness of the die. Memory dies can be stacked right on top of the processor die to provide high-speed and

low-loss memory–processor interfaces due to the lower parasitics of the TSV vertical interconnections. TSVs can be developed in an area array format thereby increasing the vertical interconnection density. They can also be used for heterogeneous integration of different IC technologies.

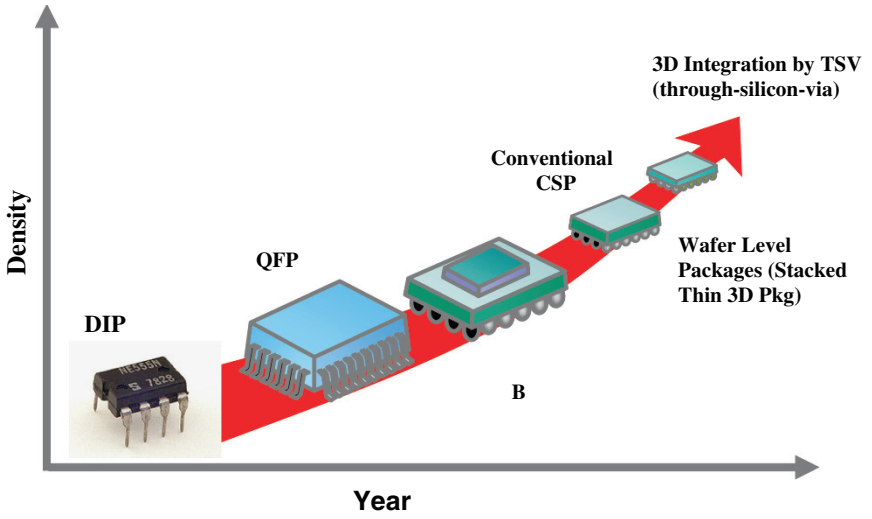

Fig. 1.5. Electronics packaging evolution

1.2 Interconnection Materials

Different levels of packaging are connected through interconnect materials. The primary purpose of interconnect materials is to electrically connect components for power, ground, and signal transmissions, with lead-containing solder alloys, especially eutectic tin/lead (Sn/Pb), has been the de facto interconnect material in most areas of electronic packaging. Such interconnection technologies include pin through hole (PTH), surface mount technology (SMT), ball grid array (BGA) package, chip-scale package (CSP), and flip chip technology [21]. Figure 1.6 shows an example of a functional surface mount component attached to a substrate via interconnect materials.

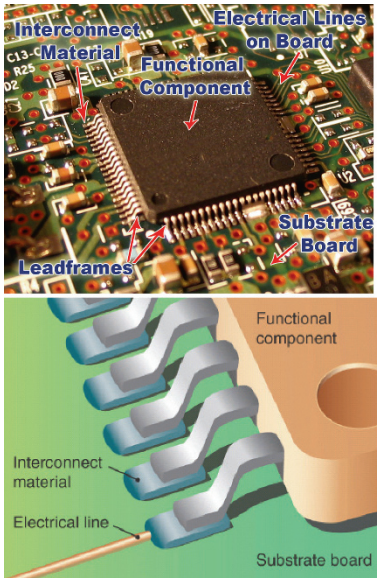

Fig. 1.6. (*Top*) Photo of a functional component that is assembled on the board substrate via interconnects. (*Bottom*) side view of the bonding between the component and the substrate via the interconnect material

1.2.1 Lead-Free Interconnect Materials

There are increasing concerns with the use of tin–lead alloy solders because the lead contained in these solders is a material hazardous to both humans and environment. Each year, thousands of tons of lead are incorporated into thousands of products with consumer products consuming the bulk of the lead. Many of these products such as cell phones, pagers, electronic toys, personal digital assistants tend to have a short life cycle on the order of 2–3 years and millions of lead-containing products simply end up in landfills. According to 2001 US Geological Survey, the total lead consumption by the US industries in 2000 was 52,400 metric tons. More than 10% of the lead, 5,430 metric tons, was used to produce alloy solders. Recycling of lead-containing consumer electronic products has proven to be very difficult, although in Japan, legislation prohibiting lead disposal in landfills and other waste disposal sites is already in place. The electronic industry is moving toward green manufacturing as a global trend. In the area of soldering, mainly driven by European RoHS (Reduction of Hazardous Substances), lead was banned effective July 1,

2006, except in some exempt items. This European legislation is followed by China RoHS which has similar list of banned materials, and its phase 1 implementation was effective March 1, 2007. In Japan, the legislative activities deal with the reclamation and recycling of electronics. The Home Electronics recycling law came into force on April 1, 2001, and applied only to TVs, refrigerators, and similar items. Although not specifically aiming at lead, this legislation effectively drove Japanese industry toward lead-free soldering process. Those legislation activities lead the trend which effectively drives the rest of the world toward lead-free soldering (see Fig. 1.7).

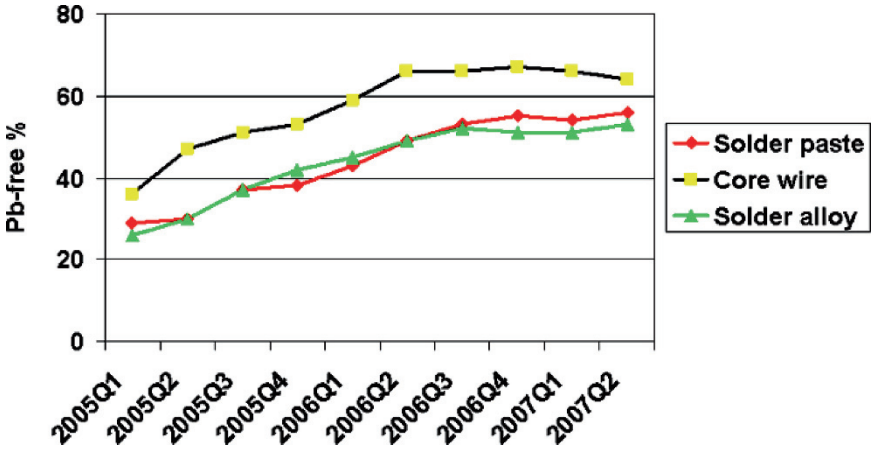

Fig. 1.7. Lead-free soldering implementation status reported by IPC [22]

The main requirements for an alternative solder alloy are the following:

1. Low melting point: The melting point should be low enough to avoid thermal damage to the assembly and high enough for the solder joint to bear the operating temperatures. The solder should retain adequate mechanical properties at these temperatures.
2. Wettability: The bond between the solder and the base metal is formed only when the solder wets the base metal properly. A high Sn content ensures this and thus forms a strong bond.
3. Availability: There should be adequate supplies or reserves available of candidate metals. Tin (Sn), zinc (Zn), copper (Cu), and antimony (Sb) are available whereas there is limited supply of indium (In).
4. Cost: Manufacturers of electronic systems are unlikely to change to an alternative solder with an increased cost unless it has demonstrated better properties or there is legislative pressure to do so.

There are strict performance requirements for solder alloys used in microelectronics. In general, the solder alloy must meet the expected levels of reliability, as well as electrical and mechanical performance [23–27].

Ever since the commencement of the research and development of Pb-free solder alloys, a large number of Pb-free solder alloys have been proposed and studied. Among the numerous lead-free solder options available, Fig. 1.8 shows the families which are of particular interest and the prevailing choices of industry: eutectic SnAg, eutectic SnCu, eutectic SnAgCu, eutectic SnZn, eutectic BiSn, along with their modifications. Also shown in Fig. 1.8 are the related applications including reflow soldering, wave soldering, and hand soldering. SnAgCu alloys are the prevailing choices, with SnCu(+Y), SnAg(+Y), and BiSn(+Y) families, where Y represents minor additive elements, also being adopted. The soldering processing window is narrower than that of eutectic tin–lead, also called Sn63 mainly due to the elevated melting temperature of SnAgCu solder and the limited high-temperature tolerance of components and board. The high surface tension of Sn aggravates the difficulty in wetting, while the high reactivity of Sn adds additional constraints to control the contact time between molten solder and base metal or solder container. Compared to Sn63, the creep rate of SnAgCu is slower at low stress, but faster at high stress. This results in a longer temperature cycling life at low joint strain applications, but a shorter cycling life at high joint strain applications. Higher Cu content stabilizes intermetallic compound (IMC) structure at interface between SnAgCu solder and NiAu bond pads. The high rigidity of SnAgCu solders enhances the fragility of joints, although significant improvement has been accomplished via low Ag or high Cu content or doping approaches [10].

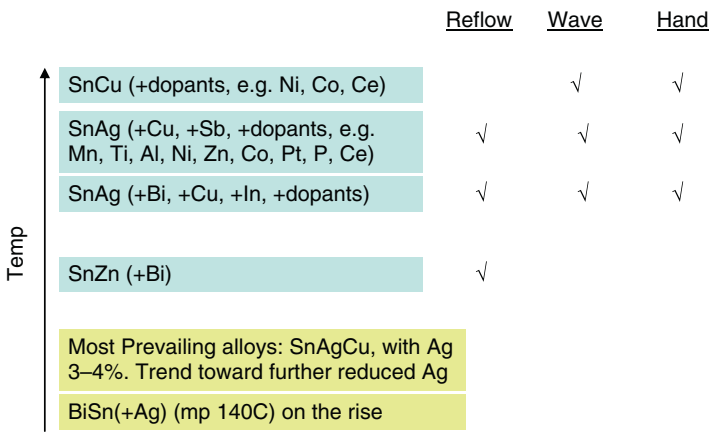

Fig. 1.8. Prevailing lead-free solder alloys and their applications [10]

Electronic devices such as notebook computers and cellular phones are required to be thin and small with complicated functions. The electronic industry has been coping with these changes, providing the necessary miniaturization of these electronic devices, and has been able to meet the required reliability. To support these changes, the interconnections provided by solder joints have become finer and finer in pitch size, and yet the reliability is maintained.

To meet the present and future strength requirements, higher strength solder alloys may be required. It is believed that composite solders would provide reinforcements to the otherwise weak solder, and researchers have been working on their development, beginning with the SnPb alloys [28–34]. These composite solders have been found to have good reliability because the reinforcing particles can suppress grain-boundary sliding, intermetallic compound (IMC) formation, grain growth, and furthermore, redistribute stress uniformly. In Pb-free composite solders, the reinforcements can be intermetallic powders of Cu_5Sn_5, Ag_3Sn or NiTi, carbon fibers, or fine oxide particles of metals such as Ni, Cu, and Ag [35–40]. Composite solder alloy development activities so far have mainly been aiming to achieve suitable physical properties and better service performance.

1.2.2 Electrically Conductive Adhesives

Other than lead-free solders, another lead-free interconnect material is electrically conductive adhesives (ECAs). ECAs mainly consist of an organic/polymeric binder matrices and conductive metal fillers. The conductive fillers provide the electrical properties and the polymeric matrices provide the physical and mechanical properties. Compared to the solder technology, ECAs offer numerous advantages such as environmental friendliness from the elimination of lead usage and flux cleaning, mild processing conditions, fewer processing steps which reduce processing cost, and finally, an increase in fine-pitch capability due to the availability of small-sized conductive fillers. There are two types of ECAs: isotropically conductive adhesives (ICAs) which are conductive equally in all directions and anisotropically conductive adhesives (ACAs) which are only conductive in one direction, typically along the *z*-axis. Figure 1.9 compares chip-to-substrate interconnects with solder joints and different ECA joints. However, like all lead-free materials, currently commercialized ECAs still have some material property limitations and challenges, including lower electrical and thermal conductivity compared to solder interconnects materials, contact resistance fatigue in reliability tests, limited current-carrying capability, metal migration fatigue in reliability and high voltage tests, and poor impact strength [40–42].

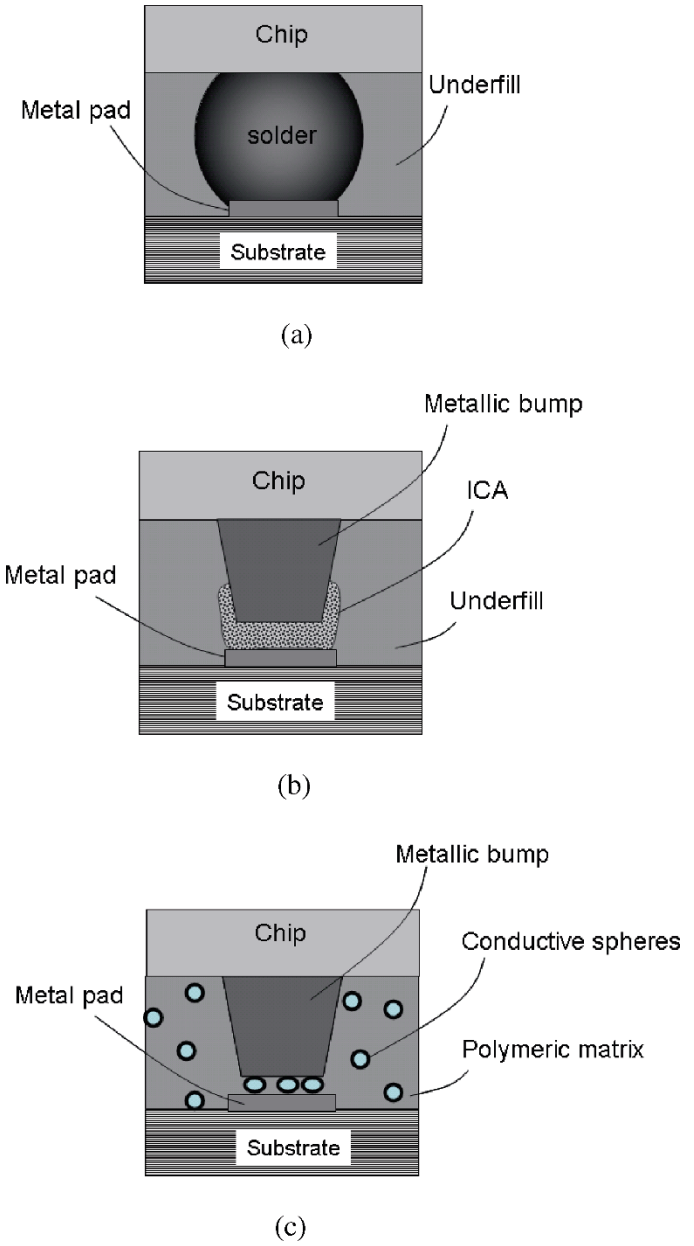

Fig. 1.9. Comparison of various types of interconnect approaches. (**a**) Solder interconnect, (**b**) isotropically conductive adhesive (ICA) interconnect, and (**c**) anisotropically conductive adhesive (ACA) interconnect

1.2.2.1 Electrically Conductive Adhesives (ECA) categories

ICAs and ACAs generally contain different types of conductive fillers and filler loadings are different too. ICAs typically are filled with 1–10 μm-sized Ag flakes and ACAs typically contain 3–5 μm-sized conductive fillers which usually are spherical in shape. Non-conductive adhesives (NCAs, typically without conductive fillers) have also become quite popular for some applications. The difference between ICA and ACA/NCA is based on the percolation theory as shown in Fig. 1.10. The percolation threshold (Pc) depends on the shape and size of the fillers, but typically in the order of 15–25% volume fraction. For ICA, the loading level of conductive fillers exceeds the percolation threshold, providing electrical conductivity in all *x*, *y*, and *z* directions. For ACAs or NCAs, the electrical conductivity is provided only in *z*-direction between the electrodes of the assembly. Figure 1.11 shows the schematics of the interconnect structures and typical cross-sectional images of flip chip joints by ICA, ACA, and NCA materials illustrating the bonding mechanism for all three adhesives.

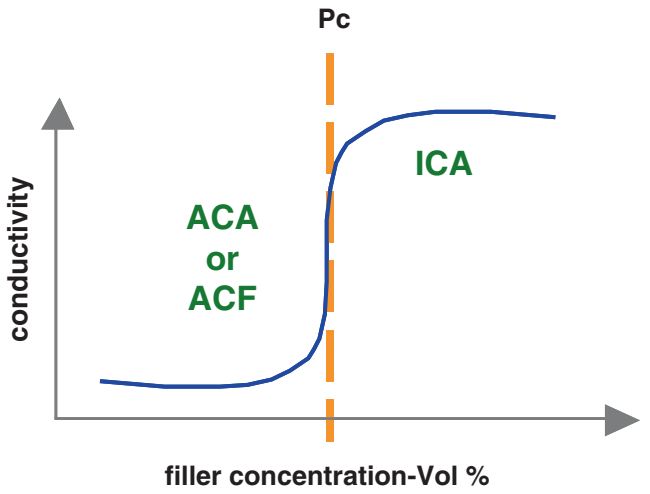

Fig. 1.10. Typical percolation curve of conductive adhesives (*P*c is the percolation threshold)

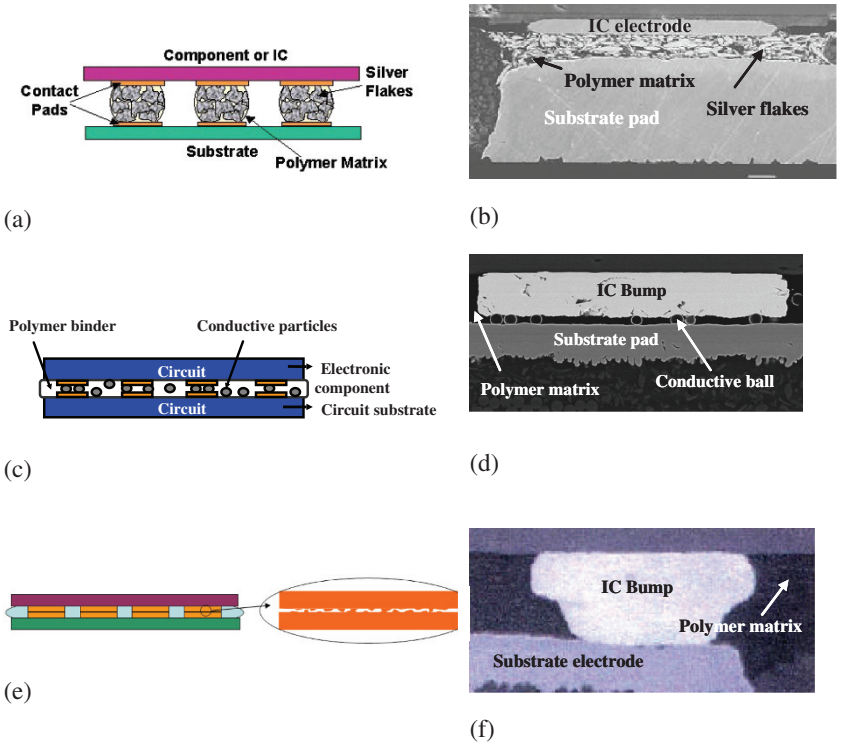

Fig. 1.11. Schematic illustrations and cross-sectional views of (**a**), (**b**) ICA, (**c**), (**d**) ACA, and (**e**), (**f**) NCA flip chip bonding

Isotropic conductive adhesives are composites of polymer resin and conductive fillers. The adhesive matrix is used to form an electrical and mechanical bond at the interconnects. With increasing filler concentrations, the electrical properties of an ICA transform it from an insulator to a conductor. ICAs have been used in the electronic packaging industry primarily as die attach adhesives [43–45]. Recently, ICAs have been proposed as an alternative to tin/lead solders in surface mount technology (SMT) [46], flip chip, and other applications.

Anisotropic conductive adhesives (ACAs) or anisotropic conductive films (ACFs) provide unidirectional electrical conductivity in the vertical or *Z*-axis. This directional conductivity is achieved by using a relatively low volume loading of conductive filler (5–20 volume percent). The low volume loading is insufficient for inter-particle contact and prevents conductivity in the *X*–*Y* plane of the adhesive. The *Z*-axis adhesive, in film or paste form, is interposed

between the surfaces to be connected. Heat and pressure are applied simultaneously to this stack-up until the particles bridge the two conductor surfaces. Recently, anisotropic conductive adhesives/films (ACAs/ACFs) are becoming popular as one of promising candidates for lead-free interconnection solutions in microelectronic packaging application due to their technical advantages such as fine-pitch capability below 40 μm, low-temperature processing ability, low cost, and environmentally friendly materials and processing. ACAs/ACFs consist of conducting particles (typically 5 ~ 10 μm in diameter) and polymer matrix that provides both attachment and electrical interconnection between electrodes [47–49]. In particular, ACFs are widely used for high-density interconnection between liquid- crystal display (LCD) panels and tape carrier packages (TCPs) to replace the traditional soldering or rubber connectors. In LCD applications, traditional soldering may not be as effective as ACFs in interconnecting materials between indium tin oxide (ITO) electrodes and TCP. ACFs have also been used as an alternative to soldering for interconnecting TCP input lead bonding to printed- circuit boards (PCBs).

1.2.2.2 Nanoelectrically Conductive Adhesives

To meet the requirements for future fine pitch and high-performance interconnects in advanced packaging, ECAs with nanomaterials or other nano-technologies are attracting more and more interest due to the special electrical, mechanical, optical, magnetic, and chemical properties that nano-sized materials can possess. There has been extensive research on nanoconductive adhesives that contain nano-filles, such as nanoparticles, nanowires, or carbon nanotubes, and nano monolayer graphenes.

A detailed review of ICAs, ACAs/ACFs, and nano-ECA will be covered in other chapters in this book.

References

[1] R. R. Tummala, E. J. Rymaszewski, and A. G. Klopfenstein, Eds., "Microelectronics Packaging Handbook," 2nd Ed., Chapman & Hall, London, 1997.

[2] L. M. Levinson, C. W. Eichelberger, R. J. Wojnarowski, and R. O. Carlson, "High-Density Interconnect Using Laser Lithography," *Proceedings International Symposium on Microelectronics*, Seattle, Washington, October 17–19, pp. 301–306, 1988.

[3] G. Lo and S. K. Sitaraman, "G-Helix: Lithography-Based, Wafer-Level Compliant Chip-to-Substrate Interconnect," *Proceedings*

54th Electronic Components and Technology Conference, Las Vegas, Nevada, June 1–4, pp. 320–325, 2004.

[4] D. B. Tuckerman, D. J. Ashkenas, E. Schmidt, and C. Smith, "Die Attach and Interconnection Technology for Hybrid WSI," *Laser Pantography States Report UCAR*, Lawrence Livermore Laboratories, pp. 10195, 1986.

[5] D. J. Ehrlich and J. Y. Tsao, "Laser Direct Writing for VLSI," *VLSI Electronics: Microstructure Science*, 7, 129–164, 1983.

[6] D. Liu, C. Zhang, J. Graves, and T. Kegresse, "Laser Direct-Write (LDW) Technology and Its Applications in Low Temperature Co-Fired Ceramic (LTTC) Electronics," *Proc. 2003 International Symposium on Microelectronics*, Nov. 18–20, pp. 298–303, 2003.

[7] V. S. Rao, A. A. O. Tay, V. Kripesh, C. T. Lim, and S. W. Yoon, "Bed of Nails-100 Microns Pitch Wafer Level Interconnections Process," *Proceedings. of the Electronic Packaging Technology Conference*, pp. 444–449, 2004.

[8] R. R. Tummala, P. M. Raj, A. Aggarwal, G. Mehrotra, S. W. Koh, and S. Bansal, "Copper interconnections for High Performance, Fine Pitch Flipchip and Ultra-Miniaturized Module Applications," *Proceedings of the Electronic Components and Technology Conference*, May 28–30, pp. 102–111, 2006.

[9] T. Wang, F. Tung, L. Foo, and V. Dutta, "Studies on a Novel Flip-Chip Interconnect Structure-Pillar Bump," *Proceedings of the Electronic Components and Technology Conference*, pp. 945–949, 2001.

[10] D. Lu and C. P. Wong, Eds., "Materials for Advanced Packaging," Springer, Berlin, 2008.

[11] I. Soga, D. Kondo, Y. Yamaguchi, T. Iwai, M. Mizukoshi, Y. Awano, K. Yube, and T. Fujii, "Carbon Nanotube Bumps for LSI Interconnect," *Proceedings of the 58th Electronic Components and Technology Conference*, pp. 1390–1394, 2008.

[12] D. Lu and C. P. Wong, "Electrical Conductive Adhesives", in Materials for Advanced Packaging, Chapter 11, D. Lu and C. P. Wong, Eds., Springer, Berlin, 2008.

[13] A. Yeoh, M. Chang, C. Pelto, T.-L. Huang, S. Balakrishnan, G. Leatherman, S. Agraharam, G. Wang, Z. Wang, D. Chiang, P. Stover, and P. Brandenburger, "Copper Die Bumps (First Level Interconnect) and Low-K Dielectrics in 65 nm High Volume Manufacturing," *Proceedings of 56th Electronic Components and Technology Conference*, 30 May–2 June, pp. 1611–1615, 2006.

[14] Z. Zhong, "Flip Chip Assemblies Using Gold Bumps and Adhesives," *Microelectronics International*, 18(3), 15–19, 2001.

[15] D. Wojciechowski, J. Vanfletern, E. Reese, and H. Hagerdorn, "Electroconductive Adhesives for High Density Package and Flip-Chip Interconnections," *Microelectronics and Reliability*, 40, 1215–1226, 2000.

[16] F. W. Kulesza and R. H. Estes, "Better Bump?," *Advanced Packaging*, 6, 26–29, 1997.

[17] C. Howard, S. Nair, S. Ang, and L. Schaper, "Investigation of Conductive Polymer-Flip Chip Attachment in Multichip Module Applications," *Proceedings Electronic Components Technology Conference*, pp. 1244–1249, 1995.

[18] L. Anon, "Polymer Flip-Chip PFC: A Solderless Bump Process," *Microwave Journal*, 38, 128–130, 1995.

[19] R. R. Tummala and V. Madisetti, "System on Chip or System on Package," *IEEE Design and Test of Computer*, 4, 48, 1999.

[20] C. P. Wong, Polymers for Electronic and Photonic Applications, Academic Press, New York, 1993.

[21] K. J. Puttlitz, K. A. Stalter, and P. T. Vianco, "Handbook of Lead-Free Solder Technology for Microelectronic Assemblies," Marcel Dekker, New York, USA, pp. 167–210, 2004.

[22] *IPC Global Solder Statistical Program Report for 2nd Quarter 2007*, August 2007.

[23] J. Cannis, "Green IC packaging," *Advanced Packaging*, 8, 33–38, 2001.

[24] L. F. A. T. White Paper: IPC-SPVC-WP-006 Round Robin Testing and Analysis, Silver, Copper, 12, "International Printed Circuit Association Solder Products Value Council," *White Paper: IPC-SPVC-WP-006 Round Robin Testing and Analysis*, Lead Free Alloys: Tin, Silver, Copper, 12, August 2003.

[25] M. Abtew and G. Selvaduray, "Lead-Free Solders in Microelectronics," *Materials Science and Engineering Report*, 27(5–6), 95–141, 2000.

[26] C. M. L. Wu, M. L. Huang, J. K. L. Lai, and Y. C. Chan, "Developing a Lead-Free Solder Alloy Sn-Bi-Ag-Cu by Mechanical Alloying," *Journal of Electronic Materials*, 29(8), pp. 1015–1020, 2000.

[27] K. Suganuma, "Advances in Lead-Free Electronics Soldering," *Current Opinion in Solid State and Materials Science*, 5, 55–64, 2001.

[28] B. Irving, "How $1-billion per Year can be Saved in the Soldering of Electronic Compounds," *Welding Journal*, 10, 54–56, 1991.

[29] J. L. Marshall and J. Calderon, "Hard-Particle Reinforced Composite Solders Part 1: Microcharacterisation," *Soldering and Surface Mount Technology*, 9(2), 22–28, 1997.

[30] R. J. Geckle, "Metallurgical Changes in Tin-Lead Platings due to Heat Aging," *IEEE Transactions on Components, Hybrids and Manufacturing Technology*, 14(4), 691–697, 1991.

[31] H. S. Betrabet, S. M. McGee, and J. K. McKinlay, "Processing Dispersion-Strengthened Sn-Pb Solders to Achieve Microstructural Refinement and Stability," Scripta Metallurgica et Materialia, 25(10), 2323–2328, 1991.

[32] D. L. D. Chung, "Carbon Fiber Reinforced Tin-Lead Alloy as a Low Thermal Expansion Solder Perform," *US Patent 5,089,356*, 1992.

[33] S. Jin and M. McCormack, "Dispersed Additions to a Pb-Free Solder for Suppression of Microstructural Coarsening," *Journal of Electronic Materials*, 23(8), 735–739, 1994.

[34] C. M. Miller, I. E. Anderson, and J. F. Smith, "A Viable Tin-Lead Solder Substitute: Sn-Ag-Cu," *Journal of Electronic Materials*, 23(7), 595–601, 1994.

[35] J. H. Lee, D. J. Park, J. N. Heo, Y. H. Lee, D. H. Shin, and Y. S. Kim, "Reflow Characteristics of Sn-Ag Matrix in-situ Composite Solders," *Scripta Materialia*, 42(8), 827–831, 2000.

[36] S. Y. Hwang, J. W. Lee, and Z. H. Lee, "Microstructure of a Lead-Free Composite Solder Produced by an in-situ Process," *Journal of Electronic Materials*, 31(11), 1304–1308, 2002.

[37] K. N. Subramanian, T. R. Bieler, and J. P. Lucas, "Microstructural Engineering of Solders," *Journal of Electronic Materials*, 28(11), 1176–1183, 1999.

[38] O. Fouassier, J. Chazelas, and J. F. Silvain, "Conception of a Consumable Copper Reaction zone for a NiTi/SnAgCu Composite Material," *Composites Part A*, 33(10), 1391–1395, 2002.

[39] C. T. Murray, R. L. Rudman, M. B. Sabade, and A. V. Pocius, "Conductive Adhesives for Electronic Assemblies," *Materials Research Bulletin*, 28, 449–454, 2003.

[40] E. P. Wood and K. L. Nimmo, "In Search of New Lead-Free Electronic Solders," *Journal of Electronic Materials*, 23(8), 709–714, 1994.

[41] Research Triangle Park, NC," *Environmental Protection Agency, National Air Quality and Emission Trend Report*, EPA-450/4-91-003, 1989.

[42] H. Kristiansen and J. Liu, "Overview of Conductive Adhesive interconnection Technologies for LCD's," *IEEE Transactions on Components Packaging and Manufacturing Technology Part A*, 21, 208–214, 1998.

[43] G. Nguyen, J. Williams, F. Gibson, and T. Winster, "Electrical Reliability of Conductive Adhesives for Surface Mount Applications," *Proceedings of International Electronic Packaging Conference*, pp. 479–486, 1993.

[44] L. Li, J. E. Morris, J. Liu, Z. Lai, L. Ljungkrona, and C. Li, "Reliability and Failure Mechanism of Isotropically Conductive Adhesives," *Proceedings of the 45th IEEE Electronic Components and Technology Conference*, May 21–24, pp. 114–120, 1995.

[45] M. A. Gaynes, R. H. Lewis, R. F. Saraf, and J. M. Roldan, "Evaluation of Contact Resistance for Isotropic Electrically Conductive Adhesives," *IEEE Transactions on Components Packaging and Manufacturing Technology Part B-Advanced Packaging*, 18, 299–304, 1995.

[46] D. Cavasin, K.Brice-Heams, and A. Arab, "Improvements in the Reliability and Manufacturability of an Integrated RF Power Amplifier Module System-In-Package, via Implementation of Conductive Epoxy Adhesive for Selected SMT Components," *Proceedings 53rd Electronic Components and Technology Conference*, pp. 1404 ~ 1407, 2003.

[47] Y. Li, K. S. Moon, and C. P. Wong, "Electronics without Lead," *Science*, 308, 1419–1420, 2005.

[48] Y. Li and C. P. Wong, "Recent Advances of Conductive Adhesives as a Lead-free Alternative in Electronic Packaging: Materials, Processing, Reliability and Applications," *Materials Science & Engineering R-Reports*, 51, 1–35, 2006.

[49] J. Lau, C. P. Wong, N. C. Lee, and S. Lee, Electronics Manufacturing: With Lead-Free, Halogen-Free, and Conductive-Adhesive Materials, McGraw Hill, New York, 2002.

Chapter 2
Nanotechnology

2.1 Introduction to Nanotechnologies and Nanopackaging

Nanotechnology is the creation of functional materials, devices, and systems through control of matter on the nanometer length scale (<100 nm) and exploitation of novel phenomena and properties (physical, chemical, biological, mechanical, electrical, etc.) at that length scale.

Nanoelectronics refer to the use of nanotechnology on electronic components. Nanoelectronics hold the promise of making computer processors more powerful than is possible with conventional semiconductor fabrication techniques. A number of approaches are currently being researched, including new forms of nanolithography, as well as the use of nanomaterials such as nanowires or small molecules in place of traditional CMOS components. Field-effect transistors have been made using both semiconducting carbon nanotubes [1] and heterostructured semiconductor nanowires [2].

Single-molecule devices are another possibility. These schemes would make heavy use of molecular self-assembly, designing the device components to construct a larger structure or even a complete system on their own. This can be very useful for reconfigurable computing.

Molecular electronics [3] is a new technology which is still in its infancy, but also brings hope for truly atomic scale electronic systems in the future. One of the more promising applications of molecular electronics was proposed by the IBM researcher Ari Aviram and the theoretical chemist Mark Ratner of North Western University in their 1974 and 1988 papers Molecules for Memory, Logic and Amplification, respectively [4, 5]. This is one of many possible ways in which a molecular-level diode/transistor might be synthesized by organic chemistry. A model system was proposed with a spiro carbon structure giving a molecular diode about half a nanometer across which could be connected by polythiophene

Y. Li et al., *Electrical Conductive Adhesives with Nanotechnologies*,
DOI 10.1007/978-0-387-88783-8_2, © Springer Science+Business Media, LLC 2010

molecular wires. Theoretical calculations showed the design to be sound in principle and there is still hope that such a system can be made to work.

Nanopackaging, i.e., the application of nanotechnologies to electronics packaging, is being explored to enhance performance and reliability electronics packages. Nanotechnology drivers are the varied ways in which materials properties change at small dimensions, and these properties can be put to work to solve past packaging problems and to develop new approaches to future nanoelectronics packaging issues. Electron transport mechanisms at small dimensions include ballistic transport where the transport of electronic signal without generating any measurable heat, severe mean mean-free path restrictions in very small nanoparticles, various forms of electron tunneling, electron hopping mechanisms, and more.

In addition, candidate next-generation nanoelectronics technologies (e.g., single-electron transistors, quantum automata, molecular electronics) are generally hyper-sensitive to dimensional change, if based on quantum mechanical electron tunneling, and appropriate packaging will be essential to the success or failure of these technologies. Packaging strategies must therefore be developed in parallel with the basic nanoelectronics device technologies in order to make informed decisions as to their commercial viabilities [6].

2.2 Nanoparticles

2.2.1 Introduction

The transition from micro-particles to nanoparticles can lead to a number of changes in physical properties. Two of the major factors are the increase in surface area to volume ratio and the size of particles moving into the realm where quantum effects predominate.

The increase of surface-area-to-volume ratio, which is a gradual progression with particles getting smaller, leads to an increasing dominance of the behavior of the atoms on the surface of the particles over that of those in the interior of the particle. This affects both the properties of a particle in isolation and its interaction with other materials. The large surface area results in lots of interactions between intermixed materials in nanocomposites, leading to special properties.

Once particles become small enough they start to exhibit quantum mechanical behavior. The property of quantum dots is a case in point, whereas these are sometimes called artificial atoms because free electrons

in them start to behave in a way similar to electrons bound by atoms in that they can only occupy certain permitted energy states.

Additionally, the fact that nanoparticles have dimensions below the critical wavelength of light make them transparent, a property that makes them very attractive for applications in packaging, cosmetics, and coatings.

2.2.2 Nanoparticle Fabrication

The nanoparticle fabrication technique to be selected depends primarily on the intended functions. Usually, chemical reduction [7–12] and physical method [13] have been developed to synthesize bimetallic nanoparticles. The chemical reduction method for the preparation of bimetallic nanoparticles can be divided into two groups: one is the co-reduction of two different kinds of metal salts. For instance, Ag/Au alloy, El-Sayed and Murphy used simultaneous reduction of silver and gold salts to form Ag/Au alloy nanoparticles with size of 18 nm and less than 10 nm, respectively. Chen et al. [14] and Zhang et al. [15] used laser irradiation of silver–gold colloidal mixture to synthesize Ag/Au alloy nanoparticles. The other method is the successive reduction of two-metal salts, which is usually carried out to prepare a core–shell structure of bimetallic nanoparticles. Mandal et al. [16] used seed-mediated techniques to synthesize core-shell type Ag/Au bimetallic nanoparticles. For the physical method, nanoparticles can be made directly from the bulk materials. Compared to the chemical reduction method, the physical method renders higher yield. Particles produced by this method are usually quite large and have a wide distribution of particle size.

Noble metal nanoparticles, for example, have been fabricated by an eco-friendly ultrasonic processing technique. Beveridge and co-workers [17, 18] have demonstrated that gold particles of nanoscale dimensions may be readily precipitated within bacterial cells by incubation of the cells with Au^{3+} ions. Klaus et al. [19–21] have shown that the bacteria *Pseudomonas stutzeri* AG259 isolated from a silver mine, when placed in a concentrated aqueous solution of $AgNO_3$, resulted in the reduction of the Ag^+ ions and formation of silver nanoparticles of well-defined size and distinct morphology within the periplasmic space of the bacteria. Taking this approach a step further, they showed that biocomposites of nanocrystalline silver and the bacteria may be thermally treated to yield a carbonaceous (cermet) nano-material with interesting optical properties for potential application in functional thin-film coatings [21]. The exact reaction mechanism leading to the formation of silver nanoparticles by this species of silver-resistant bacteria was not clear. In an interesting recent study, Nair and Pradeep [22] have demonstrated that bacteria not normally exposed to

large concentrations of metal ions may also be used to grow nanoparticles. Nair and Pradeep have shown that *Lactobacillus* strains present in buttermilk, when challenged with silver and gold ions, resulted in the large-scale production of metal nanoparticles within the bacterial cells. They also showed that exposure of lactic acid bacteria present in the whey of buttermilk to mixtures of gold and silver ions could be used to grow nanoparticles of alloys of gold and silver [22]. Recently, Jose-Yacaman and co-workers [23, 24] have shown that gold and silver nanoparticles may be synthesized in live alfalfa plants by gold and silver uptake from solid media.

A precursor may be used, e.g., $AgNO_3$ for Ag nanoparticles, and there are techniques to control the particle shapes, e.g., spherical, cubic, or wires [6, 25]. Nanoparticles tend to agglomerate, and so the crucial step is often the use of a dispersant to counter this tendency [26, 27]. The thermal or sputter evaporation of metals and condensation on an insulating substrate will also yield a surface distribution of nanoparticles [28–31].

The enhanced chemical activities of nanoparticles, which make them effective as catalysts, are due to the high surface area-to-volume ratio, and hence to the high proportion of unsatisfied chemical bonds. In addition, other physical property changes include the following:

- Melting point depression: The melting points of small metal nanoparticles drop significantly with decreasing size at dimensions under 5 nm [26].
- Sintering: The thermally activated surface self-diffusion process drives net diffusion away from convex surfaces of high curvature, and into concave surfaces, yielding low-temperature bonding between nanoparticles in contact.
- Coulomb block, or blockade: An external field or thermal source of electrostatic energy is required to charge an individual nanoparticle; this effect is the basis of single-electron transistor operation [32].
- Single grain structures, such as nanoparticles, may achieve theoretical maximum mechanical strengths [33].
- Nanoparticles one to two orders smaller than the wavelength of visible light provide unique optical scattering properties [34] and absorption peaks which "color" thin films or suspensions of such nanoparticles.

2.2.3 Nanoparticle Applications

Embedded passive components are seen to be the solution to the problem of high proportions of PWB (printed wiring board) surface space being occupied by discrete passives. The "cermet" (ceramic–metal) resistors used in specialized on-chip applications are adaptable to the embedded PWB role. The structure consists of metallic nanoparticles embedded in a

dielectric (or polymer) with electron tunneling as the transport mechanism between particles. At low fields, the coulomb block array is randomly charged by thermal energy, giving a high negative temperature coefficient of resistance (TCR), offset by the inclusion of positive TCR metallic paths. Examples of structure-related properties are provided for the $Cr_x(SiO)_{1-x}$ and $(Cr_xSi_{1-x})_{1-y}N_y$ systems.

High dielectric constant, k, and minimal thickness are required for embedded capacitors. The former requirement is met by the inclusion of high dielectric constant particulates, and the latter requirement suggests nanoparticles, e.g., barium titanate, or metals. Nanoparticle surface energies must be reduced to avoid aggregation [27]. The target k is 50–200; $k \sim 150$ has been achieved with metal nanoparticles at the expense of high leakage (dielectric loss), since this is a similar structure to the cermet resistor, albeit at lower metallic load. An ultra-high k epoxy/carbon black polymeric composite with k in excess of 13,000 has been reported by Xu and Wong [38], but the loss is quite high in 0.1. However, when the epoxy matrix resin with a loss of 0.02 was replaced with a BCB (benzocyclobutene) with a loss of 0.008, a much lower loss composite was achieved at ~0.06. An alternative approach to leakage is to use aluminum particles, to take advantage of the native oxide coating [35], with $k \sim 160$ achieved [36]. Ag/Al mixtures have also been studied [37].

Note that thermally conductive materials have very similar structural requirements to the passive components, with metallic or SiC nanoparticles as fillers [38].

Inductive components are also required, especially for RF applications. Classical magnetism theory turns out to be inapplicable for nanograin dimensions less than the ferromagnetic exchange length (tens of nanometers) which can sustain high permeability and low coercivity.

The simple addition of nanoparticles to traditional isotropic electrically conductive adhesives (ICAs) filled with micron-sized Ag fillers in an epoxy matrix might be expected to lower resistivity by providing bridges between particles, but does not in fact improve conductance, due to mean free path restrictions and added interface resistances. The same principles limit the performance of alumina-loaded thermal composites [39]. The addition of silver nanoparticles does achieve dramatic reductions, however, by sintering wide-area contacts between flakes [40], a principle also applicable to micro-via fill in PWBs [41], which can also profitably use ICA materials. Nanoparticle filler sintering is the key step in any effective use of nanoparticles in these technologies and can also improve anisotropic conductive adhesive performance [42], aided by contact conductance enhancement by the addition of self-assembly molecular surface treatments [43, 44].

PWB surface electrical interconnect is achievable by screen or "ink-jet" printing of nanoscale metal colloids in suspension [45–48]. As above, electrical continuity is established by sintering Ag nanoparticles [49–52], which can also be used for die attach.

Fused silica fillers are added to flip chip underfills to reduce the coefficient of thermal expansion, and nanoparticles resist settling better [53] and scatter light less than larger fillers, permitting UV optical curing [54] and other advantages of optical transparency [55]. The higher viscosity of the nano-filled material can be reduced by silane surface treatments. Physical properties have been successfully modeled in terms of structural parameters. Nanoparticles with functionalized surfaces may be employed to increase the modulus, glass transition temperature (T_g), and dielectric property such as voltage endurance of polymer composites due to the strong interaction between the nanoparticles and the polymeric matrix and larger interaction zone [56, 57].

The addition of Pt, Ni, or Co nanoparticles to lead-free SnAg-based solder [58, 59] eliminates Kirkendall voids, reduces intermetallic compound (IMC) growth, and reduces IMC (intermetallic compound) grain sizes, significantly improving drop-test performance [60], promoting finer grain growth, increased creep resistance, and better contact wetting [61]. Nanoparticles in solder grain boundaries also inhibit grain-boundary sliding and thermo-mechanical fatigue.

2.3 Nano Solder Particles

Compared to micron-sized solder alloy particles, the nano solder particles potentially have the following advantages:

- Depression in melting temperature
  - Reduce processing temperature
  - Reduce thermal stresses on components and substrate during processing
- Increased strength of solder alloys
  - Finer microstructure
  - Less prone to grain coarsening
  - Restriction of dislocation movement and grain-boundary sliding
- Interconnection miniaturization
  - Very fine pitch applications
  - Increase fine pitch interconnection reliability

Environmental regulations require that solder alloys for electronic components and printed wiring board interconnections be lead free. Lead-free solder alloys such as Sn/Ag/Cu have become common. However, they generally have liquidus points of 220°C or higher, compared to the 183°C melting point of eutectic tin lead solder. The high melting point alloys require higher processing temperatures, with reflow process temperatures typically above 240–260°C.

These higher reflow temperatures may create greater residual stresses in board assemblies, which potentially reduce reliability. Components may be limited to those passing high-temperature qualifications. Higher temperatures sometimes require major changes in both manufacturing equipment and processes.

Many materials, including pure metals, exhibit a change in properties as their particle sizes approach nanoscale dimensions. The increase in the surface area-to-volume ratio, which occurs naturally as particle sizes shrink, necessarily increases the relative proportion of higher energy surface atoms. The effect may include a change in reactivity, such as in sinterability, the agglomeration of metal particles by heating. It may also appear as a change in electromagnetic properties, altering electronic or optical properties.

The particle size where these changes occur – the "tipping point" – depends on both the individual element or compound and its environment. Property changes normally require particle diameters to be somewhere below 100 nm. The tipping point shows as an abrupt shift in the slope of the measured curve. Figure 2.1 illustrates a tipping point in sinterability temperature as a function of the particle size.

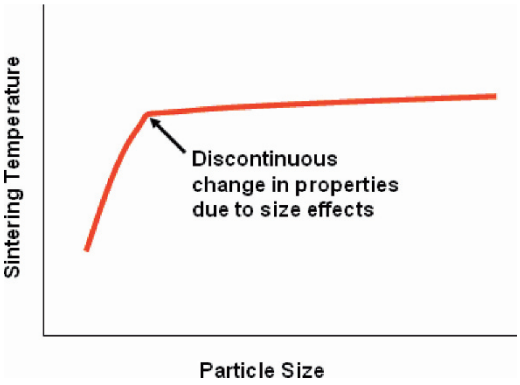

Fig. 2.1. Tipping point example

Solder materials containing nano-sized metals exploit the high surface area and high surface energy of nano-sized particles to lower the apparent melting point below the conventional melting point. Pure metals, such as Sn, Pb, and Cu, are known to show significant melting temperature depression, with the amount of temperature depression increasing as the particle size decreases. Thus the melting points of tin, silver and copper, the ingredients of lead-free solder, can all be depressed below 200°C, well below the eutectic melting point of 217°C.

Major challenges remain in developing lower temperature lead-free solders. The sub-20 nm particles must be uniform in size, well dispersed, and oxide free. However, researchers continue to show progress toward low melting point nanoparticle solder paste.

Tin (Sn) and its alloys are easily oxidized due to their low chemical potential. For nano-sized tin and its alloys, oxidation happens more easily due to the higher surface area-to-volume ratio of nanoparticles. The presence of oxides of the nanoparticles causes poor wetting and interconnection formation. Therefore, capping each nanoparticle to prevent oxidation is critical. The capping agents can cover the particle surfaces to serve as an effective barrier against the penetration of oxygen.

Jiang et al. [62] from Georgia Tech synthesized different sized 96.5Sn3.0Ag0.5Cu alloy nanoparticles by chemically reducing the precursors such as Tin (II) 2-ethylhexanoate, silver nitrate, copper nitrate. Effective capping capability can reduce or eliminate agglomeration of nanoparticles as well as protecting them from oxidation. It was found that some strong coordination agent could be an effective capping agent in forming crystalline SnAg alloy nanoparticles as shown in Fig. 2.2a, b, and c. When the SnAg alloy nanoparticles were formed, they were instantly coordinated through the pair of chelating nitrogen donor sites adjoining the two heterocyclic aromatic rings. The HRTEM characterizations (Fig. 2.2 c) showed that the particles were covered by capping agents which could provide an effective barrier against the penetration of atmospheric oxygen to the nanoparticles. At the same time, when using $NaBH_4$ as a reducing agent, hydrogen generated during a reduction reaction was found to be helpful in the creation of inert environments.

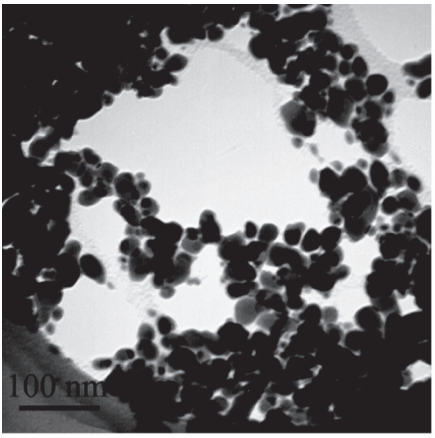

(a)

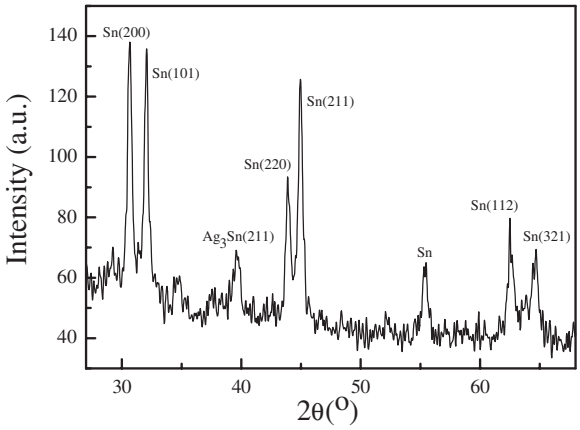

(b)

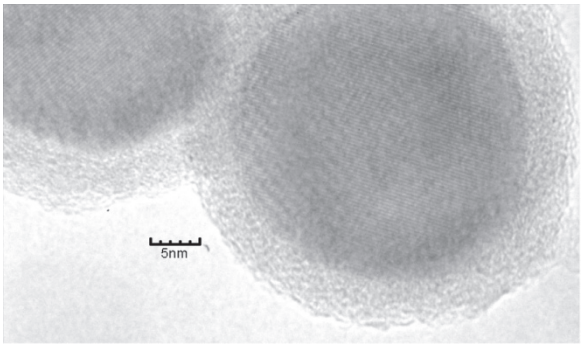

(c)

Fig. 2.2. TEM (**a**), XRD (**b**), and HRTEM (**c**) images of synthesized SnAg alloy nanoparticles

Then the author studied the melting hehavior of the synthesized SnAg alloy nanoparticles by differential scanning calorimeter (DSC). Both the particle size-dependent melting point depression and the latent heat of fusion have been observed (Fig. 2.3). As can be seen from Fig. 2.3, as much as 25°C decreasing of melting point as the SnAg particle size was reduced to about 5 nm. It has already been found that surface melting of small particles occurs in a continuous manner over a broad temperature range, whereas the homogeneous melting of the solid core occurs abruptly at the critical temperature T_m [63, 64]. For smaller size metal nanoparticles, the surface melting is strongly enhanced by curvature effects. Therefore, both the melting point and the latent heat of fusion will decrease with the particle size.

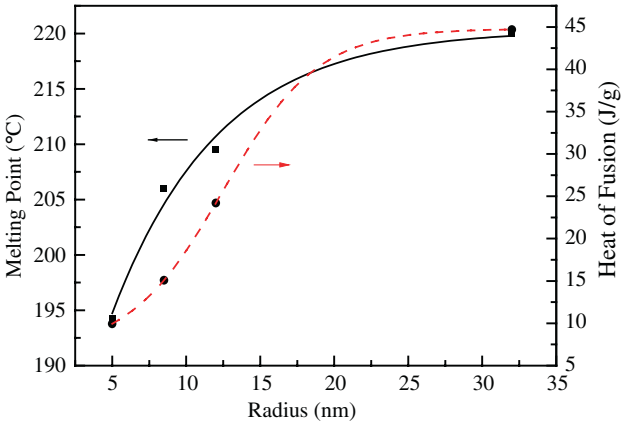

Fig. 2.3. Size-dependent melting of SnAg alloy nanoparticles by DSC

Although the nano alloys melt at a lower temperature, their wettability would be poorer than that of eutectic SnPb solders due to their intrinsically higher surface tension. Besides the intrinsic behavior of the nano alloys, the melting or sintering behavior of the nano alloy particles surrounded by liquids such as flux vehicles has not been investigated. Since all the theoretical approaches for the melting behavior of fine particles assume that the particles are placed in a free space, its behavior surrounded by the flux vehicle will be very interesting from a practical point of view.

To improve the wetting properties on the cleaned copper surface, the authors [62] formulated a nano solder paste by dispersing the SnAg alloy nanoparticles into a low viscosity acidic type flux. The synthesized particles were surface coated by capping agents to prevent oxidation. During the reflow process, the capping agents need to be debonded from the parti-

cle surfaces. Otherwise, they will hinder the wetting of particles on substrates. The desorption of these capping agents depends upon their affinity to the nanoparticle surfaces and their intrinsic thermal stability. Then the nano solder pastes were placed on top of the cleaned copper foil surface and then reflowed at 230°C in an oven with an air atmosphere for 5 min. A cross-sectional image of the sample after the reflow process was shown in Fig. 2.4. It was observed that the SnAg alloy nanoparticles with an average particle size of 64 nm completely melted and wetted on the cleaned copper foil surface. The energy dispersive spectroscopy (EDS) results revealed the formation of the intermetallic compounds (IMC) (Cu_6Sn_5), which showed scallop-like morphologies in Fig. 2.4. The thickness of the IMC was approximately 4.0 μm.

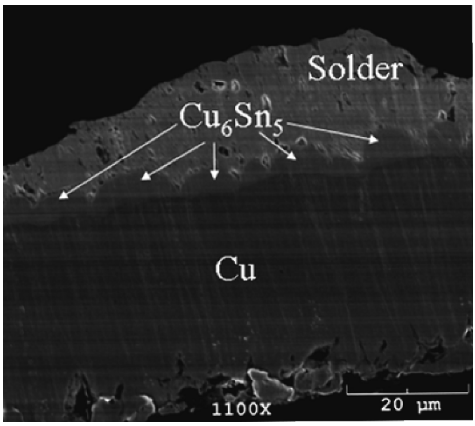

Fig. 2.4. A cross-sectional SEM image of a solder interface formed using the SnAg alloy nanoparticles (with an average particle size of 64 nm) on a cleaned copper foil surface after the reflow process

Guan et al. [65] successfully synthesized nanoparticles of Sn–4.0Ag–0.5Cu and Sn–0.4Co–0.7Cu (wt% composition) lead-free solder alloys using a top-down approach – spark erosion, also known as Consumable electrode Direct Current Arc (CDCA) or arc-discharge which has some advantages such as room temperature process, suitable for high volume production, and versatile. The manufacturing set-up, schematically shown in Fig. 2.5, shows the cathode (1), the anode (2) which are connected to a high current and low voltage power source, the bulk alloy electrodes (3 and 4), the arc discharge taking place between the electrodes (5), and the dielectric coolant (6). The nanoparticles are fabricated when the two electrodes come close enough to each other, so that a stable arc is formed. Different dielectric coolants such as liquid paraffin, glycerine, and

triethanolamine were used. Both glycerine and triethanolamine offered better oxidation protection compared to the liquid paraffin. However, due to the high viscosity of these two coolants, it became very difficult to extract the synthesized nanoparticles from the coolant. The synthesized nanoparticles were spherical in shape and with a size between 20 and 80 nm. High-resolution transmission electron microscopy (HRTEM) showed that the oxide layer thickness on the nanoparticles was about 2.5 nm. The melting point difference obtained by DSC (differential scanning calorimetry) for Sn–4.0Ag–0.5Cu and Sn–0.4Co–0.7Cu lead-free solders is between 1.1–7.8°C and 0.24–2.4°C, respectively, depending on the definition of the melting point determination by DSC.

Zhang et al. have showed that it is possible to control the particle size by changing the ultrasonic power. They have fabricated nanoparticles of Sn, Bi, and Sn–Bi by using ultrasonic vibration with a power of 900 W/cm^2 [66–68].

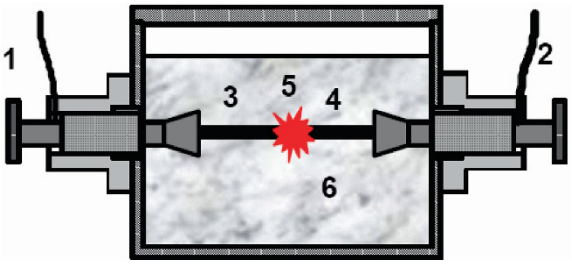

Fig. 2.5. A schematic drawing of an arc-discharge set-up for manufacturing nano solder particles

Recently there has been great research efforts to understand the effects of incorporating nanoparticles and nanotubes into the solders to the various properties of the bulk solder and also the intermetallic formation between the solder and the substrate pad finish.

Kumar et al. [69] studied the influence of nanopowders such as Ni, Cu, and Mo on the phase formation, microstructural characteristics, and mechanical behavior of conventional solder alloys (63Sn/37Pb and Sn/3.8Ag/0.7Cu). The composite solders were prepared by mechanical mixing of nickel (Ni), copper (Cu), and molybdenum (Mo) nano powders with solder alloys followed by cold compaction and sintering. It was observed that the intermetallics are uniformly distributed for the composite solders. The grain refinement of the composite solder occurs with addition of the nano sized metallic powders. The hardness of SnPb and SnAgCu composite solder increases with the increase in weight percentage of

nanopowders (Cu, Ni, and Mo). The addition of Mo to the SnPb and SnAgCu resulted in higher hardness values compared to that of adding Ni and Cu to the solders. The grain refinement and grain-boundary strengthening due to the nanopowders reinforcements are responsible for the improved deformation behavior of the composite solders.

Kumar et al. [70] investigated Sn/Ag/Cu (SAC) solders reinforced with SWCNTs, nano-nickel, and nano-Mo of varying weight percentages using a powder metallurgy method. The nanotubes were found to be homogeneously distributed at the edges of the grain boundaries of the Ag_3Sn intermetallic that are distributed evenly in the β-Sn solder matrix. Microstructure analysis revealed that the nano Ni and nano Mo particles were transformed to Ni_3Sn_4 and Mo–Sn intermetallic compounds during processing and distributed uniformly throughout the β-Sn solder matrix. When compared to the SAC solder without any reinforcement, composite solders exhibit enhanced hardness, enhanced yield strength, and enhanced ultimate tensile strength. However, the elongation to failure of the composite specimens considerably decreased. The increase in the strength of the nanocomposite solder specimens with respect to the wt% of SWCNT addition can be attributed to the critical reduction in the grain size. The enhanced mechanical properties also can be attributed to the effective load-transfer between the solder matrix and the nanotubes. The effect of brittle reinforcement content on the overall strength and ductility of the composite solder can be explained by the strengthening mechanisms such as stress gathering capability of the reinforcing particles, thermally induced matrix work hardening, a increase in dislocation density, and reduction of subgrain size.

Qi et al. [71] investigated the effects of Ni nanoparticles addition on shear property and microstructure of Sn–3.5Ag lead-free solder joint. The nickel nanocomposite Sn–3.5Ag solder was prepared by adding dispersant to the dry nanoparticles and mechanically stirred Ni nanoparticles into the Sn–3.5Ag lead-free solder paste. The shear force of the Sn–3.5Ag solder, 0.5 and 1.0wt% nickel nanocomposite solder, was tested, respectively, at reflow 120 and 240s. The result showed that adding nickel nanoparticles could improve the shear performance of the soldered joint; the shear force of the soldered joint was highest when adding 0.5wt% Ni nanoparticles at reflow 240s. The SEM observations showed that the hexagonal Cu_6Sn_5 IMC (intermetallic compound) in the inside solder is disappears gradually and the morphsa of the IMC that on the interface of the solder joint becomes planar after adding Ni nanoparticles into solder.

To study the effect of nanoparticles on the growth of intermetallic compounds during reflow processes and thermal aging and on the drop-test performance, Amagai Masazumi [72] evaluated Co, Ni, Pt, Al, P, Cu, Zn, Ge, Ag, In, Sb, or Au inclusions in Sn–Ag-based lead-free solders. Also,

these nanoparticles were studied if they can reduce the frequency of occurrence of intermetallic compound fractures in high-impact pull tests. It was found that Co, Ni, and Pt were much more effective for depressing the growth of intermetallic compounds and enhancing drop-test performance than Cu, Ag, Au, Zn, Al, In, P, Ge, and Sb.

2.4 Carbon Nanotubes (CNTs)

Since the discovery in 1991, carbon nanotubes (CNTs) have developed into a distinct branch of nano-technology, nano-material, and nano-mechanical engineering with numerous unique applications. Carbon nanotubes (CNTs) are well-ordered, all-carbon hollow graphitic nano-materials with a high aspect ratio, lengths from several hundred nanometers to several micrometers with a diameter of 0.4–2 nm for single-walled (SWNT) and 2–100 nm for coaxial multiple-walled (MWNT) carbon nanotubes.

There are mainly two types of CNT, including single-walled CNTs (SWCNT) which consist of just one layer of graphite, and multi-wall CNTs (MWCNTs) which consist of two or more concentric shells of carbon and a hollow inner capillary. The separation between the adjacent shells in MWCNTs is about 0.34 nm.

In general, CNTs can be grown by arc-discharge, laser ablation, and chemical vapor deposition (CVD) methods (Table 2.1). However, for device applications, growth of CNTs by CVD methods is particularly attractive, due to features such as selective spatial growth, large area deposition capabilities, and aligned CNT growth.

Extensive experimental and theoretical studies have shown that CNT possess extraordinary electrical, mechanical, thermal, and chemical properties with a wide range of potential applications.

Table 2.1. Summary of CNT laboratory synthesis technique

	Arc discharge	Laser ablation	CVD
Carbon source	Graphite	Graphite	Hydrocarbon, CO
Energy source	Electricity	Laser	Plasma, furnace
Growth temp	2,500–3000°C	1,200°C	600–1100°C
Yield	30wt%	Up to 70wt%	20–100wt%
Scalability	Non-scalable	Non-scalable	Scalable
Advantages	-Few or no structural defects	-Diameter control -Few defects	-Relatively low temp -Long length Diameter control
Limitations	-High temp -Short tubes	-Costly -High power -Expensive laser	-High defects -Low crystallinity

As originally proposed, Moore's law states that the number of transistors in semiconductor devices or integrated circuits (ICs) doubles approximately every 18 months [73]. One of the historical consequences of increasing the number of devices on a chip and thus microprocessor performance is an associated increase in power consumption. Heat dissipation challenges create opportunities for fundamental research in materials and thermal management strategies. Specifically, it has been suggested that future cooling approaches may be based on micro- and nanotechnologies. For thermal management applications, the distinctive properties of one-dimensional structures and materials have gained much attention. Among such materials, carbon nanotubes (CNTs), due to their unique thermal properties, give rise to new opportunities in thermal management of microelectronic devices and ICs. Also, the extraordinary electrical and mechanical properties of CNTs make them a promising candidate for electrical interconnects [74, 75].

2.4.1 Carbon Nanotubes for Electrical Interconnect Applications

2.4.1.1 Electrical Properties of Carbon Nanotubes

Previous studies have demonstrated that a carbon nanotube behaves like a quantum wire due to geometrical confinement of the tube circumference [76]. The conductance of a multi-walled nanotube (MWNT) or a single-walled nanotube (SWNT) is determined by two factors: the conducting channels per shell and the number of shells. A SWNT consists of one shell. A SWNT rope or MWNT can be viewed as a parallel assembly of single SWNTs. Due to the structural imperfection of grown CNTs, the conductance for a SWNT, a SWNT rope, or MWNT can be written as

$$G = G_0 M = (2e^2 / h) MT \tag{2.1}$$

where M is an apparent number of conducting channels and T is the transmission probability for an electron through the contacts and the tube. Ideally, T is unity and $M = 2$ for a perfect ballistic SWNT less than 1 μm long. In actual operation, T may be significantly lower than 1 due to electron–electron coupling, intertube coupling effects, scattering from defects and impurities, structural distortions, and coupling with substrates or contact pads. Therefore, the experimentally measured conductance is much lower than the quantized value. Therefore, the high electrical resistance of a single nanotube necessitates the use of nanotube bundles aligned in parallel.

2.4.1.2 Carbon Nanotubes as Interconnects

There are two types of interconnects employed in microelectronic devices: horizontal and vertical. Horizontal interconnects link transistors in different locations on an integrated circuit; many layers of these horizontal interconnects (up to 12) can exist on a state-of-the-art circuit [77]. Each layer is then separated by an interlayer dielectric, generally porous SiO_2 or SiO_2 doped with C or F to lower its dielectric constant [78]. These materials are rather weak mechanically and are thermally unstable above ~450°C. As dimensions decrease for on-chip interconnects, the current density carried by each interconnect increases. The International Technology Roadmap for Semiconductors (ITRS) predicts that in 2010 the current density will reach 5×10^6 A/cm^2, a value which can only be supported by CNTs, since they are capable of a current density of ~10^9 A/cm^2 [79].

Vertical interconnects pass through holes (vias) in the dielectrics to connect horizontal interconnects to the source, drain, or gate metallization of transistors. In existing microelectronic technology, the vias are fabricated from copper. Via regions are the most common source of failures in interconnect structures due to the high current densities and heterogeneous current distributions that cause electron-induced material transport (electromigration) [80]. Carbon nanotubes are expected to offer a substantially higher resistance to electromigration than do copper lines. Thus, CNT connections between metallization layers may solve the problems of electromigration and heat removal. Researchers from Fujitsu and Infineon have investigated this area extensively [81–83]. In one approach, a hole is etched in the interlayer dielectric, and catalyst is deposited into the bottom of the hole; excess catalyst is removed from the top of the hole. Alternatively, a catalyst layer is deposited under the interlayer dielectric and is exposed by etching a hole in the dielectric. In both approaches, CNTs are then grown within the hole by CVD or by plasma-enhanced CVD (PECVD).

When interconnects and vias are further reduced in size to meet requirements for future ICs, CNT vias will offer still more advantages. Vias consisting of only one MWNT are conceivable, since multi-walled nanotubes can be produced with diameters from 5 to 100 nm; indeed, Infineon has demonstrated such a process [81].

To take full advantage of CNT ballistic conductivity, one must open the CNT ends after growth [84] to permit better wetting and contact by Sn/Pb, etc. CNT flip chip electrical interconnection is also under study [85–88], with micrometer m-scale CNT clusters successfully developed as flip chip "nano-bumps" [89]. Au and Ag incorporation into CNTs has also been studied for electrical contacts with minimal galvanic corrosion [90]. Metal and carbon loaded polymers have long been used for high-frequency conductors in electromagnetic shielding, and both carbon fibers and multi-walled CNTs have been studied in polymer matrices for the purpose [91, 92]. CNT replacement of ICA metal filler, however, does not even match the electrical conductivity of standard materials.

2.4.1.3 Carbon Nanotubes for Thermal Management

Several investigations have indicated that CNTs have unusually high thermal conductivity in the axial direction. For example, molecular dynamics simulations of a SWNT by Berber et al. indicated that the thermal conductivity of a SWCNT can be as high as 6,600 W/mK at room temperature [93]. Dai et al. presented a method for extracting the thermal conductivity of an individual SWNT from high bias electrical measurements in the temperature range from 300 to 800K by reverse fitting the data to an existing electrothermal transport model [94]. The thermal conductivity measured was nearly 3,500 W/mK at room temperature for a SWNT of length 2.6 μm and diameter 1.7 nm. Kim et al. developed a microfabricated suspended device hybridized with MWNTs (~1 μm) to allow the study of thermal transport where no substrate contact was involved [95]. The thermal conductivity and thermoelectric power of a single carbon nanotube were measured, and the observed thermal conductivity is >3,000 W/mK at room temperature.

Hone et al. measured the thermal conductivity of aligned and unaligned SWNTs from 10 to 400K [96]. Thermal conductivity increased smoothly with increasing temperatures for both aligned and unaligned SWNTs. At room temperature, the thermal conductivity of aligned SWNTs was greater than 200 W/mK, compared to ~30 W/mK of unaligned ones; above 300K, the thermal conductivity increased and then leveled off near 400K. Yi et al. measured the thermal conductivity of millimeter-long aligned MWNTs [97]. The thermal conductivity was low, only ~25 W/mK, at room temperature, due to a large number of CNT defects. However, thermal conduc-

tivity could reach ~2,000 W/mK if the aligned MWNTs were annealed at 3,000°C to remove the defects. Yang et al. investigated the thermal conductivity of MWNT films prepared by microwave CVD using a pulsed photothermal reflectance technique [98]. The average thermal conductivity of carbon nanotube films, with the film thickness from 10 to 50 μm, was ~15 W/mK at room temperature and independent of tube length. However, by taking into account a small volume filling fraction of CNTs, the effective nanotube thermal conductivity can reach 200 W/mK.

Aligned CNTs have been grown directly on silicon surfaces for thermal management. Xu et al. grew aligned CNTs on silicon wafers using plasma-enhanced CVD [99]. The thermal testing performed was based on a one-dimensional reference bar method in high vacuum with radiation shielding, and temperature measurements were carried out with an infrared camera. Dry CNT arrays have a minimum thermal interface resistance of 19.8 mm^2K/W, while CNT arrays with a phase change material (PCM) produced a minimum resistance of 5.2 mm^2K/W. Xu et al. used a photothermal metrology to evaluate the thermal conductivity of aligned CNT arrays grown on silicon substrates by plasma-enhanced CVD [100]. The effective thermal resistance was 12 – 16 mm^2K/W, which is comparable to the resistance of commercially available thermal grease. K. Zhang et al. [101] fabricated aligned carbon nanotube (CNT) arrays from a multilayer catalyst configuration by microwave plasma-enhanced chemical vapor deposition (PECVD). One of the potential applications of CNT is thermal interface materials (TIMs). TIM is used to fill the gaps between thermal transfer surfaces, such as between microprocessors and heatsinks, in order to increase thermal transfer efficiency. These gaps are normally filled with air which is a very poor conductor. Figure 2.6 shows two typical packaging architectures used in electronics cooling [102]. For example, TIM1 between the chip and the heat spreader and TIM2 between the heat spreader and the heat sink have been introduced to fill the gap between the asperities to minimize the contact thermal resistance. The effects of the thickness and annealing of the aluminum layer on the CNT synthesis and thermal performance were investigated. It was demonstrated that the CNT–thermal interface material (CNT–TIM) reduced the thermal interfacial resistance significantly compared with state-of-the-art commercial TIM. The total thermal resistance of the CNT–TIM was only 7 $mm^2\ KW^{\cdot 1}$ and was about 10% of that of commercial silver epoxy TIM. The light performance of high-brightness light-emitting diode (HB-LED) packages using the aligned CNT–TIM was tested. The results indicated that the light output power was greatly improved with the use of the CNT–TIM. The usage of the CNT–TIM can be also extended to other microelectronics thermal management applications.

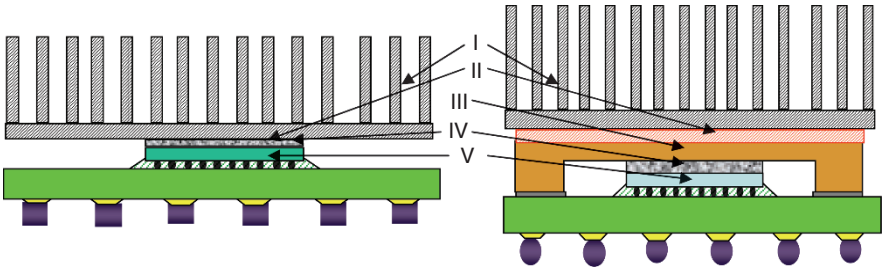

Fig. 2.6. Schematic illustration of the two thermal architectures. (**a**) Architecture I, typically used in laptop applications. (**b**) Architecture II, typically used in desktop and server applications. I, – heat sink; II, – TIM2; III, – IHS; IV, – TIM1; V, – die; VI, – underfill; VII, – package substrate [102]

The high CNT thermal conductivity is used directly for conductive cooling of chips and indirectly in convective cooling [103]. For conductive systems, CNT alignment is the problem, since the thermal conductivities of random arrays show no advantages over conventional materials. Composites filled with CNTs have also been studied for thermal interface materials, e.g., CNT/carbon black mixtures in epoxy resin. The use of a liquid crystal resin matrix can impose structural order on the CNT alignment to yield a seven-fold improvement in thermal conductivity [104]. Recently, electrospun polymer fibers filled with CNTs, or with SiC or metallic nanoparticles, have shown advances in both mechanical and thermal properties [105].

Micron-scale clusters of vertically grown nanotubes [106, 107] define microchannels for convective cooling coolant flow, similarly to the metal or silicon structures they aim to replace, with similar thermal performances. The problem is that the flowing coolant is only in contact with the outermost CNTs of the clusters, and the internal CNTs are not even in good contact with each other. The system has been modeled, and the solution is clearly to spread the CNTs apart by an optimal separation to permit coolant contact with each one. The problem then is whether individual CNTs can withstand the coolant flow pressure without detaching from the substrate.

2.4.1.4 Integration of Carbon Nanotubes into Microsystems

For electronic device applications, chemical vapor deposition (CVD) methods are particularly attractive. However, the CVD technique suffers from several drawbacks. One of the main challenges for applying CNTs to circuitry is the high growth temperature (>600°C). Such temperatures are incompatible with microelectronic processes, which are typically performed below 400–500°C in backend-of-line sequences. Another issue is the poor adhesion between CNTs and the substrates, which will result in long-term reliability issues and high contact resistance. At the device level, CNTs must be integrated and interconnected with metal electrodes to allow signal input and output. Typical approaches for CNT growth on such substrates involve the deposition of catalysts such as Fe or Ni on metal layers such Ti or Ti/Au. Unfortunately, results indicate that electrical contact is not necessarily improved, suggesting that attachment of CNTs onto the electrodes produces poor mechanical and electrical properties yielding high contact resistance. On the other hand, to meet manufacturing requirements and throughput for IC applications, a large number of CNTs must be positioned simultaneously rather than aligning CNTs one by one.

To overcome the above disadvantages, Zhu et al. at Georgia Tech proposed a methodology termed "CNT transfer technology," which is enabled by open-ended CNT structures [84]. This technique is similar to flip chip technology as illustrated schematically in Fig. 2.7.

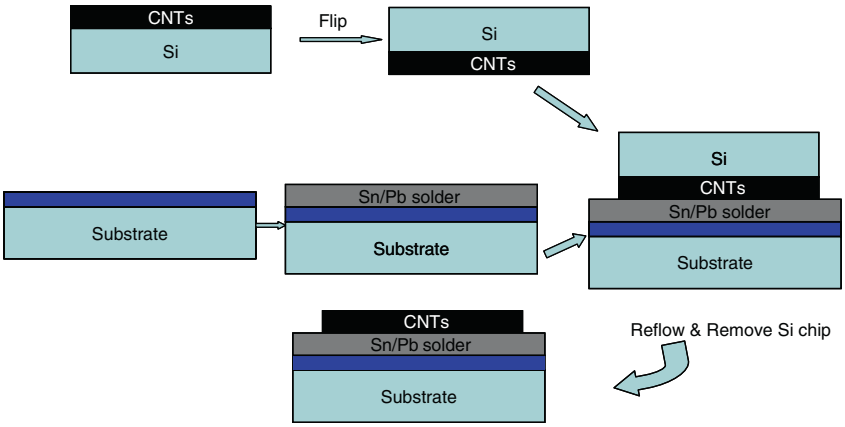

Fig. 2.7. Schematic diagram of "CNT transfer technology" [84]

The eutectic tin–lead paste is stencil printed on a copper substrate. After reflow, the tin–lead solder is polished to 30 μm thick. The silicon substrates with CNTs are then flipped and aligned to the corresponding copper substrates and reflowed in a reflow oven to simultaneously form electrical and mechanical connections. This process is straightforward to implement and offers a strategy for both assembling CNT devices and scaling up a variety of devices fabricated using nanotubes (e.g., flat panel displays). This process offers an approach to overcome the serious obstacles of integration of CNTs into integrated circuits and microelectronic device packages by offering low processing temperatures and improved adhesion of CNTs to substrates. Figure 2.8 shows the demarcation between the broken CNTs and the intact and connected ones. When pulled from the substrate, the CNTs break along the axis rather than at the CNT–solder interface. The excellent mechanical bonding strength of CNTs on the substrate anchors the CNTs and thereby improves the CNT/substrate interfacial properties.

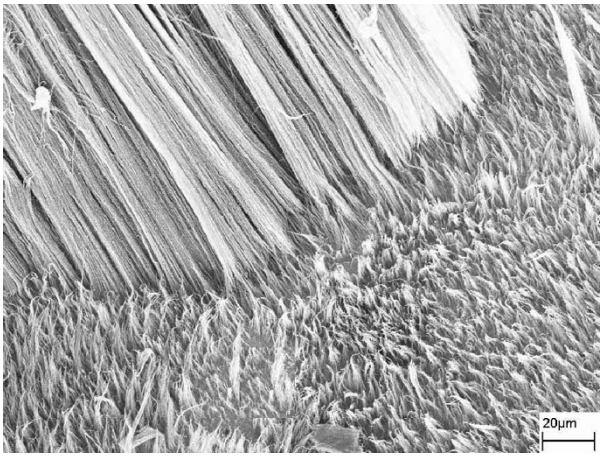

Fig. 2.8. SEM of the copper substrates on which the CNTs were assembled after some CNTs were pulled from the surface by tweezers; this figure demonstrates the excellent mechanical bond strength of CNTs transferred to the copper substrate by the solder reflow process [84]

Recently, Lin et al. from Georgia Tech proposed another new transfer technology for aligned CNT, named “chemical transfer” (Fig. 2.9). Chemical transfer is a two-step assembly process, (1) well-aligned CNTs are in situ functionalized (f-ACNTs) during the CVD growth; (2) f-ACNTs are then anchored onto the gold-coated substrate by forming covalent bonding between the f-ACNTs and the self-assembled monolayer of conjugated thiol molecules on the gold surface. The in situ functionalization process

allows for precise length control of ACNT assembly without randomly damaging the CNT structures and, equally importantly, renders the ACNT surface, especially the opened ends, chemically reactive to certain functional groups [108]. In their publication, a chemically transferred ACNT film on the gold surface with self-assembled monolayer of conjugated thiol molecules was successfully demonstrated (Fig. 2.10).

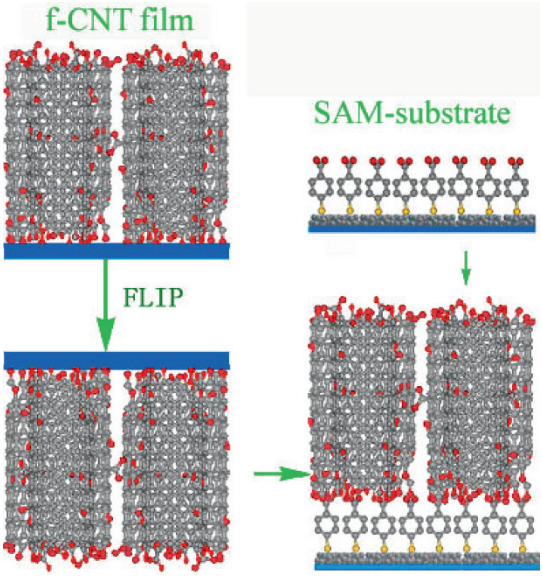

Fig. 2.9. Schematic illustration of the chemical transfer process [108]

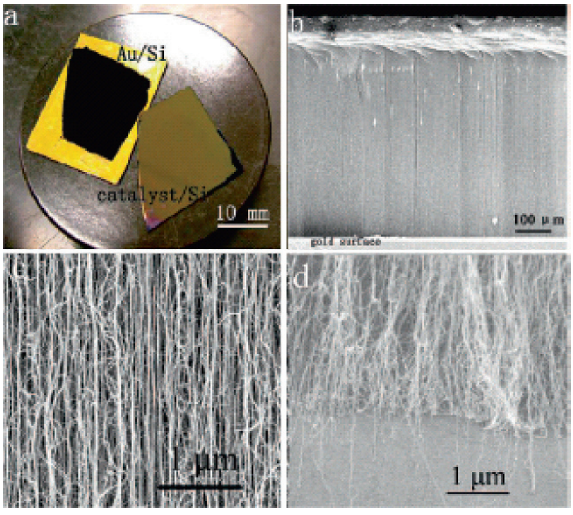

Fig. 2.10. Chemically transferred f-ACNT film on the gold surface: (**a**) photograph; (**b**) the side view SEM image (by 0.5 N/cm^2 of compressive force during transfer); (**c**) further enlargement of the CNT alignment after chemical transfer; and (**d**) the anchored f-ACNT/gold interface after part of the transferred ACNTs was removed [108]

The chemically transferred f-ACNT showed a liner current–voltage (I–*V*) curve which suggested an Ohmic contact (Fig. 2.11). The resistivity of the individual ACNT was demonstrated to be in the order of 10^{-4} Ω-cm. The authors attributed the Ohmic contact and low resistance to two factors, conjugated SAM-assisted bonding and relatively low defect density. This process offers the opportunity of using ACNT in broader applications such as electrical interconnect, thermal transport, electrodes for sensors.

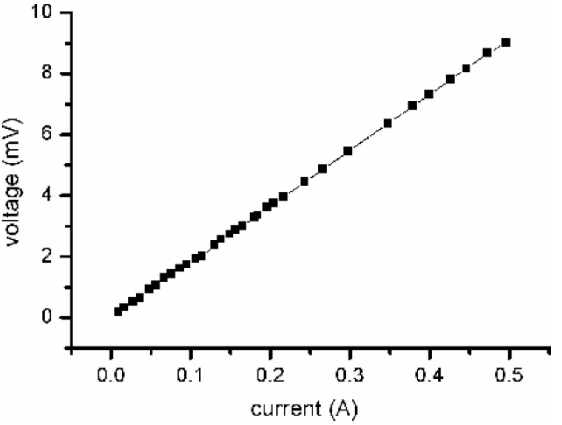

Fig. 2.11. The room temperature *I–V* curve of the f-ACNT/gold interconnect via the chemical transfer [108]

2.4.1.5 Summary and Future Needs

Scaling of microelectronic devices has led to an interest in utilizing carbon nanotubes for electrical interconnects and thermal management approaches. Carbon nanotubes are also promising for vertical interconnects (for on-chip or packaging levels) and heat removal for microelectronics packaging. CNTs may be able to meet some of the ITRS projections for device interconnects and thermal requirements. However, a number of materials and CNT process integration issues need to be addressed before a CNT technology platform can be developed, including growth of structurally perfect carbon nanotubes, chirality control of carbon nanotubes, and positioning of carbon nanotubes in predefined locations simultaneously. The barriers to CNT implementation in the packaging of microelectronic devices and ICs offer numerous opportunities for new developments and

approaches. Clearly, more effort is required in order to take CNT technologies from the research laboratory to high-volume production.

2.5 Nanocomposites

2.5.1 Recent Advances in Nanocomposites

Nanocomposites are materials that are created by introducing nanoparticulates (often referred to as filler) into a macroscopic sample material (often referred to as the matrix). This is part of the growing field of nanotechnology. After adding nanoparticulates to the matrix material, the resulting nanocomposite may exhibit drastically enhanced properties. For example, adding carbon nanotubes tends to drastically improve the electrical and thermal conductivity. Other kinds of nanoparticulates may result in enhanced optical properties, dielectric properties, or mechanical properties such as stiffness and strength. In general, the nanosubstance is dispersed into the matrix during processing. The percentage by weight (called mass fraction) of the nanoparticulates introduced can remain very low (on the order of 0.5–5%) due to the incredibly low filler percolation threshold, especially for the most commonly used non-spherical, high aspect ratio fillers (e.g., nanometer thin platelets, such as clays, or nanometer diameter cylinders, such as carbon nanotubes).

The internal surfaces are critical in determining the properties of nanofilled materials. Nanoparticles have high surface area-to-volume ratio; particularly when the size decreases below 100 nm. This high surface area-to-volume ratio means that for the same particle loading, nanocomposites will have a much greater interfacial area than microcomposites. This interfacial area leads to a significant volume fraction of polymer surrounding the particle that is affected by the particle surface and has properties different from the bulk polymer (interaction zone) [109]. Since this interaction zone is much more extensive for nanocomposites than for microcomposites, it can have significant impact on properties (shown in Fig. 2.12) [110, 111].

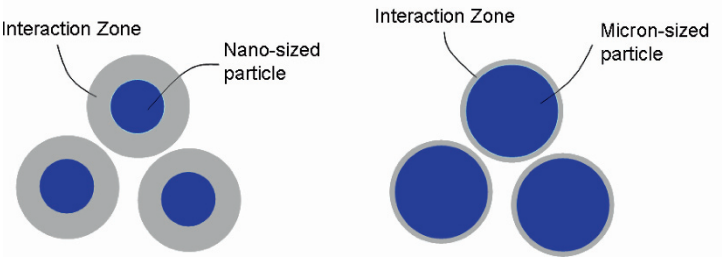

Fig. 2.12. A schematic comparison of particle and matrix interaction in nanocomposites and microcomposites

For example, depending upon the strength of the interaction between polymer and particle, this region can have a higher or lower mobility than the bulk material and result in an increase or decrease in glass transition temperature [112]. It has also been suggested that free volume in such interaction zones is altered by the introduction of nano-fillers. Since these interaction zones are likely to overlap at relatively low-volume fractions in nanocomposites, a small amount of nano-filler has been found to impact the electrical behavior [113, 114]. Some authors have emphasized that the interaction zone around the particles is a "quasi-conductive" region which partially overlaps in the nanocomposites [114]. These overlapped interface regions thus may allow charge dissipation, which, in turn, could improve the dielectric breakdown strength and voltage endurance characteristics. Introduction of a second phase can also influence the breakdown strength of the dielectrics via a scattering mechanism (i.e., an increase in path length of the carriers responsible for the breakdown processes) or, by changing the space-charge distribution [115]. It has been shown by some authors that when the size of the filler approaches the chain conformation length, they act "cooperatively" with the host structure either eliminating or suppressing Maxwell–Wagner polarization, which is well known in the case of conventionally filled materials [116]. Some recent results also suggest that it is the size of the filler that plays the most crucial role in terms of global properties (electrical, mechanical, and thermal), rather than the chemistry of the particles [117]. Finally, changes in morphology due to incorporating nanoparticles can influence the dielectric behavior of nanocomposites [118]. The large surface area can also lead to changes in the morphology of semicrystalline polymers as observed by several groups [118]. The breakdown strength of the intraspherulitic regions is higher than that of the interspherulitic regions and a change in the disorder within the spherulites or of the interspherulitic region can affect the breakdown strength. In addition, it is important to recognize that nanoparticulate/fibrous loading confers significant property improvements with very

low loading levels, traditional microparticle additives requiring much higher loading levels to achieve similar performance. This in turn can result in significant weight reductions, which is important for various military and aerospace applications, for similar performance, greater strength for similar structural dimensions and, for barrier applications, increased barrier performance for similar material thickness.

Roy et al. [56] studied the effect of interactions between the nanoparticle surface and the matrix to the electrical properties of the nanocomposite. It was found that covalent bonding between the nanoparticles and the matrix (vinylsilane treated nanoparticles) increases the temperature at which the breakdown strength decreases. The increase in interfacial region in nanocomposites creates a zone of altered polymer properties which reduces the dielectric permittivity of nanocomposites. The highest voltage endurance occurs for composites with strong covalent bonding between the matrix and the filler.

Ramanathan et al. [119] described the use of SWNTs to create low-volume fraction polymer composites with dramatically improved mechanical, thermal, and electrical properties when compared with those of the neat polymer. Composites were created with unmodified and amide-functionalized the SWNTs (a-SWNT). The formation of amide groups on the surface of SWNTs provides free amine groups to interact with PMMA, and IR spectra indicated covalent bonding between a-SWNT and PMMA. For both SWNT/PMMA and a-SWNT/PMMA composites, thermal, mechanical, and electrical data showed significantly improved properties when compared with those of the neat polymer. The experimental results also demonstrated that the a-SWNT/PMMA composite properties are consistently improved when compared with those of the SWNT/PMMA composite. The increase in thermal degradation temperature, glass transition temperature (Tg), storage modulus, and electrical conductivity confirms better interaction between the functionalized SWNTs and the polymer. Functionalized SWNT resulted in a composite where relaxation mechanisms ($tan\ \delta$) are shifted by 30°C from that of the matrix material, indicating extensive interphase regions and absence of PMMA with bulk properties. In contrast, the composite with unmodified nanotubes retained the dominant relaxation characteristics of the bulk PMMA with a broadening of the loss peak, indicating existence of discrete interphase regions near the nanotubes. The mechanical property data were compared with modeling predictions based on ideal dispersions of randomly oriented straight SWNTs in PMMA. The modulus properties for both composites significantly exceed the predicted upper bound. These results reinforce the existence of an extensive polymer interphase in both composites with altered properties. These results further demonstrate that the altered polymer near the nanotubes has increased modulus, consistent with the loss modulus

data indicating decreased mobility of the polymer in the interphase region. The consistent improvement in the properties of the a-SWNT composite when compared with those of the SWNT composite can be attributed to the increased extent of the interphase with altered properties and finer dispersion of nanotubes due to the functionalization.

The results here indicate promising potential for polymer nanocomposites with enhanced thermal, mechanical, and electrical properties. The demonstrated importance of the interphase region underscores the need for more detailed modeling and characterization to understand the changes in local polymer dynamics near nanoparticles and the percolation of these effects in distributed systems. The success of the functionalization to provide consistently improved properties in this work indicates the possibility to create designer nanocomposites with controlled interface chemistry and interphase zones and thus controlled load transfer and properties.

2.5.2 Areas of Application of Nanocomposites

The mechanical property improvements of nanocomposites have resulted in major interest in nanocomposite materials in numerous automotive and general/industrial applications. These include potential for utilization as mirror housings on various vehicle types, door handles, engine covers, and intake manifolds and timing belt covers. More general applications currently being considered include usage as impellers and blades for vacuum cleaners, power tool housings, mower hoods, and covers for portable electronic equipment such as mobile phones, pagers, etc.

The substantial gaseous barrier property improvement that can result from incorporation of relatively small quantities of nano-filler has resulted in considerable interest in nanoclay composites in food packaging applications, both flexible and rigid. The use of nanocomposite formulations would be expected to enhance considerably the shelf life of many types of food.

The ability of nanoclay incorporation to reduce solvent transmission through polymers such as polyamides has resulted in considerable interest in using these materials as both fuel tank and fuel line components for cars. Of further interest for this type of application, the reduced fuel transmission characteristics are accompanied by significant material cost reductions.

The presence of nano-filler incorporation has also been shown to have significant effects on the transparency and haze characteristics of films. In comparison to conventionally filled polymers, nanocomposite has shown to significantly enhance transparency and reduce haze. When employed to coat polymeric transparency materials, the nanocomposites can enhance both toughness and hardness of these materials without interfering with light transmission characteristics.

Kim et al. [120] investigated the moisture diffusion and barrier characteristics of epoxy-based nanocomposites containing organoclay. It was found that moisture diffusivity of nanocomposites decreased with increasing clay content. The moisture permeability showed a systematic decrease with increasing clay content. It was also observed that high aspect ratio nanoparticle showed the lowest moisture permeability because of the increased effective penetration path caused by the aspect ratio nanoparticles. Similar effects have been observed by van Es of DSM with polyamide based nanocomposites. In addition, van Es noted a significant effect of nanoclay aspect ratio on water diffusion characteristics in a polyimide nanocomposite. Specifically, increasing aspect ratio was found to diminish substantially the amount of water absorbed, thus indicating the beneficial effects likely from nanoparticle incorporation in comparison to conventional microparticle loading. Hydrophobic enhancement would clearly both improve nanocomposite properties and diminish the extent to which water would be transmitted through an underlying substrate. Thus applications in which contact with water or moist environments is likely could clearly benefit from materials incorporating nanoclay particles.

The ability of nanoclay incorporation to reduce the flammability of polymeric materials was a major theme of the paper presented by Gilman [121]. In his work Gilman demonstrated the extent to which flammability behavior could be restricted in polymers such as polypropylene with as little as 2% nanoclay loading. Although conventional microparticle filler incorporation, together with the use of flame retardant and intumescent agents would also minimize flammability behavior, this is usually accompanied by reductions in various other important properties. With the nanoclay approach, this is usually achieved while maintaining or enhancing other properties and characteristics.

2.6 Nano Interconnect

2.6.1 Carbon Nanotube Transistors

Semiconducting CNTs have been used to fabricate field-effect transistors (CNTFETs), which show promise due to their superior electrical characteristics over silicon-based MOSFETs. Since the electron mean-free path in SWCNTs can exceed 1 μm, long channel CNTFETs exhibit near-ballistic transport characteristics, resulting in high-speed devices. In fact, CNT devices are projected to be operational in the frequency range of hundreds of GHz. Recent works detailing the advantages and disadvantages of various forms of CNTFETs have also shown that the tunneling-based CNTFET offers better characteristics compared to other CNTFET structures. This device has been found to be superior in terms of subthreshold slope – a very important property for low-power applications.

Carbon nanotube field-effect transistors (CNTFETs) were fabricated with metal material (gold) and semiconductor material (bismuth telluride, Bi_2Te_3) as the source and drain materials [122]. Highly purified single-walled carbon nanotubes (CNTs) were used for the fabrication of CNTFETs. The single-walled carbon nanotubes were ultrasonically dispersed in toluene and dimethylformamide (DMF) with trifluoroacetic acid (TFA), as co-solvent. Dielectrophoresis (DEP) method was used to deposit, align, and assemble carbon nanotubes (CNTs) to bridge the gap between the source and the drain of CNTFETs to form the channel. The structure of CNTFET is similar to a conventional field-effect transistor with substrate acting as a back-side gate. Electron-beam evaporation was used to deposit gold and bismuth telluride thin films. Microfabrication techniques such as photolithography, e-beam lithography, and lift-off process were used to define and fabricate the source, drain, and gate of CNTFETs. The gap between the source and the drain varied from 800 nm to 3 μm. It was found that in the case of gold (Au) electrodes, the *I–V* curves of CNTFETs clearly show behavior of the CNT (metallic or semiconducting) aligned across the source and drain of CNTFETs, while in the case of bismuth telluride electrodes, the *I–V* curves are less dependent on the type of CNTs (metallic or semiconducting). The developed carbon nanotube field-effect transistors (CNTFETs) can be a good candidate for the application of nanoelectronics and integrated circuits with a high mobility and fast switching.

Srivastava et al. [123] evaluated CNT bundle interconnects against Cu interconnects from performance, power dissipation, and thermal management/reliability perspectives. The equivalent circuit parameters for a CNT

bundle interconnect were explicitly calculated and it was found that CNT bundles can significantly improve the performance of long global interconnects by as much as 80% with minimal additional power dissipation (for maximum metallic CNT density). Moreover, power-optimal repeater insertion methodology can be applied to CNT bundle interconnects (just as with Cu) to save power with a small delay penalty. Most importantly, it was shown that CNT bundle vias can greatly reduce interconnect temperature rise and thus, when integrated with Cu interconnects, tremendously improve Cu interconnect performance (about 30%) and lifetime (by at least two orders of magnitude) due to lower temperatures. The advantage of CNT bundle vias in controlling the back-end temperature, as shown in this work, will also have significant implications for emerging technologies such as three-dimensional ICs where thermal management is a big concern. Similarly, researchers at Rensselaer Polytechnic Institute, based on their latest results from advanced quantum mechanical computer modeling to run vast simulations on a high-powered supercomputer, concluded that the carbon nanotube bundles boasted a much smaller electrical resistance than the copper nanowires (http://www.sciencedaily.com). This lower resistance suggests carbon nanotube bundles would therefore be better suited for interconnect applications.

2.6.2 CNT Via

Some very interesting results have been achieved by Kawabata et al. [124] recently on integrating CNT in the via at a CNT growth temperature as low as 400ºC. The fabrication processes are compatible with conventional LSI processes. Briefly, a substrate with a Cu interconnect covered by a dielectric layer was first prepared. The dielectric layer was SiOC with $k = 3.0$ or $k = 2.6$ (ultra-low K dielectric). Via holes with a diameter of 160 nm were made using conventional photolithography followed by dry etching. A TaN/Ta barrier layer and a TiN contact layer were deposited by physical vapor deposition (PVD). Size-controlled Co particles with a mean diameter of about 4 nm were then deposited using a nanoparticles deposition system. MWNTs were grown by thermal CVD with C_2H_2 diluted by argon as the source gas. The substrate temperature ranged from 365ºC to 450ºC. The substrate with MWNTs was then coated with spin-on glass (SOG) and planarized by chemical mechanical polishing (CMP). The CMP condition was similar to the one used for polishing a silicon dioxide layer. Finally, a Ti top contact layer, a Ta barrier layer and a Cu wire were connected to the CNT vias by PVD. Figure 2.13a shows a schematic of via stack structure and Fig. 2.13b shows a SEM image of a via with grown CNTs. The fabricated CNT via interconnect with a diameter of 160 nm was evaluated for

its robustness over a high density current. CNTs used for fabricating vias were grown at temperatures at 400ºC. At such low temperatures, the ultra-low k dielectric layer (k = 2.6) used in the via structure was not damaged. Electrical measurement showed that the CNT via was able to sustain a current density as high as 5.0×10^6 A/cm^2 at 105ºC for 100 h without properties degradation. And we plan to measure the robustness more than higher current density. The authors are working on fabricating CNT vias at temperature lower than 400ºC which will be helpful in realizing reliable CNT vias for future LSIs.

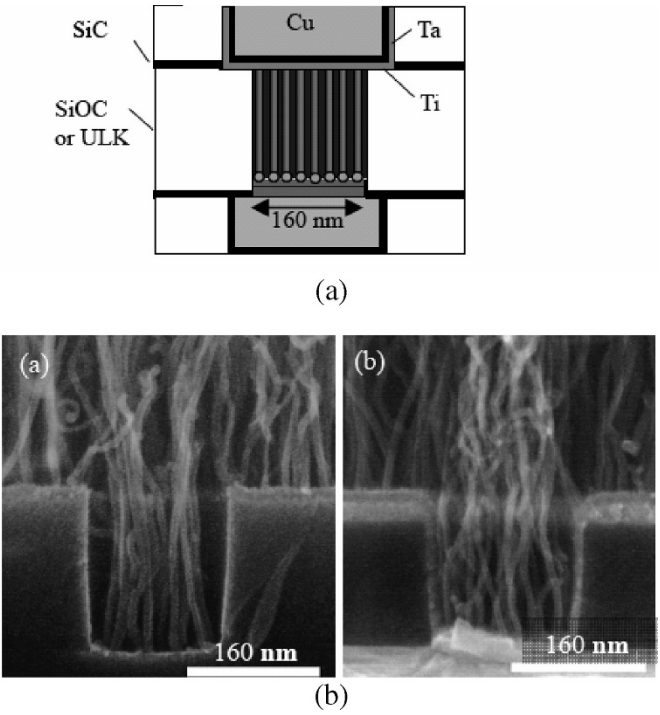

Fig. 2.13. (**a**) A schematic of via stack structure with CNTs and (**b**) SEM image of a via with CNTs which were grown at 450ºC (*left*) and 400ºC (*right*) [142]

2.6.3 CNT as Flip Chip Interconnect

Soga et al. [125] reported on CNT bumps for the flip chip interconnect instead of solder bumps. The CNT bumps were formed on the electrodes on a chip by the CNT pattern transfer process. To measure the resistance of CNT bumps, CNT bump contact chains were fabricated. It was found that

coating the CNT bumps with gold greatly improved the contact resistance of the bumps with the chip and the host substrate, resulting in a lower bump resistance of 2.3 Ω which is still too high for any practical applications. It was also demonstrated that the CNT bumps were able to absorb a displacement between the chip and the substrate up to 10 – 20% of the CNT bump height. The resilience and flexibility of CNT bumps makes them very attractive for realizing thermal stress-free flip chip structure.

Iwai et al. [126] from Fujitsu also demonstrated the use of CNT bumps to provide both electrical and thermal conductions between a high power amplifier flip chip die and a AlN substrate. The CNT bundles were grown directly on the pre-defined areas on the AlN substrate. By using the CNT bumps, heat was more effectively removed from the die and the grounding impedance was reduced significantly and, as a result, high gain was achieved.

2.6.4 Nanoparticle Interlayer for Copper to Copper Bonding

Metallic nanoparticles of copper and gold are explored and evaluated for the nanostructured bonding layers between the copper surfaces [127]. High surface energy of the nanoparticle lowers the melting temperature of the material, and hence, enhances inter-diffusion kinetics that helps in faster bonding rate. In addition, high surface energy and high grain boundary-to-volume ratio endow the particles with elaborate mobility making the diffusion kinetic even faster. It was demonstrated that the nanoparticles formed on the copper surface could reduce the bonding temperatures.

2.6.5 Interconnection Using Inkjet Printing of Nano-ink

The use of nanoparticles of metals with high electric conductivity provides new prospects for direct printing of conductive patterns. The microfabrication of conductive tracks by photolithographic and electroless techniques are time consuming, expensive processes, and there is an industrial need for direct digital printing to simplify the processes and to reduce manufacturing costs [128, 129]. Furthermore, it is desirable to fabricate onto polymeric or similar temperature sensitive substrates by solution-based printing process. Metallic conducting tracks of low resistance must be achieved at temperatures sufficiently lower so as to be compatible with organic electronics on plastic substrates.

Direct metal printing needs to be processed with ink materials that can convert to a low-resistance conductor after solvent removal and heat treatment. Two approaches have been pursued to attain these goals. The first is to use solutions of metallorganic precursors where the molecular

nature of the compound allows low-temperature reduction to the metal [130–132]. A second route is the use of suspensions of metal particles of nano-size diameters whose small size endows a reduction in melting temperature that is significantly lower than that of the bulk material [128, 133, 134]. As an example, Fuller et al. [133] reported a method to additively build three-dimensional (3-D) microelectromechanical systems (MEMS) and electrical circuitry by ink-jet printing nanoparticle gold and silver colloids. Fabricating metallic structures from nanoparticles avoids the extreme processing conditions required for standard lithographic fabrication and molten metal droplet deposition. Nanoparticles typically measure 1–100 nm in diameter and can be sintered at plastic-compatible temperatures as low as 300ºC to form material nearly indistinguishable from the bulk material. Multiple drops were deposited to leave a conductive line or surface (see Fig. 2.14). Multiple ink-jet print heads mounted to a computer-controlled 3-axis gantry deposit the 10% by weight metal colloid ink layer by layer onto a heated substrate to make two-dimensional (2-D) and three-dimensional structures. The author reported a high-Q resonant inductive coil, linear and rotary electrostatic-drive motors, and in-plane and vertical electrothermal actuators. The results suggested a route to fabricate a large-area MEMS system characterized by many layers, low cost, and data-driven fabrication for rapid turn-around time.

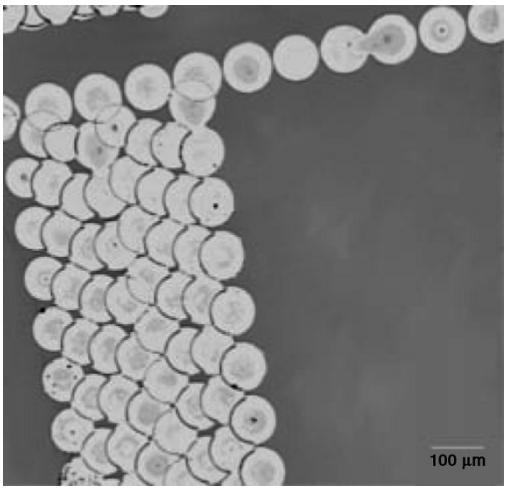

Fig. 2.14. Optical micrograph of an arrangement of sintered ink-jet printed-nanoparticle gold droplets on plastic polyimide film. Electrically conductive lines and three-dimensional structure are fabricated by printing multiple layers of droplets

Various types of printing wiring circuits are expected to become one of the key technologies for the advanced electronics packaging. The combination with metallic nanoparticles pastes can provide new tools for fine pitch and three-dimensional electronics circuits. Especially, with the combination of Ag nanoparticles pastes and ink-jet printing, one can obtain a lot of benefits as

- on-demand fabrication;
- environmental consciousness/economy;
- three-dimensional stacking;
- fine pitch lines and spaces;
- easy scale up of products;
- wide material selections and;
- small quantity but variety of products.

Kim et al. [135] demonstrated a direct metal printing of the Ag nanoparticles on plastic substrates. The granular Ag films become highly conductive, roughly 3.2 μΩ cm, when heat treated even at 200°C. The Ag particles of smaller size (21 nm) are more reactive than the larger sized particles (47 nm).

The relatively high curing temperature limits the application of nanoparticle inks only to the applications of heat-resistant substrates. K. Suganuma et al. [136] have recently developed a new type of ink for wiring metallic Ag lines. The inks are Ag carboxylate compounds designed to be decomposed at temperatures between 110 and 170ºC. Figure 2.15 shows the appearance change of a Ag carboxylate droplet during heating. Ag carboxylates are expected to be one of the metallic inks or of the sintering aids for other metallic particles. The percentages of Ag in the compounds are in the range of 30–50wt%. Excellent electric resistance (e.g., 10^{-5} Ωcm), lower than that of commercial Ag nanopaste, was achieved at a curing temperature of 160ºC.

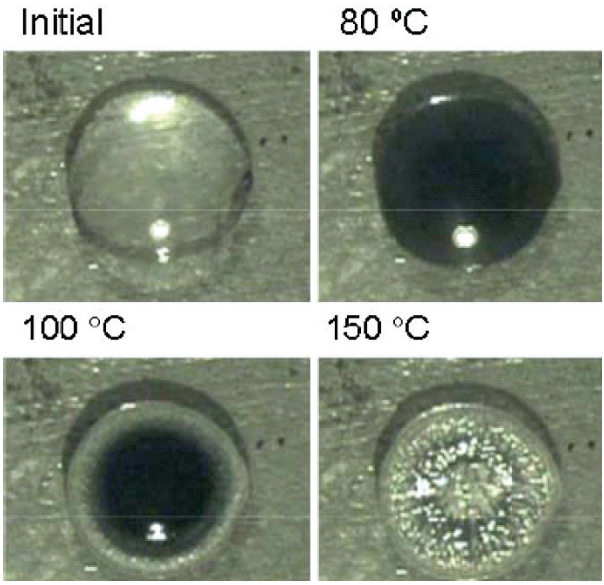

Fig. 2.15. Appearance change of an Ag carboxylate droplet during heating

Room temperature wiring is one of the last goals for printed electronics. room temperature fabrication enables to use the wide variety of functional materials into one circuit board without thermal stress or damage as well as environmental consciousness. Metallic nanoparticles can be sintered to form dense microstructure if both the surface of nanoparticles and the environment are clean without any oxidation or contamination. Ag nanoparticles are, however, usually protected by an organic layer. It is desirable to remove this organic layer by certain chemical processes with or without light heating or other kinds of energy processes, which do not have any serious damage on organic devices and substrates weak against heating.

Recently, the authors developed a new process, by which the paste of Ag nanoparticles protected with them can be successfully sintered at room temperature in air atmosphere. One of the typical organic layer is dodecylamine. In order to remove the dodecylamine layer, it was found that alcohol treatment is quite effective. For instance, Ag nanoparticles ink was printed into lines on a glass substrate and it was dipped into methanol for 10–7,200 s. As a result, sintering was immediately started and resultant Ag wires exhibited excellent low resistivity, 7.3×10^{-5} Ωcm after 7,200 s dipping. Microstructural observation on this room temperature sintering revealed that, as dipping time gets longer, Ag nanoparticles agglomerate coarsened and connection among particles becomes clearer even in a few

minutes. Thus, a novel room temperature wiring method for Ag nanoparticles has been successfully developed in air atmosphere.

2.7 Nanowires and Nanobelts

2.7.1 Introduction

A nanowire is a wire of diameter of the order of a nanometer (10^{-9} m). Alternatively, nanowires can be defined as structures that have a lateral size constrained to tens of nanometers or less and an unconstrained longitudinal size. At these scales, quantum mechanical effects are important, and hence such wires are also known as "quantum wires." Many different types of nanowires exist, including metallic (e.g., Ni, Pt, Au) [137], semiconducting (e.g., Si, InP, GaN, ZnO) [138], and insulating (e.g., SiO_2, TiO_2) [139]. Molecular nanowires are composed of repeating molecular units either organic (e.g., DNA) or inorganic (e.g., $Mo_6S_{9-x}I_x$) [140].

A common technique for creating a nanowire is the vapor–liquid–solid (VLS) synthesis method [141–143]. This technique uses as source material either laser ablated particles or a feed gas. The source is then exposed to a catalyst. For nanowires, the best catalysts are liquid metal (such as gold) nanoclusters, which can either be purchased in colloidal form or by electron-beam deposition and deposited on a substrate or self-assembled from a thin film by dewetting. This process can often produce crystalline nanowires in the case of semiconductor materials. The source enters these nanoclusters and begins to saturate it. Once supersaturation is reached, the source solidifies and grows outward from the nanocluster. The final length of the nanowires can be adjusted by simply turning off the source. Compound nanowires with super-lattices of alternating materials can be created by switching sources while still in the growth phase.

Nanowires (NWs) and nanobelts (NBs) have been demonstrated as building blocks for fabricating nanodevices, such as FET [144], gas sensor [145], diodes [146], LED [147], biosensors [148–150].

2.7.2 Applications of Nanowires

Perhaps the most obvious use for nanowires is in electronics. Some nanowires are very good conductors or semiconductors, and their minis-

cule size means that manufacturers could fit millions more transistors on a single microprocessor. As a result, computer speed would increase dramatically.

Nanowires may play an important role in the field of quantum computers. Doh et al. in the Netherlands created nanowires out of indium arsenide and attached them to aluminum electrodes [151]. At temperatures near absolute zero, aluminum becomes a superconductor, meaning it can conduct electricity without any resistance. The nanowires also became superconductors due to the proximity effect. The researchers could control the superconductivity of the nanowires by running various voltages through the substrate under the wires.

Nanowires may also play an important role in nano-size devices like nanorobots. Doctors could use the nanorobots to treat diseases like cancer. Some nanorobot designs have onboard power systems, which would require structures like nanowires to generate and conduct power.

Using piezoelectric material, nanoscientists could create nanowires that generate electricity from kinetic energy. The piezoelectric effect is a phenomenon certain materials exhibit – when you apply physical force to a piezoelectric material, it emits an electric charge. If you apply an electric charge to this same material, it vibrates. Piezoelectric nanowires might provide power to nano-size systems in the future, though at present there are no practical applications.

There are hundreds of other potential nanowire applications in electronics. Researchers in Japan are working on atomic switches that might some day replace semiconductor switches in electronic devices [152]. Scientists with the National Renewable Energy Laboratory hope that coaxial nanowires will improve the energy efficiency of solar cells [153].

2.7.2.1 Application of Nanowire in Sensor Technology

Pd as the active sensing material has unique property of interaction with hydrogen gas. Partial pressure change of hydrogen gas determines Pd's physical properties (mass, volume, electrical resistance) by forming Pd-H hydride. The difference of electrical resistance by the partial pressure change of hydrogen gas is used as the signal of hydrogen sensor. However, pure palladium has issues in sensor application such as slow response time and high detecting limit [154]. Nano-sized material has large surface-to-volume ratio for hydrogen sensing and advantages for improvement of sensor performance. Palladium nanowire has been the subject of intense interest as sensor materials and structures [155].

Yun et al. [156] demonstrated the fabrication technique involves electrodeposition to directly grow nanowires between patterned thin-film contact electrodes (Fig. 2.16). To demonstrate nanowire sensors, the author

electrochemically grown metal (Pd, Au, Pt), metal oxide (Sb_2O_3), and conducting polymer (polyaniline)-bundled nanowires. Using Pt-bundled nanowires surface modified with glucose oxidase, the author demonstrated glucose detection as a demonstration of a biomolecular sensor.

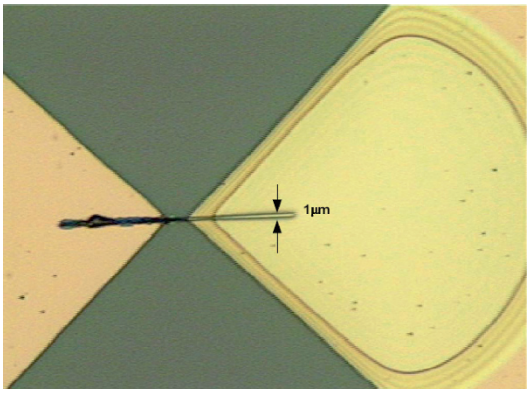

Fig. 2.16. An optical image of electrodeposited Pd wires grown between electrodes for biomedical sensor application [156]

Lee et al. [157] investigated the application of Pd–Ag nanowires as hydrogen sensor. The wire or dendrite-shaped Ag nanowire was grown by electrochemical migration method in a few minutes. The diameter of this nanowire is 50 ~ 200 nm. Pd–Ag nanowire was fabricated using Pd thin film evaporated on the Ag nanowire with 20 – 500 nm thickness. This structure can provide large surface area for sensor. The large surface area gives the reaction sites between Pd–Ag nanowire and hydrogen gas to reduce response time and increase sensitivity. The response time of Pd–Ag nanowire (with 20 nm thickness of the Pd film) is about 5 s at room temperature. The response time and sensitivity are increased according to the thickness of the Pd film on Ag nanowire. Pd–Ag nanowire is saturated and responds easily at lower concentration of hydrogen gas. The Pd film on Ag nanowire did not show the peel-off phenomenon, while pure Pd film is separated from substrate after sensing test. The mechanical stress brings this phenomenon is released by evaporating Pd film on the Ag nanowire mesh.

2.7.2.2 Nanogenerator from ZnO Nanowires

Developing novel technologies for wireless nanodevices and nanosystems is of critical importance for in situ, real-time, and implantable biosensing, remote and wireless sensing, defense technology, and commercial applications. The power sources required by such devices are highly desired to be

lifetime self-charging and in comparable small sizes. Harvesting energy from environment, including solar, thermal, and mechanical energies, provides a perfect solution for these applications. There are huge emergent needs for nanoscale sensing devices for biological sensing and defense applications. Among those possible energy sources, mechanical wave and vibration energies more ubiquitously exist under various circumstances around us [158]. Relying on the piezoelectric effect of a ceramic beam when driven to vibrate by a small mass via gravitation, mechanical energy can be converted into electricity. Many types of MEMS microgenerator have been developed using piezoelectric thin-film cantilevers [159]. However, their relatively large size, bio-incompatible nature, and low sensitivity to small vibrations seriously restrict the application in nanotechnologies and the advantages provided by nano-materials.

Nanowires (NWs) and nanobelts (NBs) of inorganic materials are the forefront in today's nanotechnology research [160]. Among the known one-dimensional nano-materials, zinc oxide (ZnO) has three key advantages [161]. First, it exhibits both semiconducting and piezoelectric properties, providing a unique material for building electro-mechanical coupled sensors and transducers [162, 163]. Second, ZnO is relatively biosafe and biocompatible, and it can be used for biomedical applications with little toxicity. Finally, ZnO exhibits the most diverse and abundant configurations of nanostructures, such as nanowires, nanobelts, nanosprings, nanorings, nanobows, and nanohelices [164]. Recently, Wang et al. at Georgia Tech developed a novel approach of converting mechanical energy into electric power using aligned ZnO nanowires. This discovery sets the foundation for nanoscale power conversion, which will potentially lead to a new adaptable, mobile, and cost-effective energy harvesting technology [165–168].

The piezoelectric nanogenerators are built on vertically aligned ZnO NWs. The operation principle relies on the piezoelectric potential generated on a bent ZnO NW. The rectifying effect of the Schottky junction between the metal electrode and the ZnO crystal can selectively accumulate and release charging, resulting in a continuous mechanical-to-electric energy conversion. The nanogenerator can convert small mechanical vibration energy and hydraulic energy into electricity under various circumstances, such as under ground, in water, or even inside human body. Wang et al. have developed an innovative approach by using ultrasonic waves to drive the motion of the NWs, leading to the production of a continuous current (Fig. 2.17) [169]. The nanogenerator worked continuously for an extended period of time of beyond 1 h. The authors were able to increase the output current to 800 nA and voltage to 10 mV.

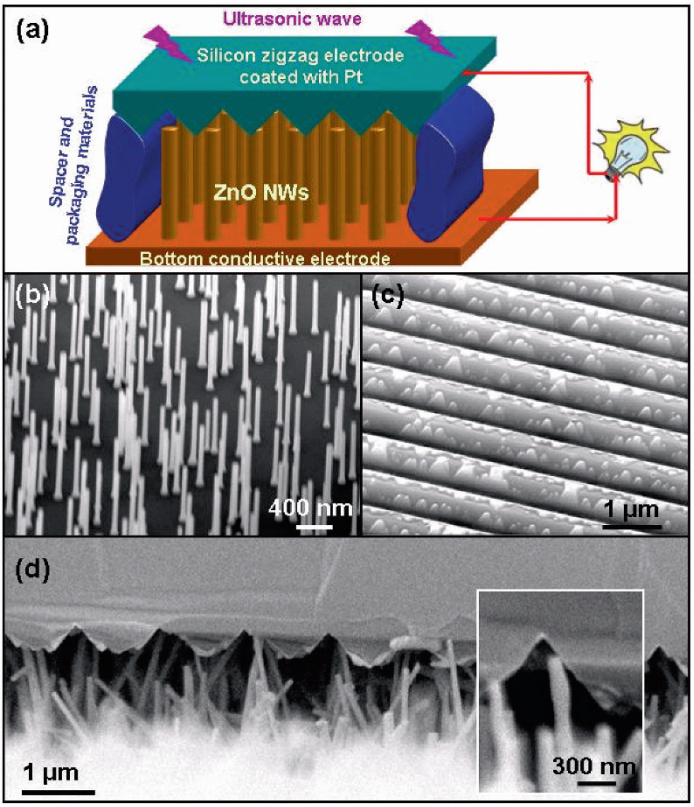

Fig. 2.17. Nanogenerators driven by an ultrasonic wave. (a) Schematic diagram showing the design and structure of the nanogenerator. (b) Low-density aligned ZnO NWs grown on a GaN substrate. (c) Zigzag trenched electrode coated with Pt. (d) Cross-sectional SEM image of the nanogenerator. Inset: A typical NW that is forced by the electrode to bend [169]

The application and the energy conversion efficiency largely depend on the fabrication and packaging techniques. In general, majority of the NWs (ideally 100%) need to be involved in power generation and all the NWs have to be well isolated from the corrosive surroundings but still have free movement. This requires a high dimensional uniformity of the NWs as well as a perfect positioning and alignment of the top electrode on the NW arrays. Upon addressing these crucial challenges, the nanogenerators can potentially become a new self-powered technology for lifetime unattended sensor systems, battery-free electronics, and even in situ, real-time, and implantable biological devices.

References

[1] H. W. C. Postma, T. Teepen, Z. Yao, M. Grifoni, and C. Dekker, "Carbon Nanotube Single-Electron Transistors at Room Temperature," Science, 293, 76–79, 2001.

[2] J. Xiang, W. Lu, Y. J. Hu, Y. Wu, H. Yan, and C. M. Lieber, "Ge/Si Nanowire Heterostructures as High-Performance Field-Effect Transistors," *Nature*, 441, 489–493, 2006.

[3] M. C. Petty, M. R. Bryce, and D. Bloor, "An Introduction to Molecular Electronics," Edward Arnold, London, 1995.

[4] A. Aviram and M. A. Ratner, "Molecular Rectifier," *Chemical Physics Letters*, 29, 277, 1974.

[5] A. Aviram, "Molecules for Memory, Logic, and Amplification," *Journal of the American Chemical Society*, 110, 5687–5692, 1988.

[6] J. E. Morris, "Nanopackaging: Nanotechnologies and Electronics Packaging," Springer, Berlin, 2008.

[7] S. H. Sun, C. B. Murray, D. Weller, L. Folks, and A. Moser, "Monodisperse FePt Nanoparticles and Ferromagnetic FePt Nanocrystal Superlattices," *Science*, 287, 1989–1992, 2000.

[8] K. W. Park, J. H. Choi, B. K. Kwon, S. A. Lee, Y. E. Sung, H. Y. Ha, S. A. Hong, H. Kim, and A. Wieckowski, "Chemical and Electronic Effects of Ni in Pt/Ni and Pt/Ru/Ni Alloy Nanoparticles in Methanol Electrooxidation," *Journal of Physical Chemistry B*, 106, 1869–1877, 2002.

[9] M. P. Mallin and C. J. Murphy, "Solution-Phase Synthesis of Sub-10 nm Au-Ag Alloy Nanoparticles," *Nano Letters*, 2, 1235–1237, 2002.

[10] A. Henglein and M. Giersig, "Radiolytic Formation of Colloidal Tin and Tin-Gold Particles in Aqueous-Solution," *Journal of Physical Chemistry*, 98, 6931–6935, 1994.

[11] P. Lu, J. Dong, and N. Toshima, "Surface-Enhanced Raman Scattering of a Cu/Pd Alloy Colloid Protected by Poly(N-vinyl-2-pyrrolidone)," *Langmuir*, 15, 7980–7992, 1999.

[12] S. Link, C. Burda, Z. L. Wang, and M. A. El-Sayed, "Electron Dynamics in Gold and Gold-Silver Alloy Nanoparticles: The Influence of a Nonequilibrium Electron Distribution and the Size Dependence of the Electron-Phonon Relaxation," *Journal of Chemical Physics*, 111, 1255–1264, 1999.

[13] Y. B. Zhao, Z. J. Zhang, and H. X. Dang, "Synthesis of In-Sn Alloy Nanoparticles by a Solution Dispersion Method," *Journal of Materials Chemistry*, 14, 299–302, 2004..

[14] Y. H. Chen and C. S. Yeh, "A New Approach for the Formation of Alloy Nanoparticles: Laser Synthesis of Gold-Silver Alloy from

Gold-Silver Colloidal Mixtures," *Chem. Commun.*, 4, 371–372, 2001.

[15] J. Zhang, J. Worley, S. Denommee, C. Kingston, Z. J. Jakubek, Y. Deslandes, M. Post, B. Simard, N. Braidy, and G. A. Botton, "Synthesis of Metal Alloy Nanoparticles in Solution by Laser Irradiation of a Metal Powder Suspension," *Journal of Physical Chemistry B*, 107, 6920–6923, 2003.

[16] M. Mandal, N. R. Jana, S. Kundu, S. K. Ghosh, M. Panigrahi, and T. Pal, "Synthesis of Au-core-Ag-shell Type Bimetallic Nanoparticles for Single Molecule Detection in Solution by SERS Method," *Journal of Nanoparticle Research*, 6, 53–61, 2004.

[17] G. Southam and T. J. Beveridge, "The Occurrence of Sulfur and Phosphorus within Bacterially Derived Crystalline and Pseudocrystalline Octahedral Gold Formed in vitro," *Geochimica Et Cosmochimica Acta*, 60, 4369–4376, 1996.

[18] D. Fortin and T. J. Beveridge, From Biology to Biotechnology and Medical Applications, in Biomineralization, E. Baeuerien, Ed., Wiley-VCH, Weinheim, pp. 7, 2000.

[19] T. Klaus, R. Joerger, E. Olsson, and C. G. Granqvist, "Silver-Based Crystalline Nanoparticles, Microbially Fabricated," *Proceedings of the National Academy of Sciences of the United States of America*, vol. 96, pp. 13611–13614, 1999.

[20] T. Klaus-Joerger, R. Joerger, E. Olsson, and C. G. Granqvist, "Bacteria as Workers in the Living Factory: Metal-Accumulating Bacteria and their Potential for Materials Science," *Trends in Biotechnology*, 19, 15–20, 2001.

[21] R. Joerger, T. Klaus, and C. G. Granqvist, "Biologically Produced Silver-Carbon Composite Materials for Optically Functional Thin-Film Coatings," *Advanced Materials*, 12, 407–409, 2000.

[22] B. Nair and T. Pradeep, "Coalescence of Nanoclusters and Formation of Submicron Crystallites Assisted by Lactobacillus Strains," *Crystal Growth & Design*, 2, 293–298, 2002.

[23] J. L. Gardea-Torresdey, J. G. Parsons, E. Gomez, J. Peralta-Videa, H. E. Troiani, P. Santiago, and M. J. Yacaman, "Formation and Growth of Au Nanoparticles Inside Live Alfalfa Plants," *Nano Letters*, 2, 397–401, 2002.

[24] J. L. Gardea-Torresdey, E. Gomez, J. R. Peralta-Videa, J. G. Parsons, H. Troiani, and M. Jose-Yacaman, "Alfalfa Sprouts: A Natural Source for the Synthesis of Silver Nanoparticles," *Langmuir*, 19, 1357–1361, 2003.

[25] M. Ohring, "Materials Science of Thin Films: Deposition & Structure," 2nd Ed., Academic Press, pp. 395–397, 2002.

[26] J. E. Morris, "Single-Electron Transistors," in The Electrical Engineering Handbook Third edition: Electronics, Power Electronics, Optoelectronics, Microwaves, Electromagnetics, and Radar, Richard C. Dorf, Ed., CRC/Taylor & Francis, Boca Raton, FL, pp. 3.53–3.64, 2006.

[27] J. Xu and C. P. Wong, "High-K Nanocomposites with Core-Shell Structured Nanoparticles for Decoupling Applications," *Proceedings of the 55th IEEE Electronic Component & Technology Conference*, pp. 1234–1240, 2005.

[28] F. Wu and J. E. Morris, "Characterizations of (SiOxCr1-x)N1-y Thin Film Resistors for Integrated Passive Applications," *53rd Electronic Components & Technology Conference*, pp. 161–166, 2003.

[29] J. E. Morris, "Recent Developments in Discontinuous Metal Thin Film Devices," *Vacuum*, 50, 107–113, 1998.

[30] J. E. Morris, F. Wu, C. Radehaus, M. Hietschold, A. Henning, K. Hofmann, and A. Kiesow, "Single Electron Transistors: Modeling and Fabrication," *Proceedings of the 7th International Conference Solid State & Integrated Circuit Technology (ICSICT)*, Beijing, pp. 634–639, 2004.

[31] H. Jiang, K. Moon, H. Dong, and F. Hua, "Thermal Properties of Oxide Free Nano Non Noble Metal for Low Temperature Interconnect Technology," *Proceedings of the56th IEEE Electronic Component & Technology Conference*, San Diego, CA, pp. 1969–1973, 2006.

[32] R. A. Flinn and P. K. Trojan, "Engineering Materials & their Applications," 2nd Ed., Houghton-Mifflin, Boston, MA, pp. 75–77, 1981.

[33] T. Yamaguchi, M. Sakai, and N. Saito, "Optical-Properties of Well-Defined Granular Metal Systems," *Physical Review B*, 32, 2126–2131, 1985.

[34] R. Das, M. Poliks, J. Lauffer, and V. Markovich, "High Capacitance, Large Area, Thin Film, Nanocomposite Based Embedded Capacitors," *Proceedings of the 56th IEEE Electronic Component & Technology Conference*, San Diego, CA, pp. 1510–1515, 2006.

[35] J. Xu and C. P. Wong, "Effects of the Low Loss Polymers on the Dielectric Behavior of Novel Aluminum-Filled High-k Nano-Composites," *Proceedings of the 54th IEEE Electronic Component & Technology Conference*, Las Vegas, pp. 496–506, 2004.

[36] J. Lu, K. Moon, and C. P. Wong, "Development of Novel Silver Nanoparticles/Polymer Composites as High K Polymer Matrix by In-Situ Photochemical Method," *Proceedings of the 56th IEEE*

Electronic Component & Technology Conference, San Diego, CA, pp. 1841–1846, 2006.

[37] L. Ekstrand, H. Kristiansen, and J. Liu, "Characterization of Thermally Conductive Epoxy Nano Composites," *Proceedings of the 28th International Spring Seminar on Electronics Technology (ISSE'05)*, Vienna, 2005.

[38] L. Fan, B. Su, J. Qu, and C. P. Wong, "Electrical and Thermal Conductivities of Polymer Composites Containing Nano-Sized Particles," *Proceedings of the 54th IEEE Electronic Component & Technology Conference*, Las Vegas, NV, pp. 148–154, 2004.

[39] H. Jiang, K. Moon, L. Zhu, J. Lu, and C. P. Wong, "The Role of Self-Assembled Monolayer (SAM) on Ag Nanoparticles for Conductive Nanocomposite," *Proceedings of the 10th IEEE/CPMT International Symposium on Advanced Packaging Materials*, Irvine, CA, pp. 266–271, 2005.

[40] R. Das, J. Lauffer, and F. Egitto, "Electrical Conductivity and Reliability of Nano- and Micro-Filled Conducting Adhesives for Z-axis Interconnections," *Proceedings of the 56th IEEE Electronic Component & Technology Conference*, San Diego, CA, pp. 112–118, 2006.

[41] K. Moon, S. Pothukuchi, Y. Li, and C. P. Wong, "Nano Metal Particles for Low Temperature Interconnect Technology," *Proceedings of the 54th IEEE Electronic Component & Technology Conference*, Las Vegas, NV, pp. 1983–1988, 2004.

[42] P. Lall, S. Islam, J. Suhling, and G. Tian, "Nano-Underfills for High-Reliability Applications in Extreme Environments," *Proceedings of the 55th IEEE Electronic Component & Technology Conference*, Orlando, FL, pp. 212–222, 2005.

[43] Y. Li, K. S. Moon, and C. P. Wong, "Adherence of Self-Assembled Monolayers on Gold and Their Effects for High-Performance Anisotropic Conductive Adhesives," *Journal of Electronic Materials*, 34, 266–271, 2005.

[44] S. Joo and D. F. Baldwin, "Demonstration for Rapid Prototyping of Micro-Systems Packaging by Data-Driven Chip-First Processing Using Nano-Particles Metal Colloids," *Proceedings of the 55th IEEE Electronic Component & Technology Conference*, Orlando, FL, PP. 1859–1863, 2005.

[45] A. Moscicki, J. Felba, T. Sobierajski, J. Kudzia, A. Arp, and W. Meyer, "Electrically Conductive Formulations Filled Nano Size Silver Filler for Ink-Jet Technology," *Proceedings of the 5th International Conference on Polymers and Adhesives in Microelectronics and Photonics*, Wroclaw, Poland, pp. 40–44, 2005.

[46] J. Kolbe, A. Arp, F. Calderone, E. M. Meyer, W. Meyer, H. Schaefer, and M. Stuve, "Inkjettable Conductive Adhesive for Use in Microelectronics and Microsystems Technology," *Proceedings of the 5th International Conference on Polymers and Adhesives in Microelectronics and Photonics*, Wroclaw, Poland, pp. 160–163, 2005.

[47] J. G. Bai, K. D. Creehan, and H. A. Kuhn, "Inkjet Printable Nanosilver Suspensions for Enhanced Sintering Quality in Rapid Manufacturing," *Nanotechnology*, 18, 1–5, 2007.

[48] W. Peng, V. Hurskainen, K. Hashizume, S. Dunford, S. Quander, and R. Vatanparast, "Flexible Circuit Creation with Nano Metal Particles," *Proceedings of the 55th IEEE Electronic Component & Technology Conference*, Orlando, FL, pp. 77–82, 2005.

[49] J. G. Bai, Z. Z. Zhang, J. N. Calata, and G. Q. Lu, "Low-Temperature Sintered Nanoscale Silver as a Novel Semiconductor Device-Metallized Substrate Interconnect Material," *IEEE Transactions on Components and Packaging Technologies*, 29, 589–593, 2006.

[50] D. Wakuda, M. Hatamura, and K. Suganuma, "Novel Room Temperature Wiring Process of Ag Nanoparticle Paste," *Proceedings of the 6th International Conference on Polymers and Adhesives in Microelectronics and Photonics*, Tokyo, pp. 110–113, 2007.

[51] A. Moscicki, J. Felba, P. Gwiazdzinski, and M. Puchalski, "Conductivity Improvement of Microstructures Made by Nano-Size-Silver Filled Formulations," *Proceedings of the 6th International Conference on Polymers and Adhesives in Microelectronics and Photonics*, Tokyo, pp. 305–310, 2007.

[52] J. G. Bai, Z. Z. Zhang, J. N. Calata, and G. Q. Lu, "Characterization of Low-Temperature Sintered Nanoscale Silver Paste for Attaching Semiconductor Devices," *Proceedings of the 7th IEEE CPMT Conference on High Density Microsystem Design and Packaging and Component Failure Analysis (HDP'05)*, Shanghai, pp. 272–276, 2005.

[53] Y. Sun, Z. Zhang, and C. P. Wong, "Photo-Definable Nanocomposite for Wafer Level Packaging," *Proceedings of the 55th IEEE Electronic Component & Technology Conference*, Orlando, FL, pp. 179–184, 2005.

[54] Y. Sun and C. P. Wong, "Study and Characterization on the Nanocomposite Underfill for Flip Chip Applications," *Proceedings of the 54th IEEE Electronic Component & Technology Conference*, Las Vegas, NV, pp. 477–483, 2004.

[55] Y. Sun, Z. Zhang, and C. P. Wong, "Fundamental Research on Surface Modification of Nano-Size Silica for Underfill Applica-

tions," *Proceedings of the 54th IEEE Electronic Component & Technology Conference*, Las Vegas, NV, pp. 754–760, 2004.

[56] M. Roy, J. K. Nelson, R. K. MacCrone, L. S. Schadler, C. W. Reed, R. Keefe, and W. Zenger, "Polymer Nanocomposite Dielectrics – The Role of the Interface," *IEEE Transactions on Dielectrics and Electrical Insulation*, 2, 629–643, 2005.

[57] W. Guan, S. C. Verma, Y. Gao, C. Andersson, Q. Zhai, and J. Liu, "Characterization of Nanoparticles of Lead Free Solder Alloys," *Proceedings of the 1st IEEE Electronics Systemintegration Technology Conference*, Dresden, Germany, 2006.

[58] K. M. Kumar, V. Kripesh, and A. A. O. Tay, "Sn-Ag-Cu Lead-free Composite Solders for Ultra-Fine-Pitch Wafer-Level Packaging," *Proceedings of the 56th IEEE Electronic Component & Technology Conference*, San Diego, CA, pp. 237–243, 2006.

[59] M. Amagai, "A Study of Nano Particles in SnAg-Based Lead Free Solders for Intermetallic Compounds and Drop Test Performance," *Proceedings of the 56th IEEE Electronic Component & Technology Conference*, San Diego CA, pp. 1170–1190, 2006.

[60] V. Kripesh, K. Mohankumar, and A. Tay, "Properties of Solders Reinforced with Nanotubes and Nanoparticles," *Proceedings of the 56th IEEE Electronic Component & Technology Conference*, San Diego, CA, 2006.

[61] K. M. Klein, J. Zheng, A. Gewirtz, D. S. Sarma, S. Rajalakshmi, and S. K. Sitaraman, "Array of Nano-Cantilevers as a Bio-Assay for Cancer Diagnosis," *Proceedings of the 55th IEEE Electronic Component & Technology Conference*, Orlando, FL, pp. 583–587, 2005.

[62] H. Jiang, K. S. Moon, F. Hua, and C. P. Wong, "Synthesis and Thermal and Wetting Properties of Tin/Silver Alloy Nanoparticles for Low Melting Point Lead-free Solders," *Chemistry of Materials*, 19, 4482–4485, 2007.

[63] R. Garrigos, P. Cheyssac, and R. Kofman, "Melting for Lead Particles of Very Small Sizes – Influence of Surface Phenomena," *Zeitschrift Fur Physik D-Atoms Molecules and Clusters*, 12, 497–500, 1989.

[64] W. Y. Hu, S. G. Xiao, J. Y. Yang, and Z. Zhang, "Melting Evolution and Diffusion Behavior of Vanadium Nanoparticles," *European Physical Journal B*, 45, 547–554, 2005.

[65] W. Guan, S. C. Verma, Y. Gao, C. Andersson, Q. Zhai, and J. Liu, "Characterization of Nanoparticles of Lead Free Solder Alloys," *Electronics Systemintegration Technology Conference*, vol. 1, pp. 7–12, 2006.

[66] Z. W. Li, X. J. Tao, Y. M. Cheng, Z. S. Wu, Z. J. Zhang, and H. X. Dang, "A Facile Way for Preparing Tin Nanoparticles from Bulk Tin via Ultrasound Dispersion," *Ultrasonics Sonochemistry*, 14, 89–92, 2007.

[67] Y. B. Zhao, Z. J. Zhang, and H. X. Dang, "A Simple Way to Prepare Bismuth Nanoparticles," *Materials Letters*, 58, 790–793, 2004.

[68] H. J. Chen, Z. W. Li, Z. S. Wu, and Z. J. Zhang, "A Novel Route to Prepare and Characterize Sn-Bi Nanoparticles," *Journal of Alloys and Compound.s*, 394, 282–285, 2005.

[69] K. Mohankumar and A. A. O. Tay, "Nanoparticle Reinforced Solders for Fine Pitch Applications," *Proceedings of Electronics Packaging Technology Conference*, pp. 455–461, 2006.

[70] K. M. Kumar, "Sn-Ag-Cu Lead-free Composite Solders for Ultra-Fine-Pitch Wafer-Level Packaging," *Proceedings of the 56th IEEE Electronic Component & Technology Conference*, San Diego, CA, pp. 237–243, 2006.

[71] F. Qi, L. Sun, Z. Hou, J. Wang, and C. Qin, *International Conference on Electronic Packaging Technology & High Density Packaging*, pp. 1–3, 2008.

[72] M. Amagai, "A Study of Nanoparticles in Sn-Ag Based Lead Free Solders," *Microelectronics Reliability*, 48, 1–16, 2008.

[73] G. E. Moore, "Progress in Digital Integrated Electronics," *International Electron Devices Meetings*, Washington D. C., pp. 11–13, 1975.

[74] F. Kreupl, A. P. Graham, G. S. Duesberg, W. Steinhogl, M. Liebau, E. Unger, and W. Honlein, "Carbon Nanotubes in Interconnect Applications," *Microelectronic Engineering*, 64, 399–408, 2002.

[75] A. P. Graham, G. S. Duesberg, W. Hoenlein, F. Kreupl, M. Liebau, R. Martin, B. Rajasekharan, W. Pamler, R. Seidel, W. Steinhoegl, and E. Unger, "How Do Carbon Nanotubes Fit into the Semiconductor Roadmap?," *Applied Physics A-Materials Science & Processing*, 80, 1141–1151, 2005.

[76] S. Frank, P. Poncharal, Z. L. Wang, and W. A. de Heer, "Carbon Nanotube Quantum Resistors," *Science*, 280, 1744–1746, 1998.

[77] T. M. Wu and E. C. Chen, "Crystallization Behavior of Poly(epsilon-caprolactone)/Multiwalled Carbon Nanotube Composites," *Journal of Polymer Science Part B-Polymer Physics*, 44, 598–606, 2006.

[78] S. Mizuno, A. Verma, H. Tran, P. Lee, and B. Nguyen, "Dielectric Constant and Stability of Fluorine Doped PECVD Silicon Oxide Thin Films," *Thin Solid Films*, 283, 30–36, 1996.

[79] B. Q. Wei, R. Vajtai, and P. M. Ajayan, "Reliability and Current Carrying Capacity of Carbon Nanotubes," *Applied Physics Letters*, 79, 1172–1174, 2001.

[80] A. P. Graham, G. S. Duesberg, R. V. Seidel, M. Liebau, E. Unger, W. Pamler, F. Kreupl, and W. Hoenlein, "Carbon Nanotubes for Microelectronics?," *Small*, 1, 382–390, 2005.

[81] M. Nihei, A. Kawabata, D. Kondo, M. Horibe, S. Sato, and Y. Awano, "Electrical Properties of Carbon Nanotube Bundles for Future via Interconnects," *Japanese Journal of Applied Physics Part 1-Regular Papers Short Notes & Review Papers*, 44, 1626–1628, 2005.

[82] W. Hoenlein, F. Kreupl, G. S. Duesberg, A. P. Graham, M. Liebau, R. Seidel, and E. Unger, "Carbon Nanotubes for Microelectronics: Status and Future Prospects," *Materials Science & Engineering C-Biomimetic and Supramolecular Systems*, 23, 663–669, 2003.

[83] Y. Awano, "Carbon Nanotube Technologies for LSI via Interconnects," *IEICE Trans. Electron.*, E89C, 1499–1503, 2006.

[84] L. B. Zhu, Y. Y. Sun, D. W. Hess, and C. P. Wong, "Well-aligned Open-ended Carbon Nanotube Architectures: An Approach for Device Assembly," *Nano Letters*, 6, 243–247, 2006.

[85] A. Naeemi, G. Huang, and J. Meindl, "Performance Modeling for Carbon Nanotube Interconnects in On-chip Power Distribution," *Proceedings of the 57th IEEE Electronic Component & Technology Conference*, Reno, NV, pp. 420–428, 2007.

[86] Y. Chai, J. Gong, K. Zhang, P. C. H. Chan, and M. M. F. Yuen, "Low Temperature Transfer of Aligned Carbon Nanotube Films Using Liftoff Technique," *Proceedings of the 57th IEEE Electronic Component & Technology Conference*, Reno, NV, pp. 429–434, 2007.

[87] C.-J. Wu, C.-Y. Chou, C.-N. Han, and K.-N. Chiang, "Simulation and Validation of CNT Mechanical Properties – The Future Interconnection Method," *Proceedings of the 57th IEEE Electronic Component & Technology Conference*, Reno, NV, pp. 447–452, 2007.

[88] A. Ruiz, E. Vega, R. Katiyar, and R. Valentin, "Novel Enabling Wire Bonding Technology," *Proceedings of the 57th IEEE Electronic Component & Technology Conference*, Reno, NV, pp. 458–462, 2007.

[89] G. A. Riley, "Nanobump Flip Chips," *Advanced Packaging*, 18–20, April, 2007.

[90] R. T. Pike, R. Dellmo, J. Wade, S. Newland, G. Hyland, and C. M. Newton, "Metallic Fullerene and MWCNT Composite Solutions

for Microelectronics Subsystem Electrical Interconnection Enhancement," *Proceedings of the 54th IEEE Electronic Component & Technology Conference*, Las Vegas, NV, pp. 461–465, 2004.

[91] J. Ding, S. Rea, D. Linton, E. Orr, and J. MacConnell, "Mixture Properties of Carbon Fibre Composite Materials for Electronics Shielding in Systems Packaging," *Proceedings of the 1st IEEE Electronics Systemintegration Technology Conference*, Dresden, Germany, pp. 19–25, 2006.

[92] J.-C. Chiu, C.-M. Chang, W.-H. Cheng, and W.-S. Jou, "High-Performance Electromagnetic Susceptibility for a 2.5Gb/s Plastic Transceiver Module Using Mutli-Wall Carbon Nanotubes," *Proceedings of the 56th IEEE Electronic Component & Technology Conference*, San Diego, CA, pp. 183–186, 2006.

[93] S. Berber, Y. K. Kwon, and D. Tomanek, "Unusually High Thermal Conductivity of Carbon Nanotubes," *Physical Review Letters*, 84, 4613–4616, 2000.

[94] E. Pop, D. Mann, Q. Wang, K. Goodson, and H. J. Dai, "Thermal Conductance of an Individual Single-wall Carbon Nanotube above Room Temperature," *Nano Letters*, 6, 96–100, 2006.

[95] P. Kim, L. Shi, A. Majumdar, and P. L. McEuen, "Thermal Transport Measurements of Individual Multiwalled Nanotubes," *Physical Review Letters*, 8721, 215502-1–215502-4, 2001.

[96] J. Hone, M. C. Llaguno, N. M. Nemes, A. T. Johnson, J. E. Fischer, D. A. Walters, M. J. Casavant, J. Schmidt, and R. E. Smalley, "Electrical and Thermal Transport Properties of Magnetically Aligned Single Wall Carbon Nanotube Films," *Applied Physics Letters*, 77, 666–668, 2000.

[97] W. Yi, L. Lu, D. L. Zhang, Z. W. Pan, and S. S. Xie, "Linear Specific Heat of Carbon Nanotubes," *Physical Review B*, 59, R9015–R9018, 1999.

[98] D. J. Yang, Q. Zhang, G. Chen, S. F. Yoon, J. Ahn, S. G. Wang, Q. Zhou, Q. Wang, and J. Q. Li, "Thermal Conductivity of Multiwalled Carbon Nanotubes," *Physical Review B*, 66, 165440.1–165440.6, 2002.

[99] J. Xu and T. S. Fisher, "Enhancement of Thermal Interface Materials with Carbon Nanotube Arrays," *International Journal of Heat and Mass Transfer*, vol49, 1658–1666, 2006.

[100] Y. Xu, Y. Zhang, E. Suhir, and X. W. Wang, "Thermal Properties of Carbon Nanotube Array Used for Integrated Circuit Cooling," *Journal of Applied Physics*, 100, 074302, 2006.

[101] K. Zhang, Y. Chai, M. M. F. Yuen, D. G. W. Xiao, and P. C. H. Chan, "Carbon Nanotube Thermal Interface Material for High-

Brightness Light-Emitting-Diode Cooling," *Nanotechnology*, 19, 215706, 2008.

[102] R. Prasher, "Thermal Interface Materials: Historical Perspective, Status, and Future Directions," *Proceedings of the IEEE*, vol. 94, pp. 1571–1586, 2006.

[103] J. Xu and T. S. Fisher, "Enhanced Thermal Contact Conductance Using Carbon Nanotube Array Interfaces," *IEEE Transactions on Components and Packaging Technologies*, 29, 261–267, 2006.

[104] T.-M. Lee, K.-C. Chiou, F.-P. Tseng, and C.-C. Huang, "High Thermal Efficiency Carbon Nanotube-Resin Matrix for Thermal Interface Materials," *Proceedings of the 55th IEEE Electronic Component & Technology Conference*, Orlando, FL, pp. 55–59, 2005.

[105] J. Liu, M. O. Olorunyomi, X. Lu, W. X. Wang, T. Aronsson, and D. Shangguan, "New Nano-Thermal Interface Material for Heat Removal in Electronics Packaging," *Proceedings of the 1st IEEE Electronics Systemintegration Technology Conference*, Dresden, Germany, pp. 1–6, 2006.

[106] Z. Mo, R. Morjan, J. Anderson, E. E. B. Campbell, and J. Liu, "Integrated Nanotube Microcooler for Microelectronics Applications," *Proceedings of the 55th IEEE Electronic Component & Technology Conference*, Orlando, FL, pp. 51–54, 2005.

[107] L. Ekstrand, Z. Mo, Y. Zhang, and J. Liu, "Modelling of Carbon Nanotubes as Heat Sink Fins in Microchannels for Microelectronics Cooling," *Proceedings of the 5th International Conference on Polymers and Adhesives in Microelectronics and Photonics*, Wroclaw, Poland, pp. 185–187, 2005.

[108] W. Lin, Y. G. Xiu, H. J. Jiang, R. W. Zhang, O. Hildreth, K. S. Moon, and C. P. Wong, "Self-Assembled Monolayer-Assisted Chemical Transfer of In Situ Functionalized Carbon Nanotubes," *Journal of the American Chemical Society*, 130, 9636–9637, 2008.

[109] B. J. Ash, R. W. Siegel, and L. S. Schadler, "Glass-Transition Temperature Behavior of Alumina/PMMA Nanocomposites," *Journal of Polymer Science Part B-Polymer Physics*, 42, 4371–4383, 2004.

[110] W. Peukert, H. C. Schwarzer, M. Gotzinger, L. Gunther, and F. Stenger, "Control of Particle Interfaces – the Critical Issue in Nanoparticle Technology," *Advanced Powder Technology*, 14, 411–426, 2003.

[111] M. F. Fréchette, M. Trudeau, H. D. Alamdari, and S. Boily, "Introductory Remarks on Nano Dielectrics," *IEEE Conference on Electrical Insulation and Dielectric Phenomena*, pp. 92–99, 2001.

[112] B. J. Ash, D. F. Rogers, C. J. Wiegand, L. S. Schadler, R. W. Siegel, B. C. Benicewicz, and T. Apple, "Mechanical Properties of Al2O3/Polymethylmethacrylate Nanocomposites," *Polym. Compos.*, 23, 1014–1025, 2002.

[113] T. Tanaka, G. C. Montanari, and R. Mulhaupt, "Polymer Nanocomposites as Dielectrics and Electrical Insulation-Perspectives for Processing Technologies, Material Characterization and Future Applications," *IEEE Transactions on Dielectrics and Electrical Insulation*, 11, 763–784, 2004.

[114] T. J. Lewis, "Nanometric Dielectrics," *IEEE Transactions on Dielectrics and Electrical Insulation*, 1, 812–825, 1994.

[115] M. S. Khalil, P. O. Henk, and M. Henriksen, "The Influence of Titanium Dioxide Additive on the Short-Term DC Breakdown Strength of Polyethylene," *IEEE Intern. Sympos. Electr. Insul., Montreal, Canada*, pp. 268–271, 1990.

[116] J. K. Nelson and J. C. Fothergill, "Internal Charge Behaviour of Nanocomposites," *Nanotechnology*, 15, 586–595, 2004.

[117] J. K. Nelson, J. C. Fothergill, and M. Fu, "Dielectric Properties of Epoxy Nanocomposites Containing TiO2, Al2O3 and ZnO Fillers," *IEEE Conference on Electrical Insulation and Dielectric Phenomena*, pp. 406–409, 2004.

[118] D. L. Ma, R. W. Siegel, J. I. Hong, L. S. Schadler, E. Martensson, and C. Onneby, "Influence of Nanoparticle Surfaces on the Electrical Breakdown Strength of Nanoparticle-Filled Low-Density Polyethylene," *Journal of Materials Research*, 19, 857–863, 2004.

[119] T. Ramanathan, H. Liu, and L. C. Brinson, "Functionalized SWNT/Polymer Nanocomposites for Dramatic Property Improvement," *Journal of Polymer Science Part B-Polymer Phys.ics*, 43, 2269–2279, 2005.

[120] J. K. Kim, C. G. Hu, R. S. C. Woo, and M. L. Sham, "Moisture Barrier Characteristics of Organoclay-Epoxy Nanocomposites," *Composites Science and Technology*, 65, 805–813, 2005.

[121] J. W. Gilman, T. Kashiwagi, and J. D. Lichtenhan, "Nanocomposites: A Revolutionary New Flame Retardant Approach," *Sampe Journal*, 33, 40–46, 1997.

[122] H. Sharma and Z. Xiao, "Fabrication of Carbon Nanotube Field-Effect Transistors with Metal and Semiconductor Electrodes," in Nanotubes and Related Nanostructures, Y. K. Yap, Ed. *(Materials Research Society Symposium Proceedings)*, vol. 1057E, 2008.

[123] N. Srivastava, R. V. Joshi, and K. Banerjee, "Carbon Nanotube Interconnects: Implications for Performance, Power Dissipation and Thermal Management," *IEEE International Electron Devices Meeting*, pp. 249–252, 2005.

[124] A. Kawabata, S. Sato, T. Nozue, T. Hyakushima, M. Norimatsu, M. Mishima, T. Murakami, D. Kondo, K. Asano, M. Ohfuti, H. Kawarada, T. Sakai, M. Nihei, and Y. Awano, "Robustness of CNT Via Interconnect Fabricated by Low Temperature Process over a High-Density Current," *International Interconnect Technology Conference,*, pp. 237–239, 2008.

[125] I. Soga, D. Kondo, Y. Yamaguchi, T. Iwai, M. Mizukoshi, Y. Awano, K. Yube, and T. Fujii, "Carbon Nanotube Bumps for LSI Interconnect," *Proceedings of Electronic Components and Technology Conference*, pp. 1390–1394, 2008.

[126] T. Iwai, "Carbon Nanotube Bumps for Thermal and Electrical Conduction in Transistor," *Fujitsu Scientific and Technical Journal*, 43, 508–515, 2007.

[127] G. Mehrotra, G. Jha, J. D. Goud, P. M. Raj, M. Venkatesan, M. Iyer, D. Hess, and R. Tummala, "Low-Temperature, Fine-Pitch Interconnections Using Self-Patternable Metallic Nanoparticles as the Bonding Layer," *Proceedings of Electronic Components and Technology Conference*, pp. 1410–1416, 2008.

[128] D. Huang, F. Liao, S. Molesa, D. Redinger, and V. Subramanian, "Plastic-Compatible Low Resistance Printable Gold Nanoparticle Conductors for Flexible Electronics," *Journal of the Electrochemical Society*, 150, G412–G417, 2003.

[129] A. Kamyshny, M. Ben-Moshe, S. Aviezer, and S. Magdassi, "Ink-Jet Printing of Metallic Nanoparticles and Microemulsions," *Macromolecular Rapid Communications*, 26, 281–288, 2005.

[130] A. L. Dearden, P. J. Smith, D. Y. Shin, N. Reis, B. Derby, and P. O'Brien, "A Low Curing Temperature Silver Ink for Use in Ink-Jet Printing and Subsequent Production of Conductive Tracks," *Macromolecular Rapid Communications*, 26, 315–318, 2005.

[131] Y. H. Byun, E. C. Hwang, S. Y. Lee, Y. Y. Lyu, J. H. Yim, J. Y. Kim, S. Chang, L. S. Pu, and J. M. Kim, "Highly Efficient Silver Patterning without Photo-Resist Using Simple Silver Precursors," *Materials Science and Engineering B-Solid State Materials for Advanced Technology*, 117, 11–16, 2005.

[132] G. G. Rozenberg, E. Bresler, S. P. Speakman, C. Jeynes, and J. H. G. Steinke, "Patterned Low Temperature Copper-Rich Deposits Using Inkjet Printing," *Applied Physics Letters*, 81, 5249–5251, 2002.

[133] S. B. Fuller, E. J. Wilhelm, and J. M. Jacobson, "Ink-Jet Printed Nanoparticle Microelectromechanical Systems," *Journal of Microelectromechanical Systems*, 11, 54–60, 2002.

[134] J. W. Chung, S. W. Ko, N. R. Bieri, C. P. Grigoropoulos, and D. Poulikakos, "Conductor Microstructures by Laser Curing of

Printed Gold Nanoparticle Ink," *Applied Physics Letters*, 84, 801–803, 2004.

[135] D. Kim and J. Moon, "Highly Conductive Ink Jet Printed Films of Nanosilver Particles for Printable Electronics," *Electrochemical and Solid State Letters*, 8, J30–J33, 2005.

[136] K. Suganuma, D. Wakuda, M. Hatamura, and K.-S. Kim, "Ink-jet Printing of Nano Materials and Processes for Electronics Applications," *Proceedings of the IEEE CPMT Conference on High Density Microsystem Design and Packaging and Component Failure Analysis*, 2007.

[137] D. J. Pena, B. Razavi, P. A. Smith, J. K. Mbindyo, M. J. Natan, T. S. Mayer, T. E. Mallouk, and C. D. Keating, "Electrochemical Synthesis of Multi-Material Nanowires as Building Blocks For Functional Nanostructures," *MRS Symposium D*, 2000.

[138] X. F. Duan and C. M. Lieber, "General Synthesis of Compound Semiconductor Nanowires," *Advanced Materials*, 12, 298–302, 2000.

[139] B. Xiang, Y. Zhang, Z. Wang, X. H. Luo, Y. W. Zhu, H. Z. Zhang, and D. P. Yu, "Field-Emission Properties of TiO2 Nanowire Arrays," *Journal of Physics D-Applied Physics*, 38, 1152–1155, 2005.

[140] M. I. Ploscaru, S. J. Kokalj, M. Uplaznik, D. Vengust, D. Turk, A. Mrzel, and D. Mihailovic, "$Mo_6S_{9-x}I_x$ Nanowire Recognitive Molecular-scale Connectivity," *Nano Letters*, 7, 1445–1448, 2007.

[141] K. K. Lew, L. Pan, E. C. Dickey, and J. M. Redwing, "Vapor-Liquid-Solid Growth of Silicon-Germanium Nanowires," *Advanced Materials*, 15, 2073–2076, 2003.

[142] P. Nguyen, S. Vaddiraju, and M. Meyyappan, "Indium and Tin Oxide Nanowires by Vapor-Liquid-Solid Growth Technique," *Journal of Electronic Materials*, 35, 200–206, 2006.

[143] S. Bhunia, T. Kawamura, S. Fujikawa, H. Nakashima, K. Furukawa, K. Torimitsu, and Y. Watanabe, "Vapor-Liquid-Solid Growth of Vertically Aligned InP Nanowires by Metalorganic Vapor Phase Epitaxy," *Thin Solid Films*, 464–465, 244–247, 2004.

[144] M. S. Arnold, P. Avouris, Z. W. Pan, and Z. L. Wang, "Field-Effect Transistors Based on Single Semiconducting Oxide Nanobelts," *Journal of Physical Chemistry B*, 107, 659–663, 2003.

[145] Q. Wan, Q. H. Li, Y. J. Chen, T. H. Wang, X. L. He, J. P. Li, and C. L. Lin, "Fabrication and Ethanol Sensing Characteristics of ZnO Nanowire Gas Sensors," *Applied Physics Letters*, 84, 3654–3656, 2004.

[146] C. S. Lao, J. Liu, P. X. Gao, L. Y. Zhang, D. Davidovic, R. Tummala, and Z. L. Wang, "ZnO Nanobelt/nanowire Schottky Diodes

Formed by Dielectrophoresis Alignment Across Au Electrodes," *Nano Letters*, 6, 263–266, 2006.

[147] F. Qian, S. Gradecak, Y. Li, C. Y. Wen, and C. M. Lieber, "Core/Multishell Nanowire Heterostructures as Multicolor, High-Efficiency Light-Emitting Diodes," *Nano Letters*, 5, 2287–2291, 2005.

[148] Y. Cui, Q. Q. Wei, H. K. Park, and C. M. Lieber, "Nanowire Nanosensors for Highly Sensitive and Selective Detection of Biological and Chemical Species," *Science*, 293, 1289–1292, 2001.

[149] Y. Huang, X. F. Duan, Q. Q. Wei, and C. M. Lieber, "Directed Assembly of One-dimensional Nanostructures into Functional Networks," *Science*, 291, 630–633, 2001.

[150] Z. H. Zhong, F. Qian, D. L. Wang, and C. M. Lieber, "Synthesis of p-Type Gallium Nitride Nanowires for Electronic and Photonic Nanodevices," *Nano Letters*, 3, 343–346, 2003.

[151] Y. J. Doh, J. A. van Dam, A. L. Roest, E. P. A. M. Bakkers, L. P. Kouwenhoven, and S. De Franceschi, "Tunable Supercurrent Through Semiconductor Nanowires," *Science*, 309, 272–275, 2005.

[152] K. Terabe, T. Hasegawa, T. Nakayama, and M. Aono, "Quantized Conductance Atomic Switch," *Nature*, 433, 47–50, 2005.

[153] B. Z. Tian, X. L. Zheng, T. J. Kempa, Y. Fang, N. F. Yu, G. H. Yu, J. L. Huang, and C. M. Lieber, "Coaxial Silicon Nanowires as Solar Cells and Nanoelectronic Power Sources," *Nature*, 449, 885–889, 2007.

[154] R. C. Hughes, W. K. Schubert, T. E. Zipperian, J. L. Rodriguez, and T. A. Plut, "Thin-Film Palladium and Silver Alloys and Layers for Metal-Insulator-Semiconductor Sensors," *J. Applied Physics*, 62, 1074–1083, 1987.

[155] M. H. Yun, N. V. Myung, R. P. Vasquez, C. S. Lee, E. Menke, and R. M. Penner, "Electrochemically Grown Wires for Individually Addressable Sensor Arrays," *Nano Letters*, 4, 419–422, 2004.

[156] M. Yun, N. V. Myung, R. P. Vasquez, J. Wang, and H. Monbouquette, "Nanowire Growth for Sensor Arrays," *Proceedings of the SPIE Nanofabrication Technologies*, vol. 5220, pp. 37–45.

[157] S.-B. Lee, E. Lee, W. Lee, and Y.-C. Joo, "Dendritic Palladium-Silver Nano-Structure Grown by Electrochemical Migration Method for Hydrogen Sensing Device," *Proceedings of Electronic Components and Technology Conference*, pp. 440–443, 2008.

[158] J. A. Paradiso and T. Starner, "Energy Scavenging for Mobile and Wireless Electronics," *IEEE Pervasive Computing*, 4, 18–27, 2005.

[159] E. K. Reilly, E. Carleton, and P. K. Wright, "Thin Film Piezoelectric Energy Scavenging Systems for Long Term Medical Monitoring," *Proceedings of the International Workshop on Wearable and Implantable Body Sensor Networks*, pp. 38–41, 2006.

[160] X. D. Wang, J. H. Song, and Z. L. Wang, "Nanowire and Nanobelt Arrays of Zinc Oxide from Synthesis to Properties and to Novel Devices," *Journal of Materials Chemistry*, 17, 711–720, 2007.

[161] Z. L. Wang, "Piezoelectric Nanostructures: From Growth Phenomena to Electric Nanogenerators," *MRS Bulletin*, 32, 109–116, 2007.

[162] Z. L. Wang, "The New Field of Nanopiezotronics," *Materials Today*, 10, 20–28, 2007.

[163] Z. L. Wang, "Nanopiezotronics," *Advanced Materials*, 19, 889–892, 2007.

[164] Z. L. Wang, "Zinc Oxide Nanostructures: Growth, Properties and Applications," *Journal of Physics-Condensed Matter*, 16, R829–R858, 2004.

[165] Z. L. Wang and J. H. Song, "Piezoelectric Nanogenerators Based on Zinc Oxide Nanowire Arrays," *Science*, 312, 242–246, 2006.

[166] Z. L. Wang, "Towards Self-Powered Nanosystems: From Nanogenerators to Nanopiezotronics," *Advanced Functional Mater.ia*, 18, 3553–3567, 2008.

[167] M. Alexe, S. Senz, M. A. Schubert, D. Hesse, and U. Gosele, "Energy Harvesting Using Nanowires?," *Advanced Materials*, 20, 4021–4026, 2008.

[168] Z. L. Wang, "Energy Harvesting Using Piezoelectric Nanowires – A Correspondence on ''Energy Harvesting Using Nanowires?'' by Alexe et al.," *Advanced Materials, Correspondence*, 20, 1–5, 2008.

[169] X. D. Wang, J. H. Song, J. Liu, and Z. L. Wang, "Direct-Current Nanogenerator Driven by Ultrasonic Waves," *Science*, 316, 102–105, 2007.

Chapter 3
Characterizations of Electrically Conductive Adhesives

3.1 Recent Advances in Polymeric Materials for Electronic Packaging

Organic polymers are widely used as structural materials and as processing aids in the electronics industry. The widespread use of polymeric materials in electronics is due to the ease in which desired engineering properties can be designed into materials by the manipulation of polymer structures and formulary compositions. In addition, the wide range of fabrication processes by which polymers can be formed into finished articles and the lower fabrication costs of polymers compared to metals or ceramics have contributed to ubiquitous use of polymers in electronic assemblies. Electronic packaging makes use of a wide variety of polymer material classes to fulfill a diverse range of engineering uses such as adhesives, substrates (printed circuit boards), encapsulants, stress buffer coatings, and interlayer dielectrics.

3.1.1 Silicones (Polyorganosiloxanes)

Silicone, with a repeating unit of alternating silicon–oxygen (Si–O) siloxane backbone, has some unique chemistry.

3.1.1.1 Room-Temperature Vulcanized (RTV) Silicones

RTV silicone is a typical condensation cure system material. The moisture-initiated catalyst-assisted (e.g., organotitanate and tin dibutyldilaurate) process generates water or alcohol as by-products, which could cause outgassing and voids. However, by careful control of the curing process, one can achieve a very reliable encapsulant. Since the silicone has a low surface tension, it tends to creep and run-over the encapsulated IC circuits. To

Y. Li et al., *Electrical Conductive Adhesives with Nanotechnologies*,
DOI 10.1007/978-0-387-88783-8_3, © Springer Science+Business Media, LLC 2010

better control the rheological properties of the material, thixotropic agents (such as fumed silica) are usually added to the formulation. The thixotropic agent provides improved yield stress, increases the G' (storage modulus), G'' (loss modulus), and η' (dynamic viscosity) of the silicone. Filler–resin and filler–filler interactions are important in obtaining a well-balanced and well-controlled encapsulant. This rheologically controlled material tends to flow evenly in all circuit edges, covers all the underchip area, and prevents wicking or run-over of the circuits, which is a critical parameter in coating production. Organic solvents such as xylenes are incorporated into the formulation to reduce the viscosity.

3.1.1.2 Heat-Curable Hydrosilation Silicones (Elastomers and Gels)

Heat-curable hydrosilation silicone (either elastomer or gel) has become an attractive polymeric material in microelectronics, such as thermal interface materials (TIM), sealants, and encapsulants. Its curing time is much shorter than the RTV-type silicone. Heat-curable silicones also tend to have slightly better stability at elevated temperatures than the conventional RTV silicone. With its jelly-like (very low modulus) intrinsic softness, silicone gel is a very attractive encapsulant in wire-bonded large-chip-size IC devices. The two-part heat-curable system, which consists of the vinyl and hydride reactive functional groups, and the platinum catalyst hydrosilation addition cure system provide a fast cure system without any by-product. To formulate a low-modulus silicone gel, a vinyl-terminated polydimethylsiloxane with a moderate low viscosity range between 200 and a few thousand centipoise (cps) and low viscosity (range from a few cps to ~100 cps) di- or multi-functional hydride-terminated polydimethylsiloxane are used in the formulation. The low viscosity hydride resin usually blends in with the higher-viscosity vinyl resin to achieve an easier mixing ratio of part A (vinyl-only portion) and part B (hydride plus some vinyl portion for cross-linking of the silicone system). This catalyst is usually incorporated in the part A vinyl portion of the polymer. However, a highly deactivated platinum catalyst system (by pre-mixing with a chelating compound for coordination) is used to formulate a one-component system. This one-component silicone gel system requires less mixing and is a problem-free production material. This solvent-less type of heat-curable silicone gel will be extensively used in electronic applications [1–12].

Electrically conductive adhesives based on silicones generally have low moisture absorption and low modulus and can be used as die attach adhesives, thermal interface materials, and interconnection materials in stress-sensitive packages.

3.1.2 Epoxies

Epoxies are one of the most utilized polymeric materials in electronics. This class of materials was first prepared in the early 1930s. Their unique chemical and physical properties (i.e., excellent chemical and corrosion resistance, superior electrical and physical properties, excellent adhesion, thermal insulation, low shrinkage, and reasonable material cost) have made epoxy resins very attractive in electronic applications. The commercial preparation of epoxies is based on bisphenol A, which, upon reaction with epichlorohydrin, produces bisphenol A epoxy:

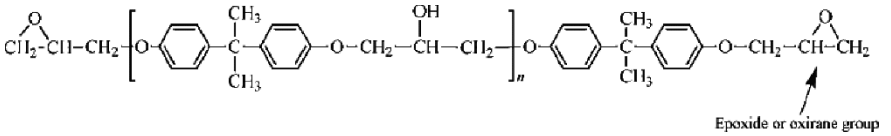

The repletion number, *n*, varies from zero (liquid) to approximately 30 (hard solid). The reactants's ratio (bisphenol A versus epichlorohydrin) determines the final viscosity of the epoxies. In addition to the bisphenol A resins, the novolac resins, with multifunctional groups that lead to higher cross-link density and better thermal and chemical resistance, have gained increasing acceptance in electronic applications.

Typical epoxy curing agents are amines, anhydrides, dicyanodiamides, melamine formaldehydes, urea formaldehydes, phenol-formaldehydes, and catalytic curing agents. Anhydrides and amines are two of the most frequently used curing agents.

Selection of the proper curing agents depends on the application techniques, curing conditions, pot-life requirement, and the desired physical properties. Besides affecting viscosity and reactivity of the epoxy formulations, curing agents determine the degree of cross-linking and the formulation of chemical bonds in the cured epoxy system. The reactivity of some anhydrides with epoxies is slow; therefore, an accelerator, usually a tertiary amine, is used to assist the cure. "Novolacs" and "Resole" are two major, commonly used phenolformaldehyde epoxies. A Novolac is a phenol-formaldehyde, acid-catalyzed epoxy polymer. The phenolic groups in the polymer are linked by a methylene bridge, which provides highly cross-linked systems for a high-temperature and excellent chemically resistant polymer. "Resole" is a base-catalyzed phenol-formaldehyde epoxy polymer. In most phenolic resins, the phenolic group is converted into an ether to give improved base resistance. Phenolic resins are cured through the secondary hydroxyl group on the epoxy backbone. High-temperature curing is required in this system, and it provides excellent chemical resistance.

High-purity epoxies have become very attractive materials in electronics. These types of resins contain greatly reduced amounts of chloride and other mobile ions, such as sodium and potassium, and have become widely used in device encapsulation and molding compounds. The incorporation of small, well-controlled spherical silica particles with narrow size distribution as fillers in the epoxy systems has drastically reduced the thermal coefficient of expansion (CTE) of these materials and makes them more compatible with the IC die-attached substrate materials. The incorporation of a small amount of an elastomeric material (such as silicone elastomeric domain particles) to the rigid epoxy has drastically reduced the elastic modulus, and the thermal stress, while increasing the toughness of the epoxy material. The low-stress epoxy has great potential applications in molding compounds, underfills, and conductive adhesives [13–22].

3.1.3 Polyurethanes

Polyurethane, commonly abbreviated as PU, is any polymer consisting of a chain of organic units joined by urethane links. Polyurethane polymers are formed by reacting a monomer containing at least two isocyanate functional groups with another monomer containing at least two alcohol groups in the presence of a catalyst. Polyurethane was first made available by Otto Bayer in the late 1920s. The early study of polyurethane was simply based on diisocyanates and diols or polyols. However, recent work is focused on the use of intermediates that are low-molecular-weight polyethers with reactive functional groups such as hydroxyl or isocyanate groups that are able to further cross-link, chain extend, or branch with other chains extended with the prepolymer (either polyester or polyether) to form polyurethanes with urea or urethane linkages, respectively. The morphology of polyurethane is well characterized. Hard and soft segments from diisocyanates and polyols, respectively, are the key to excellent physical properties of this material.

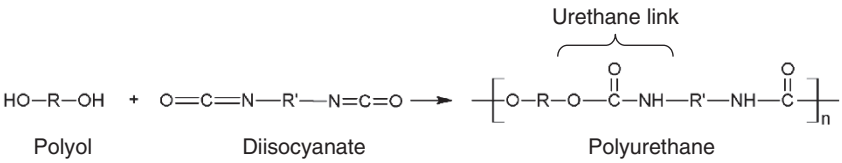

Bases are more widely used than acids as catalysts for polyurethane polymerization. The catalytic activity is increased with the basicity. Amines, such as tertiary alkylamines, and organic metal salts, such as tin or lead octoates, promote the reaction of isocyanate and hydroxyl functional groups

in the polyurethane system and accelerate the cross-linking. However, the hydrolytic stability of the polyurethane can be affected by the catalyst used. UV stabilizers are usually added to reduce the radiation sensitivity of the material. In addition, polyurethane has unique high strength, modulus, hardness, and elongation. It is one of the toughest elastomers used today. High-performance polyurethane elastomers are used in conformal coating, potting, and reactive injection molding of IC devices and adhesives.

3.1.4 Polyimides

Polyimide is one of the first low-k interlayer dielectric (k = 3.5) for IC electronic applications. It was first developed at Du Pont in the 1950s. During the past few decades, there has been tremendous interest in this material for electronic applications. The superior thermal stability (up to 600°C), mechanical, and electrical properties of polyimide have led it toward many high-performance applications, from aerospace to microelectronics. In addition, polyimides show very low electrical leakage in surface or bulk. They form excellent interlayer dielectric insulators and also provide excellent step coverage, which is very important in fabrication of the multilayer IC structures. They have excellent solvent resistance and ease of application. They can be easily either sprayed or spun on and imaged by a conventional photolithography and etch process.

Most polyimides are prepared by reacting aromatic diamine with aromatic dianhydride to form a copolymer – polyamic acid. However, by changing the diamine and dianhydride substitutes, one will derive a variety of high-performance polyimides. Polyamic acids are precursors of polyimides. Thermal cyclization (imidization) of polyamic acid is a simple curing mechanism for this material. Siemens of Germany developed the first photodefinable polyimide material. However, Ciba Geigy has a new type of photodefinable polyimide that does not require a photoinitiator. Both of these photodefinable materials are negative resist-type polyimides. A positive-resist-type polyimide that reduces the processing steps in IC fabrication has been reported by Sumitomo. An interpenetration network (IPN) of two types of polyimides is used to achieve the positive-tone material. Hitachi Chemical has developed an ultra-low thermal coefficient of expansion (CTE) polyimide that has some potential in reducing the thermal stress of the silicone chip and the polyimide encapsulant. The rigid, rod-like structure of the polyimide backbone is the key in preparing the low-CTE polyimide. By sample-blending a high- and a low-CTE polyimide, one will be able to achieve a desirable CTE material that could match the CTE on the substrate and reduce the thermal stress problem in encapsulated device temperature cycling testing. However, the susceptibility to

moisture absorption due to the carbonyl polar groups of the polyimide, a high-temperature cure, and high cost are the only drawbacks that prevent the use of polyimide in low-cost consumer electronic applications. Preimidized polyimides that cure by evaporation of solvent may avoid the drawback in high-temperature curing material. Advances in polyimide syntheses have reduced the material's moisture absorption and dielectric constant by the incorporation of siloxane segments into the polyimide backbone, which have made improvements in the polyimide, as silicone-polyimide material. This material was reported by GE Silicones in the 1960s (see next section). However, the affinity of moisture to the polyimide chemical structure is still a concern in its use in electronics. Nevertheless, polyimides are widely used as IC encapsulant, interlayer dielectrics, ion implant masks, and alpha particle getters.

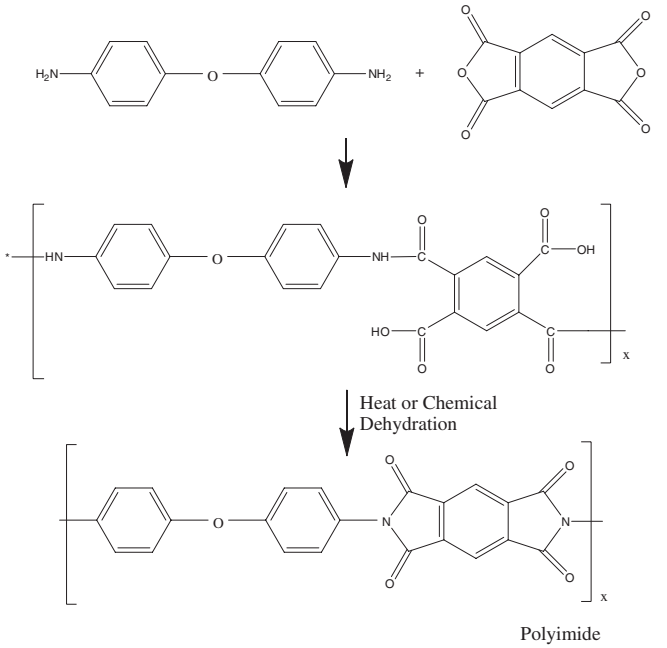

Polyimide

3.1.5 Silicone-Polyimide (SPI)

Combining the low modulus of siloxane and the high thermal stability of polyimide, the siloxane-polyimide (SPI) copolymers were first developed at General Electric. SPI copolymers have become very attractive IC device

encapsulants. Silicone-polyimides are fully imidized copolymers and are soluble in low-boiling point solvents such as diglyme. The system reduces the high processing temperature and eliminates the outgassing of water during normal polyimide imidization (cure) process, which are main drawbacks of the polyimides. Besides, the SPI has good adhesion to many materials and eliminates the need for an adhesion promoter like PI [23]. Polycondensation and polyaddition processes are used to synthesize either thermoplastic or thermosetting SPI materials. Figure 3.1 shows a process for synthesizing a poly(imide siloxane) [24, 25]. In addition, photocurable and thermocurable SPIs are also obtainable in these processes by incorporating photoreactive functional groups in these types of materials. One can control the imide and siloxane blocks within the copolymer matrix to tailor the SPI properties. As the level of the siloxane in the copolymer is increased, the polyimide blocks are shortened, T_g of the copolymer decreases and solubility increases. Since most of these are preimidized thermoplastic materials, their shelf life is very stable. These materials will have potential as IC device encapsulant, interlayer dielectrics, and passivation in microelectronic applications.

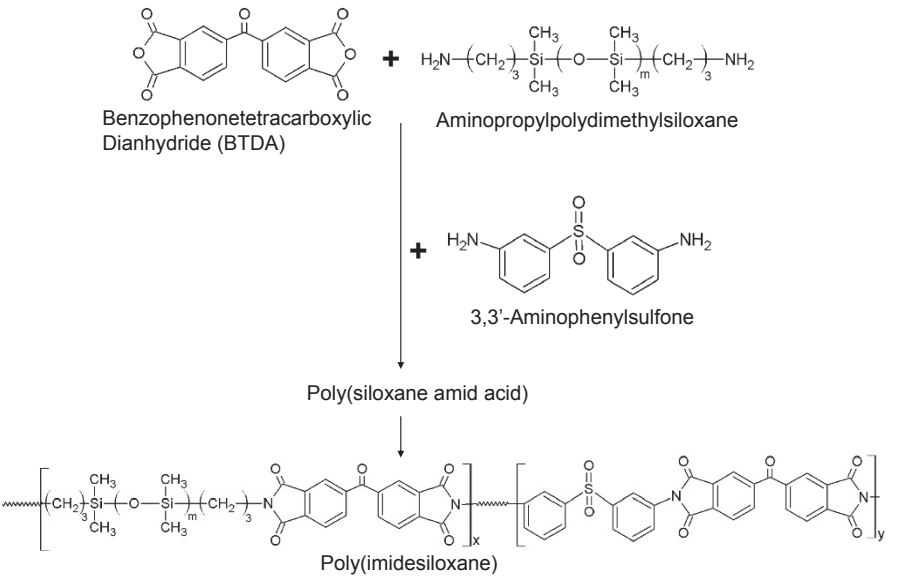

Fig. 3.1. A process for synthesizing a poly(imide siloxane)

3.1.6 Bismaleimide (BMI) Resins

Polyimide resins are a class of high-performance resins that have gained wide acceptance in a variety of applications. Bismaleimides are thermosetting polyimides that cure by addition reactions which avoid formation of volatiles. Unlike condensation polyimides which evolve volatiles during curing and are typically used as thin films, bismaleimide resins contain unsaturated double bonds which can be cured via several chemical pathways (free radical, Michael addition, or cycloaddition, such as Diels–Alder reaction). Thermal polymerization without the evolution of volatile byproducts enables bismaleimide resins to be widely applicable, ranging from electronic materials (such as die attach adhesives), coatings, films, structural adhesives, encapsulants, and high-performance fiber-reinforced composites.

Bismaleimide resins have the following generic structure:

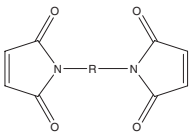

Depending on the desired properties, the R group can be either aliphatic or aromatic. For high T_g networks, aromatic bismaleimides are used. The most common component in bismaleimide resins is 4,4′ bismaleimidodiphenylmethane (BMI):

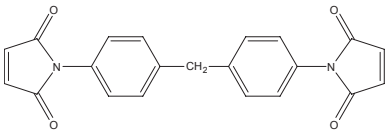

The BMI resin is a high melting point crystalline solid. When thermally cured, the resulting networks are very brittle. Bismaleimides are rarely used alone in the solid form. In most applications, reactive comonomers (e.g., vinyl and allyl compounds, allyl phenols, aromatic amines) are used to achieve the desired final properties and processing characteristics.

Liquid BMIs with long-chain aliphatic structures between the maleimide groups are used for low-modulus, low-T_g, high-flexibility applications [26]. For electronic applications, BMIs have made a significant impact in die attach adhesives. Liquid BMIs can be used to formulate high-performance die attach adhesives, owing to their very fast curing rates via free-radical polymerization with no void formation. Typical formulations

are cured with peroxides at speeds of less than 1 min (snap cure) at curing temperatures between 175 and 220°C. For these systems, a significant amount of the network formation is completed within seconds, where semiconductor chips are rapidly attached to leadframes or substrates while maintain a very high production rate at the die bonder. Additionally, the die attach formulations can be tailored to achieve low T_g, low modulus (to control stress and warpage during processing), low moisture absorption, and high adhesion at elevated temperatures. The potential drawbacks of the peroxide curing are the short work life and the need for low-temperature storage of formulated adhesive to prevent slow reaction. Typical work life (working time after thawing) is between 12 and 36 h, while premixed adhesives are typically stored at −40°C.

BMI has been used in printed circuit board manufacturing [27] and in applications where temperature requirements are somewhere between those provided by epoxy systems and those provided by polyimide systems. BMI adhesives are suitable for long-term exposure to temperatures up to 200°C and short-term exposure up to 230°C. Systems currently available are quite rigid and therefore have low peel strength.

3.1.7 Cyanate Ester Resins

Cyanate ester (CE) resins are a family of high-temperature thermosetting resins, more accurately named polycyanurate, that bridges the gap in thermal performance between engineering epoxy and high-temperature polyimides. In addition to their outstanding thermal performance, CE resins have several desirable characteristics which justify their higher cost in many applications. They possess a unique balance in properties and are particularly notable for their low dielectric constant and dielectric loss, low moisture absorption, low shrinkage, and low outgassing characteristics.

Cyanate ester resins are available as low-melt crystalline powder, liquid, semi-solid difunctional monomers and prepolymers of various molecular weights. Commercial CE resins are available in monomer and prepolymer forms with several different backbone structures. The general structure of CE resins is bisphenol, aromatic, or cycloaliphatic backbone usually with two or more ring-forming cyanate functional groups (–O–C≡N–). The cyanate group undergoes trimerization to form the *s*-triazine ring and generates a high cross-linking density, which, in combination with rigid aromatic rings, provides excellent high-temperature properties, solvent resistance, electrical properties, and mechanical strength. The following shows the cyclotrimerization reaction of bisphenol A dicyanate to form the triazine network structure:

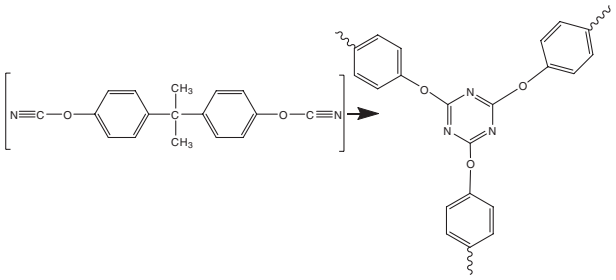

The trimerization of cyanate ester groups is normally a slow process without the presence of a catalyst. The cyclization rate can be accelerated by the presence of acids or bases [28]. A cyanate ester group contains unpaired electrons and electron-donating π bonds, which provide an excellent environment for coordination. Three types of metal coordination catalysts are used: metal naphthenates, metal acetylacetonates (AcAc), and metal octoates. Of these, Cu AcAc and Mn octoate are the most popular. Nonylphenol is also required as a co-catalyst. Cyanate ester resins show some very attractive features:

1. Stepwise addition polymerization: no void formation from condensates
2. Hot-melt processibility to liquid pourability
3. Thermally curable
4. Low cure shrinkage
5. High T_g: 260–290°C
6. Low moisture absorption: 1–3% in boiling water
7. Excellent dielectric properties
8. Excellent adhesion

For very high T_g applications, dicyanates are cured without addition of epoxy modifiers, leading to a very tight network via cyclotrimerization. The advantage of the cyanate ester family of monomers is the ability to formulate with epoxy resins. Typical resins in electronic applications are combinations of tailored epoxy monomers and oligomers along with cyanate esters.

Liquid cyanate ester monomers (bisphenol-F dicyanates) have low viscosity at 25°C and exhibit good compatibility with other cyanate ester resins, epoxy resins, and bismaleimide resins. Blending liquid cyanate ester resins with other cyanate ester and epoxy resins provided a pathway to control the rheological properties without sacrificing the final cured performance. Liquid cyanate esters enabled the development of underfill resins for chip packaging applications, where low viscosity is required during processing. After curing, cyanate ester resins provide high T_g, low coefficient

of thermal expansion, high toughness, and low moisture absorption required for underfill applications.

Materials based on cyanate esters have been used in electronic packaging such as underfill, die attach adhesives, and conductive adhesives [29].

3.2 Analytical Approaches for ECA

3.2.1 Differential Scanning Calorimeter (DSC)

Differential scanning calorimetry (DSC) is a technique for measuring the energy necessary to establish a nearly zero temperature difference between a substance and an inert reference material, as the two specimens are subjected to identical temperature regimes in an environment heated or cooled at a controlled rate.

There are two types of DSC systems in common use.

In heat-flux DSC (Fig. 3.2a), the sample and reference are connected by a low-resistance heat flow path (a metal disc). The assembly is enclosed in a single furnace. Enthalpy or heat capacity changes in the sample cause a difference in its temperature relative to the reference; the resulting heat flow is small compared with that in differential thermal analysis (DTA) because the sample and the reference are in good thermal contact. The temperature difference is recorded and related to enthalpy change in the sample using calibration experiments.

In power-compensation DSC (Fig. 3.2b), the temperatures of the sample and reference are controlled independently using separate, identical furnaces. The temperatures of the sample and the reference are made identical by varying the power input to the two furnaces; the energy required to do this is a measure of the enthalpy or heat capacity changes in the sample relative to the reference.

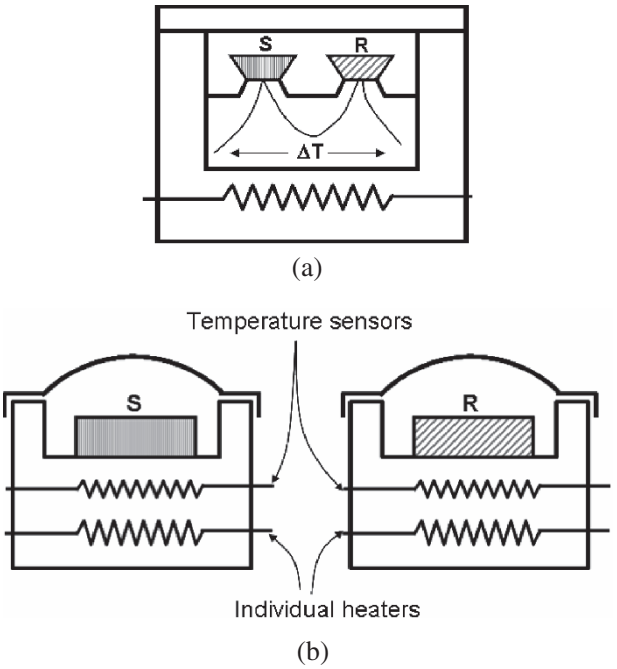

Fig. 3.2. (**a**) Heat-flux DSC; (**b**) Power-compensation DSC

The main application of DSC is studying the phase transitions, which involve energy changes or heat capacity changes that can be detected by DSC with great sensitivity. Generally, DSC is used to measure glass transitions, melting and boiling points, crystallization time and temperature, percent crystallinity, curing temperature and time, heats of fusion and reactions, specific heat capacity, oxidative/thermal stability, rate and degree of cure, reaction kinetics, etc. Figure 3.3 shows an example of a DSC curve demonstrating the appearance of several common features.

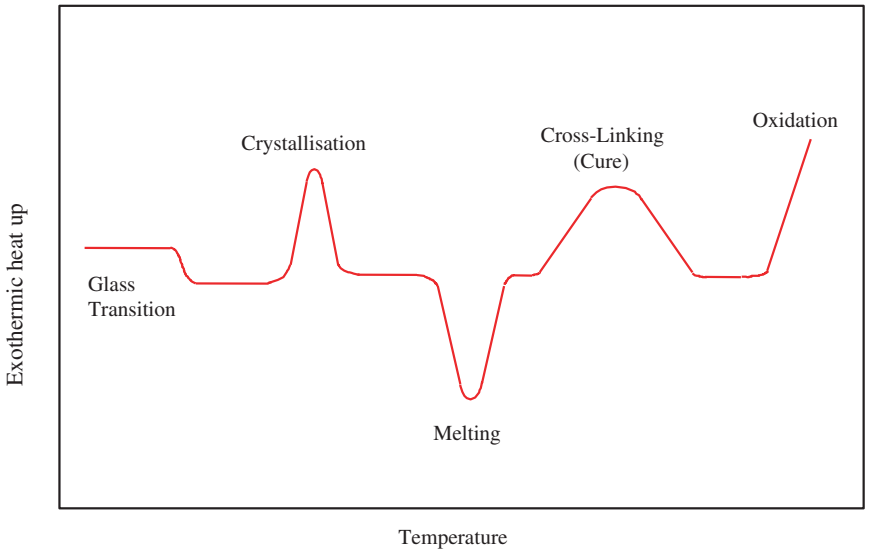

Fig. 3.3. A schematic DSC curve demonstrating the appearance of several common features

Modulated DSC provides the same qualitative and quantitative information about physical and chemical changes as conventional DSC, and it also provides unique thermochemical data that are unavailable from conventional DSC. The effects of baseline slope and curvature are reduced, increasing the sensitivity of the system. Overlapping events such as molecular relaxation and glass transitions can be separated. Heat capacity can be measured directly with modulated DSC in a minimum number of experiments.

For ECA, DSC is used to characterize the curing kinetics, heat generated during curing, and glass transition temperature (T_g) of cured sample. As examples, Figs. 3.4 and 3.5 illustrate dynamic and isothermal DSC curves which show the peak reaction temperature, glass transition temperature, and curing kinetics of three ECA samples.

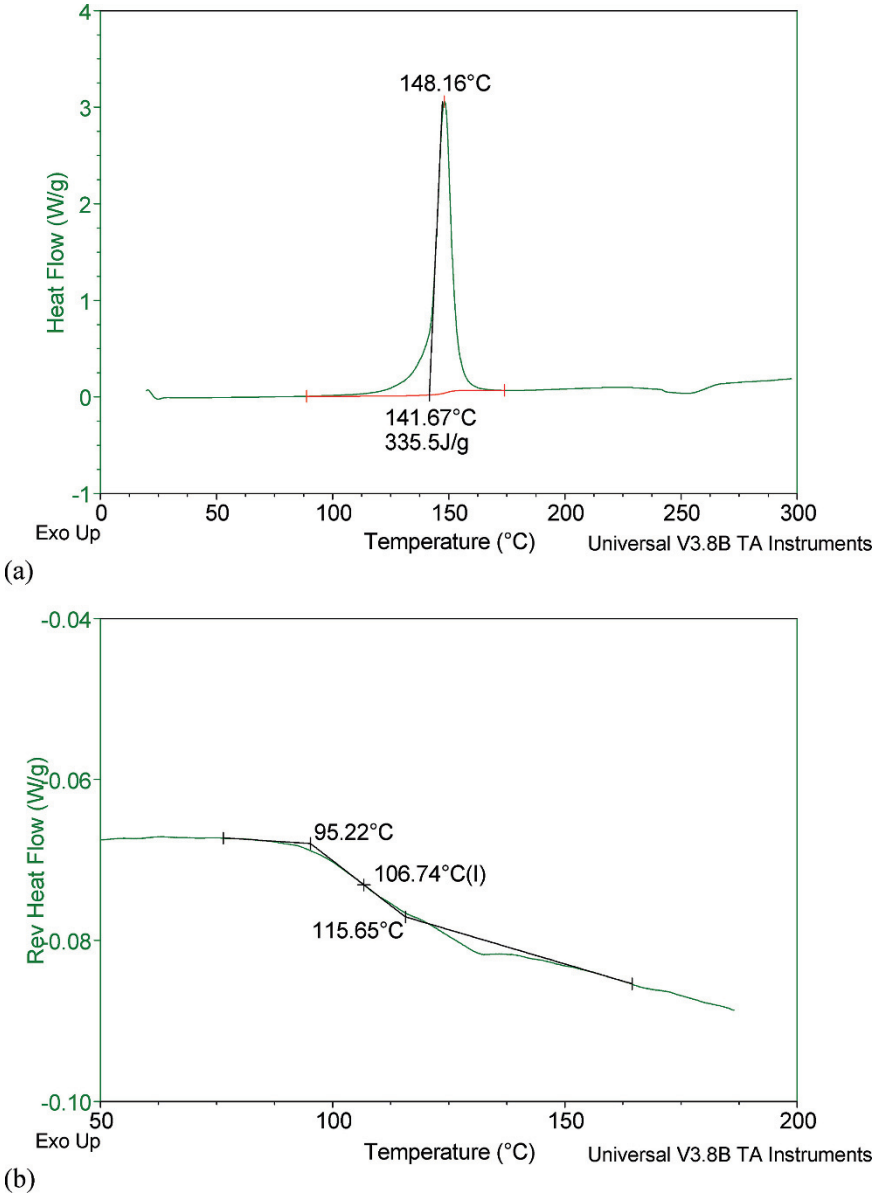

Fig. 3.4. An example of dynamic DSC curves (**a**) and glass transition temperature of three cured ECA (**b**)

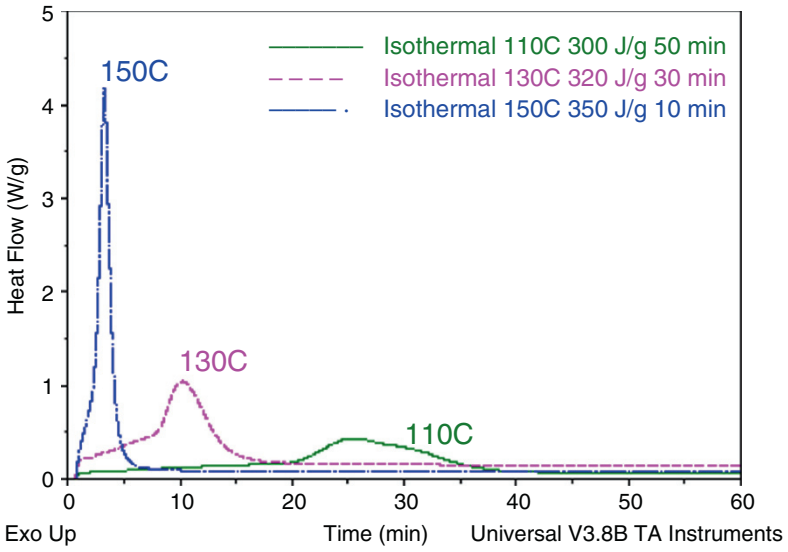

Fig. 3.5. An example of isothermal DSC curves at various temperatures

3.2.2 Thermogravimetry Analyzer (TGA)

Thermogravimetric analyzer (TGA) is performed on samples to determine changes in weight in response to changes in temperature. Such analysis relies on a high degree of precision in three measurements: weight, temperature, and temperature change. As many weight loss curves look similar, the weight loss curve may require transformation before results may be interpreted. A derivative weight loss curve can be used to tell the point at which weight loss is most apparent. Again, interpretation is limited without further modifications and deconvolution of the overlapping peaks may be required.

For ECA materials, TGA is usually employed to determine the conductive filler loadings, thermal stability and degradation of polymer matrix, and moisture absorption. TGA is also commonly used to evaluate the organic coating and debonding/decomposition temperature on fillers, as well

as the oxidation stability of conductive fillers. Figure 3.6 is a typical example of TGA curve indicating the thermal stability of a cured epoxy resin as ECA matrix.

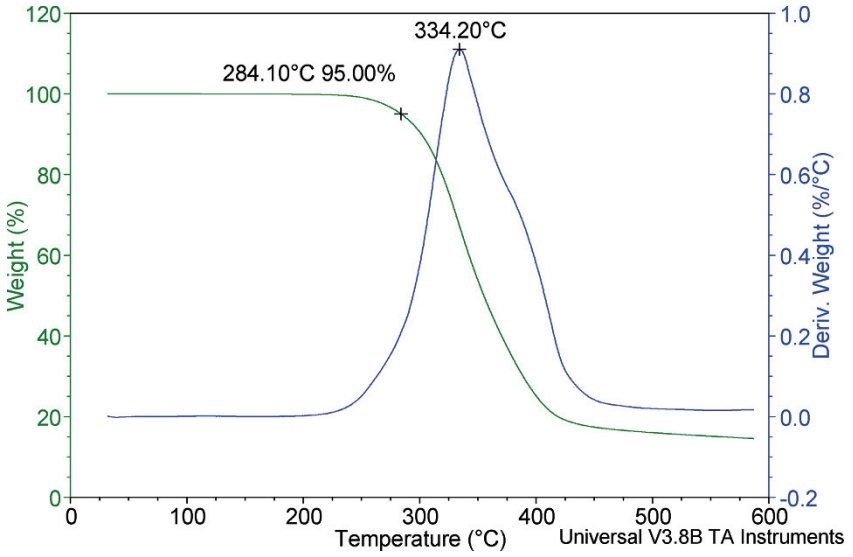

Fig. 3.6. Example of TGA curve for the thermal stability of cured epoxy

3.2.3 Dynamic Mechanical Analyzer (DMA)

DMA is a technique used to study and characterize materials, in particular, to observe the viscoelastic nature of polymers. The DMA determines changes in sample properties resulting from changes in five experimental variables: temperature, time, frequency, force, and strain. The deformation can be applied sinusoidally, in a constant (or step fashion), or under a fixed rate. The DMA uses samples that can be in bulk solid, film, fiber, gel, or viscous liquid form. Interchangeable clamps are employed to measure many properties, including modulus, damping, creep, stress relaxation, glass transitions, and softening points.

DMA measures the stiffness and damping properties of a material. The storage modulus G' (elastic response) and loss modulus G'' (viscous response) of polymers are measured as a function of temperature or time as the polymer is deformed under an oscillatory load (stress) at a controlled (isothermal or programmed) temperature in a specified atmosphere. The

stiffness depends on the mechanical properties of the material and its dimensions. It is frequently converted to a modulus to enable sample intercomparisons. The storage modulus is related to stiffness and the loss modulus to damping and energy dissipation. Damping is also expressed in terms of $\tan\delta$ and is related to the amount of energy a material can store. DMA is the most sensitive technique for monitoring relaxation events, such as glass transitions, where the mechanical properties change dramatically when relaxation behavior is observed. Glassy, viscoelastic, elastic, and liquid polymers can be differentiated by DMA, and some details of polymer structure can be inferred from the results. DMA is particularly useful for evaluating viscoelastic polymers that have mechanical properties, which exhibit time, frequency, and/or temperature effect.

For ECA materials, a typical response from a DMA shows both modulus and $\tan\delta$, as shown in Fig.3.7a and b. As the material goes through its glass transition, the modulus reduces (the material becomes less stiff) and the $\tan\delta$ *(G″/G′)* goes through a peak (the molecular reorganization of the relaxation induces less elastic behavior). The data give information on the position of the glass transition temperature, its frequency dependence, sample stiffness, and other viscoelastic properties.

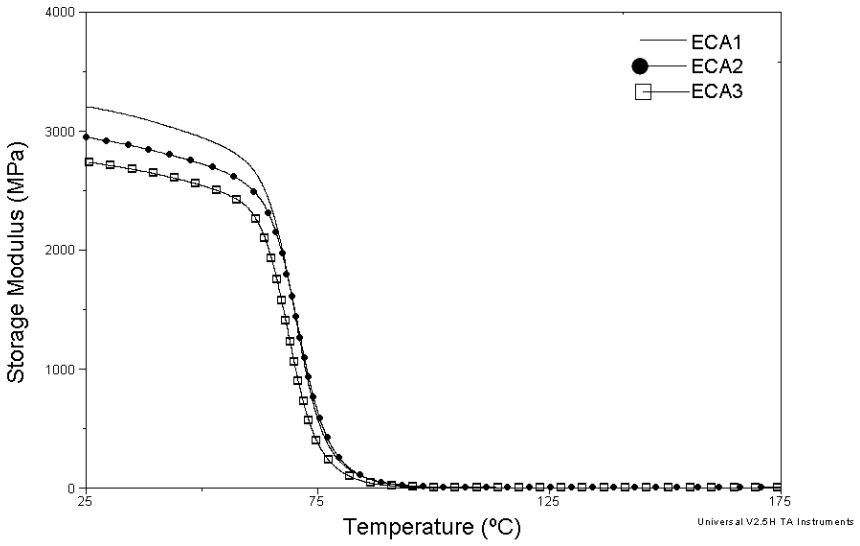

(a)

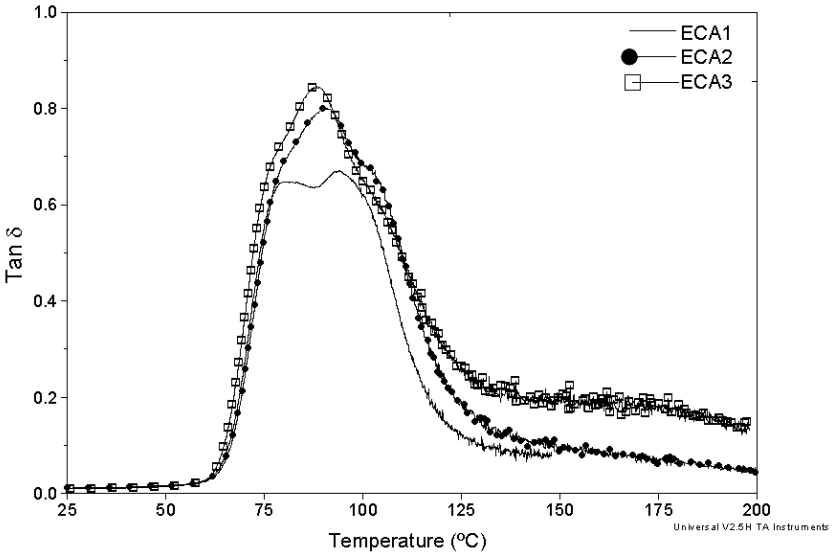

(b)

Fig. 3.7. DMA curves of three ECAs: (**a**) storage modulus and (**b**) tanδ

DMA can also be used to calculate the crosslinking density of an ECA sample. Cross-linking density, $\rho_{(E')}$, can be determined by using the kinetic theory of rubber elasticity as follows [30]:

$$\rho_{(E')} = E'/3\phi RT$$

where E' is the storage elastic modulus of cured resin at a peak temperature of tanδ + 10°C, ϕ is a front factor (assumed as $\phi = 1$), R is the gas constant, and T is the absolute temperature.

3.2.4 Thermo-mechanical Analysis (TMA)

TMA is the measurement of a change of a dimension (displacement) or a mechanical property of the sample while it is subjected to a temperature regime. The temperature regime may be heating, cooling at a rate of temperature change that can include stepwise temperature changes, linear rate of change, temperature modulation with a set frequency and amplitude, free (uncontrolled) heating or cooling, or holding the temperature constant. The sequence of temperatures with respect to time may be predetermined (temperature programmed) or sample controlled (controlled by a feedback signal from the sample response).

The major application areas of TMA are in the polymer field. A list of the main types of experiment and the information obtainable is given in Table 3.1.

Table 3.1. A list of major information obtainable from TMA

Method	Mode	Measured Quantity	As a function of	Information Obtained
Bulk sample	Flat probe/light load	Expansion	Temperature	Coefficient of thermal expansion (CTE) and T_g
Divided sample	Dilatometer	Volumetric changes	Temperature	CTE and T_g
Thin film	Penetration probe/ sgnificant load	Depth of penetration	• Force • Time • Temperature	• Modulus, cross-linking density • Creep, cure behavior • Softening, melting
Film or fiber	Tension accessory	Uniaxial extension or shrinkage	• Force • Time • Temperature	• Modulus, cross-linking density • Creep, cure behavior • Softening, melting
Fluid	Parallel plates	Distance	• Time • Temperature	• Viscosity, glation • Melting, vscosity, glation
Bulk or supported	Flexure accessory	Bending	• Time • Temperature	• Creep behavior • Softening, melting

While many other techniques exist for studying the important and informative region of the glass transition (T_g), TMA offers advantages for certain types of study. The indentation and penetration probes, for instance, can follow transitions in very thin films, such as lacquer coatings on metals. Although quantitative mechanical properties (modulus) can in principle be derived from TMA measurements, this may be difficult in practice, and Dynamic Mechanical Analysis may be preferred. TMA is better suited to comparative measurements on a range of materials and for measurements of transition temperatures and expansion coefficients on relatively small samples, in a conveniently short time.

For ECA, TMA is important to characterize the coefficient of thermal expansion (CTE) and glass transition temperature (T_g). Figure 3.8 is an example of TMA analysis of an ECA sample. The CTE before and after T_g, α_1 and α_2, respectively, can be easily calculated from the slope of the curve. The T_g is the intercept point of the slopes of α_1 and α_2.

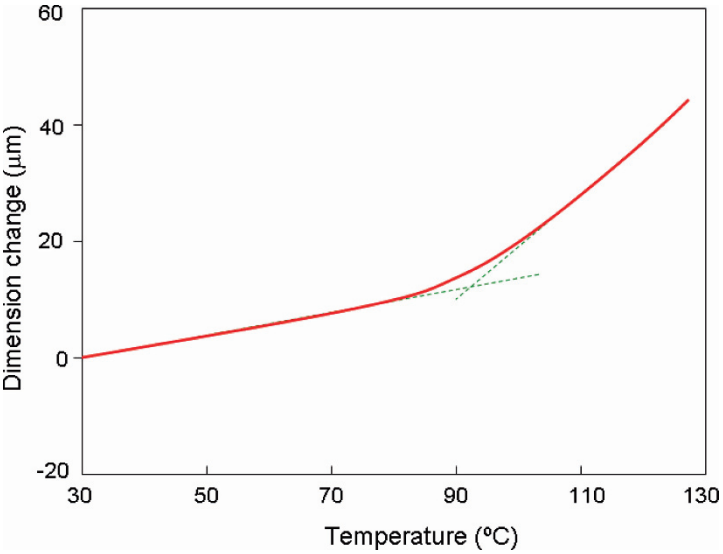

Fig. 3.8. An example of TMA curves for an ECA

3.2.5 Viscometer and Rheometer

Viscometer is an instrument used for measuring the viscosity and flow properties of fluids. Typically, it measures the force required to rotate a disc or hollow cup immersed in the specimen fluid at a predetermined speed. Of the many types, some employ rising bubbles, falling or rolling balls, and cups with orifices through which the fluid flows by gravity. Viscometers only measure under one flow condition. For liquids with viscosities which vary with flow conditions, an instrument called a rheometer is used.

A rheometer is a kind of viscometer that measures viscoelastic properties of materials beyond just viscosity. Rheology is the flow of fluids and deformation of solids under various kinds of stress and strain. A rheometer, therefore, measures material behavior such as yield stress, kinetic properties, complex viscosity, modulus, creep, and recovery.

Rheology tests are measurements of material flow and as such can reflect part of the printing process. During printing, the media is rolled under pressure from a squeegee blade traveling at approximately 10–200 mm/s. Apertures on the stencils are filled when squeegee is in close proximity, and the media is forced into the aperture and then stops moving. The final process step is when the stencil and a substrate separate as the substrate

drops away, the stencil aperture empty, and the substrate now has the printed deposits. During stencil separation the adhesive force between the deposit and the stencil walls has to be smaller than the adhesion force between printed deposit and the substrate and the cohesive force within the deposit. During printing process, the media is exposed to variable stress levels and responds in a time-dependent manner. The complex flow properties of the printing media can often be characterized by rheological test protocol illustrated in Fig. 3.9. Rheometer is widely used to evaluate the visco-elastic properties of ECAs.

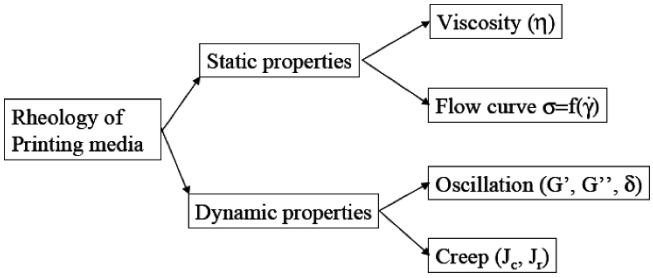

Fig. 3.9. Flow properties that can be measured by a rheometer

3.2.6 Fourier Transform Infrared (FT-IR)

Infrared (IR) absorption spectroscopy is a common technique that is used to identify the major functional groups in a compound. The identification of these groups depends on the amount of infrared radiation absorbed and the particular frequency (measured in cm^{-1}, wave numbers) at which these groups absorb. Thus, infrared absorption spectroscopy is the measurement of the wavelength and intensity of the absorption of mid-infrared light by a sample. Mid-infrared light (2.5–50 mm, 4,000–200 cm^{-1}) is energetic enough to excite molecular vibrations to higher energy levels. The wavelength of many infrared absorption bands is characteristic of specific types of chemical bonds, and infrared spectroscopy finds its greatest utility for qualitative analysis of organic and organometallic molecules. Infrared spectroscopy is used to confirm the identity of a particular compound and as a tool to help determine the structure of a molecule. Significant information for the identification of the source of an absorption band is intensity (weak, medium, or strong), shape (broad or sharp), and position (cm^{-1}) in the spectrum.

Some of the major advantages of FT-IR include the following: (1) Speed: Because all of the frequencies are measured simultaneously, most measurements by FT-IR are made in a matter of seconds rather than sev-

eral minutes. (2) Sensitivity: Sensitivity is dramatically improved with FT-IR for many reasons. The detectors employed are much more sensitive, the optical throughput is much higher (referred to as the Jacquinot advantage), which results in much lower noise levels, and the fast scans enable the co-addition of several scans in order to reduce the random measurement noise to any desired level (referred to as signal averaging). (3) Mechanical simplicity: The moving mirror in the interferometer is the only continuously moving part in the instrument. Thus, there is very little possibility of mechanical breakdown. (4) Internally calibrated: These instruments employ a HeNe laser as an internal wavelength calibration standard (referred to as the Connes advantage). These instruments are self-calibrating and never need to be calibrated by the user. These advantages make FT-IR measurement extremely accurate and reproducible. Thus, it is a very reliable technique for positive identification of virtually any sample. The sensitivity benefits enable identification of even the smallest of contaminants. This makes FT-IR an invaluable tool for quality control or quality assurance applications whether it is batch-to-batch comparisons to quality standards or analysis of an unknown contaminant. In addition, the sensitivity and accuracy of FT-IR detectors, along with a wide variety of software algorithms, have dramatically increased the practical use of infrared for quantitative analysis. Quantitative methods can be easily developed and calibrated and can be incorporated into simple procedures for routine analysis.

For conductive adhesives, FT-IR can be used to study the curing reaction of epoxy resin and optimize the ratio between new epoxy and cross-linker in reactions. In addition, FT-IR, especially diffuse reflectance infrared Fourier transform spectroscopy (DRIFTS), is widely used to evaluate the surface properties of conductive fillers of ECAs, such as the interaction between lubricant and silver flakes and the bonding between self-assembly monolayers (SAMs) and nanoconductive fillers. A schematic of the principle of the DRIFTS is shown in Fig. 3.10.

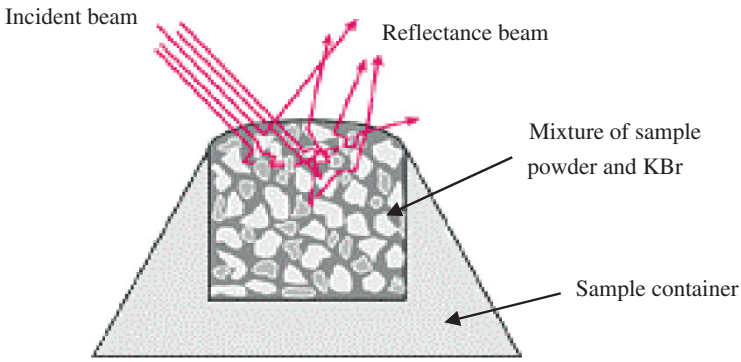

Fig. 3.10. A schematic of diffuse reflectance infrared

3.2.7 X-Ray Photoelectron Spectroscopy (XPS)

X-ray photoelectron spectroscopy (XPS) is a quantitative spectroscopic technique that measures the elemental composition, empirical formula, chemical state, and electronic state of the elements that exist within a material. XPS is a surface chemical analysis technique that can be used to analyze the surface chemistry of a material in its "s-received"state or after some treatment such as fracturing, cutting, or scraping in air or ultra-high vacuum (UHV) to expose the bulk chemistry, ion beam etching to clean off some of the surface contamination, exposure to heat to study the changes due to heating, exposure to reactive gases or solutions, exposure to ion beam implant, exposure to ultraviolet light, etc. Typically, XPS is used to measure elemental composition of the surface (1–10 nm deep), empirical formula of pure materials, elements that contaminate a surface, chemical or electronic state of each element in the surface uniformity of elemental composition across the top surface (aka, line profiling or mapping), uniformity of elemental composition as a function of ion beam etching (aka, depth profiling).

Because the energy of a particular X-ray wavelength equals a known quantity, we can determine the electron binding energy (BE) of each of the emitted electrons by using an equation that is based on the work of Ernest Rutherford:

$$E_{\text{binding}} = E_{\text{photon}} - E_{\text{kinetic}} - \Phi$$

where E_{binding} is the energy of the electron emitted from one-electron configuration within the atom, E_{photon} is the energy of the X-ray photons being used, E_{kinetic} is the kinetic energy of the emitted electron as measured by the instrument, and Φ is the work function of the spectrometer.

Compared to other analytical methods, XPS has the strength of identifying chemical state on surfaces, capable of all elements identification except for H and He, quantitative analysis, including chemical state differences between samples, applicable for a wide variety of materials, including insulating samples (paper, plastics, and glass), depth profiling with matrix-level concentrations and oxide thickness measurements.

In ECAs, XPS is typically used to analyze the surface chemistry of conductive fillers and also the fracture surface of conductive adhesive joints [31, 32].

3.2.8 X-Ray Diffraction (XRD)

X-ray diffraction (XRD) is a versatile, non-destructive technique that reveals detailed information about the chemical composition and crystallographic structure of natural and manufactured materials. XRD characterizes the geometry or shape of a molecule using X-rays. X-ray diffraction techniques are based on the elastic scattering of X-rays from structures that have long range order.

When an X-ray beam hits a sample and is diffracted, the distances between the planes of the atoms that constitute the sample can be measured by applying Bragg's law:

$$n\lambda = 2d \cdot \sin\theta$$

where the integer n is the order of the diffracted beam, λ is the wavelength of the incident X-ray beam, d is the distance between adjacent planes of atoms (the d-spacing), and θ is the angle of incidence of the X-ray beam. XRD can be used to characterize the conductive filler including nano-size fillers such as nanowires [33] and Ag-coated carbon nanotube (CNT) [34]. Figure 3.11 shows an example of the XRD spectra of a silver nanowire. It can be seen that there are four peaks which, respectively, correspond to the (111), (200), (220), and (331) planes.

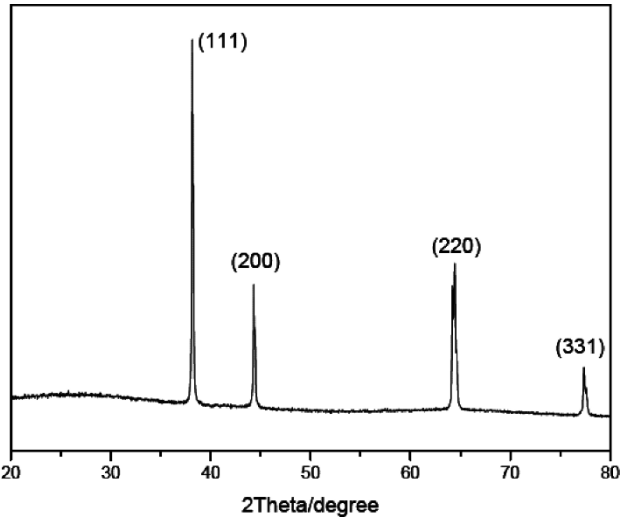

Fig. 3.11. XRD spectra of a silver nanowire

3.2.9 Transmission Electron Microscopy (TEM)

Transmission electron microscopy (TEM) is a microscopy technique whereby a beam of electrons is transmitted through an ultra-thin specimen, interacting with the specimen as they pass through. An image is formed from the interaction of the electrons transmitted through the specimen, which is magnified and focused by an objective lens and onto an imaging device, such as a fluorescent screen, as is common in most TEMs, on a layer of photographic film, or to be detected by a sensor such as a CCD camera.

Transmission electron microscopy is similar to optical microscopy, except that the photons are replaced by electrons. Since electrons have a much smaller wavelength than photons, the diffraction barrier is less of an issue and much higher resolution can be achieved. By propelling electrons at a thin sample and detecting those transmitted through it, one is able to obtain a map of the local densities of the sample, as well as diffraction information when there are ordered structures such as crystals involved.

The pros and cons of TEM are summarized as follows:

Pros

- Provides information on crystalline structures, as well as density maps.
- The resolution continues to drop as the instrument is improved.

- Theoretically, subatomic resolution should be ultimately possible.

Cons

- Requires that the sample be cut into thin slices and placed in a vacuum, possibly resulting in artifacts.
- High-resolution TEM is expensive, requiring high electron voltages.

TEM has been used to characterize conductive fillers, particle-to-particle contact, interface between conductive particle and polymer matrix, and interface between conductive adhesive and metal pads. As an example, Fig. 3.12 shows a TEM image of isotropically conductive adhesive which is filled with silver flakes.

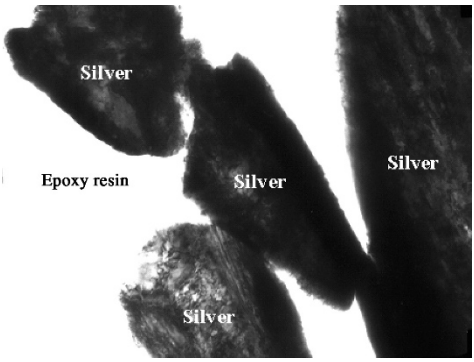

Fig. 3.12. A TEM image of a conductive adhesive (physical contact among silver flakes can be observed)

3.2.10 Scanning Electron Microscopy (SEM)

SEM operates by scanning an electron beam over the sample and measuring the electrical interactions with the surface. When the electrons hit the surface, weakly bound electrons will be ejected to produce secondary electrons. These secondary electrons can then be measured by a detector and used to calculate the color for each pixel of a SEM image. Since these secondary electrons are of low energy their trajectories can be easily influenced by electromagnetic fields. In order to avoid a charge build-up on the surface of the sample which would alter the path of the secondary electrons, the surface must be conducting. However, shadowing methods have been developed for coating non-conductive samples with a thin layer of metal so that SEM measurements become possible.

Advantages and disadvantages of SEM are summarized as follows:

Advantages

- Provides images of surface features.
- Much higher resolution than optical microscopy, due to the very small wavelength of the electron.
- Faster than scanning probe microscopy as the beam can be scanned with electromagnetic fields rather than mechanical actuators.

Disadvantages

- Requires a conductive sample (or that the surface of a non-conductive sample be metallized).
- Must be carried out in a vacuum, which is not only inconvenient but may also result in artifacts.
- Unlike SPM or interferometry, the height and chemical properties of the surface cannot be quantitatively determined by SEM.

3.2.11 Raman Spectroscopy

Raman spectroscopy is a spectroscopic technique used in condensed matter physics and chemistry to study vibrational, rotational, and other low-frequency modes in a system [35]. It relies on inelastic scattering, or Raman scattering, of monochromatic light, usually from a laser in the visible, near infrared, or near ultraviolet range. The laser light interacts with phonons or other excitations in the system, resulting in the energy of the laser photons being shifted up or down. The shift in energy gives information about the phonon modes in the system. Infrared spectroscopy yields similar, but complementary information. Figure 3.13 is a schematic energy level diagram showing the states involved in Raman signal.

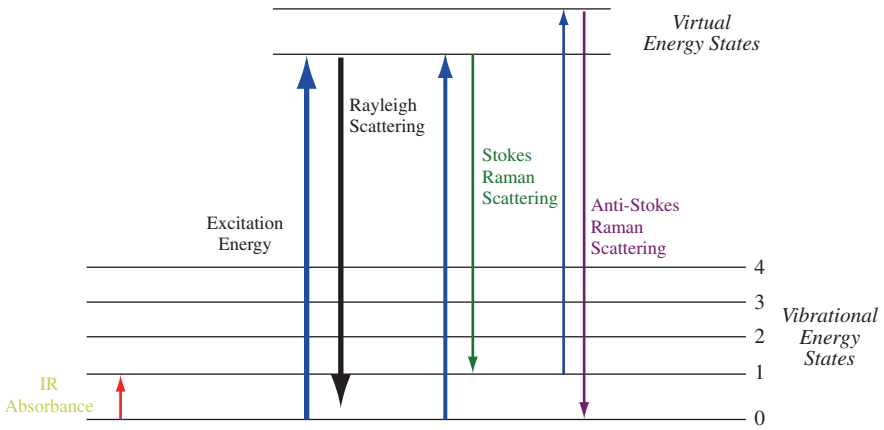

Fig. 3.13. Energy level diagram showing the states involved in Raman signal. The line thickness is roughly proportional to the signal strength from the different transitions.

Typically, a sample is illuminated with a laser beam. Light from the illuminated spot is collected with a lens and sent through a monochromator. Wavelengths close to the laser line, due to elastic Rayleigh scattering, are filtered out while the rest of the collected light is dispersed onto a detector.

The Raman effect occurs when light impinges on a molecule and interacts with the electron cloud of the bonds of that molecule. The incident photon excites one of the electrons into a virtual state. For the spontaneous Raman effect, the molecule will be excited from the ground state to a virtual energy state and relaxed into a vibrational excited state, which generates Stokes Raman scattering. If the molecule was already in an elevated vibrational energy state, the Raman scattering is then called anti-Stokes Raman scattering.

A molecular polarizability change, or amount of deformation of the electron cloud, with respect to the vibrational coordinate is required for the molecule to exhibit the Raman effect. The amount of the polarizability change will determine the Raman scattering intensity, whereas the Raman shift is equal to the vibrational level that is involved.

Raman spectroscopy is commonly used in chemistry, since vibrational information is very specific for the chemical bonds in molecules. It therefore provides a fingerprint by which the molecule can be identified. The fingerprint region of organic molecules is in the (wave number) range 500–2,000 cm^{-1}. This technique can be used to study changes in chemical bonding. For the SAM-treated ECAs, Raman spectroscopy can be used to study the orientation and alignment of the SAM molecule configuration on the conductive filler surface.

Surface-enhanced Raman spectroscopy, or Surface-enhanced Raman scattering, often abbreviated SERS, has been developed to enhance the probing of nanoparticle surface sensitivity. SERS is a surface-sensitive technique that results in the enhancement of Raman scattering by molecules adsorbed on rough metal surfaces. The enhancement factor can be as much as 10^{14}–10^{15}, which allows the technique to be sensitive enough to detect single molecules [35].

The name surface-enhanced Raman spectroscopy implies that it provides the same information that traditional Raman spectroscopy does, simply with a greatly enhanced signal. While the spectra of most SERS experiments are very similar to the non-surface enhanced spectra, there are often differences in the number of modes present. Additional modes not found in the traditional Raman spectrum can be present in the SERS spectrum, while other modes can disappear.

The modes observed in any spectroscopic experiment are dictated by the symmetry of the molecules and are usually summarized by selection rules. When molecules are adsorbed to a surface, the symmetry of the system can change, slightly modifying the symmetry of the molecule, which can lead

to differences in mode selection [36]. The symmetry of a molecule can be changed in different ways depending on the orientation in which the molecule is attached to the surface. In some experiments, it is possible to determine the orientation of adsorption to the surface from the SERS spectrum, as different modes will be present depending on the way in which the symmetry is modified [37, 38].

Raman spectroscopy has been used to characterize the organic lubricant layer on silver flake surfaces [31], and SERS was employed to study the interaction between self-assembled monolayer (SAM) and metal spheres in ACAs, and also the molecular chain orientation of the SAM molecules on the metal sphere surfaces [39].

3.2.12 Gas Chromatography/Mass Spectrometry

The GC/MS is composed of two major building blocks: the gas chromatograph (GC) and the mass spectrometer (MS) (Fig. 3.14). The gas chromatograph utilizes a capillary column which depends on the column's dimensions (length, diameter, film thickness) as well as the phase properties (e.g., 5% phenyl polysiloxane). The difference in the chemical properties between different molecules in a mixture will separate the molecules when the sample travels along the length of the column. The molecules take different amounts of time (called the retention time) to come out of (elute from) the gas chromatograph, and this allows the mass spectrometer downstream to capture, ionize, accelerate, deflect, and detect the ionized molecules separately. The mass spectrometer does this by breaking each molecule into ionized fragments and detecting these fragments using their mass to charge ratio.

For the analysis of volatile compounds, a Purge and Trap (P&T) concentrator system may be used to introduce samples. The target analytes are extracted and mixed with water and introduced into an airtight chamber. An inert gas such as nitrogen (N_2) is bubbled through the water; this is known as purging. The volatile compounds move into the headspace above the water and are drawn along a pressure gradient (caused by the introduction of the purge gas) out of the chamber. The volatile compounds are drawn along a heated line onto a “trap”, where trap is a column of adsorbent material at ambient temperature that holds the compounds by returning them to the liquid phase. The trap is then heated and the sample compounds are introduced to the GC/MS column via a volatile interface, which is a split inlet system. P&T GC/MS is particularly suited to volatile organic compounds (VOCs) and BTEX compounds (aromatic compounds associated with petroleum).

GC/MS is widely utilized to study conductive adhesives to determine the volatile species that evolve during curing and after post-cure processing, such as preseal bakeout and burn-in [40].

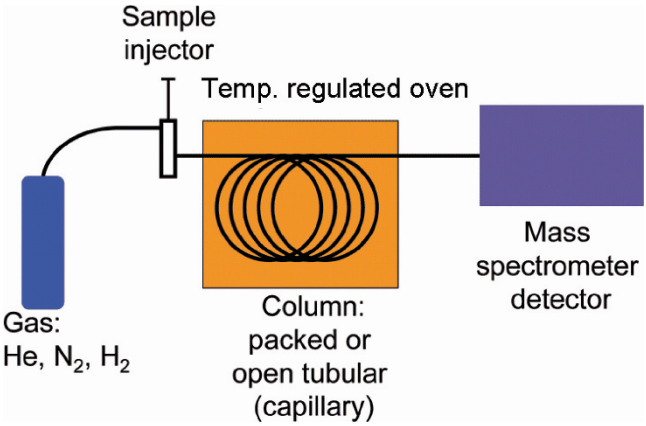

Fig. 3.14. A schematic of a GC/MS

3.2.13 Electrical Characterization of ECAs

3.2.13.1 Volume Resistivity/Bulk Resistivity

Volume resistance of a specimen is the ratio of the direct voltage to the part of the current that is distributed through the volume of the specimen. It is directly proportional to the thickness (h) and inversely proportional to the area A (cm^2) of the sample according to the equation

$$R_v = \rho_v h/A$$

where ρ_v is the proportionality constant called the volume resistivity, in ohm cm (Ω cm), which is numerically equal to the volume resistance in ohm between the opposite surfaces of a 1-cm cube of the material.

The reciprocal of volume resistivity is the volume conductivity, expressed in Siemens per centimeter (Scm^{-1}) or $\Omega^{-1}cm^{-1}$. From the equation the volume conductivity γ_v is given by

$$\gamma_v = G_v h/A$$

where G_v is the measured conductance.

Figure 3.15 shows the method used to determine the volume resistivity of conductive adhesive strip of thickness h, width w, and length l, using a

point probe approach. The four-point probe avoids this problem by using a row of four equally spaced needles. A known current is passed between the outer needles, while an open-circuit voltage reading is made between the inner needles. Because no (or very little) current flows through the voltage sensing needles, there are no errors introduced due to the contacts. The very reason for "four-point" probe measurements is to divorce the probes supplying the current from the probes measuring the voltage, so it is only necessary to consider the "voltage probes." The device used to measure the voltage is provided with a very high input impedance (ASTM F84 recommends at least $10^6 \times$ the resistivity of the specimen), thus the contact resistance is a small proportion of the resistance in the voltage measuring circuit.

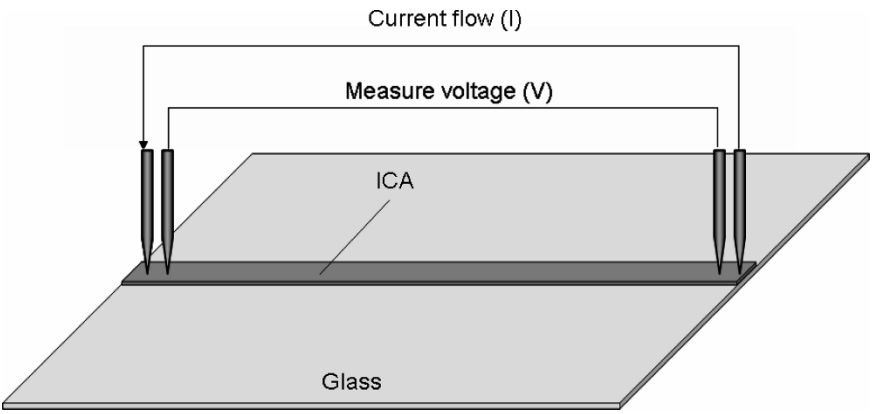

Fig. 3.15. Schematic set-up for bulk resistivity measurement

3.2.13.2 Contact Resistance

Contact resistance of an ECA joint consists of the bulk resistance of the ECA and the interfacial resistance between the ECA and the contact pads. One of the requirements for ECAs is that they must have stable contact resistance under various aging conditions including 85°C/85%RH (relative humidity) [41]. There are no standard test methods or test vehicles for contact resistance. The test vehicle you choose should represent the intended applications of the ECA. There are many test vehicles used by various researchers in the literature. Only two examples are shown here.

The test vehicle in Fig. 3.16 consists of a zero ohm resistor with metal terminations which is attached to two-metal pads using an ECA. The metal terminations of the resistor and metal pads on the substrate should be the metal surface finish which you intend to use in the real applications.

A four-wire method can be used to measure the total resistance through those two-metal pads on the substrate.

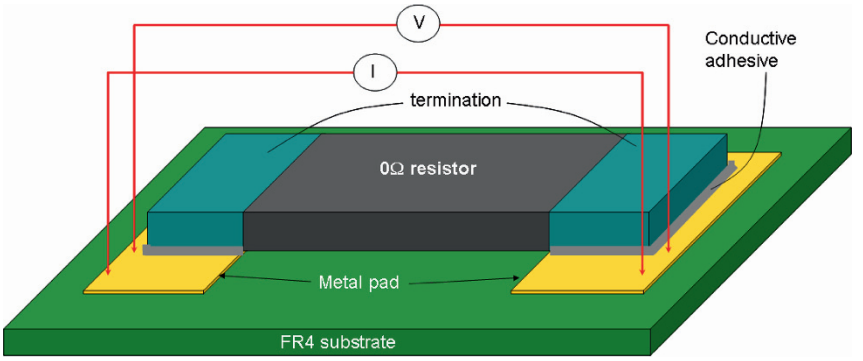

Fig. 3.16. Contact resistance test vehicle with a zero ohm resistor

Figure 3.17 shows another type of test vehicle which consists of two cross metal bars [42]. The surface of the metal bars should represent the surface finish which you are interested. A thin layer of ECA is sandwiched between these two-metal bars. A four-wire approach is used to measure the total resistance of the ECA joint. Figure 3.18 is a schematic of a test vehicle for studying the contact resistance of ACAs (anisotropically conductive adhesives).

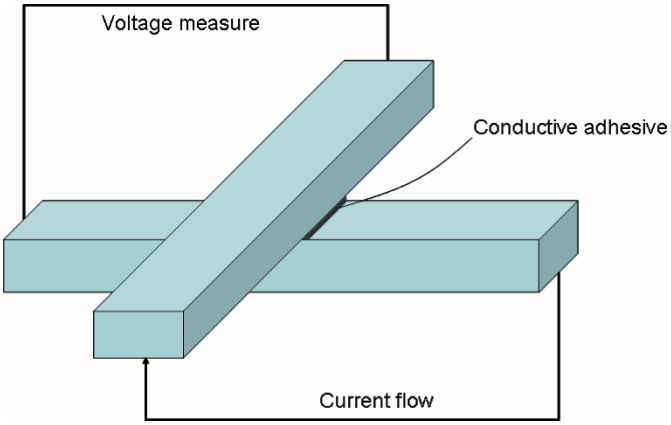

Fig. 3.17. A contact resistance test vehicle consisting of cross metal bars

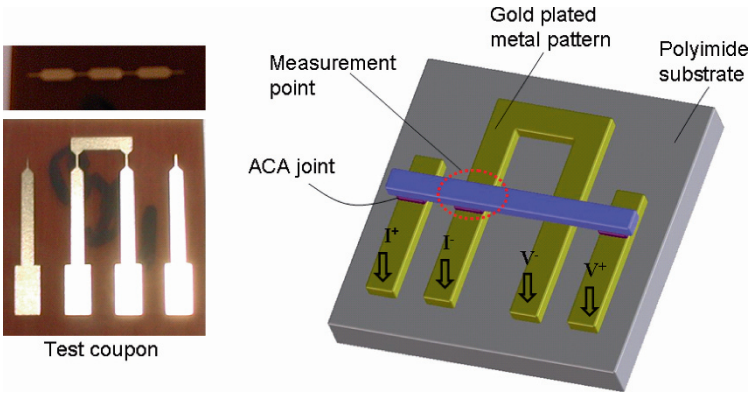

Fig. 3.18. A schematic of test set-up for measuring contact resistance of ACA joints

3.2.13.3 High-Frequency Characteristics of ECA

For wireless/RF (radiofrequency) electronic applications, a number of high-frequency (in excess of 2.45 to >10 GHz) applications and utilizations are increasing rapidly, thus it is important to characterize the cross-talk between particles, coupling with semiconductor devices and other fundamental behavior of ECAs under high-frequency conditions.

The vector network analyzer (VNA) is a form of RF network analyzer widely used for RF design applications. It can enable the RF performance of radiofrequency (RF) and microwave devices to be characterized in terms of network scattering parameters, or S parameters. The information provided by the VMA can then be used to ensure that the RF design of the circuit is optimized to provide the best performance. VNA has shown to be a useful tool to evaluate the high-frequency characteristics ACA and NCA [43].

3.2.14 Mechanical Property Characterization

3.2.14.1 Adhesion Strength

Die shear strength method (MIL-STD 883, method 2019) consists in the measurement of the force required to shear a die off a chip carrier. Although any die size can be used, a standard technique is to bond 1.27 ×12.7 mm^2 silicon die to silver-plated lead frames. The dies and lead frames are

cleaned first. A drop of a conductive adhesive paste is dispensed on the lead frames, and then dices are placed onto the conductive adhesive drops using a pick and place machine, and then the assemblies are cured. The die shear strength of each individual die is measured with a die shear tester. The die shear strength is generally calculated by averaging the results obtained on 20 individual dies tested and expressed either as a force (N) or as a stress (MPa) if the bond area is introduced in the calculation.

Lap Shear Strength Lap shear or tensile test measures the strength of the adhesive under shear. The common lap shear test method is described in ASTM D1002, and the standard test specimen is shown in Fig. 3.19. This is the most commonly used shear test for adhesives on metal substrates. Testing is carried out by pulling the ends of the overlap in tension, causing the adhesive to be stressed in shear. ASTM D3163 specifies a similar test method for rigid plastic substrates. The width of the lap shear specimen is generally 1 in. The recommended length of overlap, for metal substrates with a thickness of 0.064 in., is 0.5 ± 0.05 in. However, it is recommended that the length be chosen so that the yield point of the substrate is not exceeded.

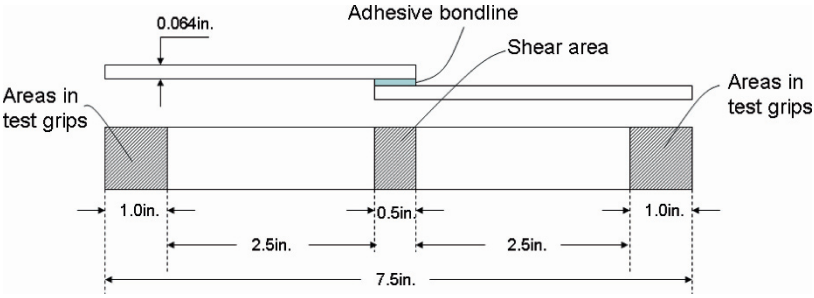

Fig. 3.19. Dimensions of a standard test sample for lap shear strength

3.2.14.2 Impact Performance

The drop test is designed to simulate the shocks experienced by PCB composites during assembly, handling, and product life. Drop-test vehicles were prepared and tested as recommended by NCMS [44]. The test vehicle is depicted in Fig. 3.20. The drop test, which was established by the National Center for Manufacturing Sciences (NCMS), has been widely used to evaluate the impact performance of conductive adhesives in the conductive adhesive industry. The drop test involves dropping mounted chip carrier and circuit board assemblies onto hard surfaces from a height of 1.5 m

(60 in.) and passing six drops as a prerequisite for the application of conductive adhesives. The drop test is easy to conduct. However, as the drop test can only qualitatively distinguish the impact performance of conductive adhesives, not much optimal information could be obtained from the drop results. To improve the impact performance of conductive adhesives, adhesive manufacturers must first accurately characterize the impact behavior of a conductive adhesive and investigate factors that may affect the impact performance of the adhesive. Therefore, it is desirable to develop a test technique that can quantitatively characterize the impact resistance of conductive adhesives at a material level and yield useful information in screening adhesives and helping formulate new conductive adhesives with more favorable impact performance.

Xu et al. [45] utilized a novel falling wedge test to quantitatively characterize the impact resistance of electrically conductive adhesives. The results obtained in this study show that the falling wedge test was able to discriminate between the impact performance of adhesives and this technique is capable of screening conductive adhesives for bonding purposes. This test technique could enable the microelectronics industry to use an adhesive specification rather than the current drop-test specification to evaluate and determine acceptance of candidate adhesive systems. The viscoelastic energy, which is a result of the internal friction created by chain motions within the adhesive material, has played an important role in the fracture behavior of the conductive adhesives. As a measure of the internal friction, the loss factor is found to be an indicator of an adhesive's ability to dissipate the mechanical energy through heat. By quantitatively relating the impact fracture energy of the adhesive joints to the loss factors of the ECAs, we have demonstrated that the impact fracture energy tends to exhibit a logarithmic relationship with the corresponding loss factor, as the increased loss factor at the test conditions consistently results in improved impact performance. This finding suggests conductive adhesive manufacturers that the impact performance of a conductive adhesive may be improved by formulating the adhesive with good damping ability under impact conditions that may be encountered in the service.

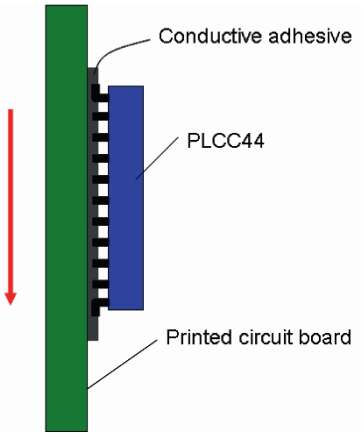

Fig. 3.20. A schematic of drop-test vehicle recommended by NCMS

3.2.14.3 Bulk Fracture Toughness

The ASTM D5045 guideline is generally followed to measure the plane strain fracture toughness of a conductive attach adhesive [46]. Fracture toughness value is determined using pre-cracked single-edge-notched (SEN) specimens in a three-point-bend fixture (3PB) (see Fig. 3.21). Pre-cracks can be introduced by scoring a razor blade at the notch tip of the specimens while at an elevated temperature such as 180°C. Upon cooling the sharp notch becomes even sharper due to thermal contraction. After precracking and conditioning, the samples are loaded in a servohydraulic materials testing machine with a 100 lb load cell and at a crosshead speed of 0.5 mm/min. K_{1C} values reported are the averages of a minimum of five tests. K_{1C} values are determined by measuring the specimen dimensions and the critical load at fracture.

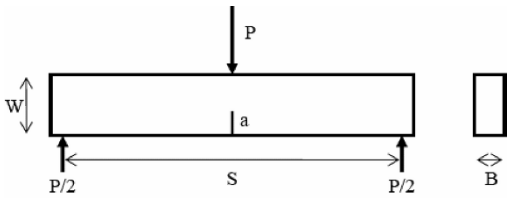

Fig. 3.21. Schematic of the loading configuration for the SENB test (*a* is the crack length, *B* is the specimen width, *W* is the specimen height, *S* is the span)

References

[1] C. P. Wong, “IC Device Encapsulants and Polymeric Reliability,” in Polymers for Electronic Applications, Chapter 3, CRC press, Boca Raton, FL, pp. 63–92, 1989.

[2] C. P. Wong, “Recent Advances in IC Passivation and Evaluation : Process Techniques and Materials,” in Polymers for Electronic and Photonic Applications, Chapter 4, C. P. Wong, Ed., Academic Press, New York, pp. 167–220, 1993.

[3] C. P. Wong and P. D’Ambra, “Embedment of Electronic Devices,” in Kirk-Othmer Encyclopedia of Chemical Technology, 4th Ed., John Wiley & Sons, New York, vol. 9, pp. 377–393, 1994.

[4] C. P. Wong, J. M. Segelken, and C. N. Robinson, “Encapsulation of Chip-on-Board,” in Handbook of Wire Bonding, Tape Automated Bonding, and Flip-Chip on Board for Multichip Module Applications, Chapter 11, J. Lau, Ed., Van Nostrand Reinhold, New York, pp. 470–503, 1994.

[5] C. P. Wong, “High Performance Silicone Gel as IC Device Encapsulants,” *Electronic Packaging Materials Science III*, 108, 175, 1988.

[6] C. P. Wong, “Silicone Gel as IC Device Encapsulants – Electrical Reliability and Cure Study,” *Polymer Science and Engineering*, 59, 480, 1988.

[7] C. P. Wong, “Materials for Electronic Packaging,” in Materials for Electronic Packaging, Chapter 12, D. Chung, Ed., Butterworth Publisher, London, pp. 281–302, 1995.

[8] C. P. Wong, A. Kumar, and K. Otsuka, “Encapsulation and Sealing,” in Microelectronics Packaging Handbook, Chapter 10, R. Tummala, E. Rymaszewski, Ed., 2nd Ed., Chapman Hall, New York, pp. 873–930, 1997.

[9] C. P. Wong, “Overview of IC Device Encapsulants as Device Packaging,” *Journal of Electronic Packaging, American Society for Mechanical Engineering*, 111, 97, 1989.

[10] C. P. Wong, “Silicone Gels as IC Encapsulants – Cure Study and Electrical Reliability,” *Polymer Materials for Electronics Packaging and Interconnects American Chemical Society*, 407, 220, 1989.

[11] C. P. Wong, J. M. Segelken, and J. W. Balde, "Understanding the Use of Silicone Gels for Nonhermetic Plastic Packaging," *IEEE Transactions on Components Hybrids and Manufacturing Technology*, 12, 421–425, 1989.

[12] C. P. Wong, "Passivating Organic Coatings with Silicone Gels: The Correlation Between the Material Cure and Its Electrical Reliability," *Electronic Packaging Materials*, 154, 195, 1990.

[13] C. P. Wong, S. H. H. Shi, and G. Jefferson, "High Performance nN-flow Underfills for Low-cost Flip-chip Applications: Material Characterization," *IEEE Transactions on Components Packaging and Manufacturing Technology Part A*, 21, 450–458, 1998.

[14] J. L. Wu, R. T. Pike, S. K. Sitaraman, and C. P. Wong, "New Reworkable High Temperature Low Modulus (in excess of 400–500°C) Adhesives for MCM-D Assembly," *Journal of Electronic Packaging*, 122, 55–60, 2000.

[15] C. P. Wong, M. B. Vincent, and S. Shi, "Fast-flow Underfill Encapsulant: Flow Rate and Coefficient of Thermal Expansion," *IEEE Transactions on Components Packaging and Manufacturing Technology Part A*, 21, 360–364, 1998.

[16] C. P. Wong, "Polymers for Encapsulation: Materials Processes and Reliability," *Chip Scale Review*, 2, 30–37, 1998.

[17] S. H. Shi and C. P. Wong, "Effects of the Complexed Moisture in Metal Acetylacetonate on the Properties of the No-flow Underfill Materials," *Journal of Applied Polymer Science*, 73, 103–111, 1999.

[18] C. P. Wong, L. J. Wang, and S. H. Shi, "Novel High Performance No Flow and Reworkable Underfills for Flip-Chip Applications," *Materials Research Innovations*, 2, 232–247, 1999.

[19] M. B. Vincent and C. P. Wong, "Enhancement of Underfill Encapsulants for Flip-chip Technology," *Soldering & Surface Mount Technology*, 11, 33–39, 1999.

[20] C. P. Wong and R. S. Bollampally, "Comparative Study of Thermally Conductive Fillers for Use in Liquid Encapsulants for Electronic Packaging," *IEEE Transactions on Advanced Packaging*, 22, 54–59, 1999.

[21] L. J. Wang and C. P. Wong, "Novel Thermally Reworkable Underfill Encapsulants for Flip-Chip Applications," *IEEE Transactions on Advanced Packaging*, 22, 46–53, 1999.

[22] L. J. Wang and C. P. Wong, "Syntheses and Characterizations of Thermally Reworkable Epoxy Resins. Part I," *Journal of Polymer Science Part A-Polymer Chemistry*, 37, 2991–3001, 1999.

[23] J. H. Kang, K. Cho, and C. E. Park, "Adhesion Strength and Mechanism of Poly(Imide-Siloxane) to Alloy 42 Leadframe," *Journal of Adhesion Science and Technology*, 15, 913–928, 2001.

[24] R. H. Bott, J. D. Summers, C. A. Arnold, L. T. Taylor, T. C. Ward, and J. E. Mcgrath, "Synthesis and Characteristics of Novel Poly(Imide Siloxane) Segmented Copolymers," *Journal of Adhesion*, 23, 67–82, 1987.

[25] J. D. Summers, C. A. Arnold, R. Bott, L. T. Taylor, T. C. Ward, and J. E. Mcgrath, "Synthesis and Characteristics of Novel Poly(Imide Siloxane) Segmented Copolymers," *Abstracts of Papers of the American Chemical Society*, vol. 192, pp. 24-Macr, 1986.

[26] C. Perabo, "BMI Resins as Low-Stress Alternatives to Epoxies for Semiconductor Package Assembly," *2003 IEEE/CPMT/SEMI 28th International Electronics Manufacturing Technology Symposium (IEMT)*, pp. 265–271, 1993.

[27] A. Takahashi, A. Nagai, A. Mukoh, M. Wajima, and K. Tsukanishi, "Low Dielectric Material for Multilayer Printed Wiring Boards," *IEEE Transactions on Components Hybrids and Manufacturing Technology*, 13, 1115–1120, 1990.

[28] R. Sundermann, G. Rottloff, and E. Grigat, *US Patent 4,195,132*, 1980.

[29] M. N. Nguyen, I. Y. Chien, M. B. Grosse, M. M. Chau, and D. A. Burkhart, "Polycyanate Die-attach Adhesives for Microelectronic Applications," *Proceedings of 45th Electronic Components and Technology Conference*, vol. 21–24 May 1995, pp. 682–687, 1995.

[30] A. V. Tobolsky, "Properties and Structure of Polymers," Wiley, New York, 1960.

[31] D. L. Markley, Q. K. Tong, D. J. Magliocca, and T. D. Hahn, "Characterization of Silver Flakes Utilized for Isotropic Conductive Adhesives," *International Symposium on Advanced Packaging Materials: Processes, Properties and Interfaces*, vol. 14–17 Mar 1999, pp. 16–20, 1999.

[32] S. Y. Xu, D. A. Dillard, and J. G. Dillard, "Environmental Aging Effects on the Durability of Electrically Conductive Adhesive Joints," *International Journal of Adhesion and Adhesives*, 23, 235–250, 2003.

[33] Y. S. Lin and S. S. Chiu, "Electrical Properties of Conductive Adhesives as Affected by Particle Compositions, Particle Shapes, and Oxidizing Temperatures of Copper Powders in a Polymer Matrix," *Journal of Applied Polymer Science*, 93, 2045–2053, 2004.

[34] H. P. Wu, X. J. Wu, M. Y. Ge, G. Q. Zhang, Y. W. Wang, and J. Z. Jiang, "Properties Investigation on Isotropical Conductive Adhesives Filled with Silver Coated Carbon Nanotubes," *Composites Science and Technology*, 67, 1182–1186, 2007.

[35] S. M. Nie and S. R. Emery, "Probing Single Molecules and Single Nanoparticles by Surface-enhanced Raman Scattering," *Science*, 275, 1102–1106, 1997.

[36] M. Moskovits and J. S. Suh, "Surface Selection Rules for Surface-enhanced Raman Spectroscopy: Calculations and Application to the Surface-enhanced Raman spectrum of Phthalazine on Silver," *The Journal of Physical Chemistry*, 88, 5526–5530, 1984.

[37] A. G. Brolo, Z. Jiang, and D. E. Irish, "The Orientation of 2,2 '-bipyridine Adsorbed at a SERS-Active Au(111) Electrode Surface," *Journal of Electroanalytical Chemistry*, 547, 163–172, 2003.

[38] A. Michota and J. Bukowska, "Surface-Enhanced Raman Scattering (SERS) of 4-Mercaptobenzoic Acid on Silver and Gold substrates," *Journal of Raman Spectroscopy*, 34, 21–25, 2003.

[39] R. W. Zhang, Y. Li, M. J. Yim, K. Moon, D. D. Lu, and C. P. Wong, "Electrically Conductive Adhesive with pi-conjugated Self-Assembled Molecular Wire Junctions for Enhanced Electrical and Thermal Properties," *58th Electronic Components and Technology Conference*, vol. 27–30 May 2008, pp. 1913–1918, 2008.

[40] R. C. Benson, T. E. Phillips, and N. DeHaas, "Volatile Species from Conductive Die Attach Adhesives," *IEEE Transactions on Components, Hybrids, and Manufacturing Technology*, 12, 571–577, 1989.

[41] M. Komagata, G. Toida, T. Hocchi, and K. Suzuki, "Conductive Adhesive for Plated Sn or SdPb Electrode," *4th International Conference on Adhesive Joining and Coating Technology in Electronics Manufacturing*, vol. 18–21 June 2000, pp. 216–220, 2000.

[42] L. C. Montemayor, "Electrically Conductive Silicone Adhesive," *Proceedings of SMTA International Conference*, Sept. 2002.

[43] Y. Li, M. J. Yim, K. S. Moon, and C. P. Wong, "Novel Nano-Scale Conductive Films With Enhanced Electrical Performance and Reliability for High Performance Fine Pitch Interconnect," *IEEE Transactions on Advanced Packaging*, 32, 123–129, 2009.

[44] M. Zwolinski, J. Hickman, H. Z. Rubin, S. Y. McCarthy, T. Hanlon, P. Arrowsmith, A. Chaudhuri, R. Hermansen, S. Lan, and D. Napp, "Electrically Conductive Adhesives for Surface Mount Solder Replacement," *IEEE Transactions an Components, Packaging, and Manufacturing Technology – Part C*, 19, 241–250, 1996.

[45] S. Y. Xu and D. A. Dillard, "Determining the Impact Resistance of Electrically Conductive Adhesives Using a Falling Wedge Test," *IEEE Transactions on Components and Packaging Technologies*, 26, 554–562, 2003.

[46] S. Gupta, R. M. Hydro, and R. A. Pearson, "Fracture Behavior of Isotropically Conductive Adhesives," *IEEE Transactions on Components and Packaging Technologies*, 22, 209–214, 1999.

Chapter 4
Isotropically Conductive Adhesives (ICAs)

4.1 Introduction

4.1.1 Percolation Theory of Conduction

Isotropic conductive adhesives, also known as "polymer solder," are composites of polymer resin and conductive fillers. The conductive fillers provide the composite with electrical conductivity through contact between the conductive particles. With increasing filler concentrations, the electrical properties of an ICA transform it from an insulator to a conductor. Percolation theory has been used to explain the electrical properties of ICA composites. At low filler concentrations, the resistivity of ICAs decreases gradually with increasing filler concentration. However, the resistivity drops dramatically above a critical filler concentration, V_c, called the percolation threshold. It is believed that at this concentration, all the conductive particles contact each other and form a three-dimensional network. The resistivity decreases only slightly with further increases in the filler concentrations [1–3]. A schematic explanation of resistivity change of ICAs based on percolation theory is shown in Fig. 4.1. In order to achieve conductivity, the volume fraction of conductive filler in an ICA must be equal to or higher than the critical volume fraction. Similar to solders, ICAs provide the dual functions of electrical connection and mechanical bond in an interconnection joint. In an ICA joint (Fig. 4.2), the polymer resin provides mechanical stability and the conductive filler provides electrical conductivity. Filler loading levels that are too high cause the mechanical integrity of adhesive joints to deteriorate. Therefore, the challenge in formulating an ICA is to maximize conductive filler content to achieve a high electrical conductivity without adversely affecting the mechanical properties. In a typical ICA formulation, the volume fraction of the conductive filler is about 25–30% [4, 5].

Y. Li et al., *Electrical Conductive Adhesives with Nanotechnologies*,
DOI 10.1007/978-0-387-88783-8_4, © Springer Science+Business Media, LLC 2010

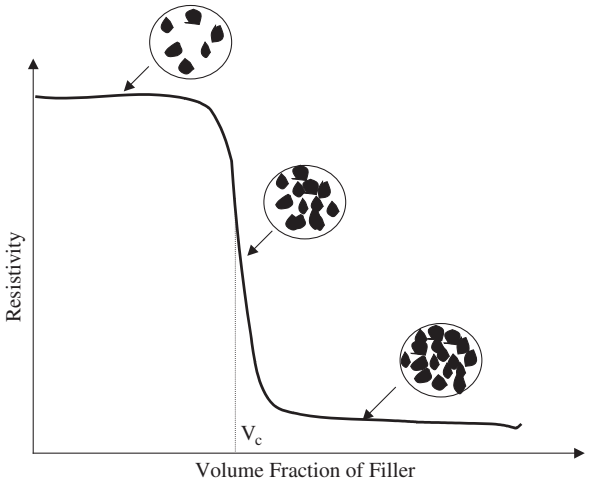

Fig. 4.1. Effect of filler volume fraction on the resistivity of ICA systems

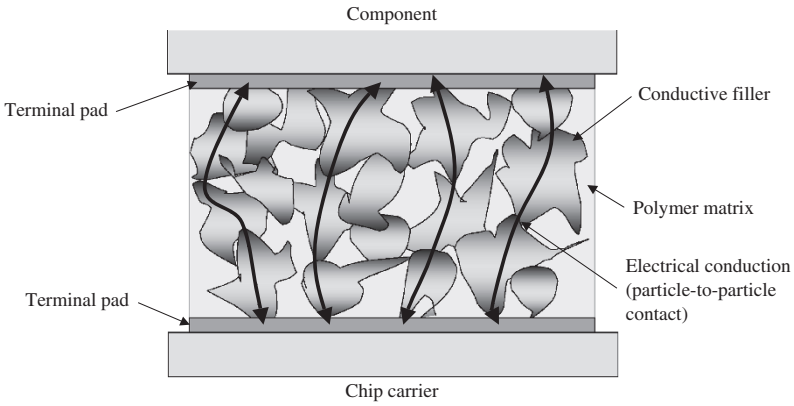

Fig. 4.2. Schematic illustration of how electrical conduction paths are established by uninterrupted particle-to-particle contact between the component and the chip carrier terminal pads in an ICA joint

4.1.2 Adhesive Matrix

An ideal polymeric matrix for ICAs should exhibit a long shelf life (good room temperature latency), fast cure, relatively high glass transition temperature (T_g), low moisture pickup, and good adhesion [6].

Both thermoplastic and thermoset resins can be used for ICA formulations. The main thermoplastic resin used for ICA formulations is polyimide resin. An attractive advantage of thermoplastic ICAs is that they are reworkable, e.g., can easily be repaired. A major drawback of thermoplastic ICAs, however, is the degradation of adhesion at high temperature. Another drawback of polyimide-based ICAs is that they generally contain solvents. During heating, voids are formed when the solvent evaporates. Most commercial ICAs are based on thermosetting resins. Epoxy resins are most commonly used in thermoset ICA formulations because they possess superior balanced properties. Silicones, cyanate esters, and cyanoacrylates are also employed in ICA formulations [7–11].

Most commercial ICAs must be kept and shipped at a very low temperature, usually –40°C, to prevent the ICAs from curing. Pot life is a very important factor for users of the ICAs. In order to achieve desirable latency at room temperature, epoxy hardeners must be carefully selected. In some commercial ICAs, solid curing agents are used, which do not dissolve in the epoxy resin at room temperature. However, these curing agents can dissolve in the epoxy at a higher temperature (curing temperature) and react with the epoxy resin. Another approach to achieve latency is to employ an encapsulated imidazole as a curing agent or catalyst. An imidazole is encapsulated inside a very fine polymer sphere. At room temperature, the polymer sphere does not dissolve or react with the epoxy resin. But at a higher temperature, after the polymer shell is broken, the imidazole is released from the sphere to cure the epoxy or catalyze the cure reaction. Fast cure is another attractive property of a desirable ICA. Shorter cure times increase throughput resulting in lower processing cost. In epoxy-based ICA formulations, proper hardeners and catalysts such as imidazoles and tertiary amines can be used to achieve rapid cure.

Conductive adhesives with low T_gs can lose electrical conductivity during thermal cycling aging [12, 13]. Electrical conductivity in metal powder- filled conductive adhesives is achieved through the contact of adjacent metal particles with each other, thus producing a continuous electrical path between a component lead and the metal pad of a chip carrier. When a joint is subjected to thermal cycling conditions, it experiences repeated cyclic shear motion of the lead relative to the chip carrier pad. The amount of shear strain is primarily dependent on the thermal cycling conditions and thermal expansion mismatch between the component and the chip carrier. Besides lead deformation and substrate compliance, the majority of the

shear strain produced is accommodated by viscoelastic or viscoplastic deformation of the conductive adhesive. When a conductive adhesive deforms to accommodate the shear strain produced, the metal particles move, thus changing the position of contact point(s) between adjacent metal particles. If the organic matrix is too compliant, it will flow to fill the area left behind the moving metal particles. When the direction of the shear strain is reversed during thermal cycling, adjacent metal particles move back to their original contact locations, which now are partially covered with the compliant, dielectric organic matrix material. As the number of thermal cycles increases, the contact resistance between adjacent particles increases, thus increasing the interconnection joint resistance [12].

Moisture absorption can influence the reliability of conductive adhesive interconnection joints. Moisture in polymer composites is known to have an adverse effect on both mechanical and electrical properties of epoxy laminates [13, 14]. Studies relating to the reliability and moisture sensitivity of electronic packages indicate similar degrading effects. It was determined that moisture absorption can cause an increase in contact resistance, especially if the metallization on the bond pads and components are not noble metals [15]. Effects of moisture absorption on conductive adhesive joints are summarized in Table 4.1. In order to achieve high reliability, conductive adhesives with low moisture absorption are required. High adhesion strength to pad and component metallization is a necessary property for conductive adhesives used for interconnections in electronic assemblies. Epoxy-based ICAs tend to have better adhesion strength than polyimide and silicone-based ICAs. However, a silicone matrix tends to have lower moisture absorption than epoxy resins [8].

Table 4.1. Effects of moisture on ICA joints

Major effects
Degrade bulk mechanical strength
Decrease interfacial adhesion strength and cause delamination
Promote the growth of voids present in joints
Give rise to swelling stress in joints
Induce the formation of metal oxide layers resulting from corrosion

4.1.3 Conductive Fillers

While polymer matrices are dielectric materials, conductive fillers in ICA formulations provide the material with electrical conductivity. In order to achieve high conductivity, the filler concentration must be at least equal to or higher than the critical concentration predicted by percolation theory.

4.1.3.1 Pure Silver versus Ag-Coated Fillers

Silver (Ag) is by far the most popular conductive filler, although gold (Au), nickel (Ni), copper (Cu), and carbon are also used in ICA formulations. Silver has the highest room temperature electrical and thermal conductivity among all the metals. Silver is unique among all of the cost-effective metals by nature of its conductive oxide (Ag_2O). Oxides of most common metals are good electrical insulators and copper powder, for example, becomes a poor conductor after aging. Nickel and copper-based conductive adhesives generally do not have good conductivity stability because they are easily oxidized. Even with antioxidants, copper-based conductive adhesives show an increase in volume resistivity on aging, especially under high-temperature and humidity conditions. Silver-plated copper has been utilized commercially in conductive inks and should also be appreciable as a filler in adhesives. While composites filled with pure silver particles often show improved electrical conductivity when exposed to elevated temperature and humidity or thermal cycling, this is not always the case with silver-plated metals, such as copper flake. Presumably, the application of heat and mechanical energy allows the particles to make more intimate contact in the case of pure silver, but silver-plated copper may have coating discontinuities that allow oxidation/corrosion of the underlying copper and thus reduce electrical paths [4].

4.1.3.2 Particle Shape and Size

The most common morphology of conductive fillers used for ICAs is flake because flakes tend to have a large surface area and more contact spots, and thus more electrical paths than spherical fillers. The particle size of ICA fillers generally ranges from 1 to 20 μm. Larger particles tend to provide the material with a higher electrical conductivity and lower viscosity [16]. A new class of silver particles, porous nano-sized silver particles, has been introduced in ICA formulations [17, 18]. ICAs made with this type of particles exhibited improved mechanical properties, but its electrical conductivity is lower than that of the ICAs filled with silver flakes. In addition, short carbon fibers have been used as conductive fillers in conductive adhesive formulations [19, 20]. However, carbon-based conductive adhesives show much lower electrical conductivity than silver-filled ones.

4.1.3.3 Nano-sized Fillers

Recently, nano-sized fillers including nanowires, nanoparticles, graphenes, and carbon nanotubes (CNTs) have also been introduced into ICA formulations. Quite some research work has been done especially on using silver-based nano-fillers such as Ag nanowires and nanoparticles for ICA

applications. The simplest and the most commonly used bulk solution synthetic method for Ag nanoparticles is the chemical reduction of metal salts (e.g., $AgNO_3$) [21–25]. Ag nanowires are generally prepared using a physical template [26, 27] or a template-less wet chemical process [28, 29]. As an example, Fig. 4.3 shows SEM images of an Ag nanowire, an Ag nanoparticle, and a micron-sized Ag flake.

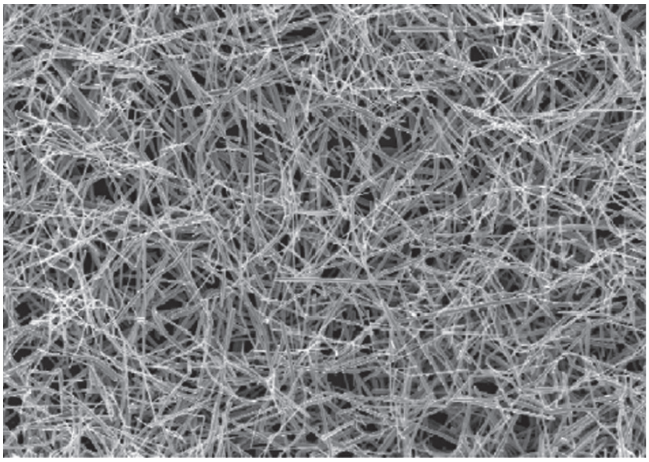

(a)

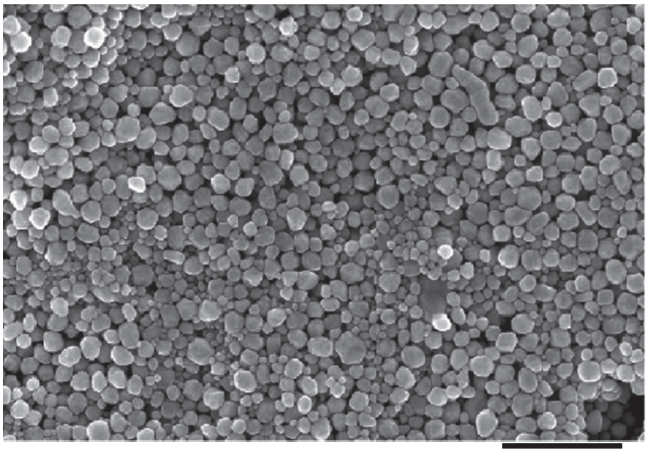

(b)

Fig. 4.3. SEM images of an Ag nanowire (**a**), an Ag nanoparticle (**b**), and a micron-sized Ag flake (**c**)

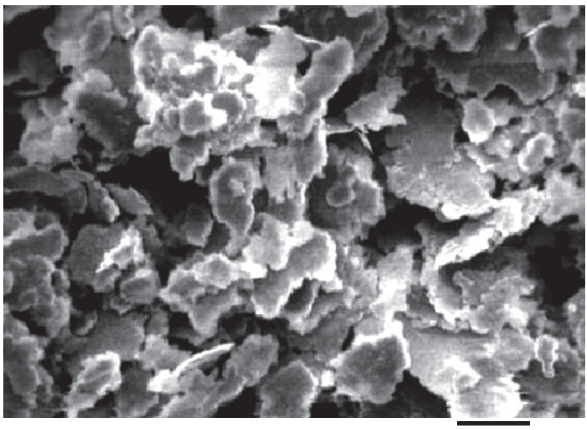

(c)

Fig. 4.3. (Continued)

4.1.3.4 Silver–Copper Fillers

Copper Conductive Fillers

Copper can be a promising candidate for conductive filler metal, due to its low resistivity, low cost, and improved electromigration performance, but oxidation causes this metal to lose its conductivity. Two approaches have been reported for surface treatment and oxidation prevention of copper fillers for ICA application. One is inorganic material coating and the other is organic material coating. For inorganic coating materials, silver, gold, and nickel/gold and solder materials, such as Sn and InSn, are some examples which are coated by electro- or electroless deposition.

For organic coating materials on copper surfaces for oxidation/corrosion protection, self-assembly monolayer (SAM) formation, such as azole or thiol compounds, and organosilicic compound formation are the representatives; however, their thermal stabilities have been the concerns, because most of the coatings lose their effectiveness when exposed to the curing condition of ICAs. Yim et al. [30] reported a Cu-filled ICA by using novel silane coupling agents for oxidation prevention of Cu fillers for conventional ICA applications. In their study, a high performance, low cost, Cu-filled ICA was demonstrated through the use of silane coupling agent and the in situ mixing with a matrix resin. The silane coupling agent was

shown to be very effective in preventing the copper powder oxidation in ICA composite materials, and the improved thermal stability of Cu-filled ICAs was achieved by using the silane coupling agents with aromatic structures. Bulk resistivity of a Cu filled ICA with a silane coupling agent was achieved at 1.28×10^{-3} Ω–cm. They also tried to use of bimodal sized fillers and an optimized concentration of same aromatic silane coupling agent, and a very low bulk resistivity of 7.5×10^{-4} Ω-cm was obtained.

Yokoyama et al. reported a powder with a specific structure as a filler for conductive adhesives in 1992 [31]. The powder particle consists of two metallic components,: copper and silver. Silver is highly concentrated on the particle surface and the concentration gradually decreases from the surface to the inner of the particle, but always contains a small amount of silver. Conductive adhesive paste filled with this powder exhibits excellent oxidation resistance, i.e., can be exposed to 100ppm of oxygen content in a nitrogen atmosphere without oxidation. It also exhibits higher solderability than commercially available copper pastes, sufficient adhesion strength even after heating and/or cooling test, and the least migration, almost the same degree as pure copper paste [31].

4.1.3.5 Low-Melt Fillers

In order to improve electrical and mechanical properties, low melting point alloy fillers have been used in ICA formulations. A conductive filler powder is coated with a low melting point metal. The conductive powder is selected from the group consisting of Au, Cu, Ag, Al, Pd, and Pt. The low melting point metal is selected from the group of fusible metals, such as Bi, In, Sn, Sb, and Zn. The filler particles are coated with the low melting point metal, which can be fused to achieve metallurgical bonding between adjacent particles or between the particles and the bond pads that are joined using the adhesive material [32, 33].

4.2 Processing of ICAs

Isotropically conductive adhesives can be applied using printing (such as stencil, screen, or inkjet printing) and dispensing. Dispensing is a continuous process where individual adhesive dots, lines, or patterns are deposited in selective areas of an interconnect substrate. The main advantage of the dispensing is its flexibility, accommodating a large variety of printed circuit boards or substrate, configurations, and design changes. Selective dispensing is the only approach that can be used once the components have

been assembled onto a board since it does not require a flat surface as does screen or stencil printing.

4.2.1 Screen and Stencil Printing

Screen and stencil printing are both batch processes that are usually less expensive and faster than selective dispensing for large production runs where few changeovers are expected.

Screen and stencil printing are the oldest and widely used processes for applying adhesives. Screen printing has been used for over 40 years in the electronics industry to apply thick film conductors and dielectrics in fabricating circuits on ceramic and organic laminate substrates. Screening printing is also used as a batch process for depositing ICAs to interconnect devices on thin-film and thick-film hybrid microcircuits.

Screen printing is a simple, low-cost process for both small and large production runs. Patterns are formed on a stainless steel mesh through a photosensitive emulsion process in which portion of the screen mesh are coated, while other areas, through which the adhesive is deposited, are left open. The photolithographically formed screen patterns, however, wear out after many runs and the screens must be reprocessed or replaced.

Stencils differ from screens in that the apertures are directly etched or cut into a metal sheet or foil. In both screens and stencil, ICA pastes are squeegeed through apertures on a substrate. The key advantages of stencils over screens, especially the laser cut and electroformed types, is the finer dimensions and smaller pitch dots that can be printed.

Even though stencil printing is widely used for ICAs and has many advantages over dispensing processes, there are several limitations:

1. Tailing or distortion can occur during snap-off.
2. Redeposition occurs on a warped substrate, leading to contamination to the adjacent pads.
3. Tooling change and added changeover time are required for design changes and new designs. Retooling cost is high.
4. Application for very fine-pitch components is limited.
5. Frequent cleaning of stencils is required to avoid clogging, missed dots, and misprints.
6. Long exposure to air and moisture decreases the pot life and increases the viscosity of the adhesive.

Desmulliez et al. demonstrated a sub-100 μm pitch stencil printing process [34]. Perfectly vertical and smooth sidewalls were produced with apertures closely following the resist sidewalls during the electroforming process. The electroforming process generated the desired mechanical

properties of the metal across the whole stencil. Apertures ranging from 1,000 μm down to 20 μm were successfully manufactured in a reproducible manner on a 50 μm nickel foil. An ICA was printed down to 50 μm pitch with reproducible results demonstrated at 90 μm pitch.

4.2.2 Dispensing

Automatic selective dispensing of adhesives includes contact and non-contact types. In the contact type, also known as syringe, needle, or machine dispensing, the adhesive is forced through a small orifice onto the substrate so that the dispensed adhesive dot makes contact with the substrate during dispensing. The adhesive is dispensed using an *x*–*y*–*z* positioning system. The dispensing process can selectively dispense reproducible amounts of adhesives with high accuracy. Multiple small dots, such as 2–5 mils in diameter, can be deposited in selected areas at rates up to 50,000 dots per hour (dph), although typical speeds are approximately 15,000–20,000 dph. These speeds are low compared with stencil printing where 50,000 dots or lines can be printed in 15–20 s.

Dispensing is particularly suitable for printed circuits board or substrate assembly where some components have already been attached. Other advantages of automated dispensing include the following:

1. Ideal for both short runs and production runs.
2. Adhesives can be dispensed on partially assembled boards.
3. Dispensers can handle a wide range of viscosities.
4. No hard tooling required.
5. Minimal setup and changeover times.
6. Less sensitive to board warpage than stencil printing.

Gaugel et al. [35] reported a micro-dispensing system which was able to produce <200 μm dots reproducibly.

4.2.3 Inkjet Printing

Areas for printing very fine-pitch matrix (e.g., very fine-pitch paths, antennas) are very attractive. But there are special requirements for ink-jet printing materials, namely the most important ones are low viscosity and very homogenous structure (like molecular fluid) to avoid sedimentation and separation during the process. Additionally, for electrical conductivity of printed structures, the liquid has to contain conductive particles, with nano-sized dimensions to avoid blocking the printing nozzle and to prevent sedimentation phenomenon. The nano-sized silver seems to be one of the

best candidates for this purpose, especially when its particle size is less than 10 nm.

Inkjet is an accepted technology for dispensing small volumes of material (50–500 picoliters). Currently traditional metal-filled conductive adhesives cannot be processed by ink jetting (due to their relatively high viscosity and the size of filler material particles). The smallest droplet size achievable by traditional dispensing techniques is in the range of 150–50 μm, yielding proportionally larger adhesive dots on the substrate. Electrically conductive inks are available on the market with metal particles (gold or silver) <20 nm suspended in a solvent at 30–50wt%. After deposition, the solvent is eliminated and electrical conductivity is enabled by a high metal ratio in the residue. Some applications include a sintering step. However, these traditional nano-filled inks do not offer an adhesive function [36, 37].

There are many requirements for an inkjettable, Ag particle-filled conductive adhesive. The silver particles must not exceed a maximum size determined by the diameter of the injection needle used. At room temperature, the adhesive should resist sedimentation for at least 8 h, preferably 24 h. A further requirement by the end user on the adhesive's proper-ties was a two-stage curing mechanism. In the first curing step the adhe-sive surface is dried and remains meltable. In this state the product may be stored for several weeks. The second curing step involves gluing the components with the previously applied adhesive. By heating and applying pressure the adhesive is re-melted and cured. Thus the processing opera-tion is similar to that required for soldering. Conductivity in the range of 10^{-4} Ω-cm in the bulk material is required. An adhesive less prone to sedimentation was formulated by using suitable additives. Furthermore the formation of filler agglomerations during deflocculation and storage was reduced. This effect was achieved by making the additives adhere to the filler particle surfaces. This requires a very sensitive balance. If the insula-tion between individual silver particles becomes too strong, overall electri-cal conductivity is significantly reduced.

Jana Kolbe et al. demonstrated feasibility of an inkjettable, isotropically conductive adhesive in the form of a silver-loaded resin with a two-step curing mechanism [38, 39]. In the first step, the adhesive was dispensed (jet-ted) and procured, leaving a "dry" surface. The second step consisted of assembly (wetting of the second part) and final curing. The attainable droplet sizes were in the range of 130 μm, but could be further reduced by using smaller (such as 50 μm or less) and more advanced nozzle shapes.

4.3 Flip Chip Applications Using ICAs

A key factor in achieving a low-cost, flip chip technology is the use of isotropic conductive adhesives. In comparison to the classical FC technologies, the use of ICAs for the bumping and joining provide-numerous advantages (Table 4.2).

Table 4.2. Advantages of flip chip technologies utilizing ICAs

Advantages
Process simplification and reduction of indexing steps by eliminating activation and purification processes
A smaller temperature load on elements and wiring carriers
The availability of a large spectrum of material combinations
A broad range of applicable adhesive systems allows the selection of processing parameters and joining characteristics
Few requirements for under bump metallization (UBM) since alloy phase formation does not have to be considered

4.3.1 ICA Process for Unbumped Chips

Motorola successfully demonstrated an ICA flip chip bumping process using stencil printing technology through both mathematical modeling and experimentation [40]. Both GaAs and Si flip chip devices with Au thin-film metallization and alumina and FR4 chip carriers also with Au metallization were used in this study. The electrical performance of chip and chip carrier combinations (i.e., GaAs/Al_2O_3, GaAs/FR4, and Si/FR4) utilizing conductive adhesive polymer bumps showed no difference from Au and AuSn bumps (all of the flip chip dies are mounted onto the chip carriers using an ICA). However, the ICA joints showed premature failure in HAST and thermal shock tests.

The polymer bumping method is a low-cost and efficient process conducted at the wafer level and suitable for large-scale production. Data of joint resistance stability under accelerated aging conditions such as 85°C/85% relative humidity and temperature cycling demonstrate polymer flip chip interconnections are capable of long-term stability. The polymer flip chip (PFC) assembly is compatible to a large range of rigid carriers, and heat-sensitive, flexible chip carriers, a key advantage of PFC over solder FC technology. Currently PFC is widely used for flip chip bonding on low-cost heat-sensitive chip carriers noted in Table 4.3 [41].

Table 4.3. Low-cost, heat-sensitive chip carriers utilized in polymer flip chip applications

Applications of polymer flip chip bonding
Microcontroller chips on PET substrates
Transponder chips on PVC/ABS/PET/PC/PI foils for smart card inlays
Circuits on flexible systems
Controller and driver circuits on polyester base materials in combination with adhesive-bonded components
Circuits on rigid and multilevel substrates such as FR4 boards or BGA's in combination with SMD components
Temperature sensitive sensors and actuators on most diverse carriers and complex microsystems

4.3.1.1 Flip Chip with Printed ICA Bumps

The PFC process is a stencil printing technology in which an ICA is printed through a metal stencil to form polymer bumps on bond pads of IC devices subsequent to the under bump metallization deposition on aluminum termination pads. The sequential processes to achieve PFC interconnects are UBM deposition, stencil printing an ICA, bump formation (ICA solidification), flip chip attach to achieve electrical connections, and underfill for enhanced mechanical and environmental integrity [40, 42].

UBM Deposition

As with virtually all flip chip processes, the Al bond pads must be protected from the formation of non-conductive aluminum oxide. This insures a low and stable resistance at bond–bond pad interface. The polymer flip chip process utilizes an electroless plating technique, Ni/Au or Pd, to cover the Al bond pads prior to polymer bumping. The typical metal thickness is 0.5–1.0 μm for Pd and 3.0–5.0 μm for Ni/Au.

ICA Printing

The PFC process combines high precision stencil printing techniques with highly conductive ICAs. These polymers can be thermosetting or thermoplastic. First, the polymer bumps are formed by deposition of an ICA through the metal mask directly onto the metallized bond pads on a wafer. Printed conductive adhesive bumps can offer an attractive alternative to the other bumping technologies in terms of low cost and manufacturability. The printing process typically involves a screen or stencil with openings through which bumps are deposited. During the printing process, the paste

is typically dispensed some distance away from the stencil apertures. Typically, the stencil is separated from a substrate by the snap-off distance. The squeegee is lowered, resulting in contact of the stencil to the substrate or wafer surface. As the squeegee moves across the stencil surface, a stable flow pattern develops in the form of a paste roll. The consequent hydrodynamic pressure developed by the squeegee pushes the paste into the patterned stencil openings. The stencil lifts away from the substrate surface with the paste remaining on the substrate.

ICA Bump Curing

The polymer bumps are then either fully cured or partially cured to the so-called B-stage for thermosetting polymer bumps. For thermoplastic polymer bumps, after stencil printing the solvent is removed to form solid bumps. Bump heights are typically 50–75 μm and process can accommodate pitches down to 5 mils. Bump density of up to 80,000 bumps/wafer has been formed with excellent coplanarity.

Once the bumped wafers are diced, chips are picked from the wafers, flipped over, and then placed on and bonded to chip carriers. Different process procedures are utilized to bond thermosetting polymer bumps to similar thermoplastic bumps as noted in Fig. 4.4. Final processing involves a heat cure for thermosetting bumps, while thermoplastic bump connections only require a few seconds under heat and pressure to melt the thermoplastic.

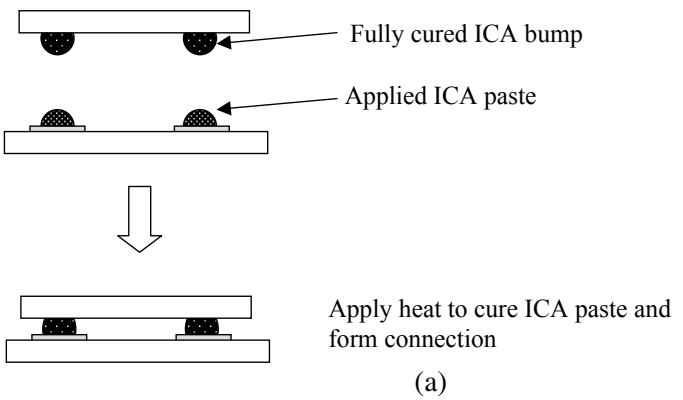

Fig. 4.4. Schematic illustrating various die attachment assembly processes utilizing ICAs. (**a**) Chip with cured ICA bumps mated with uncured ICA on carrier pads, (**b**) chip with partially cured (B-staged) ICA bumps mated with bare carrier pads, and (**c**) chip with thermoplastic ICA bumps mated with bare but preheated carrier pads

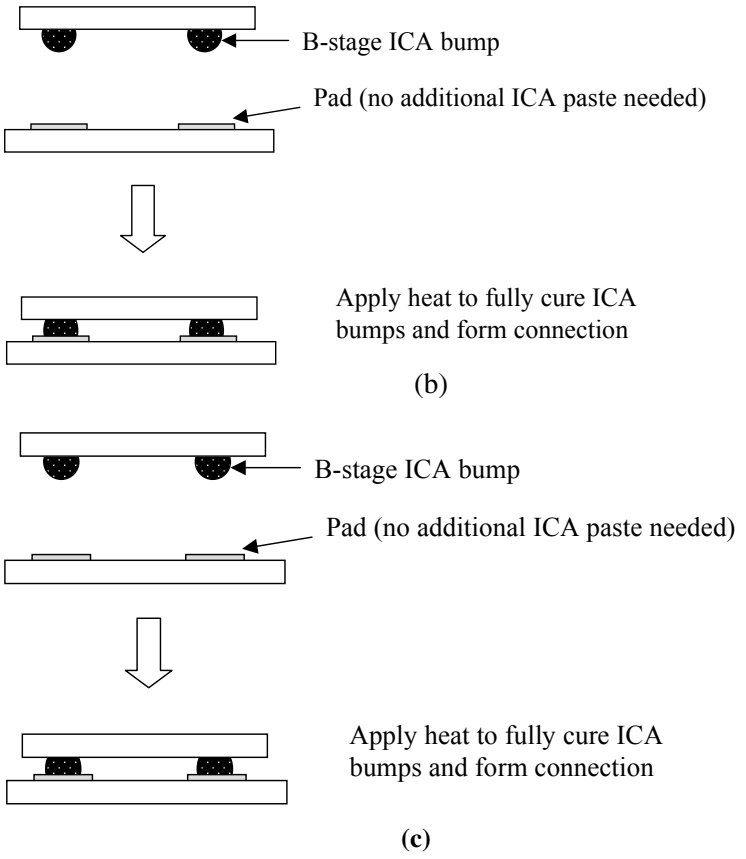

Fig. 4.4. (Continued)

Underfilling

An underfill is then injected into the gap between the chip and the chip carrier and then cured to complete the flip chip process. The function of the underfill, or encapsulation as it is sometimes referred to, is to provide mechanical integrity and environmental protection to a flip chip assembly. Studies have demonstrated that both thermoset and thermoplastic ICAs can offer low initial joint resistances of less than 5 mΩ and stable joint resistances (Au-to-Au flip chip bonding) during all the accelerated reliability

testing. The reliability results have indicated that there is no substantial difference in the performance of thermoset and thermoplastic bumps and both types of polymers offer reliable flip chip electrical interconnections [42].

4.3.1.2 Flip Chip with Micromachined ICA Bumps

Another polymer flip chip bumping process is known as micromachined bumping [43]. The bumping procedure is illustrated in Fig. 4.5. Initially Cr/Au contact metal pads for conductive-polymer bumps are deposited on Si wafers, followed by patterning a thick photoresist to create bump holes. A high aspect ratio and straight sidewall patterns are very important in shaping the conductive-polymer bumps. After the lithography, thermoplastic conductive-polymer materials, usually thermoplastic paste filled with Ag flakes, is applied by either dispensing or screen printing the paste into the bump-hole patterns. The wafer is heated in a convection oven to remove the solvent. Due to the difference in curing conditions between the thick photoresist and the conductive polymer, the photoresist can be carefully stripped to expose the dried polymer bumps. Finally, the wafer is diced into individual chips.

Chips with thermoplastic bumps are placed on chip carriers and preheated to approximately 20°C above the melting point of the polymer causing the bumps to reflow onto the matching chip carrier pads. Mechanical and electrical bonds are established as the chip carrier cools below the polymer melting temperature. To enhance the mechanical bonding strength, a small amount of pressure can be applied by placing a weight on the chip.

This flip chip bonding technique has high potential to replace conventional solder flip chip techniques for sensor and actuator systems, optical micro electromechanical systems (MEMS), optoelectronic multichip modules (OE-MCMs), and electronic system applications.

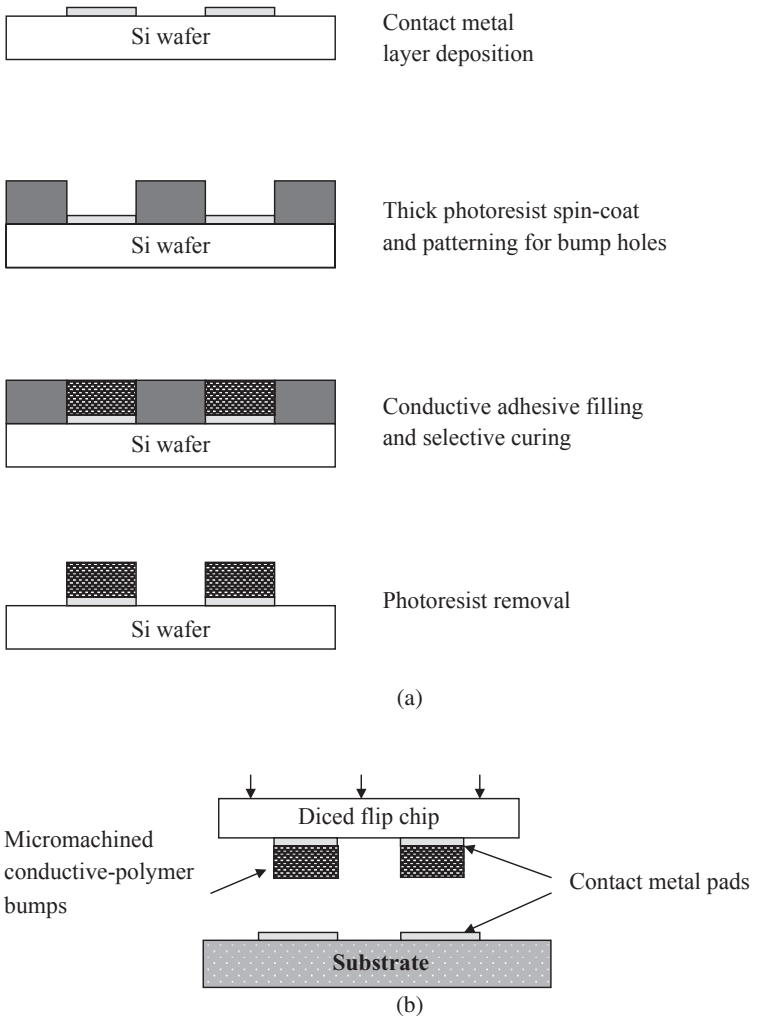

Fig. 4.5. A schematic depicting flip chip application utilizing chips with micromachined polymer bumps. (**a**) Process flow for creating micromachined polymer bumps in the wafer state. (**b**) Die attachment to a chip carrier

Saurabh K. Lohokare et al. [44] recently fabricated conductive adhesive bumps using a similar process, but with some extra polishing steps to make the bump surface flat. Flip chip interconnects formed using this new process offered lower contact resistance as compared to those of the squeegeed

bumps. Furthermore, in order to study the high-speed electrical performance characteristics of these conductive adhesive bumps, a 10-GHz p-i-n photodetector fabricated in the antimonide material system was used, and it was found that the polymer flip chip-integrated detector showed electrical performance of the conductive adhesive bumps comparable to metallic interconnects.

4.3.2 Metal-Bumped Flip Chip Joints

ICAs can also be used to form electrical interconnections with chips that have metal bumps. Isotropic conductive adhesive materials utilize much higher filler loading than ACAs to provide electrical conduction isotropically throughout the material. In order for these materials to be used for flip chip applications, they must be selectively applied to only those areas that are to be electrically interconnected. Also, the materials are not to spread during placement or curing to avoid creating electrical shorts between circuit features. Screen or stencil printing is most commonly used to precisely deposit the ICA pastes. However, to satisfy the scale and accuracy required for flip chip, bonding requires very accurate pattern alignment. To overcome this difficult requirement, Matsushita developed a transfer method [45].

Raised studs or pillars are required on either the die or the chip carrier. Matsushita uses a conventional ball bonder to form Au stud bumps. Bumping is significantly faster than creating complete wire bonds. A ball bumping process eliminates the need for traditional sputtering and plating processes used for standard bump formation. To prevent the bond area from becoming too large, the bumps are formed in a conical shape. The bumps are pressed level by a flat surface, which adjusts both height and planarity. The ICA is selectively transferred on the bump tips by contacting the face of the die to a flat thin film of the ICA which is produced by screen printing and whose transfer thickness is controlled by changing the printed film thickness. Then the die is picked, aligned, and placed on a chip carrier. The whole assembly is exposed to heat to cure the ICA and form connections between the die and the chip carrier. Finally, an underfill (an insulating adhesive) is dispensed between the die and the chip carrier and cured. This method offers the options of oven curing an assembly since bonding pressure is not required. A specially formulated ICA is used to avoid silver migration, containing 20% palladium in a silver palladium alloy. A schematic of the process flow of forming joints with stud-bumped flip chips using ICAs is shown in Fig. 4.6.

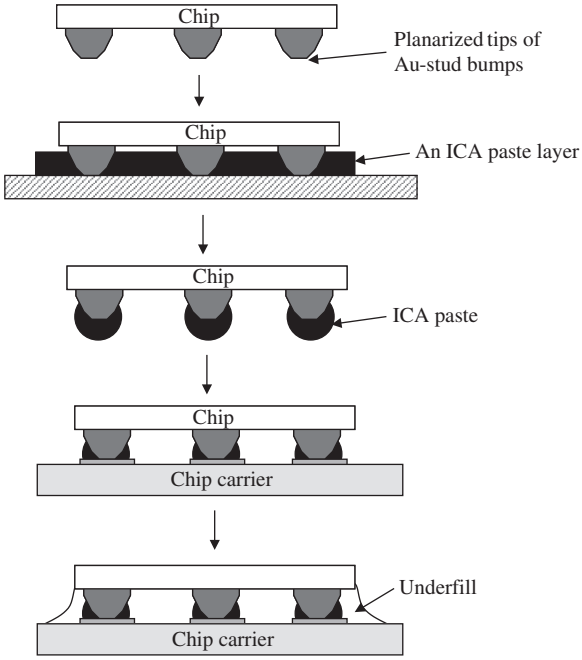

Fig. 4.6. A schematic of the process flow of joints formed with stud-bumped flip-chips using ICAs. (**a**) Tips of the gold stud bumps formed with a wire bond tool are planarized. (**b**) Planarized bumps are dipped into a thin layer of ICA. (**c**) The chip is withdrawn, leaving the bumps coated with ICA. (**d**) The chip is placed on mating pads of a chip carrier with on pressure required during curing. (**e**) An underfill (an insulating adhesive) is dispensed and cured

Another process for bonding a flip chip with metal bumps consists of screen printing an ICA on a chip carrier, aligning and placing the chip, curing the ICA to form bonds, and underfilling. By using this approach, SINTEF Electronics conducted a comparison study between an ICA-bonded and solder-bonded flip chips on FR4 chip carrier with Ni/Au metallization. The number of thermal cycles (–55 to 125°C) to failure for both solder and ICA flip chip circuits was compared. The study showed that stable contacts could be maintained for at least 1,000–2,000 cycles for ICA flip chip joints. This is comparable to the lifetime for solder flip chip joints. However, the variation among ICA samples was very high and optimization of assembly processes is needed in order to achieve more reproducible joint resistance [46].

4.4 ICAs for Surface Mount Applications

Tin–lead solders (Sn–Pb) have been the standard interconnect materials for surface mount technology (SMT) for many years. Recently, electronics industry is becoming lead free. Among the lead-free interconnect materials are electrically conductive adhesives (ECAs) and lead-free solders [47–59]. Compared to soldering technology, ECA technology can offer numerous advantages such as fewer processing steps which reduce processing cost, lower processing temperature, which makes the use of heat-sensitive and low-cost chip carriers possible, and fine-pitch capability [50].

A study of conductive adhesive joining technology on printed circuit boards (PCB) was conducted by RÖRGREN et al. [51]. Six different isotropically conductive, silver-loaded epoxies were evaluated for the surface mount process. These adhesives were used to attach electrically and mechanically 160-lead, 25-mil pitch, quad flat package (QFP) and 0805 chip components on PCB's with flash gold, passivated copper, and tin/lead metallization. The reliability of the conductive adhesive joints was evaluated in two types of environmental test: constant humidity at 60°C and 90% RH for 1,000 h, and temperature cycling for 1,000 h from −40 to 85°C. Under these conditions, both the electrical performance, in terms of contact resistance, surface insulation resistance (SIR), and the mechanical strength of the adhesive bonds were evaluated. The results show that reliable conductive adhesive joining can be achieved for both chip components and QFP components on PCB's with all three metallizations tested. Under well-controlled conditions, and with the right choice of adhesive for the application in mind, no significant increase or variation in electrical resistance during the temperature cycling test was encountered. The humidity exposure test was found to have a minor impact on both contact resistance and adhesion strength of most adhesives tested. In general, there was little difference between the different PCB metallizations used (except for SIR measurements). No evidence of silver migration could be observed after the humidity exposure for any of the adhesives tested.

Radio Frequency Identification (RFID) is quickly gaining a foothold in the identification and security industry. It is used in areas of health care, cashless ticketing system, inventory management, and security identification. Passive RFID tag is made up of a RFID chip, a coil antenna, and the substrate where the chip is attached to the coil antenna. The tag is powered up only when the coil antenna captures the signal from a reader. To produce a RFID tag, the process starts from the foundry processing where a RFID wafer consisting of thousands of complex circuits is produced. This is followed by the tag assembly which consists of the following processes. First the wafer is thinned down where excess silicon is removed using the back grinding process, a mechanical–chemical polishing technique. Next

the RFID dies are singulated from the wafer using mechanical dicing process where a diamond grit-coated blade is used. Once the chips are singulated, the die is attached to the antenna using one of the established assembly methods such as wire bonding or flip chip. Finally it would be packaged to form a complete RFID tag.

However, one critical roadblock that prevents companies in adopting RFID technologies is the manufacturing cost with assembly cost as the main contributing factor. One approach to reduce the assembly cost is using surface mount technology. Currently anisotropic conductive adhesives (ACA) and non-conductive adhesives (NCA) are being used for RFID flip chip assembly. However, these two approaches only permit series assembly which results in longer assembly time as compared to surface mount device using ICA which allows batch screen printing. Isotropic conductive adhesive (ICA) joints, however, are more sensitive to moisture and mechanical stress. Lim et al. [52] utilized an ultra-violet (UV) curable epoxy to encapsulate the chip that had been surface mounted onto the substrate so as to increase the mechanical strength of the ICA and also to reduce the exposure to moisture which degrades the joints. The assembled RFID packages performed well in all the reliability tests including thermal cycling (–40 to 125°C) and 30°C/60%RH, and active tests on detection distance.

4.5 ICAs for CSP Applications

Matsushita Electric Industrial Co., Ltd. developed solderless joining technologies using nickel-filled isotropic conductive adhesives to mount a ceramic chip-scale package (CSP-C) onto a FR4 board [53]. Nickel was selected instead of Ag because, unlike Ag, nickel does not migrate. A significant coefficient of thermal expansion (CTE) mismatch existed between the CSP-C ceramic chip carrier (CTE = 7 ppm/K) and the FR4 organic chip carrier (CTE = 16 ppm/K). This CTE mismatch resulted in large stress to be generated within the solder joints during accelerated thermal cycle (ATC) testing which led to early failure due to solder fatigue. ICAs usually exhibit better thermo-mechanical properties than solders. In addition, metal migration between joints is a great concern because the joints in a CSP area array package are arranged with a close pitch (i.e., in close proximity).

The packaging procedure was as follows: (a) the ICA was screen printed on the area array lands of the FR4 motherboard, (b) the CSP-C was mounted, and (c) the ICA was cured to form bonds. The Ni-filled conductive adhesive demonstrated a much higher resistance to metal migration

compared to Ag-filled ICAs and equivalent to solder joints. Also, the thermal fatigue life of the Ni-filled ICA joints was five times greater than comparable solder joints.

4.6 ICAs for Advanced Packaging Applications

4.6.1 Solar Cell

Thin solar cells are difficult to interconnect with standard soldering techniques. High temperature during soldering introduces stress on the joints and cells. This can cause warping and possible breakage of cells. Substituting soldering for a low-temperature joining technique would avoid building up of mechanical stress, thus increasing process yield and reliability.

A promising alternative technique is interconnection with conductive adhesives. The processing temperature is much lower, depending on the applied adhesive. Eikelboom et al. [54] studied rear-contacted solar cells interconnected with conductive adhesives. The stress on thin cells and joints between traditional soldering and conductive adhesives was compared.

Solar cells generate high currents, requiring low resistances. Long-term stability in outdoor conditions requires excellent optical and mechanical properties. High volume production demands screen printable adhesives. Contacts made on silver-plated substrates with silver plated tabs show excellent electrical properties. Contact resistances are in the milliohm range like soldered contacts.

Samples have been damp/heat tested along with soldered references. After 2,500 h at 85°C/85% humidity, no degradation occurred. Also temperature cycling, between –40°C/and +80°C, on the same samples has shown no effects after 200 cycles. No differences are measured between samples that have been encapsulated and plain samples without encapsulation. Adhesives applied to plain copper tabs or applied to screen printed and fired aluminum give low resistances directly after curing, but show rapid degradation after aging tests due to oxidation and breaking of the adhesive-to-metal bond. Porous screen-printed aluminum also soaks up the adhesive component from the paste giving poor bonding.

4.6.2 Three-Dimensional Stacking

Wire bonding process applies significant mechanical force [55, 56] in order to produce a reliable friction welded connection, often creating latent defects within a conic region of the silicon underneath bonds in die thinned below 75 μm. Wire bond-induced defects can also extend beyond the bonded die itself through underlying die attach materials and into die beneath the originally bonded die within the stack. Reverse loop bonding processes have been developed [57] to mitigate this problem in stacked die packages somewhat, although the same reliability issues often reemerge as die are further thinned below 50 μm. Wire bonding to extremely thin die presents a significant challenge, and an electrical interconnect process that dramatically reduces applied force during application will result in both enhanced yields and superior product reliability over traditional electrical interconnect methodologies.

Andrews et al. [58] demonstrated forming electrical interconnections along the edges of stacked integrated circuits by an extrusion process that utilizes automated needle dispense equipment to form local deposits of conductive adhesive paste. This vertical interconnect process was designed to form three-dimensional circuits without the imposition of significant mechanical forces that are known to cause mechanical damage to thin die or fragile substrate materials. The process was demonstrated with productivity rates that exceed 100 interconnections per minute. Figure 4.7 shows an image of a stack die package with conductive adhesive vertical interconnections. The paste extrusion process utilizes automated needle dispense equipment to produce electrically conductive structures from die to die, or die to substrate, without imposing any significant mechanical forces known to cause damage to extremely thin die or other fragile substrate materials such as GaAs or InGaP. The paste vertical interconnect process is insensitive to die type, die count (up to 128 vertical die have been demonstrated), stacking configuration, or final packaging requirement (e.g., QFN, BGA, WL-CSP).

Significant processing cost advantages were achieved by cycle-time reduction versus traditional wire bond stacked die interconnect, because serial die attach/wire bond process steps are eliminated in favor of a single staging at each process tool regardless of die count. Additional cost advantages were also found due to the elimination of gold (by eliminating the wire bonding process and reducing the gold thickness upon bondable surfaces). Further cost reduction could be achieved by adopting gang vertical interconnect methods, including but not limited to multi-needle dispense and print-based methods.

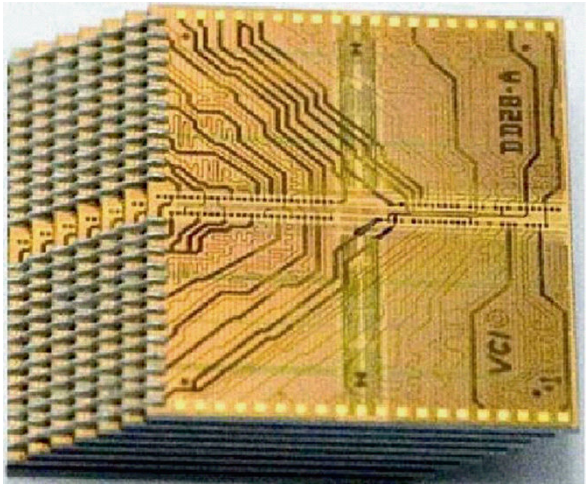

Fig. 4.7. Vertical interconnection formed by a conductive adhesive on Shingle–Tier stack

4.6.3 Microspring

Micromachined springs are attracting attentions in microsystem packaging for low-stress interconnection, high density and low-damage probing for device testing. For instance, new probe cards consisting of micromachined springs are in practical use [59] and essential for high-performance device testing, because their dimensions can easily be smaller than a few hundred micrometers. They are therefore applicable to higher pad density and smaller pad pitch chips, and capable of being effective in a test using high-speed signals above 1 GHz. Curl-up microcantilever spring probes [60] and s-type microspring probes using multilayer electroplating [61] for the probe card applications were reported in the literature.

On the other hand, microsprings may also be required for microelectronic packaging. Flip chip packages, which are utilized for high-performance microsystems, are carried out using the standard interconnect technologies, such as solder balls, gold bumps, and conductive adhesives. However, since their interconnect structures have very limited compliance, thermal expansion mismatches within the packages between the silicon integrated circuit (IC) and the package substrate can cause problems such as failures during thermal cycle testing and damages in low-k dielectrics. To overcome these, Chow et al. experimentally demonstrated that a compliant, low force (10 mgf), pressure contact using thin film microsprings [62] could

make reliable electrical contact to a gold pad [63]. Furthermore, in 0-level MEMS packaging, a commonly applicable cap wafer may need through-hole interconnect vias and microsprings to interconnect the device electrodes.

These microfabricated springs may not be suitable to microsystem packaging, because multiple photolithography procedures cause high production costs. Aiming to fabricate microspring probes without photolithography steps, Itohl et al. utilized an ultra-precise dispenser with three-axis stage system to develop a new three-dimensional microstructure forming method utilizing a continuously repeated dispensing of conductive adhesive pastes [64, 65]. The inner diameter of the nozzle used is 22 μm and the minimum dispense dot size was as small as 22 μm in diameter. High aspect ratio structures were realized by dispensing the paste dots repeatedly. By heating the substrate over 350K, the organic solvent in the paste dispensed on the substrate vaporizes and the viscosity of the paste increases. Taking advantage of this process, overhanging structures such as cantilever shapes were formed when the nozzle was moved in lateral direction as shown in Fig. 4.8. For example, in the case of the cantilever shown in Fig. 4.7b, 20 times dispensing for the post part and 40 times dispensing for the lever part were carried out. The shapes of cantilevers did not change after curing at 423–523K for 30 min. It was found that fabricated microcantilevers have probing resistance lower than 1 Ω with a low contact force of 1 mN. More complicated shapes such as spiral structure shown in Fig. 4.9 were successfully realized by controlling the dispense conditions and the substrate temperature.

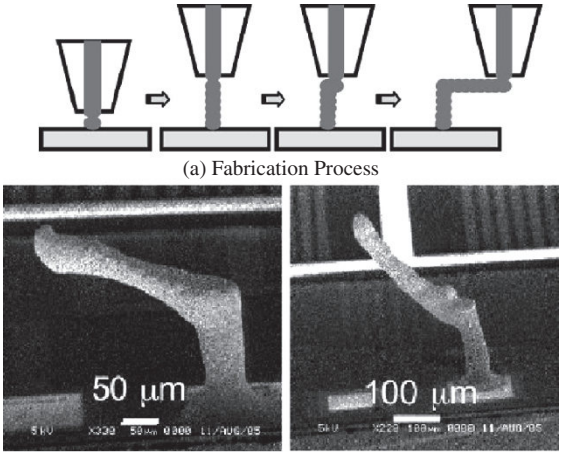

Fig. 4.8. Microcantilever springs fabricated using conductive paste continuous dispensing

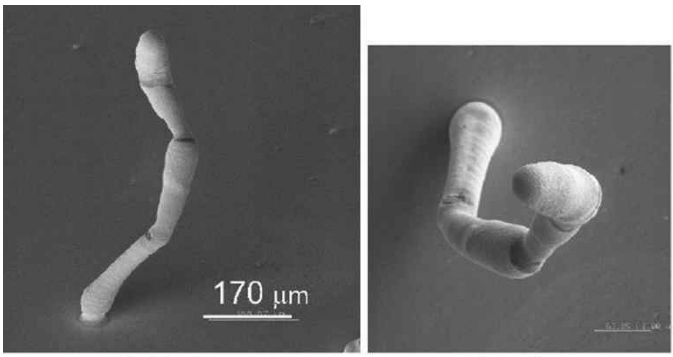

Fig. 4.9. A spiral structure fabricated using conductive adhesive dispensing

4.7 ICAs for Printed Circuit Board Applications

The electronics assembly industry has great interest in high-density PCBs (printed circuit boards) with acceptable costs. One of the key problems for more efficient use of conventionally PCBs is plated through holes (PTH), because they consume a large fraction of PCB surface area. One of the solutions that can save the PCB surface area is to use blind and buried vias in the design. Currently, many expensive plating and sequential lamination steps are needed to create most blind/buried vias. Recently, several new manufacturing technologies of PCBs have been introduced, e.g., ALIVH (any layer inner via hole) which eliminates steps mentioned above [66, 67]. Any layer interstitial via hole structure enables interconnections between any two wiring layers of the board, and thus offers benefits of downsizing, shorter wiring length for high-frequency circuit applications and ease of automatic designing. Moreover, components can be attached under the land, because via holes are filled with conductive paste. This new fabrication process uses laminate-based substrates, where holes are filled with conductive adhesive material to make reliable multilayer interconnects. This technique allows highly space-efficient circuit design and production, but requires using the laminates with special properties, adhesives, and advanced printing technologies. It will be very useful to implement the advantages of ALIVH technology into conventional double-sided PCBs. The idea of such process is based on applying electrically conduc-

tive adhesives for hole filling [68, 79]. The filling of plated through holes has been practiced for many years in order to improve the thermal performance of PCBs, particularly with BGA packages [69]. Other applications of hole-filling procedure include filling vias in inner layers and blind vias in outside layers of PCBs made by SBU (sequential build-up) technology [70]. The main requirements of electrically conductive adhesives for the via filling applications are as follows [69, 71]:

1. low viscosity to facilitate filling high aspect ratio vias (the aspect ratio is defined as a relation of hole depth to hole diameter);
2. stable enough to have a reasonable shelf life;
3. low electrical resistance: no higher than tens of milliohms electrical resistance per via (via depth 0.6 mm, aspect ratio 2:1);
4. adhere well to the walls of through holes;
5. survive reliability tests including soldering shock test, 1,000 thermal cycles of –55 to +125°C, and dump heat tests 85°C/85%RH and;
6. have stable contact resistance in combination with non-noble metals including pure Sn or Sn/Pb alloys.

Suzuki et al. [72] utilized a conductive adhesive with spherical copper powder (with an average particle size of 3–6 μm) to fill the via holes in an ALIVH. Low resistance and good reliability were achieved. Calculation and SEM image suggested the existence of metallic bond between copper particles and between copper particle and copper foil.

Kisiel et al. demonstrated filling mechanically drilled through holes with silver-filled isotropic conductive adhesives [68]. The average filling resistance of holes with a diameter of 0.6 mm and aspect ratio of 2.7:1 was about 150 mΩ. The resistance was stable after five times soldering. By changing the type of adhesives, the fill resistance was decreasing to below 100 mΩ, for the holes diameter 0.5 mm and aspect ratio 2:1 [73]. The additional advantage of applied adhesive in the holes (with a diameter of 0.5 mm) was good average fill resistance stability after 1,000 thermal cycles (–40 to +125°C); resistance changes do not exceed 20%. Unfortunately, the average fill resistance after dump heat test 85°C/85%RH significantly exceeds 100% [74]. However, the resistance of the holes of double-sided PCBs with Au metallization filled by conductive adhesives are in the range or below 50 mΩ per hole and showed stable resistance after dump heat test [75, 76]. Such resistance values can be acceptable by consumer electronic applications.

4.8 High-Frequency Performance of ICA Joints

Only limited work has been conducted to investigate the high-frequency behaviors of ICA joints. Felba et al. [67] investigated a formulation of ICA that performed well as a solder replacement in microwave applications. The study involved in various different adhesive base materials and several types of main (silver flakes, nickel, and graphite) and additional (soot and silver semiflake powder) filler materials. In order to assess the usefulness of a given adhesive formulation, an additional gap in the gold strip of a standard microstrip bandpass filter was made and bridged by an adhesive-bonded silver jumper. Both the quality factor (Q-factor) and the loss factor (L) of the filter with the bonded jumper were measured at a frequency of 3.5 GHz in a preliminary experiment and at 3.5 and 14 GHz in a final experiment. It was determined that silver flake powders are the best filler materials for ICA for microwave applications because ICAs filled with the silver flake powders exhibit the highest Q-factor and lowest loss factor. Also, addition of soot should be avoided since it decreases the quality factor [77].

A study at Georgia Tech was reported where a flip chip test vehicle was mounted on a FR4 chip carrier with a gold-plated copper transmission line [78]. The performance of eutectic Sn–Pb and ICAs was evaluated and compared using this test device. Both ICAs and eutectic Sn–Pb solder were determined to exhibit almost the same behavior at a frequency range of 45 MHz–2 GHz and the measured transmission losses for both materials were minimal. It was also found that the S_{11} characteristics of both Sn–Pb and ICAs after exposure to 85°C/85% relative humidity aging for 150 h did not vary from the signals prior to aging, but S_{12} value of the Sn–Pb joints deviated more than that of ICA joints after the aging.

Recently, Kaoru Hashimoto et al. [79] studied feasibility of the conductive adhesive joints for high-speed signal transmission, both transmission characteristics and power supply ability at the conductive adhesive joints using specially designed interconnection models which consisted of a high– speed CMOS driver LSI, a model BGA package, and a model circuit board. It was found that differential pulse signals could transmit without degradation at 12 Gbps through the eight conductive adhesive joints in daisy chain configuration, and the conductive adhesive joint exhibits waveform degradation in the case of long transition time. This was considered to be caused by its DC resistance which is about 10 times higher than that of the solder joint. However, it showed less waveform degradation in the case of short transition time. This is probably caused by the capacitive coupling interference effect due to proximity arrangement of Ag flakes in the conductive adhesive.

4.9 Reliability of ICA Joints

To date, quite some work has been published demonstrating the usefulness and limitations of isotropic adhesives to bond a variety of surface mount compounds (e.g., QFP) and passive components (R and C) under different aging conditions using various circuit and component metallizations [80]. Most of the isotropic conductive adhesives require noble metallizations (e.g., Au or AgPd) to survive harsh environmental conditions as for instance 85°C/85%RH and temperature cycling from –40 to +125°C. Most of the adhesives give bad results on SnPb surfaces, a few special types show better results in 85°C/85%RH. Deterioration of the electrical properties is due to an increase in the contact resistance. The bulk resistance of the adhesive, although considerably higher than that of solder, usually remains quite constant. On passivated Cu substrates reasonably good results were obtained.

Jon B. Nysæther et al. [81] compared the failure of flip chip on board (FCOB) with solder or ICA joints and with underfill under thermal cycling. The measurements of solder bump lifetime are compared to a lifetime model based on analytical calculations of solder strain. For two filled types of underfill with CTE nearly matched to that of solder, the measured average lifetimes vary from around 2,700 to 5,500 cycles. Measurements of the lifetime of FCOB's with ICA connections have been carried out for two different material systems. The obtained lifetimes vary between approximately 500 and 4,000 cycles. The lifetime seems to be dependent on the properties of the bump on the chip pad. Delamination, for instance at the ICA/bump interface, was found to be an important failure mechanism. The best results (>4,000 cycles) were obtained for 5 μm high Ni/Au bumps.

Aiming to understand the performance of ICA interconnects under fracture and fatigue loading, J. Constable et al. [82] investigated performance of ICA interconnects under fracture and fatigue loading by monitoring resistance changes (micro-ohm sensitivity) of ICA joints during pull and fatigue testing (cyclic loading up to 1,000 cycles). Observation of the fracture surface suggested that the ICA joint life depended upon the adhesive failure of the bond to the metal surface. It was observed that fracture strains for the ICAs were in the range of 20–38%, and resistance remained approximately constant in the elastic region, but the resistance started to increase rapidly as soon as the pull force departed from linear elastic behavior. For fatigue tests, linear displacement was ramped up the preprogrammed maximum displacement and ramped back to the starting position. It was observed that the shear strain for ICA joints surviving 1,000 cyclic loading was typically 10%, which is about an order of magnitude

greater than solders. This suggests that using conductive adhesives may be advantageous for some flip chip applications. It is believed that since silver filler particles of ICAs cannot accommodate this large strain, the silver filler particles must move relative to one another as the epoxy matrix is strained. The most common pattern of resistance change was only increased to a point corresponding to about a 70% loss in interface contact resistance before sudden failure. This was an indication that the interface crack slightly propagated into the adhesive [82].

In an effort to gain a fundamental understanding of the fatigue degradation of ICAs, R. Gomatam et al. [83] studied the behavior of ICA joints under temperature and humidity conditions. The fatigue life decreased at elevated temperature and high humidity conditions. It was also observed that the fatigue life of the ICA joints decreased considerably as the temperature cycle frequency was decreased. This effect was attributed to the fact that as the frequency was decreased, the propagating crack was exposed to higher loads for longer periods of time, effectively resulting in high creep loading [83].

M. Yamashita et al. [84] investigated the interfacial degradation mechanism between Ag-filled ICA and SnPb surface finish at elevated temperatures. It was found that, at 150ºC, the interface degradation was caused by the preferential diffusion of Sn from the plated SnPb layer into the Ag filler in the ICA. Due to this diffusion, Ag–Sn intermetallic compounds were formed on the Ag fillers adjacent to the plating layer, and many large Kirkendall voids were formed in the SnPb plating layer. Also, an interfacial debonding was observed between the ICA and the SnPb plating layer after the heat exposure.

Xu et al. [85] investigated the mechanical behavior of electrically conductive adhesive (ECA) joints exposed to elevated temperature and relative humidity conditions and failure mechanisms of conductive adhesive joints. Three silver-filled, epoxy-based adhesives were used in conjunction with printed circuit board (PCB) substrates with metallizations of Cu/Ni/Au and Cu. Double cantilever beam (DCB) tests were adopted to investigate the effects of environmental aging on ECA joints. This study revealed that conductive adhesives as well as substrate metallizations both play important roles in the durability of conductive adhesive joints. The rate of water attack on the interface of conductive adhesive joints with Cu-plated PCB substrates is faster than for those with Au/Ni/Cu metallization. A possible explanation of this phenomenon was based on considerations of surface free energy and interfacial free energy. The fracture energy of all three ICAs decreased with time under the aging condition. Following drying of the aged conductive adhesive joints, the fracture energy recovered to some extent. This recovery in the fracture energy could be attributed to the reversible effect of plasticization of the bulk adhesives, as well as the re-

gaining of bond strength between the adhesive and the substrate during drying at 150°C. However, the fracture energy of the adhesive joints showed little recovery after the metal surface was oxidized. For ECA/Cu joints, water attack on the adhesive joint may be divided into three phases: displacing the adhesive from the substrate, oxidizing copper, and weakening the copper oxide. At the end of aging, the three ECA/Cu joints exhibited different modes of failure. ECA1/Cu joints failed interfacially along the adhesive/copper oxide interface, while ECA2/Cu joints exhibited the locus of failure within the copper oxide layer. For ECA3/Cu joints, the failure occurred within the secondary layer of the adhesive, which is adjacent to the interface and is a silver-depleted layer. XPS analysis of DCB failure surfaces suggested that diffusion of Cu to the Au surface might have occurred on the Au/Ni/ Cu-plated PCB substrates during aging. Copper oxide was detected on the substrate surface upon exposure of the conductive adhesive joints to the hot/wet environment [85].

S. Kuusiluoma et al. [86] compared the reliability of isotropically conductive adhesive (ICA) attachments on liquid crystal polymer (LCP) substrate to the reliability of lead-free solder (SnAgCu) attachments on same substrate material. The assembled components were similar surface mount components and the reliability was assessed through real-time measurements of contact resistance of each connection. The devices were subjected to two environmental stress tests: a thermal cycle test and a sinusoidal vibration. Results showed that when using LCP as a substrate material, the reliabililty of the device under thermal cyclic stress is somewhat inferior to the reliability of SnAgCu solder. No significant differences could, however, be observed from the vibration test results since none of the assemblies failed in the test. The failure analysis revealed that most failures occurred at the interface between the component lead and the attachment material in both cases, but the test methods need to be developed to make further conclusions.

Ales Duraj et al. [87] investigated the influence of dynamic mechanical load (bending of testing boards) on resistance of the adhesive joints. The load was induced by a definite deflection of testing boards (fiberglass laminated PCB assembled with 1,206 SMD resistors). It was found that the applied dynamic load caused changes of basic electrical parameters of the bonds. The more the deflections applied the more changes of resistance were observed. The increase of joint resistance was not linear and was not same for all tested adhesives.

J. Lee et al. [88] studied the junction resistance variation of Ag epoxy-filled ICAs on Cu and immersion Ag-finished PWB during the 85°C/85% relative humidity aging. It was found that the junction resistances of immersion Ag PWB are lower than those of Cu-finished PWB, and the junction resistance

shift on the immersion Ag PWB was much smaller than those of Cu-finished PWB during the aging.

4.10 Recent Advances on ICAs

4.10.1 Fundamental Understanding of the Lubricant Layer on Ag Flakes

4.10.1.1 Introduction

Silver particles are the most commonly used conductive fillers in current commercial conductive adhesives because they have very high electrical conductivity and, unlike other metal oxide, silver oxide is also highly electrically conductive. In addition, compared with other noble metals such as gold, silver is relatively not expensive. The flake shape is most preferred because silver flakes tend to have more contact points which provide more electrical paths and thus higher electrical conductivity than other shapes such as powders. However, in commercial conductive adhesives, mixtures of flakes, spherical powders, and even nano-size are often used in order to achieve closer pack and better conductivity.

Silver is presently not precipitated as flake or in flake-like form. A patented chemical method describes the reduction of silver nitrate on the surface of tiny droplets of benzaldehyde suspended in an aqueous phase and the production of flake-like particles [89]. However, this method has not been used extensively. Silver flakes are generally made by mechanical milling silver powders [90, 91]. A typical flow diagram of the process of silver flake production is shown in Fig. 4.10.

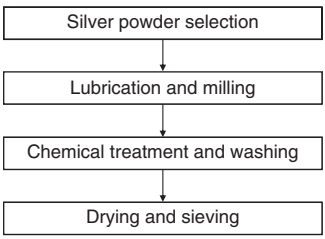

Fig. 4.10. Process of silver flake production

Silver powders are produced by three major methods: chemical precipitation, electrolytic deposition, and atomizing. Chemically precipitated silver powders are normally produced by reducing silver nitrate solutions, in an alkaline medium, with reducing agents such as sugars, aldehydes, hydrazine, and many others. This method typically yields powders with particle ranging from 0.5 to 10 μm. Electrolytic silver powders are deposited cathodically from diluted nitrate or sulfate solutions at high current densities. They are dendritic in nature and range in size from 1.2 to 50 μm. Atomized silver powders are made by disintegration a molten stream of silver with jets of very high velocity water or gas. The gas atomized silver powders are regular spheres and range in size from 5 to 100 μm. There is some difference between the silver powders produced by the above three methods. The chemical purity in general is higher with electrolytic and atomized silver powders, particularly those that have low surface areas. Most silver flakes on the market today are produced from powder made by a chemical precipitation method.

Mechanical flaking and lubrication are two process steps which are combined under one heading because mechanical flaking cannot be done without the addition of a lubricating solution. Batch-type ball mills and attritor mills are frequently used for flaking, although other types such as vibro energy, tumbling, or rod mills could also be used. In most cases the milling medium consists of small glass or metal balls. In any mill type, collisions with the mill wall and the milling media break up the silver powder and flatten it into flakes. Flaking has to be done wet and with lubricants regardless of whether the operation is done in a ball mill, attritor, or any other mill. Silver powders are very mallable, have clean surfaces, and cold weld easily. Dry milling or wet milling without a lubricant would, therefore, always lead to very large welded agglomerates that would not be useful for conductive adhesive applications. The choice of silver powder feed, milling method, weight ratios of silver powder to milling media, and the composition of the lubricant solution provides the ability to produce a wide range of physical properties of the flake product.

After completing the milling process and separating the milling medium, the flakes have to be washed to remove excess lubricant. Washing is accomplished with specific solvents for the chosen lubricant system. For conventional lubricant systems, alcohols or water are usually chosen as washing liquids.

After washing is completed, the wet flake has to be carefully dried at low temperature to prevent caking and sintering (welding). The drying is accomplished in a vacuum drier at slightly elevated temperatures.

4.10.1.2 Lubricant of Silver Flakes

Flaking of silver powder must be done in the presence of an organic lubricant. The conventional lubricants for silver flakes are saturated or unsaturated fatty acids such as stearic, oleic, linoleic, and palmitic acids. After production of silver flakes, a thin layer of lubricant remains on the silver flake surface. This layer of lubricant can affect the viscosity of conductive adhesive paste and other properties such as conductivity. The study conducted by McNeilly et al. showed that the rheological properties of silver-filled conductive adhesives strongly depend on the physical properties of the silver flake [91, 92]. Suspended in the liquid polymer, silver flakes form a three-dimensional network. The rest of the network consists of clusters of flake. The strength, size, and shape of these clusters at equilibrium determine the static viscosity of the adhesives. However, chemical nature of the lubricant layer, the interaction between the lubricant and silver flake surface, effects of this layer on electrical conductivity of ECAs, and thermal decomposition of the lubricants of the Ag flakes are not clear.

Investigation of the Interaction Between Lubricant and Silver Flakes
To study chemical nature of the lubricants on the silver flake and interaction between the lubricant and the silver flake surface, we conducted a study. In this study, a blank silver powder was lubricated with five fatty acids which had similar chemical structures but different carbon–hydrogen chain length (capric acid, lauric acid, myristic acid, palmitic acid, and stearic acid), and the lubricated Ag flakes are called Ag (10), Ag (12), Ag (14), Ag (16), and Ag (18), respectively. Based on SEM study results, it was found that, after lubrication, morphology of the Ag powders changed from spherical powders to flakes. All of the lubricated Ag powders had similar morphology. The SEM photos of the blank Ag powder and one of the lubricated powders, Ag (18) which was lubricated by stearic acid, are shown in Fig. 4.11.

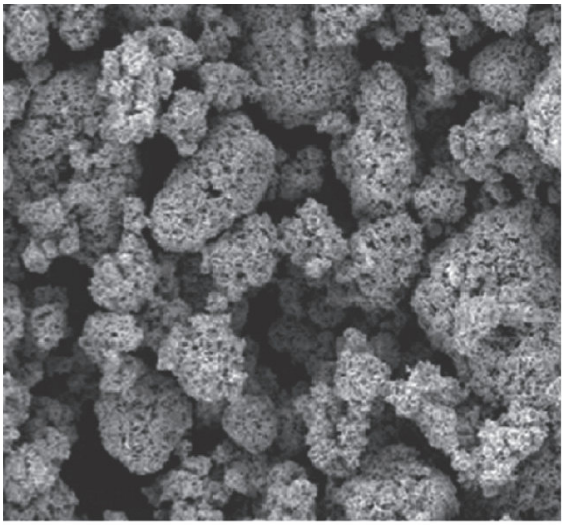

(a)

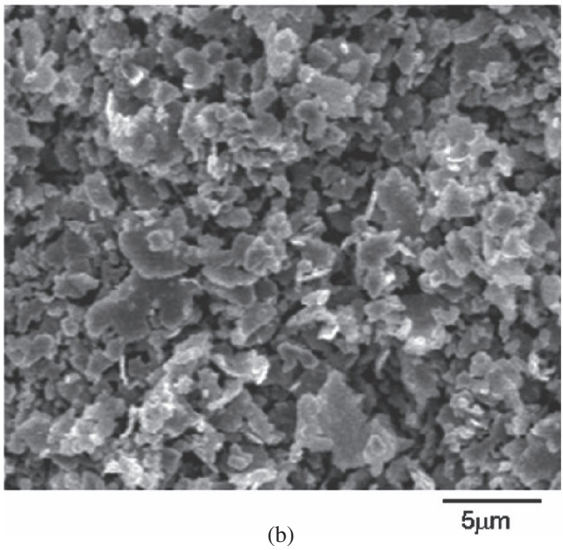

(b)

Fig. 4.11. SEM images of a silver powder (**a**) and the silver flake after lubrication process (**b**)

Thermal Study of the Lubricated Ag Particles

The blank Ag powder and the Ag flakes lubricated with different fatty acids were studied using a DSC in an air purge gas and results are given in Fig. 4.12. As can be seen from the figure, all of the Ag flakes showed two adjacent exothermic DSC peaks, one of which is broad and the other is sharp (at higher temperatures). But the blank Ag powder did not have any DSC peak. Therefore some fatty acid must have remained on the Ag flake surfaces after the lubrication process. However, in the DSC curves of these Ag flakes, there were no endothermic peaks at the temperature range of melting point of each fatty acid. This indicated the lubricant of the Ag flake surface was not in the form of free acid or no longer crystalline. The result suggested there must be some interaction between the fatty acid and the Ag flake. In addition, Ag flakes lubricated with a fatty acid of longer carbon–hydrogen chain showed the exothermic peaks at higher temperatures.

These Ag flakes were also studied by DSC dynamic scan under a nitrogen (N_2) atmosphere. All of them showed the same results: no exothermic peaks. Only the results of the Ag flake, Ag (18), are shown in Fig. 4.13 and compared. Absence of the exothermic DSC peak in nitrogen suggested that the exothermic DSC peaks in air were probably due to oxidation of the organic lubricant on the Ag flake. Weight losses of these lubricated Ag flakes and the blank Ag powder were studied using TG in an air purge gas and weight loss versus temperature is shown in Fig. 4.14. All of the Ag flakes showed much more significant weight losses than the blank Ag powder. This again indicated that some of the lubricant stays on the Ag flake surface after lubrication. The weight loss onset temperature of the Ag flake lubricated with a longer acid was higher (Fig. 4.15).

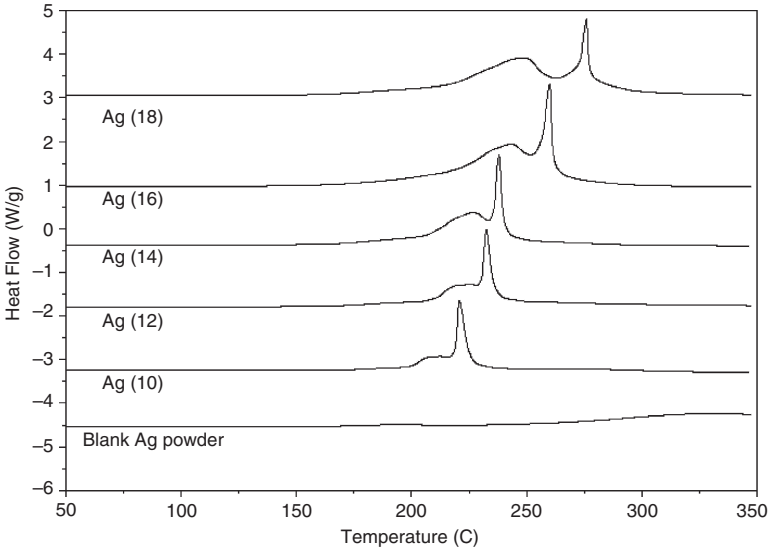

Fig. 4.12. DSC dynamic scans (in air) of a blank Ag powder and Ag flakes lubricated with five fatty acids

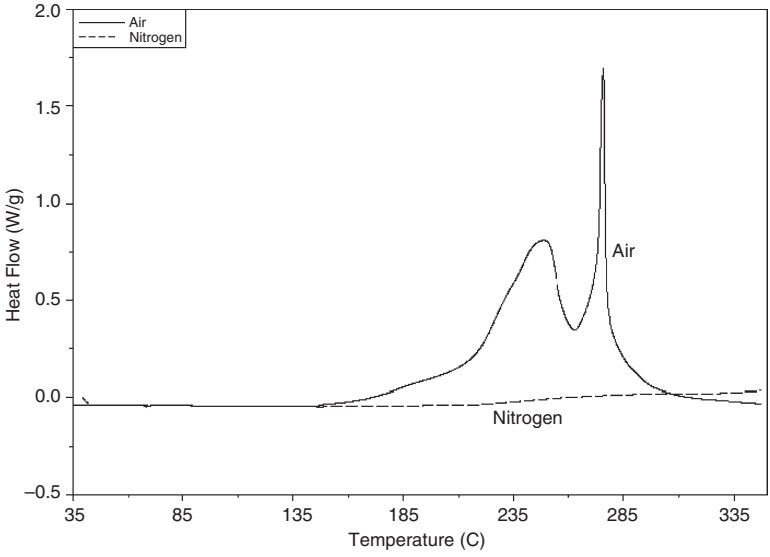

Fig. 4.13. DSC dynamic scans of Ag (18) in N_2 and air

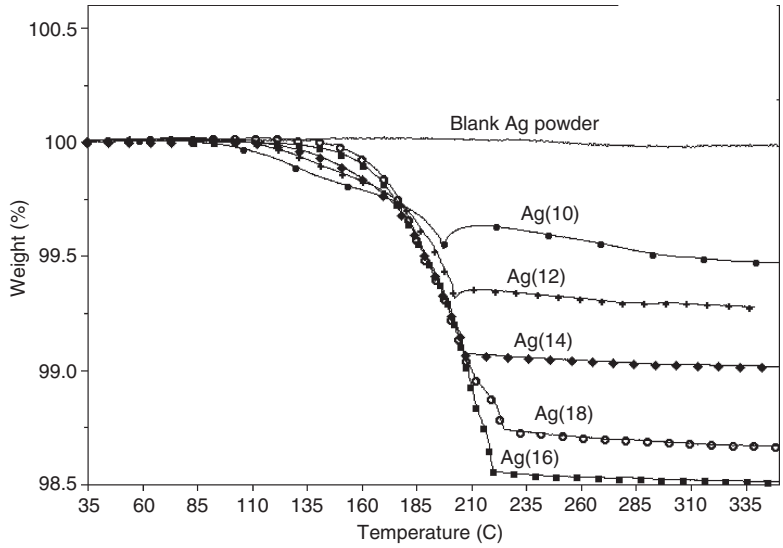

Fig. 4.14. TG dynamic scans of five Ag lubricated Ag flakes and a blank Ag powder

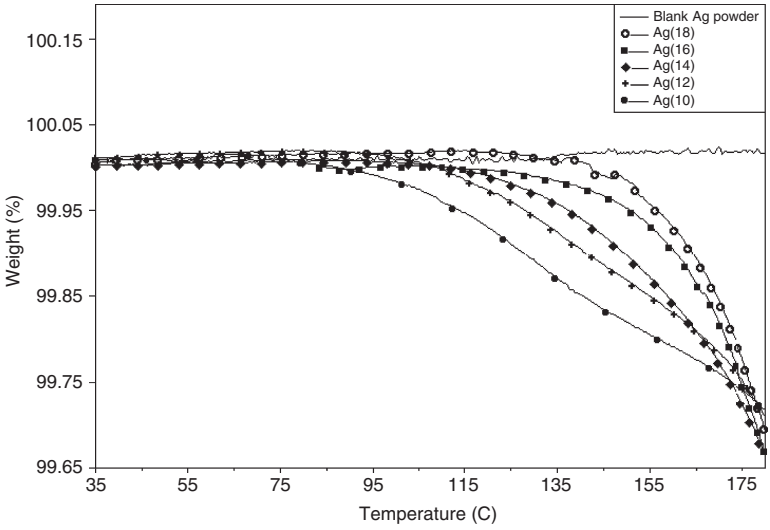

Fig. 4.15. Onsets of TG curves of five lubricated Ag flakes and a blank Ag powder

Diffuse Reflectance Infrared Fourier Transform Spectroscopy (DRIFTS) Study of Lubricated Ag Flakes

Diffuse reflectance infrared is a powerful technique to characterize the chemical nature of organic substances on powder surfaces. All of the lubricated Ag flakes and the original blank Ag powder were studied using DRIFTS. All of the lubricated Ag flakes showed similar DRIFTS spectra, therefore, only one of the Ag flakes, Ag (18), was presented here. For comparison, the DRIFTS spectra of the blank Ag powder and acid 18, stearic acid, were also collected under the same condition. The spectra of these materials are shown in Fig. 4.16. Assignments of peaks of the spectra are given in Table 4.4. The absence of a strong band near 1,700cm^{-1}, which corresponds to the C=O stretching of –COOH group, in the spectrum of Ag (18) indicates that the lubricant layer on Ag (18) was not free stearic acid. The presence of two new near bands at 1,560 and 1,410 cm^{-1}, which correspond to the asymmetric and symmetric stretching of carboxylate group –COO^{-}, respectively [93–95], in the spectrum of Ag (18) suggests that the chemistry between the carboxylic acid head group and the Ag surface yields a full conversion of the acid to a carboxylate salt, Ag stearate.

Table 4.4. Main peak assignments of DRIFTS spectra [93–95]

Chemical	Peak (cm^{-1})	Assignment
Stearic acid	2,800–2,900	C–H stretching
	1,700	C=O stretching in–COOH
	1,460	CH_2 bending
Ag (18)	2,800–2,900	C–H stretching
	1,560	Asymmetric stretching of –COO^{-}
	1,410	Symmetric stretching of –COO^{-}

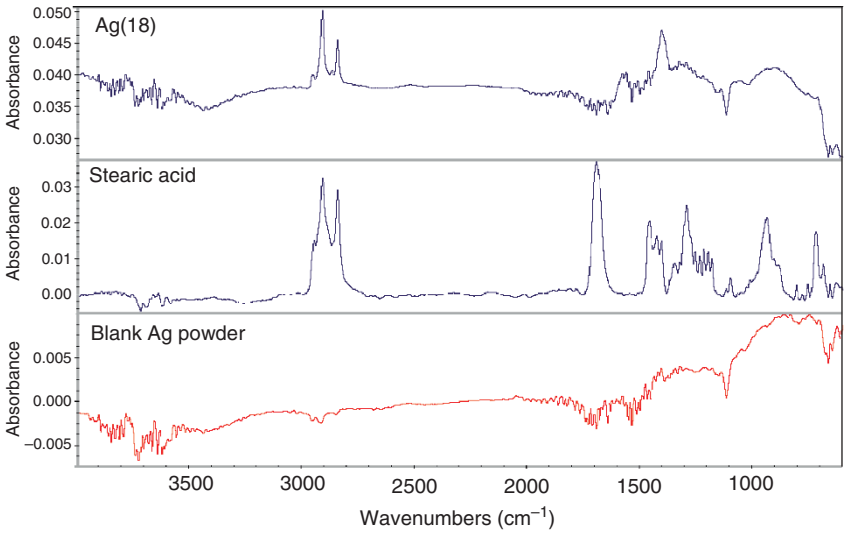

Fig. 4.16. DRIFTS spectra of a blank Ag powder, Ag (18), and stearic acid

Effects of Some Chemicals on Lubricants of Silver Flakes and Conductivity of ECAs

The organic lubricant layer on the silver flake surfaces was an insulator. They might affect electrical conductivity. Therefore, the conductivity should be improved if this lubricant somehow can be in situ removed during the curing of ECAs. One approach to remove the lubricant layer is to use some chemicals which can dissolve or wash away the lubricant layer at the temperature at which the ECA was cured. Therefore, it is of great interest to study some chemicals on the lubricant removal and electrical conductivity of ECAs.

The chemicals employed here include some solvents (methanol, acetone, and tetrahydrofuran) and short-chain acids (acetic acid and adipic acid). A sample of an Ag flake, A, was treated with these chemicals. The treatment is as follows: (i) the Ag flake was mixed with the chemicals or its solution (if it is a solid, e.g., adipic acid), (ii) the mixture was kept at room temperature overnight, (iii) the Ag flake and the chemicals were separated, (iv) the Ag flake was washed three times with a solvent, usually methanol, and (iv) after drying at 25°C and under vacuum, the treated Ag flake was studied by DSC, TGA, and DRIR.

As mentioned in the previous sections, the exothermic DSC peak of the Ag flake is probably due to the oxidation of the lubricant. It was believed that the exothermic peak is due to the oxidation of the long carbon–hydrogen chain residue which was formed after the decarboxylation of the

fatty acid lubricant [96]. Therefore, the peak area (enthalpy, ΔH, J/g) should be directly proportional to the amount of the lubricant on the Ag flake surface and the peak area can be used to estimate semi-quantitatively the relative amount of the organic lubricants present on the Ag flake surface. As for DRIR spectra of the samples, there should be no significant spectral changes after treatment if the chemical has no effect on the lubricant removal.

A Ag flake (Ag A) was treated with HAc and adipic acid methanol solution. From DSC studies, it was found that there are dramatic ΔH changes, 106 J/g for untreated Ag flake, 12 J/g for HAc-treated Ag flake, and 45 J/g for adipic acid-treated Ag flake. Either of the two processes, lubricant removal or lubricant replacement by the acids, might have happened here. If the lubricant was removed by the acids, then ΔH will decrease. If the lubricant was replaced by the short-chain acids, the ΔH also will decrease because oxidation of the short carbon–hydrogen chains of adipic acid or acetic acid will generate much less heat.

The treated Ag flakes were also studied with TGA. The result is given in Fig. 4.17. The weight loss of the Ag flake became smaller after treatment. This result indicates that the acid partially removed or replaced the lubricant and this result is consistent with the above viscosity and DSC results.

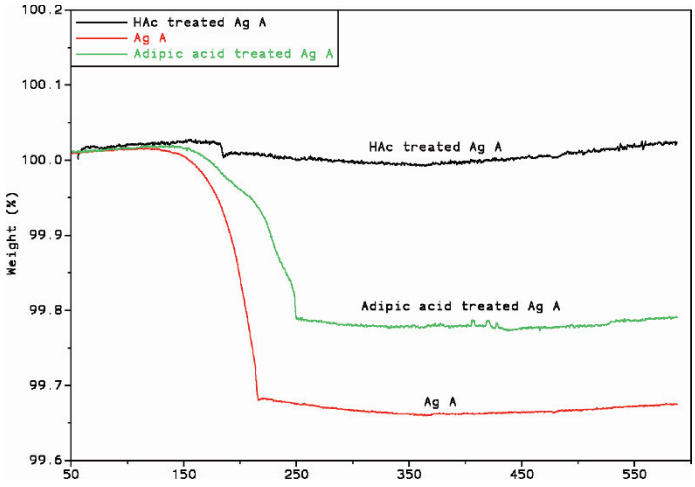

Fig. 4.17. TGA curves of the Ag A before and after treatment

The DRIR spectra of the HAc-treated and adipic acid-treated Ag flakes are shown in Fig. 4.18a, respectively. Compared to the spectrum in

Fig. 4.15, the peaks at ca. 2,800–2,900cm^{1}, which correspond to C–H stretching, disappeared after the acid treatments but other peaks remained. Compared with C–H stretching intensity of the fatty acid, the C–H stretching intensity of adipic acid and HAc is very low. However, the C=O and COO^- stretching intensities of adipic acid and HAc are similar to those of the fatty acid lubricant. If the lubricant was partially removed by the acids, then the intensities of all the peaks should decrease. However, if the lubricant was replaced by the acids, then the C–H stretching intensity will decrease dramatically but the intensities of other peaks should not change much. It seems that above DRIR results can be better explained by lubricant replacement other than lubricant removal.

The effects of these short-chain acids on electrical conductivity of a conductive adhesive were also studied. A small amount (1 part per hundred parts of resin) of the acids was introduced into an ECA formulation. The bulk resistivity of an ECA without acids, the ECA with adipic acid, and the ECA with HAc was measured and compared. The results are shown in Fig. 4.19. As can be seen from the figure, the ECAs with the acids showed lower resistivity, or better conductivity. Compared with the effects of these acids on lubricants of the silver flakes, it can be concluded that the short-chain acids improve the electrical conductivity of an ECA by replacing the long-chain lubricants of silver flake.

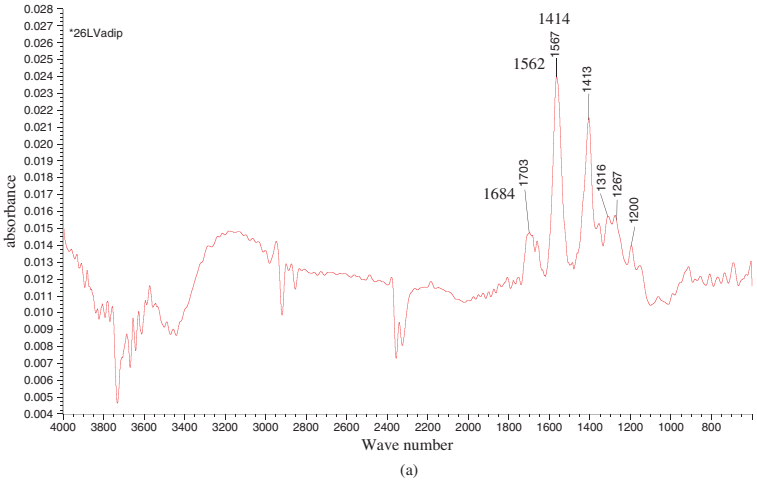

Fig. 4.18. DRIR spectra of HAc-treated (**a**) and adipic acid-treated (**b**) Ag flake A

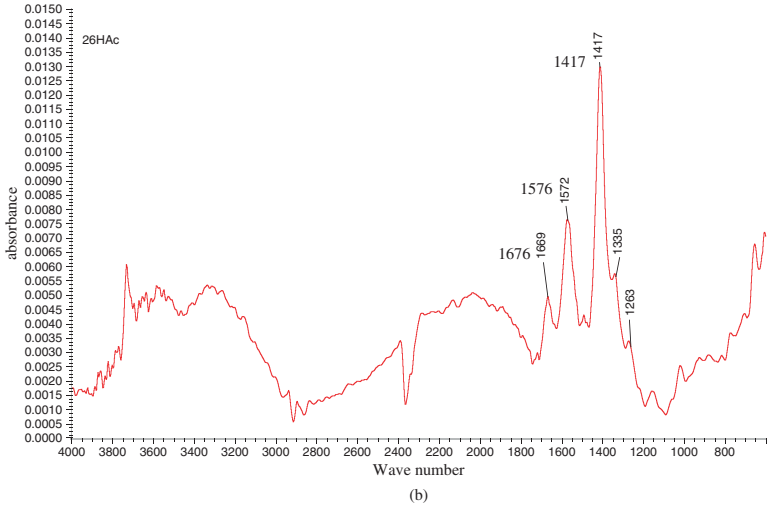

Fig. 4.18. (Continued)

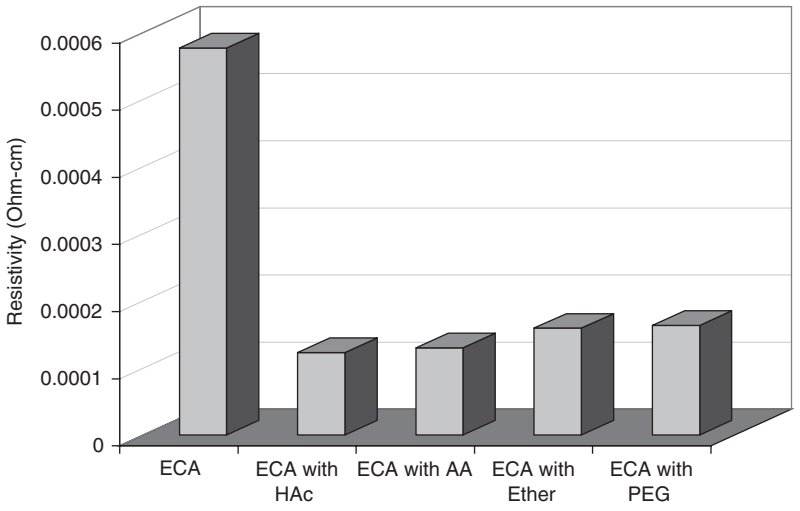

Fig. 4.19. Effects of some chemicals on conductivity of an ICA

In order to confirm that these short-chain acids improve conductivity by removing or replacing the fatty acid lubricants of the silver flake, another experiment was conducted. The HAc-and adipic acid-treated silver flake was used to formulate ECAs. The conductivity of these ECAs was compared to that of the ECA formulated with untreated silver flake. The resistivity of these ECAs is shown in Fig. 4.20. As can be seen from the figure, two ECAs-filled acid-treated silver flake exhibited lower resistivity than the ECA filled untreated silver flake A. The results further confirmed that the short-chain acids could improve electrical conductivity by removing or replacing the fatty acid lubricant of the silver flake surfaces.

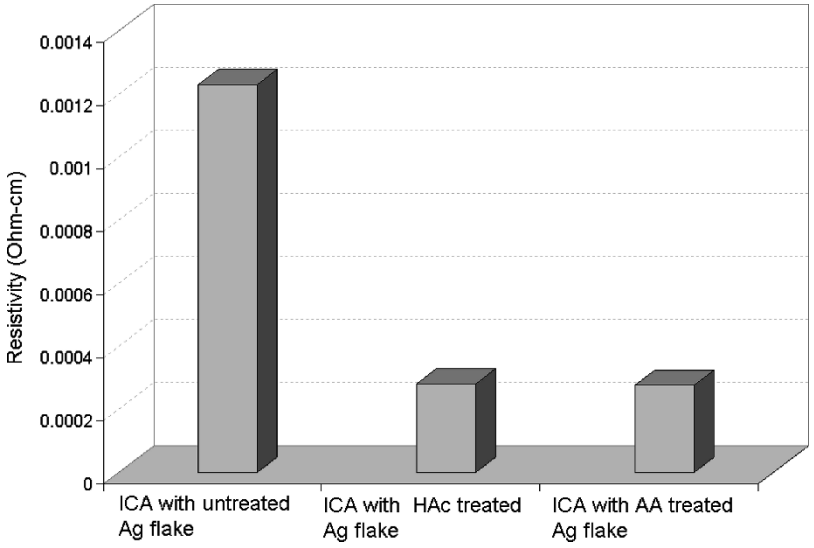

Fig. 4.20. Effects of acids on resistivity of an ICA

Ethers such as diethylene glycol butyl ether (DGBE) and a poly(ethylene glycol) (PEG) with low molecular weight (ca. 200) were used as conductivity promoters [96, 97]. Addition of a small amount of DGBE and PEG to a Ag flake-filled ECA formulation can improve electrical conductivity significantly. However, the reasons for these chemicals' conductivity improvement are still unclear at present.

Effect of these two chemicals on electrical conductivity was confirmed first. An epoxy-based ECA formulation which was filled with the Ag flake was employed in this study. The resistivity of the ECA decreased signifi-

cantly after addition of a small amount (2 parts per 100 resin) of DGBE or PEG (refer to Fig. 4.19).

The Ag flake of the above ECA formulation was treated with the ether and the polyethylene glycol. Then the treated Ag flakes were studied by DSC and DRIR. It was found that DSC peak area changed from 15 J/g (Ag flake E) to 8 J/g (ether-treated Ag flake A) and 4 J/g (PEG-treated Ag flake A), respectively. However, treated Ag flakes showed the same DRIR spectra as the untreated Ag flake. The results suggest that the lubricant was partially removed rather than replaced by the ether and PEG after treatment. Therefore, we believe that the ether and PEG improved conductivity by partially removing the lubricant on the Ag flakes. Another experiment was conducted to confirm this idea. Three ECA formulations which had the same resin formulation were filled with untreated Ag flake A, the ether-treated Ag flake A, and the PEG-treated Ag flake A, respectively. These three ECA's had the same filler loading, 80 w%. After they were cured under the same condition, bulk resistance was measured. The bulk resistivity results are given in Fig. 4.21. As can be seen in this figure, both ECA's-filled ether-treated and PEG-treated Ag flakes had lower resistivity than the ECA filled with untreated Ag flake. This study proved that the ether and the PEG improved conductivity by partially removing the Ag flake lubricant.

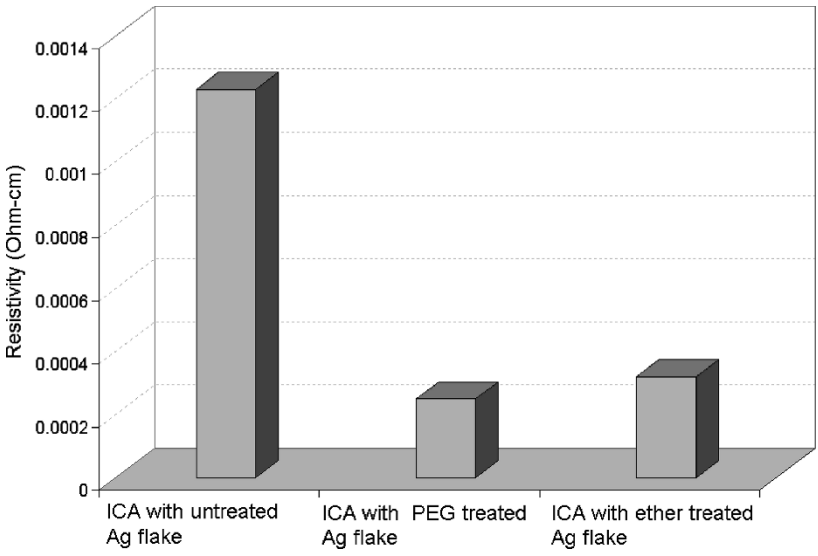

Fig. 4.21. Resistivity of ECAs filled untreated Ag flake C and treated Ag flake

4.10.2 Understanding of Conductivity Mechanism of ICAs

4.10.2.1 Introduction

Isotropic conductive adhesives (ICAs) are composed of insulating polymeric matrix and conductive fillers, generally silver flakes. The properties of composite systems are understood in terms of percolation phenomena; when a sufficient amount of conductive filler is loaded into the insulating matrix, the composite transforms from an insulator to a conductor, the result of continuous linkages of filler particles. As the volume fraction of the conductive filler is increased, the probability of continuity increases until the critical volume fraction, beyond which the electrical conductivity is high and only increases slightly with increasing volume fraction.

Although percolation theory predicts that insulators containing 20 or higher volume percent loadings of dispersed silver particles should be electrically conductive, commercial silver flake-filled epoxy adhesives failed to do so unless subjected to thermal cure and they solidify. According to percolation theory, 25–30 volume percent of a silver flake is used in almost all the isotropic conductive adhesives in order to achieve high conductivity.

However, one interesting phenomenon of ICAs is that these ICA pastes generally have very high bulk resistance but the resistance decreases dramatically after the polymeric matrix is cured and solidified. Before curing, all the silver particles should contact each other and form continuous electrical paths, based on the prediction of percolation theory. What really happens during the cure and solidifying of the ICAs is not clear.

The most popular fillers are silver (Ag) flakes that generally have a thin layer of organic lubricant on their surface to improve their dispersity. In general, conductive adhesive pastes have high resistance before cure. The adhesives can achieve high conductivity after they are cured [96, 98]. However, the conduction mechanism for isotropic conductive adhesive is still not fully understood. It was suggested that the conductivity establishment during thermal cure was the result of removal of the lubricant and that matrix shrinkage did not play a significant role either in the development or in the final value of conductivity [86]. However, there was not enough evidence to support this hypothesis in this chapter. In other literature, the effects of compressive force induced by cure shrinkage on conductivity were also mentioned [99, 100]. Again, no strong evidence was provided.

D. Lu et al. investigated the conductivity establishment mechanism of ICAs [101] by clearly studying the effects of silver flake lubricant and curing shrinkage of the polymeric resin to the conductivity establishment dur-

ing curing. By using the experimental setup (shown in Fig. 4.22), the authors studied the conductivity achievement of ICA's during cure and the silver flake alone used in this ICA. Results are shown in Fig. 4.23. Both samples showed very high resistance before heating. However, their resistance decreased dramatically above certain temperatures (T_{cond}). As can be seen in the figure, the T_{cond} of the Ag flake (230°C) is much higher than that of the adhesive (130°C). These results indicate that the epoxy resin lowered the T_{cond}. T_{cond} of the Ag flake is consistent with the onset of lubricant decomposition of the Ag flake lubricant from our previous DSC study, which is shown in Fig. 4.24. Also, it was found that the Ag particles agglomerated together after heating. This may be caused by the removal of the lubricant on the Ag flake at high temperature. Without any external pressure, Ag flakes can become conductive after the lubricants decomposed.

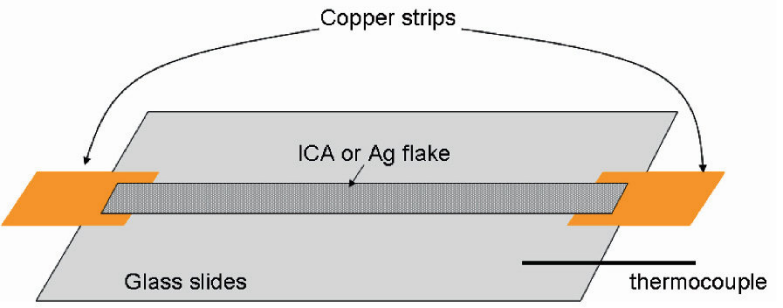

Fig. 4.22. Test device for conductivity establishment during heating

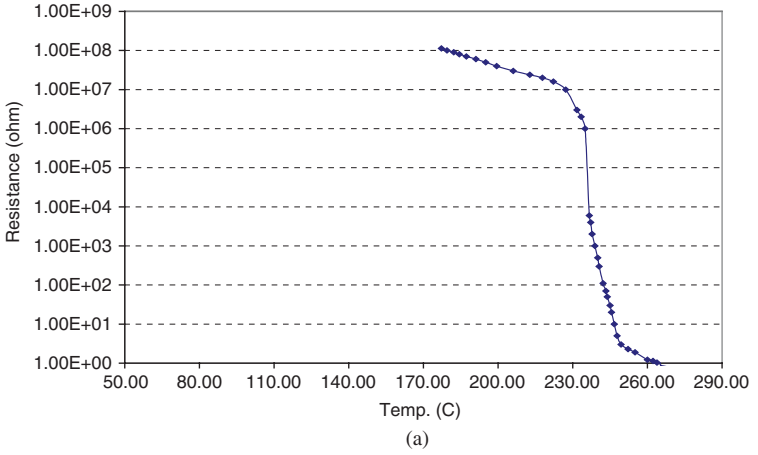

Fig. 4.23. Resistance change during heating of an Ag flake (**a**) and an ICA (**b**)

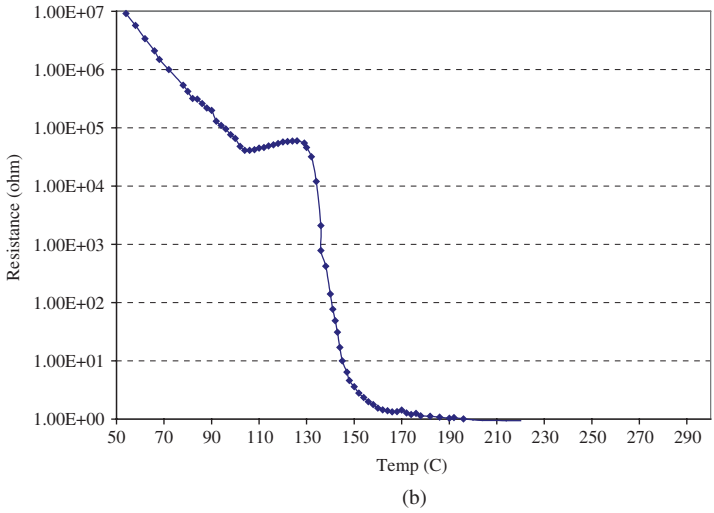

Fig. 4.23. (Continued)

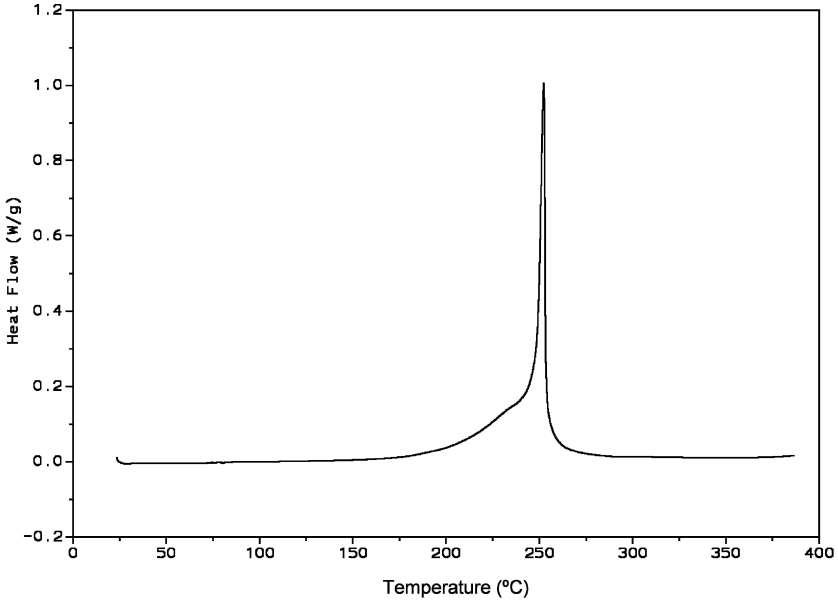

Fig. 4.24. DSC curve of an Ag flake in air

For the ICA, its T_{cond} (130ºC) is much lower than the onset of decomposition temperature of the Ag flake lubricant (approximately 230ºC). Therefore, at the T_{cond} of this ICA, the lubricant certainly did not decompose. The lubricant was either dissolved and/or reacted with the epoxy resin or remained on the Ag flake surface after cure.

During the cure of the ICA, the epoxy resin shrinks. Therefore, the Ag flakes in the adhesive would experience a compressive stress caused by resin shrinkage. This compressive stress would make the Ag flake particles closer and improve adhesive conductivity [99, 100]. The dimension changes with heating of this ICA and the sample holder (microscope cover glass) were studied using a thermo-mechanical analyzer (shown in Fig. 4.25), and the results are shown in Fig. 4.26. From this figure, the cover glass did not have obvious dimension change, but the ICA showed significant dimension decrease (cure shrinkage) at the same temperature range as that of the ICA.

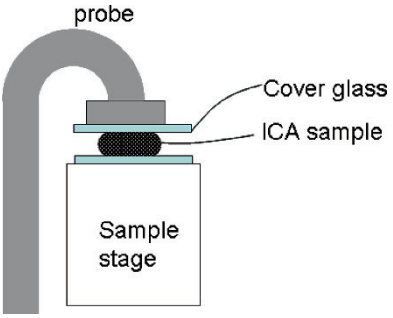

Fig. 4.25. Measurement set-up of dimension change of an ICA during thermal cure

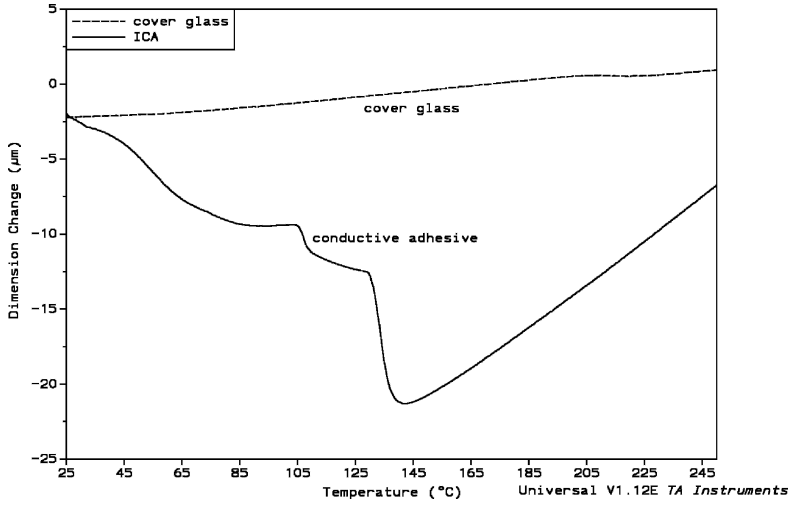

Fig. 4.26. Dimension changes of an ICA measured by using a TMA

This study indicates that resin cure shrinkage plays a very important role during conductivity establishment of a conductive adhesive. However, at this point, the possibility that the dissolution of the Ag flake lubricants by the resin at the T_{cond} of the ICA also causes conductivity development could not be eliminated.

To study the effect of curing shrinkage to the conductive establishment, the authors [101] then studied the conductivity development of Ag powders and ICA pastes with some external pressures using the apparatus shown in Fig. 4.27. A thin layer of insulating organic lubricant resulting from Ag flake production remains on Ag flakes [90,102]. The previous study indicated that this lubricant layer was a salt formed between the fatty acid lubricant and the Ag flake surface. It was believed that the low conductivity of ICA pastes was caused by this layer [96]. Two commercially lubricated Ag flakes (Ag A and B), both of which have lubricants and a Ag powder without lubricant (Ag C), were tested. The results are shown in Fig. 4.28. The Ag particles were packed very loosely in the tube of the test device at the initial stage when they were first placed into the tube. After applying a very small force through the aluminum bars, the Ag particles were packed more densely and low-resistance values were obtained. The resistance decreased only slightly with further increase in external pressures. These tests were done at room temperature; therefore, the lubricants of the Ag flakes were not thermally removed. Also, under these low pressures, the lubricants were not mechanically removed either. The fact that

blank Ag powder (Ag C) showed similar resistance behavior to these two Ag flakes suggests that lubricants do not affect electrical conductivity significantly in this case. Therefore, the conductivity establishments of these Ag particles were the result of intimate contacts between the Ag particles caused by the small external pressures. The results demonstrated that the conductivity of the Ag flakes could be achieved just by applying very small pressures to the material without lubricant removal. The result also implies that adhesive pastes might achieve conductivity just by resin cure shrinkage.

In addition, conductivity establishment of an ICA paste with external pressure was also studied using this test device. It was observed the ICA remained highly insulating with external pressure. This was probably because the ICA paste was not compressible (no shrinkage) and the Ag flakes were not brought closer even though an external pressure was applied. This study further proved that ICA pastes could not become conductive unless the Ag particles are pushed closer together.

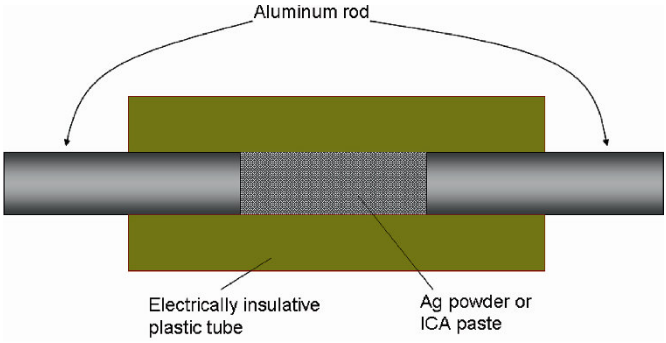

Fig. 4.27. Apparatus for studying conductivity development with external pressures

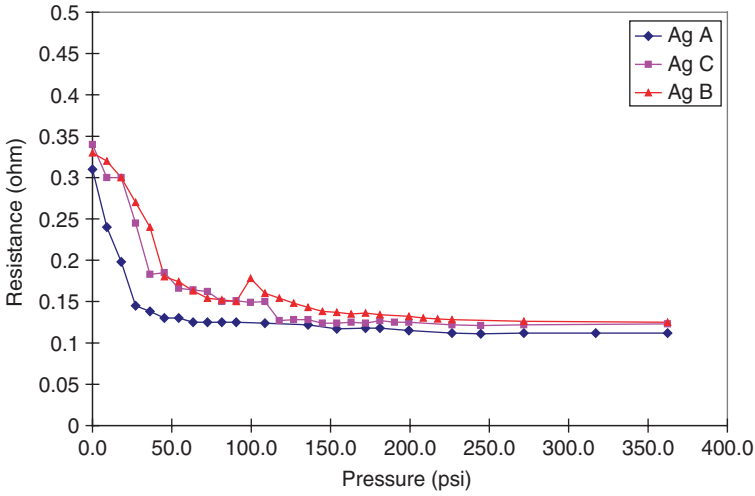

Fig. 4.28. Resistance change of some Ag particles with external pressure

A Ag flake-filled conductive adhesive was cured at 25°C in order to ensure that the lubricant was not thermally removed after cure. The resistivity of the adhesive before cure was beyond the measurement limits of the multimeter. After cure, the resistivity changed to 10^{-3} Ω-cm. Because the ICA was cured at room temperature, the lubricant on the Ag flakes was not thermally removed. Therefore, the conductivity was due to either dissolution of the insulating lubricant layer by the resin or intimate contact between the Ag flakes caused by the resin cure shrinkage.

The shrinkage of the resin part of this adhesive was calculated from the densities of the uncured and cured resin. The densities of the resin before cure and after cure were measured with a gravity bottle. An ether, diethylene glycol butyl ether, was used as the medium in the density measurement of the cured resin. Assuming no significant weight change during the cure of the resin, resin cure shrinkage can be calculated using the following equation:

$$Shrinkage = [(1/d_l - 1/d_s) / d_l\,] \times 100$$

where d_l is the density of the uncured resin and d_s is the density of the cured resin. Based on the above equation, the resin cure shrinkage of this adhesive was 3.42%.

In order to find out if the Ag flake lubricant remained on the Ag flake surfaces after the adhesive was cured at room temperature, another parallel experiment was conducted. Two samples were prepared: one contained the same Ag flake with the epoxy resin and the other contained the Ag flake and 6wt% hardener methanol solution. Methanol was used as a solvent because it would not remove the Ag flake lubricants [94]. The mixtures were kept at room temperature for the same period of time as the cure time of the ICA. Then, the mixtures were washed with tetrahydrofuran (THF) three times to remove the resin and hardener. Previous study showed that THF also did not wash away the lubricants [101]. After drying at room temperature and under vacuum, the recovered Ag flakes were studied by DSC in an air atmosphere and compared with the same Ag flake which was just washed three times with THF. The peak area (ΔH, J/g) of the exothermic peak in the DSC curves of the Ag flakes was used to estimate the amount of the lubricants semi-quantitatively [103]. For each Ag flake, three samples were studied. The average and standard deviation for each of the Ag flakes are given in Table 4.5.

Table 4.5. ΔH values of Ag flakes

Ag flakes	Average ΔH(J/g)	Standard deviation
Recovered from epoxy	50.0	0.4
Recovered from 2E4MZ-CN methanol solution	46.6	0.5
Untreated	48.4	0.8

As can be seen from the above table, ΔH values of the recovered Ag flakes are the same as that of the original Ag flake within experimental error. The result indicates that the Ag flake lubricant was not removed after being exposed to the epoxy or hardener under the cure condition of the ICA, a week at room temperature. The result suggested that the lubricant remained on the Ag flake surfaces after the ICA was cured at room temperature for a week. Therefore, high conductivity of this conductive adhesive was achieved only through resin cure shrinkage. It can be concluded from this experiment that conductivity of ICAs can be achieved just by resin cure shrinkage even though lubricant removal may contribute to the high conductivity [103]. Therefore, lubricant removal is not a prerequisite for conductivity achievement.

In a conductive composite, once filler loading reaches the percolation threshold, a significant number of percolated linkages are formed. Each percolated linkage should be thought as a series of resistors, with each particle and each particle–[particle contact contributing to the total resistance in the linkage. There are two important contributions to the particle–

particle contact resistance: a constriction resistance and a tunneling resistance. Constriction resistance $R_{cr} = \rho_i/d$, where ρ_i is the intrinsic filler resistivity and d is the diameter of the contact spot. For particles with a layer of thin film coated on their surfaces, if the thickness of the film is on the order of 100 Å or less, quantum mechanical tunneling can occur, resulting in lower resistivities [99]. Tunneling resistance $R = \rho_t/a$, where ρ_t is the tunneling resistivity and a is the contact area. The resistivity of the film is not a factor in tunneling, so that organics, polymers, and oxides will have similar tunneling resistivities for similar thicknesses. The dependence of tunneling resistivities on the insulating film thickness can be described by a general tunneling curve (shown in Fig. 4.29) [99]. The particle–particle–contact resistance is the sum of these two separate effects, $R_c = \rho_i/d + \rho_t/a$. In general, the tunneling resistance term dominates R_c.

Before cure, in an ICA formulation, a thin layer of epoxy resin covers each Ag particle surface besides the lubricant layer even though theoretically the particle should contact each other according to percolation theory. Each percolated linkage has high total resistance, and thus the ICA has high resistance before cure. When the ICA cures, the resin shrinks and compresses the particles bringing all the particles closer together. Therefore, the insulating film thickness is decreased, and thus tunneling resistivity decreases dramatically. Also, particle–particle contact area, a, and contact diameter, d, increase after cure. The increases of a and d cause R_{cr} and R_t both to decrease. Therefore, the total contact resistance, R_c, decreases. A schematic explanation is given in Fig. 4.30.

In summary, ICA's become highly conductive only after they are cured and solidified. ICA pastes can achieve high conductivity through resin cure shrinkage alone. Therefore, resin cure shrinkage rather than lubricant removal is the prerequisite for conductivity achievement of ICA's even though lubricant removal may contribute to conductivity. The resin probably compresses and causes Ag flakes to contact more intimately with the resin shrinkage during a thermal cure. The decrease of distance between the flakes caused the dramatic drop of particle–particle contact resistance. Thus, the total resistance of a percolation linkage decreased dramatically during a thermal cure.

In order to eliminate the effect of lubricant and elucidate the effects of shrinkage on conductivity, a blank Ag powder without lubricant was used in this study. A trifunctional epoxy was employed to vary the cross-linking density and shrinkage of ICA formulations. Three ICAs were formulated with above three resin formulations and the blank Ag powder (filler loading was 70w%). Bulk resistance of these ICAs after cure was measured and compared. Cross-linking density, cure shrinkage, and bulk resistivity of these three ICAs are given in Table 4.6. As can be seen from the table, formulations with higher cross-linking density had higher cure shrinkage

and lower resistivity [95]. Because there is no lubricant on the Ag particles, the bulk resistance difference was only due to the different cure shrinkage of these samples.

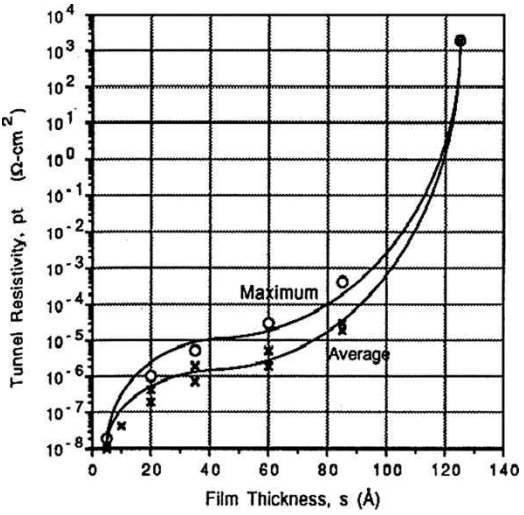

Fig. 4.29. Tunnel resistivity for thin films as a function of film thickness [99]

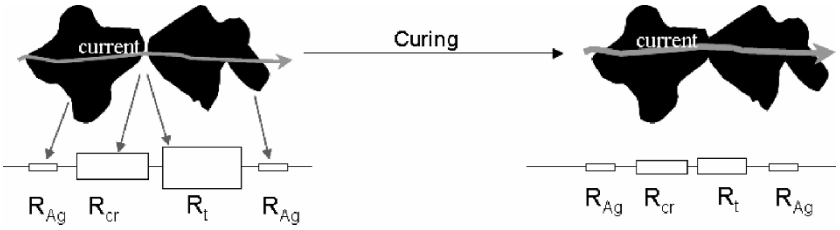

Fig. 4.30. Change of a particle–particle contact resistance due to the more intimate contact between two Ag flakes caused by shrinkage of the polymeric matrix (R_{Ag}–bulk resistance of Ag)

Table 4.6. Cross-linking density, cure shrinkage, and volume resistivity of three ICA formulations

Formulation	Cross-linking density (10^{-3}mol/cm^3)	Shrinkage (%)	Bulk resistivity (mΩ-cm)
ICA1	4.50	2.98	3.0
ICA2	5.33	3.75	1.2
ICA3	5.85	4.33	0.58

4.10.3 Improvement of Electrical Conductivity of ICAs

Electrical conductivity of ICAs is inferior to solders [95]. Even though the conductivity of ICAs is adequate for most applications, a higher electrical conductivity of ICAs is still needed. To develop a novel ICA for modern electronic interconnect applications, a thorough understanding of the materials is required.

4.10.3.1 Silver Flake Lubrication Removal

The lubricant layer on a silver flake of an ICA plays an important role in the performance of ICAs, including the dispersion of Ag flakes in adhesives and the rheology of the adhesive formulations [90, 104–107]. The organic layer consists of a Ag salt formed between the Ag surface and the lubricant, which typically is a fatty acid such as stearic acid [102, 103]. This lubricant layer affects the conductivity of an ICA because it is electrically insulating [103, 106]. To improve conductivity, the organic lubricant layer must be partially or fully removed through the use of chemical substances that can dissolve the organic lubricant layer [96, 103, 104]. However, the viscosity of an ICA paste may increase if the lubricant layer is removed. An ideal chemical substance (or lubricant remover) should be latent (does not remove the lubricant layer) at room temperature, but be active (capable of removing the lubricant layer) at a temperature slightly below the cure temperature of the polymer binder. The lubricant remover can be a solid short-chain acid, a high boiling point ether such as diethylene glycol monobutyl ether or diethylene glycol monoethyl ether acetate, and a polyethylene glycol with a low molecular weight [96, 103]. These chemical substances can improve electrical conductivity of ICAs by removing the lubricant layer on the Ag flake surfaces and providing an intimate flake-flake contact [101,103].

4.10.3.2 Increase Shrinkage

In general, ICA pastes exhibit low electrical conductivity before cure, but the conductivity increases dramatically after they are cured. ICAs achieve electrical conductivity during the cure process, mainly through a more intimate contact between Ag flakes caused by the shrinkage of polymer binder [101]. Accordingly, ICAs with high cure shrinkage generally exhibit the best conductivity. Therefore, increasing the cure shrinkage of a polymer binder is another method for improving electrical conductivity. For ICAs based on epoxy resins, a small amount of a multifunctional epoxy resin can be added into the formulation to increase cross-linking density, shrinkage, and thus increase conductivity [101].

4.10.3.3 Transient Liquid Phase Fillers

Another approach for improving electrical conductivity is to incorporate transient liquid-phase sintering metallic fillers into ICA formulations. The filler used is a mixture of a high melting point metal powder (such as Cu) and a low melting point alloy powder (such as Sn–Pb). Upon reaching its melting point, the low melt point powder liquefies dissolving the high melting point particles. The liquid exists only for a short period of time and then forms an alloy and solidifies. The electrical conductivity is established through a plurality of metallurgical connections formed in situ from these two powders in a polymer binder. The polymer binder fluxes both the metal powders and the metals to be joined and facilitates the transient liquid bonding of the powders to form a stable metallurgical network for electrical conduction, and also forms an interpenetrating polymer network providing adhesion. High electrical conductivity can be achieved using this method [101, 107–109]. The ICA joints formed include metallurgical alloying to the junctions as well as within the adhesive itself. This provides a stable electrical connection during elevated temperature and humidity aging. In addition, the ICA joints showed good impact strength due to the metallurgical interconnection between the conductive adhesive and the components. One critical limitation of this technology is that the numbers of combinations of low-melt and high-melt fillers are limited. Only certain combinations of metallic fillers that are mutually soluble exist to form this type of metallurgical interconnections.

4.10.3.4 Incorporation of Reducing Agent in Conductive Adhesives

Another approach to improve the conductivity of Ag-filled ICA is the incorporation of reducing agents [110]. Even if the silver oxide showed much better conductivity than most of the other metal oxides which are basically insulative, the conductivity of silver oxide is still inferior to metal itself. Therefore, incorporation of reducing agents would further improve the electrical conductivity of ICAs. Aldehydes were introduced into a typical ICA formulation and obviously improved conductivity was achieved due to reaction between aldehydes and silver oxides that exist on the surface of metal fillers in ECAs during the curing process (Equation 4.1).

$$R–CHO+Ag_2O \rightarrow R–COOH+2Ag \qquad (4.1)$$

The oxidation product of aldehydes, carboxylic acids, which are stronger acids and have shorter molecular length than stearic acid, can also partially replace or remove the stearic acid on Ag flakes and contribute to the improved electrical conductivity.

4.10.4 Mechanism Underlying Unstable Contact Resistance of ICA Joints

Electrically conductive adhesives (ECAs) are an environmentally friendly alternative to lead-bearing solders. ECAs are superior to their counterpart, eutectic Sn/Pb solders, in many respects, including reduced environmental impact, improved processing characteristics, and increased resistance of thermal fatigue [6, 50, 111, 112]. However, compared to the mature soldering technology, conductive adhesive technology still has limitations and concerns that greatly hinder its wide application. One critical limitation of current commercial ECAs is that contact resistance between the ECAs and the nonnoble metal surfaces increases significantly during high temperature and high humidity aging, particularly 85°C/85% relative humidity (RH) aging. It is commonly accepted that metal oxide formation at the interface between the ECA and the non-noble metal surface is responsible for the contact resistance shift [98, 112–115]. Oxides such as Cu oxide and Pb oxide were found at the interfaces between ECAs and Cu and Sn/Pb-finished components, respectively, after 85°C/85%RH aging [116]. Two mechanisms, simple oxidation and galvanic corrosion, both of which can

cause the formation of metal oxide, were suggested as the possible mechanisms behind the unstable contact resistance phenomenon [49, 111, 117, 118]. Since oxidation and galvanic corrosion are two different processes, different approaches should be employed to prevent them. Therefore, in order to stabilize contact resistance by preventing metal oxide formation, it is essential to identify the dominant mechanism for the metal oxide formation and for the contact resistance shift. However, no prior work has been conducted to identify the main mechanism underlying the contact resistance shift phenomenon, and no prior study has been conclusive. In this study, a series of experiments were carefully designed to differentiate these two mechanisms and to elucidate the dominant one responsible for metal oxide formation and contact resistance shift.

Even though above investigations did not show consistent results, they did indicate one important issue: contact resistance increase is mainly due to the oxide formation at the interface of conductive adhesives and non-noble metals. However, there are two possible mechanisms which can cause oxide formation: simple oxidation and electrochemical corrosion of the non-noble metals.

A brief introduction about oxidation and electrochemical corrosion, especially galvanic corrosion, is given here. Oxidation is a reaction between a material (metals in this case) and oxygen. It can happen under both dry and wet conditions and generally at high temperatures. However, a galvanic corrosion process will happen only when the following conditions are met: (1) two metals which have different electrochemical potentials are present and connected, (2) an aqueous phase with electrolyte exists, and (3) one of the two metals has electrochemical potential lower than the potential of the reaction ($H_2O + 4e^- + O_2 = 4\ OH^{\bullet}$), which is 0.4 V under the standard condition. When two different metals contact under a wet condition, a galvanic corrosion (electrochemical corrosion) occurs. The less noble metal (with an electrochemical potential less than 0.4 V) acts as an anode and loses electrons. The anode metal becomes ions ($M \bullet ne^- = M^{n+}$) and dissolves in the aqueous medium. The noble metal (with higher electrochemical potential) acts as a cathode and, under many conditions, the reaction on this electrode is generally $H_2O - 4e^{\bullet} - O_2 = 4\ OH^{\bullet}$. In this mechanism, oxygen is also involved in the reaction but not directly reacted with the anode metal. The metal ion M^{n-} will combine with the OH^- and form a metal hydroxide which is usually unstable and becomes a metal oxide. Therefore, electrochemical corrosion can only occur under wet condition between two different metals. Theoretically, if only metal is involved or if under a dry condition, galvanic corrosion is insignificant.

Clearly simple oxidation and electrochemical corrosion are two different processes. In order to prevent the oxide formation at the interface between an ECA and non-noble metals, it is of critical importance to differentiate

these two mechanisms and elucidate which one mechanism is the dominant one. No prior work has been done to elucidate the main mechanism and no prior work has been conclusive.

4.10.4.1 Contact Resistance Shift Phenomenon

The total contact resistance of an ICA joint consists of the bulk resistance of the ICA material (R_{bulk}), and the interfacial resistance (R_{int}.) between the ICA and the metal (refer to Fig. 4.31). The change of bulk resistance of an ICA material during aging was studied first.

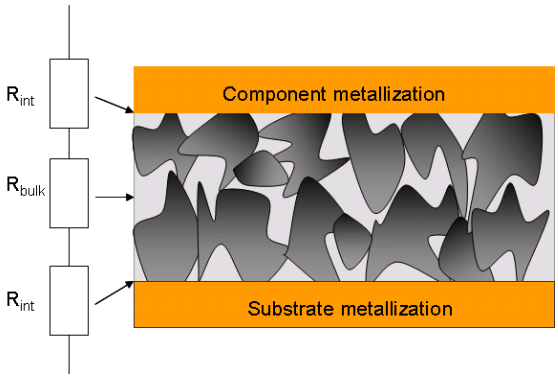

Fig. 4.31. The contact resistance of an ICA joint

Bulk resistance shifts of five commercial conductive adhesives (ECA-1, ECA-2, ECA-3, ECA-4, ECA-5) during 85°C/85%RH aging were studied and results are shown in Fig. 4.32. All of the five ECAs are silver flake-filled and epoxy-based conductive adhesives and are from four different manufacturers. As can be seen from this figure, bulk resistance of all the ECAs decreased slightly in the early stage of the aging and remained stable thereafter. The initial decrease of bulk resistance may be due to further cure of the ECAs. The bulk resistance of silver-filled ECAs did not change during aging because silver flakes are not susceptible to oxidize or corrode and silver oxide is still electrically conductive even after silver is oxidized. It can be concluded from this study that a conductive adhesive showed stable bulk resistance during an elevated temperature and humidity aging as long as the ECA was filled with silver flakes. In other words, silver flake-filled conductive adhesives have stable bulk resistance during aging.

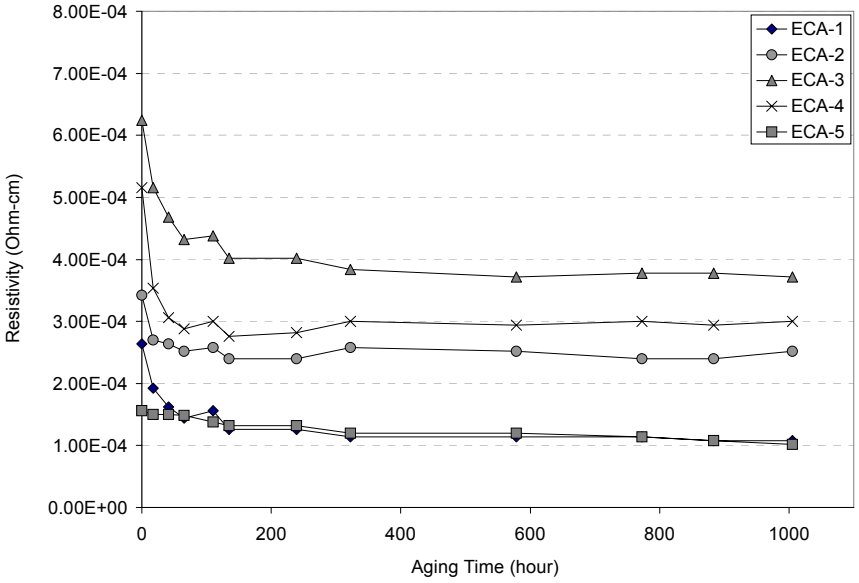

Fig. 4.32. Bulk resistance shifts of ECAs during aging

Contact resistance was measured using an in-house test vehicle shown in Fig. 4.33. It consists of metal wire segments (about 1 cm long) that are separated by approximately 1 mm gaps. The metal wires were used here to simulate the metallization of printed circuit board and surface finish of surface mount components. Conductive adhesive pastes were applied to the gaps to connect all the metal wire segments. After cure, the total contact resistance of a specimen was then measured.

Above five commercial conductive adhesives were also used in this study. Contact resistance between these ECAs with different metal wires was studied with the contact resistance test device described in previous section. Shifts of the contact resistance during 85° C /85%RH aging were recorded. After 500-h aging, if the increase of the contact resistance is larger than 20%, the contact resistance is defined as "unstable." But if the increase is less than 20% after 500-h aging, the contact resistance is considered as "stable" [118]. It was found that all five ECAs exhibited the same trend of contact resistance change during aging. As an example, results of only one of those ECAs are given in Table 4.7. As can be seen from the table, this ECA showed stable contact resistance on noble metals Ag, Pt, and Au but showed significant contact resistance shifts on non-noble metals Ni, Sn, and Sn/Pb. The results are consistent with those from other researchers, which indicate that our in-house test vehicle is valid and reliable [113, 115, 116].

The fact that bulk resistance of all these ECAs remained stable and contact resistance of these ECAs on non-noble metals increased during aging indicated that the contact resistance increase was caused by the increase of the interfacial resistance ($R_{int.}$) between the ECA and the metal. Therefore, the main task in this section is to elucidate the reasons for the increase of $R_{int.}$ during aging.

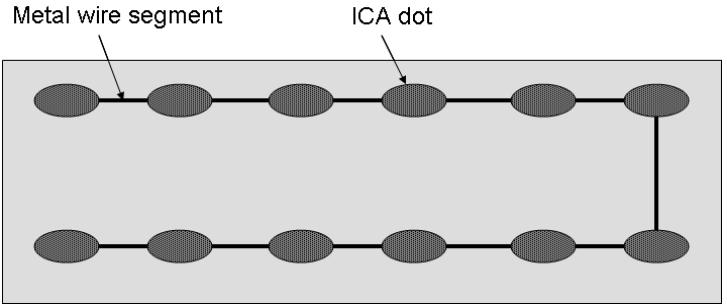

Fig. 4.33. In-house contact resistance test device

Table 4.7. Shifts of the contact resistance between an ICA with different metals

Metal wires	Contact resistance change during aging
Pt	Stable
Au	Stable
Ag	Stable
Sn	Unstable
Sn/Pb	Unstable
Ni	Unstable

4.10.4.2 Investigation of Mechanisms Underlying the Unstable Contact Resistance Phenomenon

In order to focus on the mechanism of study, ICA formulations used in this study were kept as simple as possible. A base resin formulation was composed of just a bisphenol-F-type epoxy, a hardener, and a catalyst. Other components such as an adhesion promoter, conductivity enhancer, and diluent were omitted from these formulations.

An ICA was formulated using the above base resin formulation. The filler was a Ni flake, and filler loading was 70w%. Different metal wires, Ni, Sn, Cu, and Ag, were selected and employed in the test vehicles shown in Fig. 4.34. The contact resistance changes of these samples during

85°C/85%RH aging are shown in Fig. 4.33. It was found that all the contact resistance increased with aging time, but the contact resistance with Ag wire increased much more significantly than that with Ni, Sn, and Cu. This result suggested that the contact resistance change is not due to simple oxidation of the non-noble metals. For if it were, the contact resistance with Ni, Sn, and Cu wires should have increased more dramatically than that with Ag wire.

The ICA used in this study was also a Ni flake-filled epoxy adhesive. By using two different metal wires, Ni and Ag, simple oxidation and galvanic corrosion mechanisms could be differentiated. Therefore, two different samples were tested here: Ni flake-filled ICA with Ni wire (referred as Ni/Ni combination in later sections) and Ni flake-filled ICA with Ag wire (referred as Ni/Ag combination). Six specimens were fabricated for each sample. The specimens were aged under two different conditions: 85°C/dry and 85°C/85%RH. Three of the specimens were exposed to 85°C/dry and the other three were exposed to 85°C/85%RH. The contact resistance of each specimen was collected periodically during the aging. The results of these specimens were reported for each sample. The resistance changes of the samples during 85°C/dry and 85°C/85%RH aging are shown in Figs. 4.35 and 4.36, respectively.

As can be seen from Fig. 4.35, upon exposure to 85°C/dry, both Ni/Ni and Ni/Ag combinations showed no significant contact resistance change. From Fig. 4.35, it was found that during 85°C/85%RH aging, contact resistance of Ni/Ni combination was relatively stable, but contact resistance of the Ni/Ag combination increased dramatically. Under the 85°C/dry aging condition, galvanic corrosion is negligible; therefore, simple oxidation of the metals is the only possible mechanism. Insignificant contact resistance shifts for both samples indicates that simple oxidation is not dominant at 85°C. Under the aging condition of 85°C/85%RH, both simple oxidation and galvanic corrosion can happen. If simple oxidation dominated, then the Ni/Ni combination should have had a larger resistance shift than the Ni/Ag combination. The fact that the Ni/Ag combination showed much significant resistance shifts indicates that simple oxidation of the non-noble metals is not a dominant mechanism for contact resistance shifts during 85°C /85%RH aging.

Three conductive adhesives (ECA-1, ECA-2, and ECA-3) were formulated with the base resin formulation mentioned in the previous section. These three ECAs are exactly the same except for the fact that their fillers were different. ECA-1 was filled with Ni flake. ECA-2 was filled Ag flake. ECA-3 was filled with a mixture of the Ni flake and the Ag flake (weight ratio of the Ni flake and the Ag flake was 95:5). Again, six specimens were tested for each sample. Three of them were exposed to 85°C/dry and the other three were aged under the condition of 85°C/85%RH. Bulk

resistance of each specimen was measured periodically during the aging. Results of these three specimens for each sample were reported.

Shifts of bulk resistance of these samples under 85°C/dry and 85°C/85%RH conditions are shown in Figs. 4.37 and 4.38, respectively. It can be seen that (1) during 85°C/dry aging, all of the samples showed relatively stable resistance and (2) under the aging condition of 85°C/85%RH, ECA-3, was filled with the mixture of Ni and Ag flakes and much larger resistance increase than ECA-1 and ECA-2.

Based on the above results, it can be summarized that

1) under the aging condition of 85°C/dry, regardless the metals involved, all samples showed relatively stable resistance, even though the metals involved included an easily oxidizable metal such as Ni;
2) under the aging condition of 85°C/85%RH, if only one type of metal was involved, the samples showed stable resistance, even for commonly known oxidizable metals such as Ni.

However, the resistance increased dramatically if two different metals were involved. These results strongly indicate that galvanic corrosion rather than simple oxidation is the dominant mechanism for the unstable contact resistance phenomenon during high-temperature and high-humidity aging.

The experimental results of above sections are consistent with galvanic corrosion mechanism [119]. A schematic explanation is given in Fig. 4.39. When a Ni flake contacts with a Ag wire or a Ag flake, particularly under wet condition, moisture and oxygen diffuse into the interface and then the moisture condenses into water. The accumulated water could dissolve some impurities from the resin and form an electrolyte solution. All the requirements for a galvanic corrosion are met. Therefore, microgalvanic cells are formed at the interface. The less noble metal Ni acts as an anode, loses electrons, and becomes Ni^{2+}. The reaction can be represented as $Ni - 2e^- = Ni^{2+}$. The noble metal Ag acts as a cathode and the reaction on this electrode is $2H_2O + 4e^- + O_2 = 4OH^-$. Ni^{2+} combines with the OH^- and form a nickel hydroxide, $Ni(OH)_2$, that is usually unstable and becomes nickel oxide. As a result, a layer of Ni oxide is formed at the interface.

Because this oxide layer has much higher resistance than the nickel, the contact resistance increased significantly after aging. Galvanic corrosion can happen only if the potential of a metal which acts as an anode is lower than the potential of the cathodic reaction, $2H_2O + 4e^- + O_2 = 4OH^-$ which is 0.4 V under standard conditions [119]. According to Table 4.8, normal potentials of Ag, Au, and Pt are higher than the potential of the cathodic reaction. No galvanic corrosion occurs and thus no metal oxide is formed at the interface. As a result, the contact resistance between the Ag-filled ECA with these noble metals remained stable during aging. In con-

trast, the other metals, Ni, Sn, and Sn/Pb all have lower potentials than the cathodic reaction. Galvanic corrosion happens and the non-noble metals are corroded to form insulating metal oxides at the interface. Therefore, the contact resistance between the Ag flake-filled ECA with these metals increased dramatically upon aging.

All of the above results indicated that shift of the contact resistance between an ECA and non-noble metals is mainly due to the metal oxide formation which is caused by galvanic corrosion of the non-noble metal at the interface.

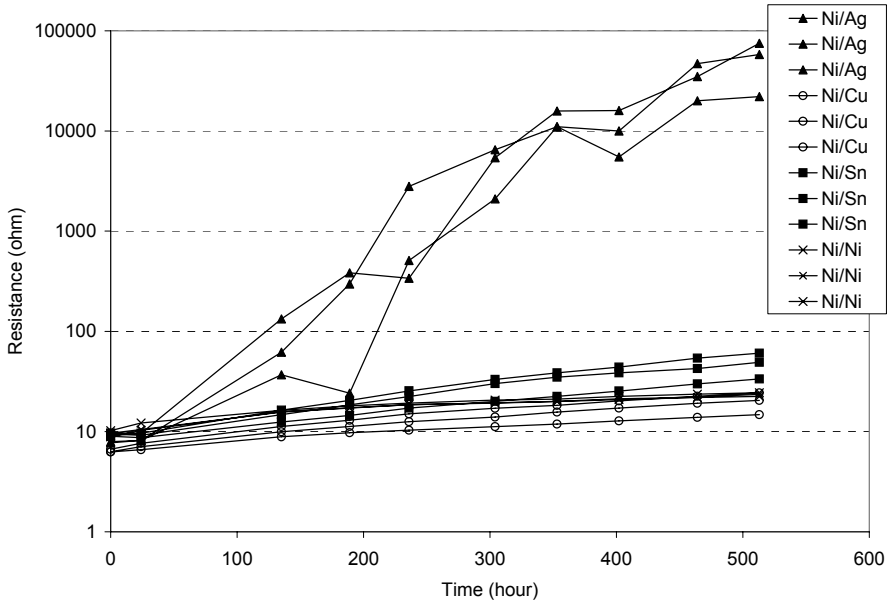

Fig. 4.34. Shifts of contact resistance of nickel-filled ECAs on different metal wires

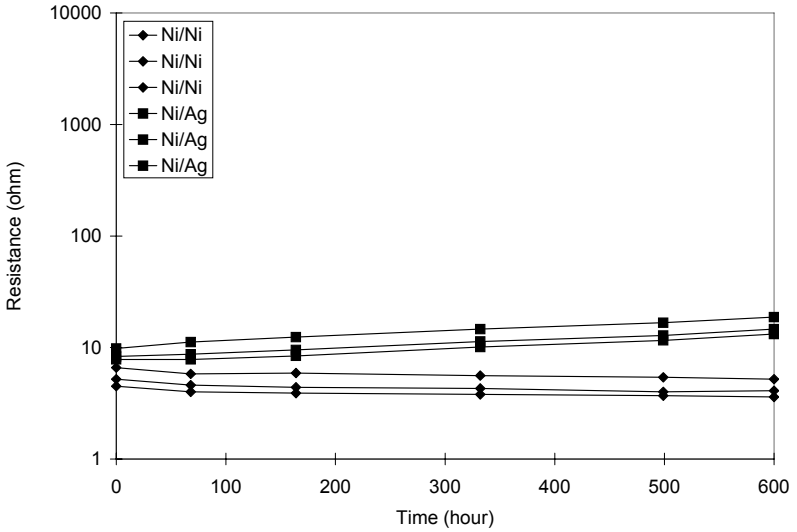

Fig. 4.35. Contact resistance shifts of a Ni flake-filled ICA with Ni and Ag wires under 85°C/dry aging condition

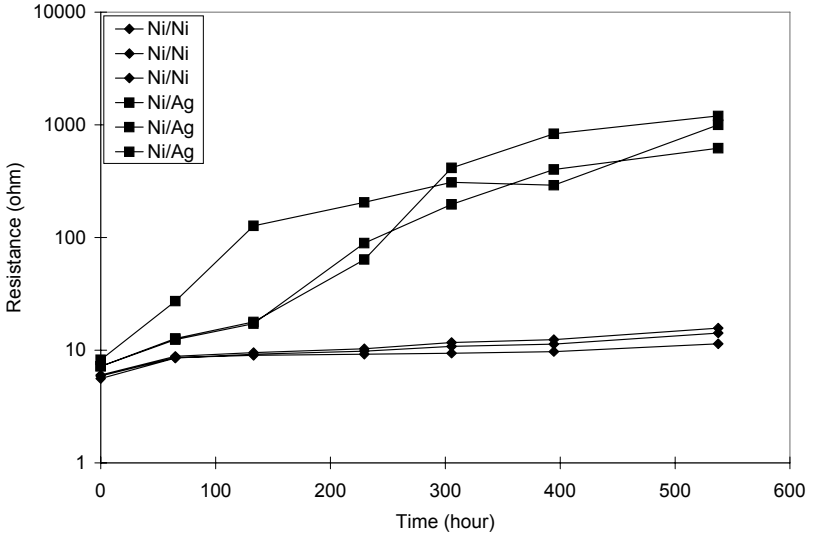

Fig. 4.36. Contact resistance shifts of a Ni flake-filled ICA with Ni and Ag wires under 85°C/85%RH aging condition

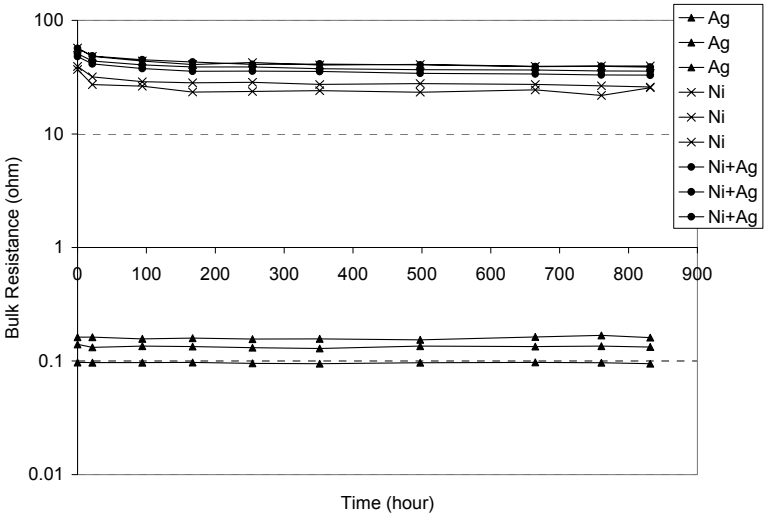

Fig. 4.37. Bulk resistance shifts of three ICAs with different fillers under 85° C/dry aging condition

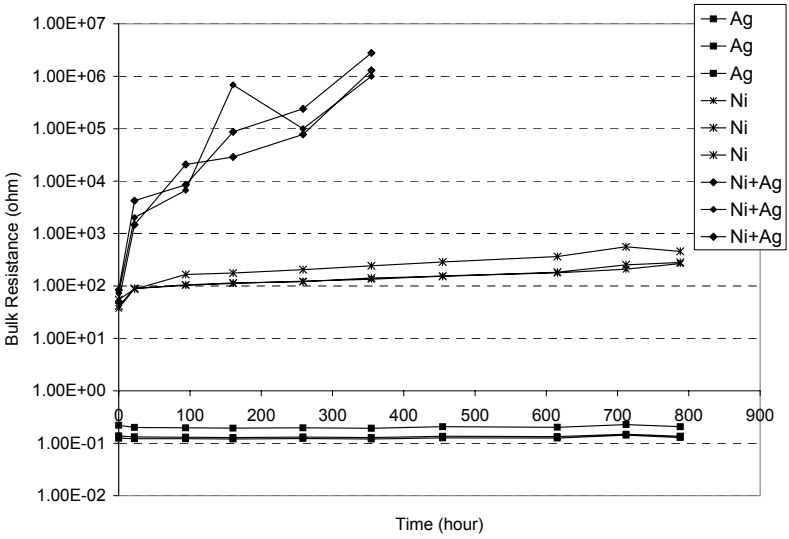

Fig. 4.38. Bulk resistance shifts of three ICAs with different fillers under 85°C/85%RH aging condition

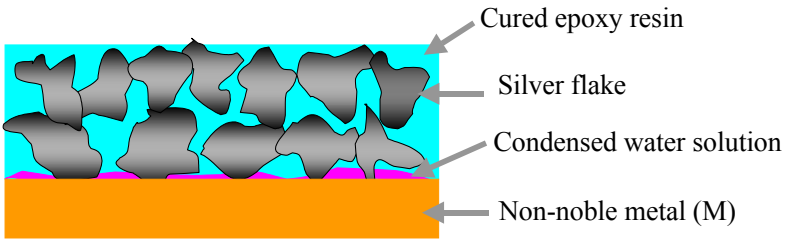

Fig. 4.39. A schematic explanation of galvanic corrosion at the interface between metal flake (such as Ni) and metal wire (such as Ag) during 85ºC/85%RH aging

Table 4.8. Normal potentials of some electrode reactions [120]

Electrode reaction	Normal potential (v) (normal hydrogen scale)
$Au - 3e = Au^{3+}$	1.50
$Pt - 2e = Pt^{2+}$	1.20
$Ag - e = Ag^{+}$	0.80
$H_2O + O_2 + 4e = 4OH^{-}$	0.40
$Cu - e = Cu^{+}$	0.34
$Cu - 2e = Cu^{2+}$	0.52
$Pb - 2e = Pb^{2+}$	–0.13
$Sn - 2e = Sn^{2+}$	–0.14
$Ni - 2e = Ni^{2+}$	–0.25

Metal oxide formation resulting from galvanic corrosion has been identified as the main mechanism for the unstable contact resistance. In this study, the metal oxide formation at the interface between an ECA and a non-noble metal (Sn/Pb was selected here) during aging was observed using TEM with energy dispersive X-ray (EDX) with ultra-thin window technique. A TEM image of a cross-sectional interface between an ECA and Sn/Pb is shown in Fig. 4.40. From the images, it can be observed clearly that a metal oxide layer was formed at the interface.

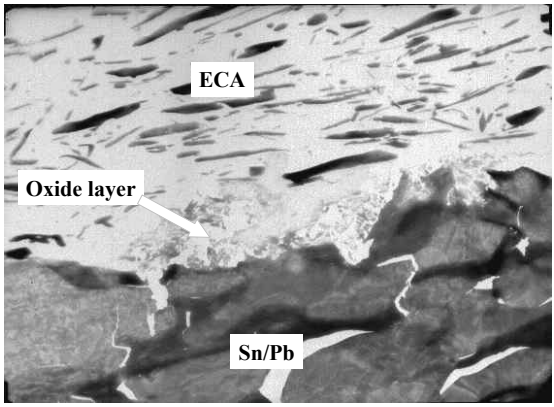

Fig. 4.40. TEM images of a cross-sectional interface between an ECA and Sn/Pb

4.10.5 Improvement of Contact Resistance Stability

4.10.5.1 Effects of Electrolytes on Contact Resistance Shifts

An electrolyte solution is one of the requirements for galvanic corrosion. Electrolytes should increase the electrical conductivity of the solution, accelerate galvanic corrosion, and cause larger contact resistance increase. The effects of four electrolytes, sodium chloride (NaCl), sodium acetate (NaAc), ammonium chloride (NH_4Cl), ammonium sulfate ($(NH_4)_2SO_4$), on contact resistance shifts of an ECA on Sn/Pb metal were investigated. The concentration of each electrolyte was 0.5 part of each electrolyte per 100 parts of the resin of the ECA. The contact resistance of the ECAs with and without the electrolytes was measured periodically during 85ºC/85% RH aging. The results are shown in Fig. 4.41.

As can be seen from Fig. 4.41, the ICAs with the electrolytes showed faster increase of contact resistance than the ECA without electrolytes. Electrolytes can increase electrical conductivity of the solution and accelerate galvanic corrosion. It can be concluded from this study that, in order to stabilize contact resistance during aging, resins, hardeners, and other ingredients with low impurity contents should be used to formulate ICAs.

Fig. 4.41. Effects of electrolytes on contact resistance shift of ICAs on Sn/Pb surface

4.10.5.2 Effect of Moisture Adsorption on Contact Resistance Shifts

The water condensed from the adsorbed moisture at the interface between an ECA and the metal formed the electrolyte solution which was required for galvanic corrosion to occur. Therefore, an ICA with lower moisture absorption should show slower contact resistance shift during aging due to its slower corrosion rate at the interface.

Three ICA formulations were formulated with different epoxy resins but the same hardener and catalyst. These three ICAs had similar properties but different levels of moisture absorption. The moisture absorption of the cured resins of these ICAs is shown in Fig. 4.41. The contact resistance shifts of these ICAs on Sn/Pb were compared and are shown in Fig. 4.42. Comparing Figs. 4.42 and 4.43, it was found that the ICA with the highest moisture absorption (ECA-III) showed the fastest contact resistance shift and the ICA with the lowest moisture absorption (ECA-I) showed the slowest contact resistance shift during aging. Thus, there is a correlation between moisture absorption and contact resistance shift. Therefore, one of the approaches to formulate an ICA with more stable contact resistance is

to select epoxy and hardener combinations which can provide ICAs with lowest moisture absorption.

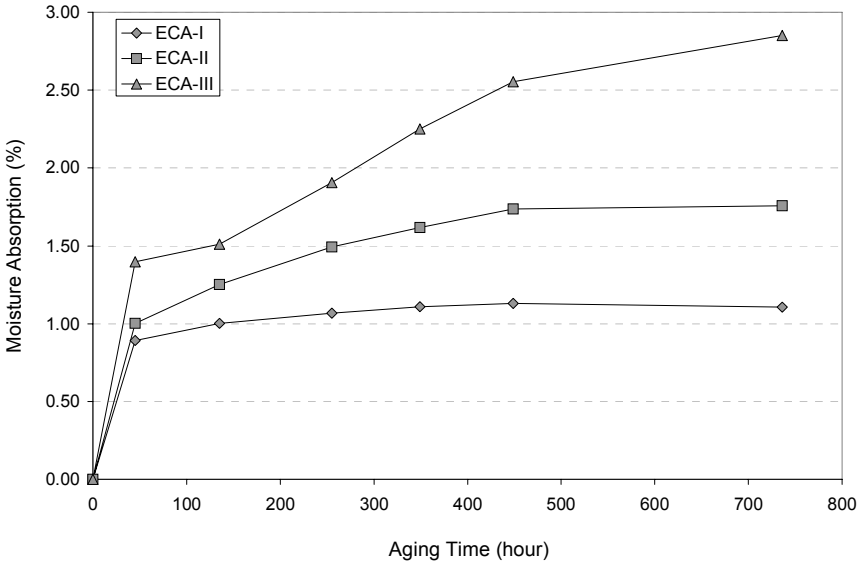

Fig. 4.42. Moisture absorption of three ICAs (ECA-I, ECA-II, and ECA-III)

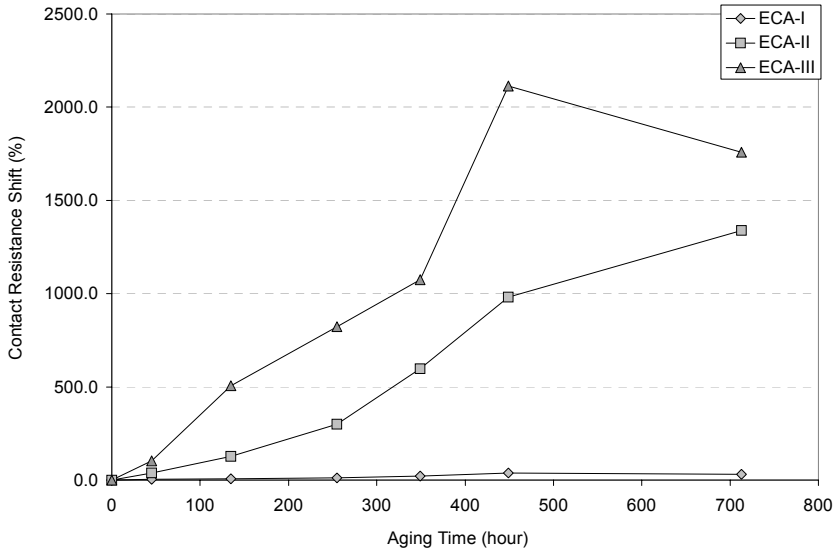

Fig. 4.43. Contact resistance shift of three ICAs (ECA-I, ECA-II, and ECA-III)

4.10.5.3 Approaches to Improve Contact Resistance Stability

Galvanic corrosion happens only in wet conditions. An electrolyte solution must be formed at the interface before galvanic corrosion can happen. Therefore, one way to prevent galvanic corrosion at the interface between an ICA and the non-noble metal surface is to lower the moisture pickup of the ICA. ICAs that have low moisture absorption generally show more stable contact resistance on non-noble surfaces [121]. Without an electrolyte, galvanic corrosion rate is very low. The electrolyte in this case is mainly from the impurity of the polymer binder (generally epoxy resins). Therefore, ICAs formulated with resins of high purity should perform better.

The second method of preventing galvanic corrosion is to incorporate some organic corrosion inhibitors into ICA formulations [122–123]. In general, organic corrosion inhibitors act as a barrier layer between the metal and the environment by being adsorbed as a film over the metal surfaces [124–125]. Some chelating compounds are especially effective in preventing metal corrosion [125]. Most of the organics were studied using the UV-visible spectrometry.

Two corrosion inhibitors (INH1) and (INH2) were used in this study. The shifts of contact resistance of the ICAs without and with corrosion inhibitors on Sn/Pb-finished substrates during 85°C/85% RH aging were measured and the results are shown in Fig. 4.44. From the figure, it can be seen that both inhibitors could slow the contact resistance increase. The ICA with INH1 showed stable contact resistance after the initial decrease even after 1,400-h 85 ° C/85% RH aging. INH2 was not as effective as INH1.

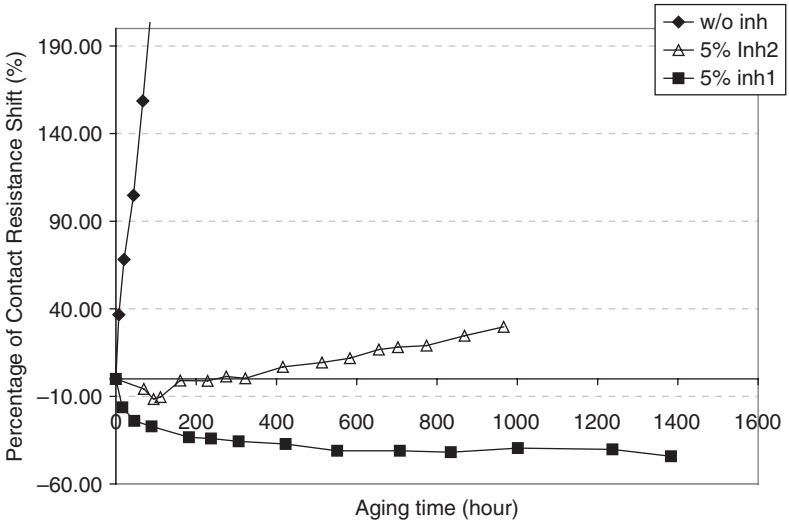

Fig. 4.44. Shifts of contact resistance of conductive adhesives with and without corrosion inhibitors

The main mechanism of chelating corrosion inhibitors such as INH1 is that they may adsorb on a specific metal surface and form a complex film which plays an essential role in the inhibition of the metal corrosion. The absorbance of each of corrosion inhibitor solutions was scanned for the wavelength from 600 to 190 nm. It was found that the INH1 and INH2 showed characteristic absorbance peaks at wavelengths of 235 and 263 nm, respectively. These two wavelengths were selected as the fixed wavelengths in the later measurement of the corrosion inhibitor concentrations.
A small amount (2 g) of a Sn/Pb powder was placed into 8 ml aqueous solution of INH1 and INH2 (concentration was $3 \times 10^{\cdot 5}$ g/ml). The mixtures were kept at room temperature for 24 h. After the Sn/Pb powder settled down, the upper clear solution was studied using the UV-visible spectrometry. The absorbance of the original solutions of these corrosion inhibitors and the upper solutions from the mixtures was measured and compared. Three samplings were collected for each solution, and results are shown in Table 4.9. From the absorbance data in this table, it can be clearly seen that INH1 concentration in the solution decreased significantly after mixing with Sn/Pb powder for some time, but INH2 concentration did not change much. This result indicated that INH1 was adsorbed on the Sn/Pb surface easily but INH2 did not. The strong absorbance of INH1 on Sn/Pb may be the reason that INH1 could effectively stabilize the contact resistance of ECAs on Sn/Pb surfaces.

Table 4.9. Absorbance from the UV spectra of INH1 and INH2 solutions

	INH1 (at 235 nm)		INH2 (at 263 nm)	
	INH1 solution before mixing with Sn/Pb powder	INH1 solution before mixing with Sn/Pb powder	INH2 solution before mixing with Sn/Pb powder	INH2 solution before mixing with Sn/Pb powder
1	3.586	0.846	3.488	3.294
2	3.556	0.851	3.399	3.285
3	3.575	0.860	3.442	3.296
Average	3.572	0.852	3.443	3.291

Table 4.10. Polarization resistance (Rp) and polarization conductance (1/Rp) of Sn/Pb in electrolyte solutions with and without inhibitors

Electrolyte solution	R_p ($\Omega\ cm^2 \times 10^{-3}$)	$1/R_p$ ($\Omega^{-1}cm^{-2} \times 10^6$)
0.2 M NaCl	3.265	306
0.2 M NaCl + 0.001 M INH2	4.101	244
0.2 M NaCl + 0.001 M INH1	7.464	134

Electrochemical study can elucidate the effects of corrosion inhibitors on decreasing the corrosion rate. Polarization resistance (*R*p) was determined as the slope of the potentiostatic polarization curves of Sn/Pb measured in the vicinity of the zero current. The polarization conductance (1/*Rp*), which is directly proportional to the corrosion current, was measured on Sn/Pb electrodes in the solutions. Therefore, if the Sn/Pb shows a higher polarization conductance in a solution, it is more susceptible to corrode in that solution. The polarization resistance and polarization conductance of the Sn/Pb in the electrolyte solutions without or with the inhibitors are shown in Table 4.10. As can be seen from the table, Sn/Pb had a much lower polarization conductance in the electrolyte solution with INH1 added than the one without an inhibitor. But Sn/Pb showed a slightly lower polarization conductance in INH2 electrolyte solution than in the electrolyte solution without an inhibitor. The results clearly indicated that Sn/Pb showed a much slower corrosion rate in NaCl solution with INH1 than INH2. Therefore, INH1 could stabilize contact resistance of ECAs on Sn/Pb much more effectively than INH2.

The effectiveness of the corrosion inhibitors is also highly dependent on the types of contact surfaces. For different surface finishes, specific corrosion inhibitors with different functional groups are needed to stabilize the contact resistance. Effective corrosion inhibitors have been reported for Cu, Al, and Sn surfaces as well [126, 127].

Some silane coupling agents, besides their traditional use as surface modifiers for adhesion improvement, can act as corrosion inhibitors to stabilize electrical contact resistance of conductive adhesive joints. Matienzo et al. [127] demonstrated that conductive adhesive joints were electrically stable for up to 137.5 h under 85°C/85% RH condition by treating the aluminum substrate surface with a thin layer (less than 5 nm) of an organosilane coupling agent, which is a material capable of bonding chemically with the aluminum oxide surface layer and potentially bonding with the polymer binder in the adhesive.

Oxygen can accelerate galvanic corrosion. Therefore, another way to slow down the corrosion process is to incorporate some oxygen scavengers into ICA formulations [128]. When an oxygen molecule diffuses through the polymer binder, it reacts with the oxygen scavenger and is consumed. However, when the oxygen scavenger is depleted completely, then oxygen still can diffuse into the interface and accelerate the corrosion process. Therefore, oxygen scavengers can only delay galvanic corrosion process for some time. Similarly, the oxygen scavengers used must not react with epoxy resin at its cure temperature. Common oxygen scavengers include hydrazine, carbohydrazide, hydroquinone, gallic acid, propyl gallate, hydroxylamines and related compounds, dihydroxyacetone, 1,2-dihydro-1,2,4,5-tetrazines, erythorbic acid, and oximes [128–130].

Incorporating a low melting alloy (LMA) filler into Ag-filled ICA can stabilize the contact resistance [131]. For comparison purpose, another ICA (ICA-1) was formulated using the same resin but only with silver flakes. As shown in Fig. 4.45, metallurgical connections between the Ag particles were formed in the ICA filled with LMA, but only physical contacts between Ag flakes were found in the ICA-1. An acid was incorporated in the ICA formulations to act as a fluxing agent. During the cure of the ICAs, the fluxing agent removed the oxide from the Ag flake surfaces, and the LMA particles melted and wetted the silver flakes and connected the silver lakes together. Due to this metallurgical connection, a lower bulk resistance was expected for the LMA-filled ICA than the ICA-1. The interconnection between the CA and the Ni metal surface was also observed using the SEM. From Fig. 4.46, it can be seen that a good metallurgical connection was formed at the interface between the ICA and the Ni surface. However, for ICA containing only silver flakes (ICA-1), only physical contacts between the Ag flakes and the Ni metal were observed. Therefore, a lower contact resistance should be expected for the LMA-filled ICA than the ICA-1. It was found that the ICA with the LMA filler showed much lower initial contact resistance (0.15 Ω) than the ICA with only the silver flakes (8.90 Ω). The metallurgical interconnection formed between the silver flakes and the substrate (Ni) resulted in a lowered contact resistance.

The contact resistance shift during 85°C/85% RH aging of these two ICAs was also compared and the results are shown in Fig. 4.47. As can be seen from the figure, the ICA filled with silver flakes and LMA filler showed much more stable contact resistance on Ni than the ICA filled with silver flakes only. The resistance increase of the ICA filled only with silver flakes was also due to the metal oxide formation caused by galvanic corrosion during aging. However, because there were metallurgical connections between the silver flakes and the substrate (Ni), the contact resistance remained stable during the elevated temperature and humidity aging.

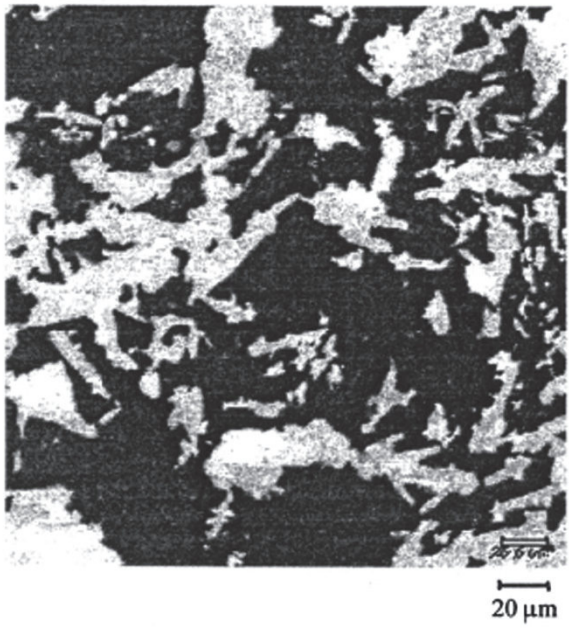

(a)

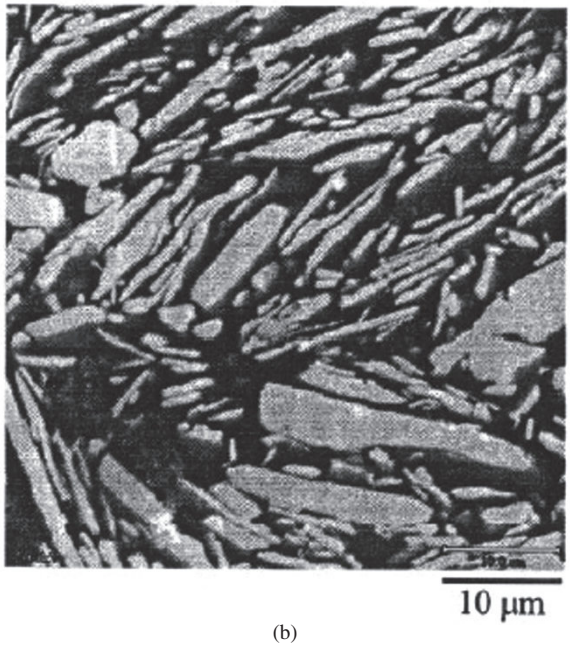

(b)

Fig. 4.45. SEM micrographs of (**a**) an ICA filled with Ag flakes and a LMA filler and (**b**) an ICA filled only with Ag flakes

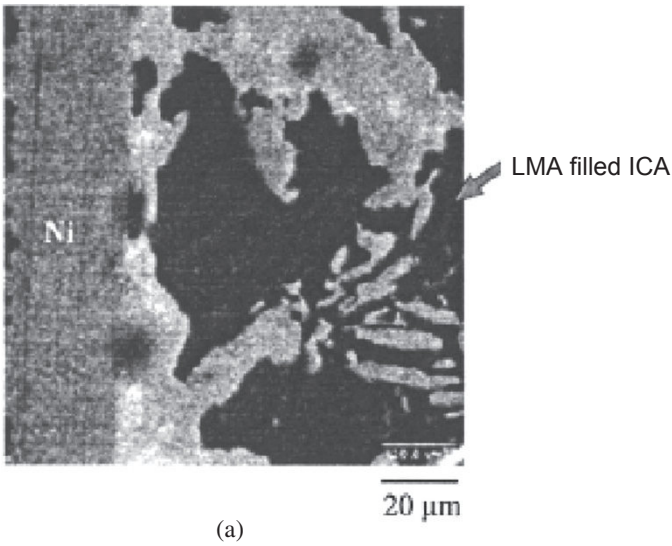

(a)

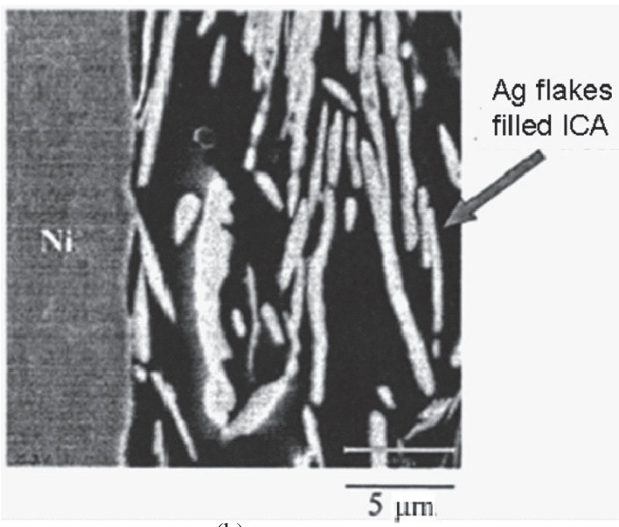

(b)

Fig. 4.46. SEM micrographs of joints formed between (**a**) a Ni substrate and an ICA filled with Ag flakes and LMA and (**b**) an ICA filled with only Ag flakes

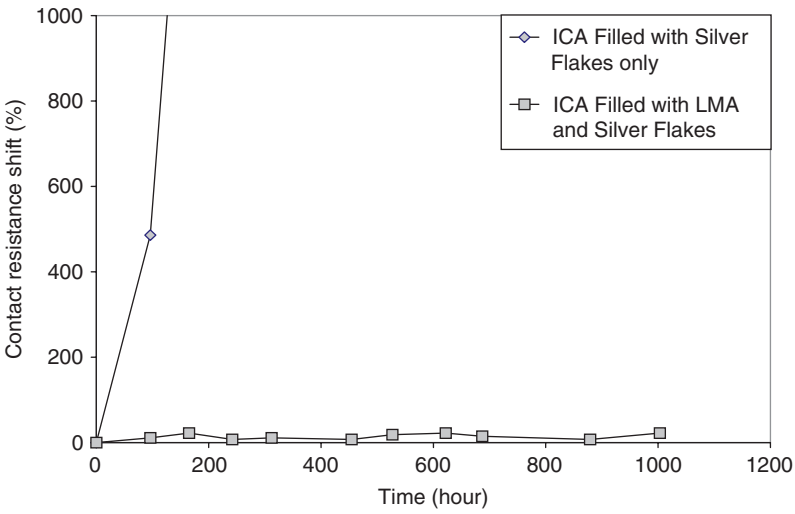

Fig. 4.47. Shifts of contact resistance of an ICA on nickel surface

To improve the contact resistance stability, applying a sacrificial anode is another efficient method. For galvanic corrosion of ECAs during aging, the larger the difference in electrochemical potential, the faster the corrosion develops. Also, the self-corrosion rates of both metals will change; the comparably active metal (the anode) corrodes faster, while the other (the cathode) corrodes slowly. Generally, metals with a low potential tend to corrode faster and show increased contact resistance than those with a high potential value. Therefore, when applying sacrificial materials with lower electrochemical potential than those of electrode metal pads into ECAs, the sacrificial materials are preferably corroded first and, thus, can protect the metal finishes [132] (Fig. 4.48). This corrosion control is very important in reliability issues of the conductive adhesive joints. The addition of low corrosion potential individual metals, metal mixtures, or metal alloys greatly reduces the electrode potential of ECAs, or in other words, narrows down the potential gap between the ECA and the metal finishes. Thus, these sacrificial anode materials act as an anode in this configuration and they are corroded first instead of the metal finishes, resulting in protecting the surfaces at the cathode [132–134].

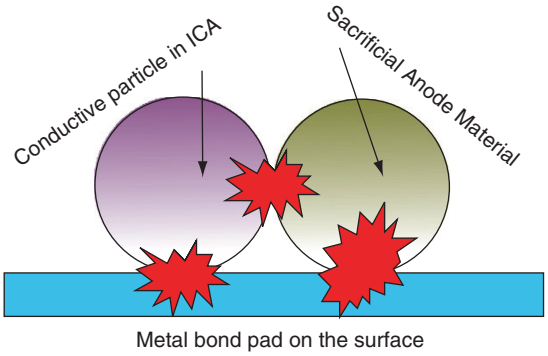

Fig. 4.48 A schematic illustration of sacrificial materials in protection of metal fillers and metal bond pad for corrosion control

Another approach of improving contact resistance stability during aging is to incorporate some electrically conductive particles, which have sharp edges, into the ICA formulations. The particle is called oxide-penetrating filler. Force must be provided to drive the oxide-penetrating particles through oxide layer and hold them against the adherend materials. This can be accomplished by employing polymer binders that show high shrinkage when cured [135] (Fig. 4.49). This concept is used in polymer solder which has good contact resistance stability with standard surface-mounted devices (SMDs) on both solder-coated and bare circuit boards.

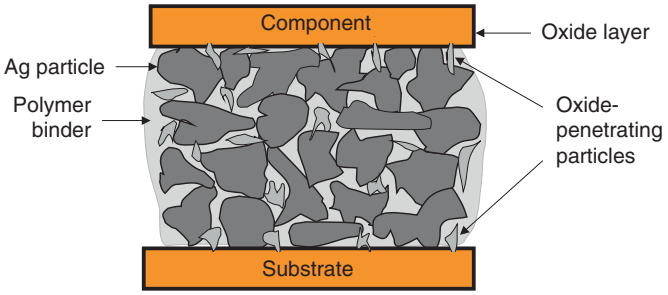

Fig. 4.49. A joint connected with an ICA containing oxide-penetrating particles and silver powders

4.10.6 Impact Performance

Impact performance is a critical property of solder replacement ICAs. There has been continuing efforts in developing ICAs that have better impact strength to pass the drop test, a standard test used to evaluate the impact strength of ICAs.

Nano-sized metal particles were used in ICAs to improve the electrical conduction and mechanical strength. Using nano-sized particles, agglomerates are formed due to surface tension effect [136]. Another approach is simply to decrease the filler loading to improve the impact strength. However, such a process reduces the electrical properties of the conductive adhesives. A recent development was reported where conductive adhesives were developed using resins of low modulus so that this class of conductive adhesives could absorb the impact energy developed during the drop test [137]. However, the electrical properties of these materials were not mentioned in the chapter. Conformal coating of the surface-mounted devices was used to improve mechanical strength. It was demonstrated that conformal coating could improve the impact strength of conductive adhesives joints [138].

Rao et al. study indicated that the impact performance of an ICA is highly dependent on its damping property (loss factor, tan δ) [139].

More recently, Xu et al. [140] designed a novel falling wedge test to quantitatively characterize the impact resistance of electrically conductive adhesives. The viscoelastic energy, which is a result of the internal friction created by chain motions within the adhesive material, has played an important role in the fracture behavior of the conductive adhesives. As a measure of the internal friction, the loss factor was found to be an indicator of an adhesive's ability to dissipate the mechanical energy through heat. By quantitatively relating the impact fracture energy of the adhesive joints to the loss factors of the ECAs, the author demonstrated that the impact fracture energy tends to exhibit a logarithmic relationship with the corresponding loss factor, as the increased loss factor at the test conditions consistently results in the improved impact performance. This finding suggests that the impact performance of a conductive adhesive may be improved by formulating the adhesive with good damping ability under impact conditions that may be encountered in the service.

Aiming at formulating ICAs with high damping property, D. Lu et al. developed a new class of conductive adhesives which is based on an epoxide-terminated polyurethane (ETPU) [141, 142]. This class of conductive adhesives has the properties of polyurethane materials, such as high toughness and good adhesion. The modulus and glass transition temperature of the ICAs can be adjusted by incorporating some epoxy resins such as bisphenol-F epoxy resin. Conductive adhesives based on the ETPU

showed a broad loss factor (tan δ) peak with temperature and a high tan δ value at room temperature. The tan δ value of a material is a good indication of the damping property and impact performance of the material. In general, the higher the tan δ value, the better the damping property (impact strength) of the material. As an example, changes in tan δ and modulus with temperature of an ETPU-based ICA which were measured by a dynamic mechanical analyzer (DMA) are shown in Fig. 4.50. ICA based on ETPU resin also showed much higher loss factor (tan δ) in a wide frequency range than the ICA based on bisphenol-F epoxy resin (Fig. 4.51). This indicated that the ICAs based on ETPU resin should exhibit good damping property and improved impact performance in different electronic packages. This class of conductive adhesives showed superior impact performance and substantially stable contact resistance with non-noble metal surfaces, such as Sn/Pb, Sn, and Cu.

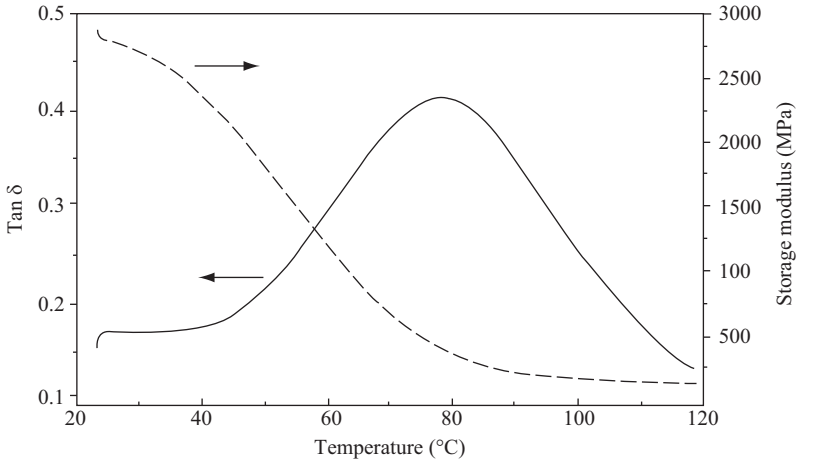

Fig. 4.50. Changes of tan δ and storage modulus with temperature of an ETPU-based conductive adhesive

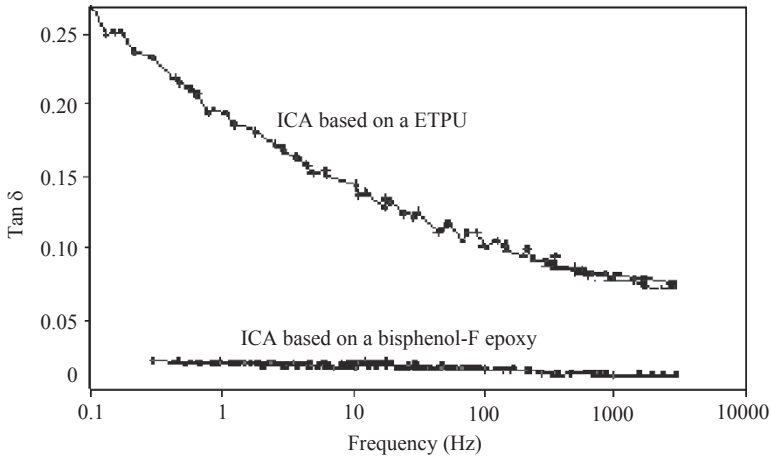

Fig. 4.51. Loss factor (tan δ) versus frequency of two ICAs

4.10.7 Adhesion Strength

Another critical aspect of conductive adhesive is the adhesion strength. High adhesion strength is a critical parameter in fine-pitch interconnection that is fragile to shocks encountered during assembly, handling, and lifetime.

There are two types of adhesion mechanisms, physical bonding and chemical bonding, which contribute to the overall adhesion strength of polymer on a surface [143]. Chemical bonding involves the formation of covalent or ionic bonds to link between the polymer and the substrate. In other words, a chemical reaction must take place for the formation of chemical bonds. Physical bonding involves mechanical interlocking or physical adsorption between the polymer and the surface of substrate. In cases where the molecules of the polymer are highly compatible with the molecules of the substrate, they interact to form an inter-diffusion layer. In mechanical interlocking, polymer and substrate interact on a more macroscopic level, where the polymer flows into the crevices and the pores of substrate surface to establish adhesion. Therefore, a polymer is expected to have better adhesion on a rougher surface because there is more surface area and "anchors" to allow for interlocking between the polymer and the substrate. This section summarizes the efforts on the adhesion improvement of conductive adhesives.

4.10.7.1 Plasma Cleaning and Vacuum Process

Plasma cleaning of surfaces has been considered as one of the effective approaches to enhance the adhesion strength of conductive adhesives [144]. During the plasma etching process, the plasma radicals react with the contaminants and those long-chain organic molecules can be broken down into small gaseous ones (mostly gaseous water and carbon-oxide conjunctions). These particles can be evacuated from the system by the vacuum pump. After the surface is cleaned of oxide, a layer of atoms available in the chamber will deposit on the clean surface, protecting the metal from new oxidation. Furthermore, the plasma can also etch the surface to enhance the mechanical interlocking mechanism for adhesion improvement. With plasma treatment, the adhesion strength of conductive adhesives could be improved. However, the improvement also requires a high vacuum process due to the possible corrosion on the highly cleaned surface caused by the moisture in ECAs. After vacuum process, the surface was changed by removal of air and water and the contraction of adhesives.

4.10.7.2 Application of Coupling Agents in ECA

Another approach to improve adhesion is by using coupling agents [145]. Coupling agents are organofunctional compounds based on silicon, titanium, or zirconium. For example, R– × –$(O–R')_3$, where , X=Si, Ti, or Zr, R = organic chain that interacts with the polymer, and R′= organic chain that interacts with the substrate. A coupling agent consists of two parts and acts as intermediary to "couple" the inorganic substrate and polymer.

There are a few theories about how coupling agents can enhance bonding. The first is the chemical bonding theory, where the R′ groups of the coupling agent can form hydrogen bonds to the surface, and then condense to form covalent bonds to the surface. Then, the R group of the coupling agent would react with the polymer during the curing reaction. Another theory is based on how coupling agents affect the wetting capability of the surface and its surface energy. Good wetting is necessary for good adhesion, and for a liquid or a polymer to wet a surface, its surface tension must be lower than that of the substrate [146]. Generally, inorganic surfaces have high surface tension, while organic liquids have surface tension less than 100 dynes/cm^2 (i.e.,10 N/m^2). However, inorganic surfaces can be hydrophilic and a layer of water may accumulate on it, thus causing the surface tension of the surface to decrease. Polymers with some polar characteristics can displace water molecules on the surface and good wetting can still take place. In the case of non-polar polymers, coupling agents may help to reduce surface tension of the polymer.

Silane coupling agents have been commonly used to improve the adhesion performance. For example, chemically etched 304 stainless steel can react with γ-aminopropyltrimethoxysilane. The methoxy groups of the silane coupling agent can first hydrolyze to hydroxyl groups which are quite reactive and can react with the metal surface metal hydroxyl groups, forming a metal oxygen silane chemical bond. The other organo-reactive group (amine end of the coupling agent) can react with polyamic acid, a precursor of the polyimide polymer, to form a better and strong metal–polymer interfacial bonding. As such, it produces mechanically stronger polyimide/stainless steel interfaces. Other approaches use the formation of a thick metal oxide layer prior to application of the silane coupling agent to improve adhesion to organic films [127, 147, 148]. Silane coupling agents have also been shown to reduce the rate of hydration of aluminum surfaces and improve adhesion to organic films [149, 150]. In conductive adhesives, application of specific silane coupling agents with appropriate concentration can increase the adhesion strength on different metal surfaces.

Although silane coupling agents are mostly used, some other coupling agents with various functional groups, such as thiol, carboxylate coupling agents, are also used [151].

4.10.7.3 Roughening of Contact Surfaces

It has been reported that surface roughness affects the adhesion strength of conductive adhesives. Surface with larger roughness typically shows higher adhesion strength. Roughening of surfaces, for example, by sand blasting, chemical etching, plasma treatment, or anodization to specific morphologies, has been employed to enhance the adhesion strength and provide structural durability in humid or corrosion environments [152].

4.10.7.4 Optimization of Elastic Modulus

In order to enhance the adhesion, another approach is to lower the elastic modulus of adhesive resins. By using low elastic modulus resins, the thermal stress at the adhesion interface can be reduced and, thus, the improved the adhesion strength [153–54]. Figure 4.52 shows the relationship between the adhesion strength against COF (chip on flex) and the elastic modulus. The adhesion strength increases with lowering the elastic modulus. However, too low modulus value deteriorates the cohesive force and thus decreases the adhesion strength. Therefore, the elastic modulus needs to be optimized to improve the adhesion properties.

In addition to the methods listed above, some other factors such as curing conditions and structures of IC packaging may also affect the adhesion strength of conductive adhesives.

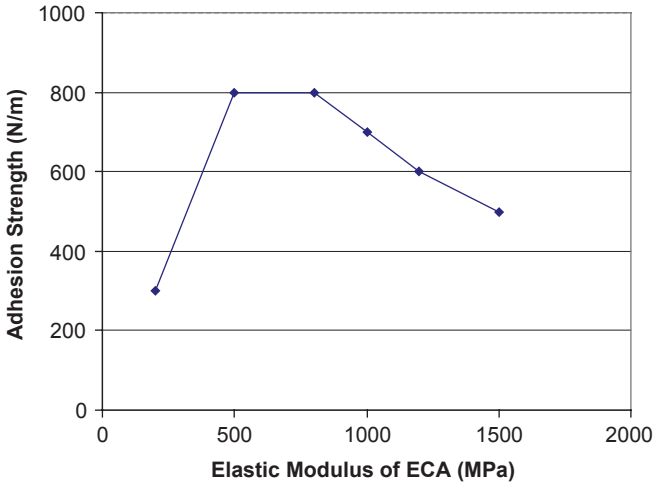

Fig. 4.52. The relationship between the adhesion strength and the elastic modulus of ECA

4.10.8 Recent Advances on Nano-ICAs

To meet the requirements for future fine-pitch and high-performance interconnects in advanced packaging, ECAs with nano-material or nano-technology attract more and more interests due to the specific electrical, mechanical, optical, magnetic, and chemical properties. There has been extensive research on nano-conductive adhesives which contain nano-filler such as nano particles, nanowires, carbon nanotubes, and graphenes. This chapter will provide a comprehensive review of most recent research results on nano-conductive adhesives.

4.10.8.1 ICAs with Silver Nano-wires

Wu et al. [155] developed an epoxy-based ICA filled with silver nano-wires and compared the electrical and mechanical properties of this nano-ICA to two other ICAs filled with micrometer-sized (roughly 1 μm and 100 nm) silver particles. The nano-wires had a diameter of roughly 30 nm and a length up to 1.5 μm, and the nano-wires were polycrystalline in nature. It was found that at a low filler loading (e.g., 56wt%), the bulk resistivity of ICA filled with the Ag nano-wires was significantly lower than the ICAs filled with 1 μm or 100 nm silver particles. The better electrical

conductivity of the ICA-filled nano-wires was contributed by the lower contact resistance between nano-wires and a more significant contribution from the tunneling effect among the nano-wires. It was also found that at the same filler loading (e.g., 56wt%), the ICAs filled with Ag nano-wires showed shear strength similar to that of the ICAs filled with the 1 μm and 100 nm silver particles. However, to achieve the same level of electrical conductivity, the filler loading must be increased to at least 75wt% for the ICA filled with micrometer-sized Ag particles, and the shear strength of these ICAs is then decreased (lower than that of the ICAs filled with 56wt% nano-wires) due to the higher filler loading.

4.10.8.2 Effect of Nano-sized Silver Particles on the Conductivity of ICAs

Lee et al. [156] studied the effect of nano-sized filler on the conductivity of conductive adhesives by substituting nano-sized Ag colloids for micro-sized Ag particles partially or wholly in a polymeric system (poly(vinyl acetate) – PVAc). Electrical resistivity was then measured as a function of silver volume fraction. It was found that when nano-sized silver particles were added into the system at 2.5wt% increment, the resistivity increased in almost all cases, except when the quantity of micro-sized silver was slightly lower than the percolation threshold value. At that point, the addition of the about 2.5wt% brought about significant decrease in resistivity. Near the percolation threshold, when the micro-sized silver particles are still not connected, the addition of a small amount of nano-sized sliver particles helps to build the conductive network and thus lowers the resistivity of the composite. However, when the filler loading is above the percolation threshold and all the micro-sized particles are connected, the addition of nanoparticles seems only to increase the relative contribution of contact resistance between the particles. Due to its small size, for a fixed amount of addition, the nano-sized silver colloid contains a larger number of particles when compared with micro-sized particles. This large number of particles should be beneficial to the interconnection between particles. However, it also inevitably increases the contact resistance. As a result, the overall effect is an increase in resistivity upon the addition of nano-sized silver colloids.

Ye et al. [157] also reported a similar phenomenon, i.e., the addition of nanoparticles showed a negative effect on electrical conductivity. They proposed two types of contact resistance, i.e., restriction resistance due to small contact area and tunneling resistance when nanoparticles are included in the system. It was believed that the conductivity of micro-sized Ag particle-filled adhesives was dominated by constriction resistance, while that of the nanoparticle-containing conductive adhesives was controlled by

tunneling and even thermionic emission. Fan et al. [158] and Mach et al. [159] also observed a similar phenomenon (adding nano-size particles reduced electrical conductivity).

Lee et al. [156] also studied the effect of temperature on the conductivity of ICAs. Heating the composite to a higher temperature can reduce the resistivity quite significantly. This is likely due to the high activity of nano-sized particles. For microsized paste, this temperature effect was considered negligible. The inter-diffusion of silver atoms among nano-sized particles helped to reduce the contact resistance quite significantly and the resistivity reached 5×10^{-5} Ω cm after treatment at 190°C for 30 min. Jiang et al. [160] showed that when suitable surfactant was used in the nano-Ag containing ICA, the dispersion and inter-diffusion of silver atoms among nano-sized particles could be facilitated and the resistivity of ICA could be reduced to 5×10^{-6} Ω cm.

4.10.8.3 ICAs Filled with Aggregates of Nano-sized Ag Particles

To improve the mechanical properties under thermal cycling conditions while still maintaining an acceptably high level of electric conductivity, Kotthaus et al. [161] studied an epoxy-based ICA material system filled with aggregates of nano-sized Ag particles. The idea was to develop a new filler material which did not deteriorate the mechanical property of the polymer matrix to a great extent. A highly porous Ag powder was attempted to fulfill this requirement. The Ag powder was produced by the inert gas condensation (IGC) method. The powder consisted of sintered networks of ultra-fine particles in the size range from 50 to 150 nm. The mean diameter of these aggregates could be adjusted up to some micrometers. The as-sieved powder was characterized by a low level of impurity content, an internal porosity of about 60%, and a good ability for resin infiltration. Using the above nano-sized Ag powder instead of Ag flakes is more likely to retain the properties of the resin matrix because of the infiltration of the resin into the pores. Measurements of the shear stress–strain behavior indicated that the thermo-mechanical properties of bonded joints could be improved by up to a factor of 2, irrespective of the chosen resin matrix.

Resistance measurements on filled adhesives were performed in a temperature range from 10 to 325K. The specific resistance of the nano-sized Ag powder-filled adhesive was about 10^{-2} Ω cm and did not achieve the typical value of commercially available adhesives of about 10^{-4} Ω cm. The reason may be that Ag nanoparticles are more or less spherical in shape, which provides fewer conduction paths than Ag flakes, and have the intrinsically lower specific conductivity. For certain applications where mechanical stress plays an important role, this conductivity may be sufficient,

and therefore, the porous Ag could be suitable as a new filler material for conductive adhesives.

4.10.8.4 ICAs Filled with Nano-sized Ni Particles

It is generally known that metal powders present properties that are different from those of bulk metals when their particle size is made as small as nanometer size. Powders are classified into particles, micro-particles, and nanoparticles according to size. Although the classification criterion is not clear, particles with diameter smaller than 100 nm are generally called nanoparticles. This classification is based on the fact that when particle size is smaller than 100 nm, the particle possesses properties that are not found in the micro-particles larger than 100 nm. For example, when the particle diameter of such magnetic materials as iron and nickel is near 100 nm, their magnetic domains change from multiple to single, and their magnetic properties also change [162]. Majima et al. [162] reported an application example of metal nanoparticles to conductive pastes, focusing on the properties of a new conductive adhesive that were not found in conventional ICAs. Sumitomo Electric Industries, Ltd. (SEI) has developed a new liquid-phase deposition process using plating technology [162]. This new nanoparticle fabrication process achieves purity greater than 99.9% and allows easy control of particle diameter and shape. The particle's crystallite size calculated from the results of X-ray diffraction measurement is 1.7 nm, which leads to an assumption that the size of primary particles is extremely small. When the particle size of nickel and other magnetic metals becomes smaller than 100 nm, they change from multi-domain particles to single-domain particles, and thus their magnetic properties change. That is, if the diameter of nickel particles is around 50 nm, each particle acts like a regular magnet, and magnetically connects with each other to form chain-like clusters. When the chain-like clusters are incorporated into a conductive paste, electrical conduction of the paste is expected to be better than the original paste. The chain-like nickel particles developed were mixed with a pre-defined amount of poly(vinylidene difluoride) (PVdF) that acted as an adhesive. Then, *n*-methyl-2-pyrrolidone was added to this mixture to make a conductive paste. This paste was applied on a polyimide film and then dried to make a conductive sheet. Specific volume resistivity of the fabricated conductive sheet was measured by the quadrupole method. The same measurement was also conducted on the conductive sheet that used paste made of conventional spherical nickel particles. Measurement of the sheet resistance immediately after paste application indicated that the developed chain-like nickel powder had low resistance of about one-eighth of that of the conventionally available spherical nickel particles. This result showed that when the newly developed chain-like nickel particles

were incorporated in the conductive paste, high conductivity could be achieved without pressing the sheet. SEI tested and developed the metal nanoparticles and investigated the possibility of their application in a conductive paste.

4.10.8.5 Nano-ICAs Filled with CNT

Electrical and Mechanical Characterization of CNT-Filled ICAs

The density of commercially available silver-filled conductive adhesives is around 4.5 g/cm^3 after cure. Metal-filled electrically conductive adhesives offer an alternative to typical lead–tin soldering with the advantages of being simple to process at lower temperatures without toxic lead or corrosive flux. The disadvantage of conventional metal-filled conductive adhesives is that a high loading of filler decreases the mechanical impact strength, while a low filler loading results in poor electrical properties. Carbon nanotubes are a new form of carbon, which was first identified in 1991 by Sumio Iijima of NEC, Japan [163]. Nanotubes are sheets of graphene rolled into seamless cylinders. Besides growing single wall nanotubes (SWNTs), nanotubes can also have multiple walls (MWNTs) – cylinders inside other cylinders. A carbon nanotube can be 1–50 nm in diameter and up to a few centimeters in length, with each end "capped" with half of a fullerene dome consisting of five or six member rings. Along the sidewalls and cap, additional molecules can be attached to functionalize the nanotube to adjust its properties. CNTs are chiral structures with a degree of twist such that the graphene rings join into cylinders. The chirality determines whether a nanotube will conduct in a metallic or semiconducting manner. Carbon nanotubes possess many unique and remarkable properties. The measured electrical conductivity of metallic carbon nanotubes is in the order of 10^4 S/cm (ballistic transport) [168]. The thermal conductivity of carbon nanotubes at room temperature can be as high as 3,000–6,600 W/mK [164]. The Young's modulus of carbon nanotubes is about 1 TPa. The maximum tensile strength of carbon nanotubes is close to 30 GPa, with some reported at TPa [165]. The density of MWNTs is 2.6 g/cm^3 and the density of SWNTs ranges from 1.33 to 1.40 g/cm^3 depending on the chirality [166]. Since carbon nanotubes have very low density and long aspect ratios, they have the potential of reaching the percolation threshold at very low weight percent loading in the polymer matrix. Wu et al. [167] developed a process to prepare silver-coated carbon nanotubes (SCCNTs), and then used the SCCNTs to formulate an ICA and compare its electrical and mechanical properties to ICAs filled with traditional multi-walled carbon nanotubes (CNTs) and micrometer-sized Ag particles. It was found that the ICA filled with SSCNTs had a lower bulk resistivity ($2.21 \times 10^{\cdot 4}$

Ω cm) and higher shear strength than that of the Ag–particle filled ICA at the same filler volume content (28%).

Experiments conducted by Qian et al. [168] showed 36–42% and 25% increases in elastic modulus and tensile strength, respectively, in polystyrene (PS)/CNT composites. The TEM observations in their experiments showed that cracks propagated along weak CNT–polymer interfaces or relatively low CNT density regions and caused failure. If the outer layer of MWNTs can be functionalized to form strong chemical bonds with the polymer matrix, the CNT/polymer composites can be further improved in mechanical strength and have controllable thermal and electrical properties.

Effect of Adding CNTs to the Electrical Properties of ICAs

Lin and Lin [169] studied the effect of adding CNTs on the electrical conductivity of silver-filled conductive adhesives which had epoxy as the base resin and had various filler loadings. It was found that the CNTs could enhance the electrical conductivity of the conductive adhesives greatly when the silver filler loading was still below the percolation threshold. For example, the 66.5wt% filled silver conductive adhesive without CNTs had a resistivity of 10^{4} Ω cm, but showed a resistivity of 10^{-3} Ω cm after adding 0.27wt% CNTs. Therefore, it is possible to achieve the same level of electrical conductivity by adding a small amount of CNTs instead of the silver fillers.

Composites Filled with Surface-Treated CNT

Although CNTs have exceptional physical properties, incorporating them into other materials has been very challenging due to their non-polar and hydrophobic surfaces. Problems such as phase separation, aggregation, poor dispersion in the matrix, and poor adhesion to the matrix must be overcome. Zyvex Corporation [170] claimed that they had overcome these restrictions by developing a new surface treatment technology that optimizes the interaction between CNTs and the host matrix. A multifunctional bridge was created between the CNT sidewalls and the host matrix. The power of this bridge was demonstrated by comparing the fracture behavior of the polycarbonate, polystyrene, or epoxy composites filled with untreated and surface-treated nanotubes. It was observed that the untreated nanotubes interacted poorly with the polymer matrix and thus left behind voids in the matrix after fracture. However, for the composite filled with treated nanotubes, the nanotubes remained in the matrix even after the fracture, indicating strong interaction with the matrix. Due to their superior dispersion in the polymer matrix, the treated nanotubes achieved the same level of electrical conductivity at much lower loadings than the untreated nanotubes [171, 172].

References

[1] P. B. Jana, S. Chaudhuri, A. K. Pal, and S. K. De., "Electrical Conductivity of Short Carbon Fiber-Reinforced Carbon Polychloroprene Rubber and Mechanism of Conduction," *Polymer Engineering and Science*, 32, 448–456, 1992.

[2] Malliaris and D. T. Turner, "Influence of Particle Size on the Electrical Resistivity of Compacted Mixtures of Poly-mers and Metallic Powders," *Journal of Applied Physics*, 42, 614–618, 1971.

[3] G. R. Ruschau, S. Yoshikawa, and R. E. Newnham, "Resistivities of Conductive Composites," *Journal of Applied Physics*, 73(3), 953–959, 1992.

[4] K. Gilleo, "Assembly with Conductive Adhesives," *Soldering and Surface Mount Technology*, 19, 12–17, Feb. 1995.

[5] P. G. Hariss, "Conductive Adhesives: A Critical Review of Progress to Date," *Soldering and Surface Mount Technology*, 20, 19–21, May 1995.

[6] J. C. Jagt, "Reliability of Electrically Conductive Adhesive Joints for Surface Mount Applications: A Summary of the State of the Art," *IEEE Transactions on Components, Packaging, and Manufacturing Technology, Part A*, 21(2), 215–225, 1998.

[7] M. A. Lutz and R. L. Cole, "High Performance Electrically Conductive Adhesives," *Hybrid Circuits*, 23, 27–30, Sep. 1990.

[8] J. M. Pujol, C. Prud'homme, M. E. Quenneson, and R. Cassat, "Electroconductive Adhesives: Comparison of Three Different Polymer Matrices. Epoxy, Polyimide, and Silicone," *Journal of Adhesion*, 27, 213–229, 1989.

[9] J. I. J. Gonzales and M. G. Mena, "Moisture and Thermal Degradation of Cyanate-ester-based Die Attach Material," *Proceedings of 47th Electronic Components and Technology Conference*, San Jose, CA, pp. 525–535, May 1997.

[10] Y. Chien and M. N. Nguyen, "Low Stress Polymer Die Attach Adhesive for Plastic Packages," *Proceedings of 1994 Electronic Components and Technology Conference*, San Diego, pp. 580–584, May 1994.

[11] D. P. Galloway, M. Grosse, M. N. Nguyen, and A. Burkhart, "Reliability of Novel Die Attach Adhesive for Snap Curing," *Proceedings of the IEEE/CPMT International Electronic Manufacturing Technology (IEMT) Symposium*, Austin, TX, pp. 141–147, Oct. 1995.

[12] R. L. Keusseyan and J. L. Dilday, "Electric Contact Phenomena in Conductive Adhesive Interconnections," *International Journal of Microcircuits and Electronic Packaging*, 17(3), 236–242, 1994.

[13] M. K. Antoon and J. L. Koenig, "Fourier-Transform Infrared Study Of The Reversible Interaction of Water and a Crosslinked Epoxy Matrix," *Journal of Polymer Science (Physics)*, 19, 1567–1575, 1981.

[14] M. K. Antoon and. J. L. Koenig, "Irreversible Effects of Moisture on the Epoxy Matrix in Glass-Reinforced Composites," *Journal of Polymer Science (Physics)*, 19, 197–212, 1981.

[15] C. G. L. Khoo and J. Liu, "Moisture Sorption in Some Popular Conductive Adhesives," *Circuit World*, 22(4), 9–15, 1996

[16] S. M. Pandiri, "The Behavior of Silver Flakes in Conductive Epoxy Adhesives," *Adhesives Age*, 30, 31–35, 1987.

[17] B. Günther and H. Schäfer, "Porous Metal Powders for Conductive Adhesives," *Proceedings of the 2nd International Conference on Adhesive Joining & Coating Technology in Electronics Manufacturing*, Stockholm, Sweden, pp. 55–59, June 1996.

[18] S. Kotthaus, B. H. Gunther, R. Haug, and H. Schafer, "Study of Isotropically Conductive Adhesives Filled with Aggregates of Nano-Sized Ag-Particles," *Proceedings of the 2nd International Conference on Adhesive Joining & Coating Technology in Electronics Manufacturing*, Stockholm, Sweden, pp. 14–17, June 1996.

[19] P. K. Pramanik, D. Khastgir, S. K. De, and T. N. Saha, "Pressure-sensitive Electrically Conductive Nitrile Rubber Composites Filled with Particulate Carbon Black and Short Carbon Fibre," *Journal of Materials Science*, 25, 3848–3853, 1990.

[20] P. B. Jana, S. Chaudhuri, and A. K. Pal, "Electrical Conductivity of Short Carbon Fiber-Reinforced Poly-chloroprene Rubber and Mechanism of Conduction," *Polymer Engineering and Science*, 32(6), 448–456, 1992.

[21] V. R. Chaudhari, S. K. Haram, and S. K. Kulshreshtha, "Micelle Assisted Morphological Evolution of Silver Nanoparticles," *Colloids and Surfaces, A*, 301, 475–480, 2007.

[22] Pal, S. Shah, and S. Devi, "Synthesis of Au, Ag and Au–Ag Alloy Nanoparticles in Aqueous Polymer Solution," *Colloids and Surfaces, A*, 302, 51–57, 2007.

[23] Z. Chen and L. Gao, "A Facile and Novel Way for the Synthesis of Nearly Monodisperse Silver Nanoparticles" *Materials Research Bulletin*, 42, 1657–1661, 2007.

[24] Kumar, H. Joshi, R. Pasricha, A. B. Mandale, and M. Sastry, "Phase Transfer of Silver Nanoparticles from Aqueous to Organic

Solutions Using Fatty Amine Molecules," *Journal of Colloid and Interface Science*, 264, 396–401, 2003.

[25] M. G. Guzmán, J. Dille, and S. Godet, "Synthesis of Silver Nanoparticles by Chemical Reduction Method and Their Antibacterial Activity," *Proceedings of World Academy of Science, Engineering and Technology*, vol. 33, pp. 367 – 374, 2008.

[26] Z. Hu, T. Xu, R. Liu, and H. Li, "Template Preparation of High-Density, and Large-Area Ag Nanowire Array by Acetaldehyde Reduction," *Materials Science & Engineering A*, 371, 236–240, 2004.

[27] Y. Sun, Y. Yin, B. Mayers, T. Herricks, and Y. Xia, "Uniform Silver Nanowires Synthesis by Reducing $AgNO_3$ with Ethylene Glycol in the Presence of Seeds and Poly(vinyl pyrrolidone)," *Chemistry of Materials*, 14, 4736–4745, 2002

[28] E. A. Hernandez, B. Posada, R. Irizarry, and M. E. Castro, "A New Wet Chemical Approach for Selective Synthesis of Silver Nanowires," *NSTI-Nanotech 2004*, 3, 156 – 158, 2004.

[29] E. Korte, S. E. Skrabalak, and Y. Xia, "Rapid Synthesis of Silver Nanowires through a CuCl- or CuCl2-mediated Polyol Process," *Journal of Materials Chemistry*, 18, 437–441, 2008.

[30] M. J. Yim, Y. Li, K. Moon, and C. P. Wong, "Oxidation Prevention and Electrical Property Enhancement of Copper-Filled Isotropically Conductive Adhesives*", Journal of Electronic Materials*, 36(10), 1341–1347, 2007.

[31] Yokoyama, T. Katsumata, A. Fujii, and T. Yoneyama, "New Copper Paste for CTF Applications," *IMC Proceedings*, pp. 376–381, 1992.

[32] S. K. Kang, R. Rai, and S. Purushothaman, "Development of High Conductivity Lead (Pb)-Free Conducting Adhesives," *Proceedings of 47th Electronic Components and Technology Conference*, San Jose, CA, pp. 565–570, May 1997.

[33] S. K. Kang, R. Rai, and S. Purushothaman, "Development of High Conductivity Lead (Pb)-Free Conducting Adhesives," *IEEE Transactions on Components, Packaging and Manufacturing Technology, Part A*, 21(1), 18–22, Mar. 1998

[34] M. P. Y. Desmulliez, R. W. Kay, S. Stoyanov, and C. Bailey, "Stencil Printing at Sub-100 microns Pitch," *Proceedings of Electronics Packaging Technology Conference*, pp. 354 – 358, 2004.

[35] T. Gaugel, S. Bechtel, and J. Neumann-Rodekirch, "Advanced Micro-dispensing System for Conductive Adhesives," *Proceedings of 1st International IEEE Conference on Polymers and Adhesives in Microelectronics and Photonics*, pp. 40 – 45, 2001.

[36] Kamyshny, M. Ben-Moshe, S. Aviezer, and S. Magdassi, "Ink-Jet Printing of Metallic Nanoparticles and Microemulsions," *Macromolecular Rapid Communications*, 26, 281–288, 2005.

[37] D. Cibis, and U. Currle, "Inkjet Printing of Conductive Silver Paths," *2nd International Workshop on Inkjet Printing of Functional Polymers and Materials. Eindhoven, The Netherlands*, 2005

[38] Kolbe, A. Arp, F. Calderone, E. M. Meyer, W. Meyer, H. Schaefer, and M. Stuve, "Inkjettable Conductive Adhesive for Use in Microelectronics and Microsystems Technology," *Proceedings of IEEE Polytronic 2005 Conference.* Wroclaw, Poland, pp. 1–4, 2005.

[39] Moscicki, J. Felba, T. Sobierajski, J. Kudzia, A. Arp, and W. Meyer, "Electrically Conductive Formulations Filled Nano Size Silver Filler for Ink-Jet Technology," *Proceedings of IEEE Polytronic 2005 Conference,* Wroclaw, Poland, pp. 40–44, 2005.

[40] J. K. Lin, J. Drye, W. Lytle, T. Scharr, R. Subrahmanyan, and R. Sharma, "Conductive Polymer Bump Interconnects," *Proceedings of 46th Electronic Components and Technology Conference*, Orlando, FL, pp. 1059–1068, May 1996.

[41] T. Seidowski, F. Kriebel, and N. Neumann, "Polymer Flip Chip Technology on Flexible Substrates-Development and Applications," *Proceedings of 3rd international Conference on Adhesive Joining and Coating Technology in Electronics Manufacturing*, Binghamton, New York, pp. 240–243, September 1998.

[42] R. H. Estes, "Process and Reliability Characteristics of Polymer Flip Chip Assemblies Utilizing Stencil Printed Thermosets and Thermoplastics," *Proceedings of 3rd International Conference on Adhesive Joining and Coating Technology in Electronics Manufacturing*, Binghamton, New York, pp. 229–239, September 1998.

[43] E. Oh, "Flip Chip Packaging with Micromachined Conductive Polymer Bumps", *IEEE Journal on Selected Topics in Quantum Electronics*, 5(1), 119–126, January–February 1999.

[44] S. K. Lohokare, Z. Lu, C. A. Schuetz, and D. W. Prather, "Electrical Characterization of Flip-Chip Interconnects Formed Using a Novel Conductive-Adhesive-Based Process," *IEEE Transactions on Advanced Packaging*, 29(3), 542–547, 2006.

[45] Gaynes, R. Kodnani, M. Pierson, P. Hoontrakul, and M. Paquette, "Flip Chip Attach with Thermoplastic Electrically Conductive Adhesive," *Proceedings of 3rd International Conference on Adhesive Joining and Coating Technology in Electronics Manufacturing*, Binghamton, New York, pp. 244–251, September 1998.

[46] Y. Bessho, "Chip on Glass Mounting Technology of Lsis for LCD Module," *Proceedings of International Microelectronics Conference*, pp. 183–189, May 1990

[47] J. B. Nysaether, Z. Lai, and J. Liu, "Isotropically Conductive Adhesives and Solder Bumps for Flip Chip on Board Circuits – A Comparison of Lifetime Under Thermal Cycling," *Proceedings of 3rd International Conference on Adhesive Joining and Coating Technology in Electronics Manufacturing*, Binghamton, New York, pp. 125–131, September 1998.

[48] B. Trumble, "Get the Lead Out!," *IEEE Spectrum*, pp. 55–60, May 1998.

[49] B. T. Alpert and A. J. Schoenberg, "Conductive Adhesives as a Soldering Alternative," *Electronic Packaging & Production*, 31, 130–132, November 1991.

[50] G. P. Nguyen, J. R. Williams, F. W. Gibson, and T. Winster, "Electrical Reliability of Conductive Adhesives for Surface Mount Applications," *Proceedings of International Electronic Packaging Conference*, San Diego, CA, pp. 479–486, September 1993.

[51] S. Rorgren and J. Liu, "Reliability Assessment of Isotropically Conductive Adhesive Joints in Surface-Mount Applications," *IEEE Transactions on Components, Packaging, and Manufacturing Technology, Part B*, 18(2), 305–312, 1995.

[52] S. Y. L. LIM, S. C. Chong, L. Guo, and W. Y. Hnin, "Surface Mountable Low Cost Packaging for RFID Device," *Proceedings of Electronic Packaging and Technology Conference*, pp. 255–259, 2006.

[53] H. Takezawa, M. Itagaki, T. Mitani, Y. Bessho, and K. Eda, "Development of Solderless Joining Technologies Using Conductive Adhesives," *Proceedings of 4th International Symposium and Exhibition on Advanced Packaging Materials, Processes, Properties and Interfaces*, Braselton, GA, pp. 11–15, March 1999.

[54] D. W. K. Eikelboom, J. H. Bultman, A. Schönecker, M. H. H. Meuwissen, M. A. J. C. Van Den Nieuwenhof, and D. L. Meier, "Conductive Adhesives for Low-Stress Interconnection of Thin Back-Contact Solar Cells," *29th IEEE Photovoltaic Specialists Conference*, pp. 403 – 406, May 2002.

[55] S. K Prasad, Advanced Wirebond Interconnection Technology, Springer, New York, 2004.

[56] G. G. Harman, Wirebonding in Microelectronics: Materials, Processes, Reliability and Yield, 2nd Ed., McGraw Hill, New York, 1997.

[57] F. Carson, "Advanced 3D Packaging and Interconnect Schemes," *Kulicke and Soffa Symposium at Semicon*, San Francisco, CA, July 2007.

[58] L. D. Andrews, T. C. Caskey, and S. J. S. McElrea, "3D Electrical Interconnection Using Extrusion Dispensed Conductive Adhesives," *International Electronics Manufacturing Technology Symposium*, pp. 96–100, 2007.

[59] http:Hwww.formfactor.com/

[60] K. Kataoka, S. Kawamura, T. Itoh, T. Suga, K. Ishikawa, and H. Honma, "Low Contact-Force and Compliant MEMS Probe Card Utilizing Fritting Contact," *Proceedings 15th International Conference on Micro Electro Mechanical Systems (MEMS'02)*, Las Vegas, January 20–24, pp. 364–367, 2002

[61] K. Kataoka, T. Itoh, K. Inoue, and T. Suga, "Multi-Layer Electroplated Micro-Spring Array for MEMS Probe Card," *Proceedings 17th International Conference on Micro Electro Mechanical Systems (MEMS'04)*, Maastricht, Jan. 25–29, pp. 733–736, 2004

[62] D. L. Smith and A. S. Alimonda, "A New Flip-Chip Technology for High-Density Packaging," *Proceedings 46th Electronic Components and Technology Conference*, Orlando, May 28–31, pp. 1069–1073, 1996.

[63] E. M. Chow, C. Chua, T. Hantschel, K. van Schuylenbergh, and D. K. Fork, "Solder-Free Pressure Contact Micro-springs in High-Density Flip-Chip Packages," *Proceedings 55th Electronic Components and Technology Conference*, Lake Buena Vista, Florida, May 31–June 3, pp. 1119–1126, 2005.

[64] T. Itoh, K. Kataoka, and T. Suga, "Fabrication of Microspring Probes Using Conductive Paste Dispensing," *Proceedings 19th International Conference on Micro Electro Mechanical Systems (MEMS'06)*, Istanbul, January 22–26, pp. 258–261, 2006.

[65] T. Itoh, T. Suga, and K. Kataoka, "Microstructure Fabrication with Conductive Paste Dispensing," *Proceedings of the 2nd IEEE International Conference on Nano/Micro Engineered and Molecular Systems*, Bangkok, Thailand, pp. 1003–1006, January 2007.

[66] Motoaki Itou, "High-Density PCBs Provided for More Portable De-sign," *Nikkei Electronics Asia*, vol. 8, No. 11, 1999 www.nikkeibp.com/nea/nov99/tech/index.html

[67] P. J. Savolanien, "Advanced Substrates for Wireless Terminals," *Proceedings of 4th International Conference on Adhesive Joining & Coating Technology in Electronics Manufacturing, Adhesives in Electronics*, Espoo, Finland, June 18–21, pp. 264–268, 2000.

[68] R. Kisiel, A. Markowski, and M. Lubiak, "Conductive Adhesive Fillets for Double Sided PCBs," *Proceedings of IEEE Interna-*

tional Conference on Polymer & Adhesives, Zalagerszeg, Hungary, pp. 13–16, June 2002.

[69] J. J. Felten and S. A. Padlewski, "Electrically Conductive Via Plug Material for PWB Applications," *IPC Printed Circuits Expo* 1997, San Jose, California, pp. S6-6-1–S6-6-4, March 1997.

[70] S. Wakabayashi, S. Koyama, T. Iijima, M. Nakazawa, and N. Kaneko, "A Build-up Substrate Utilizing a New via Fill Technology by Electroplating," *Proceedings of 4th International Conference on Adhesive Joining & Coating Technology in Electronics Manufacturing*, Espoo, Finland, pp. 280–288, June 2000.

[71] G. Dreezen, E. Deckx, and Luyckx, "Solder Alternative: Electrically Conductive Adhesives with Stable Contact Resistance in Combination with Non-Noble Metallizations," *Proceedings of European Microelectronics and Packaging Symposium*, Prague, pp. 284–292, June 2004.

[72] T. Suzuki, S. Tomekawa, T. Ogawa, D. Andoh, M. Tanahashi, and T. Ishida, "Interconnection Technique of ALIVH Substrate," *2001 International Symposium on Advanced Packaging Materials*, pp. 23–28, 2001.

[73] R. Kisiel, J. Borecki, J. Felba, and A. Moscicki, "Technological Aspects of Applying Conductive Adhesives for Inner Connections in PCB," *2004 4th IEEE International Conference on Polymers and Adhesives in Microelectronics and Photonics*, Portland, OR, pp. 121 – 125, September 2004.

[74] R. Kisiel, J. Borecki, G. Koziol, and J. Felba, "Conductive adhesives for through holes and blind vias metallization," *Proceedings of XXVIII International Conference IMAPS Poland Chapter*, Wrocław, Poland, September 2005.

[75] R. Kisiel, J. Borecki, J. Felba, and A. Moscicki, "Electrically Conductive Adhesives as Vias Fill in PCBs: The Influence of Fill Shape and Contact Metallization on Vias Resistance Stability," *28th International Spring Seminar on Electronics Technology*, pp. 193–198, 2005

[76] R. Kisiel, J. Borecki, G. Koziol, and J. Felba, "Conductive Adhesives for Through Holes and Blind Vias Metallization," *Microelectronics Reliability*, 45(12), 1935–1940, 2005.

[77] J. Felba, K. P. Friedel, and A. Moscicki, "Characterization and Performance of Electrically Conductive Adhesives for Micro-Wave Applications," *Proceedings of 4th International Conference on Adhesive Joining and Coating Technology in Electronics manufacturing*, Helsinki, Finland, pp. 232–239, June 2000

[78] S. Liong, Z. Zhang, and C. P. Wong, "High Frequency Measurement for Isotropically Conductive Adhesives," *Proceedings of 51st Electronic Components and Technology Conference*, Orlando, FL, pp. 1236–1240, May 2001.

[79] K. Hashimoto, Y. Akiyama, and K. Otsuka, "Transmission Characteristics in GHz Region at the Conductive Adhesive Joints," *Proceedings of Electronic Components and Technology Conference*, pp. 2067–2072, 2008.

[80] J. C. Jagt, "Reliability of Electrically Conductive Adhesive Joints for Surface Mount Applications: A Summary of the State of the Art," *IEEE Transactions on Components, Packaging, and Manufacturing Technology, Part A*, 21(2), 215–225, June 1998.

[81] J. B. Nysaether, Z. Lai, and J. Liu, "Thermal Cycling Lifetime of Flip Chip on Board Circuits with Solder Bumps and Isotropically Conductive Adhesive Joints," *IEEE Transactions on Advanced Packaging*, 23(4), 743–749, 2000.

[82] J. H. Constable, T. Kache, H. Teichmann, S. Muhle, and M. A. Gaynes, "Continuous Electrical Resistance Monitoring, Pull Strength, and Fatigue Life of Isotropically Conductive Adhesive Joints," *IEEE Transactions on Components and Packaging Technology*, 22(2), 191–199, 1999.

[83] R. Gomatam, E. Sancaktar, D. Boismier, D. Schue, and I. Malik, "Behavior of Electrically Conductive Adhesive Filled Adhesive Joints Under Cyclic Loading, Part I: Experimental Approach," *Proceedings of 4th International Symposium and Exhibition on Advanced Packaging Materials, Processes, Properties and Interfaces*, Braselton, GA, pp. 6–12, March 2001.

[84] Yamashita and K. Suganuma, "Degradation Mechanism of Conductive Adhesive/Sn-Pb Plating Interface by Heat Exposure," *Journal of Electronic Materials*, 31, 551 - 556, 2002.

[85] S. Xu, D. A. Dillard, and J. G. Dillard, "Environmental Aging Effects on the Durability of Electrically Conductive Adhesive Joints," *International Journal of Adhesion & Adhesives*, 23, 235–250, 2003.

[86] S. Kuusiluoma and J. Kiilunen, "The Reliability of Isotropically Conductive Adhesive as Solder Replacement – a Case Study Using LCP Substrate," *Proceedings of Electronic Packaging and Technology Conference (EPTC)*, pp. 774–779, 2005.

[87] Duraj and P. Mach, "Stability of Electrical Resistance of Isotropic Conductive Adhesives within Mechanical Stress," *International Conference on Applied Electronics, Pilsen*, 35–38, Sept, 2006.

[88] L. Jeahuck, C. S. Cho, and J. E. Morris, "Electrical and Reliability Properties of Isotropic Conductive Adhesives (ICAs) on Immersion Silver Printed Wiring Boards (PWBs)," *Proceedings of International Conference on Electronic Materials and Packaging*, 19–22, pp. 1–4, November 2007.

[89] J. E. Ehrreich, "Novel Electroconductive Compositions and Powder for Use Therein" *US Patent 4,407,674*, October 1983.

[90] E. M. Jost and K. McNeilly, "Silver Flake Production and Optimization for Use in Conductive Polymers," *Proceedings of ISHM, (Bournemouth, England)*, pp. 548–553, 1987.

[91] E. M. Jost and K. McNeilly, "Silver Flake Increases Performance of Conductive Adhesives," *Advanced Packaging*, pp. 42–46, June/July, 1999,

[92] K. McNeilly and E. M. Jost, "Effect of Lubricant Solvent Systems on the Rheological Properties of Silver Filled Polymers," *Proceedings International Microelectronics Conference*, pp. 299–303, 1996.

[93] E. Schlotter, M. D. Porter, T. B. Bright, and D. L. Allara, "Formation and Structure of a Spontaneously Absorbed Monolayer of Arachidic on Silver," *Chemical Physics Letters*, 132(1), 93–98, 1986.

[94] C. Naselli, J. F. Rabolt, and J. D. Swalen, "Order-Disorder Transitions in Langmuir-Blodgett Monolayers. I. Studies of Two-Dimensional Melting by Infrared Spectroscopy," *Journal of Chemical Physics*, 82(4), 2136–2140, 1985.

[95] L. J. Bellamy, The Infrared Spectra of Complex Molecules, Wily, New York, 1975.

[96] J. Lovinger, "Development of Electrical Conduction in Silver-Filled Epoxy Adhesives," *Journal of Adhesion*, 10, 1, 1979.

[97] J. Lovinger, "Conductive Adhesive System Including a Conductivity Enhancer", *US Patent 4,356,505*, 1982.

[98] P. Wong, D. Lu, L. Meyers, S. A. Jr. Vona, and Q. K. Tong, "Fundamental Study of Electrically Conductive Adhesives," *Proceedings 1st IEEE International Polymeric Electronics Packaging*, p. 80, 1997.

[99] G. R. Ruschau, S. Yoshikawa, and R. E. Newnham, "Resistivities of Conductive Composites," *Journal Applied Physics*, 72(3), 953–959, 1992.

[100] E. Sancaktar and Y. Wei, "The Effect of Pressure on the Initial Establishment of Conductive Paths in Electronically Conductive Adhesives," *Journal of Adhesion Science and Technology*, 10(11), 1221–1235, 1996.

[101] Lu, Q. Tong, and C. P. Wong, "A Study of Lubricants of Ag Flake for Microelectronics Conductive Adhesives," *IEEE Transactions on Components, Packaging, and Manufacturing Technology, Part A*, 22(3), 365–371, 1999.

[102] P. Wong, D. Lu, and Q. K. Tong, "Lubricants of Silver Fillers for Conductive Adhesive Applications," *Proceedings of the third international conference on adhesive joining and coating technology in electronics manufacturing*, Binghamton, New York, vol. 184. pp. 184–192, September 1998.

[103] Lu and C. P. Wong, "A Fundamental Study on Silver Flakes for Conductive Adhesives," *Proceedings of 4th International Symposium Advanced Packaging Materials*, pp. 256–260, 1998.

[104] D. Lu and C. P. Wong, "Effect of Shrinkage on Conductivity of Isotropic Conductive Adhesives," *International Journal of Adhesives and Adhesion*, 20(3), 189–193, 2000.

[105] L. Smith-Vargo, "Adhesives that Posses a Science all Their Own," *Electronic Packaging & Production*, 48–50, August 1986.

[106] S. M. Pandiri, "The Behavior of Silver Flakes in Conductive Epoxy Adhesives," *Adhesives Age*, 30, 31–35, October 1987.

[107] C. Gallagher, G. Matijasevic, and J. F. Maguire, "Transient Liquid Phase Sintering Conductive Adhesives as Solder Replacement," *Proceedings of 47th Electronic Components and Technology Conference*, San Jose, CA, pp. 554–560, May 1997.

[108] J. Roman and T. Eagar, "Low Stress Die Attach by Low Temperature Transient Liquid Phase Bonding," *Proceedings of ISHM*, San Francisco, CA, pp. 52–57, October 1992.

[109] C. Gallagher, G. Matijasevic, and A. Capote, "Transient Liquid Phase Sintering Conductive Adhesives," *US Patent 5863622*, August 1998.

[110] Y. Li, K. Moon, A. Whitman, and C. P. Wong, "Enhancement of Electrical Properties of Electrically Conductive Adhesives (ECAs) by Using Novel Aldehydes", *IEEE Transactions on Components and Packaging Technologies*, 29(4), 758–763, 2006.

[111] Nguyen, J. Williams, and F. Gibson, "Conductive Adhesives: Reliable and Economical Alternatives to Solder Paste for Electrical Applications," *Proceedings ISHM*, pp. 510–517, 1992.

[112] J. C. Jagt, P. J. M. Beric, and G. F. C. M. Lijten, "Electrically Conductive Adhesives: A Prospective Alternative for SMD Soldering," *IEEE Transactions on Components, Packaging, and Manufacturing Technology B*, 18, 292–298, May 1995.

[113] M. A. Gaynes, R. H. Lewis, R. F. Saraf, and J. M. Roldan, "Evaluation of Contact Resistance for Isotropic electrically Con-

ductive Adhesives," *IEEE Transactions on Components, Packaging, and Manufacturing Technology B*, 18, 299–304, May 1995.

[114] M. Zwolinski, J. Hickman, H. Rubin, Y. Zaks, S. McCarthy, T. Hanlon, P. Arrowsmith, A. Chaudhuri, R. Hermansen, S. Lan, and D. Napp, "Electrically Conductive Adhesives for Surface Mount Solder Replacement," *Proceedings of the 2nd International Conference on Adhesive Joining and Coating Technology in Electronics Manufacturing*, Stockholm, Sweden, June 3–5, pp. 333–340, 1996.

[115] Botter, "Factors that Influence the Electrical Contact Resistance of Isotropic Conductive Adhesive Joints During Climate Chamber Testing," *in Proceedings of the 2nd International Conference on Adhesive Joining and Coating Technology in Electronics Manufacturing*, Stockholm, Sweden, June 3–5, pp. 30–37, 1996.

[116] J. Liu, K. Gustafsson, Z. Lai, and C. Li, "Surface Characteristics, Reliability and Failure Mechanisms of Tin, Copper and Gold Metallizations," *Proceedings of the 2nd International Conference on Adhesive Joining and Coating Technology in Electronics Manufacturing*, Stockholm, Sweden, June 3–5, pp. 141–153, 1996.

[117] K. Gilleo, "Evaluating Polymer Solders for Lead Free Assembly, Part I," *Circuits Assembly*, pp. 50–51, 1994.

[118] K. Gilleo, "Evaluating Polymer Solders for Lead Free Assembly, Part II," *Circuits Assembly*, pp. 51–53, 1994.

[119] U. R. Evans, "The Corrosion and Oxidation of Metals: Scientific Principles and Practical Applications," Edward Arnold, London, UK, 1960.

[120] Milazzo, "Electrochemistry: Theoretical Principles and Practical Applications," Elsevier, New York, 1963.

[121] D. Lu and C. P. Wong, "Novel Conductive Adhesives for Surface Mount Applications," *Journal of Applied Polymer Science,* 74, 399–406, 1999.

[122] Tong, D. Markley, G. Fredrickson, R. Kuder, and D. Lu, *Proceedings of the 49th IEEE Electronic Components and Technology Conference*, San Diego, CA, pp. 347–352, 1999.

[123] C. M. Cheng, G. Fredrickson, Y. Xiao, Q. K. Tong, and D. Lu, *US Patent 6,344,157* 2002.

[124] G. Trabanelli and V. Carassiti, "Mechanism and Phenomenology of Organic Inhibitors," in Advanced Corrosion Science and Technology, M. G. Fontana and R. W. Staehle, Eds., Plenum Press, New York, Vol. 1, pp. 147–229, 1970

[125] G. Trabanelli, Corrosion Mechanisms, F. Mansfeld, Ed., Marcel Dekker, New York, pp. 119–164, 1987.

[126] Y. Li, K. Moon, and C. P. Wong, "Reliability Improvement of Conductive Adhesives on Tin (Sn) Surfaces," *Journal of Adhesion Science and Technology*, 19(16), 1427–1444, 2005.

[127] L. J. Matienzo1, F. D. Egitto1, and P. E. Logan, "The Use of Silane Coupling Agents in the Design of Electrically Stable Interfaces of 6061 T6 Aluminum Alloy Surfaces and Epoxy-based Electrically Conductive Adhesives," *Journal of Materials Science*, 38, 4381–4843, 2003.

[128] Reardon, Proceedings Corrosion'86, Paper no. 175, NACE, Houston, TX, 1986.

[129] M. G. Noack, Proceedings Corrosion'89, Paper no. 436, NACE, Houston, TX, 1989.

[130] P. A. Reardon and W. E. Bernahl, "New Insight into Oxygen Corrosion Control," Corrosion '87, Paper no. 438, NACE, Houston, TX, 1987.

[131] D. Lu and C. P. Wong, "Isotropic Conductive Adhesives Filled with Low-Melting-Point Alloy Fillers," *IEEE Transactions on Electronics Packaging Manufacturing*, 23(3), 185–190, 2000.

[132] Li, K. Moon, and C. P. Wong, "A Novel Approach to Stabilize Contact Resistance of Electrically Conductive Adhesives on Lead-Free Alloy Surfaces," *Journal of Electronic Materials*, 33, 106–113, 2004.

[133] H. Takezawa, T. Mitani, T. Kitae, H. Sogo, S. Kobayashi, and Y. Bessho, *Proceedings of 8th IEEE International Symposium on Advanced Packaging Materials: Processes, Properties and Interfaces*, Atlanta, GA, March 3–6, 2002, pp. 39–143, 2002.

[134] S. Moon, S. Liong, H. Li, and C. P. Wong, "Stabilizing Contact Resistance of Isotropically Conductive Adhesives (ICA) on Various Metal Surfaces by Incorporating Sacrificial Anode Materials", *Journal of Electronic Materials*, 33(4), 1381–1388, 2004.

[135] D. Durand, D. Vieau, A. L. Chu, and T. S. Weiu, *US Patent 5180523* 1989.

[136] Kotthaus, R. Haug, H. Schafer, and O. D. Hennemann, *Proceedings of 1st IEEE International Symposium on Polymeric Electronics Packaging*, Norrkoping, Sweden, pp. 64–69, 1997.

[137] Vona and Q. K. Tong, *Proceedings of 4th International Symposium and Exhibition on Advanced Packaging Materials, Processes, Properties and Interfaces*, Braselton, GA, pp. 261–267, 1998

[138] Liu, and B. Weman, *Proceedings of the 2nd International Symposium on Electronics Packaging Technology*, Shanghai, China, pp. 313–319, 1996

[139] Y. Rao, D. Lu, and C. P. Wong, "A Study of Impact Performance of Conductive Adhesives," *International Journal of Adhesion and Adhesives*, 24(5), 449–453, 2004.

[140] Zwolinski, J. Hickman, H. Rubin, Y. Zaks, S. McCarthy, T. Hanlon, P. Arrowsmith, A. Chaudhuri, R. Hermansen, S. Lan, and D. Napp, "Electrically Conductive Adhesives for Surface Mount Solder Replacement"; *IEEE Transactions an Components, Packaging, and Manufacturing Technology – Part C*, 19(4), 241–250, October 1996.

[141] D. Lu and C. P. Wong, *US Patent No. 6,740,192*, 2004

[142] Y. Rao, D. Lu, and C. P. Wong, "A Study of Impact Performance of Conductive Adhesives," *International Journal of Adhesion and Adhesives*, 24(5), 449–453, 2004.

[143] N. Gent and G. R. Hamed, "Adhesion," in Encyclopedia of Polymer Science and Technology, J. I. Kroschwitz, H. F. Mark, N. M. Bikales, C. G. Overberger, and G. Menges, Eds., Wiley, New York, Vol. 1, 1985.

[144] J. E. Morris and S. Probsthain, *Proceedings of the 4th IEEE International Conference on Adhesive Joining and Coating Technology in Electronics Manufacturing*, June 8–21, pp. 41–45, 2000.

[145] Liong, C. P. Wong, and W. F. Burgoyne, "Adhesion Improvement of Thermoplastic Isotropically Conductive Adhesive," *IEEE Transactions on Components and Packaging Technologies*, 28(2), 327–336, 2005.

[146] E. P. Plueddemann, Silane Coupling Agents, 2nd Ed., Plenum, New York, 1991.

[147] S. R. Culler, *US Patent 5 393 362,* 1995.

[148] R. A. Cayless, *US Patent 5 437 937*, 1995.

[149] H. W. Eichner and W. E. Schowalter, Report No. 1813, Forest Products Laboratory, Madison, Wisconsin, 1950.

[150] J. A. Marceau, R. H. Firminhac, and Y. Moji, *US Patent 4 085 012*, 1979.

[151] K. Moon, C. Rocket, and C. P. Wong, "Adhesion Improvement of Thermoplastic-Based Isotropic Conductive Adhesives under Humid Environment using Self-Assembled Monolayer Compounds," *Journal of Adhesion Science and Technology*, 18(2), 153–167, 2004.

[152] G. D. Davis and J. D. Venables, in Durability of Structural Adhesive, A. J. Kinloch, Ed., Applied Science, Essex, UK, p. 43, 1983.

[153] Nagai, K. Takemura, K. Isaka, O. Watanabe, K. Kojima, K. Matsuda, and I. Watanabe, *2nd IEMT/IMC Symposium*, April 15–17, pp. 353–357, 1998.

[154] Watanabe, T. Fujinawa, M. Arifuku, M. Fujii, and Y. Gotoh, *Proceedings of 9th IEEE International Symposium on Advanced Packaging Materials: Processes, Properties and Interfaces*, Atlanta, GA, March 24–26, pp. 11–16, 2004.

[155] H. P. Wu, X. J. Wu, J. F. Liu, G. Q. Zhang, and Y. W. Wang, "Development of a Novel Isotropic Conductive Adhesive Filled with Silver Nanowires", *Journal of Composite Materials*, 40(21), 1961–1968, 2005.

[156] H. H. Lee and K. S. Choua, "Effect of Nano-Sized Silver Particles on the Resistivity of Polymeric Conductive Adhesives", *International Journal of Adhesion & Adhesives*, 25, 437–441, 2005.

[157] Ye, Z. Lai, L. Johan, and A. Tholen, "Effect of Ag Particle Size on Electrical Conductivity of Isotropically Conductive Adhesives", *IEEE Transactions on Electronics Packaging Manufacturing*, 22(4), 299–302, 1999.

[158] L. Fan, B. Su, J. Qu, and C. P. Wong, "Electrical and Thermal Conductivities of Polymer Composites Containing Nano-Sized Particles," *Proceedings of Electronic Components and Technology Conference*, Las Vegas, NV, pp. 148–154, 2004.

[159] P. Mach, R. Radev, and A. Pietrikova, "Electrically Conductive Adhesive Filled with Mixture of Silver Nano and Microparticles," *Proceedings of 2nd Electronics System Integration Technology Conference*, pp. 1141–1146, 2008.

[160] H. Jiang, K. S. Moon, Y. Li, and C. P. Wong, "Surface Functionalized Silver Nanoparticles for Ultrahigh Conductive Polymer Composites," *Chemistry of Materials*, 18(13), 2969–2973, 2006.

[161] S. Kotthous, B. H. Günther, R. Hang, and H. Schafer, "Study of Isotropically Conductive Bondings Filled with Aggregates of Nano-Sized Ag-Particles," *IEEE Transactions on Components, Packaging, and Manufacturing Technology, Part A*, 20(1), 15–20, 1997.

[162] Majima, K. Koyama, Y. Tani, H. Toshioka, M. Osoegawa, H. Kashihara, and S. Inazawa, "Development of Conductive Material Using Metal Nano Particles," *SEI Technical Review*, 54, 25–27, 2002.

[163] S. Iijima, "Helical Microtubules of Graphitic Carbon", *Nature*, 354, 56, 1991.

[164] S. Berber, Y. K. Kwon, and D. Tománek, "Unusually High Thermal Conductivity of Carbon Nanotubes," *Physical Review Letters*, 84(20), 4613–4616, 2000.

[165] M. F. Yu, B. S. Files, S. Arepalli, and R. S. Ruoff1, "Tensile Loading of Ropes of Single Wall Carbon Nanotubes and their Mechanical Properties," *Physical Review Letters*, 84(24), 5552–5555, 2000.

[166] G. Gao, T. Cagin, and W. A. Goddard, "Energetics, Structure, Mechanical and Vibrational Properties of Single Walled Carbon Nano-Tubes (SWNT)," *Nanotechnology*, 9, 184–191, 1998.

[167] H. P. Wu, X. J. Wu, M. Y. Ge, G. Q. Zhang, Y. W. Wang, and J. Z. Jiang, "Properties Investigation on Isotropical Conductive Adhesives Filled with Silver Coated Carbon Nanotubes," *Composites Science and Technology*, 67, 1182–1186, 2007.

[168] D. Qian, E. C. Dickey, R. Andrews, and T. Rantell, "Load Transfer and Deformation Mechanisms in Carbon Nanotube Polystyrene Composites," *Applied Physics Letters*, 76, 2868, 2000.

[169] X. Lin and F. Lin, "Improvement on the Properties of Silver-Containing Conductive Adhesives by the Addition of Carbon Nanotube," *Proceedings of High Density Microsystem Design and Packaging*, Shanghai, China, pp. 382–384, 2004.

[170] M. Rutkofsky, M. Banash, R. Rajagopal, and C. Jian, "Using a Carbon Nanotube Additive to Make Electrically Conductive Commercial Polymer Composites," *S.A.M.P.E. Journal*, 41(2), 54–55, 2005.

[171] W. Lin, Y. Xiu, H. Jiang, R. Zhang, O. Hildreth, K. Moon, and C. P. Wong, "Self-Assembled-Monolayer-Assisted Chemical Transfer of in-situ Functionalized Carbon Nanotubes," *Journal of the American Chemical Society*, 130(30), 9636–9637, 2008.

[172] W. Lin, K. Moon, and C. P. Wong, "A Combined Process of *in-situ* functionalization and Microwave Treatment to Achieve Ultra-Small Thermal Expansion of Aligned Carbon Nanotube/Polymer Nanocomposites: Toward Applications as Thermal Interface Materials," *Advanced Materials*, 21, 2421–2424, 2009.

Chapter 5
Anisotropically Conductive Adhesives/Films (ACA/ACF)

5.1 Introduction

Anisotropic conductive adhesives (ACAs) or anisotropic conductive films (ACFs) are generally composed of polymer-based matrix with conductive fillers such as metallic particles or metal-coated polymer spheres. ACAs/ACFs provide unidirectional electrical conductivity in the vertical or *Z*-axis. This directional conductivity is achieved by using a relatively low-volume loading of conductive filler (5–20 volume percent) [1–3]. The low-volume loading is insufficient for inter-particle contact and prevents conductivity in the *X–Y* plane of the adhesive. The *Z*-axis adhesive, in film or paste form, is interposed between the surfaces to be connected. In the ACF interconnection, the conductive particles are trapped in the *z*-direction, allowing the metal layers of conductive particles to conduct electricity from the IC to the substrate while preventing short -circuiting in the *x–y* direction. The electrical conduction path is formed by mechanical contact between the conductive particle and the substrate. These contacts are retained by the adhesion strength of the cured polymer adhesive. Heat and pressure are applied simultaneously to this stack-up until the particles bridge the two conductor surfaces. Because of the anisotropy, ACA/ACF may be deposited over the entire contact region, greatly facilitating materials application. Also, an ultra-fine- pitch interconnection (<0.04 mm) could be achieved easily. The fine-pitch capability of ACA/ACF would be limited by the particle size of the conductive filler, which can be a few microns or a few nanometers in diameter. A cross-section of a joint formed by an ACA between two components is shown in Fig. 5.1.

Y. Li et al., *Electrical Conductive Adhesives with Nanotechnologies*,
DOI 10.1007/978-0-387-88783-8_5, © Springer Science+Business Media, LLC 2010

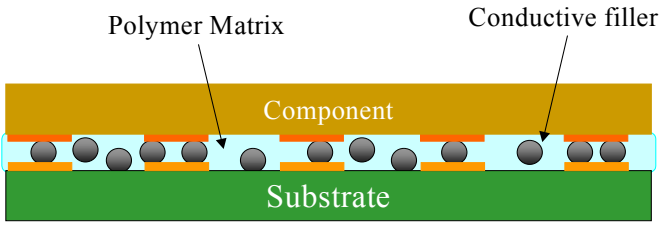

Fig. 5.1. A cross-section of an ACA joint

Anisotropic conductive adhesives (ACAs) are becoming popular as one of the promising candidates for lead-free interconnection solutions. In particular, ACFs are widely used for high density interconnection between liquid crystal display (LCD) panels and tape carrier packages (TCPs) to replace the traditional soldering or rubber connectors. In LCD applications, traditional soldering may not be as effective as ACFs in interconnecting materials between indium-tin- oxide (ITO) electrodes and TCP. Recently, ACFs have also been used as an alternative to soldering for interconnecting TCP input lead bonding to printed circuit boards (PCBs).

5.2 ACA Materials and Processing

5.2.1 ACA Materials

When designing materials to achieve fine-pitch interconnections, several important variables must be considered which are application dependent. These variables include adhesive characteristics as well as particle types.
Two basic types of adhesives are available: thermosetting and thermoplastic materials. Thermoplastic adhesives are rigid materials at temperatures below the glass transition temperature (T_g) of a polymer. Above T_g, polymers exhibit flow characteristics. When using this type of material, assembly temperatures must exceed the T_g to achieve good adhesion. The principal advantage of the thermoplastic adhesives is the relative ease with which the interconnection can be disassembled for repair operations. Thermosetting adhesives, such as epoxies and silicones, form a three-dimensional cross-linked structure when cured under specific conditions. Curing techniques include heat, UV light, and added catalyst. As a result of this irreversible cure reaction, the initial uncross-linked material is transformed into a rigid solid. The curing reaction is not reversible, as such, it may hinder disassembly and interconnection repair. The ability to

maintain strength at high temperatures and the deformation of robust adhesive bonds are the principal advantages of these materials. For the selection of the adhesive, the robust bonds should be formed to all surfaces involved in the interconnection. Numerous materials surfaces can be found in the interconnection region including SiO_2, Si_3N_4, SiON, polyester, polyimide, FR-4, glass, gold, copper, and aluminum. Adhesion to these surfaces must be preserved after standard tests such as temperature–humidity bias aging and temperature cycling. Some surfaces may require chemical treatment to achieve good adhesion. In addition, the adhesive must not contain ionic impurities that would degrade electrical performance of the interconnections.

The materials used as conductive particles must also be carefully selected. Silver (Ag) offers moderate cost, high electrical conductivity, high current-carrying ability – even its oxide is still electrical conductive – and low chemical reactivity. Therefore, silver is the most commonly used conductive fillers for ICAs. However, problems with electromigration, especially under high bias condition, may occur. Besides silver, gold (Au) is also a widely used conductive filler due to its high conductivity and inertness nature. However, it is a noble metal and costs may be prohibitive for large-volume applications. Copper (Cu) due to its high conductivity and low cost appears to be another logical choice, but the challenge of easy oxidation under heat and humidity conditions somewhat limits the wide applications in conductive adhesives unless plating or complexing approaches are used. Nickel (Ni) is a lower cost alternative, but corrosion and oxidation of nickel surfaces have been found during accelerated aging tests. Metals (Ni and Au) -plated polymeric particles may offer the best combination of properties at moderate cost and therefore are commonly used in fine-pitch interconnection. Some ACA/ACF materials used solder (Sn/Pb) particles to ensure electrical contacts with high reliability by creating a metallurgical bond.

5.2.2 Processing

ACF assembly process requires the application of pressure during adhesive cure. Curing of adhesive needs standard method to supply the energy and initiate the chemical reaction. Heat is the typically used method while sometimes ultra-violet (UV) radiation is also used to initiate the reaction. These energy sources are easily incorporated into the process. Special equipment is needed to apply pressure during cure. Typically, heat is supplied from the thermode used for component pickup, whereas UV is usually brought through the substrate by optical fiber bundles. The chip would

be aligned to the contact pads on the substrate prior to being heated and pressed during assembly process. Therefore, an ultra-fine-pitch interconnection can be achieved easily using ACF.

Important process parameters for ACA/ACF assembly are temperature, pressure load, tacking time (time needed for the adhesive to soften and flow), and bonding time (final cure time). For typical ACA/ACF processes, one of the interconnecting parts is preheated to a temperature below the ACA/ACF bonding temperature, but high enough to partially soften the film so that it has the ability to flow and fill void areas. The bonding load should be high enough to allow the conductive spheres to make good physical contact between conductors but not high enough to damage any of the parts. Finally, the tacking time should be sufficient to give adequate time for the film to flow before curing begins so that it seals the contact area during the final bonding process. Many parameters can affect the bonding quality during the ACA/ACF bonding process, including

- curing temperature and time;
- bonding temperature and time;
- temperature ramp rate;
- alignment accuracy;
- pressure value, pressure distribution, and pressure application rate;
- bump height and uniformity; and
- board planarity and stiffness of the contact interfaces.

ACF bonding process is thermo-compression bonding (TCB) as shown in Fig. 5.2. In the case of thermo-compression bonding, an ACF material is attached to the glass substrate after film removal. Then final bonding is established by thermal cure of ACF resin, typically at 180^{o}C, 20 s, and 30 kgf/cm^{2} and conductive particle deformation between the electrodes of TCP and glass substrate by applied bonding pressure.

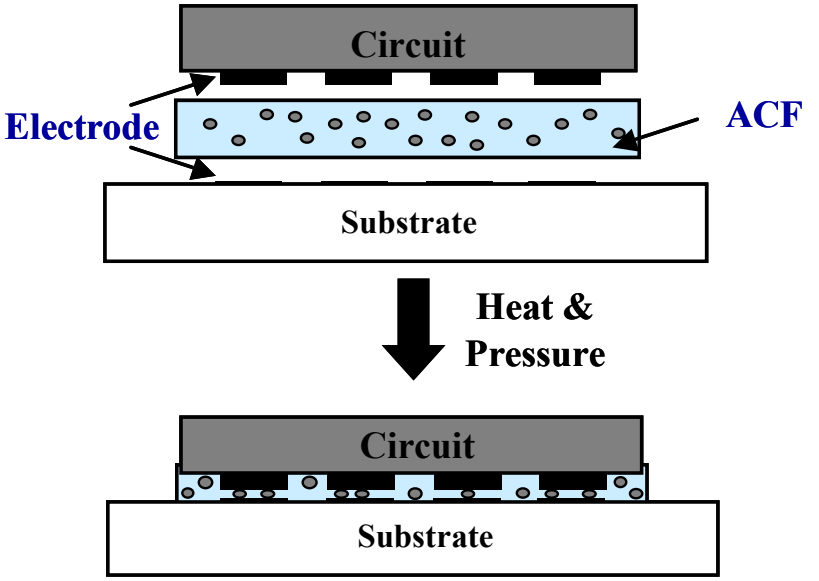

Fig. 5.2. Thermo-compression bonding using ACF

5.3 Applications of ACA/ACF

5.3.1 ACAs/ACFs for Flat Panel Displays

Interconnection technologies using ACFs are major packaging methods for flat panel display modules that need to be of high resolution, light weight, thin profile, and low consumption power. The technology has already been successfully implemented in the forms of out lead bonding (OLB), flex to PCB bonding, reliable direct chip attach such as Chip-On-Glass (COG), Chip-On-Film (COF) for flat panel display modules [4, 5], including liquid crystal display (LCD), plasma display panel (PDP), and organic light emitting diode display (OLED). As for the small and fine-pitched bump of driver ICs to be packaged, fine-pitch capability of ACF interconnection is much more desired for COG, COF, and even OLB assemblies. There have been advances in development for improved material system and design rule for ACF materials to meet fine-pitch capability and better adhesion characteristics of ACF interconnection for flat panel displays.

In addition to the LCD industry, ACA/ACF is now finding applications in flex circuits and surface mount technology (SMT) for chip-scale package

(CSP), application-specific integrated circuit (ASIC), and flip chip attachment for cell phones, radios, personal digital assistants (PDAs), sensor chip in digital cameras, and memory chip in laptop computers. Figure 5.3 shows various packaging technologies using ACF for LCD modules, tape carrier packages (TCP), COG, and COF bonding. Since connection pitch of driver IC electrode has been decreased and the number of output electrodes per IC increased for the progress of high-resolution LCD modules, ACF materials and packaging technologies have also been developed to meet high- density interconnection capability.

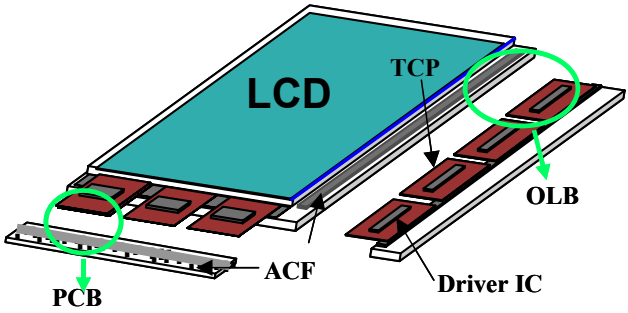

(a)

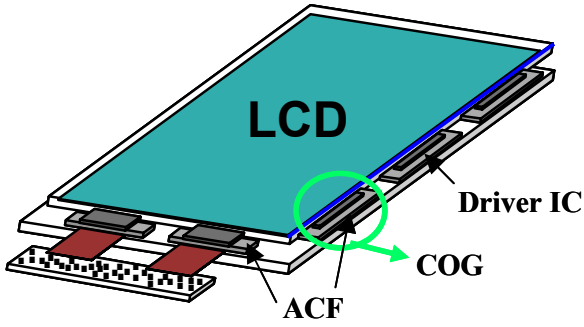

(b)

Fig. 5.3. Various packaging technologies using ACF in LCD modules (**a**) TCP outer lead bonding (OLB), and PCB bonding; (**b**) COG bonding; and (**c**) COF bonding

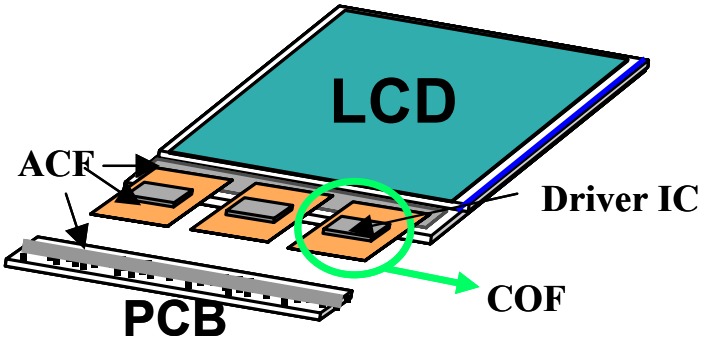

(c)

Fig. 5.3. (Continued)

The kind, size, density of conductive fillers and adhesive resin systems are different according to packaging technologies for LCD module. When TCP is mounted using ACF on LCD glass substrate, the CTE mismatch between TCP and the panel should be considered for thermal bonding, and this is more serious for finer pitch TCP bonding below 50 μm.

In COG technology, the bare driver ICs are flip chip bonded on glass substrate using ACF, and it is the most advantageous technology for low cost and compact size LCD module production [6]. The CTE difference between driver IC and glass substrate is relatively small compared with that in TCP applications and it provides more reliable COG connections.

COF, another ACF bonding area, is a relatively new technology compared with COG and COB in the production of flat panel module. LCD module production using COF technology is in an upgrowing stage due to its advantages of fine pitch interconnection, low contact resistance, and pre-test capability compared with COG in the high-density, multi-functional LCD module. In COF technologies, there are several alternatives for interconnect materials and processes, such as Au–Sn joining [7], stud bump bonding (SBB) joining [8], ACF joining, NCF and NCP joining. Among them, ACF joining method has been applied as main bonding method similar to COG technology.

For flex to glass bonding below 50 μm pitch, COF using ACF becomes more popular due to several advantages like fine-pitch capability, design flexibility, and low CTE base material. ACFs are also used in attaching

fine-pitched driver IC on COF substrates. The geometry of COF is very similar to that of TCP. However, the substrate is different, which is a two-layer structure, normally Cu and polyimide (PI) which is thinner, of higher density, better flexible, and more durable in high temperature than TCP with a three-layer structure (Cu, adhesive, and PI). COF's two-layer structure has normally weak adhesion property with ACF materials. Therefore, there has been development in ACF adhesion improvement to two-layer COF substrate.

Triple-layered ACF has been developed, which has adhesion layers on both sides of conventional ACF layer to improve interface adhesion and control bonding property for fine-pitch application during thermo-compression bonding as shown in Fig. 5.4 and the resulting reliability enhancement of COF module assembly [9].

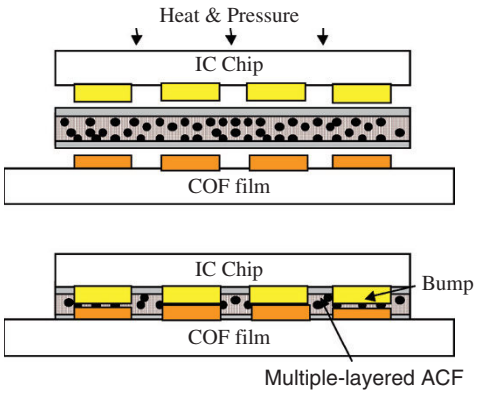

Fig. 5.4. COF bonding process using triple-layered ACFs [9]

5.3.2 ACAs/ACFs for Fine-Pitch Interconnections

As the function of driver IC for high-resolution LCD module increases, the bump density on IC also increases and this means bump size and pitch are reduced. For fine-pitch COG connection using ACF, the number of conductive particles trapped between the bump and the substrate pad should be enough. Therefore, conductive particle density of ACF for COG is much higher than that of ACF for TCP OLB. But due to high density of conductive particles, there is high possibility of electrical short circuit between adjacent bumps, mainly due to conductive particle accumulation by being flowed into the bump gap during COG bonding process. Therefore, double-layer ACF, which is composed of ACF layer and NCF layer with-

out conductive filler, was developed to have high electrical conductivity between bump and ITO electrode and electrical insulation between adjacent bumps [10]. As bump size and pitch of driver IC decreased, insulating layer-coated conductive particle was introduced instead of conventional conductive particles in ACF layer, and non-conductive fillers were incorporated together with conductive particles to ensure electrical insulation [11].

Figure 5.5 shows the relationship between the short circuit rate and the type of conductive particle. The double-layer ACF with conventional conductive particle and insulating layer-coated conductive particle are both 4 μm in diameter and of 35,000/mm^2 density. Insulating-coated conductive filler ACF is more advantageous than normal conductive particle ACF by reducing electrical short more effectively, and it achieved insulation capability at 10 μm gap level. In double-layer ACF structure, ACF and NCF layer thicknesses are 7 and 18 μm, respectively. The viscosity, formulation, thickness of adhesive layers, conductive filler density, type, and hardness should be optimized for high-performance COG package.

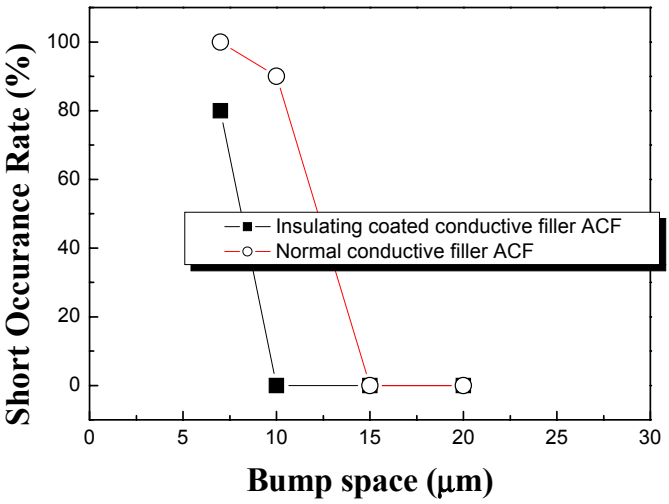

Fig. 5.5. The relationship between the short circuit rate and the type of conductive particle [11]

5.3.3 ACA/ACF in Flip Chip Applications

Conventional flip chip assembly involves two main steps: solder reflow and application of underfill, which is an organic adhesive placed between

the IC chip and the substrate to improve mechanical reliability. In recent years, ACA flip chip (where the active IC is bonded face down toward the substrate) technology has been employed in many applications where flip chips are bonded to rigid chip carriers [5, 8]. This includes personal digital assistants (PDAs), sensor chip in digital cameras, and memory chip in laptop computers. In all the applications, the common feature is that ACA flip chip technology is used to assembly bare chips where the pitch is extremely fine, normally less than 100 μm. For those fine applications, it is apparently the use of ACA flip chip instead of soldering that is more cost-effective.

ACA flip chip bonding exhibits better reliability on flexible chip carriers because the ability of flex provides compliance to relieve stresses. For example, the internal stress generated during resin curing can be absorbed by the deformation of the chip carrier. ACA joint stress analysis conducted by Wu et al. indicated that the residual stress is larger on rigid substrates than on flexible substrates after bonding [12]. Furthermore, the interconnect profile is much smaller, improves the miniaturization of the electronics, and reduces the processing temperature; as such, it reduces the thermal stress of the electronic components and enhances the product reliability and performance.

5.3.3.1 ACF Flip Chip Interconnection for Flip Chip Devices

As already stated, ACF provides a simpler flip chip interconnection process because there is no need for an underfill encapsulant process, compared to solder joints. However, thermal and mechanical stresses and strains induced by CTE (coefficient of thermal expansion) mismatches between the chip and the organic substrates need to be considered in flip chip interconnections to organic substrates such as FR-4 PCBs (printed circuit boards) and FPCs (flexible printed circuits). In order to apply ACF to flip chip interconnection to PCBs, the reliability of adhesive resins has been improved by formulating with epoxy resins, modifiers, and flexbilizing agents. It is also of concern that contact resistance may not be low since interconnection using ACF relies on mechanical contact as described earlier, unlike the metal bonding of soldering. Bonding process parameters such as temperature, pressure, and curing time have an important influence on the interconnection resistance between both electrodes. For example, if the bonding temperature is too low, the mechanical contact between bonding electrodes is not maintained. Also, conducting particles dispersed in adhesive films cannot make good electrical contacts with bonding electrodes.

5.3.3.2 ACF Flip Chip Interconnection for Bumpless Devices

ACF can be applied for bumpless flip chip interconnection to FR-4 PCBs, when bumps are produced on substrate electrodes. The use of bumpless chips allows a reduction in the cost of the flip chip bonding process, since Au bumping on the chip is not required. In addition, bumpless chip technology can provide fine pitch interconnection by reducing packages height significantly and allowing ultra-thin packages to be produced. For unbumped flip chips, a pressure-engaged contact must be established by bringing the particles to the aluminum chip pads rather than a bump. The pressure must be sufficient to break the oxide on the aluminum pads. A sufficient quantity of particles must be trapped in the contact pad area and remain in place during bonding and curing to achieve a reliable interconnection. In addition to maximizing the number of particles in the contact area the number of particles located between adjacent pads must be minimized to prevent electrical shorts. An additional factor that must be in the case of unbumped flip chip devices is adhesive flow during bonding and curing. It is essential to control the heating temperature to be sufficiently slow when the polymeric resin is cured so the conductive filler particles can migrate from the chip carrier side to the chip side pad [13].

5.4 Recent Advances of ACA/ACF and Nano-ACA/ACF

ACAs/ACFs are becoming popular as one of the promising candidates for lead-free interconnection solutions due to their technical advantages such as fine-pitch capability (<40 μm pitch), low temperature processing ability, low cost, and environmentally friendly materials and process. However, there are some key issues that hinder their implementation as interconnect materials for high-performance devices such as microprocessor and application-specific integrated circuit (ASIC) applications. The ACA/ACF joints have lower electrical conductivity and poor current-carrying capability because there is only mechanical/physical contact between the joints and no metallurgical contact of interconnects. To ensure low contact resistance and high current density, interface between conductive fillers and electrode should be improved. There have been extensive efforts on the research and development of high-performance ACA during the last two decades. The efforts so far have been mainly addressed on various material properties and assembly aspects. In particular with the rapid advancement of nano-technology, tremendous activities are also being pursued in high-performance ACA/ACF materials with nano-technology. The results of

their studies would allow development of ACA joints using fine-pitch flip chips on flexible/rigid substrates with better reliability and performance.

5.4.1 Low-Temperature Sintering of Nano-Ag- Filled ACA/ACF

One of the concerns for ACA/ACF is the higher joint resistance since interconnection using ACA/ACF relies on mechanical contact, unlike the metal bonding of soldering. The limited mechanical bonding restricts the electrical, thermal, and current flow along the ACA/ACF joints. As such, ACA/ACF cannot be used in high- power devices yet. An approach to minimize the joint resistance of ACA/ACF is to make the conductive fillers fuse each other and form metallic joints such as metal solder joints. However, fusing metal fillers in polymers does not appear feasible, since a typical organic printed circuit board (T_g ~125^{o}C), on which the metal-filled polymer is applied, cannot withstand such a high temperature; the melting temperature (T_m) of Ag, for example, is around 960^{o}C. Research showed that T_m and sintering temperatures of materials could be dramatically reduced by decreasing the size of the materials [14–17] (Fig. 5.6). It has also been reported that the surface premelting and sintering processes are a primary mechanism of the T_m depression of the fine nano particles (<100 nm). For nano-sized particles, sintering behavior could occur at much lower temperatures, as such, the use of the fine metal particles in ACAs would be promising for fabricating high electrical performance ACA joints through eliminating the interface between metal fillers. The application of nano-sized particles can also increase the number of conductive fillers on each bond pad and result in more contact area between fillers and bond pads. Therefore, application of nano-sized particles has potentials to improve the current density of the ACA joints by distributing current into more conductive paths (Fig. 5.7).

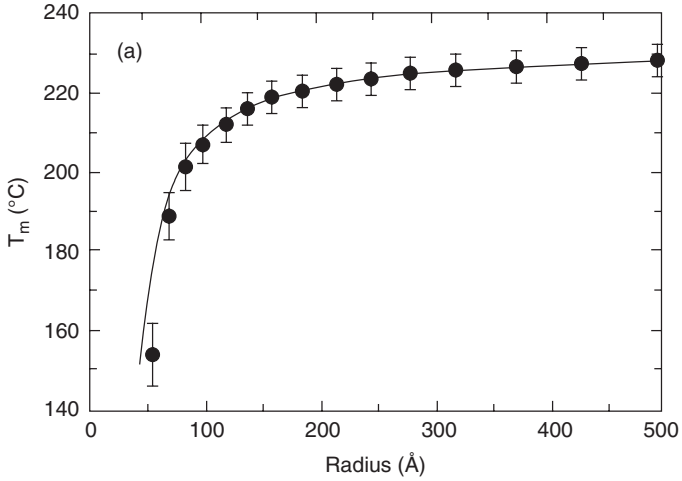

Fig. 5.6. Size dependence of the melting points of Sn particles [15]

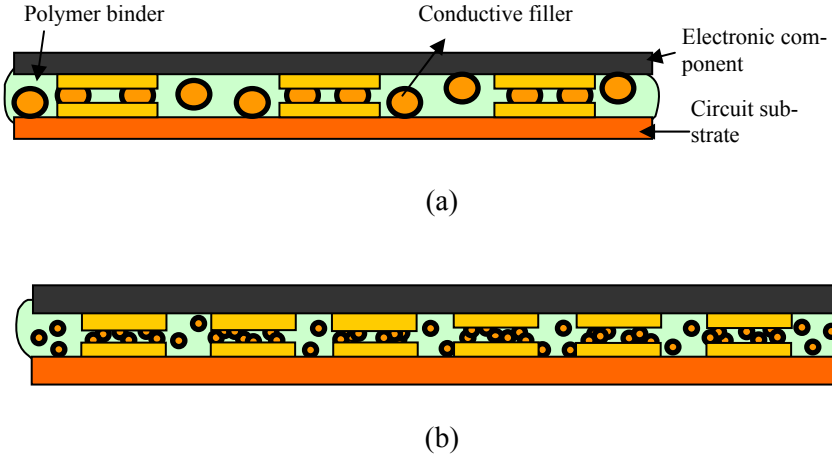

Fig. 5.7. Illustration of a chip and substrate assembled by ACA. (**a**) Traditional ACA with micron-sized fillers and (**b**) novel ACA with nano-fillers

Figure 5.8 shows the SEM photographs of nano-Ag particles annealed at various temperatures. Although very fine particles (20 nm) were observed for as-synthesized (in Fig. 5.8a) and 100°C treated particles (in Fig. 5.8b), dramatically larger particles were observed after heat treatment at 150°C and above. With increasing temperatures, the particles became larger and appeared as a solid matter rather than porous particles or agglomerates. The particles shown in Fig. 5.8c–e were fused through their surface and many dumbbell- type particles could be found. The morphology was similar to a typical morphology of the initial stage in the typical sintering process of ceramic, metal, and polymer powders. This low-temperature sintering behavior of the nano particles is attributed to the extremely high inter-diffusivity of the nano particle surface atoms, due to the significantly energetically unstable surface status of the nano-sized particles with large proportion of the surface area to the entire particle volume.

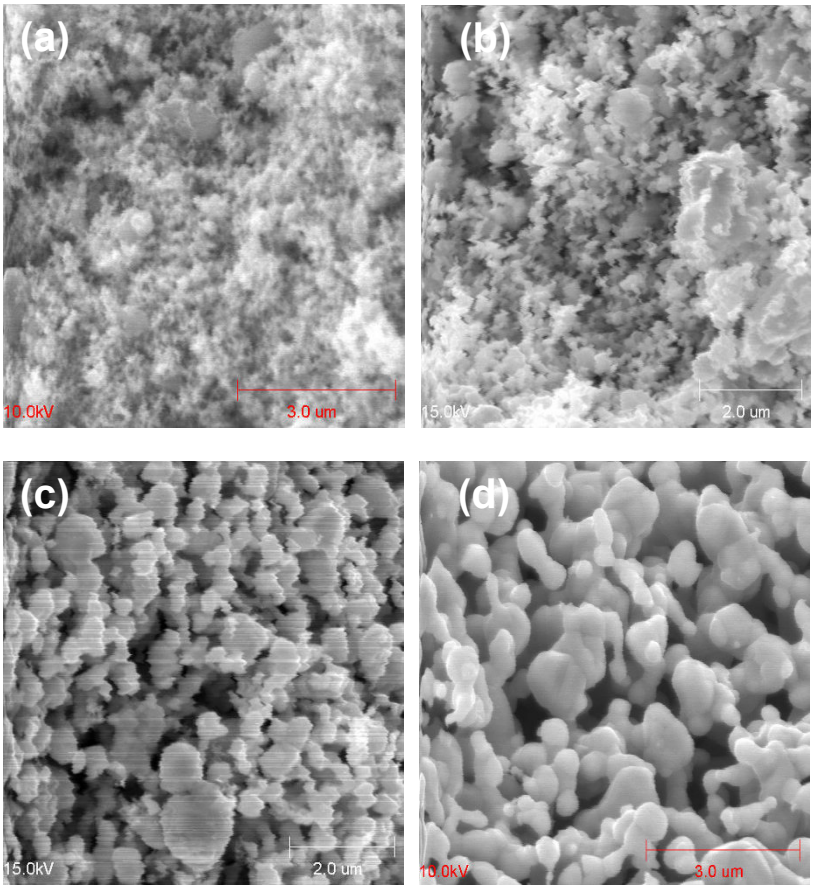

Fig. 5.8. SEM photographs of 20 nm-sized Ag particles annealed at different temperatures for 30 min: (**a**) room temperature (no annealing); (**b**) annealed at 100°C; (**c**) annealed at 150°C; (**d**) annealed at 200°C, and (**e**) annealed at 250°C [16]

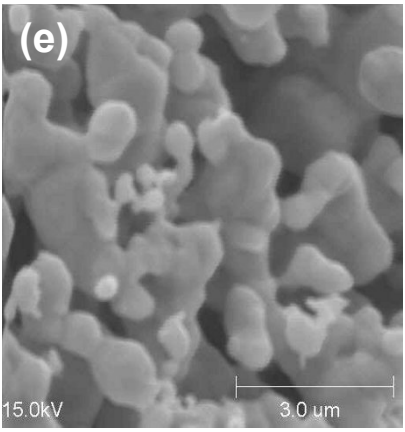

Fig. 5.8. (Continued)

For the sintering reaction in a certain material system, temperature and duration are the most important parameters; in particular, the sintering temperature. Current–resistance (I–R) relationship of the nano-Ag-filled ACA is shown in Fig. 5.9. With increasing curing temperatures, the resistance of the ACA joints decreased significantly, from 10^{-3} Ω to 5×10^{-5} Ω. Also, higher curing temperature ACA samples exhibited higher current-carrying capability than the low-temperature samples. This phenomenon suggested that more sintering of nano-Ag particles and subsequently superior interfacial properties between fillers and metal bond pads were achieved at higher temperatures [18], yet the *x*–*y* direction of the ACF maintains an excellent dielectric property for electrical insulation.

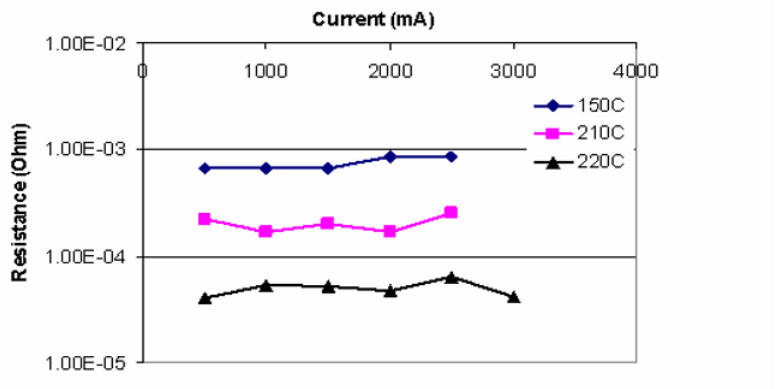

Fig. 5.9. Current–resistance (I–R) relationship of nano-Ag-filled ACAs with different curing temperatures [18]

5.4.2 ACA Joints with Low Melting Point (LMP) Filler

In order to conquer the limitation of conventional solders and adhesives used in electronics packaging, a self-organized joining process using conductive adhesive with low melting point alloy was reported [19]. In their process, adhesive which has an oxygen-reductive capability was mixed with fusible fillers (Sn–In alloy) and then heated to the temperature in between the melting point of fillers and the curing peak point of the resin. Motion of fillers occurred in the joint due to the thermal effect and hydrodynamic resin flow. Then, the adjoining fillers contacted and partly coalesced and even grew to form a large spherical blob by wetting. Finally, the joint was held in the temperature range over the curing peak point of the resin until the resin was fully cured. For a conduction path with a large volume fraction of filler, the filler adjoins with adjacent fillers and the morphology was isotropic. On the other hand, when the coalesced filler size exceeded the joint height, a conduction path forms and wetness developed on both sides of the electrode. Although a wide conduction path could be formed, the connection was unidirectional along the electrodes and the connection was anisotropic. An arrayed conduction path was achieved by combining materials which could form the anisotropic type only in the direction normal to the small electrodes shown in Fig. 5.10. Between horizontal electrodes, the insulation could also be maintained with self-organizing characteristics.

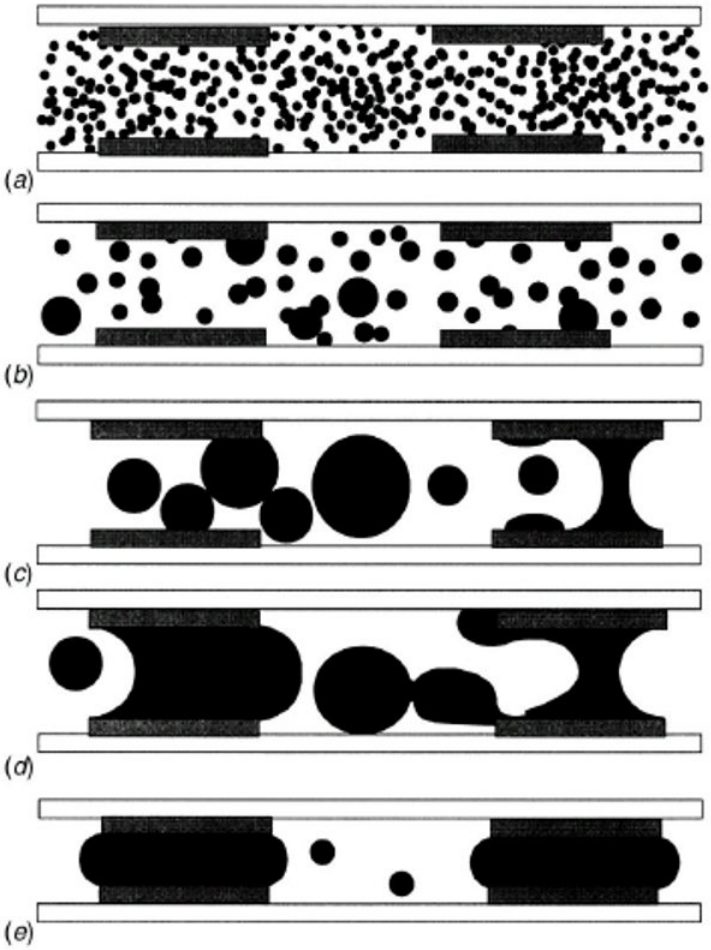

Fig. 5.10. Self-interconnection process using LMP (low melting point) alloy adhesive application. (**a**) Filler dispersion in resin, (**b**) filler coalescence and adhesion wetting on pads, (**c**) filler growth up to joint height and bridge formation between pads, (**d**) lateral flow by capillary force, and (**e**) completion of the interconnect [19].

5.4.3 Self-Assembled Molecular Wires for Nano-ACA/ACF

Self-assembled monolayers (SAMs) of small molecules, polymers, and proteins have attracted much attention in both experimental and theoretical fields for about two decades, and they offer the means to alter and control the chemical nature of surfaces. Self-assembled monolayers (SAMs) provide a convenient, flexible, and simple system with which to tailor the interfacial properties of metals, metal oxides, and semiconductors. SAMs are organic assemblies formed by the adsorption of molecular constituents from solution or the gas phase onto the surface of solids or in regular arrays on the surface of liquids (in the case of mercury and probably other liquid metals and alloys); the adsorbates organize spontaneously (and sometimes epitaxially) into crystalline (or semicrystalline) structures. The molecules or ligands that form SAMs have a chemical functionality, or "head group," with a specific affinity for a substrate; in many cases, the head group also has a high affinity for the surface and displaces adsorbed adventitious organic materials from the surface [20, 21]. There are a number of head groups that bind to specific metals, metal oxides, and semiconductors. The most well-studied SAMs are those prepared by the adsorption of alkanethiols ($CH_3(CH_2)_nSH$) on gold [22–29]. When adsorbed from the solution onto the Au (111) surface, alkanethiols form well-ordered monolayers possessing a ($\sqrt{3} \times \sqrt{3}$) R30° structure, wherein the sulfur atoms are bound to the three-fold hollow sites of the Au (111) surface [30]. On silver, the hydrocarbon chain is tilted much less, at about 13° from the surface normal. The adsorption of carboxylic acids ($CH_3(CH_2)_nCOOH$) has also been studied on silver surface and some experimental results suggested an epitaxial film with an in-plane structure of p (2×2) overlayer structure on Ag (111) surface. The bonding between carboxylic acids and Ag is considered as an acid–base reaction, and the driving force is the formation of a surface salt between the carboxylate anion and a surface metal cation [31–37]. As an example, Fig. 5. 11 is a schematic diagram of an ideal, single-crystalline SAM of alkanethiolates supported on a gold surface with a (111) texture [21]. The thickness of a SAM is typically 1–3 nm; they are the most elementary form of a nanometer-scale organic thin-film material. The composition of the molecular components of SAM determines the atomic composition of the SAM perpendicular to the surface; this characteristic makes it possible to use organic synthesis to tailor organic and organometallic structures at the surface with positional control approaching 0.1 nm.

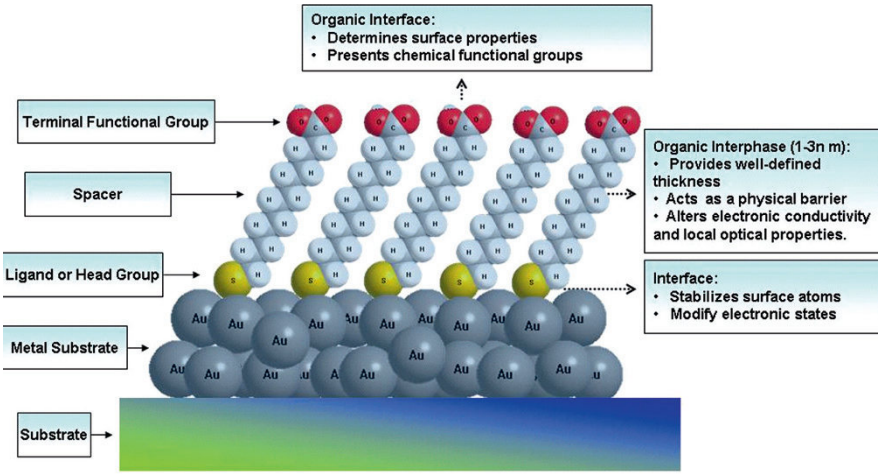

Fig. 5.11. Schematic diagram of an ideal, single-crystalline SAM of alkanethiolates supported on a gold surface with a (111) texture. The anatomy and characteristics of the SAM are highlighted [21]

Self-assembled monolayers (SAMs) offer unique opportunities to increase fundamental understanding of self-organization, structure–property relationships, and interfacial phenomena. The ability to tailor both head and tail groups of the constituent molecules makes SAMs excellent systems for a more fundamental understanding of phenomena affected by competing intermolecular, molecular-substrates and molecule–solvent interactions like ordering and growth, wetting, adhesion, lubrication, and corrosion. The thermal stability and structural properties of SAMs are governed by both the substrate–acid interactions and chain–chain interactions in the adsorbed layer. The structural features of these SAMs have been studied in detail by several experimental techniques such as IR spectroscopy, X-ray diffraction, surface-enhanced Raman spectroscopy (SERS), and X-ray photoemission spectroscopy (XPS). These experimental studies reveal that the ordered or crystalline nature of the SAMs is a function of the temperature and chain length. At room temperature, SAMs with longer chain lengths prefer a more ordered structure as compared to shorter chains,

which show no preferred tilt direction. At higher temperatures, the melting point can be reached which is chain length dependent.

In ACA/ACF interconnections, if SAM molecules can be introduced and monitored as electrical junctions or molecular wires, the interface properties between the conductive fillers and the contact pad are expected to be enhanced (Fig. 5.12). Some recent studies have introduced self-assembled molecular wires (SAM) into the interface between metal fillers and metal-finished bond pad of ACAs [38, 39]. These organic molecules adhere to the metal surface and form physi-chemical bonds, which allow electrons to flow, as such, it reduces electrical resistance and enables a high current flow. The unique electrical properties are due to their tuning of metal work functions by those organic monolayers. The metal surfaces can be chemically modified by the organic monoalyers and the reduced work functions can be achieved by using suitable organic monolayer coatings. An important consideration when examining the advantages of organic monolayers pertains to the affinity of organic compounds to specific metal surfaces. Table 5.1 gives the examples of molecules preferred for maximum interactions with specific metal finishes; although only molecules with symmetrical functionalities for both head and tail groups are shown, molecules and derivatives with different head and tail functional groups are possible for interfaces concerning different metal surfaces.

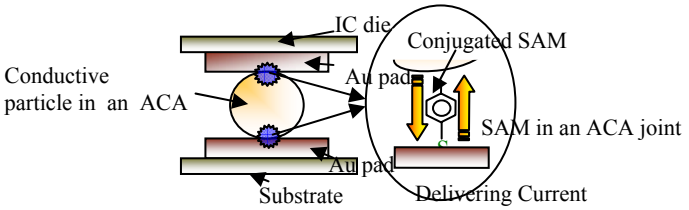

Fig. 5.12. Schematic illustration of SAM molecule formed in an ACA joint

Table 5.1. Potential organic monolayer interfacial modifiers for different metal finishes

Formula	Compound	Metal finish
H-S-R-S-H	Dithiols	Au, Ag, Sn, Zn
N•C-R-C•N	Dicyanides	Cu, Ni, Au
O=C=N-R-N=C=O	Diisocyanates	Pt, Pd, Rh, Ru
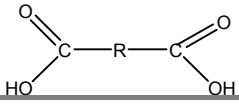	Dicarboxylates	Fe, Co, Ni, Al, Ag

Table 5.1. (Continued)

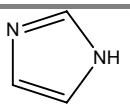	Imidazole and derivatives	Cu
$R\text{-}Si(OH)_3$	Organo-silane derivatives	SiO_2, Al_2O_3, quartz, glass, mica, ZnSe, GeO_2, Au

R denotes alkyl and aromatic groups

Different organic molecular wires, dicarboxylic acid and dithiol have been introduced into ACA/ACF joints. For SAM-incorporated ACA with micron-sized gold/polymer or gold/nickel fillers, lower joint resistance was achieved for low-temperature curable ACA (<100°C) (Fig. 5.13a). For high curing temperature ACA (150°C), however, the improvement was not as significant as low curing temperature ACAs, due to the partial desorption/degradation of organic monolayer coating at relatively high temperature (Fig. 5.13b) [38].

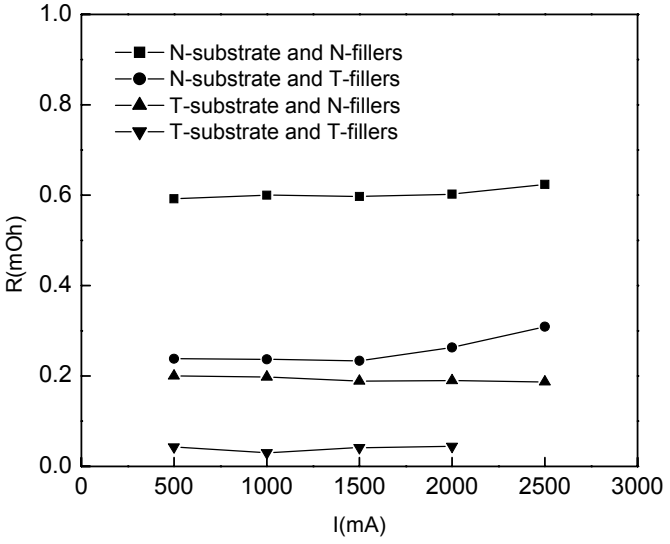

(a)

Fig. 5.13. Electrical properties of (**a**) low-temperature curable ACA with untreated (N) and treated (T) conductive fillers and substrates and (**b**) high-temperature curable ACA with untreated (N) and treated (T) conductive fillers and substrates [38]

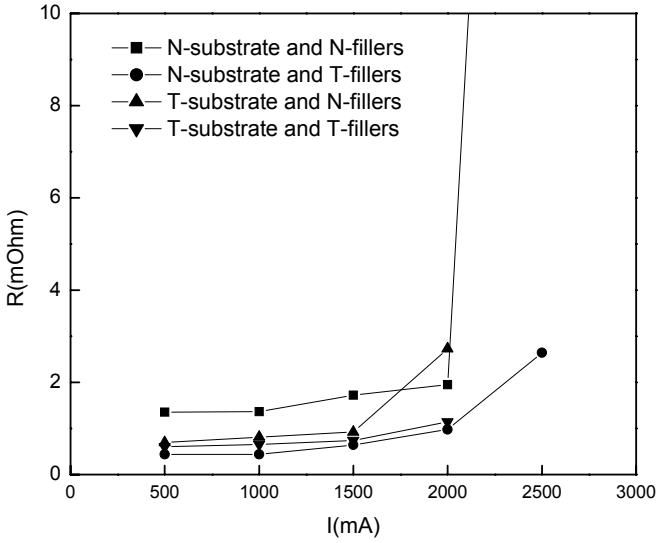

(b)

Fig. 5.13. (Continued)

However, when dicarboxylic acid or dithiol was introduced into the interface of nano-silver-filled ACAs, significantly improved electrical properties could be achieved at high-temperature curable ACA/ACF, suggesting the coated molecular wires did not suffer degradation on silver nanoparticles at the curing temperature (Fig. 5.14). For the untreated nano-Ag-filled ACAs, the electrical resistance of the ACA joints was around 10^{-3} Ω and the highest current applied without inducing joint failure (maximum allowable current) was 2.5 A. Over 2.5 A, the adhesive joints could not survive and the adhesive joints was burned and damaged. With the introduction of monolayer-protected silver nanofillers, the slope of *I–V* curve decreased dramatically, indicating a significantly improved conductivity of the joint. For the dithiol-treated nano-Ag-filled ACAs, the joint resistance decreased to 10^{-4} Ω, but the current carrying capability was the same as untreated samples. Increasing current over 2.5 A led to the failure of adhesive joints. For the acid M-treated ACA samples, dramatically decreased joint resistance was achieved as low as 10^{-5} Ω. The resistance value was comparable or even lower than some of the metallic solder joints. ($10^{-4} \sim 10^{-5}$ Ω). Moreover, the maximum allowable current of acid M-treated samples also increased significantly, from 2.5 to 3.5 A. Interestingly, at

current higher than 4 A when failure occurred, the failure location was between the probe tip and the substrate rather than the adhesive joints. This observation suggested that acid M-treated nano-Ag ACA joints had the potential to carry even higher current, provided a suitable or optimized test vehicle could be designed and used in this study. The improved electrical properties for SAM-coated nano-Ag ACA may be due to higher thermal stability of the SAM compounds on the silver nanoparticles. Those SAM compounds can also help the dispersion of silver nanoparticles in the epoxy resin and protect the metal fillers. The SAM compounds adhere to the conductive fillers, forming physi-chemical bondings and allowing electrons to freely flow/tunnel through the interfaces, as such, it reduces electrical resistance and can also carry a high current flow for ACA joints. Unlike the SAMs on micro-sized metal fillers which suffered degradation at temperatures higher than 100°C, the larger surface area and higher surface energy of nano particles enabled the SAMs to be more readily coated and relatively thermally stable on the metal surfaces. The stronger bonding between SAM and silver nanoparticles and the superior thermal stability made it more effectively improve the electrical properties of ACA cured at relatively higher temperature (e.g., 150°C) [39].

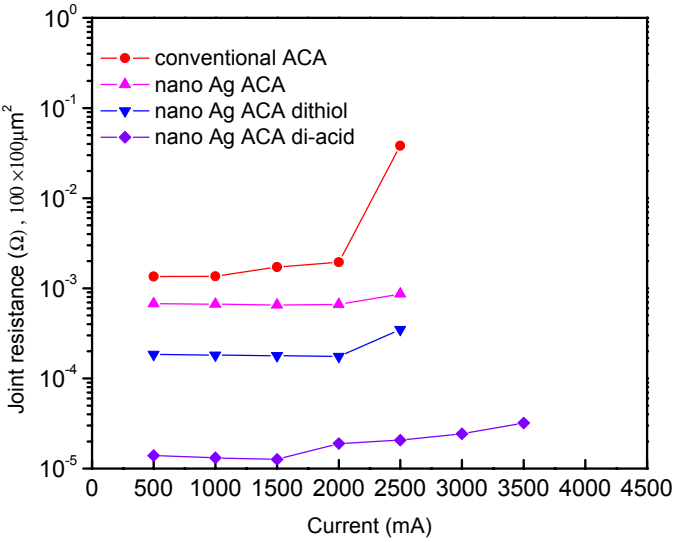

Fig. 5.14. Electrical properties of nano-Ag-filled ACA with dithol or dicarboxylic acid [39]

5.4.4 Silver Migration Control in Nano-silver filled ACA

Silver is the most widely used conductive fillers in ICAs and currently also considered as a potential candidate for ACA/ACF fillers because of the many unique properties of silver particles, in particular, the silver nano particles. Silver has the highest room temperature electrical and thermal conductivity among all the metals. Furthermore, silver is also unique among all the cost-effective metals by nature of its conductive oxide (Ag_2O). In addition, silver nano particles are relatively easy to be manufactured into different sizes (a few nano-meters to 100 nm) and shapes (such as spheres, rods, wires, disks, flakes) and well dispersed in a variety of matrice materials. Therefore, silver nanocomposites are considered as a promising material in electronic industry, such as nano-Ag ACA/ACF as a fine-pitch lead-free interconnect and high dielectric constant composites in embedded passives. However, a major problem that impedes the use of silver-containing materials in electronics is the electrochemical migration of silver in the presence of moisture and applied bias. In microelectronic devices, silver migration usually occurs between adjacent conductors, which leads to the formation of dendrites, growing from the cathode to the anode, and finally accumulating with an electrical short-circuit failure. To avoid short circuit, self-passivated aluminum (Al) has long been used in semiconductor devices, while copper (Cu) is being used in most electronic devices in recent years due to the better electrical conductance. However, copper is easily oxidized and a lot of efforts are needed to prevent the oxidation problem. Silver is the most promising metal for next-generation semiconductor devices because of the excellent electrical and thermal properties. By solving the migration issue for silver, it will have great potential to be used for next-generation high-performance advanced semiconductor devices.

Metal migration is an electrochemical process, which requires chemical interaction between the surroundings and the metal (generating metal ions); a polar transport electrolyte in aqueous conditions through which ionic migration occurs; and under an electric field. In fact, this situation prevails in most electronic packages where three conditions are present. It is considered that a threshold voltage exists above which the migration starts. When a potential is applied across the electrodes, a chemical reaction takes place at the positively biased electrode where positive metal ions are formed ($Ag \rightarrow Ag^+ e^-$). These ions, through ionic conduction, migrate toward the negatively charged cathode, where over time, they accumulate to form metallic dendrites ($Ag^+ e^- \rightarrow Ag$). As the dendrite growth increases, a reduction of electrical spacing occurs. Eventually, the silver growth reaches the anode

and creates a metal bridge between the electrodes, resulting in an electrical short circuit [40]. In particular in metal–polymer nano–composites, polymers tend to absorb water and other ionic pollutants from the environment, i.e., H_2S, HNO_3, CO_2, and tend to migrate between electrodes under the driving force of an electric field. Therefore, the insulation resistance of the polymer is curtailed. Water can not only act as the solvent and vehicle for ionic transport, but also participate pervasively in the conduction through electrolysis, especially at higher voltages.

Although other metals may also migrate under specific environment, silver has been the most prominent on the metal migration species, mainly due to the high solubility of silver ion in water, low activation energy for silver migration, high tendency to form dendrite, and low propensity/possibility to form stable passivation oxide layer like aluminum [41–43]. The rate of metal migration is increased by (1) an increase in the applied potential, (2) an increase in the time of the applied potentials, (3) an increase in the level of relative humidity, (4) an increase in the presence of ionic and hydroscopic contaminants on the surface of the substrate, and (5) a decrease in the distance between electrodes of the opposite polarity. Metal migration can be considered as a two-step process involving ionization and diffusion of the migrating species. DiGiacomo [41, 43] proposed a semi-empirical model of metal migration based on the electrochemistry of solutions, theory of adsorption and condensation, and transport through water films and polymers characterized by the products of four functions. In Eq. 3.1, migration is characterized by the current density:

$$\begin{aligned} J &= ZFDC_0\left(1-\exp\left(-\frac{ZFDE}{RT}t\right)\right) \\ &= ZFC_0D_0\exp(-\Delta H_D/kT)\left(1-\exp\left(-\frac{ZFD_0\exp(-\Delta H_D/kT)E}{RT}t\right)\right) \end{aligned} \tag{3.1}$$

where Z is the valence; F is Faraday's electrochemical equivalent, D is the diffusitivity of migration component, $D = D_0 \exp(-\Delta H_D/kT)$, where ΔH_D is activation energy of diffusion component, C_0 is the ionic concentration of migration component; $E = V/d$ is the electric field, where V is the applied voltage, d is the distance between electrodes; t is time; k and R are Boltzmann constant and molar gas constant, respectively.

In order to reduce silver migration, several methods have been reported. The methods include (1) alloying the silver with an anodically stable metal such as palladium [40] or platinum [44] or even tin [45]; (2) using hydrophobic coating over the PWB to shield its surface from humidity and ionic contamination, since water and contaminates can act as a transport medium and increase the rate of migration; (3) plating of silver with metals, such as tin, nickel, or gold, to protect the silver fillers and reduce migration; (4) coating the substrate with polymer [46]; (5) applying benzotriazole (BTA) and its derivatives in the environment [47]; (6) employing siloxane epoxy polymers as diffusion barriers due to the excellent adhesion of siloxane epoxy polymers to conductive metals [48]; (7) chelating silver fillers in ECAs with molecular monolayers [49]. As an example shown in Fig. 5.15, with carboxylic acids and forming chelating compounds with silver ions, the silver migration behavior (leakage current) could be significantly reduced and controlled. The obvious stabilized current leakage and subsequently the well-controlled electrochemical migration is due to the protection of silver ions with carboxylic acids by forming the chelating compounds. The adsorption of carboxylic acids on silver has been widely studied. The reaction is considered as an acid–base reaction, and the driving force is the formation of chelating bond/complex between the carboxylate anion and a surface silver ion (Equation 3.2).

$$Ag - e^- \rightarrow Ag^+; \quad Ag^+ + COO^- \rightarrow Ag^+ \ldots COO^- \tag{3.2}$$

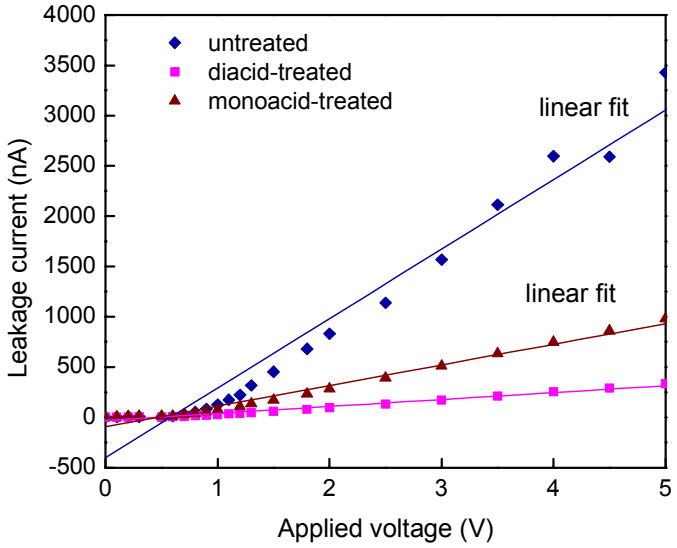

(a)

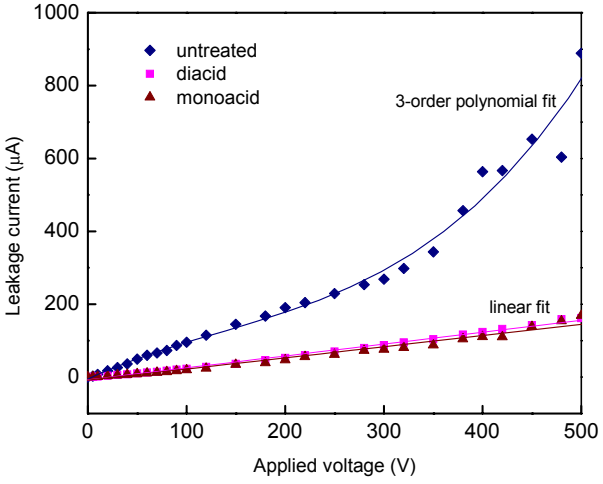

(b)

Fig. 5.15. Leakage current–voltage relationship of nano-Ag conductive adhesives at (**a**) low voltages and (**b**) high voltages [49]

The silver migration control in nano-ACA can also be observed from the morphology of ACA after high voltage test. Figure. 5.16 shows the photographs of test boards in the vicinity of nano-Ag ECAs after current–voltage tests up to 500 V. Obvious silver dendrites with several branches were observed for untreated nano-Ag ECAs, indicating the severe Ag migration. For the dicarboxylic acid incorporated nano-Ag ECA, however, no obvious dendrites were detected. The dark area around the edge of nano-Ag ECAs is considered to be from the typical inter-diffusion between different materials (nano-ECA and test board) rather than the ionic migration.

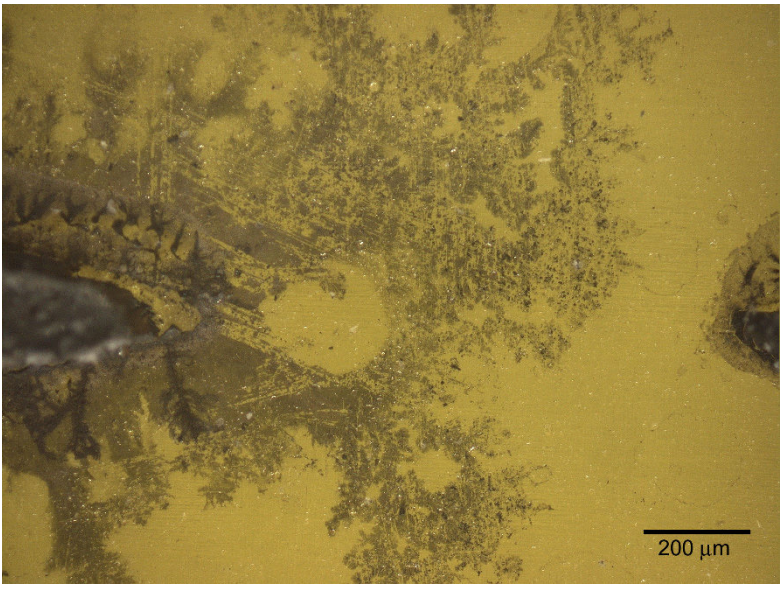

(a)

Fig. 5.16. Morphology in the vicinity of silver nano-Ag ECA after high-voltage migration tests. (**a**) Untreated nano-Ag ECA and (**b**) dicarboxylic acid-incorporated nano-Ag ECA [49]

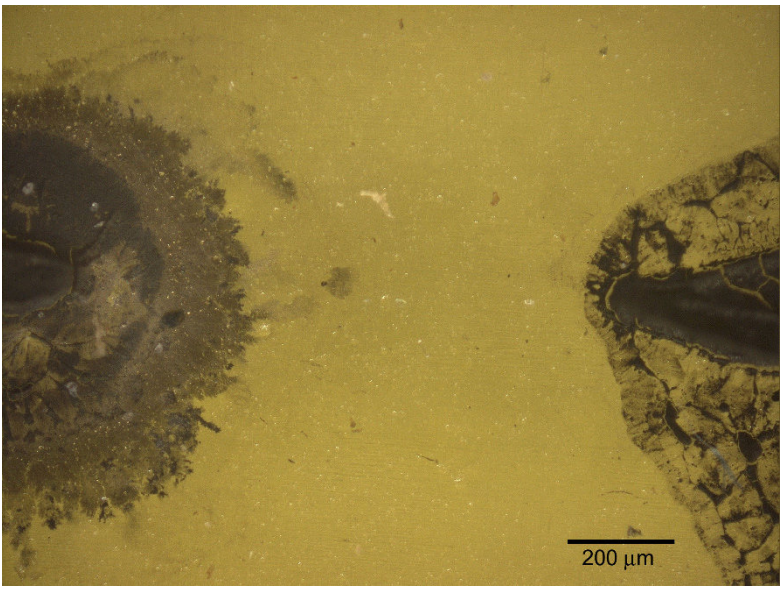

(b)

Fig. 5.16. (Continued)

5.4.5 ACA/ACF with Ferromagnetic Conductive Fillers

ACAs offer electrical conductivity in only vertical direction between the component termination and the pad. During the curing process, the ACA needs the application of pressure in order to capture a monolayer of particles between the mating pads. This requires specialized tooling and also sequential assembly. The application of pressure has been identified as a major factor in the performance of ACAs. Any surface variations in the component and pad and the extent of particle deformation influence the performance and long-term reliability of the assemblies.

In order to minimize or eliminate the required bonding pressure for ACA/ACF, researchers [50–54] have investigated *Z*-direction conductive adhesives based on magnetic alignment of ferromagnetic metal particles dispersed in a nonconductive adhesive polymer. As shown in Fig. 5.17, the presence of the magnetic field aligns the particles distributed within the matrix into columns between the mating pads. The electrical connection between the mating pads is formed by the build-up of the chain, wherein

the particles contact each other and form a continuous path. The columns are held in place by curing of the adhesive matrix while holding the magnetic field. This arrangement of columns enables conduction between the component and the substrate and eliminates the need for sequential assembly and pressure during cure. In addition, this technique could accommodate varying lead/interconnect geometries and coplanarity errors. The number of conductive particles in each column is dependent on the thickness of the adhesive printed and the average particle diameter. The interparticular resistance is expected to have a major influence on the contact resistance of the column and the performance of the ACA joint. The formation of the conductive columns may also provide good thermal dissipation paths and accommodate for the coefficient of thermal expansion mismatch when used with flip chip and other chip-scale devices. The epoxy matrix could also serve as an underfill and provide the necessary strength to hold components in place during fatigue loading and impact testing.

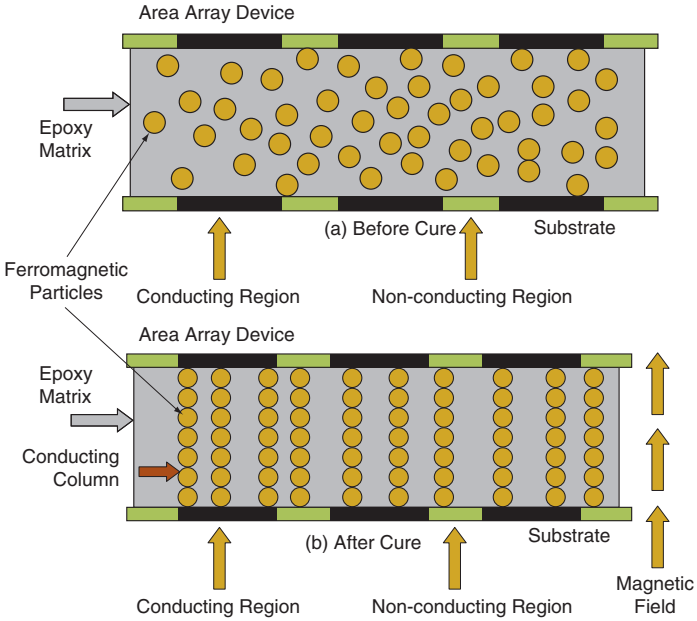

Fig. 5.17. Schematic illustration of ACA with aligned ferromagnetic particle columns under magnetic field

Jin et al. from AT&T Bell Labs found that the strength of the magnetic field could affect the formation of the chains [50, 51]. If the magnetic field applied was too strong, the magnetic aligning force in the columns overwhelms the surface tension on the top surface of the composite mixture, and the columns continue to grow into a dendrite structure above the surface. If the magnetic field is not strong enough, many columns fail to reach the top surface. It was also discovered that with finer particles, the assemblies revealed uniformity of resistance values when compared to large particles.

Sancaktar et al. investigated the effects of the type of magnetic and conductive nickel fillers, resin viscosity, and the magnitude of the aligning magnetic field on the electrical properties of the resulting anisotropic adhesive joints [52]. They also noticed the influence of the magnetic field strength in the formation of the columns. The authors have suggested that the optimum volume fraction of the filler and the optimal field strength have to be employed for the formation of a desirable magnetically distributed column structure. The authors also identified that the contact resistance decreased with an increase in magnetic field strength and the directional conductivity of the ACA increased with the increase in volume fraction of filler particles.

Breval et al. reported an ACF consisting of iron particles [53]. The influence of magnetic field strength on the formation of conductive columns was also discussed. The authors also observed that the elongated particles rotated to align lengthwise.

Ramkumar et al. recently investigated the applicability of this magnetic alignment of ferromagnetic metal particles in ACF for fine and ultra-fine-pitch mixed technology surface mount electronics packaging applications [54]. The authors found that the formation of conductive columns within the polymer matrix could provide a very high insulation resistance between adjacent conductors. It could also enable mass curing of the adhesive and eliminate the need for sequential assembly. The novel ACA with aligned ferromagnetic particles was found to be very effective in providing the interconnection for surface mount technology (SMT) passives and leaded, bumped, or bumpless integrated circuit packages. The requirement for precise stencil printing was eliminated, as the application of magnetic field aligned the conductive columns in the *Z*-axis direction eliminating any lateral conductivity. The ability to mass cure the adhesive while applying the magnetic field reduced the assembly time considerably. Placement accuracy was still found to be very critical. It was also found in this chapter that shear testing of adhesive joints after thermal aging showed significance past 500 h and after temperature–humidity aging showed significance within the first 100 h. I–V characteristics of the Daisy chained ball

grid array devices assembled with and without bumps revealed considerable difference in the breakdown current. The correlation between the initial contact resistance of the Daisy chain and the final breakdown current was also determined. As shown in Fig. 5.18, Daisy chains that had higher initial resistance showed lower breakdown current.

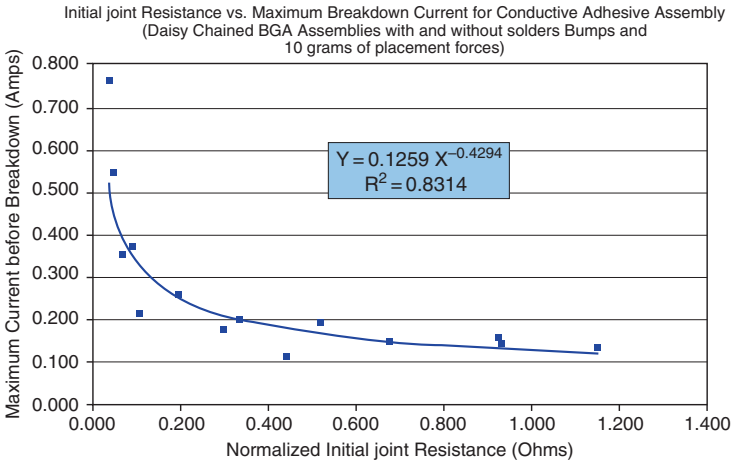

Fig. 5.18. Initial joint resistance versus maximum breakdown current for adhesive joint [54]

Sumitomo Electric recently developed a new-concept ACF using nickel nano particles with a straight-chain-like structure as conductive fillers [55]. They applied the formulated straight-chain-like nickel nano particles and solvent in a mixture of epoxy resin on a substrate film. Then the particles were made to orient toward the vertical direction of the film surface and fixed in resin by evaporating the solvent. In the estimation using 30 μm-pitch IC chips and glass substrates (the area of Au bumps was 2,000 μm^2, the distance of space between neighboring bumps was 10 μm), the new ACF showed excellent reliability of electrical connection after high-temperature, high humidity (60°C/90%RH) test and thermal cycle test (between −40°C and 85°C). The samples were also exposed to high temperature and high humidity (60°C/90%RH) for insulation ability estimation. Although the distance between two electrodes was only 10 μm, ion migration did not occur and insulation resistance has been maintained at over 1 GΩ for 500 h. This result showed that the new ACF has superior insulation reliability. This indicates that this new ACF has potential to be applied in very fine interconnections.

5.4.6 Nanowire ACF for Ultra-fine-pitch Flip Chip Interconnection

In order to satisfy the reduced I/O pitch and avoid electric shorting, a possible solution is to use high aspect ratio metal post. Nanowires exhibit high possibilities due to the small size and extremely high aspect ratio. In literature, nanowires could be applied in FET sensor for gas detection, magnetic hard disk, nanoelectrodes for electrochemical sensor, thermal-electric device for thermal dissipation, temperature control, etc. [56–58]. To prepare nanowires, it is important to define nano structures on photoresist. Many expensive methods such as e-beam, X-ray, or scanning probe lithography have been used but the length of nanowires cannot be achieved to micrometerscale. Another less expensive alternative is electrodeposition of metal into nano-porous template such as anodic aluminum oxide (AAO) [59] or block-copolymer self-assembly template [60]. The disadvantages of block-copolymer template include thin thickness (that means short nanowires), nonuniform distribution, and poor parallelism of nano-pores. However, AAO has benefits of higher thickness (>10 μm), uniform pore size and density, larger size, and very parallel pores. A new ACF with nanowires was recently reported, which used AAO templates to obtain silver and cobalt nanowires array by electrodeposition [61]. And then low viscous polyimide (PI) was spread over and filled into the gaps of nanowires array after surface treatment. The bimetallic Ag/Co nanowires could be kept parallel during fabrication by magnetic interaction between cobalt and applied magnetic field. The silver and cobalt nanowires/polyimide composite films could be obtained with diameter of nanowire about 200 nm and maximum film thickness up to 50 μm. The *X*–*Y* insulation resistance is about 4 – 6 GΩ and *Z*-direction resistance including the trace resistance (3 mm length) is less than 0.2 Ω. They also demonstrated the evaluation of this nanowire composite film by stress simulation. They found that the most important factor for designing nanowire ACF was the volume ratio of nanowires. But actually the ratio of naowires cannot be too small to influence the electric conductance. They concluded that it is important to get a balance between electric conductance and thermal–mechanical performance by increasing film thickness or decreasing modulus of polymer matrix instead of reducing ratio of nanowires.

5.4.7 Thermal Performance of ACA/ACF

As the current density at the ACA flip chip assembly is increasing for high current and high power dissipation device applications, the current-carrying capability of ACA is one of the important properties and has been characterized [62]. ACA, a normally thermally poor conductor, is required to be a thermal transfer medium which allows the board to act as new heat sink for the flip chip package and improve the lifetime of ACA flip chip joint under high current density application. The effect of thermal conductivity of ACA on the current-carrying capability of flip chip joints was investigated [63]. Figure. 5.19 shows comparison result of *I–V* characteristics when ACA flip chip joints is bias-stressed at a pair of Au stud bumps/ACA joints between conventional ACA without any thermal filler and thermally conductive ACA with SiC fillers. The conventional ACA flip chip joint shows the typical *I–V* curve with maximum allowable current level of 4.53 A. In contrast, flip chip joint using thermally conductive ACA shows almost linear increase of current as increase of voltage and maximum allowable current level is 6.71 A. Therefore, the current-carrying capability of ACA flip chip joint was improved by the use of thermally conductive ACA material. Figure. 5.20 shows the resistance changes of flip chip joints using conventional ACA and thermally conductive ACA as a function of time under constant current of 4.1 A. The contact resistances of conventional ACA flip chip joints increased abruptly as time passed 50 h and had open circuits before 100 h. But the thermally conductive ACA flip chip joints showed stable contact resistance behaviors without any open circuit. The failure or degradation mechanism of ACA flip chip joints under current biasing test is suggested as follows: (1) Au–Al IMCs formation, (2) crack formation and propagation along the Au/IMC interface, and (3) Al or Au depletion due to electromigration. All these causes of electrical degradation of ACA flip chip joints are due to heat accumulation at the Au stud bumps/PCB pads and thermal degradation of adhesive due to joule heating under high current bias. Similar discussion on the heat-induced failure mechanism of flip chip joint using isotropic conductive adhesive (ICA) under high current density was presented [64].

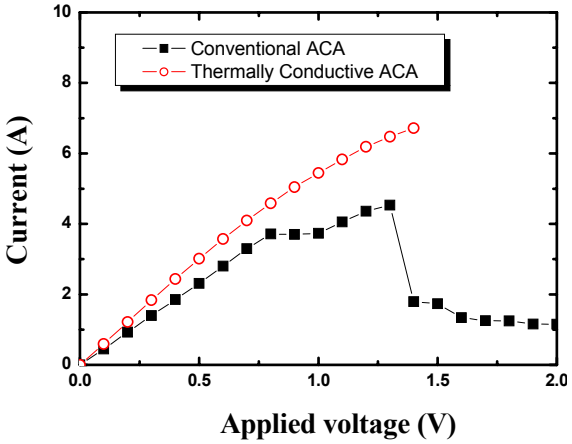

Fig. 5.19. *I–V* test (bias stressing) results at Au stud bumps/flip chip joints by conventional ACA and thermally conductive ACA [63]

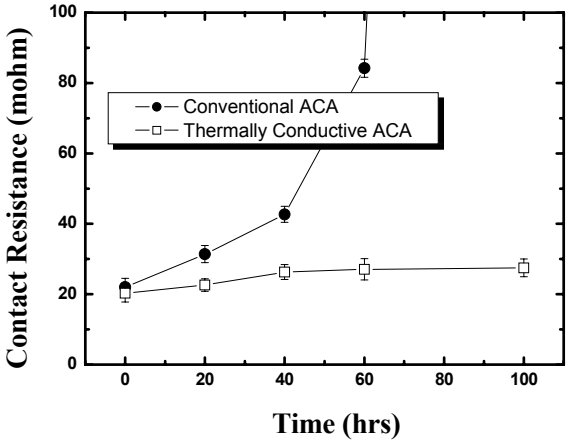

Fig. 5.20. Contact resistance changes of Au stud bump/flip chip joints using conventional ACA and thermally conductive ACA after 20, 40, 60, 100 h under bias current [63]

If the local temperature of flip chip joint by ACA/Au stud bump is relatively low due to effective heat dissipation throughout thermally conductive ACA, the thermal degradation process due to local joule heating and thermal degradation is slowed down, and electrical stability is obtained. This is verified by the behavior of junction temperature on the surface of

flip chip IC assemblies under current stressing condition as a function of time in Fig. 5.21.

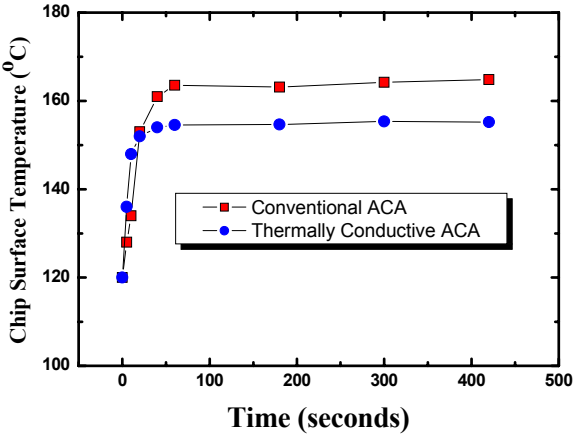

Fig. 5.21. Maximum chip surface temperature of flip chip assemblies using conventional and thermally conductive ACAs as a function of time under high current bias condition [63]

Ekstrand et al. also conducted research on thermally conductive ACA with incorporation of electrically insulating but thermally conductive fillers, including nano and micro scale particles of alumina oxide, silicon carbide, and carbon nanotubes (CNTs), used with and without surface treatment [64]. In this chapter, some experimental values are compared with the theoretical calculation based on Lewis–Nielsen theory (Fig. 5.22). From the theoretical calculations, carbon nanotubes and needle-shaped SiC (1:35 and 1:10 diameter to length ratio, respectively, is assumed) influenced the thermal conductivity of the composite more than the spherical SiC and Al_2O_3. The experimental values for Al_2O_3 composite were higher than the theoretical value, which was explained as the polydisperse of powders and therefore easier to form conductive network. On the contrary, the experimental values of the CNT composites were lower than the calculated value, which could be attributed to the poor dispersion of CNT into polymers.

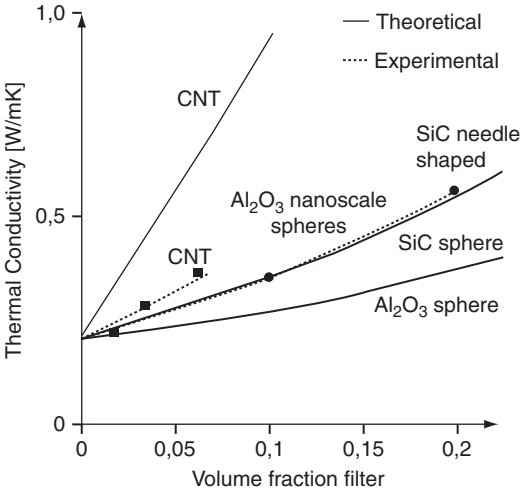

Fig. 5.22. Comparison of theoretical (according to Lewis–Nielsen theory) thermal conductivity and experimental values for polymer–nanocomposite [64]

The maximum chip surface temperature increases abruptly and become stable at around 50 s of high current applying time. The chip surface using thermally conductive ACA became hot faster than conventional ACA joint, which means thermally conductive adhesive dissipates the heat from the source more easily than conventional ACA does. The maximum temperature of chip surface of flip chip joint using thermally conductive ACA is lower than that of conventional ACA under constant current stressing. Therefore, the electrical reliability of flip chip joint under high current bias condition can be improved by dissipating the heat from hot spot and keeping the chip temperature as cool as possible. To further enhance the thermal performance of ACA/ACF, carbon nanotubes, with high thermal conductivity (>3,000 W/k from theoretical calculations), can also be aligned within the composite matrix to enhance the thermal conductivity.

5.5 ACA/ACF Reliability

Reliability is always one of the most important considerations to determine the value of materials. Reliability behavior of interconnection is characterized by performing accelerated aging tests such as high and low temperature storages, temperature cycling, and humidity storage. In the past few

years, several issues dealing with reliability of joints have been studied. Some main degradation mechanisms have been found, including oxide growth on less noble metallization causing increased contact resistance, stresses due to the thermal load or influence of humidity-inducing cracks within, or delamination of the adhesive layer.

5.5.1 Effects of Bonding Conditions

Bonding conditions of ACF, such as bonding temperature, temperature ramping rate, and pressure, affect the curing of ACF materials and the bonding quality of ACF joints. It has been reported that higher bonding temperatures resulted in better cross-linking density and stronger adhesion strength of ACF [65–67]. The increased adhesion strength with increasing bonding temperature is considered to be due to the inter-diffusion and/or reaction between the ACF polymeric material and the flex. In addition, it has been found that ACF assemblies with higher degrees of curing showed smaller increase in contact resistance after aging. At lower bonding temperatures and subsequently lower degree of cure, the conductive particles are able to move in the polymer layer. Therefore, there is a possibility of the conductive particles to squeeze due to the applied pressure through the soft adhesive. As a result, in some joints, higher and unstable contact resistance and even some open joints were found. At higher bonding temperature and higher degree of cure, the conductive particles remain stable throughout the ACF joints. A reliable interconnect with metal-to-metal contact could be achieved with less increase in contact resistance [68].

The bonding pressure also affects the reliability of ACF joints significantly. The lower the pressure used, the lower the stress accumulated at the interface and consequently better reliability after thermal cycling test. However, pressure has to be large enough to achieve good electrical conductivity and strong bonding.

5.5.2 Effect of Mechanical Properties on the Reliability of ACF Joints

Since stresses due to the thermal load or influence of humidity-induced cracks are one of the main degradation mechanisms of ACF joints, the mechanical properties of ACF materials play a significant role in the terminal deformation and reliability performance during thermal cycling testing [69, 70]. Generally, materials with a combination of high Young's modulus and low CTE (coefficient of thermal expansion) should show an improved reli-

ability in temperature cycling [71]. This is because matched CTE between the matching electrode pairs of the IC and the substrate (two contact partners) is necessary to minimize thermo-mechanical stresses on conductive joints within the polymeric layer, and sufficient Young's modulus prevents the assembly from bending (Fig. 5.23).

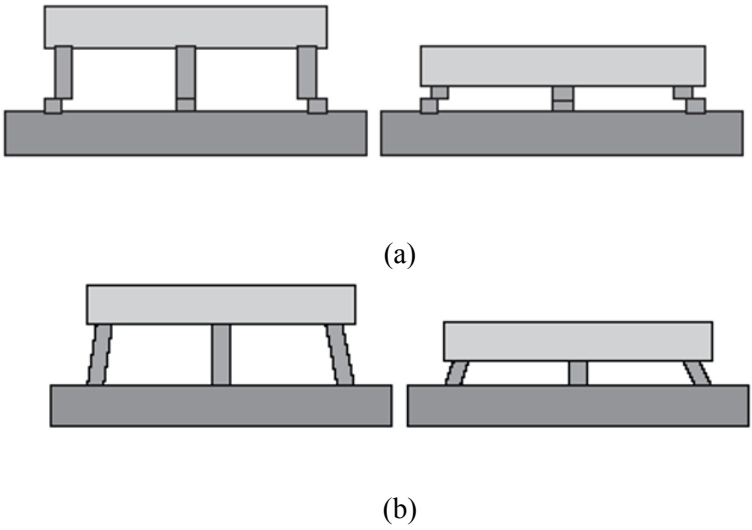

Fig. 5.23. (**a**) Deformation mechanism of the ACA joint due to thermally induced stress and (**b**) schematic diagram showing that thermal mismatch strain reduces as solder bump height increases [68]

Flip chip using anisotropic conductive adhesive should provide acceptable reliability level in harsh environments together with good processability. It requires the use of polymer materials which have close CTE value to the chip and the board and strong adhesion for better reliability. To enhance the reliability of ACA flip chip assemblies, non-conductive fillers, such as silica fillers, were added in the ACA materials [72] with different filler loadings. As the content of filler increased, CTE values decreased with increased storage modulus.

For the test IC chip and substrate, the gold stud bumps were formed on each I/O pad of test chips and 1 mm-thick FR-4 substrates were prepared. Flip chip assembly was performed by bonding the chip on the substrate with an appropriate bonding pressure of 50 kgf/cm^2 at 180°C for 30 s. The

chip was electrically connected to the substrate via the contacts between compressed gold stud bumps and conductive fillers in the ACA. Non-conductive fillers with smaller size than conductive fillers do not contribute the electrical contacts and instead affect other properties such as Young's modulus and CTE.

Reliability tests in terms of temperature cycling, high humidity and temperature, and high-temperature and dry condition test were performed by measurement of contact resistance variation. Figure. 5.24 showed that flip chip assembly using modified ACA composites with lower CTEs and higher modulus by loading non-conducting fillers exhibited better contact resistance behavior than conventional ACAs without non-conducting fillers. An ACF with a lower CTE and higher modulus can reduce the thermally induced shear strain in ACF layer measured by moiré interferometry during thermal cycling environment as shown in Fig. 5.25 and thus can increase the overall thermal cycling lifetime of ACF joints [70]. There are still more demanding issues for reliability enhancements such as low moisture absorption, effects of reflow temperature, process void, cure density, and interface stability of adhesion strength in ACA.

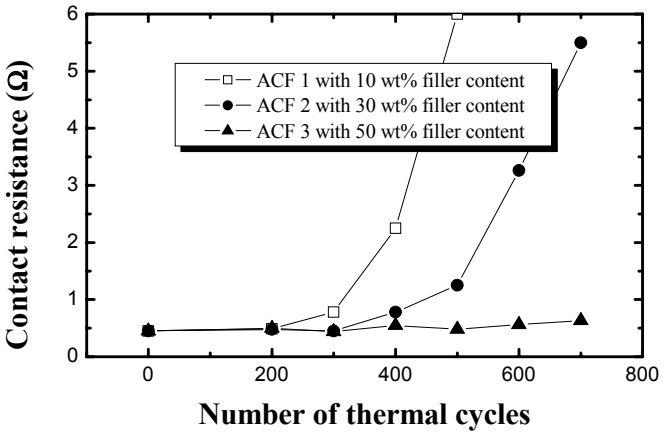

Fig. 5.24. Contact resistance of flip chip interconnects using ACA with different filler content during thermal cycling test from –60°C o 150°C for 700 cycles [72]

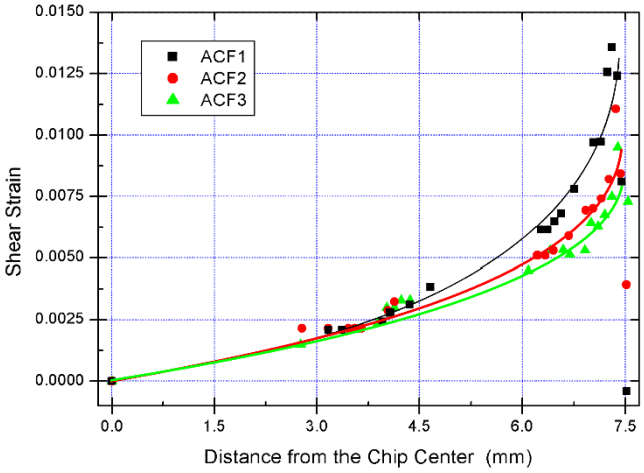

Fig. 5.25. Thermal shear strain of ACF layer between chip and FR-4 substrate of flip chip assembly [72]

5.5.3 Effects of Bump Height on the Reliability of ACA Joints

For ACA joining, the bumps and pads are made of hard materials such as Ni or Cu. The bumps and the pads are mechanically very strong that they cannot easily be deformed by the external stresses. The interface between the bump and the pad will play an important role in determining the juncture of the ACA joint and the joint strength. In particular, the height of the bumps can change the deformation characteristics and hence the reliability of the interconnection in the FC assembly. To study the effect of the adhesive volume in the structure indirectly Lai et al. [73] have investigated the effect of bump height on the reliability of ACA joints with FR4 rigid and polyimide flexible substrate. Their experiments indicated that for joints with rigid substrate an excessively high bump could induce poor reliability. They concluded that reliability problems of having high bump could occur since excessively high bump could easily cause a porous structure in the ACA layers.

Pinardi et al. [74] also reported work on the effects of bump height on the strain variation during the thermal cycling test of ACA flip-chip joints. The results showed that effect of bump height was significant only in the interface between the bumps and the pads. Bigger volume area of high strain was found for higher bump. There was practically no effect of the bump height on the strain changes in the bumps and in the pads. The effect of bump height was different for ACA joints than for solder joints, which

showed an increase of fatigue life of joints with high bump height (stand-off) because a high bump can relax the shear stresses in the corner regions of the solder.

5.6 Future Advances of ACA/ACF

Significant research has been conducted on ACA/ACF as a potential solder replacement for some electronics packaging applications. However, there are still challenges of ACA bonding in electronic assemblies. Sufficient conducting particles must be trapped during the bonding process to guarantee a reliable electrical contact. Failure mechanisms of ACA/ACF joints under various conditions need to be addressed and resolved. High current capability/density and self-alignment during the interconnect process, etc., must be better understood in order for this technology to be widely used to replace lead-bearing solders.

5.6.1 Materials Development

It is important to develop new ACA/ACF materials with high-performance dielectric properties, high purity, good adhesion, reasonable T_g, fast curing, storage stability at ambient, and stable contact resistance after various conditions frequently encountered in the field such as thermal aging and cycling, thermal shock, high temperature/high humidity/bias. Also, ACAs with low CTE are required. Commercially available ACAs typically exhibit very high CTEs because of the low filler loading levels utilized. Some preliminary studies have shown that ACAs with a low CTE created by introducing non-conductive fused silica fillers (with a TCE of 0.5 ppm) have a lower shear strain and better contact resistance stability during thermal cycling test. In addition to CTE mismatch, the current-carrying capability of ACF needs to be improved for high-power device applications, such as microprocessor and application specific integrated circuit (ASIC) applications.

5.6.2 High-Frequency Compatibility

For wireless/RF (radio frequency) electronic applications, a number of high-frequency (in excess of 2.45 to >10 GHz) applications and utilizations are increasing rapidly, thus it is important to characterize the cross-talk between particles, coupling with semiconductor devices, and other fundamental behavior of ACAs under high-frequency conditions. It is also necessary to maximize the current- carrying capability of ACAs at high-

frequency range and after exposure to various environmental tests. Good dielectrics with low loss factor (tan δ) and low dielectric constant (k) are critically needed.

5.6.3 Reliability

It is necessary to understand the effect of the chip carrier material on ACF join reliability. This is a key issue before ACF technology is widely utilized in manufacturing (i.e., in high-volume and low-cost applications). It is also necessary to establish failure rate prediction models for ACF joints for a wide variety of field conditions. It is essential to gain full understanding on effects of high current and high power on ACF joints; degradation and stress relaxation of polymeric matrices; and the effects of temperature, humidity, and other environments on matrix materials and the effects of fillers.

5.6.4 Wafer-Level Application

Flip chip technology is extending its applications to the fields of smart cards, displays, computers, mobile phones, communication systems, etc. However, the flip chip technology has a drawback that the production efficiency is poor in terms of process complexity and product cost because it requires conventional solder using complex connection processes, that is, solder flux coating, chip/board arranging, solder bump reflowing, flux removing, underfilling, and cure process. In order to reduce these complex processes, particular attention has recently been paid to wafer-level packaging technology in which wafers are coated with polymeric materials having flux and underfill functions [75, 76]. More recently, in developing new, improved flip chip connection technology, advantage has been taken of conductive adhesives, which are of a lower price than solders and enable the formation of ultra-fine pitches with the potential to realize environmental friendly, fluxless, and low-temperature processes.

In spite of extensive research activities, flip chip technology using these environmental friendly ACF or ACP as connecting materials suffer from the disadvantage of being inefficient in production costs requiring many processes, including chip design and bump formation for ACA flip chip packaging, mass production of connecting materials, and automation of connecting processes. Therefore, wafer-level flip chip package using ACA was developed to provide advantages in terms of production cost by simplifying the processes subsequent to the fabrication of conventional solder bump flip chip packages [77, 78].

Fabrication of wafer-level flip chip package using ACA comprised of forming a low-priced non-solder bump on an I/O pad of each chip of a wafer, coating the ACA over the wafer, dicing the ACA-coated wafer into individual chips by use of a wafer dicing machine, and subjecting the individual chips to flip chip bonding as shown in Fig. 5.26. The application of ACA to the bump-formed wafer can be achieved in a spraying, a doctor blade, or a meniscus coating process using ACP solution, and lamination of ACF. The film was laminated on the wafer in a thickness of 20–50 μm.

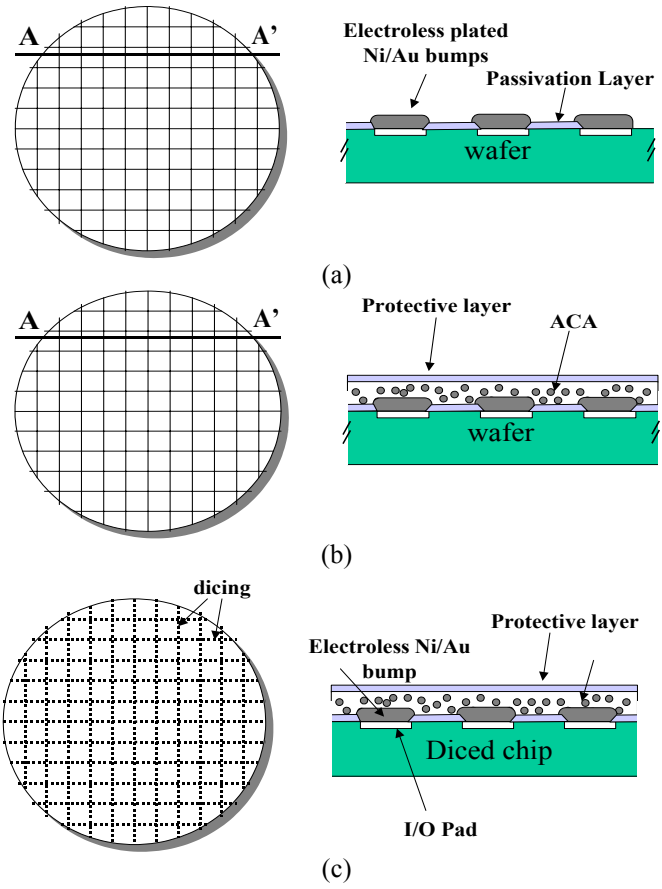

Fig. 5.26. (**a**) Schematic views showing a wafer with non-solder bump formation and cross-section view along the line A–A', (**b**) schematic views showing a wafer after ACA deposition on bump-formed wafer and its cross-section as view, and (**c**) schematic views showing a dicing process and cross section of diced chip with ACA deposition [77]

In wafer dicing process, the wafer with pre-applied ACA is mounted on a wafer dicing machine to confirm the scribe line of the wafer, after which the wafer is diced into individual chips. In this regard, ACA is required to be transparent and have such high adhesion as not to exhibit delamination during the process. After removing the protective layer from the diced chips, it is heat pressed against a circuit board so that the individual chips are electrically connected via the conductive particles of ACA onto the substrate pads. Wafer-level flip chip package using ACA is economically favorable owing to its simplicity and environmental friendly process.

References

[1] Y. Li, K. S. Moon, and C. P. Wong, "Electronics without Lead," *Science*, 308, 1419–1420, 2005.

[2] Y. Li and C. P. Wong, "Recent Advances of Conductive Adhesives as a Lead-Free Alternative in Electronic Packaging: Materials, Processing, Reliability and Applications," *Materials Science & Engineering R-Reports*, 51, 1–35, 2006.

[3] K. Gilleo, "Assembly with Conductive Adhesives," *Soldering & Surface Mount Technology*, 19, 12–17, 1995.

[4] H. Nishida, K. Sakamoto, H. Ogawa, and H. Ogawa, "Micropitch Connection Using Anisotropic Conductive Materials for Driver IC Attachment to a Liquid Crystal Display," *IBM Journal of Research and Development*, 42, 517–525, 1998.

[5] J. Liu, A. Tolvgard, J. Malmodin, and Z. H. Lai, "A Reliable and Environmentally Friendly Packaging Technology – Flip-Chip Joining Using Anisotropically Conductive Adhesive," *IEEE Transactions on Components and Packaging Technologies*, 22, 186–190, 1999.

[6] R. Joshi, "Chip on Glass-Interconnect for Row/Column Driver Packaging," *Microelectronics Journal*, 29, 343–349, 1998.

[7] J. Tjandra, C. L. Wong, J. How, S. Peana, M. Mita, and G. Murakami, "Au-Sn Microsoldering on Flexible Circuit," *Proceedings of Electronics Packaging Technology Conference,* pp. 52–57, 1997.

[8] Y. Kumano, Y. Tomura, M. Itagaki, and Y. Bessho, "Development of Chip-on-Flex Using SBB Flip-Chip Technology," *Microelectronics Reliability*, 41, 525–530, 2001.

[9] M. J. Yim, J. S. Hwang, J. G. Kim, J. Y. Ahn, H. J. Kim, W. S. Kwon, and K. W. Paik, "Highly Reliable Flip-Chip-on-Flex Package Using Multilayered Anisotropic Conductive Film," *Journal of Electronic Materials*, 33, 76–82, 2004.

[10] I. Watanabe, K. Takemura, N. Shiozawa, and T. Ohta, Chapter 9, "Flip chip interconnection technology using anisotropic conductive adhesive films," in *Flip Chip Technologies*, J. H. Lau, Ed., McGraw Hill, New York, 1996.

[11] M. J. Yim and K. W. Paik, "Recent Advances on Anisotropic Conductive Adhesives (ACAs) for Flat Panel Displays and Semiconductor Packaging Applications," *International Journal of Adhesion and Adhesives*, 26, 304–313, 2006.

[12] C. M. L. Wu, J. Liu, and N. H. Yeung, "Reliability of ACF in Flip-Chip with Various Bump Heigh," *Proceedings of 4th International Conference on Adhesive Joining and Coating Technology in Electronics Manufacturing,* Helsinki, Finland, pp. 101–106, 2000.

[13] K. Gustafsson, S. Mannan, J. Liu, Z. Lai, D. Whalley, and D. Williams, "The Effect on Ramping Rate on the Flip Chip Joint Quality and Reliability Using Anisotropically Conductive Adhesive Film on FR4 Substrate," *Proceedings of 47th Electronic Components and Technology Conference*, San Jose, CA, pp. 561–566, 1997.

[14] G. L. Allen, R. A. Bayles, W. W. Gile, and W. A. Jesser, "Small Particle Melting of Pure Metals," *Thin Solid Films*, 144, 297–308, 1986.

[15] S. L. Lai, J. Y. Guo, V. Petrova, G. Ramanath, and L. H. Allen, "Size-Dependent Melting Properties of Small Tin Particles: Nanocalorimetric measurements," *Physical Review Letters*, 77, 99–102, 1996.

[16] K. S. Moon, H. Dong, R. Maric, S. Pothukuchi, A. Hunt, Y. Li, and C. P. Wong, "Thermal Behavior of Silver Nanoparticles for Low-Temperature Interconnect Applications," *Journal of Electronic Materials*, 34, 168–175, 2005.

[17] M. Y. Efremov, F. Schiettekatte, M. Zhang, E. A. Olson, A. T. Kwan, R. S. Berry, and L. H. Allen, "Discrete Periodic Melting Point Observations for Nanostructure Ensembles," *Physical Review Letters*, 85, 3560–3563, 2000.

[18] Y. Li, K. S. Moon, and C. P. Wong, "Enhancement of Electrical Properties of Anisotropically Conductive Adhesive Joints via Low Temperature Sintering," *Journal of Applied Polymer Science*, 99, 1665–1673, 2006.

[19] K. Yasuda, J. M. Kim, and K. Fujimoto, "Adhesive Joining Process and Joint Property with Low Melting Point Filler," *Journal of Electronic Packaging*, 127, 12–17, 2005.

[20] A. Ulman, "Formation and Structure of Self-Assembled Monolayers," *Chemical Reviews*, 96, 1533–1554, 1996.

[21] J. C. Love, L. A. Estroff, J. K. Kriebel, R. G. Nuzzo, and G. M. Whitesides, "Self-Assembled Monolayers of Thiolates on Metals as a Form of Nanotechnology," *Chemical Reviews*, 105, 1103–1169, 2005.

[22] G. E. Poirier and E. D. Pylant, "The Self-Assembly Mechanism of Alkanethiols on Au(111)," *Science*, 272, 1145–1148, 1996.

[23] M. D. Porter, T. B. Bright, D. L. Allara, and C. E. D. Chidsey, "Spontaneously Organized Molecular Assemblies 4. Structural Characterization of Normal-Alkyl Thiol Monolayers on Gold by Optical Ellipsometry, Infrared-Spectroscopy, and Electrochemistry," *Journal of the American Chemical Society*, 109, 3559–3568, 1987.

[24] L. H. Dubois and R. G. Nuzzo, "Synthesis, Structure, and Properties of Model Organic-Surfaces," *Annual Review of Physical Chemistry*, 43, 437–463, 1992.

[25] C. D. Bain, H. A. Biebuyck, and G. M. Whitesides, "Comparison of Self-Assembled Monolayers on Gold – Coadsorption of Thiols and Disulfides," *Langmuir*, 5, 723–727, 1989.

[26] C. D. Bain, E. B. Troughton, Y. T. Tao, J. Evall, G. M. Whitesides, and R. G. Nuzzo, "Formation of Monolayer Films by the Spontaneous Assembly of Organic Thiols from Solution onto Gold," *Journal of the American Chemical Society*, 111, 321–335, 1989.

[27] C. D. Bain and G. M. Whitesides, "Formation of Monolayers by the Coadsorption of Thiols on Gold – Variation in the Length of the Alkyl Chain," *Journal of the American Chemical Society*, 111, 7164–7175, 1989.

[28] C. D. Bain and G. M. Whitesides, "Molecular-Level Control over Surface Order in Self-Assembled Monolayer Films of Thiols on Gold," *Science*, 240, 62–63, 1988.

[29] L. H. Dubois, B. R. Zegarski, and R. G. Nuzzo, "Molecular Ordering of Organosulfur Compounds on Au(111) and Au(100) – Adsorption from Solution and in Ultrahigh-Vacuum," *Journal of Chemical Physics*, 98, 678–688, 1993.

[30] G. E. Poirier, "Characterization of Organosulfur Molecular Monolayers on Au(111) Using Scanning Tunneling Microscopy," *Chemical Reviews*, 97, 1117–1127, 1997.

[31] N. E. Schlotter, M. D. Porter, T. B. Bright, and D. L. Allara, "Formation and Structure of a Spontaneously Adsorbed Monolayer of Arachidic on Silver," *Chemical Physics Letters*, 132, 93–98, 1986.

[32] Y. T. Tao, M. T. Lee, and S. C. Chang, "Effect of Biphenyl and Naphthyl Groups on the Structure of Self-Assembled Monolayers – Packing, Orientation, and Wetting Properties," *Journal of the American Chemical Society*, 115, 9547–9555, 1993.

[33] M. G. Samant, C. A. Brown, and J. G. Gordon, "An Epitaxial Organic Film – the Self-Assembled Monolayer of Docosanoic Acid on Silver(111)," *Langmuir*, 9, 1082–1085, 1993.

[34] S. W. Joo, S. W. Han, H. S. Han, and K. Kim, "Adsorption and Stability of Phthalic Acid on a Colloidal Silver Surface: Surface-Enhanced Raman Scattering Study," *Journal of Raman Spectroscopy*, 31, 145–150, 2000.

[35] M. Moskovits and J. S. Suh, "Conformation of Mono-Carboxylic and Dicarboxylic-Acids Adsorbed on Silver Surfaces," *Journal of the American Chemical Society*, 107, 6826–6829, 1985.

[36] K. Bandyopadhyay, V. Patil, K. Vijayamohanan, and M. Sastry, "Adsorption of Silver Colloidal Particles Through Covalent Linkage to Self-Assembled Monolayers," *Langmuir*, 13, 5244–5248, 1997.

[37] K. Bandyopadhyay, M. Sastry, V. Paul, and K. Vijayamohanan, "Formation of a Redox Active Self-Assembled Monolayer: Naphtho[1,8-cd]-1,2-dithiol on gold," *Langmuir*, 13, 866–869, 1997.

[38] Y. Li, K. S. Moon, and C. P. Wong, "Adherence of Self-Assembled Monolayers on Gold and Their Effects for High-Performance Anisotropic Conductive Adhesives," *Journal of Electronic Materials*, 34, 266–271, 2005.

[39] Y. Li, K. S. Moon, and C. P. Wong, "Monolayer-Protected Silver Nano-Particle-Based Anisotropic Conductive Adhesives: Enhancement of Electrical and Thermal Properties," *Journal of Electronic Materials*, 34, 1573–1578, 2005.

[40] G. Ripka and G. Harsanyi, "Electrochemical Migration in Thick-Film ICs," *Electrocomponent Science and Technology*, 11, 281–290, 1985.

[41] G. D. Giacomo, Chapter 6, "Electrochemical Migration," in *Electrochemistry of Semiconductors and Electronics: Processes and Devices*, J. McHardy and F. Ludwig, Eds., Noyes Publications Park Ridge, NJ, USA, pp. 255–295, 1992.

[42] R. Manepalli, F. Stepaniak, S. A. Bidstrup-Allen, and P. A. Kohl, "Silver Metallization for Advanced Interconnects," *IEEE Transactions on Advanced Packaging*, 22, 4–8, 1999.

[43] G. D. Giacomo, "Reliability of Electronic Packages and Semiconductor Devices," Chapter 9, McGraw-Hill, New York, USA, 1997.

[44] R. Wassink, "Notes on the Effects of Metalization of Surface Mounted Components on Soldering," *Hybrid Circuits*, 13, 9–13, 1987.

[45] Y. Shirai, M. Komagata, and K. Suzuki, "Non-Migration Conductive Adhesives," *1st International IEEE Conference on Polymers and Adhesives in Microelectronics and Photonics*, pp. 79–83, 2001.

[46] H. Schonhorn and L. H. Sharpe, "Prevention of Surface Mass Migration by a Polymeric Surface Coating," *US Patent 4377619*, 1983.

[47] V. Brusic, G. S. Frankel, J. Roldan, and R. Saraf, "Corrosion and Protection of a Conductive Silver Paste," *Journal of the Electrochemical Society*, 142, 2591–2594, 1995.

[48] P.-I. Wang, T.-M. Lu, S. P. Murarka, and R. Ghoshal, *US Patent No. 20050236711*, 2005.

[49] Y. Li and C. P. Wong, "Monolayer Protection for Eletrochemical Migration Control in Silver Nanocomposite," *Applied Physics Letters*, 89, 112112, 2006.

[50] S. Jin, R. C. Sherwood, J. J. Mottine, T. H. Tiefel, R. L. Opila, and J. A. Fulton, "New, Z-Direction Anisotropically Conductive Composites," *Journal of Applied Physics*, 64, 6008–6010, 1988.

[51] S. Jin, T. H. Tiefel, and R. Wolfe, "Directionally-Conductive, Optically-Transparent Composites by Magnetic Alignment," *IEEE Transactions on Magnetics*, 28, 2211–2213, 1992.

[52] E. Sancaktar and N. Dilsiz, "Anisotropic Alignment of Nickel Particles in a Magnetic Field for Electronically Conductive Adhesives Applications," *Journal of Adhesion Science and Technology*, 11, 155–166, 1997.

[53] E. Breval, M. Klimkiewicz, Y. T. Shi, D. Arakaki, and J. P. Dougherty, "Magnetic Alignment of Particles in Composite Films," *Journal of Materials Science*, 38, 1347–1351, 2003.

[54] S. M. Ramkumar and K. Srihari, "A Novel Anisotropic Conductive Adhesive for Lead-Free Surface Mount Electronics Packaging," *Journal of Electronic Packaging*, 129, 149–156, 2007.

[55] H. Toshioka, M. Kobayashi, K. Koyama, K. Nakatsugi, T. Kuwabara, M. Yamamoto, and H. Kashihara, *SEI Technical Review*, 62, 58–61, 2006.

[56] Y. Cui, Q. Q. Wei, H. K. Park, and C. M. Lieber, "Nanowire Nanosensors for Highly Sensitive and Selective Detection of Biological and Chemical Species," *Science*, 293, 1289–1292, 2001.

[57] G. A. Prinz, "Device Physics – Magnetoelectronics," *Science*, 282, 1660–1663, 1998.

[58] V. P. Menon and C. R. Martin, "Fabrication and Evaluation of Nanoelectrode Ensembles," *Analytical Chemistry*, 67, 1920–1928, 1995.

[59] A. J. Yin, J. Li, W. Jian, A. J. Bennett, and J. M. Xu, "Fabrication of Highly Ordered Metallic Nanowire Arrays by Electrodeposition," *Applied Physics Letters*, 79, 1039–1041, 2001.

[60] T. Thurn-Albrecht, J. Schotter, C. A. Kastle, N. Emley, T. Shibauchi, L. Krusin-Elbaum, K. Guarini, C. T. Black, M. T. Tuominen, and T. P. Russell, "Ultrahigh-Density Nanowire Arrays Grown in Self-Assembled Diblock Copolymer Templates," *Science*, 290, 2126–2129, 2000.

[61] R.-J. Lin, Y.-Y. Hsu, R.-C. Fan, Y.-C. Chen, S.-Y. Cheng, C.-T. Huang, and R.-H. Uang, "Design of Nanowire Anisotropic Conductive Film for Ultra-Fine Pitch Flip Chip Interconnection," *in: Proceedings of 6th Electronics Packaging Technology Conference*, Singapore, pp. 120–125, 2004.

[62] S. H. Fan and Y. C. Chan, "Current-Carrying Capacity of Anisotropic-Conductive Film Joints for the Flip Chip on Flex Applications," *Journal of Electronic Materials*, 32, 101–108, 2003.

[63] M. J. Yim, H. J. Kim, and K. W. Paik, "Anisotropic Conductive Adhesives with Enhanced Thermal Conductivity for Flip Chip Applications," *Journal of Electronic Materials*, 34, 1165–1171, 2005.

[64] L. Ekstrand, H. Kristiansen, and J. Liu, "Characterization of Thermally Conductive Epoxy Nano Composites," *28th IEEE International Spring Seminar on the Challenges of Electronics Technology Progress*, pp. 35–39, 2005.

[65] J. Haberland, B. Pahl, S. Schmitz, C. Kallmayer, R. Aschenbrenner, and H. Reichl, *in: 4th Electronics Packaging Technology Conference*, pp. 144–149, 2002.

[66] Y. C. Chan and D. Y. Luk, "Effects of Bonding Parameters on the Reliability Performance of Anisotropic Conductive Adhesive Interconnects for Flip-Chip-on-Flex Packages Assembly I. Different Bonding Temperature," *Microelectronics Reliability*, 42, 1185–1194, 2002.

[67] Y. C. Chan and D. Y. Luk, "Effects of Bonding Parameters on the Reliability Performance of Anisotropic Conductive Adhesive Interconnects for Flip-Chip-on-Flex Packages Assembly II. Different Bonding Pressure," *Microelectronics Reliability*, 42, 1195–1204, 2002.

[68] M. A. Uddin, M. O. Alam, Y. C. Chan, and H. P. Chan, "Adhesion Strength and Contact Resistance of Flip Chip on Flex Packages – Effect of Curing Degree of Anisotropic Conductive Film," *Microelectronics Reliability*, 44, 505–514, 2004.

[69] M. F. Rizvi, Y. C. Chan, C. Bailey, H. Lu, and A. Sharif, "The Effect of Curing on the Performance of ACF Bonded Chip-on-Flex Assemblies After Thermal Ageing," *Soldering & Surface Mount Technology*, 17, 40–48, 2005.

[70] L. Q. Cao, Z. H. Lai, and J. H. Liu, "Interfacial Adhesion of Anisotropic Conductive Adhesives on Polyimide Substrate," *Journal of Electronic Packaging*, 127, 43–46, 2005.

[71] R. A. Islam, Y. C. Chan, and B. Ralph, "Effect of Drop Impact Energy on Contact Resistance of Anisotropic Conductive Adhesive Film Joints," *Journal of Materials Research*, 19, 1662–1668, 2004.

[72] M. J. Yim and K. W. Paik, "Effect of Nonconducting Filler Additions on ACA Properties and the Reliability of ACA Flip-Chip on Organic Substrates," *IEEE Transactions on Components and Packaging Technologies*, 24, 24–32, 2001.

[73] Z. H. Lai, R. Y. Lai, K. Persson, and J. Liu, "Effect of Bump Height on the Reliability of ACA Flip Chip Joining with FR4 Rigid and Polyimide Flexible Substrate," *Journal of Electronics Manufacturing*, 8, 217–224, 1998.

[74] K. Pinardi, Z. H. Lai, D. Vogel, Y. L. Kang, J. Liu, S. Liu, R. Haug, and M. Willander, "Effect of Bump Height on the Strain Variation during the Thermal Cycling Test of ACA Flip-Chip Joints," *IEEE Transactions on Components and Packaging Technologies*, 23, 447–451, 2000.

[75] P. Garrou, "Wafer Level Chip Scale Packaging (WL-CSP): An Overview," *IEEE Transactions on Advanced Packaging*, 23, 198–205, 2000.

[76] Q. Tong, B. Ma, S. Hong, L. Nguyen, H. Nguyen, and A. Negasi, "Encapsulant Materials and Processes for Wafer Level-Chip Scale Packaging (WL-CSP)," *in: Proceedings of 52nd Electronic Components and Technology Conference*, pp. 1366–1372, 2002.

[77] K. W. Paik and M. J. Yim, *US Patent No. 6,518,097*, 2003.

[78] H. Y. Son, C. K. Chung, M. J. Yim, J. S. Hwang, K. W. Paik, G. J. Jung, and J. K. Lee, "Wafer-Level Flip Chip Packages Using Pre-applied Anisotropic Conductive Films (ACFs)," *IEEE Transactions on Electronics Packaging Manufacturing*, 30, 221–227, 2007.

Chapter 6
Non-conductive Adhesives/Films (NCA/NCF)

6.1 Introduction

Electrically conductive adhesive joints can be formed using unfilled organic adhesives, i.e., without any conductive filler particles. The electrical connection of non-conductive adhesives/films (NCA/NCF) is achieved by sealing the two contact partners under pressure and heat. Thus, the small gap contact is created, approaching the two surfaces to the distance of the surface asperities. The formation of contact spots depends on the surface roughness of the contact partners [1–5]. Approaching the two surfaces enables a small number of contact spots to form which allows the electric current to flow. When the parts are pressed together during the sealing process, the number and area of the single contact spots are increased according to the macroscopic elasticity or flexibility of the parts and the microhardness and plasticity of the surfaces, respectively.

Recently, non-conductive adhesives/films (NCAs/NCFs) are considered as a low-cost option for flip-chip assemblies. Conductive joints with non-conductive adhesives provide a number of advantages compared to other adhesive bonding techniques. NCA joints avoid short circuiting and are not limited, in terms of particle size or percolation phenomena, to a reduction of connector pitches. Further advantages include cost-effectiveness, ease of processing regarding the possibility of non-structured adhesive application, good compatibility with a wide range of contact materials, and low temperature cure. In fact, the pitch size of the NCA joint can be limited only by the pitch pattern of the bond pad, rather than the adhesive materials. Contacts between the nanoscale rough structures of the bottom and top surfaces lead to the electrical conduction between the two pads. NCA flip-chip interconnection provides a solution for the ultra-fine pitch interconnection and has recently found its application in the manufacturing of LCDs, LED array modules, smart cards, etc. NCA/NCF requires no conductive fillers, but needs a relatively high bonding pressure between the IC chip and the substrate coupled with heat. During bonding, the heat and

Y. Li et al., *Electrical Conductive Adhesives with Nanotechnologies*,
DOI 10.1007/978-0-387-88783-8_6, © Springer Science+Business Media, LLC 2010

pressure are applied and the direct physical contacts between the two surfaces of the IC bump and the substrate bond pad can be achieved. The electrical contact resistance of an NCA/NCF joint is controlled by the processing pressure, surface roughness, and NCA/NCF material properties. The NCA has showed higher current-carrying capability than the ACA joints. Figure 6.1 shows the schematic illustration of flip-chip CSP using NCF as first-level interconnection and its cross-section view of Au stud bump joint.

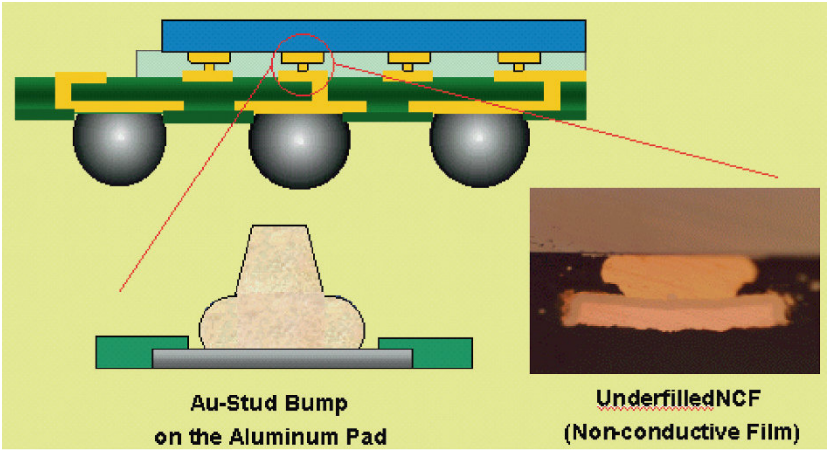

Fig. 6.1. Schematic illustration of flip-chip CSP using NCF and cross-section of NCF interconnection.

In spite of the advantages of NCF joints, there are still some challenging properties of NCF. Since the electrical conductivity of NCF is achieved through physical/mechanical contact and no metallurgical joints are formed, it has limited electrical conductance and current-carrying capability as well as restricted reliability performance under high-temperature/humidity environment or thermal cycling. Low contact resistance, high current-carrying capability, and high reliability of NCF joints are demanding properties for lead-free solder alternatives and high current density application.

6.2 Electrical Properties of NCA/NCF Joints

6.2.1 Contact Resistance of NCA/NCF Joints

To ensure low contact resistance and high current density, interface between electrodes plays important role. The interfaces between electrodes for NCF joints must be defect free and occupy the stable contact area even under high electrical current and harsh environments. This interface control in NCF joints contributes to performance and reliability of their joints in electronic packaging. In most NCF joints, electrical conductance between contacts is dependent on the constriction resistance and tunneling resistance due to the presence of ultra-thin insulating film between contacts. The control of the tunneling resistance is important in reducing the contact resistance for NCF joints [6–8]. In order to understand the contact resistance of NCA/NCF joints, our group at Georgia Tech conducted the study combining the theoretical calculation and experimental characterization [9]. A model was established to calculate the contact resistance of NCA joints. Tunnel resistance is identified as the major contributor to the overall contact resistance, and the electron-injection barrier has been considered important in controlling the tunnel resistivity. The conclusion from this study provides guidance for future work on improving electrical performance and reliability of NCF joints.
Experimental investigation of Williamson et al. established that many of the manufacturing processes produce surfaces with an isotopic Gaussian distribution of heights of the surface asperities [10]. In most analyses of the microcontact involving two rough Gaussian surfaces, the analysis can be simplified by considering the contact between a single surface (with effective surface roughness characteristics) and a perfectly flat surface.

In order to obtain the electrical resistance of an NCA/NCF joint, the resistance of a physical contact needs to be determined. For a microcontact, the contact resistance is composed of constriction and tunnel resistance [6]. Constriction resistance occurs as the electrical current must squeeze through the asperities to cross the interface. Tunnel resistance is due to the intermediate layer between the metal surfaces. The total resistance of a physical contact can be written as Equation 6.1:

$$R = R_c + R_t = (\rho_1 / 4a + \rho_2 / 4a) + \xi / \pi a^2 \tag{6.1}$$

where R_c is the constriction resistance, R_t is the tunnel resistance, ρ_1 and ρ_2 are the bulk electrical resistivity of the two contacting bodies, a is the radius of contact area, and ξ is the tunnel resistivity of the interface.

Tunnel resistance is due to the intermediate layer between the metal surfaces. The intermediate layer may consist of a thin film of NCA/NCF material. Tunnel resistivity is a function of the film thickness s, the work function Φ for electron emission from metal into film (electron-injection barrier), and the relative permittivity ε_r of the material of the film. It can be expressed as Equation 6.2

$$\xi = 0.5 \times 10^{-12} \frac{A^2 \exp(AB)}{1 - AB} \left(\Omega \cdot \mathrm{cm}^2\right) \tag{6.2}$$

where $A = 7.32(s\text{-}7.2/\phi)$, $B = 0.1265\sqrt{\phi - \frac{10}{s\varepsilon_r}}$ with ϕ in eV and s in Å.

Based on Equation 6.1, the electrical resistance of an NCA/NCF joint can be written as Equation 6.3 by assuming all physical contacts have average contact area.

$$R_{jo\,\mathrm{int}} = R / n_s = [(\rho_1 / 4a + \rho_2 / 4a) + \xi / \pi a^2] / n_s \tag{6.3}$$

where n_s is the number of physical contacts of an NCA/NCF joint, which can be calculated from surface roughness, material hardness, and applied external pressure. Therefore, the contact resistance of a NCA/NCF joint is dependent on surface morphology, processing pressure, and material properties.

From some experimental characterizations, we found that constriction resistance only composed a negligible amount of an NCA/NCF joint resistance, while tunnel resistance is the main source for the joint resistance. In order to increase the performance of NCA/NCF material, one needs to decrease the tunnel resistivity (ξ). Tunnel resistivity is dependent on the film thickness, electron-injection barrier, and dielectric constant of the intermediate layer material. The thickness of the film is dependent on the applied processing pressure and it cannot be increased further due to process requirement. The parameters one can control are electron-injection barrier and dielectric constant.

Figure 6.2 shows the effect of film dielectric constant on tunnel resistivity at different film thickness. The electron-injection barrier is 2.7 eV. As one can tell tunnel resistivity remains almost unchanged when the dielectric constant is changed from 2.5 to 5.

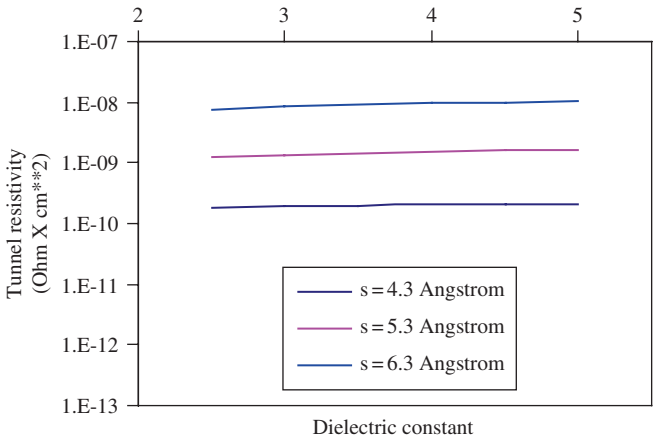

Fig. 6.2. Effect of dielectric constant on tunnel resistivity (electron-injection barrier = 2.7 eV) [9]

However, the effect of electron-injection barrier is much more significant. As one can see from Fig. 6.3, the tunnel resistivity decreased with the decreasing of electron-injection barrier. For all film thickness, the tunnel resistivity was reduced by two magnitudes when the electron-injection barrier was changed from 1.5 to 3.5 eV. Therefore, there is not much one can do in order to improve the electrical performance by modifying the dielectric property of resin system. More research should be focused on the reduction of tunnel resistivity by decreasing the electron-injection barrier.

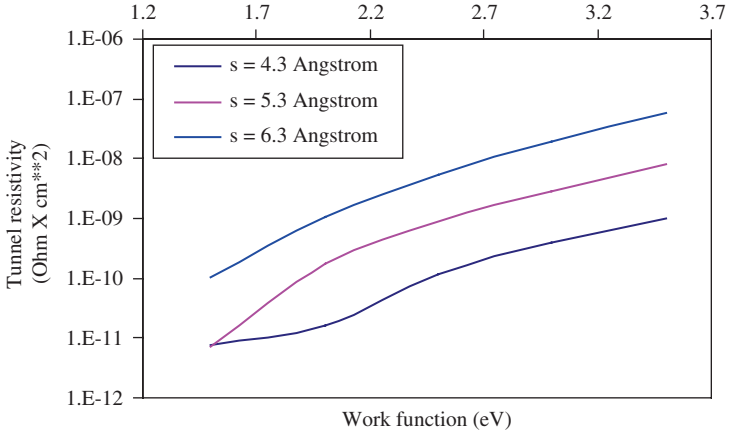

Fig. 6.3. Effect of electron-injection barrier on tunnel resistivity (dielectric constant = 3.5) [9]

Various flip-chip configurations arising from different bump types and adhesives are possible and have been reported in literatures [11–14]. Selection of flip-chip joint configuration and adhesives materials is also important to meet desired performance criteria. Min et al. [15] evaluated the effects of some different combinations of commonly available bump types, adhesives, and substrate finishing on the joint resistance and ACF and NCF joints. Their results showed that direct contact of bumps to substrate pads was the preferred flip-chip joint configuration for stable contact resistance readings after assembly. To achieve this, the compatibility of the bump and adhesive types was important. Their reliability results showed a strong dependence on the adhesive types. Adhesive pastes (NCP and ACP) demonstrated better reliability results compared to film (ACF/NCF). They also reported that stable contact resistances could be attained in the absence of conductive particles in the polymer matrix. ENIG with the inert Au plating was still the preferred pad finishing for direct contact with Au bumps. With OSP pad finishing, degradation of resistance readings was observed after assembly and reliability stress testing.

6.3 Reliability of NCA/NCF Joints

As the most recent emerged conductive adhesives technology, fully understanding of the performance, in particular, the reliability and failure mode of NCA/NCF joints are needed. Finite element method (FEM) was applied by researchers to investigate the shear stress distribution induced by coefficient of thermal expansion (CTE) mismatch. Caers et al. [4] investigated the moisture-induced failure mechanisms on flip chip on flex interconnect with NCA using FEM simulations and materials characterizations. Their study showed that flip chip on flex interconnections with NCA was quite stable under steady-state humid conditions, but the interconnections are probably more sensitive to sudden changes of temperature or humidity environments than steady-state conditions.

Teh et al. evaluated the reliability performance of NCA flip chips in various environmental tests [16]. They characterized the hygro-thermo-mechanical and stress relaxation properties to identify the impact of material properties on reliability. They also performed finite element analysis to understand the results. Their studies revealed that the robustness of NCA flip-chip assembly was primarily limited by the NCA's sensitivity to moisture. The characterizations indicated that the primary modes of failure in NCA assembly for moisture sensitivity test (MST) and pressure cooking test (PCT) were interfacial delamination and bump/pad opening. Delamination appeared to initiate in the middle of the package, spreading outward to the die edge. It was postulated that PCT failures were induced mainly by the hygroscopic swelling stress, whereas MST failures were induced by hygroscopic swelling mismatch superimposed with thermal mismatch stresses, followed by vapor pressure at reflow temperature. In both cases, the delamination was aided by the weakening of interfacial strength due to the presence of moisture and high temperature. These factors affect the degradation of the compressive force that maintains the mechanical contact in NCA flip-chip structure. The common failure modes include interfacial delamination, bump/pad opening as well as cracking.

As illustrated in Fig. 6.4, the in-plane hygroscopic swelling of the substrate and the adhesive could cause bowing of the package that induces tension in the center of the package as well as compression at the edge of the package.

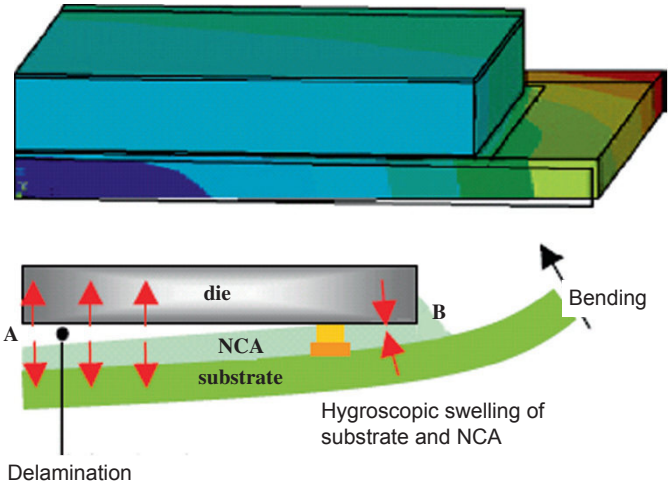

Fig. 6.4. Hygroscopic swelling induces bowing and delamination in PCT

Chung et al. [17] investigated the effects of the functional groups of NCFs on materials properties and thermal cycling reliability of NCFs-bonded FCOB assemblies. They found that NCFs with multi-functional epoxies showed improved thermo-mechanical properties such as lower CTE, higher modulus at high temperate region, and higher Tg. These effects were considered to be caused by increasing chain cross-linking due to the increase of functionality. Their results indicated that the enhanced thermo-mechanical properties improved the thermal cycling reliability and could reduce the shear deformation between bumps and pads in the high-temperature region. They concluded that adequate materials design guideline should be provided for highly reliable NCFs.

Kim et al. [18–21] examined the effect of bonding force on the electrical conductivity of ACAs and NCAs to obtain the optimum bonding force for a reliable flip chip on a flexible substrate. Figure 6.5 shows the connection resistance versus bonding force relationship for both ACF and NCF in their study. Increasing the bonding force reduced the connection resistance in both cases of ACF and NCF. However, quantitative values of connection resistance differed between ACF and NCF showed that the contact resistances of the ACF joints were more than an order of magnitude larger than those of the NCF joints.

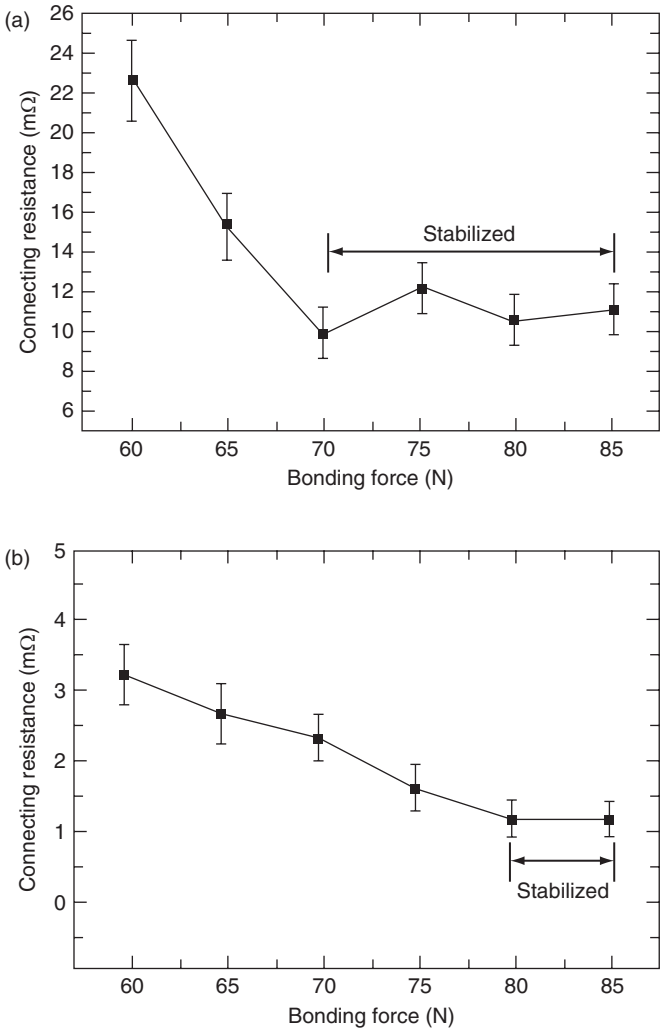

Fig. 6.5. Variations of connection resistance with bonding force: (**a**) ACF joints and (**b**) NCF joints [19]

Kim et al. also compared the reliability of ACF and NCF under different conditions such as reflow process [19], thermal shocking [21], and temperature–humidity testing (THT) [20]. For all the above conditions, they observed two kinds of conduction behaviors: increased connection resistance and Ohmic behavior termination. The increased connection resis-

tance was considered to be due to the decreased contact area caused by directional swelling of the adhesives, while the Ohmic behavior termination was considered to be due to either contact opening in the NCF joints or interface cracking.

6.4 Recent Advances of NCA/NCF

6.4.1 Low-Temperature Assembly of NCF

To form the electrical junctions with NCF, temperature and pressure need to be applied simultaneously to ensure the polymer curing and mechanical bonding. Bonding temperature, time, and pressure are important conditions to determine the resistance and reliability of NCF joints. In general, higher bonding temperature usually induced higher cross-linking density of NCA/NCF, and therefore could improve the physical properties such as glass transition temperature (Tg), adhesion strength, impact performance, etc. However, when some low-cost substrates are used for a total cost control purpose, the base materials of the substrates may not be able to tolerate the typical bonding temperature of NCF. For example, when a PET-based substrate is used in smart card fabrication, it is recommended that the applied temperature during the assembly process be kept under 160°C to prevent any warpage or even damage of the substrate. Ma et al. [22] evaluated the NCF bonding under the precondition of a reduced processing temperature in order to minimize thermally induced damage to the low-cost flexible substrates. In their study, the assembly process was modified and investigated with an emphasis on the effect of the bonding force on the electrical performance and the reliability of the NCA joints. For the modified assembly process, the NCF was first laminated onto the substrate after warming up at room temperature for 1 h and prebonded at 90°C for 10 s at a bonding pressure of 30 kPa. The cover layer on the NCA was then carefully peeled off and bonding was performed between 140°C and 180°C for 10 s instead of the regular assembly temperature of 220°C. Finally, all the bonded assemblies were inserted into a high-temperature chamber to post-cure at 140°C for 2 min to obtain sufficient thermal energy to get adequately cured. They found that the lower the temperature, the larger the bonding force required to achieve good electrical performance in terms of small joint resistance. However, when a higher bonding pressure was applied, there was a higher risk of interfacial delamination failure. Therefore, a reduced processing temperature and a moderately increased bonding force need to be optimized to enable good electrical conductivity for low cost flexible substrates.

6.4.2 Improvement of Electrical Properties of NCA/NCF Joints with π-Conjugated Molecular Wires

Self-assembled monolayer (SAM) has been extensively studied in the last decade, and recent discoveries on the capability of SAM to functionalize the materials and tune their physical and chemical properties have attracted more interests in the research area. In particular, conjugated molecules have smaller band gaps between the highest occupied molecular orbital (HOMO) also called valence band and the lowest unoccupied molecular orbital (LUMO) also called conduction band and possess delocalized conjugated π-lectrons that can contribute to conduction. In semiconductors, self-assembled molecular wires have seen importance in tuning the metal work function (Φ) and electrical conduction of metal–molecule contact [23–30]. In Chapter 5, we have reviewed the application of self-assembled monolayer on the electrical and thermal performance and ACA/ACF. SAM molecules with specific functional groups and structures could significantly reduce the electrical resistance of ACA joints and improve the interface properties. In NCF joints, improved interface properties were also discovered by using appropriate π-conjugated molecular wires from both theoretical calculation and experimental validation [9, 31].

As discussed in this chapter, contact resistance of NCF joints is mainly dominated by the tunnel resistivity (ξ), which is dependent on the film thickness, electron-injection barrier, and dielectric constant of the intermediate layer material. Experimental measurements and computational calculations by different authors [23, 28, 29, 32–34] have demonstrated that the metal work function (i.e., Au in this case) can be tuned by using polar molecules that can self-assemble on the metal and changing the electronic surface dipole. Therefore, incorporation of π-conjugated molecular wires could reduce the tunnel resistance and consequently the overall contact resistance of NCF joints.

Our group recently introduced some thiol (–SH)-terminated conjugated molecular wires into the NCF joints [31]. It was shown that thiol (–SH)-terminated molecular wires could be well assembled on the Au electrodes and improve the interfacial properties of the NCF joints. Molecular wires with more aromatic rings in the structure (such as biphenyldithiol (BPD)) exhibits higher thermal stability after curing condition (150°C) than those with single aromatic ring (such as 1,4-benezenedithiol (BDT)). The current–voltage (I–V) relationship and correspondingly current–resistance (I–R) relationship of NCF joints with π-conjugated thiol molecules are compared in Fig. 6.6. The untreated NCF joints showed a contact resistance of 0.15×10^{-3} Ω and current-carrying capability (maximum current below

which the I–V relationship remains linear) of 2.7 A. After incorporating conjugated molecular wires, the joint resistance of NCF could be reduced to 0.1 $\times 10^{-3}$ Ω and 0.05 $\times 10^{-3}$ Ω with BDT and BPD, respectively. In addition, the current-carrying capability of BDT- and BPD-incorporated NCF was also increased to 2.9 and 3.1 A, respectively. The significantly improved electrical properties of NCF could be attributed to the enhanced interface properties with molecular wires and the conjugated molecular wires assisted the electrons tunneling and current flow between the joints.

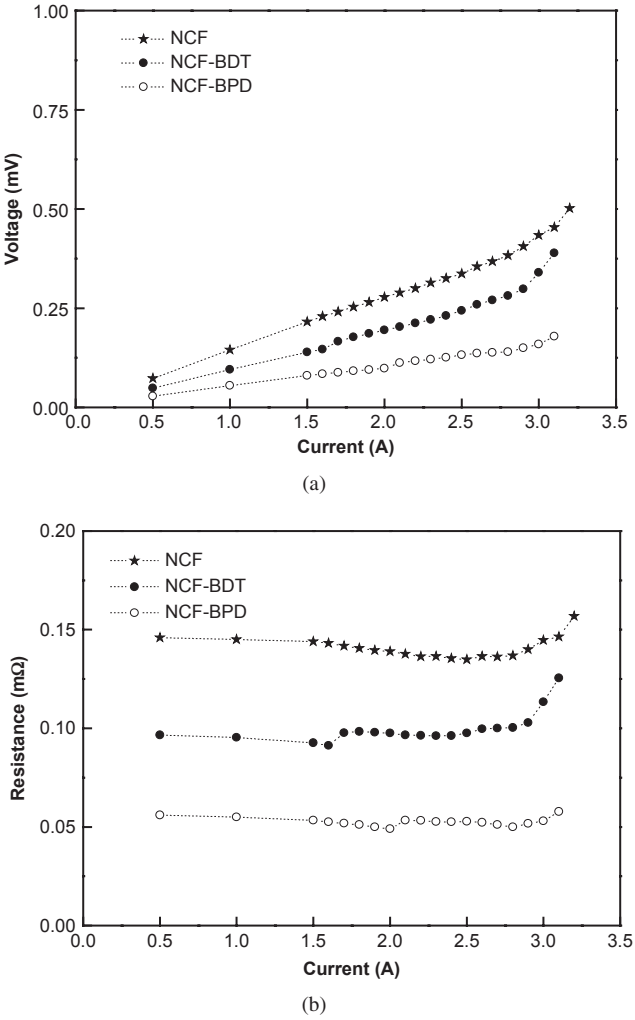

Fig. 6.6. Electrical properties of NCF joints with molecular wires. (**a**) I–V relationship of NCF joints and (**b**) corresponding I–R relationship of NCF joints [31]

6.4.3 NCA/NCF with Fillers

NCA/NCF usually does not contain any conductive fillers in the formulation. Instead, a much higher bonding pressure than ACF is needed to achieve a reliable interconnect joints. In addition, due to the high CTE of unfilled NCF materials, there have been problems on the flip-chip failure under thermal cycling due to the CTE mismatch between chip and substrates. In recent years, there has been some research on the incorporation of low loading of nano-fillers such as silver, gold particles, or non-conductive fillers such as silica, aluminum nitride, silicon carbide in NCA/NCF for improving electrical performance and reliability of NCF joints.

6.4.3.1 Nano-NCA/NCF

To solve the issues (high bonding pressure and lower electrical performance) of traditional ACF/NCF while maintaining the advantages of ultra-fine pitch and low cost, we investigated a novel NCF material incorporated with very low loading of nanoscale conductive fillers (nano-silver particles) [35]. This novel interconnect film (as illustrated in Fig. 6.7) combines the electrical conduction along the z-direction (ACF-like) and the ultra-fine pitch (<100 nm) capability (NCF-like). Unlike typical ACF which requires 1–5 vol% of conductive fillers, the NCF only needs less than 0.1 vol% conductive fillers to achieve good electrical conductance in the z-direction.

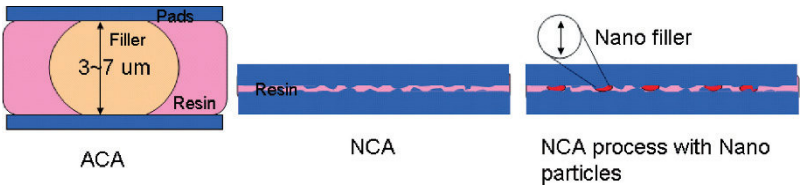

Fig. 6.7. Comparisons of ACA, NCA, and nano-NCA

The conductive nanoparticles can be added into the polymer matrix via two ways. One is the in situ formation of the nanoparticles in the polymer matrix [36] and the other is the incorporation of pre-made conducting nanoparticles [35]. These nanoparticles can fill the gap in between the surface bonding, therefore, the nano-NCF could allow a lower bonding pressure than NCF to achieve a much lower joint resistance (over two orders of magnitude lower than typical ACF joints) and higher current-carrying capability. As shown in Fig. 6.8, as the bonding pressure increased, the

contact resistance of ACF/NCF joint generally decreased due to the contact area increment. For adhesives joints, there was a critical (minimum) pressure below which the contact resistance remained high. The minimum bonding pressure was reduced from 200 MP for NCF to150 MPa for nano-NCF.

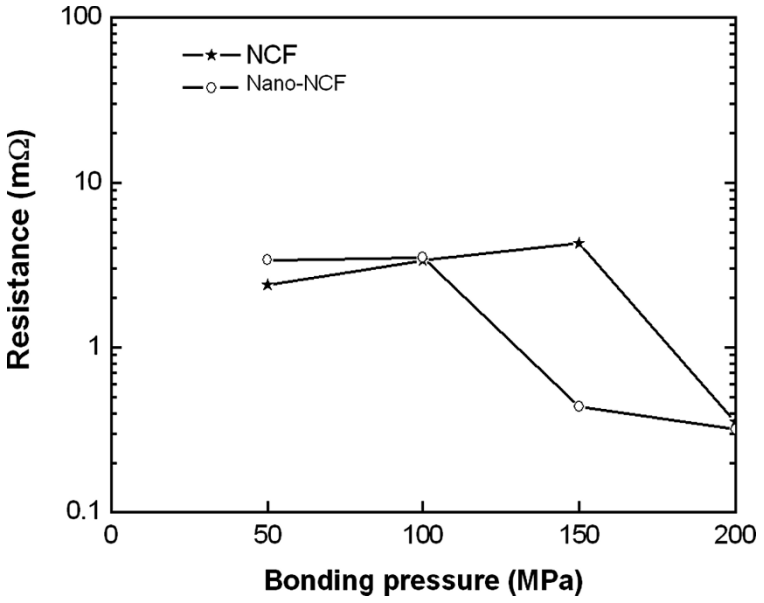

Fig. 6.8. Effects of bonding pressure on the joint resistance of NCF and nano-NCF [35]

When comparing the I–R relationship of NCF, ACF, and nano-NCF (Fig. 6.9), it was shown that the joint resistance of the nano-NCF could be much lower than that of the conventional ACF with optimized processing conditions. In addition, the current-carrying capability could also be enhanced. The joint resistance and current-carrying capability shown in this study were even better than those of the NCF and lead-free solder joints, due to the lower resistance of Ag fillers compared to the lead-free solders [35].

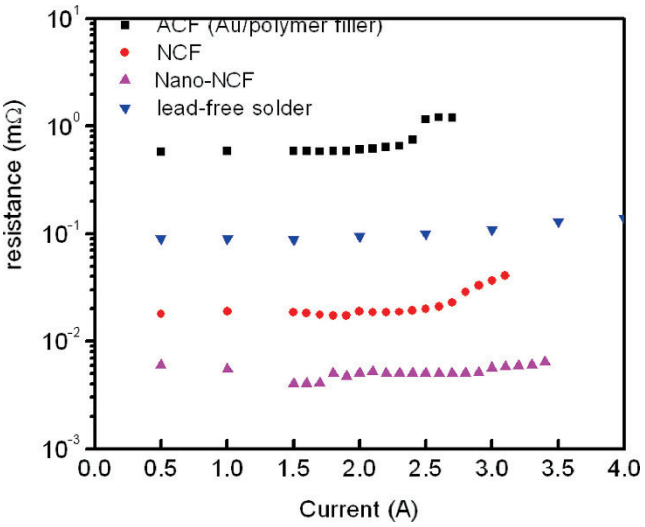

Fig. 6.9. Comparison of current–resistance (I–R) relationships of typical ACF, NCF, lead-free solder, and nano-NCF [35]

6.4.4 Incorporation of Non-conductive Fillers in NCA/NCF

For the full implementation of flip chip using NCA, it is necessary to provide good reliability to prove availability of NCA in flip-chip technology. NCA usually has high CTE values, which introduces problems/failures under thermal cycling due to the CTE mismatch between chip and substrates. In order to reduce thermal and mechanical stress and strain induced by CTE mismatch while maintaining the ultra-fine-pitch capability of NCA, Yim et al. [37] introduced electrically non-conductive but thermally conductive fillers, such as silica in NCA. In addition to provide *z*-direction electrical conductivity, the new NCA also function like underfill. In this chapter, by optimizing the filler content, the materials properties such as CTE modulus and adhesion could be adjusted, and the formulated NCA could exhibit good electrical, mechanical, and reliability characteristics.

6.4.5 Multi-layer ACF/NCF

The principle of ACF bonding is that the electrical connections are established through conductive particles and the mechanical interconnections are maintained by the adhesive. However, the need for higher resolution and larger capacity displays is driving the need for finer pitch interconnection. As the bumps of the driver IC grow less and less to an ultra-fine pitch, an electrical short is sometimes generated between the adjacent bumps due to the electrical bridging by agglomeration of conductive particles between the bumps. Also, as the interval between the bumps goes to the ultra-fine pitch, the cross-sectional area of the bump decreases. Since it is requested that many conductive particles form mechanical contacts between small bumps of driver IC and the electrode of the LCD panel, the density of conductive particles in the anisotropic conductive film becomes high, and therefore, the probability of the electrical short increases.

In order to meet the requirement for fine-pitch interconnect, Hitachi has developed a double-layer ACF/NCF which consists of an ACF layer and a NCF layer [38, 39]. Conventional ACF has only one layer of adhesive in which the conductive particles are dispersed in a random distribution, while conventional NCF does not contain any conductive fillers but requires a higher bonding pressure to achieve electrical conductivity. In Hitachi's double-layer structure, the conductive particle layer and the adhesive layer are formed separately and attached together later (as shown in Fig. 6.10). The conductive particle layer is thin and has a high viscosity thermosetting material. The adhesive layer is thick and has a low viscosity pure thermosetting resin. The double-layer design is reported to increase the number of particles on the interconnection electrodes and help in improving the fine-pitch capability.

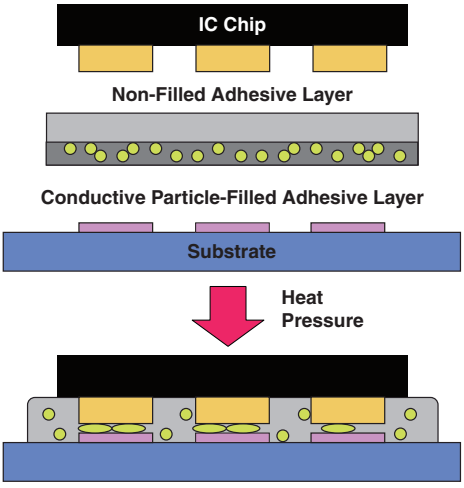

Fig. 6.10. Schematics of Hitachi double-layer ACF process

Jia et al. evaluated a double-layer ACF/NCF for ultra-fine pitch COG applications [40]. From their study, the double-layer ACF/NCF performed a better particle capturing capability than the single-layer ACF although it has a lower particle density (Fig. 6.11). It was also found that the particles agglomerated between adjacent bumps were less for the resin from the NCF layer squeezes the particles out of the bump gap during the thermocompression bonding, which reduced the short-circuiting failures. In addition, they also reported that the double-layer ACF/NCF had a more stable and lower contact resistance than the conventional ACF in both of the environmental tests under different bump areas.

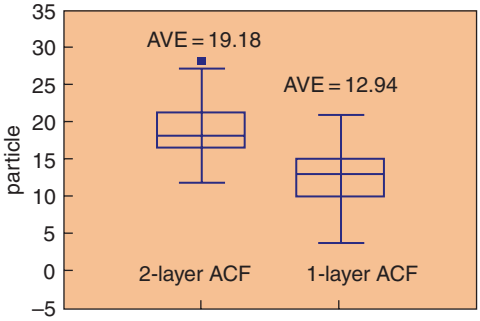

Fig. 6.11. Comparison of conductive particles trapped under one bump [40]

Yim et al. [41] present a triple-layer ACF that has functional layers (NCF layers) on both sides of a conventional ACF layer to improve interface adhesion and control the bonding property during thermocompression bonding and the resulting reliability of the interconnection for COF module assembly. Figure 6.12a and b shows the multi layered ACF with functional layers on both sides of the ACF layer. In their design, functional layers had no particles inside the layer and good flow properties during thermocompression bonding. The functional layers had a low modulus before cure to be flowed easily on the fine-pitched surface of the COF substrate. Figure 6.12c shows the COF bonding process using the multi-layered (triple-layered structure) ACF in their study.

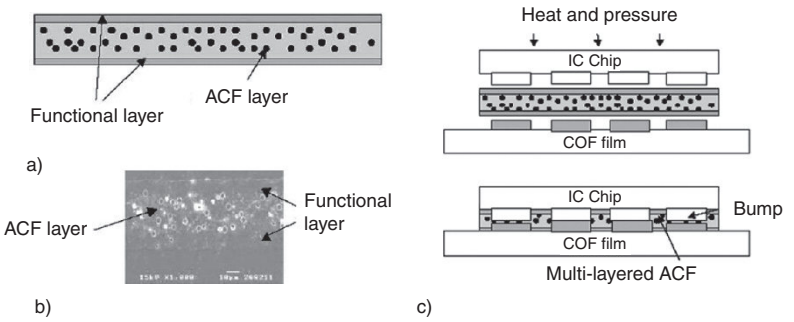

Fig. 6.12. Schematic drawings of (**a**) multiple-layered ACF, (**b**) cross-section view of ACF by SEM, and (**c**) COF-bonding process using developed ACFs [41]

In their paper, they also investigated the effect of bonding pressure, time, and temperature on contact resistance of the triple-layer ACF and correlated its behavior with the number of conductive particles on the bump and reaction rate of the resin. The reliability tests of the COF assemblies of the multi-layered ACF compared with the single-layered ACF showed that adhesion and electrical properties of multilayered ACF joints were superior to those of the single-layered ACF because of improved adhesion characteristics on the two-layer flex substrates.

6.4.6 Wafer-Level NCF

Wafer-level process is becoming widely used in LSI packaging production due to the advantage of size minimization and process cost reduction. Recently, the concept of wafer-level NCF has been developed [42–45]. In conventional COG assembly process, ACF is used as a bonding adhesive between IC chip and glass substrate. In this process ACF narrow tape of 2 mm or less width is pasted and cut to 20 mm long or so on LCD module substrate one by one. After that driver IC chip is mounted on it one by one again. Both of them need alignment processes (Fig. 6.13a).
In contrast to the ACF process the WL-NCF process is that where first NCF is laminated on a whole area of active side of LSI wafer with bumps (Fig. 6.13b). And then wafer with NCF is cut into chips by dicing. After that the chips are aligned and bonded on substrates one by one. The WL-NCF assembly contains only single one by one process compared with the conventional ACF process which has double of it. The NCF cut with just the chip size has an effect of minimizing the foot print of IC assembly, which is good for narrowing the frame of LCD panel. The size of ACF on a substrate is usually larger than that of a chip for an alignment margin.

The concept of WL-NCF could help shortening of lead time and minimization of bonding area.

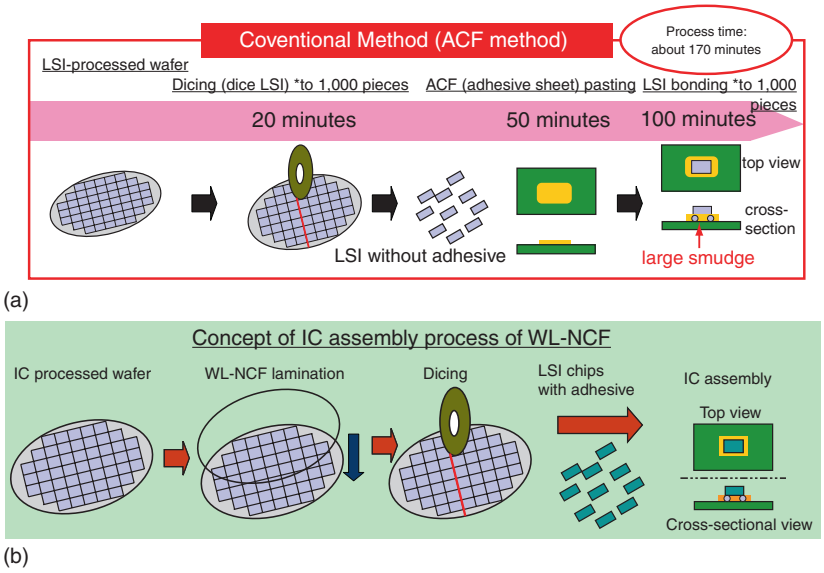

Fig. 6.13. Comparison of ACF bonding (**a**) and wafer-level NCF bonding (**b**)

References

[1] H. Yu, S. G. Mhaisalkar, and E. H. Wong, "Effect of Temperature on the Cure Shrinkage Measurement of Non-conductive Adhesives for Flip Chip Interconnects," *Journal of Materials Research*, 20, 1324–1329, 2005.

[2] H. Yu, S. G. Mhaisalkar, and E. H. Wong, "Cure Shrinkage Measurement of Nonconductive Adhesives by Means of a Thermomechanical Analyzer," *Journal of Electronic Materials*, 34, 1177–1182, 2005.

[3] S. Ito, M. Mizutani, H. Noro, M. Kuwamura, and A. Prabhu, "A Novel Flip Chip Technology using Non-conductive Resin Sheet," *Proceedings of the 48th IEEE Electronic Components and Technology Conference*, pp. 1047–1051, 1998.

[4] J. Caers, X. J. Zhao, E. H. Wong, C. K. Ong, Z. X. Wu, and R. Ranjan, "Prediction of Moisture Induced Failures in Flip Chip on Flex Interconnections with Non-conductive Adhesives," *Proceedings of the 53rd IEEE Electronic Components and Technology Conference*, pp. 1176–1180, 2003.

[5] R. D. Pendse, K.-M. Kim, and S. Tam, "A New Flip Chip Packaging Technology for the Mid-Range Application Space," *Proceedings of the 52nd IEEE Electronic Components and Technology Conference*, pp. 100–104, 2002.

[6] R. Holm, "Theory and Application," *In Electrical Contacts, Springer, New York*, 1967.

[7] M. Chin, K. A. Iyer, and S. J. Hu, "Prediction of Electrical Contact Resistance for Anisotropic Conductive Adhesive Assemblies," *IEEE Transactions on Components and Packaging Technologies*, 27, 317–326, 2004.

[8] L. Kogut and K. Komvopoulos, "Electrical Contact Resistance Theory for Conductive Rough Surfaces Separated by a Thin Insulating Film," *Journal of Applied Physics*, 95, 576–585, 2004.

[9] H. Dong, Y. Li, M. J. Yim, K. S. Moon, and C. P. Wong, "Investigation of Electrical Contact Resistance for Nonconductive Film Functionalized with pi-Conjugated Self-Assembled Molecules," *Applied Physics Letters*, 90, 092102, 2007.

[10] J. B. Williamson, J. Pullen, R. T. Hunt, and D. Leonard, "The shape of solid surfaces," *Surface Mechanics, ASME, New York*, pp. 24, 1969.

[11] R. Miessner, R. Aschenbrenner, H. Reichi, S. Ling, B. Le;, A. Lew, R. Benson, and E. Nhan, "Comparison of Flip Chip Technologies on Rigid Polyimide with Respect to Reliability and Manufacturing Costs," *Proceedings 50th Electronic Components and Technology Conference*, pp. 1133–1138, 2000.

[12] R. Miessner, R. Aschenbrenner, and H. Reichl, "Reliability Study of Flip Chip on FR4 Interconnections with ACA," *Proceedings 49th Electronic Components and Technology Conferences*, pp. 595–601, 1999.

[13] J. Liu, A. Tolvgard, J. Malmodin, and Z. H. Lai, "A Reliable and Environmentally Friendly Packaging Technology - Flip-Chip Joining Using Anisotropically Conductive Adhesive," *IEEE Transactions on Components and Packaging Technologies*, 22, 186–190, 1999.

[14] Y. Okada, T. Katahira, N. Masuda, T. Koseki, and T. Takai, "Material Characterization and in-situ Process Monitoring for a Robust

ACF Base Flip Chip Technology," *IEEE Transactions on Components and Packaging Technologies*, 24, 713–720, 2001.

[15] A. M. Tan, S. P.-S. L. Lim, A. Yeo, and C. Lee, "Influence of Bump Geometry, Adhesives and Pad Finishings on the Joint Resistance of Au Bump and A/NCA Flip Chip Interconnection," *Proceedings of Electronic Packaging Technology Conference*, pp. 797–801, 2005.

[16] L. K. Teh, E. Anto, C. C. Wong, S. G. Mhaisalkar, E. H. Wong, P. S. Teo, and Z. Chen, "Development and Reliability of Nonconductive Adhesive Flip-Chip Packages," *Thin Solid Films*, 462 (63), 446–453, 2004.

[17] C.-K. Chung, W.-S. Kwon, J.-H. Park, S.-B. Lee, and K.-W. Paik, "Effects of the Functional Groups of Nonconductive Films (NCFs) on Materials Properties and Reliability of NCF Flip-Chip-on-Organic Boards," *2005 International Symposium on Electronics Materials and Packaging (EMAP2005)*, pp. 156–161, 2005.

[18] J. W. Kim, Y. C. Lee, and S. B. Jung, "Effect of Bonding Conditions on Conduction Behavior of Anisotropic Conductive Film Interconnection," *Metals and Materials International*, 14, 373–379, 2008.

[19] J. W. Kim, D. G. Kim, Y. C. Lee, and S. B. Jung, "Analysis of Failure Mechanism in Anisotropic Conductive and Nonconductive Film Interconnections," *IEEE Transactions on Components and Packaging Technologies*, 31, 65–73, 2008.

[20] J. W. Kim, Y. C. Lee, and S. B. Jung, "Reliability of Conductive Adhesives as a Pb-free Alternative in Flip-chip Applications," *Journal of Electronic Materials*, 37, 9–16, 2008.

[21] J. W. Kim, Y. C. Lee, D. G. Kim, and S. B. Jung, "Reliability of Adhesive Interconnections for Application in Display Module," *Microelectronic Engineering*, 84, 2691–2696, 2007.

[22] Y. Ma and Y. C. Chan, "The Effect of Bonding Force on the Electrical Performance and Reliability of NCA Joints Processed at a Lowered Temperature," *Journal of Materials Science*, 42, 6658–6664, 2007.

[23] B. de Boer, A. Hadipour, M. M. Mandoc, T. van Woudenbergh, and P. W. M. Blom, "Tuning of Metal Work Functions with Self-Assembled Monolayers," *Advanced Materials*, 17, 621–625, 2005.

[24] T. Dadosh, Y. Gordin, R. Krahne, I. Khivrich, D. Mahalu, V. Frydman, J. Sperling, A. Yacoby, and I. Bar-Joseph, "Measurement of the Conductance of Single Conjugated Molecules," *Nature*, 436, 677–680, 2005.

[25] C. Joachim, J. K. Gimzewski, and A. Aviram, "Electronics Using Hybrid-Molecular and Mono-Molecular Devices," *Nature*, 408, 541–548, 2000.

[26] Q. Sun, A. Selloni, and G. Scoles, "Electronic Structure of Metal/Molecule/Metal Junctions: A Density Functional Theory Study of the Influence of the Molecular Terminal Group," *Journal of Physical Chemistry B*, 110, 3493–3498, 2006.

[27] Y. H. Kim, S. S. Jang, and W. A. Goddard, "Conformations and Charge Transport Characteristics of Biphenyldithiol Self-Assembled-Monolayer Molecular Electronic Devices: A Multiscale Computational Study," *Journal of Chemical Physics*, 122, 244703, 2005.

[28] N. Koch, A. Kahn, J. Ghijsen, J. J. Pireaux, J. Schwartz, R. L. Johnson, and A. Elschner, "Conjugated Organic Molecules on Metal Versus Polymer Electrodes: Demonstration of a Key Energy Level Alignment Mechanism," *Applied Physics Letters*, 82, 70–72, 2003.

[29] G. Heimel, L. Romaner, J. L. Bredas, and E. Zojer, "Interface Energetics and Level Alignment at Covalent Metal-Molecule Junctions: pi-conjugated Thiols on Gold," *Physical Review Letters*, 96, 196806, 2006.

[30] B. de Boer, M. M. Frank, Y. J. Chabal, W. R. Jiang, E. Garfunkel, and Z. Bao, "Metallic Contact Formation for Molecular Electronics: Interactions between Vapor-deposited Metals and Self-Assembled Monolayers of Conjugated Mono- and Dithiols," *Langmuir*, 20, 1539–1542, 2004.

[31] Y. Li, M. J. Yim, and C. P. Wong, "High Performance Nonconductive Film with pi-conjugated Self-Assembled Molecular Wires for Fine Pitch Interconnect Applications," *Journal of Electronic Materials*, 36, 549–554, 2007.

[32] X. Crispin, V. Geskin, A. Crispin, J. Cornil, R. Lazzaroni, W. R. Salaneck, and J. L. Bredas, "Characterization of the Interface Dipole at Organic/Metal Interfaces," *Journal of the American Chemical Society*, 124, 8131–8141, 2002.

[33] P. S. Bagus, V. Staemmler, and C. Woll, "Exchangelike Effects for Closed-shell Adsorbates: Interface Dipole and Work Function," *Physical Review Letters*, 89, 096104/1–096104/4, 2002.

[34] L. Yan, N. J. Watkins, S. Zorba, Y. L. Gao, and C. W. Tang, "Thermodynamic Equilibrium and Metal-organic Interface Dipole," *Applied Physics Letters*, 81, 2752–2754, 2002.

[35] Y. Li, M. J. Yim, K. S. Moon, and C. P. Wong, "Novel Nano-Scale Conductive Films With Enhanced Electrical Performance

and Reliability for High Performance Fine Pitch Interconnect," *Ieee Transactions on Advanced Packaging*, 32, 123–129, 2009.

[36] S. Pothukuchi, Y. Li, and C. P. Wong, "Development of a Novel Polymer-Metal Nanocomposite Obtained through the Route of in situ Reduction for Integral Capacitor Application," *Journal of Applied Polymer Science*, 93, 1531–1538, 2004.

[37] M. J. Yim, J. S. Hwang, W. Kwon, K. W. Jang, and K. W. Paik, "Highly Reliable Non-conductive Adhesives for Flip Chip CSP Applications," *IEEE Transactions on Electronics Packaging Manufacturing*, 26, 150–155, 2003.

[38] I. Watanabe, "Development of Double-layer Anisotropic Conductive Adhesive Films," *Hitachi Chemical Technical Report*, 26, 13–16, 1996.

[39] J. Liu, "Conductive Adhesives for Electronics Packaging," *Ed., Chapter 15, Electrochemical Publications*, pp. 386–387, 1999.

[40] L. Jia, H. Ding, X. Sheng, and B. Xie, "Evaluation of a Double-layer Anisotropic Conductive Film (ACF) for Fine Pitch Chip-on-glass (COG) Interconnection," *6th International Conference on Electronic Packaging Technology*, pp. 344–347, 2005.

[41] M. J. Yim, J. S. Hwang, J. G. Kim, J. Y. Ahn, H. J. Kim, W. S. Kwon, and K. W. Paik, "Highly Reliable Flip-chip-on-flex Package using Multilayered Anisotropic Conductive Film," *Journal of Electronic Materials*, 33, 76–82, 2004.

[42] T. Nonaka, K. Fujimsru, N. Asahi, K.-i. Kasumi, and Y. Matsumoto, "Development of Wafer Level NCF (Non Conductive Film)," Proceedings of 58th IEEE Electronic Components and Technology Conference, pp. 1550–1555, 2008.

[43] Z. Q. Zhang, Y. Y. Sun, L. H. Fan, and C. P. Wong, "Study on B-stage Properties of Wafer Level Underfills," *Journal of Adhesion Science and Technology*, 18, 361–380, 2004.

[44] Q. Tong, B. Ma, A. Savoca, L. Nguyen, C. Quentin, S. Luo, and C. P. Wong, "Recent Advances on a Wafer-Level Flip Chip Packaging Process," *IEEE Proceedings of the 50th Electronic Components and Technology Conference*, pp. 101–106, 2000.

[45] S. Shi and C. P. Wong, "The Process and Materials for Low-Cost Flip-Chip Solder Interconnect Structure for Wafer Level No Flow Process," *US Patent 6,746,896*, 2004.

Chapter 7
Conductive Nano-Inks

7.1 Introduction

7.1.1. An Overview of Conventional Patterning of Electronics

Patterning of electronics to obtain specific designs is conventionally carried out on wafer or substrates by photolithography. This is a process to transfer images and patterns from a mask to the surface of a wafer or substrate. The steps typically involved in the photolithographic process are wafer or substrate cleaning, barrier layer formation, photoresist application, soft baking, mask alignment, exposure and development, and hard-baking.

Y. Li et al., *Electrical Conductive Adhesives with Nanotechnologies*,
DOI 10.1007/978-0-387-88783-8_7, © Springer Science+Business Media, LLC 2010

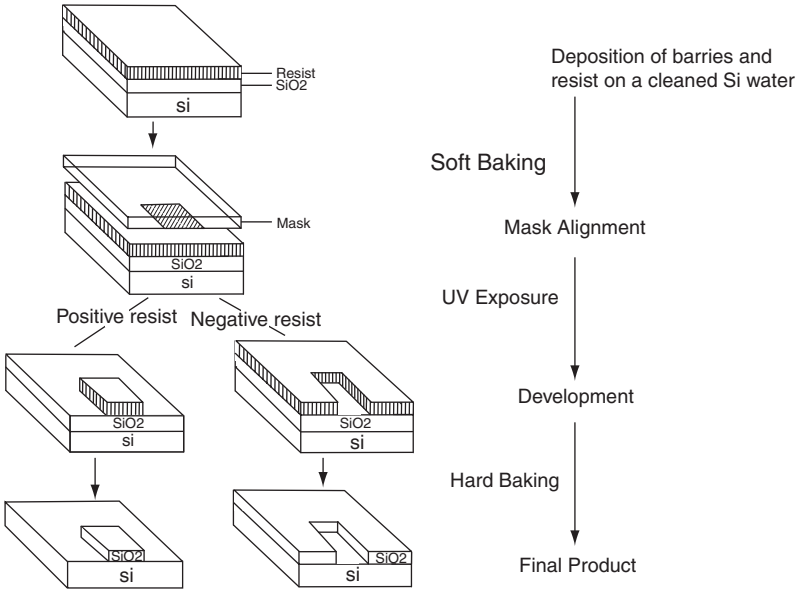

Fig. 7.1. Conventional silicon processing [1]

The basic process is illustrated in Fig. 7.1. The silicon wafers are first chemically treated in order to remove particulate matter, organic contaminants, and ionic and metallic impurities. Next, a passive silicon oxide barrier layer is grown across the surface of the wafer. A layer of either a positive or negative photoresist is then applied by spin coating. Soft-baking plays a very critical role in photo-imaging. In the soft-baking step, most of the solvent is removed from the photoresist coating. The photoresist layer is then covered with an appropriate mask and is exposed to a radiation. After photo-exposure and post-exposure bake, the resist is developed by a selective solvent to reveal a negative or positive image of the pattern on the mask (positive: exposed material is removed, negative: unexposed material is removed). In the final step, the wafer is hard-baked in order to remove residual solvent from the photoresist and improve adhesion of the photoresist to the wafer surface. The resist protects the surface of the wafer and allows selective etching, doping, ion implantation, or metallization. Recent improvements and technological advances in the field of photolithography have made it possible to obtain circuitry of near-nanoscale dimensions [1].

Photolithographic patterning requires a large infrastructure. The industry, however, is well established and has benefited from continuing improvements in pattern resolution. Photolithography has been used in the

production of electronic components, integrated circuits, and devices. While it is a complex, expensive, and capital-intensive process, given economies of scale ever lower cost microelectronics have been realized. Electronic circuits and devices patterned on crystalline silicon are, however, constrained by limitations of wafer size. Accordingly this process on silicon does not lend itself to wide format applications like those in which novel plastic semi-conductive materials can be leveraged [2]. Increased research in the field of printable electronics is being conducted because lithographic processes must accommodate serious environmental hazards like acidic and high heavy metal content effluents and use of volatile organic compounds (VOCs) in photoresist developers [3]. The environmental impact of photolithographic process is significant. The overall processing and development of photolithographic patterns consumes much more material than that contained in circuits and devices produced thereby [4]. The disposal of circuit boards is also a problem. Resin laminate substrates can contain fungicides, fire retardants, and organic compound and toxic residues from soldering operations. These constituents necessitate recycling operations and disposal [5].

7.1.2 Introduction of Printed Electronics

Printed electronics may employ any of a number of printing technologies or processes to create electronic circuits, devices, electrical components, and interconnects. Printed electronics can be used alone or in combination with conventional microelectronic components such as silicon chips for a range of different applications. Printing technologies have received increased interest recently because of their ability to pattern a variety of functional materials. Printing technology also allows use of various types of substrates including flexible media. Materials such as conductive and semi-conductive electronically functional polymers can be patterned using printable technologies. Direct printing of electronic features may create new markets and new low-cost microelectronic products.

Today, there are a number of low resolution circuits and electronic devices that can be produced by printing. This field is opening up a wide array of novel applications that could be commercially and economically feasible in the future. The key is to make it efficient and affordable. Printing offers unique features including [6]

1) Customization in volume production
- short cycle time from design to manufacturing;
- fast manufacturing runs;
- Reduced logistics costs;

2) Production advantages
- Ergonomic user interface solutions;
- Environmentally friendly;

3) Applicability in novel products
- Flexible structures;
- Low end integrated electronics.

Printing may be the optimum process for production of many plastic-based electronic circuits, large-area devices, and flexible electronics. Printing enables the production of disposable, thin, and wearable electronics. Some of the interesting end applications for printable electronics are identification, antennas, displays, radio frequency identifications (RFIDs), sensors, batteries, security devices, and quality indicators. Among the unique characteristics of printable electronics are that it has a low environmental impact, low cost, and may be the optimal process for production of disposable devices, single use devices, smart packaging, flexible electronics, and large-area devices [7].

Techniques and processes that have been explored in regard to their utility in printed electronics include inkjet printing, screen printing, flexography, lithography, spray printing, stamping, etc. The majority of the work in this area has involved inkjet [8] and screen printing technologies [9]. The major high volume printing processes currently in use are offset lithography and flexography [3, 5, 10]. Printing of conductive inks to fabricate circuits [5], LEDs [11], sensors [12], microwave integrated circuits (MIC) [13], radio frequency circulator components on a wide range of flexible materials [14], etc., have been reported using offset lithography. Conductors, resistors, anodes/emitting layers, and organic light-emitting diodes (OLEDs) [15] have been fabricated using flexography and gravure printing.

Key requirements for printable electronics include need for functional fluid materials to build logics, a suitable high-speed and large-volume printing process that makes ease of production and low cost feasible and adaptation to the process to print electronics. The key benefit of printed electronics is that it offers the possibility of using electronics in applications where the cost of silicon would make it impossible or the brittleness of silicon would make it inadequate.

7.1.3 Utility of High Volume Printing Processes in Printable Electronics

Extensive research has been carried out in printable electronics in inkjet and screen printing technologies. However, screen and inkjet printing are relatively slow, limiting their productivity and use in high volume manufacturing [8]. A number of "soft lithographic" techniques have been used to make devices like transistors, RFID tags, wearable electronics and other novel applications [16, 17]. They too are, however, slow and have a limited production volume. Some of the major advantages of high volume printing processes are

- high volume, high speed;
- additivity;
- substrate latitude (including flexible substrates);
- large–area printing;
- demonstrated repeatability;
- negligible waste;
- commercial availability of functional materials and infrastructure;
- utility in short run lengths;
- quick changeover/make ready systems.

There are, however, some challenges. The following properties have to be appropriately optimized for offset lithography and flexography.

- particle sizes distribution in the inks;
- solvent evaporation rate;
- rheological properties;
- substrate surface energy;
- printing speed.

The major high volume printing processes are offset lithography and flexography. These two important printing processes are discussed briefly below along with the ink considerations for such processes.

7.1.3.1 Offset Lithography

Offset lithography is a process that relies on two dissimilar wetting characteristics to produce an image. It may use photographic processes to make negatives. A schematic of the process can be seen in Fig. 7.2.

The lithography plate is a flexible aluminum or plastic printing plate. Modern printing plates have a brushed or roughened texture and are covered with a photosensitive emulsion. A photographic negative of the desired

image is placed in contact with the emulsion and the plate is exposed to light. After development, the emulsion shows a reverse of the negative image, which is thus a duplicate of the original (positive) image. The plate is then chemically treated so the positive image is receptive to printing inks. The plate is affixed to a drum on a printing press. Rollers apply water (in form of the fountain solution), which wets the non-image areas of the plate, and ink, which adheres to the positive image areas. If this image were directly transferred to a substrate, it would create a positive image, but this would wet the substrate as well. Instead, the plate rolls against a drum covered with a rubber blanket, which squeezes away the water and picks up the ink. The substrate rolls across the blanket drum and the image is transferred to the substrate. Because the image is first transferred, or offset to the rubber drum, this reproduction method is known as offset lithography or offset printing.

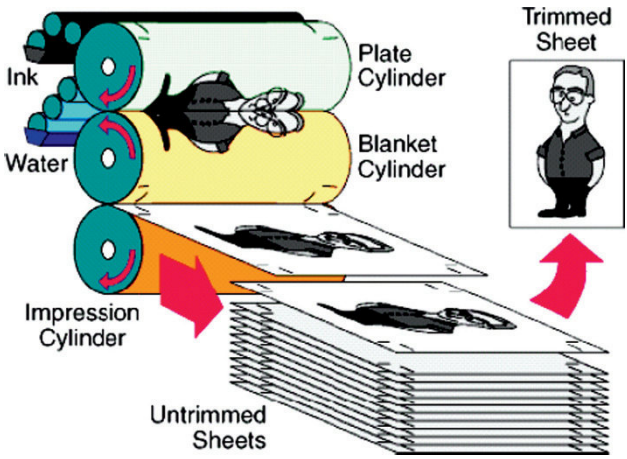

Fig. 7.2. Schematic of a Lithographic Printing Process (http://www.bobs.co.uk/print/Offset.html)

The pros: This process has excellent control of registration and resolution in printing of circuit patterns. The commercial printing presses can be used for printing electronics. Conductive lithographic inks are also commercially available. Low ink volume is required for any given pattern. With the advent of waterless/UV inks, there is a substantial development potential in lithography. Waterless lithography makes use purely of the difference of surface energy of the image area and non-image areas for ink

transfer to image areas. With current printing developments, circuit components of up to 25 μm lines/gap have been achieved and thinner lines/gaps are being aimed for.

The cons: Offset lithography has very high start-up costs. The single printed ink layers are very thin (~1 μm). This makes multiple passes imperative especially in obtaining sufficient thickness for conductivity in ink films. The start-up waste on very short runs is high. The lithographic process requires stringent control on the ink rheology. Thus the inks have to be highly viscous. Therefore, most available commercial inks are resins loaded with conductive materials like silver/copper particles or flakes or carbon black. It is difficult to formulate organic inks meeting such requirements [18]. Also ink drying speed and water balance in the printing process have to be optimized well.

7.1.3.2 Flexography

Flexographic printing process is a rotary relief method of printing. A schematic of the process can be seen in Fig. 7.3. It uses a printing plate made of rubber, plastic, or some other flexible material. Recently photopolymers are also being used to increase the resolution and lifetime. The image pattern is raised on the plate like the raised areas on a rubber stamp. The plate is attached to a plate cylinder so that it can print in a rotary fashion. Ink is applied to a raised image on the plate using an engraved roller called anilox. The anilox roller has small cells or wells all over its surface, which transfer a precise volume of ink. Excess ink is wiped off by a doctor blade before printing. This helps in depositing a controlled amount of the ink to the substrate. Only the raised part (image part) on the plate receives the ink and the pattern is transferred to the substrate by the pressure of the impression cylinder. Non-image areas are below the printing surface and do not reproduce. The thickness of the film can be adjusted by controlling the rotating speed and the pressure applied on the substrate.

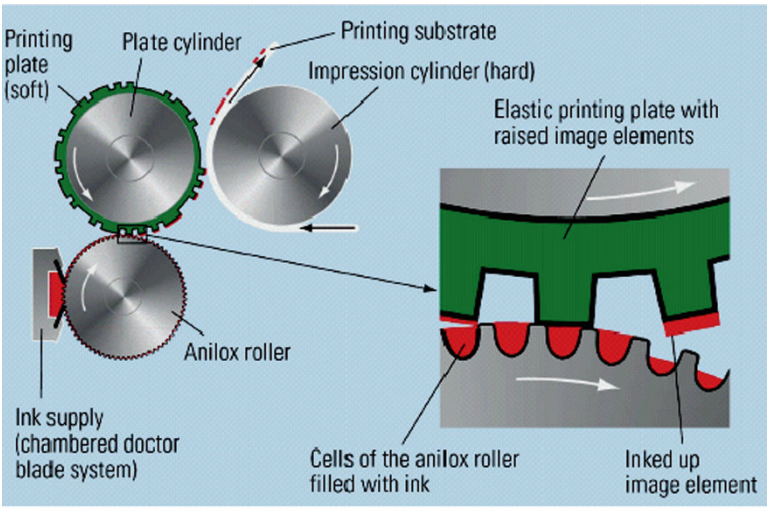

Fig. 7.3. Schematic of a flexographic printing process (H. Kipphan, Handbook of Print Media)

The pros: Flexography is a relatively easy and reliable process. The ink film thickness control can be a useful tool in obtaining uniform coverage over large areas. The fast drying inks used in flexography make it ideal for printing on materials like plastics and foils. This makes flexography the predominant method used for printing flexible bags, wrappers, and similar forms of packaging. The soft rubber plates are also well suited to printing on thick, compressible surfaces such as cardboard packaging. Inks used in flexography may be either water based or solvent based. The process uses only a fraction of ink used in other techniques due to the anilox roll which meters ink quantities and the ink cures fully within hours. The process is relatively simple and convenient in that it exhibits excellent handling characteristics pre-press, on-press, and post-press. This process also shows tremendous room for development in improving results. Recently hard polymer capped plates or cushioned plates are being used to avoid dot gain (spread of ink outside the image areas due to squeezing of flexo plate during printing) or halo effects.

The cons: The raised image of the plate expands due to printing pressure leading to a gain in the image areas (dot gain). This leads to difficulty in registration and size monitoring. One of the problems of flexography is the halo obtained around the actual printed edges. Therefore, only macro features are practically possible in flexography. Flexography can be used to print conductive traces, but the resolution obtained is limited.

7.1.3.3 Inks

The inks for the specialized field of printable electronics have to be specially designed. Both the intended application and the desired printing process will govern the composition of the ink. The physical properties of the wet ink are important in some applications but not in some others, and similarly the physical properties of the dry ink film are important in some applications but not all. Identifying the function of a dry ink layer that is necessary to enable a desired application requires an understanding of the print process requirements and therefore the wet ink. The rheology and surface energy of inks determine the viscosity, applicable substrate, dry ink structure, adhesion, cohesion, and surface properties of the final print. The correct rheology of the ink depends not only on the intended printing process but also on the specific printing equipment, ambient conditions, production speed, and production parameters.

There are a number of factors to be considered when formulating a specific ink (for both polymeric and metal particles filled inks):

- methods and ingredients for making conductive inks;
- conductive polymers;
- silver and other metal particles;
- factors affecting ink performance;
- factors affecting conductivity.

It is difficult to correlate the rheological data collected under very controlled conditions with a printing process. The printing speed, scale, geometry, press setting, substrate, chemical contaminants, etc., make it difficult to analyze the exact working conditions. Shear rates can be significantly higher in printing processes than in a rheometer. Thus indirect correlation is sometimes necessary to deduce projected behavior when transitioning from lab to press. Properties of the dry ink are also important to the functionality of a device constructed from electronic inks. Tests like adhesion, rub resistance, and solvent resistance provide an indication of the robustness of the printed materials. However, due to variability in processes, applications, and substrates, there are no well-defined standard ranges for such properties [19].

Most commercially available conductive inks are comprised of finely dispersed conductive particles in a non-conductive resin matrix which bind the particles. The particles may be metallic copper, silver, or aluminum or non-metallic, conductive carbon blacks. The volume fraction of the conductive particles is generally maintained above the percolation threshold, the minimum volume fraction require for inter-particle connectivity. The inks may be used to produce conductive patterns on flexible and rigid substrates. The flexo/gravure inks are generally water based and the litho inks are oil based.

Conductive inks are compatible with a variety of blankets, plates, and substrates. These inks have low volatile organic chemical content and are considered to be environmental friendly. Line resolution of 50 μm is achievable with the flexo/gravure inks, and 40 μm with the litho inks. The inks have sheet resistance as low as 100 Ω/□ (Ohms per square) at a film thickness of approximately 8 μm. For printed resistors, ink formulations can be tuned to cover a wide range of sheet resistance (100Ω/□ – 500Ω/□) at a film thickness of 2 μm or less [20]. The conductivity in a given ink formulation is governed by the printing process, drying method, substrate, etc. The conductivity measurements are typically analyzed in terms of sheet resistivity (ρ_s):

ρ_s = *{(resistance of a rectangular region of the printed conductor) * (width of region)}/(length of region)*

The length of the conductive region divided by the width implies number of equal-sided squares being measured. Hence sheet resistivity is reported in ohms per square (Ω/□).

Lithographic inks: These are highly viscous inks (paste inks). The tack or splitting of the ink between two rolls is an important property to be considered in multi-impression printing. Lithographic conductive inks must be designed such that they do not chemically dissolve in image or non-image areas on the printing plate. A common problem with lithographic inks is that splitting of ink filaments can lead to uneven texture. Inks should exhibit the phenomenon of "trapping." In this phenomenon, the first layer printed onto the substrate shows the ability to become more receptive to subsequent printed layers.

Flexographic inks: These are relatively low viscosity inks (fluid inks). Low viscosity is necessary because the ink needs to flow into the cells of the anilox rolls of the press. The inks must be designed to be readily redispersible over the lifetime of the product. Various dispersing agents and binders may be used to obtain optimum properties [19].

7.2 Conventional Conductive Inks

Conventional conductive inks are primarily composed of metallic flakes, usually silver or copper, or carbon flakes that are suspended in a retaining matrix. A retaining matrix is typically made of polymers, which are known as polymer thick films (PTFs). The retaining matrix is not inherently conductive although it may be weakly conductive.

Once the ink is printed, the retaining matrix must be reduced to allow the ink to be conductive. The ink becomes conductive when the retaining matrix is removed and the metallic or carbon particles come in contact with each other. This process of reducing the retaining matrix is known as curing. In conductive inks, this can be performed through a number of methods (e.g., UV, heat curing). Typically, PTF ink formulations have a lower curing temperature of 150°C, which allows for more options for substrate selection and is particularly useful with flexible polymer films [21]. Flexographic conductive inks, since they are water based, typically cure through evaporation of the solvent into the air. Unsaturated polyester, acrylics, epoxy, and thiolene resins can be used as the matrix for UV curable ink [20].

The difference between carbon- and metallic-based conductive inks is that carbon inks are generally less conductive than metallic inks and therefore provide for a weaker signal and less read range when used in RFID applications. However, carbon-based inks are more economical to produce and are less environmentally hazardous than metallic-based inks.

Carbon inks are typically used in electro magnetic interference (EMI)/RF shielding applications, such as their use in speakers and monitor screens because of their weak conductivity [21]. Currently, much research is being done to improve and develop better carbon and organic-based inks because they are much more environmentally compatible and would require less regulation and containment in production of printed electronic products.

Metallic inks are currently used in a wide array of printed electronic applications such as membrane switches and circuits, RFID tag antennas, smart package and tamper evidence packaging, and printed battery testers [21]. Applications of conductive metallic inks that are currently in the research and development stage that will enter production are printed RFID chips, flexible photovoltaic arrays, and printed batteries, among others [22].

Conductive inks, both metallic and organic, are typically formulated to provide properties to suit a specific substrate and printing process. Currently, conductive inks have been developed for use in all forms of print methods (ink-jet, screen, flexography, gravure, offset litho) with the exception of toner-based electrostatic printing.

7.2.1 Metallic Ink

Metallic-based inks are commonly used for membrane switches and circuits and now increasingly for RFID tag antennas. In the case of RFID, the conductivity of metal particle inks is typically more than sufficient. Therefore, curing can be done at relatively low temperatures for a few seconds using a heated press. Other applications include the use of conductive ink

for connections on smart blister packs, which record when a pill is popped (because a circuit is broken), and for tamper evidence packs which work on a similar principle. As another example, tens of millions of printed battery testers have been sold, based on a conductive ink.

Conductive inks are also being used to fabricate printed antennas for automotive applications (Fig. 7.4) [23]. Silver particle filled inks were printed on the thin-film substrate. For dimensional stability reasons, only pre-shrunk films can be used. For better adhesion the films may be pretreated. After printing, the drying parameters must be considered because an accurate thermal treatment is essential to enhance the conductivity and adhesion. A very essential part of the research work was to specify the most appropriate inks. The inks properties such as rheology and printability have been tested thoroughly using test patterns. The performance of the antenna relies very much on the silver content. On the other hand, the silver content is the factor which has a great influence on the price. Also the particle geometry is important. Flakes or spheres are typically available. For the integration purpose the binder system is crucial, too. As well as having many advantages and attractiveness, the printed antenna must be competitive against the classical rod antenna. It was shown that inks are most suitable whose silver content does not exceed a certain limit, and the printed antennas

- show superior performance;
- are more flexible;
- are adaptable to different geometries;
- are cheaper (in most cases).

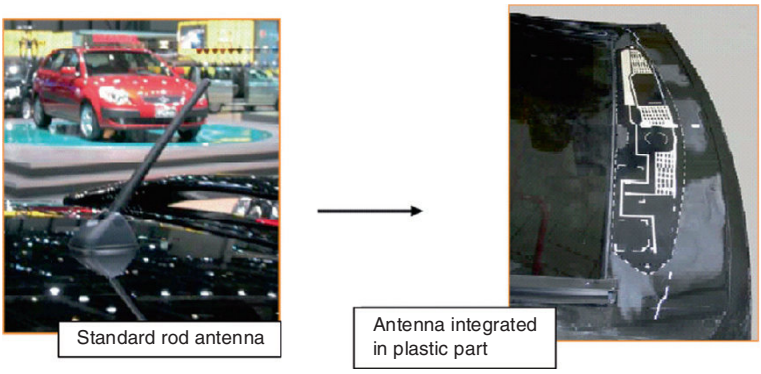

Fig. 7.4. Comparison of standard rod antenna and the antenna printed with conductive inks

Conductive inks have been used widely for forming the antenna RFID tags. RFID is basically a method of storing and retrieving information from a tiny silicon chip on a tag attached to an object. There are two general categories of RFID tags, passive tags and active tags. The active tags have a battery to power the tag circuitry. The battery allows for greater memory capacity in the tag, increases the linear range from which the tag can be read, and allows the tag to independently announce its presence by periodically transmitting its ID code. These tags are more expensive, but have advantages for tracking large, complex items. For example, active tags are used to identify seal and shipping containers, and the entire contents of the container can be stored in the tag's memory.

The more common type, however, is the passive tag, so-called because it has no internal battery power. Passive tags are powered by "free space" energy drawn from the RF carrier wave transmitted by an RFID interrogator.

In its simplest form, a passive RFID tag is an assembly of two major components:

1. a small antenna circuit tuned to the RF carrier frequency and
2. a silicon integrated circuit (IC chip) programmed with unique identification codes and communication protocols.

RFID system performance hinges, in large part, on tag performance. And the tag, in turn, relies on a handful of elements that determine its performance–the antenna being an especially critical one. An RFID tag antenna circuit is made of a conductive material–such as copper, aluminum, or silver–bonded to a substrate material. The substrate can be fiberglass (down to 1/64″ thickness) or a flexible polymer such as PET or Kapton in sheets or rolls. There are a number of approaches to forming the conductive antenna image onto the substrate:

- subtractive etching;
- printing with conductive inks;
  - screen printing;
  - gravure, also called intaglio or dry offset;
  - offset (oil-based inks);
- vapor deposition.

The earliest method of antenna fabrication has been subtractive etching of a metal-plated substrate (e.g., copper-clad FR4 fiberglass). The antenna design is printed onto a clear film as a positive image (black on clear). The image can be laser, ink-jet or photographically printed. The film positive is placed over the copper plating, which has been coated with a photoresist and exposed to light. The copper-clad board is then processed in photographic development solution, which removes the resist from the exposed

areas. The developed board is immersed in an etching bath (e.g., ferric chloride) until the exposed areas are etched away. Subtractive etching has matured to the point where it has become a low-tech process requiring inexpensive off-the-shelf materials and equipment. The process can be done in anyone's garage. That is fine for prototype development; however, for larger production runs, etching creates significant amounts of metal salt and chemical waste products, incurring increased costs due to regulatory fees, reclamation charges, and trucking expenses. By comparison, printing and vapor deposition methods differ primarily in that they are additive methods, resulting in reduced process steps, waste, and cost.

The simplest additive method is screen printing with conductive ink. Screen printing is widely available and inexpensive; however, it does have limitations. Screen printing is not well suited to very large production runs because it is relatively slow and the screens are not as durable as gravure or offset. Also, an important consideration in forming an antenna circuit on a substrate is image resolution or how much fine detail is achievable with a given printing method. One RFID industry goal is tag miniaturization, because a smaller tag is less obtrusive when applied to a product, uses less materials, and more tags can be ganged on a given area of substrate. But as a tag antenna design gets smaller, proper tuning to the RF carrier wave frequency demands that the antenna dimensions be reproduced precisely. A spacing of 230 threads per inch is common for screens, capable of printing a circuit trace of 0.5 mm (127 mil) in width, but that is an order of magnitude coarser than is achievable with gravure. The trade-off is that, when using screen printing, a thicker deposit of ink can flow onto the substrate than is possible with gravure, resulting in higher conductivity (lower resistance) values.

Gravure printing has traditionally been the preferred method for reproducing high-quality photography and art on a mass scale. Gravure printing with conductive ink is capable of producing resolutions of 50 μm. Gravure is suited to very large production runs: the engraved plates are durable and throughput as high as 900 m/min. Conductive inks are typically fine metal particles of silver or copper suspended in a polymer vehicle. A conductive ink's characteristic properties of flow, adhesion, and cohesion are crucial to resolution of fine detail. In addition to fine detail, however, it is paramount that the printed image has the lowest possible resistance to electromagnetic energy. Metal particle density determines the conductivity of the printed antenna–that is, how efficiently the RF energy can be captured and returned by the RFID tag assembly. The higher the particle density of the metallization, the better the conductivity. But as the particle density increases so does the ink's viscosity, resulting in a thicker ink that is difficult to apply. An ink with a lower viscosity could have the opposite problems: dimensional instability, poor adherence, and a higher electrical resistance.

To solve that problem, a new ink was developed [24]. Metallic particles are suspended in an organic carrier that decomposes after printing, leaving a 99% pure metal coating. It was claimed this organic ink is 3–10 times more conductive than polymer-based inks (Fig. 7.5).

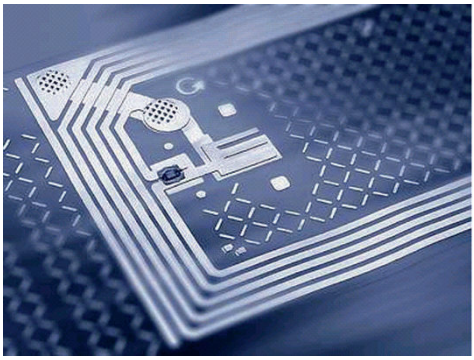

Fig. 7.5. An optical image of the printed RFID antenna [24]

7.2.2 Conductive Carbon Ink

7.2.2.1 Introduction

Carbon-based inks, which are only weak conductors, have typically been used for EMI/RF shielding, such as on monitor screens and speakers. Permanent cost saving is a must in the printed circuit board industry, like in all other industries. At the same time, however, the quality standards have to be maintained. With printed circuit boards (PCBs) that are produced in medium and large volume, cost saving proves a particular asset. These PCBs, mainly for consumer electronics, are subject to the greatest price pressure and cost saving in the production process is one of the decisive factors for the economy and competitiveness of the end product.

Costs can be saved by replacing expensive raw materials with more economical ones and by a simplification of the production process. The employment of carbon-conductive inks in the production of printed circuit boards combines both the use of economical materials and the simplification/rationalization of the production process.

The substitution of gold by carbon-conductive ink on contact points not only eliminates the necessity of using the extremely expensive raw mate-

rial "gold" but also the labor-intensive plating process. When double-sided, plated through hole circuits are replaced by single-sided printed circuit boards with cross-over carbon conductors, the savings are even more substantial because besides the cost for the wet processing in the course of the through-hole plating also the separate treatment of the two printed circuit board sides can be disregarded. Furthermore, single-sided base material can be used instead of the double-sided copper-clad base material.

If carbon-conductive inks are used to print resistors directly onto the base material the effort involved in assembling the printed circuit boards is reduced and in the case of multilayers it may even be possible to save on layers.

7.2.2.2 Theoretical Fundamentals

Carbon-conductive inks consist of one or more paint binding agents (polymers), solvents, and carbon particles. After application of the ink, the solvents evaporate and following a curing mechanism, a polymer film remains on the substrate into which the carbon particles are homogeneously embedded.

The concentration of the conducting particles must be high enough that a contact of the individual particles enables the flow of current within the ink system. The concentration in which the resistance drops significantly is called the percolation threshold.

The maximum concentration of the conducting particles is mainly dependent on their structure and the specific surface. Only so many conductive solids can be added to the ink as can be homogeneously embedded by the polymer. This is the only method of achieving a firmly adhesive, nonporous (dense), and closed coating.

Generally, metal or carbon powders are used as conducting particles. Compared to carbon powders, metal or precious metal powders yield conductance that is higher mainly due to the higher specific conductivity of metals and also to the smaller specific surface of metallic powders so that higher particle loading in the ink is possible.

On the other hand, metal powders have the problems of oxidation/corrosion and migration as in the case of the frequently used silver. Furthermore, the high material price of metal powders adversely influences the cost of the ink.

Decomposition of organic matter with the exclusion of air or incomplete combustion results in carbon in a third amorphous form, either in coarse masses as coal or in finest dispersion as carbon-black (soot).

The individual character of soots is determined in particular by the specific surface and the structure. The specific surface of 80–1,200 m^2/g decides the percentual amount of soot to be used. The structure is determined

by the coalescence of the primary particles during the production process and is one of the decisive factors for the necessary packing density in the ink coating.

Since soots are produced synthetically, structure and specific surface can be easily controlled during the production process. From the large variety of different soot types available, the most suitable types for the production of conductive inks have to be selected on the strength of structure and specific surface.

On account of the more amorphous structure, however, an adequate packing density cannot be obtained with soots alone, and thus graphites with a more stratified structure are added, however, recent studies have shown that a few layers (1–10) graphene layers material may have higher conductivity than the conventional graphites. The combination results in conductive inks which meet the aforementioned requirements in the cured ink coating, i.e., direct contact of the conducting particles.

By selecting the suitable polymers, the following properties can be achieved:

- easy processing (1-pack system);
- good adhesion to different substrates;
- high mechanical and chemical resistance;
- nearly no change in resistance after soldering processes and/or after hot-air leveling;
- favorable curing conditions, i.e., lowest possible curing temperature and short curing times.

7.2.2.3 Use of Carbon-Conductive Inks

In addition to the printed circuit board technology, carbon-conductive inks are also employed in other sectors of electronics/electrical engineering. By means of carbon-conductive inks, static electricity can be discharged from plastic components and other insulators, such as paint coatings. This application is mainly used in the housing industry (television and computer housings) with the paint being relatively fluid and sheet-sprayed onto the components.

Carbon-Conductive Inks For Laminate Keyboards

Carbon-conductive inks are used for the production of laminate keyboards. The entire conductor pattern and the contact areas are printed on plastic film, such as polyester or polyimide, using carbon-conductive inks. For this application, either two separate films are used or one film, the two sections of which are folded together. There is an insulating separator film

between the two films and the entire laminate keyboard is masked by a printed cover foil.

The switch contact is affected by finger pressure on previously determined areas of the film at which the separator film is cut out. The contact is affected by touching of the upper and lower films and it is interrupted again as soon as the pressure is relieved. A service life of up to 25,000,000 switching cycles has been established in laboratory tests. This field of application is mainly related to keyboards for computers and control units as well as electronic games.

When selecting suitable carbon-conductive inks for this range of application, special attention must be paid to good adhesion to the substrates used, adequate elasticity as well as high abrasion resistance.

Carbon-Conductive Inks as Contact Materials, Substitution for Gold

Traditionally, nickel/gold plating has been applied over copper tracks used for keyboard contacts or edge fingers. This provides a conductive, corrosion resistant, environmentally stable coating. Replacement of gold plating by carbon ink offers the following additional advantages [25]:

- Cost – Replacing gold with carbon reduces material costs and replacing the electrolytic bath with a simple screen printing process reduces process costs.
- Robustness – Tests have shown that a typical carbon ink is hard enough to withstand >1 million pushbutton operations (keypad) or 100 insertion operations with a 75 g force (edge connector) without showing wear or increased resistance.
- Resistance – The above advantages are gained without a significant increase in loop resistance of the closed circuit using the graphite pill.

The thin print of carbon ink (typically 15 μm has a low resistance, less than the resistance across the graphite pill. Figure 7.6 is an example of carbon ink over a copper keypad.

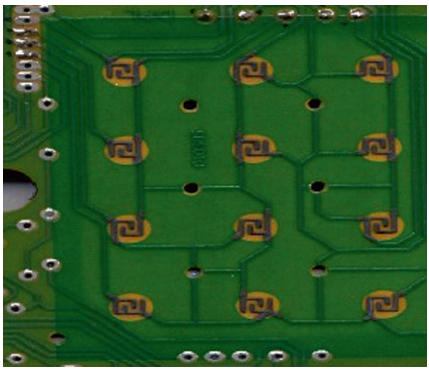

Fig. 7.6. Example of carbon ink over a copper keypad

A partial gold plating on printed circuit boards is mainly effected for the purpose of protecting contact points such as edge connectors, tip contacts, and sliding contacts from mechanical and chemical attacks in order to achieve a long service life. In the case of tip contacts, the use of carbon-conductive ink eliminates the need for gold plating.

This means substantial cost saving because the following operations are required for a partial gold plating:

- covering the areas that are not to be gold plated;
- electrodeposition of nickel;
- electrodeposition of gold;
- stripping of the plating resist (mostly in solvents);
- coating the areas that are not gold plated with solder resist for subsequent soldering processes.

With their increasing abrasion resistance carbon-conductive inks conquered a further field of application as sliding contacts, for instance for automotive applications. Within the scope of the necessary cost reduction expensive gold contacts are also being replaced by printed carbon-conductive ink sliding contacts in this sector. With optimum process parameters up to 125,000 contact cycles can be realized.

Carbon-Conductive Inks as Components

Used as components carbon-conductive inks can considerably contribute to the miniaturization of a PCB.

Carbon-conductive inks can be printed as resistances on outer and inner layers. Moreover, they can assume the function of a potentiometer or are conditionally suitable for shielding purposes.

Further advantages are
- improved layout design;
- single-sided assembly, thus one-time reflow soldering;
- low inductivities on account of short network connections;
- all resistances required are created at the same time.

Carbon-Conductive Inks as Etch Resists
Carbon-conductive ink can also be used as an etch resist. In this process, the entire conductive pattern including the contact areas are printed on copper-clad base material using carbon-conductive ink. The uncoated copper is removed and the finished circuit with carbon-conductive ink-protected conductors and contact areas is available. Besides the careful adjustment of the etching baths to the conductive ink used, patent rights have to be observed with respect to this process.

Manufacturing Heating Elements with Carbon-Conductive Inks
For applications such as heated mirrors in automobile electronics, a layer of carbon-conductive ink can be printed on the relevant parts which heats up when exposed to electric current. This is an economical method of heating wing-mirrors. However, when selecting a suitable carbon-conductive ink, care must be taken that the resistance does not change with the increasing number of heating phases such that a heating effect is no longer achieved.

7.3 Conductive Nano-Inks

7.3.1 Metallic Nano-Inks

Recently conductive nano-inks which contain nano-sized metallic particles have been attracting much attention. Electrically conductive inks are available on the market with metal particles (gold or silver) < 20 nm suspended in a solvent at 30–50wt%. After deposition, the solvent is eliminated and electrical conductivity is enabled by a high metal ratio in the residue. In addition, some applications also require the silver particles to be sintered on the substrate at elevated temperatures in order to obtain the required electrical conductivity [26]. The nano–inks can be applied by inkjet printing to form fine metal lines and features with high electrical conductivity.

The physical properties of nanoparticles are a subject of intense recent interest [27–30]. As the size of low-dimensional materials decreases to the

nanometer size range, electronic, magnetic, optic, catalytic, and thermodynamic properties of the materials are significantly altered from those of either the bulk or a single molecule. Especially, metal nanoparticles have very unique properties which directly relate to their dimensions and to the fact that a large ratio of the atoms in the particle are in the surface of the particle. The melting behavior of finite systems have been of considerable theoretical and experimental interest for many years, and it has been found that the melting point (T_m) of materials can be dramatically lowered by decreasing the size of the material when compared to their bulk counterparts. Their low melting temperature, which results in low sintering temperatures, makes them potentially suitable for use in printed electronics, since they may potentially be annealed at low temperatures to form conductive films of low resistance.

Printable electronics manufactured using roll-to-roll processes will offer the unique opportunities for mass production of large format and inexpensive flexible electronics [31]. Metallic nano-ink is a popular choice for forming metal conductors for printed electronics because it could be printed to substrates from solutions and sintered to conductive films at low temperatures because of the size effect [32]. Particularly, silver nanoparticles (Ag-NPs) are considered to be the most important precursor candidate for printed conductors for the good balance of cost and performance [33–35]. On the other hand, gold nanoparticles (Au-NPs) are desirable because Au has better chemical stability and high work function. Copper nanoparticles are also very attractive because they potentially offer lower cost than both Ag and Au.

Generally, gold nanoparticles are easily produced in a liquid ("liquid chemical methods") by the reduction of chloroauric acid ($HAuCl_4$) with strong reducing agent such as sodium boron hydride (NaBH), although more advanced and precise methods exist. As the neutral gold atoms form, the solution becomes supersaturated, and gold gradually starts to precipitate in the form of nanoparticles. To prevent the particles from further aggregation, stabilizing agents that bind to the nanoparticle surface are essential. Such agents can be organic ligands to create organic –inorganic hybrids with advanced functionality [36–46], allowing one to tune their material properties. Such hybrid materials may have significant applications in a wide variety of areas, including electronics, and (nano) biotechnology.

Nanoparticle science and technology have received an important advancement by Schmid et al., who formerly synthesized ligand-stabilized gold nanoparticles [47] opening the right way to Brust et al. [48] to prepare monolayer-protected gold nanoparticles. The organic monolayers on the surface of metal nanoparticles prevent aggregation and oxidation [49]. Many organic compounds with reactive head groups, such as thiol, sulphide,

thiosulfate, xanthate, amine, selenide, and isocyanide, have been utilized to protect by self-assembly different metal nanoparticles including Au, Ag, Cu, Pt, Pd, Ni, and bimetallics. The synthesis of metal nanoparticles protected with various monolayers containing different reactive head and functional tail groups is of high significance to improve their chemical and biochemical technological applications. Because of the expected marked electronic and optical properties of copper nanoparticles, there has been an increased interest in the preparation of stable monolayer-protected copper nanoparticles. Alkyl xanthates, alkylamines, tetraalkyl ammonium complexes, and alkanethiol ligands have been utilized to protect copper nanoparticles. However, a limited progress has been obtained because of the high instability of copper nanoparticles. Chen and Sommers [50] have prepared copper nanoparticles protected by alkanethiolate in one-phase system. Their prepared spherical (1–2 nm in diameter) Cu particle bound hexanethiolate monolayers underwent oxidation of copper core, morphological evolution, and irreversible aggregation process. Long-chain alkanethiols, which have been found to self-assemble into compact monolayers (i.e., three-dimensional self-assembled monolayers) on metallic nanoparticles [51–53], can not only induce metallic nanoparticles to be readily isolated but also reduce their conductivity.

Bhat et al. [54] synthesized and characterized steroid capped noble metal nanoparticles (silver and gold) by reducing their precursors gold trichloride ($AuCl_3$) and $AgNO_3$. It was demonstrated that bile acid-derived thiols can cap and stabilize the metal nanoparticles as efficiently as long alkyl chain thiols. The maximum particle sizes of Ag and Au nanoparticles are 3 and 5 nm, respectively. These capped nanoparticles could be easily dispersed in many nonpolar solvents in the presence of an alcohol and their dispersions are stable for more than a year.

Yang et al. [55] reported a novel chemical process for producing hydrophobic nano-copper particles with satisfied anti-oxidation property. Well-dispersed nano-copper particles with satisfied surface properties were obtained from the water/organic solution. In this process, oleic acid acts as both a phase transfer agent and a particle protector coordinating their carboxyl end groups on the newly generated copper particles surface, and the hydrophobic carbon tails of the oleic acids are pointed outward from the surface of particles. In addition, this organic film also plays an important role for preventing the newly generated copper particles from oxidation.

Foresti et al. [56] synthesized copper 3-(6-mercaptohexyl)thiophene-protected nanoparticles in a one-phase system utilizing an $NaBH_4$/LiCl mixture in diglyme as the reducing reagent and avoiding water medium in dissolving copper salts. TEM investigation carried out on the Cu T6SH nanoparticles immediately after synthesis and after different periods up to 6 months long of storage at low temperature has put in evidence that their

spherical shape of about 5–6 nm in diameter does not vary appreciably (Fig. 7.7).

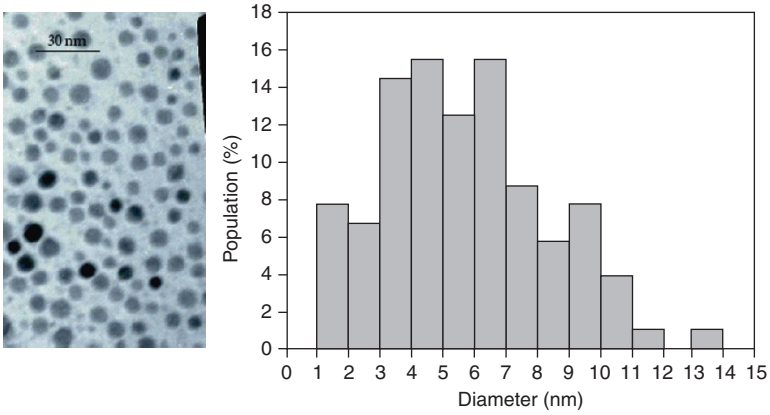

Fig. 7.7. TEM image (**a**) of the fresh Cu T6SH nanoparticles synthesized by $NaBH_4$/LiCl mixture in diglyme as the reducing reagent and (**b**) the depict of the nanoparticle size histogram is reported [56]

Kanninen et al. [57] studied the stability and oxidation of copper nanoparticles stabilized with various ligands. Lauric acid-capped copper nanoparticles were prepared by a modified Brust–Schiffrin method. Then, ligand exchange with an excess of different capping agents was performed. Oxidation and stability were studied by UV-vis, XRD, and TEM. Alkanethiols and oleic acid were found to improve air stability. The oxidation resistance of thiol-capped copper nanoparticles was found to increase with the chain length of the thiol. After oxidation, no traces of the ligand-exchanged particles were found, suggesting their dissolution due to excess ligand. Oleic acid protected the particles against oxidation better than the tested thiols at large excess (ligand-copper ratio 20:1).

Murai et al. [58] explored a different approach to cap copper nanoparticles with organic long chain acids by evaporation of a copper wire in an oleic acid vapor/mist. The thickness of the coating layer was a few nanometers. The median diameter of the powder was 25 nm, and became 10 nm smaller than that without the coating because of the inhibition of particle growth by the formation of the coating. From phase identification by transmission electron microscopy and X-ray diffraction analysis, it was found that the copper nanoparticles have been passivated and have not been oxidized in over 2 months.

Luechinger et al. [59] synthesized metallic copper nanoparticles by a bottom-up approach, and in situ coated with protective shells of graphene in order to get a metal nanopowder of high air stability and chemical inertness. Using an amphiphilic surfactant, a water-based copper nanocolloid could be prepared and successfully printed onto a polymer substrate by conventional inkjet printing using household printers. The dried printed patterns exhibited strong metallic gloss and an electrical conductivity of >1 S/cm without the need for a sintering or densification step. This conductivity currently limits use in electronics to low current application or shielding and decorative effects. The high stability of graphene-coated copper nanoparticles makes them economically a most attractive alternative to silver or gold nanocolloids and will strongly facilitate the industrial use of metal nanocolloids in consumer goods.

Woo et al. [60] developed a Cu/Ag-based mixed metal conductive ink from which highly conductive tracks were formed on a flexible substrate after annealing at low temperature. Addition of small Ag particles significantly improves the particle packing density by filling the interstices formed between the larger Cu particles, which in turn improved electrical conductivity compared to pure Cu metal film. The particle size and volume ratio of the Ag particles added need to be carefully controlled to achieve maximum packing density in the bimodal particle system. In addition, the authors demonstrated direct writing of complex patterns that exhibit high conductivity by inkjet printing followed by annealing at sufficiently low temperature (175−210°C) to not damage the transparent plastic substrate such as polyethersulfone (PES).

7.3.2 Conducting Polymer-Based Inks

Intrinsically conducting polymers have also been utilized to formulate conductive inks [61]. Nelson et al. [62] used poly3,4-ethylenedioxythiophene doped with poly(styrene sulfonate) (PEDOT:PSS), a commercially available conductive polymer, to fabricate electrodes for disposable sensors. The authors successfully printed the electrodes using an ink-jet printer that utilizes piezoelectric nozzles to dispense the polymer. Printing on silicon wafer and photographic paper yielded good quality electrodes. To achieve a lower resistance for electrodes that will be used in devices, the following method was used: one layer of PEDOT: PSS was printed, and then a second layer was printed on top of the first one. The resistance of the two-layered electrode was around 30 kΩ compared to 80 kΩ for one layer of the conducting polymer.

Montbach et al. [63] reported the first flexible cholesteric display made with ink-jet-printed conducting polymers ink as top and bottom electrodes

on thin plastic substrates. Inkjet-printed conductive polymer (CP) electrodes provide ease of patterning as well as enable highly flexible displays. The main components of the CP mixture are polyethylenedioxy thiophene (PEDOT)/PSS (poly (3,4) ethylenedioxythiophene/polystyrenesulfore acid). The initial CP mixture was modified to better control the rate of evaporation of the solutions, allowing for more uniform and flat electrodes, along with less clogging of the nozzles after the printer sat idle for any extended period of time resulting in longer print head lifetimes. The display characteristics with CP electrodes are very similar to a display made with ITO electrodes, demonstrating the compatibility of inkjet printed CP as a viable transparent electrode for flexible cholesteric displays. It was demonstrated that inkjetting of PEDOT/PSS materials is a viable approach to making highly flexible cholesteric displays of high brightness and contrast on very thin plastic substrates. Conductive polymer is a very attractive alternative electrode material for flexible displays and works better then expected; however, the current relationship between transmission and sheet resistance results in slightly altered display performance parameters.

Conducting polymer inks have also been used for fabricating active electroluminescent devices. Bharathan et al. [64] successfully demonstrated using ink-jet printing an aqueous solution of polyethylenedioxy thiophene (PEDOT) to form a light-emitting logo.

Anupama Karwa et al. [65] developed a different type of conducting polymer inks. PANI nanofibers (shown in Fig. 7.8) obtained by interfacial polymerization method were used in various formulations to obtain flexo water-based and solvent-based printable inks. Interfacial polymerization of aniline is a practical synthetic method capable of making pure, uniform, and template-free PANI nanostructures with small diameters (sub-100 nm) in bulk quantities. The method does not necessitate a need for any special dopant or solvent. The nanofibers produced by this method have been reported to have nearly uniform diameters between 30 and 50 nm with lengths varying from 500 nm to several micrometers [66, 67]. An all-printed chemical vapor sensor was successfully fabricated by printing a PANI layer on silver interdigitated electrodes using flexographic printing. The ink showed better adhesion on coated paper substrate than on flexible plastic substrates.

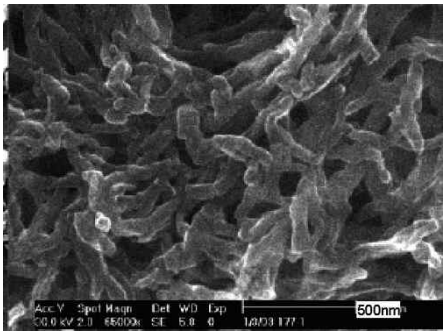

Fig. 7.8. PANI nanofibers obtained by interfacial polymerization method

7.3.3 Organometallic Ink

Organometallic inks are also called metal organic decomposition (MOD) inks. The dry organometallic compounds, such as silver (hexafluoroacetylacetonate), 1,5-cyclooctadiene, or $Cu_2(CH_3COO)_4$, are dissolved in an organic solvent such as toluene, ethanol, or butanol. The ink is delivered by spraying or is ink-jet printed on a heated substrate in the desired pattern. A metallic film forms upon solvent evaporation and decomposition of the printed precursor at elevated temperature (~300° C) (Fig. 7.9). Gaseous by-products of decomposition leave the system, providing contamination-free metal films.

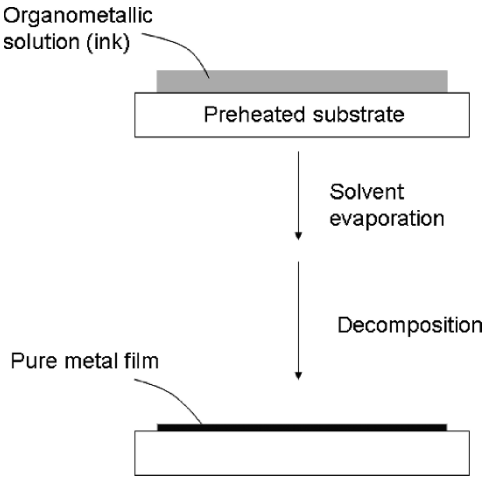

Fig. 7.9. Schematic showing the process of forming a metal film from an organometallic ink

7.3.3.1 Chemical Vapor Deposition (CVD)

Copper films have been deposited by low pressure chemical vapor deposition from mixtures of the Cu^{+1} precursor copper hexafluoroacetylacetonate vinyltrimethylsilane and water vapor [68]. The addition of water vapor at the optimum concentration more than doubles the deposition rate and substantially reduces the nucleation time without adversely affecting the copper film resistivity, but excess amounts of water vapor significantly increase the copper resistivity. Auger electron spectroscopy analysis detected no impurities in copper films deposited under optimum water conditions, but detected oxygen in films deposited under excess water conditions, suggesting copper oxide formation.

7.3.3.2 Excimer Laser-Induced CVD Deposition

Izquierdo et al. [69] demonstrated to deposit high purity metallic copper on TiN and fluoropolymer substrates using excimer laser-induced CVD and copper(hexafluoroacetylacetonate)(trimethylvinylsilane(Cu(hfac)(TMVS)) as the precursor and H_2 as carrier gas.

To increase the silver loading of the ink and obtain higher deposition rates, silver or other metal nanoparticles may be added to the ink along with the organometallic precursor. In this configuration, silver particles comprise the main conducting volume of the resultant coating, while the organometallic constituent acts as a glue for the silver particles, providing enhanced electrical and mechanical bonding of the metal particles with the substrate and between themselves. Fine, deagglomerated nanoparticulate metal powders must be used in this ink so as to avoid clogging the 10–50 μm orifice of the ink-jet. In addition, active constituents, such as adhesion promoters, surface activators, precursors of n-type dopants for selective emitters, or possibly nanosized glass frits, may be added to the ink to achieve the required electronic and mechanical properties of the contact. Curtis et al. [70] demonstrated direct-write technologies offer the potential for low-cost materials efficient deposition of contact metallizations for photovoltaics. The author reported on the ink-jet printing of metal organic decomposition (MOD) inks with and without nanoparticle additions. The substrate was preheated to an elevated temperature such as 100°C so that the solvent evaporated right away after the ink deposition to prevent the ink from spreading on the substrate surface. A high-temperature (300°C) annealing was conducted to decompose the organometallic compound into Ag. Near-bulk conductivity of printed and sprayed metal films has been achieved for Ag and Ag nanocomposites. Good adhesion and ohmic contacts with a measured contact resistance of 400 $\mu\Omega\bullet cm^2$ have been observed between the sprayed silver films and a heavily doped n-type layer

of Si. Ink-jet-printed films show adhesion differences as a function of the process temperature and solvent (Fig. 7.10). Silver lines with good adhesion and conductivity have been printed on glass with 100 μm resolution.

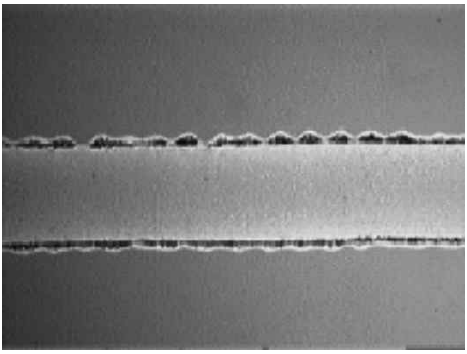

Fig. 7.10. Single line pattern printed on glass with a ink-jet printer using Ag(hfa)(COD)-based ink. The width of the line is 200 μm

Majumder et al. [71] used a capillary bridge printing technique to deposit copper interconnects using homogeneous solutions of a Cu(II) precursor in a series of low boiling primary alcohols. The rheological properties of the solutions have been measured first to determine their printability. The as-printed lines with subsequent annealing at relatively low temperatures (~200°C), in order to evaporate the volatile solvents and facilitate dissociation of the precursor deposit, produced conducting interconnects. The precursor has been demonstrated to be self-reducing and requires no reducing environment (e.g., H_2) thus making the interconnect formation easier. Moreover, successful decomposition of the precursor into metallic Cu at such low temperatures holds promise for applications involving flexible polymer substrates.

Wehner et al. [72] demonstrated organometallic precursors containing gold or copper are dissolved in a variety of solvents and spilled onto the substrate. Dimethylenglycoldimethylether, DME, exhibited best properties with respect to a high solubility of the precursor and slow evaporation of the solvent. With second harmonic Nd:YAG or argon ion laser radiation of 150 mW power metal lines were written on polyimide from organo-gold (I) and copper compounds with a writing speed of 0.6 mm/s.

7.3.3.3 Photo Silver Patterning Without Photoresist

Without use of photoresist, highly efficient method for silver patterning is developed by using photosensitive organo-silver precursors, which are

prepared by a reaction of silver(I) salts and excess of amines [73]. The organo-silver precursors produce the metallic silver patterns via the photodecomposition of precursor molecules under controlled conditions. Broadband UV irradiation through a photo-mask on the precursor thin film produces a partially reduced and insoluble silver species in a short time. After development, the irradiated areas were treated with a reducing agent to obtain pure metallic patterns. Subsequently, annealing step was followed at 100–350°C to increase the adhesion of interface and cohesion of silver particles. Figure 7.11 shows the schematic of the patterning process. The line resolution of 5 μm was obtained by the present silver precursors. (Fig. 7.12). Film thickness was also controllable from 50 to 250 nm by repetition of the above procedure. The average electrical conductivity was in the range of 3–43 Ω•cm, measured by four-point probe technique. AES depth profile of the silver pattern thus obtained showed carbon and oxygen contents are less than 1% through the whole range. Even though sulfur contaminant exists on the surface, it was believed that nearly pure silver pattern was generated. It is believed that the silver patterning technique using the organo-silver precursors is cost-effective and simple to make metallic line patterns, compared to the conventional photolithography methods.

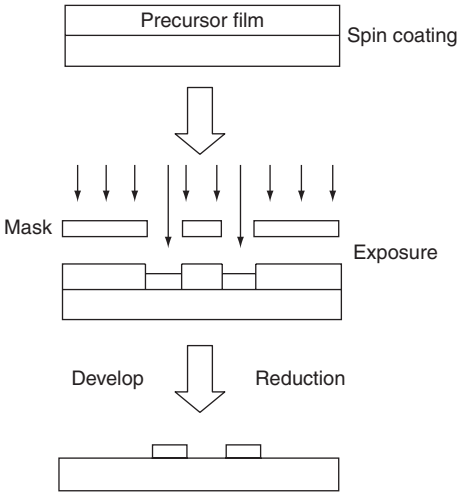

Fig. 7.11. Schematic diagram for spin-on process

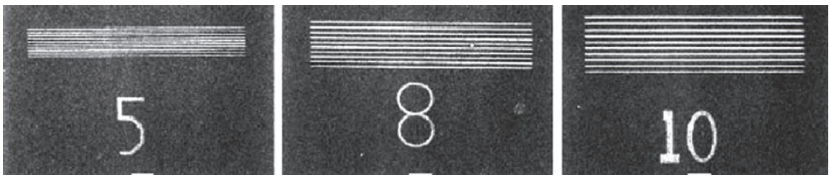

(a) 5 μm pattern (b) 8 μm pattern (c) 10 μm pattern

Fig. 7.12. SEM of photolithographic pattern of silver on a glass substrate using a Ag precursor

7.3.3.4 Effect of Organometallic Compounds on Silver Inks

Lu et al. [74] studied the effects of metalloorganic decomposition (MOD) compounds to properties of low-temperature-curing conventional silver paste inks which were prepared from silver flake, α-terpineol. Results indicated that 2-ethylhexanoate possesses the lowest decomposition temperature (190.3°C) among the MOD agents studied, and it forms silver particles to promote the linking of silver flake powders and thus reduces the resistivity to <13 μ ·cm at a temperature as low as 200°C.

Lu et al. [75] also attempted to modify the curing conditions of MOD silver pastes through the substitutions of silver flakes with silver(I) oxide (Ag_2O) and silver(II) oxide (AgO). Differential thermal analysis (DTA), derivative thermogravimetric analysis (DTG), and X-ray diffraction (XRD) results indicated that the presence of residual silver oxide, which effectively catalyzes the evaporation of α-terpineol and the decomposition of silver 2-ethylhexanoate, decreases the curing temperature and shortens the soaking time. The reduced silver and the remaining Ag_2O enhance the connectivity and packing density of the silver flakes, and thus increase the electrical conductivity of the films. For films prepared from pastes with 20wt% Ag_2O or AgO, resistivities of 14×10^{-6} and $19 \times 10^{-6}\,\Omega$·cm, respectively, were successfully achieved after being cured at 200°C for 5 min.

7.4 Processing of Nano Ink

7.4.1 Ink-jet Printing

In the last two decades ink-jet printing has grown to a major topic in scientific research, especially drop-on-demand (DOD) ink-jet printing systems [76–78]. DOD ink-jet printing has progressed from printing text and

graphics, where it started originally, to a tool for (rapid) manufacturing technology.

During the last years, the fabrication of narrow conductive tracks by methods of ink-jet printing has been investigated extensively [26, 79–81]. Printing of flexible electronics and minimizing their feature size dramatically lowers the production costs of electronic devices, because material can be positioned on-demand, which reduces the amount of necessary material. The main bottleneck in ink-jet-printed features on flexible (polymeric) substrates is the low softening point (glass transition temperature-T_g) of the substrate, which limits the processing temperature. The T_g of commonly used polymeric substrates, like poly(ethylene terephthalate) (PET) or polycarbonate (PC), is below 150°C. Typically, colloidal suspensions of conductive materials need a sintering temperature of >200°C, which is, hence, not compatible with most polymeric substrates. Feasible products of flexible electronics include, for example, interconnections for circuitry on a printed circuit board (PCB) [82], electrodes for thin-film transistor (TFT) circuits [83], organic light-emitting diodes (OLEDs) [84], or disposable displays and radio frequency identification (RFID) tags [85, 86]. Furthermore, printing large-area displays is also a possibility [8]. The typical dimensions of ink-jet-printed features depend on the nozzle diameter and are usually not below 100 μm [35, 87]. The most obvious way to minimize the feature size, that is, line width, is by reducing the nozzle diameter [88]. However, this introduces a narrow window with respect to surface tension and viscosity of the inks and thereby limits the choice of inks that can be printed. Furthermore, when printing suspensions the particles should be sufficiently smaller than the nozzle diameter; otherwise nozzle clogging occurs. When using piezoelectric-based DOD ink-jet printers, smaller droplets can also be produced by modifying the waveform.

Besides a decrease in nozzle size, and thus a higher print resolution, further decrease in line diameter was realized by heating the sample holder of the printer to its maximum temperature (60°C), which stimulates evaporation of the solvent and prevents broadening of the lines [87, 89]. This resulted in the direct ink-jet printing of lines with a diameter of 40 μm. The silver tracks were sintered at 200°C for 1 h, which resulted in a conductivity of 13–23%, compared to bulk silver. The as-printed narrow silver tracks can be used in, for example, (plastic) electronic applications such as radio frequency identification (RFID) tags or electrodes for thin-film transistor (TFT) circuits.

The NRI has succeeded in developing a new ink-jet, which we call the super ink-jet, able to form fine patterns less than 1/10th the size of conventional ink-jet patterns [90]. Using a liquid containing metal nanoparticles as ink, the Super ink-jet forms lines less than 1μm thick without any pretreatment on the substrate's surface (Fig. 7.13).

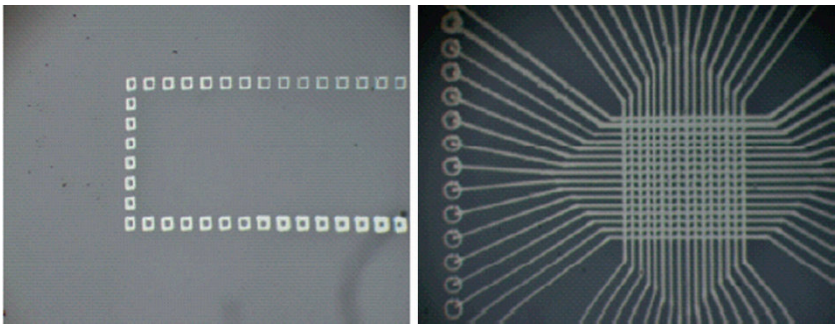

Fig. 7.13. Ultra-fine wiring plotted directly on a glass substrate with a metal nanopaste using the super ink-jet; (*left*) squares 25 μm long on each side and (*right*) line 3 μm wide

Muarta et al. [91] reported the development of a super fine ink-jet system which allows arrangements of dots with a minimum size of less than 1 μm. Using the ultra-fine silver paste, the authors achieved the direct print of ultra-fine metallic wire of only a few micrometers in width without any prepatterning treatment on the substrate. Furthermore, using the transition metal nano-particles as catalyst-ink, patterned array of carbon nano-tubes were successfully obtained. A field emission from the patterned carbon nano-tubes is also confirmed. All these processes can be carried out at atmospheric pressure on the desktop without special treatment on the substrate to achieve the ultra-fine line width of about 3.6 μm and line space of 1.4 μm using a silver nanopaste, and circuit pattern using a conducting polymer, MEH-PPV (Poly[(2-methoxy-5-(2'-ethylhexyloxy))-1,4-phenylenevinylene]) (see Fig. 7.14).

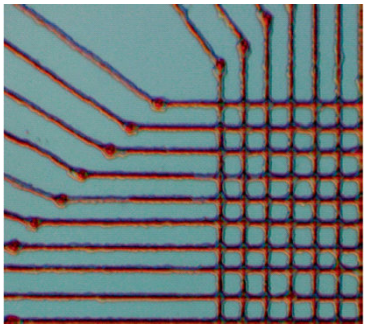

Fig. 7.14. Fine circuit of conducting polymer (line width 3 μm, 10 μm pitch in the lattice area)

A major challenge in applying ink-jet processes for direct writing is formulating suitable inks. The inks must contain the appropriate precursors and a carrier vehicle. In addition, they may contain various binders, dispersants, and adhesion promoters, depending on the nature of the precursor and the particular application. In the case of inks for metallization, the content of the metallic ink must be adjusted to provide the required resolution, with good adhesion and the desired electronic properties for the conducting lines. Ink composition is critical because it defines the way in which the ink can be jetted, the adhesion to the substrate, and the line resolution and profile, and it can control the mechanism of metal formation.

Self-aligned printing (SAP) technique is a recently developed bottom-up printing technique which utilizes the unique droplet motion on heterogeneous surfaces to define sub100-nm critical features and surpasses the resolution which can commonly be achieved by direct printing by two orders of magnitude. It has been applied to fabricate field-effective transistors (FETs) using conducting polymer electrodes based on poly (3,4-ethylenedioxithiophene) doped with poly(styrenesulfonate) (PEDOT/PSS) and fabricate FETs with nano gold inks [92].

7.4.1.1 Sintering

Generally two different techniques, heating and laser, have been used to sinter printed nanoparticle structures. Conventional radiation–conduction–convection heating is the most commonly used method, wherein the sintering temperatures are typically above 200°C [79]. Therefore, many potentially interesting substrate materials, such as thermoplastic polymers or paper, cannot be used. In fact, one of the very few, if not the only, organic substrate that can be used is (expensive) polyimide (PI). The long sintering times required – usually 60 min or more – also imply that the technique is not feasible for fast industrial production. As an alternative, a laser sintering method was developed [93–95]. The laser follows the conductive tracks and sinters these selectively, without affecting the substrate. However, this method is costly and complex from a technical point of view. Thus, there is a clear need for a fast, simple, and cost-effective technique that would allow the sintering of the printed structures by the selective heating of only the printed components. Microwave heating fulfills these requirements [96].

Niizeki et al. [97] reported a novel coating technology by means of sintering the silver nano-ink by a laser beam. The novelty lies in the use of a conventional Nd:YAG laser to metallize nanoparticles as an alternative to furnace sintering. Silver nanoparticles with 5 nm in average diameter dis-

persed in the silver nano-ink are successfully sintered on the Cu substrate by this method. Laser sintering proceeds from the paste surface into the Cu substrate, and the maximum film thickness obtained by laser sintering is about 0.2 μm. Multi-step sintering by the repletion of spin coating and laser metallization enabled a thicker Ag pad of around 1 μm (Fig. 7.15). No peeling of the laser-sintered Ag film from the substrate was observed. Its adhesive strength is higher than that of a furnace-sintered sample. The Ag film thus fabricated can be used as pads for wire bonding, being an alternative to electroplating.

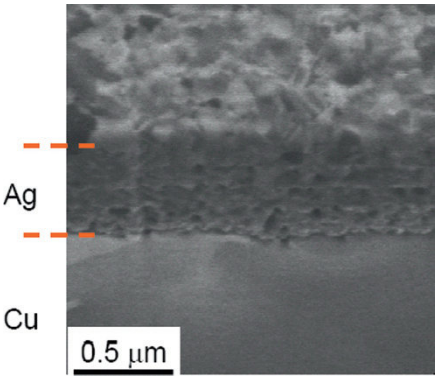

Fig. 7.15. A cross-sectional image of a five-layered Ag film on a copper substrate

Microwave sintering Microwave heating is widely used for the sintering of dielectric materials [98] and in synthetic chemistry [99, 100]. It offers advantages such as uniform, fast, and volumetric heating. Microwave radiation is absorbed due to coupling with charge carriers or rotating dipoles. At normal incidence, the amplitude is an exponentially decaying function of the distance, characterized by a penetration depth d_p,

$$d_p = c\varepsilon_0/(2\pi f\varepsilon'') = (\pi f\mu\sigma)^{-1/2}$$

where σ is the conductance, f the frequency of the microwave radiation, ε'' the dielectric loss factor, μ the permeability of the material and, ε_0 the permittivity of free space.

Highly conductive materials (e.g., metals) can be sintered by microwave radiation [101, 102], but have a very small penetration depth: the penetration depth at 2.54 GHz for silver, gold, and copper ranges from 1.3 to 1.6 μm [103]. The microwave sintering of metals is therefore non-trivial and can only be successful if the dimension of the object perpendicular to the plane of incidence is of the same order as the penetration depth. Inkjet printed conductive tracks fulfill this requirement. On the other hand, the rotational freedom of any dipoles present in thermoplastic polymers below the glass transition temperature (T_g) is limited, and therefore the absorption of microwave radiation by these species is negligible.

Perelaer et al. [87] developed a new method for the preparation of conductive silver tracks on a PI polymer substrate by using microwave radiation to sinter the silver nanoparticles. Since the polymer substrate is virtually transparent to microwave radiation, a negligible amount of energy is absorbed by the substrate, whereas the conducting silver nanoparticles, with a high dielectric loss factor, absorb the microwaves strongly. The resistivity of the material as calculated from the resistance and the cross-sectional area of a line is 3.0×10^{-7} Ω m, which is 5% of the value of bulk silver. This method shortens the sintering time of silver nanoparticles by a factor of 20. Figure 7.16 shows scanning electron microscopy (SEM) images of an inkjet-printed silver track on polyimide (PI), before and after sintering in the microwave reactor. The structure of the unsintered silver tracks is homogeneous at all length scales. The sintered lines consist of clusters of silver (nano)particles with a diameter of about 500 nm. Since the original size of the nanoparticles ranges from 5 to 10 nm, the clusters in the sintered tracks must have been formed by melting these particles after the decomposition of the organic binder around the nanoparticles.

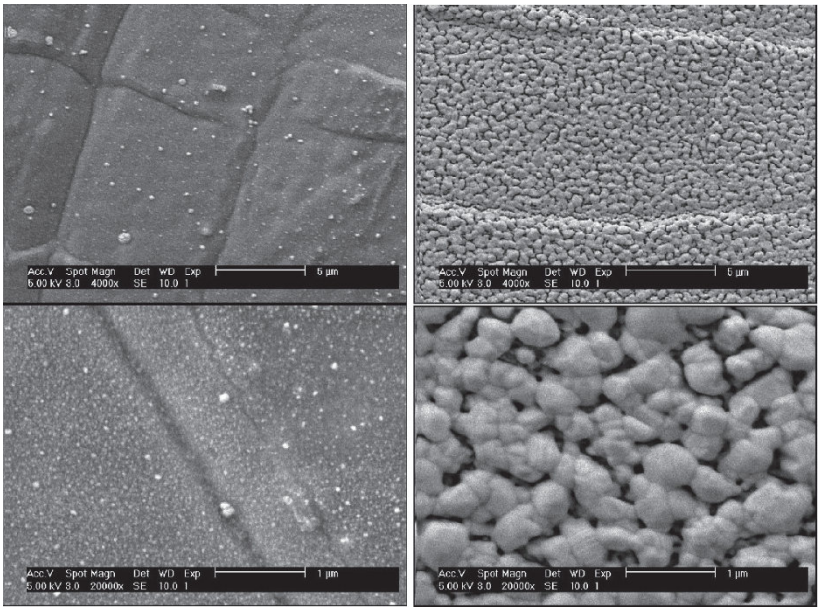

(a) (b)

Fig. 7.16. SEM images of inkjet-printed silver tracks on polyimide (PI), before and after sintering in the microwave. (**a**) Unsintered silver tracks and (**b**) sintered silver tracks. The magnification from *top* to *bottom* is 4,000× and 20,000×, respectively

7.4.2 Pyrolytic Printing

Oosterhuis et al. [104] reported preliminary results on pyrolytic printing of conductive inks. Pyrolytic metal printing provides a powerful alternative to existing printing techniques for metal track production. Existing techniques generally exhibit drawbacks like limited resolution, multiple process steps, high heat load on the substrate, or the necessity of chemical treatments that affect the whole substrate.

Pyrolytic printing starts with the generation of droplets of a solution of some precursor salt, such as silver nitrate ($AgNO_3$), or copper acetate ($Cu_2(CH_3COO)_4$). This precursor solution has a viscosity and surface tension which are mainly defined by the solvent properties. Therefore, any conventional jetting device that yields mono-disperse droplets can generate the droplets. A nitrogen flow leads the droplets into a furnace that heats the droplets, which leads to evaporation of the solvent followed by pyrolysis of the precursor material. In this way liquid metal particles are generated. At the outlet of the furnace, aerodynamic focusing assures accurate deposi-

tion of the molten metal droplets, which yields 20 µm wide conductive metal tracks directly onto the substrate. The process is particularly innovative as it allows a combination of rather high melting point metals with substrates that are restricted to a low thermal load, such as silver printed on polymer foil. Furthermore, the combination of a drop-on-demand generator and aerodynamic focusing yields unprecedented deposition accuracy. Applications are in the field of dedicated electronic circuits, strain-gauges, RF-ID tags, electronics on foil, through-silicon vias, OLEDS, and solar cells.

The printing set-up comprises a drop-on-demand jetting device (http://www.microfab.com/equipment/devices.html) that creates 30–100 µm droplets of a 10–20%w/w (mass percentage) aqueous $AgNO_3$ solution. The generated droplets pass through an inspection chamber followed by a ceramic tube furnace with a temperature up to 1500°C. A nitrogen flow guides the droplets through the furnace. The substrate located several millimeters below the orifice is placed upon an *x*–*y* stage to be able to generate two-dimensional patterns.

A pyrolytic printing process consists of the following consecutive steps (Fig. 7.17):

- Droplet generation: The droplet is generated using a mono-disperse droplet generator. For the printing of two-dimensional or three-dimensional structures, a drop-on-demand print head is required. For high-speed production of straight lines, a continuous head may be used.
- Droplet heat-up: Once the droplet is generated, the nitrogen flow carries it into the furnace where it is heated by infrared radiation.
- Solvent evaporation: Once the droplet temperature approaches the boiling point of the solvent, the solvent will quickly evaporate, until only solid salt particles remain.
- Pyrolysis: Further heating will cause the salt to melt after which it reaches the pyrolysis temperature of $AgNO_3$. Then, the reaction $AgNO_3(l) \rightarrow Ag(s) + NO(g) + O_2(g)$ takes place, which yields solid silver.
- Melting silver: Following the pyrolysis step, the solid silver particles are heated further, up to the melting point of silver. Once molten, the droplet may be heated further until it leaves the furnace. In this phase, the heat input needs to be controlled in order to control the droplet temperature on impact, which highly influences the final track size and quality.
- Focusing: Near the outlet of the furnace, the droplets may deviate from their initial course as a result of the preceding process steps. Therefore, aerodynamic focusing is required to (re-)concentrate the droplets in the center of the printed track. Focusing is achieved by accelerating the flow through a contraction at the end of the tube. During this acceleration of the gas flow, the droplet velocity also increases as a result of drag forces.

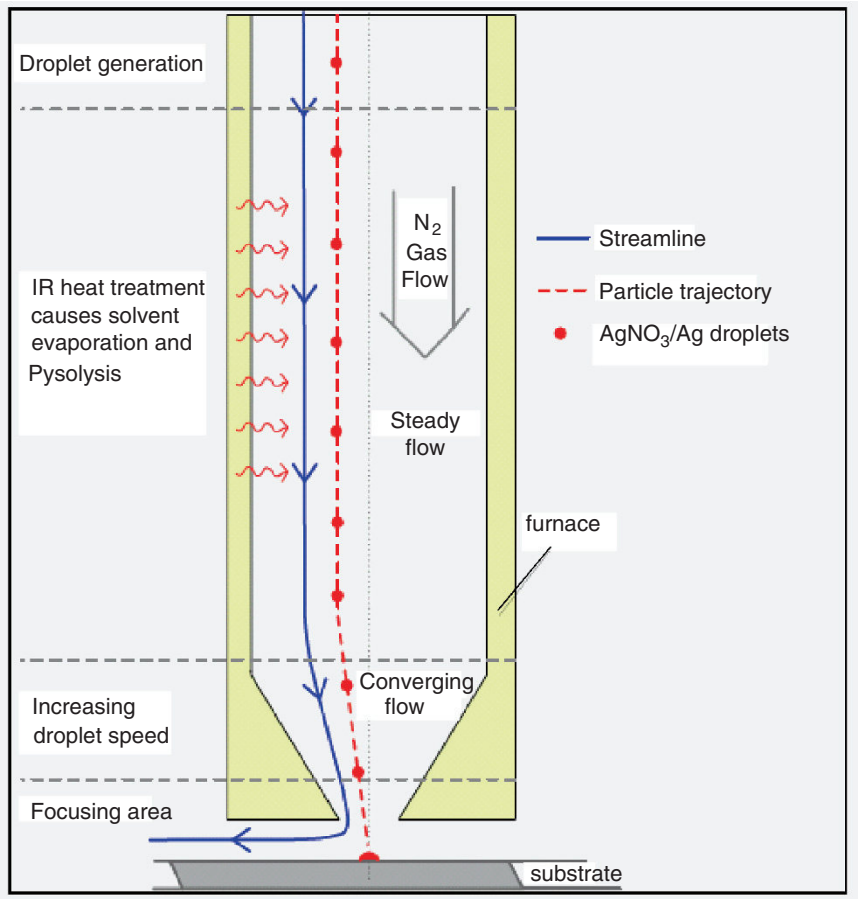

Fig. 7.17. Schematic overview of the pyrolytic printing process

Currently, printing with this setup was successful up to the pyrolysis temperature of $AgNO_3$. A deposition accuracy of 5 µm was also demonstrated. This is illustrated by a printed free-standing pillar of 20 µm diameter and 2 mm height (Fig. 7.18a). Silver tracks with full metal conductivity was successfully printed on SiO_2 and glass. The track width is 0.3 ± 0.1 mm (Fig.7.18b).

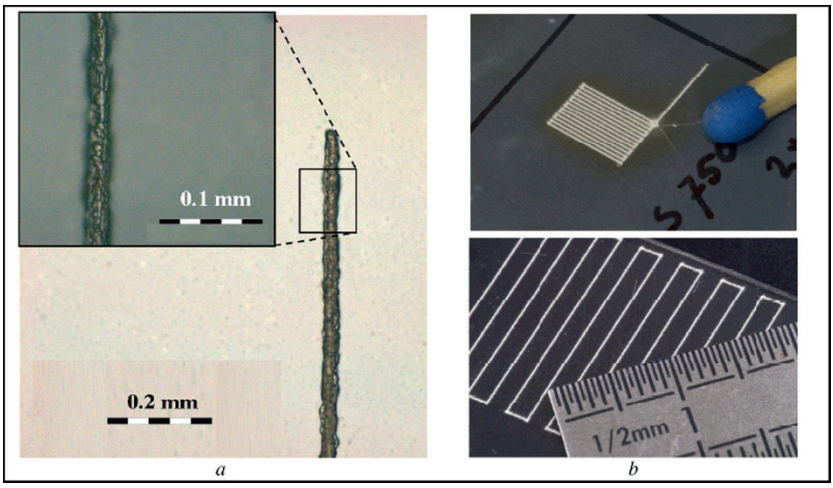

Fig. 7.18. Experimental printing results. (**a**) Aerodynamic focusing; a free-standing pillar could be printed of 2 mm high and 20 μm wide. (**b**) Silver tracks with full metal-conductivity, printed on SiO_2 (*top*) and glass (*bottom*). The track width is 0.3 ± 0.1 mm

7.4.3 Gravure Printing

Gravure printing is the inverse of flexo-printing process. Ink is transferred to a patterned plate (Gravure cylinder), but the plate is designed to hold ink in the grooves between elevated lines and areas instead of on the highest points like in flexo-printing. The ink is scraped from the elevated regions on the printing plate by a doctor blade before the plate contacts the substrate, as illustrated in Fig. 7.19.

The gravure process is typically chosen because of the printing speed that can be achieved. To transfer ink at high speed, extremely low viscosity is required. Solvents such as toluene, xylene, and alcohols are often used, sometimes in conjunction with water.

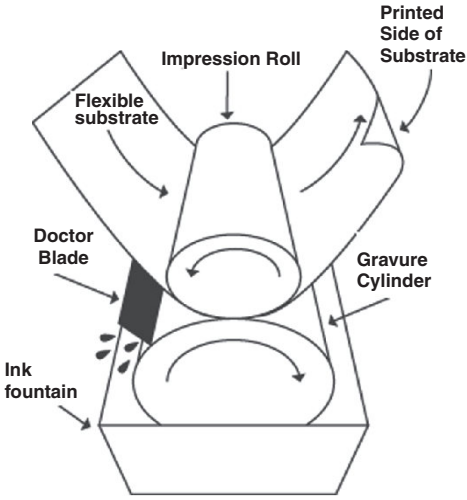

Fig. 7.19. Schematic set-up of a gravure printing

Among conventional printing processes, gravure printing is the premier process in terms of high quality and ability to print at very high speeds. Robustness of its image carrier is also advantageous, contributing to very good printing stability over time. These advantages of gravure printing make it a very promising process for electronics manufacture, smart packaging, and RFID [105]. There are specific requirements to be met in order to achieve the best print quality possible. These include both the substrate properties (smoothness, compressibility, porosity and ink receptivity, wettability, etc.) and the ink properties (ink chemistry, viscosity, rheological behavior, solvent evaporation rate, drying, etc.). Furthermore, process parameters, such as doctor blade angle and pressure, impression pressure, and speed, have tremendous effect on quality of printed ink films [106]. In addition, the engraving method used to prepare the image carrier is an important factor, because ink release from engraved cells will depend on the width and depth of cells and their overall shape [107].

There are many advantages and challenges of using printing processes in the manufacture of electronic devices. The main advantages include high-speed fabrication, low-cost manufacturing, and possibility of using flexible substrates, less waste, and roll-to-roll capability. On the other hand, each of the available printing processes has its limitations, such as resolution, registration, and uniformity of the printed layer. Among printing processes, gravure printing is considered to deliver the highest quality print and thus it is believed that it also has a big potential in printed elec-

tronics. Gravure printing and materials are very well established for printing of visual images. However, very little is known about the printability of materials needed for electronic devices. Therefore, there is a need for further investigation of conductive inks properties and performance. Working properties of inks, such as surface tension, rate of evaporation, and rheology, are very important in the process of evaluating new functional materials for electronics printing. In addition, the effect of different additives used in optimization of ink's press performance on quality and electrical properties of printed layers needs to be evaluated.

Pudas et al. [108] developed a roto-gravure printing technique for printing conductive lines on paper and plastic films. The inks contained metal particles in an organic medium and were cured in temperatures of 70–120°C, limited by the substrate durability. The printed conductor line properties were characterized for different substrates: resistance, yield as a function of line width, coil inductance, folding endurance, adhesion, printed antenna properties, and maximum current density. A printed resistance down to 50 mΩ/□ was obtained, with conductor lines 4–7 μm thick. Minimum line resolution and resistance were affected by smoothness of substrates. Adhesion properties were adequate for the studied components.

7.5 Applications of Conductive Inks

7.5.1 Die Attach for High Power Devices

For high power applications the thermal impedance of the die attach layer can play a significant role in the ultimate operating temperature. Therefore, one would like to use the highest thermal conductivity die attach material consistent with the overall package manufacturing process. Package manufacturing processes are typically below 350°C. This has precluded the use of high conductivity silver or gold metal pastes for standard die attachment because they typically require heating the paste to at least 500–600°C in order to obtain the high thermal conductivities typical of these metal foils.

Polymer-matrix composites (e.g., silver-filled epoxies) have low processing temperatures and low elastic moduli for low mechanical stresses on devices, but they have relatively low thermal and electrical conductivities and low operating temperature (typically lower than 200°C). Soft solders (e.g., lead–tin or indium-based alloys) are susceptible to fatigue failure under thermal cycling conditions. On the other hand, hard solders (e.g., gold-based eutectic alloys) and glass matrix composites (e.g., silver-filled glasses) are used to enable devices to run at higher junction temperatures,

but their higher elastic moduli and processing temperatures can generate high mechanical stresses in devices, and these materials also have relatively low thermal and electrical conductivity.

Bai et al. [109] reported a low-temperature (as low as 275°C), pressureless (i.e., no externally applied pressure) sintering technology that utilizes nano-silver paste to provide superior electrical, thermal, and mechanical properties, and high-temperature capability to device attachments and interconnections. The silver paste was prepared by mixing nanoscale silver particles with carefully selected organic components which can burn out within the low-temperature firing range. Once the material is sintered at 275°C it will not melt unless it is heated to 961°C (the melting point of silver), such that the paste can be used for subsequent die attachments as well as other interconnections in a packaging process that involves multiple joining steps. This eliminates the need to design a hierarchy of process temperatures that is required to accommodate different reflow schedules for a series of solder alloys. The sintered material showed a thermal conductivity of 2.4 W/K-cm. Results demonstrated the low-temperature silver sintering as an effective die attach method for high-temperature electronic packaging.

Figure 7.20 shows microstructure of solder and sintered nano- Ag paste die attached layers.

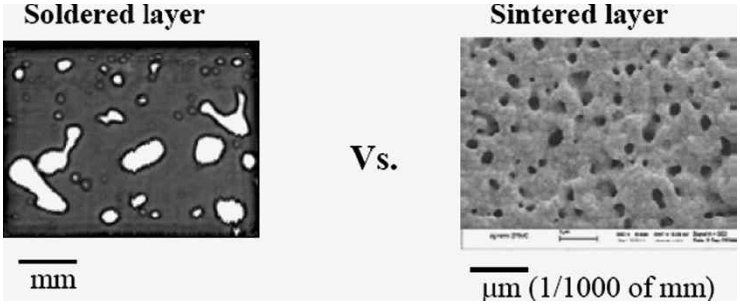

Fig. 7.20. Microstructure comparison of solder and sintered nano-Ag paste die attach layers: Sintered nano-Ag showed uniformly distributed micron-sized voids; solder layer showed much larger voids

7.5.2 Printed Low-resistance Metal Conductors for Printed Electronics

Low-resistance conductors are crucial for the development of ultra-low-cost electronic systems such as radio frequency identification (RFID) tags.

Low-resistance conductors are required to enable the fabrication of high-Q (quality factor) inductors, capacitors, tuned circuits, and interconnects. The fabrication of these circuits by printing will enable a dramatic reduction in cost, through the elimination of lithography, vacuum processing, and the need for high-cost substrates. Conductive inks with organic-encapsulated metallic nanoparticles (such as Au, Ag, or Cu) or organometallic inks may be printed and subsequently annealed to form low-resistance conductor patterns. One of the key challenges is that the conductor fabrication process cannot impose excessive heat to the low-cost flexible substrates which generally cannot withstand high temperatures. Microwave sintering, pyrolytic printing, laser sintering, and pressure-assisted sintering [110] all showed certain promises.

Another trend is to develop novel inks with much lower sintering temperatures. Huang et al. [86] demonstrate a thiol-derivatized gold nanocluster technology suitable for use in printed circuits on plastic. By reducing the alkane chain length, the authors were able to significantly lower the processing temperature requirements necessary to convert solution deposited nanoparticles into low-resistance, continuous films. Using 4- or 6 carbon chain length thiols, it is possible to produce Au nanocrystals that anneal at plastic-compatible temperatures. Figure 7.21 shows the TEM images of two type of nano-gold particles fabricated. The anneal conditions are independent of anneal ambient, and low-resistance films are uniformly achieved provided a sufficient anneal is used to completely drive off the encapsulant. There is a trade-off between stability and anneal temperature due to the instability of thiols with short alkane chains. However, optimization of the process revealed that 1.5 nm gold nanoclusters encapsulated with hexanethiol showed good stability and are suitable for use as printed conductors on plastic. Ink-jet-printed conductor patterns formed on plastic using this material (sintered at 150°C) resulted in low-resistance lines with conductivities as high as 70% of bulk gold, attesting to the quality of this process.

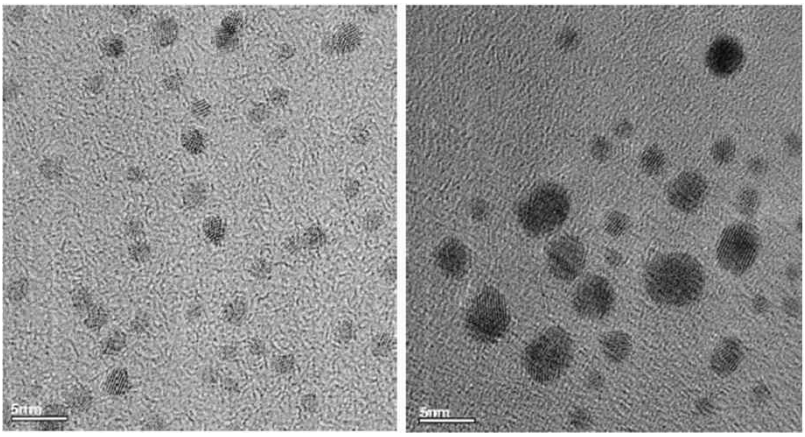

Fig. 7.21. TEM images of hexanethiol-encapsulated nanocrystals synthesized with a gold/thiol mole ratio of 1:4 (*left*) and 1:1/12 (*right*)

It was also reported that silver ink with a particle size of 5–6 nm can be sintered to form a solid silver film with a high conductivity at a temperature of 150°C (see Fig. 7.22). Wang et al. [111] recently studied the sintering behavior of a silver nano-ink (with silver particle size of 4.6 nm) under various sintering conditions. The effect of sintering temperature is illustrated in Fig. 7.23 for Ag-NP films after 3 min sintering at various temperatures. It was found that the lowest sintering temperature which provided high-conductivity Ag film is 130°C.

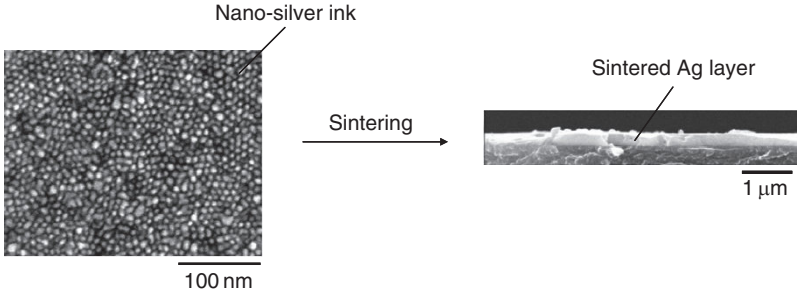

Fig. 7.22. Ag layer formed by sintering a nano-silver ink at 150°C (http://www.nanoparticles.org/pdf/YangZ.pdf)

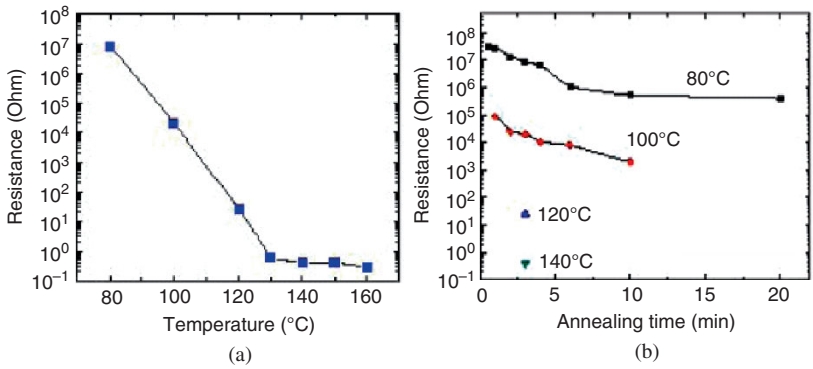

Fig. 7.23. The electrical resistance of Ag-NP films (*right*) sintered at various temperatures for various times, and (*left*) sintered at various temperatures for 3 min [111]

7.5.3 Micro-bump

When droplet becomes smaller, the solvent evaporation rate also increases. Super fine droplet shows rapid solvent evaporation. Murata et al. [112] applied this principle to form three-dimensional structures using super fine droplet nano-inks. A pillar with high aspect ratio could be formed by simply ejecting super fine droplets at the same spot. In the case of normal ink-jet process, the liquid spot at the landing point will spread into a large puddle. From scanning electron microscope (SEM) observations, the diameter of the formed pillar was about 0.6 μm. Since the process is quite stable and reproducible, micro-bump array of 50 μm pitch could be fabricated and it was found that the height is linearly proportional to the ejecting time, and thus the height of the pillar can be easily controlled by the ejecting time. The inner structures of the micro-bumps (pillars) were studied by using a focused ion-beam technique. Figure 7.24 shows cross-section SEM image of a gold micro-bump which is formed by super fine ink jet and gold nanopaste. It should be noted that the bump is uniform, high-density gold. A diameter of about 6 μm is difficult to achieve by a conventional stud bumping techniques and a typical bump pad requires at least a 100 μm^2. Our micron-scale bumps might be useful for high density ultrasonic bonding interconnection. Three-dimensional structures can be formed on any arbitrary point on a substrate, by simply ejecting super fine droplet at the same spot. The process is not limited to creating bumps, however. By moving the inkjet head the authors were able to create more complicated microstructures. Figure 7.25a shows representative result of cylinder-like structure formed by super fine ink-jet and a silver nanopaste. The process

is quite stable and repeatable, thus the cylinder array could be achieved. Any shape could be controlled by nozzle movement. The micro cylinder might be useful as micro socket array, Fig. 7.25b shows micro-bump array of 50 μm pitch. These bumps can be used as micro-plug for the micro-socket of Fig. 7.25a.

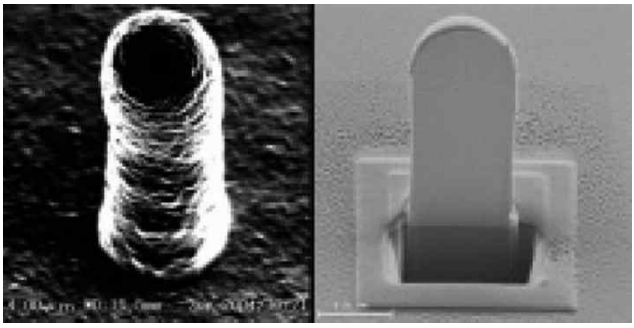

Fig. 7.24. SEM image of a gold micro bump fabricated by super fine ink-jet system on Si substrate (*left*) and cross-sectional image (*right*)

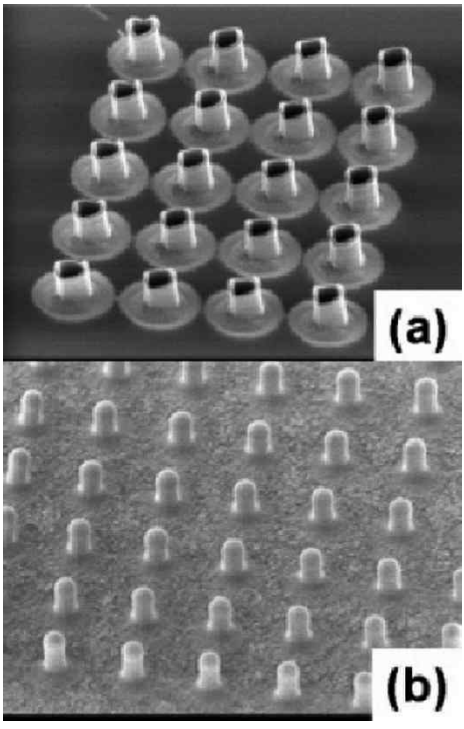

Fig. 7.25. SEM image of a micro-plug (**a**) and micro-socket (**b**) fabricated by super fine ink-jet system on Si and gold substrates, respectively

7.5.4 Interconnect for System-in-Package (SiP)

Mäntysalo et al. [113] presented a concept of ink-jet deposited system-in-Package (SiP). The SiP package contains bare ICs and discrete passive components that are encapsulated with resin mold. Encapsulation material works as a substrate for interconnections, which are directly deposited on top of the mold. All connections between the components and connections to the I/O pins are formed by ink-jetting silver nanoparticle inks. Silver nanoparticles are sintered in an oven at 220°C and resistivity values lower than 5 μΩ·cm are reported. Precuring of a substrate at a higher temperature than the sintering temperature of silver nanoparticles decreases the resistivity of the lines. As a conclusion, the sintering profile needs to be considered carefully in order to achieve resistance requirements set by the design. This chapter focuses on interconnections and system integration design aspects.

The process of making the SiP module is shown in Fig. 7.26. At the beginning, components are assembled on an adhesive carrier. Contact areas of the components must be placed toward the carrier. After the component assembly, the carrier is placed in the molding cast and the epoxy resin is poured inside the case.

After the molding process, the module is ready for the printing of the nano-inks. The silver nanopaste used in this study requires sintering temperature of 220–230°C for a period of 1 h [114], which will introduce quite a tough thermal stress for the components. Thus, material selection must be considered. In order to reduce heat stresses, more advantage sintering methods, such as laser or microwave sintering, can be used [87, 115]. Figure 7.27 shows an example of encapsulated components with first-level interconnections. This module has a size of 17 mm × 17 mm × 1.0 mm, containing 4 bare ICs and over 50 discrete passive components.

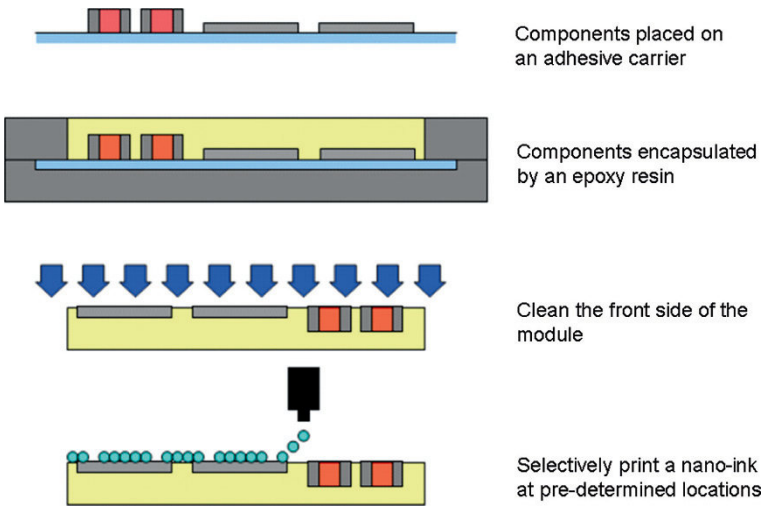

Fig. 7.26. Process steps of ink-jet-printed system-in-package manufacturing

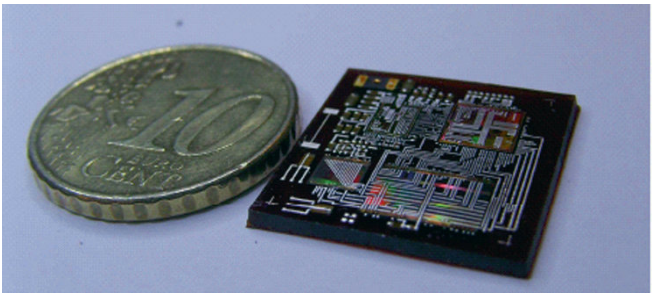

Fig. 7.27. Encapsulated components and first-level interconnections ink-jetted. Module has a size of 17 mm × 17 mm × 1 mm

References

[1] http://www.ece.gatech.edu/research/labs/vc/theory/photolith.html

[2] R. F. Service, "Patterning Electronics on the Cheap," *Science*, 278, 383–384, 1997.

[3] D. Harrison, B. J. Ramsey, P. Sidney, and A. Evans, *US Patent* # 6,356,234.

[4] C. Edward, "PEDs are Coming, Printable Electronics and Displays," Printed Electronics, New Orleans. USA, 2004.

[5] B. J. Ramsey, P. S. A. Evans, and D. Harrison, "A Novel Circuit Fabrication Technique Using Offset Lithography," *Journal of Electronics Manufacturing*, 7, 63–67, 1997.

[6] S. Pienimaa and R. Ronkka, "Towards Printed Products," Printed Electronics Europe 2005, Cambridge, UK, 2005.

[7] T. Remonen, "Organic Electronics: From Basic Research to Production," Printed Electronics, Pira International, Thistle Marble Arch, London, UK, Sept 14–15, 2004.

[8] P. Calvert, "Inkjet Printing for Materials and Devices," *Chemistry of Materials*, 13, 3299–3305, 2001.

[9] H. Sirringhaus and T. Shimoda, "Inkjet Printing of Functional Materials," *MRS Bulletin*, 28, 802–803, 2003.

[10] R. Sangoi, C. G. Smith, M. D. Seymour, J. N. Venkataraman, D. M. Clark, M. L. Kleper, and B. E. Kahn, "Printing Radio Frequency Identification (RFID) Tag Antennas Using Inks Containing Silver Dispersions," *Journal of Dispersion Science and Technology*, 25, 513–521, 2004.

[11] D. Lochun and M. Kilitziraki, "Post-Processing of Conductive Lithographic Films for Multilayer Device Fabrication," *IEEE/CPMT International Electronics Manufacturing Technology Symposium*, pp. 287–293, 1999.

[12] P. M. Harrey, B. J. Ramsey, P. S. A. Evans, and D. J. Harrison, "Capacitive-Type Humidity Sensors Fabricated Using the Offset Lithographic Printing Process," *Sensors and Actuators B-Chemical*, 87, 226–232, 2002.

[13] P. R. Shepherd, P. S. A. Evans, B. J. Ramsey, and D. J. Harrison, "Lithographic Technology for Microwave Integrated Circuits," *Electronics Letters*, 33, 483–484, 1997.

[14] P. S. A. Evans, P. M. Harrey, B. J. Ramsey, and D. J. Harrison, "RF Circulator Structures via Offset Lithography," *Electronics Letters*, 35, 1634–1636, 1999.

[15] R. Weiss and R. Baumann, *Changing Offset Printing: From Color to Functionality, Latest Technology & Applications for Printed Electronics- Impact on Printing and Packaging*, 2004.

[16] H. Sirringhaus, T. Kawase, R. H. Friend, T. Shimoda, M. Inbasekaran, W. Wu, and E. P. Woo, "High-Resolution Inkjet Printing of All-Polymer Transistor Circuits," *Science*, 290, 2123–2126, 2000.

[17] L. Torsi, A. Tafuri, N. Cioffi, M. C. Gallazzi, A. Sassella, L. Sabbatini, and P. G. Zambonin, "Regioregular Polythiophene Field-Effect Transistors Employed as Chemical Sensors," *Sensors and Actuators B-Chemical*, 93, 257–262, 2003.

[18] J. Parker, "Practical Considerations of Printing Conductive Materials," IMAPS 3rd Advanced Technology Workshop on Printing an Intelligent Future: Printed Organic and Molecular Electronics Technologies, Annapolis, Maryland, 2004.

[19] D. R. Gamota, P. Brazis, K. Kalyanasundaram, and J. Zhang, "Printed Organic and Molecular Electronics," Kluwer Academic Publishers (Boston/Dordrecht/New York/London), Springer, 2004.

[20] D. A. Bolon, G. M. Lucas, and S. H. Schroeter, "Radiation Curable Conductive Ink," *IEEE Transactions on Electrical Insulation*, 13, 116–121, 1978.

[21] "Metallic Conductive Inks," *Printed Electronics Review*, 2006.

[22] D. Carli, "A Bright Future for the Growth of Gravure: Printed Electronics," *Gravure Magazine*, vol. 2, pp. 46–51, 2006.

[23] G. Huebner and I. Petersen, "Printed Antennas for Automotive Applications," *Science & Technology*, 1, 35–39, 2008.

[24] R. Moscatiello, "A Reflection of the Future: RFID Today," *SGIA Journal*, first Quarter, 25–29, 2005.

[25] D. J. Fearns, "Applications of Polymer Thick Film Inks in Surface Mount Technology," *Circuit World*, 14, 27–30, 1988.

[26] A. Kamyshny, M. Ben-Moshe, S. Aviezer, and S. Magdassi, "Ink-Jet Printing of Metallic Nanoparticles and Microemulsions," *Macromolecular Rapid Communications*, 26, 281–288, 2005.

[27] G. L. Allen, R. A. Bayles, W. W. Gile, and W. A. Jesser, "Small Particle Melting of Pure Metals," *Thin Solid Films*, 144, 297–308, 1986.

[28] Q. Jiang, S. Zhang, and M. Zhao, "Size-Dependent Melting Point of Noble Metals," *Materials Chemistry and Physics*, 82, 225–227, 2003.

[29] K. Dick, T. Dhanasekaran, Z. Y. Zhang, and D. Meisel, "Size-Dependent Melting of Silica-Encapsulated Gold Nanoparticles," *Journal of the American Chemical Society*, 124, 2312–2317, 2002.

[30] Z. Zhang, J. C. Li, and Q. Jiang, "Modelling for Size-Dependent and Dimension-Dependent Melting of Nanocrystals," *Journal of Physics D-Applied Physics*, 33, 2653–2656, 2000.

[31] G. P. Crawford, Ed., Flexible Flat Panel Display, Wiley, New York, 2005.

[32] P. Buffat and J.-P. Borel, "Size Effect on the Melting Temperature of Gold Particles," *Physical Review* A, 13, 2287–2298, 1976.

[33] J. W. Park and S. G. Baek, "Thermal Behavior of Direct-Printed Lines of Silver Nanoparticles," *Scripta Materialia*, 55, 1139–1142, 2006.

[34] D. Wakuda, M. Hatamura, and K. Suganuma, "Novel Method for Room Temperature Sintering of Ag Nanoparticle Paste in Air," *Chemical Physics Letters*, 441, 305–308, 2007.

[35] D. Kim, S. Jeong, J. Moon, and K. Kang, "Ink-Jet Printing of Silver Conductive Tracks on Flexible Substrates," *Molecular Crystals and Liquid Crystals*, 459, 45–55, 2006.

[36] T. Yonezawa, K. Yasui, and N. Kimizuka, "Controlled Formation of Smaller Gold Nanoparticles by the Use of Four-Chained Disulfide Stabilizer," *Langmuir*, 17, 271–273, 2001.

[37] T. Hasobe, H. Imahori, P. V. Kamat, T. K. Ahn, S. K. Kim, D. Kim, A. Fujimoto, T. Hirakawa, and S. Fukuzumi, "Photovoltaic Cells Using Composite Nanoclusters of Porphyrins and Fullerenes with Gold Nanoparticles," *Journal of the American Chemical Society*, 127, 1216–1228, 2005.

[38] E. E. Foos, A. W. Snow, M. E. Twigg, and M. G. Ancona, "Thiol-Terminated Di-, Tri-, and Tetraethylene Oxide Functionalized Gold Nanoparticles: A Water-Soluble, Charge-Neutral Cluster," *Chemistry of Materials*, 14, 2401–2408, 2002.

[39] S. U. Son, Y. Jang, K. Y. Yoon, E. Kang, and T. Hyeon, "Facile Synthesis of Various Phosphine-Stabilized Monodisperse Palladium Nanoparticles Through the Understanding of Coordination Chemistry of the Nanoparticles," *Nano Letters*, 4, 1147–1151, 2004.

[40] V. J. Gandubert and R. B. Lennox, "Assessment of 4-(Dimethylamino)pyridine as a Capping Agent for Gold Nanoparticles," *Langmuir*, 21, 6532–6539, 2005.

[41] C. K. Yee, A. Ulman, J. D. Ruiz, A. Parikh, H. White, and M. Rafailovich, "Alkyl Selenide- and Alkyl Thiolate-Functionalized Gold Nanoparticles: Chain Packing and Bond Nature," *Langmuir*, 19, 9450–9458, 2003.

[42] P. Ahonen, T. Laaksonen, A. Nykanen, J. Ruokolainen, and K. Kontturi, "Formation of Stable Ag-Nanoparticle Aggregates Induced by Dithiol Cross-Linking," *Journal of Physical Chemistry B*, 110, 12954–12958, 2006.

[43] S. Ray, A. K. Das, M. G. B. Drew, and A. Banerjee, "A Short Water-Soluble Self-Assembling Peptide Forms Amyloid-Like Fibrils," *Chemical Communications*, 40, 4230–4232, 2006.

[44] P. K. Vemula and G. John, "Smart Amphiphiles: Hydro/Organogelators for In Situ Reduction of Gold," *Chemical Communications*, 21, 2218–2220, 2006.

[45] X. D. Wang, C. E. Egan, M. F. Zhou, K. Prince, D. R. G. Mitchell, and R. A. Caruso, "Effective Gel for Gold Nanoparticle Formation, Support and Metal Oxide Templating," *Chemical Communications*, 29, 3060–3062, 2007.

[46] I. Doudevski and D. K. Schwartz, "Mechanisms of Self-Assembled Monolayer Desorption Determined Using In Situ Atomic Force Microscopy," *Langmuir*, 16, 9381–9384, 2000.

[47] G. Schmid, R. Pfeil, and R. Boese, "Au55[P(C6H5)3]12Cl6-a Gold Cluster of Unusual Size," *Chemische Berichte*, 114, 3634–3642, 1981.

[48] M. Brust, M. Walker, D. Bethell, D. J. Schiffrin, and R. Whyman, "Synthesis of Thiol-Derivatized Gold Nanoparticles in a 2-Phase Liquid-Liquid System," *Journal of the Chemical Society-Chemical Communications*, 7, 801–802, 1994.

[49] M. C. Daniel and D. Astruc, "Gold Nanoparticles: Assembly, Supramolecular Chemistry, Quantum-Size-Related Properties, and Applications Toward Biology, Catalysis, and Nanotechnology," *Chemical Reviews*, 104, 293–346, 2004.

[50] S. W. Chen and J. M. Sommers, "Alkanethiolate-Protected Copper Nanoparticles: Spectroscopy, Electrochemistry, and Solid-State Morphological Evolution," *Journal of Physical Chemistry* B, 105, 8816–8820, 2001.

[51] N. Sandhyarani and T. Pradeep, "Crystalline Solids of Alloy Clusters," *Chemistry of Materials*, 12, 1755–1761, 2000.

[52] N. Sandhyarani, M. R. Resmi, R. Unnikrishnan, K. Vidyasagar, S. G. Ma, M. P. Antony, G. P. Selvam, V. Visalakshi, N. Chandrakumar, K. Pandian, Y. T. Tao, and T. Pradeep, "Monolayer-Protected Cluster Superlattices: Structural, Spectroscopic, Calorimetric, and Conductivity Studies," *Chemistry of Materials*, 12, 104–113, 2000.

[53] J. C. Love, L. A. Estroff, J. K. Kriebel, R. G. Nuzzo, and G. M. Whitesides, "Self-Assembled Monolayers of Thiolates on Metals as a Form of Nanotechnology," *Chemical Reviews*, 105, 1103–1169, 2005.

[54] S. Bhat and U. Maitra, "Facially Amphiphilic Thiol Capped Gold and Silver Nanoparticles," *Journal of Chemical Sciences*, 120, 507–513, 2008.

[55] J. G. Yang, Y. L. Zhou, T. Okamoto, T. Bessho, S. Satake, R. Ichino, and M. Okido, "Preparation of Oleic Acid-Capped Copper Nanoparticles," *Chemistry Letters*, 35, 1190–1191, 2006.

[56] E. Foresti, G. Fracasso, M. Lanzi, I. G. Lesci, L. Paganin, T. Zuccheri, and N. Roveri, "New Thiophene Monolayer-Protected Copper Nanoparticles: Synthesis and Chemical-Physical Characterization," *Journal of Nanomaterials*, 2008(3), 1–6, 2008.

[57] P. Kanninen, C. Johans, J. Merta, and K. Kontturi, "Influence of Ligand Structure on the Stability and Oxidation of Copper Nanoparticles," *Journal of Colloid and Interface Science*, 318, 88–95, 2008.

[58] K. Murai, Y. Watanabe, Y. Saito, T. Nakayama, H. Suematsu, W. Jiang, K. Yatsui, K. H. Shim, and K. Niihara, "Preparation of Copper Nanoparticles with an Organic Coating by a Pulsed Wire Discharge Method," *Journal of Ceramic Processing Research*, 8, 114–118, 2007.

[59] N. A. Luechinger, E. K. Athanassiou, and W. J. Stark, "Graphene-Stabilized Copper Nanoparticles as an Air-Stable Substitute for Silver and Gold in Low-Cost Ink-Jet Printable Electronics," *Nanotechnology*, 19, 445201, 2008.

[60] K. Woo, D. Kim, J. S. Kim, S. Lim, and J. Moon, "Ink-Jet Printing of Cu-Ag-Based Highly Conductive Tracks on a Transparent Substrate," *Langmuir*, 25, 429–433, 2009.

[61] R. A. de Barros, C. R. Martins, and W. M. de Azevedo, "Writing with Conducting Polymer," *Synthetic Metals*, 155, 35–38, 2005.

[62] F. Nelson, "Materials Ink Jet Printing of Electronic Structures," *National Nanotechnology Infrastructure Network, 2007 REU Research Accomplishments*, pp. 70–71, 2007.

[63] E. Montbach, D. Marhefka, D. J. Davis, M. Lightfoot, S. Green, N. Venkataraman, T. Schneider, A. Khan, and J. W. Doane, "Flexible Ink Jet Printed Conductive Polymer Electrode Cholesteric Display," *SID Digest*, pp. 1737–1740, 2006.

[64] J. Bharathan and Y. Yang, "Polymer Electroluminescent Devices Processed by Inkjet Printing: I. Polymer Light-Emitting Logo," *Applied Physics Letters*, 72, 2660–2662, 1998.

[65] A. Karwa, "Printing Studies with Conductive Inks and Exploration of New Conducting Polymer Compositions," *Rochester Institute of Technology, March 2006, Master Thesis*, 2006.

[66] J. X. Huang, S. Virji, B. H. Weiller, and R. B. Kaner, "Polyaniline Nanofibers: Facile Synthesis and Chemical Sensors," *Journal of the American Chemical Society*, 125, 314–315, 2003.

[67] J. X. Huang and R. B. Kaner, "Nanofiber Formation in the Chemical Polymerization of Aniline: A Mechanistic Study," *Angewandte Chemie-International Edition*, 43, 5817–5821, 2004.

[68] A. V. Gelatos, R. Marsh, M. Kottke, and C. J. Mogab, "Chemical-Vapor-Deposition of Copper from Cu+1 Precursors in the Presence of Water-Vapor," *Applied Physics Letters*, 63, 2842–2844, 1993.

[69] R. Izquierdo, J. Bertomeu, M. Suys, E. Sacher, and M. Meunier, "Excimer Laser-Induced Deposition of Copper from Cu(Hfac)(Tmvs)," *Applied Surface Science*, 86, 509–513, 1995.

[70] C. Curtis, T. Rivkin, A. Miedaner, J. Alleman, J. Perkins, L. Smith, and D. Ginley, "Metallizations by Direct-Write Inkjet Printing," Colorado, October 2001.

[71] P. Majumder, M. Tiwari, C. Megaridis, J. McAndrew, M. Xu, J. Belot, and C. G. Takoudis, "Evaluation and Testing of Organometallic Precursor for Copper Direct-Write," *MRS Spring Meeting, Symposium N, Paper #: 1002-N07-23, 2007*.

[72] M. Wehner, F. Legewie, B. Theisen, and E. Beyer, "Direct Writing of Gold and Copper Lines from Solutions," *International Conference on Photo-Excited Processes and Applications No. 2*, Jerusalem, ISRAEL, vol. 106, pp. 406–411, 1996.

[73] Y. H. Byun, E. C. Hwang, S. Y. Lee, Y. Y. Lyu, J. H. Yim, J. Y. Kim, S. Chang, L. S. Pu, and J. M. Kim, "Highly Efficient Silver Patterning without Photo-Resist Using Simple Silver Precursors," *Materials Science and Engineering B-Solid State Materials for Advanced Technology*, 117, 11–16, 2005.

[74] C. A. Lu, P. Lin, H. C. Lin, and S. F. Wang, "Effects of Metallo-Organic Decomposition Agents on Thermal Decomposition and Electrical Conductivity of Low-Temperature-Curing Silver Paste," *Japanese Journal of Applied Physics Part 1-Regular Papers Brief Communications & Review Papers*, 45, 6987–6992, 2006.

[75] C. A. Lu, P. Lin, H. C. Lin, and S. F. Wang, "Effects of Silver Oxide Addition on the Electrical Resistivity and Microstructure of Low-Temperature-Curing Metallo-Organic Decomposition Silver Pastes," *Japanese Journal of Applied Physics Part 1-Regular Papers Brief Communications & Review Papers*, 46, 4179–4183, 2007.

[76] B. J. de Gans, P. C. Duineveld, and U. S. Schubert, "Inkjet Printing of Polymers: State of the Art and Future Developments," *Advanced Materials*, 16, 203–213, 2004.

[77] H. M. Dong, W. W. Carr, and J. F. Morris, "An Experimental Study of Drop-on-Demand Drop Formation," *Physics of Fluids*, 18, 072102, 2006.

[78] N. Reis, C. Ainsley, and B. Derby, "Ink-Jet Delivery of Particle Suspensions by Piezoelectric Droplet Ejectors," *Journal of Applied* Physics, 97, 094903, 2005.

[79] K. Cheng, M. H. Yang, W. W. W. Chiu, C. Y. Huang, J. Chang, T. F. Ying, and Y. Yang, "Ink-Jet Printing, Self-Assembled Polyelectrolytes, and Electroless Plating: Low Cost Fabrication of Circuits on a Flexible Substrate at Room Temperature," *Macromolecular Rapid Communications*, 26, 247–264, 2005.

[80] P. J. Smith, D. Y. Shin, J. E. Stringer, B. Derby, and N. Reis, "Direct Ink-Jet Printing and Low Temperature Conversion of Conductive Silver Patterns," *Journal of Materials Science*, 41, 4153–4158, 2006.

[81] H. H. Lee, K. S. Chou, and K. C. Huang, "Inkjet Printing of Nanosized Silver Colloids," *Nanotechnology*, 16, 2436–2441, 2005.

[82] J. B. Szczech, C. M. Megaridis, D. R. Gamota, and J. Zhang, "Fine-line Conductor Manufacturing Using Drop-on-Demand PZT Printing Technology," *IEEE Transactions on Electronics Packaging Manufacturing*, 25, 26–33, 2002.

[83] Y. L. Wu, Y. N. Li, and B. S. Ong, "Printed Silver Ohmic Contacts for High-mobility Organic Thin-Film Transistors," *Journal of the American Chemical Society*, 128, 4202–4203, 2006.

[84] Y. Yoshioka, P. D. Calvert, and G. E. Jabbour, "Simple Modification of Sheet Resistivity of Conducting Polymeric Anodes via Combinatorial Ink-Jet Printing Techniques," *Macromolecular Rapid Communications*, 26, 238–246, 2005.

[85] S. B. Fuller, E. J. Wilhelm, and J. M. Jacobson, "Ink-Jet Printed Nanoparticle Microelectromechanical Systems," *Journal of Microelectromechanical Systems*, 11, 54–60, 2002.

[86] D. Huang, F. Liao, S. Molesa, D. Redinger, and V. Subramanian, "Plastic-Compatible Low Resistance Printable Gold Nanoparticle Conductors for Flexible Electronics," *Journal of the Electrochemical Society*, 150, 412–417, 2003.

[87] J. Perelaer, B. J. de Gans, and U. S. Schubert, "Ink-Jet Printing and Microwave Sintering of Conductive Silver Tracks," *Advanced Materials*, 18, 2101–2104, 2006.

[88] C. Kung, M. D. Barnes, N. Lermer, W. B. Whitten, and J. M. Ramsey, "Single-Molecule Analysis of Ultradilute Solutions with Guided Streams of 1-mu m Water Droplets," *Applied Optics*, 38, 1481–1487, 1999.

[89] T. H. J. van Osch, J. Perelaer, A. W. M. de Laat, and U. S. Schubert, "Inkjet Printing of Narrow Conductive Tracks on Untreated Polymeric Substrates," *Advanced Materials*, 20, 343–345, 2008.

[90] H. Yokoyama, "Nanotechnology: A Breakthrough toward a Resource & Energy Compatible Society of 21st Century," *AIST Today International Edition* No.10, Nanotechnology, 2003.

[91] K. Murata, "Super-fine Ink-jet Printing for Nanotechnology," *Proceedings of the International Conference on MEMS, NANO and Smart Systems*, 2003.

[92] N. Zhao, M. Chiesa, H. Sirringhausa, Y. N. Li, and Y. L. Wu, "Self-Aligned Inkjet Printing of Highly Conducting Gold Electrodes with Submicron Resolution," *Journal of Applied Physics*, 101, 064513, 2007.

[93] N. R. Bieri, J. Chung, D. Poulikakos, and C. P. Grigoropoulos, "Manufacturing of Nanoscale Thickness Gold Lines by Laser Curing of a Discretely Deposited Nanoparticle Suspension," *Superlattices and Microstructures*, 35, 437–444, 2004.

[94] T. Y. Choi, D. Poulikakos, and C. P. Grigoropoulos, "Fountain-pen-based Laser Microstructuring with Gold Nanoparticle Inks," *Applied Physics Letters*, 85, 13–15, 2004.

[95] J. W. Chung, S. W. Ko, N. R. Bieri, C. P. Grigoropoulos, and D. Poulikakos, "Conductor Microstructures by Laser Curing of Printed Gold Nanoparticle Ink," *Applied Physics Letters*, 84, 801–803, 2004.

[96] M. Nuchter, B. Ondruschka, W. Bonrath, and A. Gum, "Microwave Assisted Synthesis – A Critical Technology Overview," *Green Chemistry*, 6, 128–141, 2004.

[97] T. Niizeki, K. Maekawa, M. Mita, K. Yamasaki, Y. Matsuba, N. Terada, and H. Saito, "Laser Sintering of Ag Nanopaste Film and Its Application to Bond-Pad Formation," *Proceedings of the 58th IEEE Electronic Components and Technology Conference*, pp. 1745–1750, 2008.

[98] K. J. Rao, B. Vaidhyanathan, M. Ganguli, and P. A. Ramakrishnan, "Synthesis of Inorganic Solids Using Microwaves," *Chemistry of Materials*, 11, 882–895, 1999.

[99] P. Lidstrom, J. Tierney, B. Wathey, and J. Westman, "Microwave Assisted Organic Synthesis – A Review," *Tetrahedron*, 57, 9225–9283, 2001.

[100] F. Wiesbrock, R. Hoogenboom, and U. S. Schubert, "Microwave-Assisted Polymer Synthesis: State-of-the-Art and Future Perspectives," *Macromolecular Rapid Communications*, 25, 1739–1764, 2004.

[101] Y. Fang, M. T. Lanagan, D. K. Agrawal, G. Y. Yang, C. A. Randall, T. R. Shrout, A. Henderson, M. Randall, and A. Tajuddin, "An Investigation Demonstrating the Feasibility of Microwave Sintering of Base-Metal-Electrode Multilayer Capacitors," *Journal of Electroceramics*, 15, 13–19, 2005.

[102] R. M. Anklekar, K. Bauer, D. K. Agrawal, and R. Roy, "Improved Mechanical Properties and Microstructural Development of Microwave Sintered Copper and Nickel Steel PM Parts," *Powder Metallurgy*, 48, 39–46, 2005.

[103] E. T. Thostenson and T. W. Chou, "Microwave Processing: Fundamentals and Applications," *Composites Part A-Applied Science and Manufacturing*, 30, 1055–1071, 1999.

[104] G. Oosterhuis and F. K. Feenstra, "Pyrolytic Printing, the Holy Grail in Metal Printing?," *5th European Thermal-Sciences Conference*, The Netherlands, 2008.

[105] T. C. Claypole, E. Jewell, G. Davies, and V. Vigne, "The Effect of Speed and Viscosity on Line Quality in Rotogravure Printing with Reference to Printed Electronics," *IARIGAI's 32nd International Research Conference on Digitalization and Print Media, Porvoo, Finland*, pp. 93–99, 2005.

[106] M. F. Bohan, T. C. Claypole, and D. T. Gethin, "The Effect of Process Parameters on Product Quality of Rotogravure Printing," *Proceedings of the Institution of Mechanical Engineers, Part B, Journal of Engineering Manufacture*, vol. 214, pp. 205–219, 2000.

[107] K. Gillett, Gravure – Process and Technology, GAA and GEF, 2nd Ed., Rochester, New York: Gravure Association of America, Gravure Education Foundation, 2003.

[108] M. Pudas, N. Halonen, P. Granat, and J. Vahakangas, "Gravure Printing of Conductive Particulate Polymer Inks on Flexible Substrates," *Progress in Organic Coatings*, 54, 310–316, 2005.

[109] J. G. F. Bai, R. Yin, Z. Y. Zhang, G. Q. Lu, and J. D. van Wyk, "High-temperature Operation of SiC Power Devices by Low-temperature Sintered Silver Die-attachment," *IEEE Transactions on Advanced Packaging*, 30, 506–510, 2007.

[110] A. D. Albert, M. F. Becker, J. W. Keto, and D. Kovar, "Low Temperature, Pressure-Assisted Sintering of Nanoparticulate Silver Films," *Acta Materialia*, 56, 1820–1829, 2008.

[111] H. Wang, L. Huang, Z. Xu, C. Xu, R. J. Composto, and Z. Yang, "Sintering Metal Nanoparticle Films," *Flexible Electronics and Displays Conference and Exhibition*, pp. 1–3, 2008.

[112] K. Murata and K. Shimizu, "Micro Bump Formation by Using a Super Fine Inkjet System," *35th International Symposium on Microelectronics IMAPS*, San Diego, TP66, 2006.

[113] M. Mäntysalo and P. Mansikkamäki, "Inkjet-Deposited Interconnections for Electronic Packaging," *NIP23 and Digital Fabrication*, pp. 813–817, 2007.

[114] H. Saito and Y. Matsuba, "Liquid Wiring Technology by Ink-Jet Printing Using NanoPaste," *Proceedings of the 39th International Symposium on Microelectronics*, San Diego, USA, 2006.

[115] N. R. Bieri, J. Chung, S. E. Haferl, D. Poulikakos, and C. P. Grigoropoulos, "Microstructuring by Printing and Laser Curing of Nanoparticle Solutions," *Applied Physics Letters*, 82, 3529–3531, 2003.

Chapter 8
Intrinsically Conducting Polymers (ICPs)

8.1 Basics of Intrinsically Conducting Polymers

8.1.1 Introduction

Synthetic polymers, whose long molecules string together hundreds of identical structural units, have been insulating electric equipment since the turn of the century. The later fabrication, in the 1970s, of polymers with usefully high electrical conductivity stirred intense interest in the research and development community. By now these polymers are showing commercial promise in such areas as power equipment, batteries, microelectronics, shielding against electromagnetic interference, and coatings, not to mention micromachines and adhesives.

The addition of conducting fillers such as copper and carbon black to conventional polymers has been the primary approach to produce easy-to-process materials having some measurable electrical conductivity. The cost of the technique is undoubtedly low, but problems can arise in the form of surface corrosion, uneven mixing, reduced mechanical properties, and incompatibility of the filler with the polymer matrix. Careful selection of materials and processing methods for a given application can reduce the consequences of these problems.

Intrinsically conducting polymers (ICPs) are generally synthetic "metals" because they have electrical, magnetic, and optical properties typical of metals and semiconductors. These characteristics arise from the conjugation of their backbone, namely a regular succession of single and double bonds [1]. This configuration causes the formation of high-energy orbitals in which electrons are loosely bonded to their corresponding atom. Charge movement within the material can be induced by the application of an electric or magnetic field. There are two energy levels, HOMO (highest occupied molecular orbital, also called valence band) at lower energy,

Y. Li et al., *Electrical Conductive Adhesives with Nanotechnologies*,
DOI 10.1007/978-0-387-88783-8_8, © Springer Science+Business Media, LLC 2010

which can give up electrons, and the LUMO (lowest unoccupied molecular orbital, also called conducting band) at higher energy, which can attract electrons. These bands are separated by an energy gap, also called band gap, corresponding to the forbidden energy levels. The distance between the HOMO and LUMO determines the conducting, semiconducting, or insulating character of the material. The conduction mechanism is generated by the carrier movement (or jump) from the HOMO to the LUMO, which is easier if the HOMO–LUMO energy gap is small. Actually, most of the conducting polymers display semi conducting properties, and an oxidizing doping such as $KMnO_4$ or iodine is needed to generate the radical cations, coupled with the dopant counter anion, the so-called "polarons" to improve the mobility of charge carriers by decreasing the HOMO to LUMO energy band gap.

Electrically conducting polymer is composed of macromolecules having fully conjugated sequences of double bonds along the chains. Conducting polymers are prepared in two steps, which can be simultaneous or sequential. First, the polymer is formed from its starting material by a conventional chemical polymerization process. The molecular structure of such polymers typically has considerable delocalization of electrons along the polymer chains. This structure is also conducive to formation of energy bands, from and to which charge carriers can be easily removed or added.

Common classes of organic conductive polymers include poly(acetylene)s, poly(pyrrole)s, poly(thiophene)s, poly(aniline)s, poly (3,4-ethylene dioxythiophene), and poly (phenyl vinylene) as shown in Fig. 8.1. Conductivity in the simplest semiconducting and metallic organic polymer, polyacetylene, is partially based on sp^2 hybridized linear carbon chains. The carbon atom has six electrons outside the nucleus, of which four are valence electrons; i.e., four (the 2s and the 2p electrons) take part in chemical bonds. In free space, or where the potential is spherically symmetric, the 1s and 2s orbitals of the carbon atom are filled, and the 2p orbitals are occupied with two electrons. In order to lower the total energy and form spatially directed chemical bonds, in molecules and crystals, carbon can form two primary hybrid structures tetrahedrally directed covalent bonds (sp^3 hybridized) as in diamond and saturated polymers: and hexagonally directed covalent bonds (sp^2 hybridized) as in graphite and conjugated polymers.

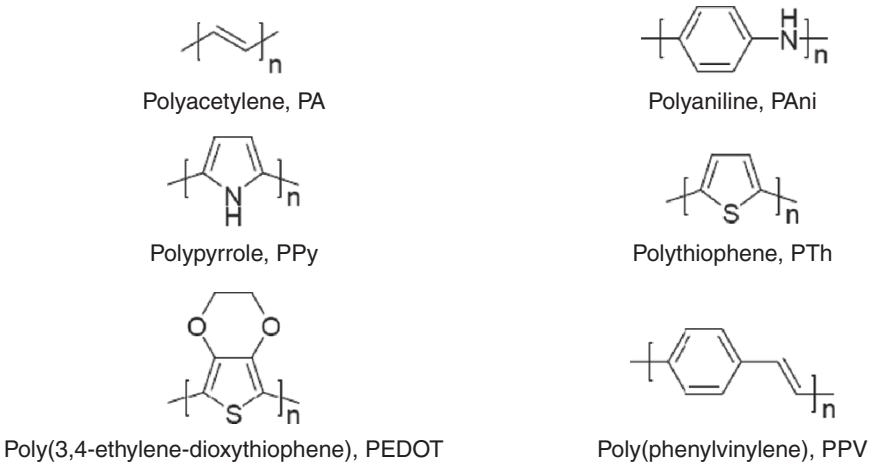

Fig. 8.1. Examples of conductive polymers

Traditional polymers such as polyethylenes are electrical insulators. Since all of the valence electrons are bound in sp^3 hybridized covalent bonds, there are no mobile electrons to participate in electronic transport. Conjugated, conducting polymers are formed from sp^2 hybridized carbons. Polyacetylene is the simplest conjugated polymer $(CH)_x$. In polyacetylene, the three in-plane sigma orbitals of the sp^2 hybridized carbon create the "backbone"; two of them bonded to the neighboring carbons and the third sigma orbital bonded to a hydrogen atom. The fourth electron resides in the Pz orbital, and because of its orthogonality to the plane defined by the other three sigma bonds it is in first approximation independent of them. This one-electron picture of the Pz electron being decoupled from the backbone sigma orbitals gives these polymers special electronic properties.

Although the π-electrons in polyacetylene are delocalized along the chain, pristine polyacetylene is not a metal. The polymerization of polyacetylene from the monomer acetylene yields a dimerized (bond alternating) structure. The resulting polymer is insoluble and intractable. Consequently, the molecular weight cannot be directly determined. Thus, because the

Staudinger index, *N*, is unknown, polyacetylene is typically designated as $(CH)_x$. The molecular structure of "real" polyacetylene has alternating single and double bonds which are, respectively, longer and shorter than the equilibrium value of the bond length in uniform $(CH)_x$. In this structure, the π-electrons on neighboring carbon atoms form a weak π–π bond resulting in the bond alternating structure (short bond length associated with and indicative of the pi bond). The bond alternation has been determined from analysis of X-ray diffraction data and from analysis of nuclear magnetic resonance data; the shorter bond length is 1.35 Å and the longer bond length is 1.45 Å. Such a bond alternating structure doubles the unit cell thereby opening a gap in the electronic structure. As a result, because of the bond alternating structure, polyacetylene is a semiconductor in its ground state. Semiconducting polymers can be doped to sufficiently high carrier densities that metallic polymers are obtained. The metallic state of doped conjugated polymers (conducting polymers) is stabilized by interchain interactions sufficiently strong that the systems are anisotropic three-dimensional metals.

When charge carriers (from the addition or removal of electrons) are introduced into the conduction or valence bands (see below) the electrical conductivity increases dramatically. The most notable difference between conductive polymers and inorganic semiconductors is the mobility, which until very recently was dramatically lower in conductive polymers than their inorganic counterparts, though recent advancements in molecular self-assembly are closing that gap. This low charge carrier mobility is related to amorphous and disordered nature of the solid state nanostructure in the conducting polymers. In fact, as with inorganic amorphous semiconductors, conduction in such relatively disordered materials is mostly a function of "mobility gaps" with phonon-assisted hopping, polaron-assisted tunneling, etc., between localized states.

Typically "doping" the conductive polymers involves actually oxidizing/reducing of the compound. Conductive organic polymers associated with a protic solvent may also be "self-doped". Melanin is the classic example of both types of doping, being both an oxidized polyacetylene and likewise commonly being hydrated.

The conjugated polymers in their undoped, pristine state are semiconductors/insulators. As such the energy gap is around 2 eV and higher and is too big for a considerable excitation of the charge carriers thermally. Therefore, the undoped conjugated polymer, such as polythiophene, polyacetylene etc., has only a conductivity of around 10^{-10} to 10^{-8} S/cm. Upon doping the conjugated polymers there is a rapid increase of electrical conductivity of several orders of magnitude up to values of around 10^{-1} S/cm even at a very low level of doping such as < 1%. Subsequent doping of the conducting polymers will result in saturation of the conductivity at values

around 100–10^5 S/cm for different polymers [2]. Highest values reported up to now are for the conductivity of stretch-oriented polyacetylene with confirmed values of around 10^5 S/cm [2].

Poly(phenylene vinylene), PPV, is an alternating copolymer of the repeat units of polyacetylene and poly(paraphenylene). PPV and its soluble derivatives have emerged as the prototypical luminescent semiconducting polymers. Today, poly(3-alkylthiophenes) are the archetypical materials for solar cells and transistors.

8.1.2 Doping

In silicon semiconductors, a few of the silicon atoms are replaced by electron-rich (e.g., phosphorus) or electron-poor (e.g. boron) atoms to create n-type and p-type semiconductors, respectively. It should be pointed out that all these polymers are semiconductors with a fairly large bandgap in their pristine or undoped state. Only by doping are they transformed into "synthetic metal". In contrast, there are two primary methods of doping a conductive polymer, both through a reduction–oxidation (redox) process. The purpose of doping is to reduce the band gap energy between HOMO and LUMO and thus make charge carrier movement easier. The doping agents are incorporated during redox polymerization reaction. Indeed, the dopant anion is attracted, via local resonance, to the radical formed during oxidation and acts as a counterion [3]. The radical cation coupled with the counter anion–dopant combination is called a polaron and it represents the actual charge carrier in the conducting polymers. The polaron formation induces a local distortion of the chain [3] and the formation of energy levels within the band gap. In this way, charge carriers can move easily from the HOMO to the LUMO, promoting the electron mobility along the molecular chain. For polyacetylene, solitons also play an important role for converting polyacetylene from semiconductor to near metallic conductor [4].

The first approach is chemical doping which involves exposing a polymer, such as melanin (typically a thin film), to an oxidant (typically iodine or bromine) or reductant (far less common, but typically involves alkali metals such as Li or Na). The second method is electrochemical doping in which a polymer-coated, working electrode is suspended in an electrolyte solution in which the polymer is insoluble along with separate counter and reference electrodes. An electric potential difference is created between the electrodes which causes a charge (and the appropriate counterion from the electrolyte) to enter the polymer in the form of electron addition (n doping) or removal (p doping). Polymers may also be self-doped, e.g., when associated with a protonic solvent such as water or an alcohol.

The reason n-type doping is so much less common is that Earth's atmosphere is oxygen rich, which creates an oxidizing environment. An electron-rich n-type polymer will react immediately with elemental oxygen to de-dope (re-oxidize to the neutral state) the polymer. Thus, chemical n-type doping has to be done in an environment of inert gas (e.g., argon). Electrochemical n-type doping is far less common in research, because it is much more difficult to exclude oxygen from a solvent in a sealed flask; therefore, although very useful, there are likely to be no commercialized n-type conductive polymers.

Different polymers and polymer derivatives, doped with a weak oxidation agent or reducing agent resulting in various conjugated polymers, had brought about the understanding of charge storage and charge transfer mechanisms. The electrical conductivities of the intrinsically conducting polymer systems range from those typical of insulators ($<10^{-10}$ S/cm) to those typical of semiconductors such as silicon ($\sim 10^{-5}$ S/cm) to those greater than 10^4 S/cm [5]. Conductivities of various conducting polymers are shown in Fig. 8.2. However, the main problems of these polymers are their processability and stability. The development of highly conducting polymers with good stability and acceptable processing attributes are the main focuses of many recent research works.

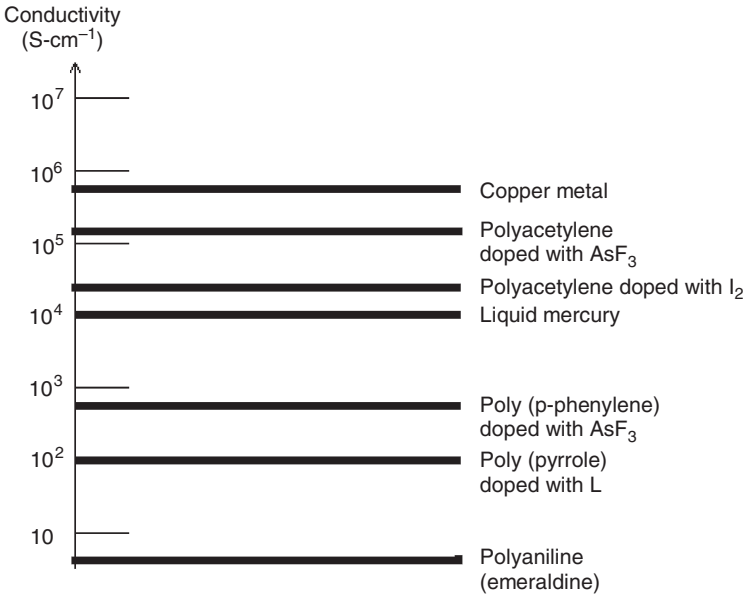

Fig. 8.2. Logarithmic conductivity ladder of conducting polymers and metals

The concept of doping is the central theme which distinguished conducting polymers from all other polymers [6]. Conducting polymers can be doped by redox reaction or protonation, in which the latter is only applicable to polyaniline (PAni). Figure 8.3 demonstrates the oxidation process of PPy. Some electrons are removed from polypyrrole (PPy) backbones by chemical or electrochemical oxidations, leaving positive charges on them. The resulting radical cations are called polarons, which acts as the charge carriers. Counterions, X^-, are also induced close to the polymer chains to balance the positive charges. Doped conducting polymers are semiconductors or conductors (~100–105 S/cm). This doping process is reversible, that is, the doped PPy can be turned into its undoped state by chemical or electrochemical reductions.

For PANI, the doping process is different. PAni structure shown in Fig. 8.4 is in a totally reduced state [7]. Generally, PAni chains consist of two types of structural units: Quinod and Benzenoid. These two units can be transformed into each other by redox. Not all types of doped PAni are conductors; the protonated PAni is electrically conductive only when x:y = 1:1 (Benzenoid: Quinod = 3:1). The protonic acid doping process is illustrated in Scheme 3B. Doping and undoping play key roles in the sensing mechanism of conducting polymer-based sensors.

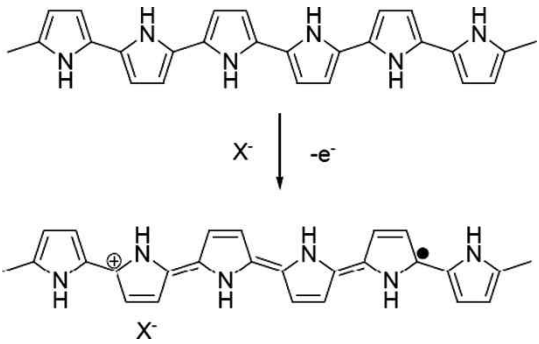

Fig. 8.3. Oxidation doping of PPy

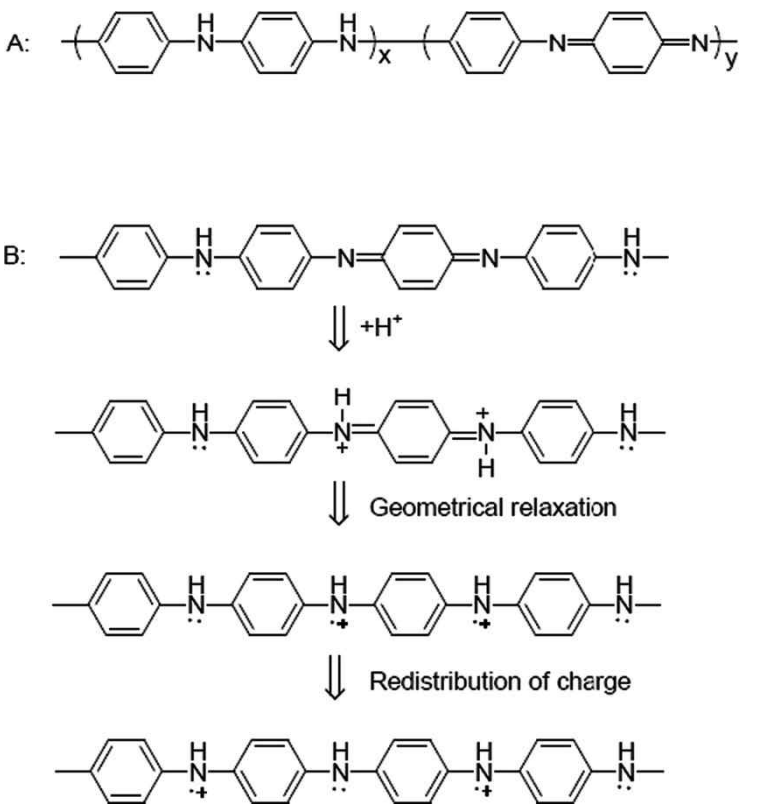

Fig. 8.4. Structure (a) and protonic acid doping process (b) of polyaniline(PAni)

8.1.3 Polyacetylene

In the early 1970s, Shirakawa et al. [8] succeeded in synthesizing polyacetylene films with metallic luster, which initiated a new field of research on conducting polymers. In the late 1970s, it was found that conductivity of the polyacetylene could be increased dramatically by chemical doping. Since then, polyacetylene has been studied extensively from scientific and technological viewpoints. Many conjugated polymers such as polypyrrole, polythiophene, and polyphenylenevinylene have been synthesized and found to be conductive upon doping.

Among all the conducting polymers, polyacetylene is the simplest conjugated polymer and has been of primary interest. The attainable conductivity of this polymer has been rising steadily through the improvement synthesis

and doping techniques. Although a vast amount of information of the polymer has been accumulated, the conductivity mechanism, especially for the heavily doped polymers, is far from being well understood. This is due to the complexity of the conduction process in the polymeric system, where macromolecular, intermolecular, intermetallic domain, and interfibrillar processes all contribute somewhat to the conductivity. Activation type of temperature dependence of the conductivity, which is commonly observed for majority of the doped conducting polymers, suggests that the intermolecular and/or intermetallic domain processes still play a major role in the measured conductivity [9]. In such a system, metallic conductivity appears difficult to correlate with DC conductivity, as the hoping process between localized states dominates essentially the carrier transport.

In early 1980s, the observed conductivity range of polyacetylene was 10^2–10^3 S/cm [10]. The conductivity of polyacetylene has increased steadily with the improvement of the polymerization techniques. By polymerizing the acetylene in oriented liquid crystals, Akagi et al. [11], Ribet et al. [12], and Aldissi et al. [13] have achieved highly oriented polyacetylene, which exhibited a conductivity of more than 10^4 S/cm along the orientation ($\sigma_{\parallel}$). On the other hand, Schimmel et al. [14] prepared a highly stretchable polyacetylene by using the Shirakawa catalyst aged at 120° C and silicone oil as solvent, and attained a conductivity of about 10^4 S/cm. Thereafter, Naarmann and Thcophilou succeeded in preparing metallic conductive polyacetylene yielding a conductivity of over 10^5 S/cm by their improved procedure, the so-called adding reducing agent (ARA) method. Moreover, Tsukamoto et al. [15] obtained metallic-conductive polyacetylene by making some modifications on Naarmann and Thcophilou's method.

8.2 Applications of Conducting Polymers

8.2.1 Lithography

8.2.1.1 Background

Lithographic techniques delineate the intricate patterns necessary to form the doped regions of silicon on a chip or interconnections on a substrate

[16, 17]. Lithography relies on radiation-sensitive photoresist which, when irradiated through a quartz/chrome mask containing the pattern to be transferred undergo chain scissioning (positive tone), cross-linking (negative tone), de protection, or molecular rearrangement, thereby creating a difference in solubility between the irradiated or exposed areas and the non-irradiated or unexposed areas of the polymer. In a subsequent development step, the more soluble regions of the resist are selectively removed. This pattern is subsequently transferred to the underlying substrate (e.g., silicon dioxide, silicon nitride, silicon, or metal) by various etching processes, followed by removal of the photoresist [18].

Photoresists may be patterned with photons at different wavelengths (365 nm, 248 nm, 193 nm), electron beams, X-rays, and ion beams [19]. Photolithography has been the dominant technology in the industry to date. However, electron-beam (e-beam) technology is used to fabricate masks for photolithography and for high-resolution, low-volume specialty chips, and it is currently being considered as a next-generation projection lithography option for semiconductor device fabrication [20]. The dimensions that must be delineated are rapidly decreasing. As the industry continues to require improved resolution, new materials, processes, and tools must evolve to sustain this trend.

8.2.1.2 Charge Dissipators for Electron-Beam Lithography

E-beam lithography is a direct-write method in which a focused beam of electrons is directly scanned over the resist; no mask is required because the pattern is computer generated. It is a technology capable of extremely high resolution, since the beam of electrons can be focused to tens of nanometers, and capable also of excellent alignment of level-to-level pattern overlays. However, because it is a step and repeat process which is time consuming, coupled with the high cost of the e-beam equipment, E-beam lithography is a high cost lithography process when compared to the general flood exposure process.

During the e-beam patterning process, charging of the resist can be problematic [21, 22]. The trapped charge and surface charge can deflect the path of the electron beam and result in image distortion as well as errors in level-to-level registration. To circumvent this problem, conducting materials which function as discharge layers are incorporated into resist systems as coatings above or below the imaging resist. Indium-tin-oxide films, amorphous carbon films produced by plasma chemical vapor deposition, and thin metal coatings can eliminate charging. However, these solutions are not ideal, since evaporative processes are needed to deposit the films. The actual conditions of evaporation may generate heat or stray

irradiation, degrading the lithographic performance of the resist. In addition, the subsequent removal of these layers is difficult if not impossible.

The conducting, water-soluble ammonium poly(p-styrenesulfonate) [23, 24] has also been reported as a charge dissipator for e-beam lithography. It has the advantage of ease of processability, since it can be spin applied. However, its conductivity is low, and thus its effectiveness at eliminating resist charging is marginal [25].

Intrinsically conducting polymers, particularly the soluble derivatives, are attractive alternative charge dissipators for e-beam lithography. These materials combine high conductivity with ease of processability. The first conducting polymer to be evaluated in this type of application is polyaniline. These materials are generally doped with protonic acids such as aqueous hydrochloric acid (HCl) to give a conductivity of the order of 1 S/cm [26, 27]. Polyanilines are the preferred conducting polymer system for many applications, since this family of polymers offers a number of advantages over other conducting polymers. They are generally soluble [28–32], environmentally stable polymers that are fabricated by a one-step synthesis involving inexpensive raw materials [33]. They offer extensive chemical versatility, allowing the properties of the polymer to be tuned to more appropriately meet the needs of a given application. Indeed, many polyaniline derivatives exist today as a result of chemical modification of their polymer backbone [34–40], the introduction of dopant [32, 41–44], or changes in their oxidation state [45, 46].

When polyaniline was first evaluated as an e-beam discharge layer, the polymer was incorporated into a multilayer resist system (Fig. 8.5) as a conducting interlayer between the imaging resist and a planarizing underlayer. It has been demonstrated that polyaniline is very effective at eliminating resist charging, even though it is used as a thin interlayer between thick insulating layers in this nongrounded configuration; however, the silicon wafer substrate is grounded with connections made at the top and bottom surfaces of the wafer. The polyaniline functions by bleeding off charges from the resist and preventing charge build-up in the resist layer, which otherwise deflects the e-beam and creates placement errors.

In this first evaluation of polyaniline as a charge dissipator in resist systems, the polymer was processed in two steps. The base form of the polyaniline, which is generally the more soluble, was first spin -applied onto a surface. The sample was then converted in to the conducting form by dipping it into an aqueous acid solution. The doping reaction takes several hours to ensure the diffusion of the dopant into the bulk of the film. This process is not desirable because it increases the number of steps and prolongs the exposure of substrates to acid solutions, posing contamination, reliability, and corrosion concerns.

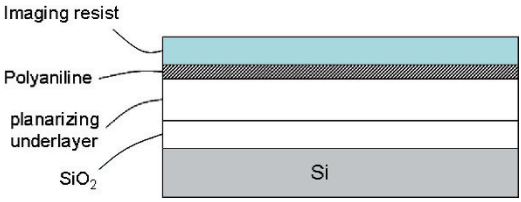

Fig. 8.5. Multilayer photoresist system incorporating polyaniline as a conducting interlayer

In a subsequent study [47], a simplified one-step process for applying the polyaniline to resist systems was reported. A method of inducing the doping in situ in the polymer was developed, thereby eliminating the need for external acid solutions. This was accomplished by incorporating salts in the polymer which would decompose upon irradiation or thermal treatment to generate the active dopant species, i.e., a protonic acid, in situ in the material [47–49].

In the studies described thus far, the polyaniline is incorporated below the imaging resist. In these systems, once the resist is exposed and developed, the polyaniline remains in the open areas, as shown in Fig. 8.6a. To transfer the pattern to the underlying substrate, the exposed polyaniline is removed by reactive ion etching (RIE) with oxygen.

Although the method of utilizing polyaniline below the resist works quite well, an easier and more optimum approach is to apply the conducting layer on top of the resist and to have the conductor removed simultaneously with the development of the resist. This configuration and process are depicted in Fig. 8.6b. Because the conductor in this case is applied directly on the resist, it must meet certain requirements. First, the solvent used to coat the conducting polymer must not dissolve the resist nor induce any interfacial problems. The conducting polymer must not degrade the lithographic performance of the resist. It should not introduce any contamination. In addition, it should be cleanly removed, and if possible, during the development of the resist. Since most resists currently used in the industry are developed in aqueous systems, the conducting polymer must be soluble in these systems.

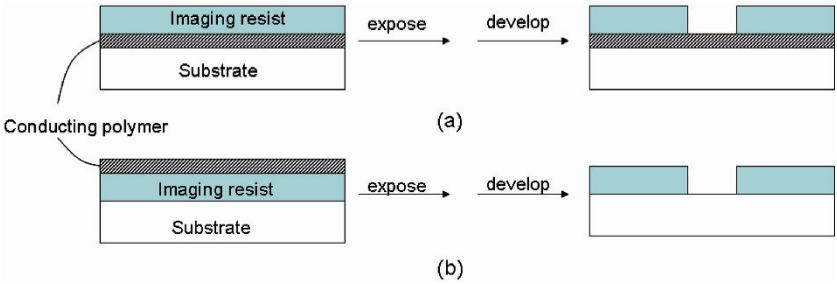

Fig. 8.6. (**a**) Multilayer resist structure incorporating polyaniline as an interlayer. After resist is exposed and developed, polyaniline remains in open areas. Etching of polyaniline is required to transfer image. (**b**) Multilayer resist structure in which the conducting polymer is applied as a topcoat discharge layer. The conducting polymer is removed during resist develop

In recent years, a number of polyaniline derivatives have been developed which are soluble in the conducting form. A few of these derivatives are soluble in water [34, 44, 50, 51]. One method of introducing water solubility has been the incorporation of sulfonate groups onto the polymer backbone.

Another conducting polymer that has been of interest for charge dissipation in e-beam lithography is the water-soluble, self-doped polythiophenes such as the sulfonated derivatives [52–54].

As the microelectronics industry continues to move toward increased circuit density, with a continuous decrease in device geometries, higher precision in e-beam writing will be required. Any surface charge on the resist can reduce the precision of the writing. Thus, discharge layers will probably be necessary in the future. The water-soluble conducting polymers have been shown to offer not only an effective approach to eliminating resist charging, but also much simpler processing than do currently used materials such as metal coatings.

8.2.1.3 Conducting Resists

In the applications discussed in the previous sections, the conducting polymers function as added charge-dissipative layers which are subsequently removed. The resists which are used to delineate the circuitry patterns are insulators. If the resists were conducting, there would be no need for an additional dissipative layer – only one polymer coating would be necessary. A sensitive, high-resolution, water-developable conducting resist would offer significant process simplification.

Recently there has been considerable effort on developing conducting resists. The first report [48] of such a polymer was based on the radiation-induced doping of the unsubstituted polyaniline base with onium salts. These salts have been shown to decompose readily upon irradiation to generate protonic acids. The polyaniline and the onium salt (e.g., triphenylsulfonium hexafluoroantimonate) are dissolved in *N*-methylpryolidone (NMP) and processed into a film. Upon exposure of the film to ultraviolet radiation or to an e-beam, the generated acid dopes the polymer. Since the doped polymer is no longer soluble, a solubility difference is created between exposed and unexposed regions. Thus, a negative conducting resist developed in a mixture of NMP/diglyme was attained [47–49]. Using an e-beam, 0.25-mm-wide conducting lines in a 0.25-mm-thick film.

A water-developable, negative conducting resist was more recently reported [44]. Cross-linkable functionality was incorporated into the polyaniline backbone so that, upon e-beam irradiation, the polyaniline cross-linked and became water-insoluble. Images of conducting lines 1.0 mm wide in a 0.75-mm-thick film, which were patterned with an e-beam at a dose of 200 mC/cm^2, were then developed with water (Fig. 8.7). Lines of 250 nm wide were also delineated. This resist is quite promising because it is a water-developable conducting resist, but its lithographic performance requires significant improvement. Much higher sensitivity and resolution are required.

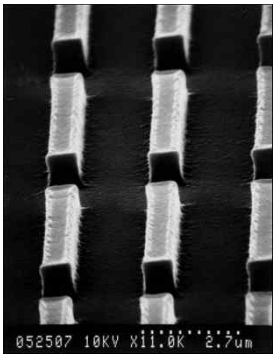

Fig. 8.7. Conducting polyaniline lines (1.0 μm wide) in a 0.75 μm thick film patterned with a e-beam irradiation [44]

Conducting resists have also been reported with polythiophenes. One of the first examples [55, 56] was based on poly(3-octylthiophene) (P3OT). The nondoped form of the polymer was combined with a cross-linking

reagent, ethylene 1,2-bis(4-azido-2,3,5,6-tetrafluorobenzoate). Upon exposure to deep UV, cross-linking through the octyl side chain was induced. This system cross-linked upon e-beam irradiation as well. In addition, the polymer without the cross-linker was also noted to cross-link with e-beam irradiation.

An extension of the substituted thiophene work involved the incorporation of methacrylate functionality onto the thiophene backbone [57]. Methacrylates are widely known to undergo free-radical polymerizations. Poly(3-2-(methacryloyloxyethyl)thiophene) and copolymers with other substituted thiophenes with the basic structure depicted as Fig. 8.8 were synthesized. The polymers undergo cross-linking through the methacrylate side chains upon irradiation. Negative images developed in organic solvents were obtained, and 3-mm-wide lines in a 75-nm-thick film were written. The resist had good sensitivity (14 mJ/cm^2) at a wavelength of 313 nm [57]. In this system, as in the previous polythiophene examples, the imaged patterns must subsequently be doped to make the patterns conducting.

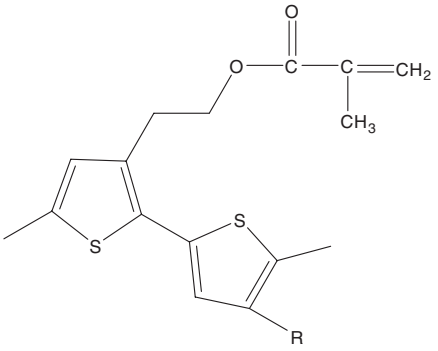

Fig. 8.8. Polythiophene–methacrylate structure (from [57])

Methods of imaging conducting polymers either directly in the conducting form or in the precursor, nondoped form have been developed. These methods are appropriate in applications in which the conducting polymer must be patterned to a certain geometry. However, for these imageable conducting polymer methods to be utilized in lithography, the lithographic performance of the conducting resists must be improved, because they are currently not competitive with conventional resists in terms of resolution, sensitivity, and contrast. Further work in this area is required to bring the conducting polymer-based resists closer in performance to conventional resists.

8.3 Metallization

In microelectronics, the term metallization generally refers to a patterned film of conducting material deposited on a substrate to form interconnections between electronic components. Over the last few years, conducting polymers have been demonstrated to provide a new route to metallization, particularly in printed circuit board (PCB) technology [58, 59]. In general, conducting polymers can be utilized for both electrolytic and electroless metallization. The conducting polymers that have been of interest in this area include polyaniline, polypyrrole, and polythiophene.

The complexity of PCBs [60–62] varies from single-sided boards, where circuitry is found on only one side, to double-sided boards, to boards comprising multiple layers of circuitry. The degree of complexity depends on the specific interconnection requirements for a given product. Connections between the two sides of a board and layer-to-layer connections are made with copper-plated throughholes (PTHs), allowing greater circuit density because they provide cross-over capability. A circuit crosses over another by simply entering a PTH, continuing on the other side, and so on.

The through holes are drilled into the laminate substrate and are then copper-plated. Figure 8.9 depicts two common metallization schemes for PCBs [60–62]. In one method (Fig. 8.9a), a conducting "strike" layer (generally a thin layer of copper) is deposited by electroless plating. This copper layer renders the surface sufficiently conducting to allow a thicker copper layer to be electrolytically deposited in selected regions defined by a photoresist process. In an alternate method (Fig. 8.9 b), an all-electroless process is used. The current processes have certain disadvantages. Electroless deposition requires the use of expensive noble metal salts, such as $PdCl_2$, as seeds. The salts are applied to the PCB surface followed by reduction of the noble metal to the zero-valent state. The zero-valent noble metal particles are the active sites for heterogeneous copper reduction in electroless plating.

Electroless baths are generally unstable and require close monitoring. The baths can fluctuate between being too stable, resulting in PTH voids, and being too active, resulting in homogeneous decomposition of the bath. Formaldehyde, the most commonly used reducing agent in electroless baths, is toxic and poses environmental concerns.

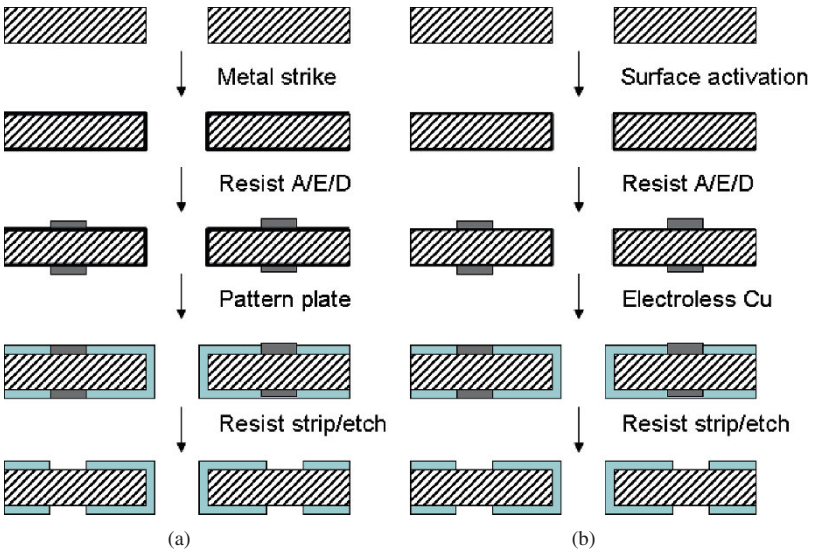

Fig. 8.9. Two types of metallization schemes for PCBs: (**a**) Initial conducting strike layer deposition followed by electrolytic pattern plating; (**b**) All-electroless process. A/E/P stands for application, exposure, and development

An alternative to current methods is the use of a conducting polymer as an electrode for direct electrolytic metallization of copper. In one study [58], a PCB was coated with a 1 μm-thick layer of polyaniline applied from an aqueous acetic acid solution. The polyaniline-coated board was electrolytically copper plated. The copper started to plate on the hole wall from the two contact sides and grew inward until the copper front met at the center of the hole wall. As the plating process continued, a thicker, uniform copper coating was deposited on the polyaniline surface (Fig. 8.10). Today, as a result of the many soluble polyaniline derivatives that have been developed, a variety of solvents including water can be used to apply the polymer.

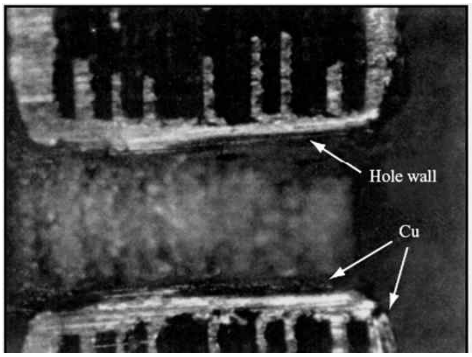

Fig. 8.10. Micrograph depicting a cross-section of a polyaniline through hole that has a continuous copper deposit (from [58])

Another variation to the use of conducting polymers for metallization was based on spontaneous noble metal deposition induced by a conducting polymer [58]. It was found that polyaniline can spontaneously reduce noble metal ions such as Pd^{+} and Ag^{1+} to their zero-valent state upon immersion of the polymer in an aqueous solution of the corresponding metal salt. Thin films of Pd and Ag deposit on the polymer surface without an external reducing agent. While this approach does not preclude the use of a precious metal, it does eliminate the need for subsequent activation of the metal. The Pd-coated polyaniline can be used for subsequent electrolytic as well as electroless metallization.

It should be pointed out that the use of imageable conducting polymers described in the previous section is applicable to metallization. A conducting polymer could be applied to the circuit board surface and directly imaged, thereby eliminating an additional photoresist process. Electroplating could then occur selectively on the patterned conducting polymer.

8.4 Corrosion Protection of Metals

Metals such as copper (Cu) and silver (Ag) are widely used in microelectronics for wiring and EMI shielding. They readily corrode in a variety of ambients [63–66]. In oxygen-saturated water, Ag and Cu dissolve with a measurable corrosion rate of about 0.002 and 0.2 nm/min, as determined from the potentiodynamic polarization curves [64, 65, 67]. In the presence of an applied potential and humidity, these metals dissolve from the more electrically positive metallic part of the device and plate at the more negative part as dendrites, which can cause shorts. In addition, with increasing line density and decreasing dimensions, ion accumulation alone without

dendrite formation can destroy the designed electrical performance of the product. Inhibitors such as benzotriazole (BTA), a common used organic soldering preservative (OSP) on PCB, provide excellent corrosion protection for Cu and Ag metals. However, these azole-type inhibitors do not provide protection at high temperature (i.e., in a soldering application), nor do they protect against an applied potential [64, 65]. Therefore, new materials are needed to protect Ag and Cu against corrosion and dissolution, particularly at high temperatures and in the presence of an applied potential.

For more than a decade, the use of polyaniline for corrosion protection of metals, such as stainless steel, has been investigated. In the first study by DeBerry [68], polyaniline was electrochemically deposited on ferritic stainless steels and was found to provide anodic protection that significantly reduced corrosion rates in acid solutions. Numerous studies since then have confirmed the corrosion-protective properties of polyanilines [67, 69–73].

Non-electrochemical methods of applying polyaniline have been demonstrated. In one recent study, dispersions based on doped polyaniline passivated mild steel, stainless steel, and copper [71].

The use of polyaniline to protect Cu and Ag at high temperature and under an applied potential, which is of interest to the microelectronics industry, was extensively studied by Brusic et al. [64, 65, 67]. A number of soluble polyanilines were evaluated in both the nondoped and doped forms. These materials were tested by two procedures which were designed to closely simulate conditions to which these metals may be exposed during actual use in an electronic product (as in, for example, a PCB). In most cases, the corrosive environment would vary depending on the relative humidity, i.e., the amount of adsorbed water on the surface.

Soluble poly-o-phenetidine, particularly in the nondoped form, which is highly soluble in a variety of organic solvents, was found to provide excellent protection for Cu and Ag and was superior to the unsubstituted polyaniline base. Homogeneous and adherent films 184, 339, and 477 nm thick were spin applied onto Ag and Cu surfaces from an NMP or gamma-butyrolactone solution and evaluated. Even the thinnest film provided a perfect barrier to oxygen, since the electrochemical data indicate no current dependence attributable to oxygen reduction. Oxygen reduction (generally the main cause of Cu and Ag corrosion) is completely inhibited. The anodic current metal dissolution is greatly reduced by a factor which increases with film thickness. The protection is substantial, especially at high potentials, where Cu dissolution is about four orders of magnitude lower than that measured on bare Cu. Similar results were observed with Ag.

In terms of dendrite formation, it was found that poly-o-phenetidine provided exceptional protection. Bare Cu and Ag were observed to form dendrites within seconds of an applied potential, as evidenced by shorting of the lines. BTA was found to be ineffective, since BTA protected metal lines formed dendrites within seconds as well. Metal lines that were coated with poly-o-phenetidine-base passivation did not form dendrites, even after 30 min of applied potential of 5 V. The coated lines were also tested at elevated temperature (220°C for 30 min); dendrites were not formed under these conditions. A temperature/humidity study was performed in which the poly-o-phenetidine-coated metal was stored for 1,000 h at 85°C and 80% relative humidity; again, no dendrites were observed. In a more drastic test, a 5-V potential was applied to the coated metal while at 85°C and at 80% relative humidity for 1,000 h. No failure was observed under these conditions as well.

The poly-o-phenetidine provides excellent corrosion protection for Cu and Ag at elevated temperatures as well as under an applied potential. The superior protection offered by this polyaniline derivative may stem from its excellent coverage and adhesion to the metal surface. It has good solubility and forms very uniform films. In addition, the ethoxy group can complex with the metal and enhance its adhesion characteristics. Indeed, peel test results show adhesion strength in excess of 60 g/mm [67]. Generally, values greater than 50 g/mm for polymer-to-metal adhesion are considered to be excellent.

8.5 Electrostatic Discharge (ESD) Protection for Electronic Components

Electrostatic charge (ESC) and electrostatic discharge (ESD) constitute a serious and expensive problem for many industries – in particular for microelectronics [74]. It has been estimated that $15 billion a year is attributed by the US electronics industry to ESD damage alone.

Electrostatic charge can accumulate to thousands of volts. The static charge can attract airborne particles, as is often observed on cathode ray tubes (CRTs). This becomes a significant contamination concern if particles are attracted to critical surfaces such as device wafers. The accumulated charge will eventually discharge in the form of a “lightning bolt” which can destroy devices on ICs. As IC circuit density continues to increase and the area and thickness of the active device elements continue to shrink, device sensitivity to the destructive effects of ESD will continue to increase.

To protect devices against ESC and ESD, conducting materials are used extensively in clean rooms during their manufacture. In addition, conductors are incorporated into plastic packages which are used to transport sensitive electronic components such as chips, modules, and PCBs. The materials currently used include ionic conductors, carbon- or metal-filled resins, and, in certain cases, metal coatings. The use of ionic conductors is not a reliable method for ESD protection. Electrical conductors, on the other hand, are stable systems with conductivities that are not humidity dependent. However, the use of these materials is a more expensive alternative. Carbon-filled systems pose contamination concerns because of sloughing of the carbon particles. In addition, relatively high loading levels are required to attain a given level of conductivity. Such high loading can degrade the mechanical/physical properties of the host polymer. With high loadings, recyclability of the plastic carriers becomes more difficult.

Conducting polymers offer a new alternative for ESD protection, with numerous advantages over current materials. The conductivity of such polymers can be tuned, can easily meet the high end of the dissipative range, and is stable in comparison to ionic conductors. By appropriate design of the conducting polymer, contamination concerns can be eliminated. In addition, conducting polymers can offer a high degree of transparency. Polyaniline, polypyrrole, and, more recently, polythiophene have been the predominant conducting polymers of interest for ESD protection. These polymers have been used as fillers in a number of host resins. In addition, coating formulations have been developed which can be applied directly onto plastic surfaces.

Pyrrole has been in situ polymerized onto the surface of textile fabrics [75, 76]. Polyaniline in the form of a dispersible powder has been blended with a number of thermoplastic and thermoset resins, resulting in blends which have excellent ESD properties [77–80]. Soluble polyanilines have also been blended with appropriate polymers [81, 82]. In the latter systems, very low loadings have been reported to be necessary to reach a certain level of conductivity.

8.6 Field-Effect Transistors (FET)

The field-effect transistor (FET) is a type of transistor that relies on an electric field to control the shape and hence the conductivity of a “channel” of one type of charge carrier in a semiconductor material. FETs are sometimes called unipolar transistors to contrast their single-carrier-type operation with the dual-carrier-type operation of bipolar (junction)

transistors (BJT). An organic field-effect transistor (OFET) is a field-effect transistor using an organic semiconductor (such as conducting polymers) in its channel. OFETs can be prepared either by vacuum evaporation of small molecules, or by solution-casting of polymers or small molecules. These devices have been developed to realize low-cost, large-area electronic products.

Xue et al. [83] fabricated two polymer field-effect transistors (FET) fabricated by both spin-coating and ink-jet-printing techniques using conducting polymer polypyrrole (PPy) as a semiconductor material. These thin film polymer field-effect transistors operate in the depletion mode. The measured turn-off threshold voltage is around 20 V for both the spin-coated and ink-jet-printed PPy FET transistors. The device performance of the spin-coated transistors is slightly better than that of the ink-jet printed transistors. This is mainly due to high surface roughness of the printed polymer film and printed dot boundaries, leading to low charge carrier mobility in the printed polymer FET transistors.

Covington et al. [84] demonstrated the fabrication of polymer FET for gas sensor applications. The development of ultra-low power CMOS compatible gas sensors has been the goal of many research groups for a number of years. Such sensors benefit from both a low fabrication cost and an ease of integration with any associated transducer or signal processing circuitry. A sensor with these attributes consists of a conducting polymer gate which operates at ambient temperature. Both electrochemically deposited and polymer composite materials have been deposited to form the gate electrode of an n-channel enhanced MOSFET (ECFET and PCFET, respectively). The authors presented the first full characterization of these sensors in terms of their response to pulses of ethanol and toluene vapor in air. In addition, environmental effects of temperature and humidity on both the baseline signal (i.e., zero vapor) and vapor response were investigated. The PCFET and ECFET vapor sensitivities (operating at constant current) were found to be up to 5.5 μV/ppm and –2.3 μV/ppm for toluene and 0.6 μV/ppm and 4.5 μV/ppm for ethanol, respectively. The relative selectivity of the sensors was observed to be up to 564 for these two organics, with an observed sign change with certain polymers. In addition, the detection limits were estimated to be below 1 ppm of toluene and ethanol vapor in air.

Ashizawa et al. [85] fabricated a metal–insulator–semiconductor field-effect transistor (MISFET) using poly(3,4-ethylenedioxythiophene) doped with poly(4-styrenesulfonate) as an active channel by multiple line patterning, one of the most simple, rapid, and inexpensive methods capable of making patterns of conducting polymers, insulators, and metals using a standard laser printer. The MISFET operated both in the depletion

and enhancement modes in response to positive and negative gate voltages, respectively, where the gate current was crucial to the performance of the device. Furthermore, a novel device, metal–semiconductor field-effect transistor (MESFET) using a Schottky barrier formed at the interface between aluminum and PEDOT/PSS instead of the polymer insulator was fabricated.

Liu et al. [86] fabricated an all-polymer field-effect transistor (FET) using an ink-jet printing technique. Poly(3,4-ethylenedioxythiophene) works as the source/drain/gate electrode material because of its good conductivity. Polypyrrole acts as the semiconducting layer. Poly(vinyl pyrrolidone), an insulating polymer with a dielectric constant of 60, operates as the dielectric layer. All the polymers were diluted with deionized water and printed with a piezoelectric ink-jet printing system. It was shown that the fabricated device functions at a depletion mode with low operation voltage and has a field-effect mobility of 0.1 $cm^2 \cdot V^{-1} \cdot s^{-1}$, an on/off ratio of 2.9×10^3, and a sub-threshold slope of 2.81 $V \cdot decade^{-1}$.

8.7 Sensors

The electronic nose was developed in order to mimic human olfaction that functions as a non-separative mechanism, i.e., an odor/flavor is perceived as a global fingerprint. Electronic noses include three major parts: a sample delivery system, a detection system, and a computing system.

The sample delivery system enables the generation of the headspace (volatile compounds) of a sample, which is the fraction analyzed. The system then injects this headspace into the detection system of the electronic nose. The sample delivery system is essential to guarantee constant operating conditions.

The detection system, which consists of a sensor set, is the "reactive" part of the instrument. When in contact with volatile compounds, the sensors react, which means they experience a change of electrical properties. Each sensor is sensitive to all volatile molecules but each in their specific way. Most electronic noses use sensor arrays that react to volatile compounds on contact: the adsorption of volatile compounds on the sensor surface causes a physical change of the sensor. A specific response is recorded by the electronic interface transforming the signal into a digital value. Recorded data are then computed based on statistical models.

The more commonly used sensors include metal-oxide semiconductors (MOS), conducting polymers (CP), quartz crystal microbalance (QCM), surface acoustic wave (SAW), and field-effect transistors (MOSFET).

The physical properties of conducting polymers strongly depend on their doping levels. Fortunately, the doping levels of conducting polymers can be easily changed by chemical reactions with many analytes at room temperature, and this provides a simple technique to detect the analytes. Most of the conducting polymers are doped/undoped by redox reactions; therefore, their doping level can be altered by transferring electrons from or to the analytes. Electron transferring can cause the changes in resistance and work function of the sensing material. The work function of a conducting polymer is defined as the minimal energy needed to remove an electron from bulk to vacuum energy level. This process occurred when PPy, PTh, and in some cases PAni films were exposed in NH_3, NO_2, I_2, H_2S, and other redox-active gases [87–95]. Electron acceptors, such as NO_2 and I_2, can remove electrons from the aromatic rings of conducting polymers. When this occurs at a p-type conducting polymer, the doping level as well as the electric conductance of the conducting polymer is enhanced. An opposite process will occur when detecting an electrodonating gas. However, this mechanism has not been understood clearly. Except for the pure redox reactions, partial charge transferring also leads to an alternation in the conductivity of a conducting polymer [96]. In some cases, a catalyst incorporated in to the conducting polymer film can help in detecting some inert analytes. Athawale et al. prepared nanocomposite of Pd/PAni and found its electrical resistance responses rapidly and reversibly in the presence of methanol [97].

8.7.1 Film Sensors

Bai et al. [7] reviewed the gas sensors fabricated by using conducting polymers such as polyaniline (PAni), polypyrrole (PPy), and poly (3,4-ethylenedioxythiophene) (PEDOT) as the active layers. The conducting polymer films were fabricated using electrochemical deposition, dip-coating, spin coating, etc. Various sensor configurations including chemiresistor and transistor and diode sensors were discussed. Figure 8.11 shows a common type of chemiresistor which can be fabricated through a cheap and convenient process. A chemiresistor is a resistor, whose electric resistance is sensitive to the chemical environment [84]. Two types of conducting polymer transistor, classified by whether the current flow through the polymer [98, 99], were used to detect gases as illustrated in Fig. 8.11. Figure 8.12a shows the configuration of a thin film transistor (TFT), whose active layer is made of conducting polymer, and Fig. 8.12b represents the structure of insulated gate field-effect transistor (IGFET), whose gate electrode is made of conducting polymer and the current flows through the other semiconducting layer, e. g. silicon.

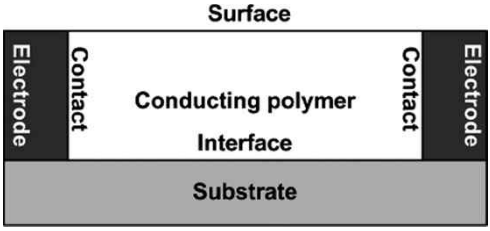

Fig. 8.11. Configuration of a chemiresistor

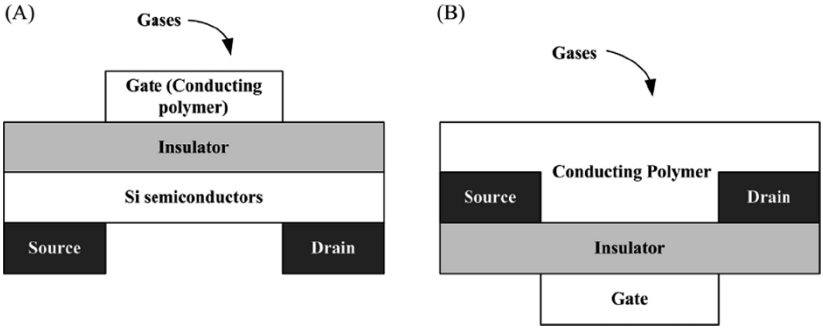

Fig. 8.12. Configuration of TFT (**A**) and IGFET (**B**)

Shrivas et al. [100] studied toxic gas sensing property by polyaniline thin film conducting polymer for ammonia gas. In this work, the precipitate of the conducting polymer has been synthesized by chemical method. The conducting polymer film which acts as an active layer of sensor was prepared with the help of the precipitate (of the conducting polymer) by spin-coating technique. The deposited films were characterized by FT-IR spectroscopy and four-probe method. The study indicates that the resistance of the film decreases with the increase in concentration of ammonia at the known volume.

8.7.2 Conducting Polymer Nanofibers for Gas Sensor

Conducting polymer nanofibers are promising one-dimensional nanostructured materials due to their chemical doping specificities, adjustable transport properties, large surface areas, light weights, low cost, easy processing, and scalable productions. The nanofibrillar morphology

significantly improves the performance of conducting polymer in many conventional applications involving polymer interactions with its environment. This leads to much faster and more responsive chemical sensors. Such nanostructured materials are very promising in applications including chemical sensors [98, 101, 102], biosensing [103], nanoelectronics, catalysis, and scaffolds for tissue engineering.

Wei et al. [104] developed a template-free solution method in which the diameter of the tube could be controlled by the dopant functionality and amount. Zhang et al. [105] described a nanofiber seeding method for synthesizing bulk quantities of nanofibers of PAni. Furthermore, Chiou et al. [106] reported a simple and scalable approach to produce polyaniline nanofibers in dilute chemical polymerization without the aid of specific templates. The high quality, small diameter PAni nanofibers were produced in large quantities.

Huang et al. [107, 108] recently developed two facile approaches–interfacial polymerization and rapidly mixed reactions–that readily produce high-quality nanofibers (Fig. 8.13). In a typical PAni chemiresistor, a thin film of PAni is coated (usually by spin coating or drop casting) on electrodes as the sensitive layer for chemical vapors. On exposure to chemical vapors, a change in the film resistance can be readily recorded by a computer-controlled circuit. The performance of such chemiresistors is determined by the interactions between vapor molecules and polymer. Poor diffusion of the vapor molecules can readily outweigh any improvements made to the polymer chains since most of the material other than the limited number of surface sites is unavailable for interacting with the vapor, thus degrading sensitivity. An immediate advantage of using nanofibers of PAni is that they shrink the diffusional path length for vapor molecules from the thickness of the film to the diameter of the nanofibers. For example, improvements in both sensitivity and time response of many orders of magnitude are now observed using the nanofibers [107, 109]. A great variety of chemical vapors including hydrochloric acid, ammonia, organic amines, hydrazine, chloroform, methanol, and hydrogen sulfide have been tested and categorized. Five different mechanisms have been elucidated [110]. For each mechanistic type, significantly enhanced performance of nanofiber films over conventional materials is observed. The three-dimensional open structure of the nanofiber films also leads to some novel sensing properties. For example, for conventional film sensors, the response is strongly affected by the film thickness; however, the response of the porous nanofiber films is essentially thickness independent [107, 109].

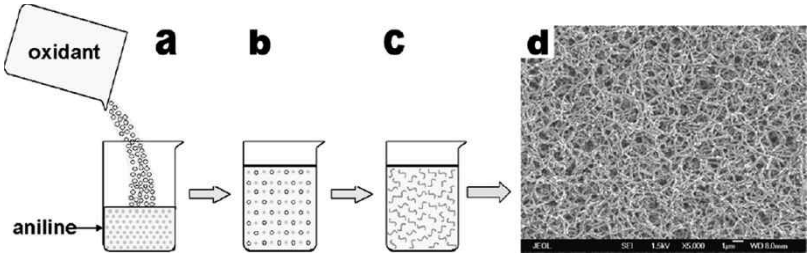

Fig. 8.13. Pure polyaniline nanofibers can also be made by rapidly mixed reactions. In a typical reaction: (**a**) the initiator and monomer solutions in 1 M HCl are rapidly mixed together all at once. Therefore (**b, c**) the initiator molecules are depleted during the formation of nanofibers, disabling further polymerization leading to overgrowth. (**d**) A typical scanning electron microscopy (SEM) image of nanofibers prepared in this manner (Adapted from ref. [111])

Cai et al. [112] synthesized nanostructured conducting polymers using dilute chemical polymerization method, a template-free approach, to obtain nanofibers of PAni. The aqueous solution of nanofibers shows a stable colloid dispersion, which is spread into an interdigitated electrode resulting a porous film for DC test; the film is also embed into a cavity element for RF analyzer. In the presence of specific chemical reagents, the conducting polymer materials will undergo conductivity changes to several orders of magnitude, which finally induce the change of film resistance and RF conductivity for sensing. The sensor response is strongly dependent upon the film morphology, porosity, and humidity. The devices show a quick response (i.e., less than 60 s in 100 ppm concentration) and are significantly sensitive to various chemical gases (e.g., HCl and NH_3) at the concentrations of 10–1000 ppm. Such novel emerging chemoresistive RF technology will potentially open the challenge for the remote wireless detection of explosives and other chemical agents.

8.7.3. Biosensor

A basic requirement for a chemical or biological sensor is to convert a molecular binding event into a measurable signal. Conducting polymers are attractive for sensor applications because they can directly convert the binding event into an electrical signal. In addition they can be modified chemically with appropriate functional groups for specific recognition and detection of different analytes and scaled all the way down to the nanoscale or even a single-molecule dimension, which provides one with a unique opportunity to study molecular binding events on the nanoscale. Because of these unique properties, many groups have applied conducting polymers to chemical and biosensors [113–115].

Forzani et al. [116] presented different chemical sensor applications based on nanoscale functionalized conducting polymer junction arrays. Each junction is formed by bridging a pair of gold electrodes separated with a small gap 20–60 nm with polyanilines or PEDOT functionalized with enzymes, oligopeptides, or oligonucleotides for detection of glucose, heavy metal ions, nerve agent simulants, or RNA sequences (Fig. 8.14). When an analyte binds the polymer nanojunction modified with the selective recognizing element, it induces a change in the conductance via changes in polymer conformation, local pH, or charge distribution. Unique features of the nanojunction array sensors include:

(1) By reducing the junctions down to nanoscale, the conductance of even a poorly conductive polymer is measurable. This is important because a polymer is often much less conductive once a molecular probe is attached to it, which makes the conductance measurement difficult if one uses films or micron-scale junctions. This is also significant for polymers, e.g., polyaniline that are poorly conductive under physiological conditions near neutral pH.

(2) The nanojunctions have a large surface to volume ratio which rises to extremely high sensitivity and fast response time.

(3) The reduced dimension requires only small amounts of probes and samples and promises a highly integrated device.

(4) When oligopeptides are used as probes, the number of different oligopeptides that can be attached is virtually unlimited by choosing different amino acid sequences which allows one to tune the specificity of the sensor via the combinatorial chemistry approach.

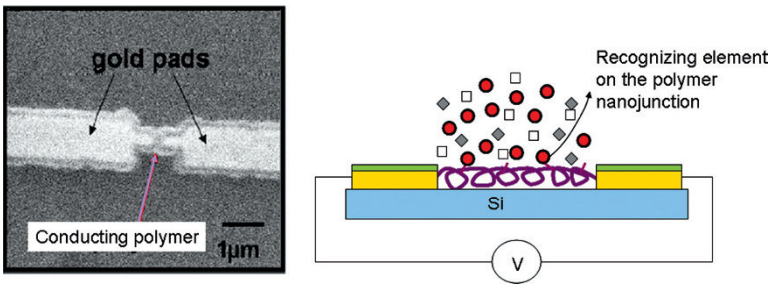

Fig. 8.14. SEM image of a polymer nanojunction and schematic of a recognizing element-modified polymer nanojunction for sensing applications (from [116])

A critical step in the development of biosensors based on ICPs is achieving the immobilization of biological molecules without a significant change in their properties. In the case of DNA immobilization, widely used methods are electrostatic entrapment [117, 118] and covalent attachment [119–121]. Polypyrrole and polythiophene are commonly used ICPs for DNA sensor preparation. Garnier et al. developed a process of functionalizing a conjugated polymer which involves the preparation of a precursor polymer film bearing a leaving group, such as an activated ester, at its 3-position, which can be substituted by an appropriate functional group [122]. Other different functionalized pyrrole and thiophene monomers were used in the preparation of DNA sensors [123–125]. Recently, Peng et al. [126] prepared DNA sensors based on functionalized polypyrrole and polythiophene films and their performances were studied by electrochemical impedance spectroscopy (EIS). Conducting polymers of functionalized monomers of PAA, PPDA, and 3-((2′:2″,5″:2‴-terthiophene)-3′′-yl) acrylic acid (TAA) were synthesized for this purpose. The results implied that polypyrrole functionalized with longer unsaturated carbon side chains provides better DNA-sensing properties. The sensor based on poly(TAA) shows a qualitatively different response compared with polypyrrole sensors. It was shown that this difference was caused by differences in dominant ion movement at the interface of film and electrolyte.

8.7.4 Chemical Sensor

Li et al. [127] studied the sensors based on arrays of regioregular polythiophenes (rr-PTs), which has an air-stable conducting property that makes them suitable as chemiresistive sensing materials. Their solubility in a variety of organic solvents also enables them to be ink-jet printed for device fabrication; chemiresistors were demonstrated to be viable options for detection and discrimination of volatile organic compounds (VOCs). The family of rr-PT-based conductive polymers and copolymers with various side chains and end groups were synthesized and tested. Their responses showed a variety of distinct new patterns that might significantly enhance sensor discrimination capability between VOCs. Possible sensing mechanisms and interactions between the VOC vapors and the variety of rr-PT chemistries that might account for the observed electrical property changes were described. This work provides the foundation for further research and development to design chemical structures to optimally respond to a given analyte.

8.8 Microfluid Pump

Methods for manipulation of fluid in the micro-scale are widely used in areas ranging from chemistry, biology to materials science. For a microfluidic analytical system, the main function is to provide a manifold of interconnecting channels to control the reagent/sample delivery and analyte detection within a single integrated platform. The basic building blocks consist of channels in which the fluid flows, valves which control the direction of flow, and one or more pumps that provide the driving force to move the fluid. Numerous microfluidic devices such as microfluidic chips, flow sensors, microvalves, and micropumps have been reported [128, 129].

For driving the liquid movement, well-known methods include piezoelectric [130], thermopneumatic [131], electrostatic [132], and electromagnetic actuation [133]. Besides the mechanically driven reciprocating micropump, there are continuous flow-type micro-pumps based on electro-osmosis (EO), electrohydrodynamics (EHD), and magnetichydrodynamics (MHD). While there are many micropump designs available for micro-nano-scale liquid delivery, they generally require high operation voltages and high running current and therefore are very power hungry [134–138].

Kim et al. [139] reported the development of a micropump for small-volume fluid delivery. The pump has small size and low power, and potentially can be easily integrated into microfluidic devices for, e.g., lab-on-a-chip applications. This design employs polypyrrole (PPy) as the electrochemical actuator to produce the mechanical movements required for the pumping action.

Figure 8.15 illustrates the typical configuration of such a micropump which is composed of a sealed pump chamber, a diaphragm, and check valves for controlling fluid inlet and outlet. Reciprocating movement of the diaphragm generates a two-mode pump cycle that results in a periodic volume change that creates positive and negative pressures in the pump chamber. During the prime mode, a negative pressure is generated by the upward movement of the diaphragm to close the outlet check valve and lift the inlet check valve to suck fluid into the pump chamber. During the following pump mode, the downward diaphragm movement generates positive pressure to force the inlet check valve to close and push the outlet check valve to open and excrete fluid into the outlet. Hence, the actuator diaphragm provides driving force for the fluid movement and the check valves at the inlet and outlet direct the flow to create a continuous flow in one specific direction.

The diaphragm employed was a conductive polymer membrane/ polydimethylsiloxane (PDMS) bilayer membrane which can be electro-

chemically actuated to provide the mechanical movements. Inherently conductive polymers such as polypyrrole (PPy) undergo reversible volume change during electrochemical redox reactions as a result of insertion/removal of either dopant ions or the solvated counterions that are present in the immediate environment to maintain electrical balance [140]. When specific voltages are applied alternatively across the PPy membrane, the membrane deforms to a convex and concave form to drive the diaphragm to perform continuous push and pull actions. This bending-type actuator produces large deformations, but the generated pressure is relatively small compared to a conventional solenoid pump. For this reason, custom-designed check valves were fabricated that would operate effectively at low actuation pressures. It was demonstrated that the fabricated actuator pump was capable of producing a maximum flow rate of 52 μL/min and a nominal minimum flow rate of 18 μL/min when operated at ±1.5 V power supply. The back pressure it generates is 11mBar. This device consumes very low power, 55 mW/stroke.

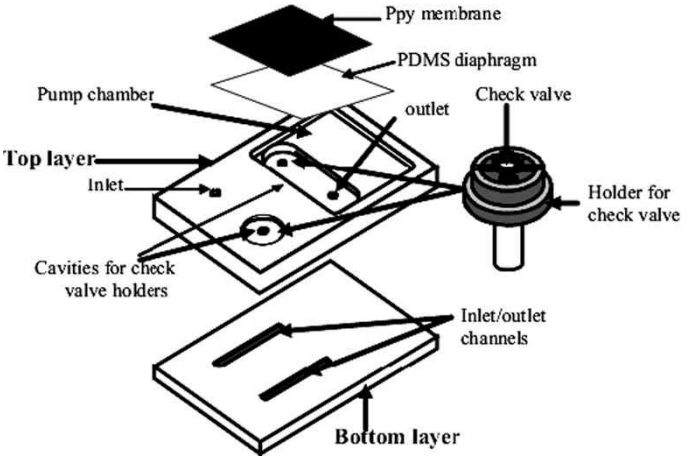

Fig. 8.15. Scheme of the pump assembly (from [139])

Wu et al. [140] developed a low voltage fluid movement system for microfluidic channels utilizing the electromechanical actuation properties of polypyrrole. A confined concentric arrangement of polypyrrole actuators is used to induce fluid movement through an inner channel in a single unit. Series connection of these units and appropriate electrical connection/

stimulation induces a novel peristaltic action that enables fluids to be pumped in a predetermined direction. Flow rates of up to 2.5 μl/min can be achieved against a back pressure of 50 mbar, which is sufficient to enable fluid movement in a glass capillary channel (diameter: 266 μm, length: 12.8 cm). The mechanism of fluid movement enables the use of low voltage devices (1 V) to drive fluid with an average power requirement of 8.7 mW.

8.9. Shielding of Electromagnetic Interference (EMI)

EMI (electromagnetic interference) can be defined as spurious voltages and currents induced in electronic circuitry by external sources. In recent years, EMI problem or electromagnetic pollution has received wide attention because of the malfunctioning of the electronic equipments from the radiations generated from the source or emanating from other electronic equipments. Research in the past decade has established the ability of polymer composites made with electrically conducting polymers to be suitable as a shield against the electromagnetic interference [77, 141–144].

So far conducting composites were made by adding metallic fillers, C-black, or metallic powders. However because of certain disadvantages like labour intensity, relatively high cost, and time consumption besides the galvanic corrosion phenomenon observed when dissimilar metals are joined, conducting polymer composites were being made which were found suitable for EMI shielding and for the dissipation of electrostatic charge.

Conducting polyaniline forms an important family of electronic polymers with a developed potential application for a number of areas because of their flexible chemistry, processibility, environmental stability, and ease of forming composites. The electromagnetic interference shielding effectiveness of conducting polyaniline (PANI) – ABS composites was studied at 101 GHz. It was observed that shielding effectiveness of the PANI–ABS composites increases with the increase in the loading levels of the conducting polymer doped with hybrid dopants. The lower loading of PANI doped with hybrid dopants in the molded conducting composites can be effectively used for the dissipation of electrostatic charge. However, with higher loadings, a shielding effectiveness of 60 dB has been achieved which makes the conducting composites a potential EMI shielding material for its application in encapsulation of electronic equipments in electronic and in high tech applications.

Koul et al. [145] studied the electromagnetic interference shielding effectiveness of conducting PANI–ABS composites at 101 GHz. It was observed that shielding effectiveness of the composites increases with the increase in the loading levels of the conducting polymer doped with hybrid dopants. The lower loading of PAni doped with hybrid dopants in the moulded conducting composites can be effectively used for the dissipation of electrostatic charge. However, with higher loadings, a shielding effectiveness of 60 dB has been achieved which makes the conducting composites a potential EMI shielding material for its application in encapsulation of electronic equipments in electronic and in high tech applications.

Kim et al. [146] prepared intrinsically conducting polymer(ICP)/PET textile composites by chemical and electrochemical polymerization of ICP on a PET fabric in sequence, and investigated the effects of the chemical or electrochemical polymerization conditions on the properties of resulting composites such as electrical conductivity and electromagnetic interference shielding effectiveness (EMI SE). The ICP/PET composite prepared in this study was highly electrically conducting, showing 0.3 Ω-cm of the specific volume resistivity and about 35 dB of EMI SE (shielding efficiency) over a wide frequency range.

ICPs are new alternative candidates for EMI shielding applications due to their lightweight, corrosion resistance, ease of processing, and tunable conductivities when compared with typical metals. More importantly, the dominant shielding characteristic of absorption other than that of reflection for metals render ICPs more promising materials in applications requiring not only high EMI shielding effectiveness but also shielding by absorption, such as in stealth technology [147].

8.10 Nanofiber-Based Nanocomposites And Devices

Owing to the redox-active nature of polyaniline, metal nanoparticles can be deposited on polyaniline nanofibers through a direct reaction between polyaniline nanofibers and oxidizing metal ions, such as Au^{3+} and Ag^{+} [108]. The nanofibers can serve as a template to guide the growth of metal nanoparticles and/or confine them in the polymer matrix [108]. The uniform diameters of the nanofibers lead to relatively narrow size distributions of the metal nanoparticles. For example, treating de-doped polyaniline nanofibers with a 10 mM $AgNO_3$ solution at room temperature (~25°C) readily yields Ag nanoparticle-decorated nanofibers in a dot-ON-fiber fashion (Fig. 8.16b). When the same reaction was refluxed in water at ~100°C, three morphologies – dot-ON-fiber, dot-IN-

fiber, and silver shells on nanofibers – were obtained (Fig. 8.16c, d). This can be explained by understanding the diffusion and chemical processes occurring during the reaction (Fig. 8.16a). At reflux temperature, the rates of both the reduction reaction with polyaniline and the diffusion of Ag^{+} into the nanofibers are enhanced; hence, some Ag+ may be forced into the nanofibers before the reaction is complete. Therefore, both dot-ON-fiber and dot-IN-fiber structures are obtained. The Ag nanoparticles outside the nanofiber can merge into neighboring particles and form a continuous shell on the nanofiber due to Ostwald ripening. Under properly designed reaction conditions, it should be possible to have either the diffusion or the reaction overwhelm the other, leading to pure dot-ON-fiber or dot-IN-fiber types of Ag–polyaniline composites. Such composites should be promising materials for biosensing, catalysis, and nanoelectronics.

Huang et al. [108] obtained pure dot-ON-fiber and dot-IN-fiber types of Au–polyaniline nanocomposites, respectively. As shown in Fig. 8.17, an interesting electrical bistability (Fig. 8.17d) has been discovered for the dot-IN-fiber type of nanocomposite (Fig. 8.17a, b). When the potential across the sandwich-type device (Fig. 8.17c) is increased to +3 V, an abrupt increase in current is observed. This changes the device from a low-conductivity OFF state to a high-conductivity ON state (Fig. 8.17d, curve A). The device is stable in the ON state when the potential is lowered back to 0 V (Fig. 8.17d, curve B). The high conductivity of the ON state can be changed back to the OFF state by applying a reverse bias of –5 V. The device is then stable in the OFF state until +3 V is applied, at which point it returns to the ON state (Fig. 8.17d, curve C). This electrical bistability can potentially be used to construct polyaniline-based nonvolatile memory devices (PANI-MEM). Such devices are found to have nanosecond switching times (Fig. 8.17e), high on/off ratios, and potentially low manufacturing costs, making them promising for faster and less expensive nonvolatile data storage media than what is currently available (e.g., flash memory).

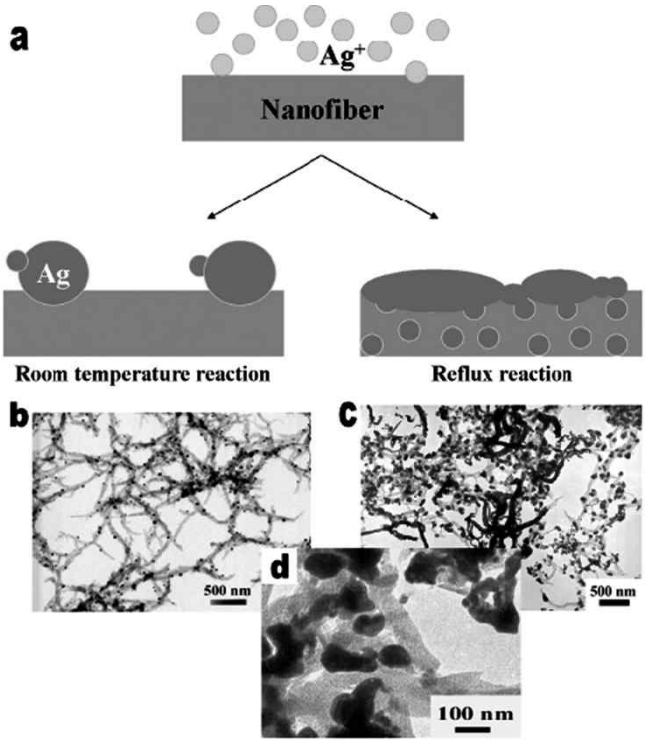

Fig. 8.16. Polyaniline nanofibers can guide the deposition of metal nanoparticles. (**a**) Schematic showing two types of Ag–polyaniline composites obtained at ~25°C and under reflux conditions (~100°C, in water), respectively. (**b**) At room temperature, Ag nanoparticles (20–30 nm) are deposited on the nanofibers. (**c, d**) At boiling temperature, continuous Ag coating outside the nanofibers as well as small Ag nanoparticles (<10 nm) [108]

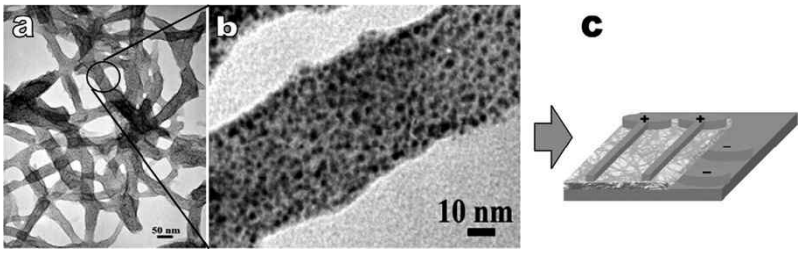

Fig. 8.17. Au–polyaniline nanocomposite (**a, b**) is a promising material for making ultra-fast nonvolatile memory devices (**c**). (**c**) A schematic showing the sandwich type of device structure. (**d**) I–V characteristics of the polyaniline nanofiber/Au nanoparticle device. The potential is scanned from (A) 0 to +4 V, (B) +4 to 0 V, and (C) 0 to +4 V. (**e**) I–V characteristics of the OFF and the ON states of the device before and after the application of a voltage pulse of 4 V with a width of 25 ns as shown in the inset (Adapted from ref. [108])

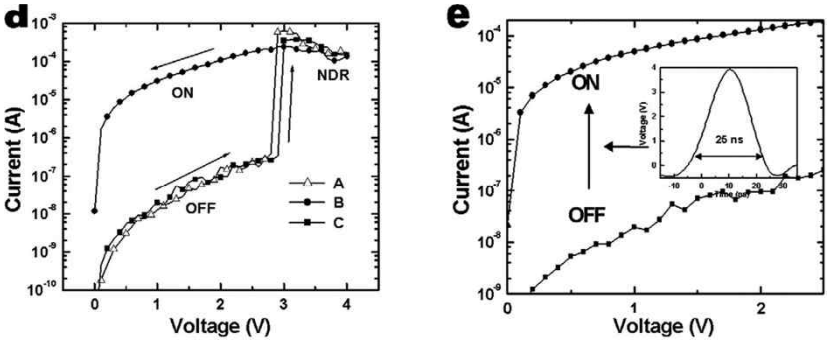

Fig. 8.17. (Continued)

8.11 Polymer Light-Emitting Diodes (PLEDs)

Conjugated polymers derive their semiconducting properties from having delocalized π-electron bonding along the polymer chain. The π bonding and π * antibonding orbitals form delocalized valence and conduction wavefunctions, which support mobile charge carriers. Electroluminescence from conjugated polymers was first reported [148] using poly(phenylene vinylene) (PPV) as the single semiconductor layer between metallic electrodes, as is illustrated in Fig. 8.18.

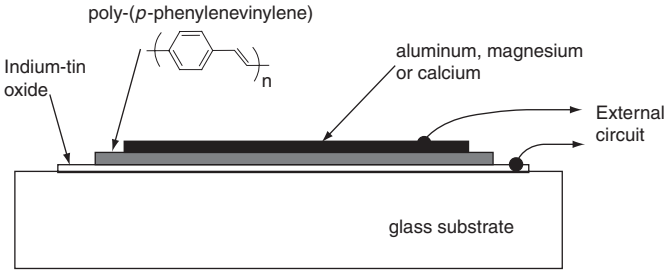

Fig. 8.18. Structure of a polymer LED fabricated with poly(phenylenevinylene) (PPV) as the active semiconductor

In this structure, the indium–tin oxide (ITO) layer functions as a transparent electrode and allows the light generated within the diode to leave the device. The top electrode is conveniently formed by thermal evaporation of a metal. LED operation is achieved when the diode is biased sufficiently to achieve injection of positive and negative charge carriers from opposite electrodes. Capture of oppositely charged carriers within the region of the polymer layer can then result in photon emission.

Diodes of this type can be readily fabricated by solution processing the semiconducting polymer onto the ITO-coated glass, even though the film thickness is no more than typically 100 nm. Spin coating from solution has been demonstrated to be capable of producing highly uniform layer thickness, with no more than a few Ångstrom thickness spread over several square centimeters. Electrodes are chosen to facilitate charge injection; ITO has a relatively high work function and is therefore suitable for use as a hole-injecting electrode, and low work-function metals such as Al, Mg, or Ca are suitable for injection of electrons.

PPV has an energy gap between π and π * states of about 2.5 eV and produces yellow-green luminescence in a band below this energy, with the same spectrum as that produced by photoexcitation. Note that it shows broadening due to vibronic coupling, as is characteristic for optical transitions in molecular semiconductors where the excited state is confined to the molecular unit and is described as an exciton.

The levels of efficiency of the first, simple LEDs based on PPV, which were fabricated with aluminum negative electrodes, were relatively low, of order 0.01% photon generated within the device per electron injected. These values have risen rapidly over the past 5 years as improved understanding of the operation of these devices, aided in considerable measure by parallel developments made with sublimed molecular film devices [149], has allowed considerable optimization of the device characteristics. More recently, much higher efficiencies have been reported for diodes made with similar structures to that shown in Fig. 8.19, but with a layer of poly(dioxyethylene thienylene) doped with polystyrene sulfonic acid (see Fig. 8.19) between ITO and emissive polymer layers. Efficiencies in the green part of the spectrum up to 22 lumen/W for emissive polymers based on polyfluorene [150]. Such devices are well matched to drive from standard silicon circuits, showing typical display brightness (100 cd/m^2) below 3 V.

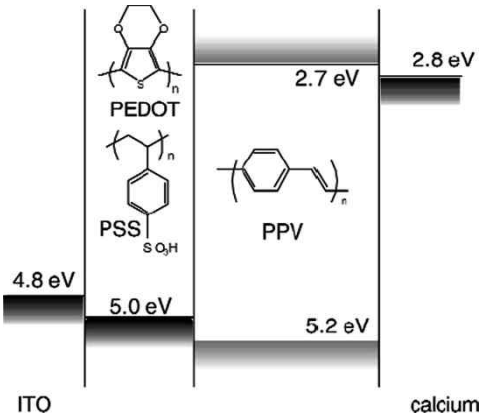

Fig. 8.19. Schematic of the energy levels for a polymer LED formed with a layer of the conducting polymer system PEDOT-PSS, which acts as hole-injecting electrode, formed on glass coated with indium–tin oxide (ITO). The cathode is formed with vacuum-sublimed calcium. The figure shows energies for the metal work-functions, and for the ionization potential and electron affinity for the semiconducting polymer (Adapted from ref. [150])

There has been very considerable progress made with chemical modification of conjugated polymers to tune color of emission so that full-color displays can be fabricated. Blue emission is achieved in a wide range of polymers, including the poly(fluorene)s (see, e.g., [151]), and red-emitting polymers have been developed by the Dow Chemical Company and others. In general, blue-emitting materials suffer from the tendency to form aggregate states which show red-shifted emission, and it is generally found that this effect is enhanced for electroluminescence in comparison with photoluminescence.

There is much interest in understanding what determines the limit to LED efficiency. The internal quantum efficiency, η_{internal}, is usually expressed as the product of the efficiency of electron–hole capture within the semiconductor layers, γ, the fraction of excitons produced as singlets (rather than triplets), r_{st}, the fraction of singlet excitons which decay radiatively; q (which is often set equal to the photoluminescence quantum efficiency), $\eta_{\text{internal}} = \gamma_{\text{st}}\, q$.

The process of double-charge injection, the requirement to balance electron and hole currents, and the requirement to achieve electron–hole recombination within the active semiconductor layer (and appropriately spaced away from the electrodes) have proved to be more tractable to engineering of electrodes and semiconducting polymers than was earlier considered feasible, and it seems that the value of γ is

close to 100% for the better-performing devices now made. As discussed below, one important approach is to construct heterostructure architectures, with two polymers used to transport either electrons or holes, with recombination forced to occur close to the heterojunction [152]. There has also been much work on the improvement of the process of charge injection at the two electrodes, and devices which retain the simple single-semiconductor layer architecture can also show very high efficiencies [153]. One approach to this is to arrange that the barrier for hole injection, which is shown as a single discontinuous step in Fig. 8.19, is formed by a graded-composition of self-assembled polymer bilayers, so that the barrier for injection takes the form of a series of smaller steps.

Radiative decay rates for singlet excitons in semiconducting polymers are now relatively high in many of the materials used in LEDs, often above 50%. Though this is now well accepted, there had been considerable concern that intermolecular interactions would lead to solid-state quenching (through, for example, the formation of Davydov-split intermolecular excitons), and the reasons why this is not found for the polymers are being investigated. The third term that enters the expression for the internal quantum efficiency is the fraction of excitons that form as emissive singlet excitons. It had generally been assumed that this would be set by spin statistics, with 25% of electron–hole pairs forming singlets and 75% forming triplets. Given that the exchange energy for these materials is large (>0.5 eV), intersystem crossing is unimportant, so this would limit device efficiency to 25% of the product of γ and q. However, experiments now show that this value can be considerably higher of order 45% [153, 154], and there is considerable interest in identifying possible models for spin-dependent electron–hole recombination [155].

The external quantum efficiency depends on the out-coupling light generated in the device in the forward direction, and is modeled and measured for devices that are made as described above to be as high as $1.2/n^2$ where n is the substrate refractive index (this is the case when the radiative dipole moments lie parallel to the plane of the device, as is found for many of the spin-coated polymer semiconductors) [156].

8.11.1 Polymer Displays

The obvious attraction of these solution-processed polymer LEDs is that they can be coated over large areas, so that arrays of devices can be conveniently assembled. Passive-matrix addressing provides a particularly

convenient arrangement for assembling a display. For this, the bottom electrode (ITO) is arranged as a series of columns, the polymer layers are deposited by spin-coating and do not require lateral patterning (since cross-talk via these polymer layers can be arranged to be unimportant), and the cathode electrode is arranged as a series of rows. Addressing is done by powering each row in sequence, while holding the column voltages as required. The rectifying characteristics of these diodes remove cross-talk and give good performance for displays with no more than "intermediate" information content, e.g., 1/4 VGA (320 × 240 pixels).

Beyond this, the need to drive each row for shorter times to higher peak currents becomes limiting, and there is now interest in using the active-matrix schemes used for high-quality liquid crystal displays (LCDs). These use amorphous silicon thin-film transistor circuits to provide a latch circuit at each pixel, which maintains the correct potential at the liquid crystal cell throughout the refresh cycle. To extend this drive scheme to the organic LEDs requires that the transistor circuit be able to drive current through the LED, and this is not easily accomplished with amorphous silicon transistors because carrier mobilities are low. However, amorphous silicon can be re-crystallized in situ, particularly by laser annealing, to form polycrystalline silicon, and this shows much improved mobilities for the field-effect charges, and hence improved speed and current-carrying capacity. This has been developed for the LCD displays in order to allow the address decoding to be performed by circuitry on the glass substrate, but turns out to be well matched for the polymer LEDs [157].

The final step in producing a full-color display is the patterning of red, green, and blue pixels onto such an active-matrix array. One particularly attractive approach is to print the three polymer systems required for each color directly in place onto the back plane, and in this way avoid the need to employ photolithographic processes. Ink-jet printing is particularly suitable for this and is now demonstrated [157].

8.11.2 Heterojunctions

The use of heterojunctions formed between dissimilar semiconducting polymers has proved to be very powerful, both in applications for LEDs and also for photovoltaic devices. A schematic view of such a heterojunction is shown in Fig. 8.20. In this scheme, two polymers with similar energy gaps differ in their electronegativities, with CN-PPV selected as a high electron-affinity material, and the two PPVs selected as low ionization potential materials. The offset in band-edge positions is about 0.5 eV for these systems (larger for the dialkoxy–PPV, MEH-PPV than for the unsubstituted PPV). The energetics of charges and of excitons in the vicinity of such a heterojunction have been modeled by the Mons group and

compared with experiments on model junctions [158]. What is found is that when the band-edge offsets are larger than the binding energy of the intrachain singlet exciton, such an exciton is ionized to place the electron on the CN-PPV and the hole on the PPV. This then gives useful photovoltaic operation, particularly when the two polymers are mixed together to form a large surface area heterojunction device. This is achieved between CN-PPV as shown in Fig. 8.20 and the dialkoxy-substituted PPV, MEH-PPV [159]. Efficiencies of such devices have been raised to relatively high values, with quantum efficiencies toward 30% and energy conversion efficiencies of order 2% in AM 1.5 conditions [160, 161].

In contrast, when the band-edge offset is smaller than the singlet exciton binding energy, the exciton is still stable at the heterojunction (though it will move to the lower energy gap side of the junction), and there is little charge generation. This is the case for the heterojunction formed between PPV without the dialkoxy substitution and CN-PPV, and such structures are very effective for use in LEDs, in which electrons and holes are transported from either side of the device, and are trapped at the heterojunction, allowing very efficient electron–hole capture.

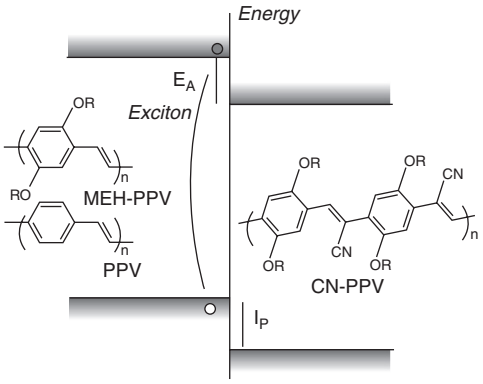

Fig. 8.20. Schematic of a heterojunction formed between two semiconducting polymers. As discussed in the text, the offset in band-edge position is sufficient to cause exciton ionization in the case of MEH-PPV versus CN-PPV, so that photovoltaic operation is achieved, whereas for the junction formed between PPV and CN-PPV, exciton energy transfer to the lower-gap material, CN-PPV, occurs (Adapted from ref. [158])

8.12 Solar Cells

Polymer solar cells are a type of organic solar cell (also called plastic solar cell) that produce electricity from sunlight using polymers. It is a relatively novel technology, being researched by universities, national laboratories, and industries around the world.

Currently, many solar cells in the world are made from a refined, highly purified silicon crystal, both crystalline and amorphous similar to those used in the manufacture of integrated circuits. The high cost of these silicon solar cells and their complex production process has generated interest in developing alternative photovoltaic technologies. Compared to silicon-based devices, polymer solar cells are lightweight (which is important for small autonomous sensors), disposable, inexpensive to fabricate (sometimes using printed electronics), flexible, customizable on the molecular level, and have lower potential for negative environmental impact.

The following discussion is based primarily on Mayer et al.'s review cited below. Organic photovoltaics (PV) are comprised of electron donor and electron acceptor materials rather than semiconductor p–n junctions. The molecules forming the electron donor region of organic PV cells, where exciton electron–hole pairs are generated, are generally conjugated polymers possessing delocalized π electrons that result from carbon p orbital hybridization. These π electrons can be excited by light in or near the visible part of the spectrum from the molecule's highest occupied molecular orbital (HOMO) to the lowest unoccupied molecular orbital (LUMO), denoted by a $\pi - \pi^*$ charge transition. The energy bandgap between these orbitals determines which wavelength of light can be absorbed.

Unlike in an inorganic crystalline PV cell material, with its band structure and delocalized electrons, excitons in organic photovoltaics are strongly bound with an energy between 0.1 and 1.4 eV. This strong binding occurs because electronic wavefunctions in organic molecules are more localized, and electrostatic attraction can thus keep the electron and hole together as an exciton. The electron and hole can be dissociated by providing an interface across which the chemical potential of electrons decreases. The material that absorbed the photon is the donor, and the material acquiring the electron is called the acceptor. After dissociation has taken place, the electron and hole may still be joined as a geminate pair and an electric field is then required to separate them.

After exciton dissociation, the electron and hole must be collected at contacts. However, charge carrier mobility now begins to play a major role: if mobility is not sufficiently high, the carriers will not reach the contacts and will instead recombine at trap sites or remain in the device as undesirable space charges that oppose the drift of new carriers. The latter

problem can occur if electron and hole mobilities are highly imbalanced, such that one species is much more mobile than the other. In that case, space-charge limited photocurrent (SCLP) hampers device performance.

As an example of the processes involved in device operation, organic photovoltaics can be fabricated with an active polymer and a fullerene (C_{60})-based electron acceptor. The illumination of this system by visible light leads to electron transfer from the polymer chain to a fullerene molecule. As a result, the formation of a photoinduced [quasiparticle] or polaron (P+) occurs on the polymer chain and the fullerene becomes an ion-radical C_{60}- . Polarons are highly mobile along the length of the polymer chain and can diffuse away. Both the polaron and ion-radical possess spin $S = ½$, so the charge photoinduction and separation processes can be controlled by the electron paramagnetic resonance method.

The simplest architecture that may be used for an organic PV device is a planar heterojunction. A film of active polymer (donor) and a film of electron acceptor are sandwiched between contacts in a planar configuration. Excitons created in the donor region may diffuse to the junction and separate, with the hole remaining behind and the electron passing into the acceptor. However, planar heterojunctions are inherently inefficient; because charge carriers have diffusion lengths of just 3–10 nm in typical organic semiconductors, planar cells must be thin to enable successful diffusion to contacts, but the thinner the cell, the less light it can absorb.

Bulk heterojunctions (BHJs) address this shortcoming. In a BHJ, the electron donor and acceptor materials are blended together and cast as a mixture that then phase-separates. Regions of each material in the device are separated by only several nanometers, a distance optimized for carrier diffusion. Although devices based on BHJs are a significant improvement over planar designs, BHJs require sensitive control over materials morphology on the nanoscale. A great number of variables, including choice of materials, solvents, and the donor–acceptor weight ratio can dramatically affect the BHJ structure that results. These factors can make rationally optimizing BHJs difficult.

The next logical step beyond BHJs are ordered nanomaterials for solar cells or ordered heterojunctions (OHJs). This paradigm eliminates much of the variability associated with BHJs. OHJs are generally hybrids of ordered inorganic materials and organic active regions. For example, a photovoltaic polymer can be deposited into pores in a ceramic such as TiO_2. Holes still must diffuse along the length of the pore through the polymer to a contact, so OHJs do have thickness limitations. Mitigating the hole mobility bottleneck will thus be key to further enhancing OHJ device performance, but controlling morphology inside the confines of the pores is challenging.

Engineers at the University of California, San Diego (UCSD) have employed "nanowires" to boost the efficiency of organic solar cells (http://ucsdnews.ucsd.edu/newsrel/science/05-08Nanowires.asp). Indium phosphide (InP) nanowires can serve as electron superhighways that carry electrons kicked loose by photons of light directly to the device's electron-attracting electrode – and this scenario could boost thin-film solar cell efficiency. The new design (shown in Fig. 8.21) increases the number of electrons that make it from the light-absorbing polymer to an electrode. By reducing electron–hole recombination, the UC San Diego engineers have demonstrated a way to increase the efficiency with which sunlight can be converted in to electricity in thin-film photovoltaics. Recently, Grimes et al. [162] at Penn State University show that using Foster-type resonance energy transfer can improve the efficiency of the solar cell by extending the sun light beyond the present UV/Vis regime (350–650 nm) into the near IR regime (>650 nm) which can enhance the solar harvest efficiency by utilizing a ruthenium polypyridine complex acceptor anchored to the surface of the TiO_2 nanowires.

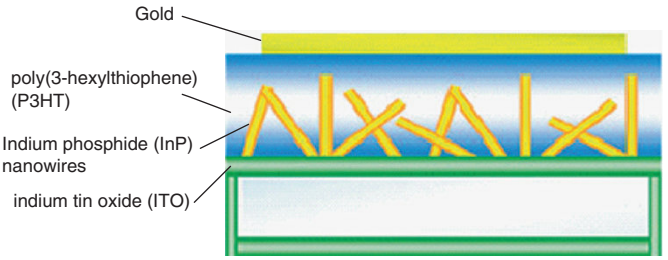

Fig. 8.21. Schematic of the nanowire–polymer hybrid device created by UC San Diego engineers and described in the Journal of *Nano Letters*

8.13 Three-Dimensional Interconnect

By the use of templates like porous membranes during polymerization, conducting molecular wires can be formed with highly anisotropic properties which might be used as interconnecting layers in a three-dimensional (3D)-chip stacking (Fig. 8.22). Ackermann et al. reported preliminary results on forming polypyrrole (PPy) molecular wires in isolating porous polycarbonate membranes as self-supporting layers using directional electrochemical polymerization (DEP) technique. The DEP process which had a structured cathode turned out to be a powerful technique to perform a micropatterning of the membrane with polymer wires. The DEP-processed

polymer micro-wires demonstrated a conductivity of 0.5 S/cm, but without any cross-talk, which is very important for a perfect signal transfer in the 3D-chip stacking.

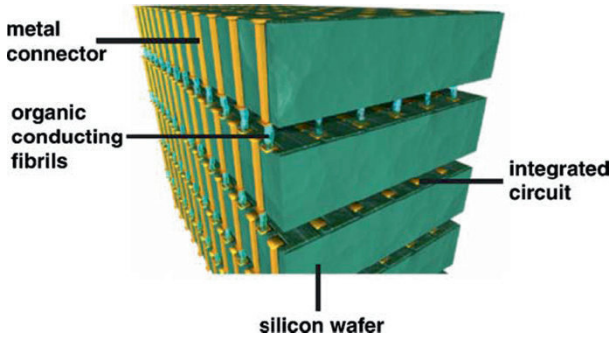

Fig. 8.22. Cortex 3D-chip stacking with chip interconnections accomplished by organic conducting fibrils (from [162])

8.14 Conducting Polymer Artificial Muscles

Although the use of conducting polymers as artificial muscles was first demonstrated by Baughman and co-workers in 1990 [163], advances in performance have been continuously made until now and further improvements are both desirable and achievable. These conducting polymer artificial muscles use the dimensional changes resulting from electrochemical ion insertion and deinsertion, possibly along with associated solvating species. Since both electrodes can comprise conducting polymers, both can be used as artificial muscles. Depending upon the conducting polymer/electrolyte system used, the initial state, and the rate of potential change used for actuation, electron insertion into one electrode can be accompanied by a volume increase as cations are inserted or a volume decrease as anions are removed. Similar processes can occur at the counter electrode. This feature, as well as possible time-dependent changes of the intercalated/deintercalated species, can complicate the control of actuation [164, 165]. Expansion appears to be primarily perpendicular to the polymer chain orientation for oriented polymers, suggesting to the first order that ions and accompanying solvent are slotted between chains [166, 167]. The polymers most often used in actuation are polypyrrole, polyaniline, and polythiophene derivatives. Rates of actuation tend to be low (<<1%/s) because of the relatively slow transport of ions within the polymer and the large degree of doping sometimes used [168], but they can exceed 10%/s using

metal contacts, porous polymers, fast charging methods, or thin films and fibers [169–171]. High-quality electrochemically grown films and solution-spun fibers have tensile strengths on the order of 100 MPa or higher, and adding carbon nanotubes (CNTs) can further increase strength and reduce problematic creep [172]. Work densities [173] approach 100 MJ/m^3. Operating voltages are ~2 V, though higher voltages of up to 10 V are sometimes used to increase actuation rate. Such high voltages will ultimately cause degradation of the electrolyte and/or polymer unless the voltage profile as a function of time is properly provided [169], so that excess voltage over the redox stability range is resistively dissipated at the beginning of a voltage pulse and the applied voltage is progressively decreased as the current decreases.

The advantage of conducting polymers over electronic electric electroactive polymers (EAPs) is their low operating voltage. They feature higher strains and low cost. But the electromechanical coupling is low (<1%). Much of the input electrical energy can be recovered, but the need to shunt relatively large amounts of electrical energy can slow actuation and push the limits of power supplies, making large-scale applications (e.g. robotic arms) challenging. One promising means of improving coupling is to design conjugated molecules that fold and expand in response to changes in oxidation state, bringing artificial muscle a little closer to the elegance of real muscle [174]. Applications being considered include blood vessel reconnection, dynamic Braille displays, valves, and actuated catheters [175].

8.15 ICP as Interconnect Materials

Lam et al. [176] studied the possibilities of employing intrinsically conducting polymers (ICPs) in place of electrical conductive-polymer composites (ECPs) for applications involving electrical contacts and reported a preliminary investigation made on two types of ICPs namely poly(3,4-ethylenedioxythiophene) (PEDOT) and polyaniline (PANI). The ICPs were doped with different ratios of solvents and prepared under certain conditions to achieve improvements in the mechanical structure, processibility, and conductivity. Experiments were carried out to measure the contact resistances using four-wire resistance measurement techniques while subjected to a normal force. In this primary study, the optimum conductivity levels for the ICPs were found in the 10^{-2} Scm^{-1} range. Although these values are comparatively low with respect to extrinsic conducting polymers and metals, ICPs have shown initial potentials in conductivity enhancement and possible implementations as an electrical contact or conductive coating.

Conductive polymer blends and composites can be prepared by combining an insulating polymer or copolymer with an intrinsically conductive polymer, such as polypyrrole, polythiophene, and polyaniline. Cooper and Vincent [177] prepared electrically conductive films by casting mixed dispersion of Emeraldine Salt (ES) particles (needles) with film-forming latex particles. They studied the effects of concentration of the conducting particles on the conductivity of resulting films and concluded that the percolation threshold was ~20wt% in the case of ES particles.

Sancaktar et al. [178] conducted study on ES-filled composite adhesive. Data illustrated the effect of filler loading on electrical conduction with a critical percolation concentration at about 30% by volume for dispersion in nitrocellulose solution. Experimental results with the ES-filled composite adhesive also revealed that the adhesive/substrate interphase had a strong influence on the electrical conduction behavior in bonded joints. We believe that there is a redox reaction occurring at the adhesive interphases with aluminum and zinc substrates, resulting in the formation of a dense, nonconductive layer of metallic oxide (Al_2O_3 for Al, and ZnO for Zn plated) catalyzed by ES particles, eventually preventing the electron flow necessary for the formation of a continuous, conductive network between the adhesive and the substrate. Mechanical experiments performed using single lap joints bonded with nitrocellulose adhesive filled 40% by volume with ES powder revealed a relatively brittle behavior for the composite adhesive, with failure occurring mostly in the interfacial mode.

Corsat et al. [179] demonstrated nano-imprinting conducting polymer to form pyramid-shaped bumps. The conjugated polymers are relatively soft compared to other polymers. To allow the imprinting of such materials, conductive polyaniline (PANI) was blended with thermoplastic polymethylmethacrylate (PMMA) plasticized with di-octylphthlate to decrease the glass transition temperature of the PMMA. Depending on the concentration of PANI and plasticizer, it is possible to adjust the conductivity of the blend between 0.5 and 50 S/cm and the glass transition temperature between 30 and 110°C. To avoid thermo-mechanical stresses at cooling due to CTE mismatch, a low temperature process was developed to address a very low pitch with a relatively low cost. The process flow is presented in Fig. 8.23 and imprinted pyramid is shown in Fig. 8.24. The softness (deformability) of the conductive-polymer pyramid was utilized to make the electrical contact to the metal pads of the substrate under pressure and temperature. However, the electrical testing showed that the interconnection was not functional on the full interconnect area and more work has to be done to make the interconnections fully functional.

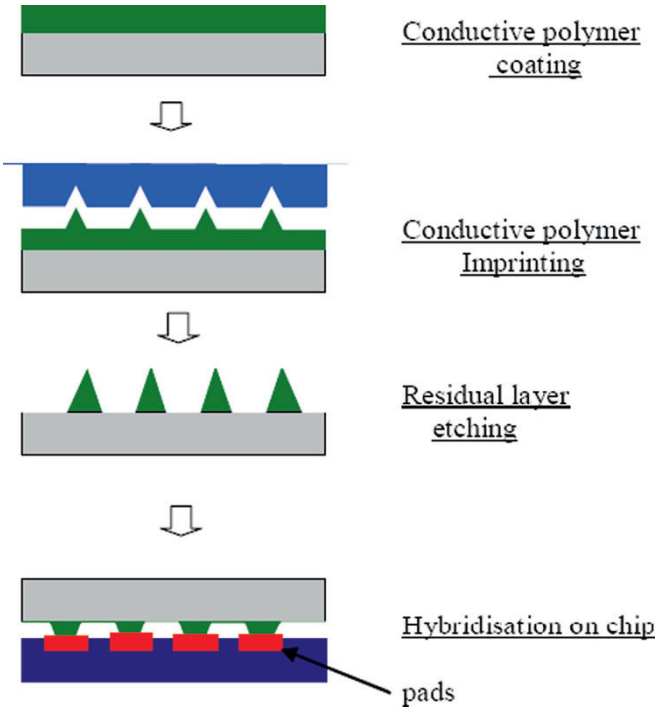

Fig. 8.23. Low temperature interconnection process between a die and a substrate

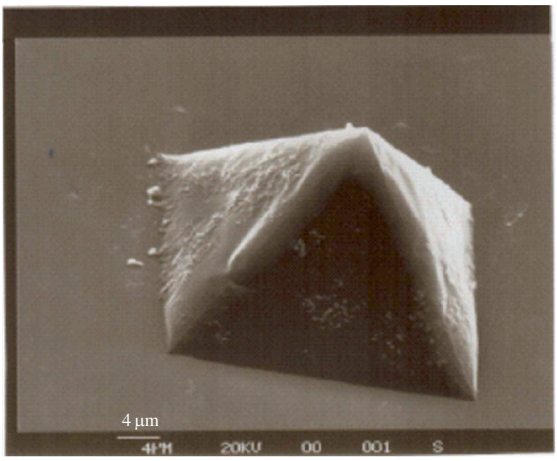

Fig. 8.24. Conducting polymer pyramid after plasma etching

Chow et al. [180] demonstrated the feasibility of using a thermoplastic intrinsically conductive polymer based on doped polyaniline (PANI) as an interconnect material with low processing temperatures. PANI samples were sandwiched between gold substrates and the contact resistance of the PANI samples was measured in situ under 85°C/85%RH aging. It was found that the doped-PAN1 dissolved in Cresol gives the lowest initial and stable resistance and no corrosion to gold surface.

Kuechenmeister et al. [181] investigated using polypyrrole as the interlayer between an ICA bump and aluminum pad. A unique and cost competitive procedure was developed for the activation of aluminum bond pads using polypyrrole as conductive interlayer. Low contact resistance (< 1 Ω) was achieved in the layer system aluminum/polypyrrole/copper.

Electron-dense multiple double and triple chemical bonds are typically used in the ICP structure. However, their multi-bond structures tend to produce rigid, insoluble polymers that are difficult to use. The multiple bonds and fused ring structures found in all of the common ICPs tend to be sensitive to oxidation. The instability in air, brittleness, and difficulty of application make ICPs mostly a lab curiosity at this stage, but there is hope that new conductive structures may someday lead to useful products. Recently, Lu at al. [182] have used ICP such as polyaniline (PANI) coupled with an in situ formation of nanoAg particles to develop an ultra-high *k*(dielectric constant) composite for potential embedded capacitor applications.

In conclusion, with the continuous research and development on ICPs, there will be more applications in the near future.

References

[1] A.-J. Attias, "Polymères Conjugués et Polymères Conducteurs Electroniques," *Techniques de l'Ingénieur – Traité Électronique*, 1862, 1–20, 2002.

[2] H. Naarmann and N. Theophilou, "New Process for the Production of Metal-Like, Stable Polyacetylene," *Synthetic Metals*, 22, 1–8, 1987.

[3] V. Shaktawat, N. Jain, R. Saxena, N. S. Saxena, K. Sharma, and T. P. Sharma, "Temperature Dependence of Electrical Conduction in Pure and Doped Polypyrrole," *Polymer Bulletin*, 57, 535–543, 2006.

[4] A. J. Epstein, H. Rommelmann, R. Bigelow, H. W. Gibson, D. M. Hoffmann, and D. B. Tanner, "Role of Solitons in Nearly Metallic Polyacetylene," *Physical Review Letters*, 50, 1866–1869, 1983.

[5] N. Basescu, Z. X. Liu, D. Moses, A. J. Heeger, H. Naarmann, and N. Theophilou, "High Electrical-Conductivity in Doped Polyacetylene," *Nature*, 327, 403–405, 1987.

[6] A. G. MacDiarmid, "Synthetic Metals: A Novel Role for Organic Oolymers (Nobel lecture)," *Angewandte Chemie-International Edition*, 40, 2581–2590, 2001.

[7] H. Bai and G. Q. Shi, "Gas Sensors Based on Conducting Polymers," *Sensors*, 7, 267–307, 2007.

[8] T. Ito, H. Shirakawa, and S. Ikeda, "Thermal cis-trans isomerization and decomposition of polyacetylene," *Journal of Polymer Science, Polymer Chemistry*, 13, 1943–1950, 1975.

[9] S. Roth, G. Mahler, Y. Shen, and F. Coter, "Molecular Electronics of Conducting Polymers," *Synthetic Metals*, 28, C815–C822, 1989.

[10] S. Pekker and A. Janossay, Chapter 2, "Chemistry of Doping in Polyacetylene," Handbook of Conducting Polymers, T. A. Skotherm, Ed., Marcel Dekker, New York, vol. 2, 1986.

[11] K. Akagi, H. Shirakawa, K. Araya, A. Mukoh, and T. Narahara, "Highly Conducting Polyacetylene Films Prepared in a Liquid-Crystal Solvent," *Polymer Journal*, 19, 185–189, 1987.

[12] J. L. Ribet, M. Rolland, A. Montaner, M. Galtier, Z. Lakhliai, J. L. Sauvajol, M. Brunet, R. Almairac, and P. Bernier, "Synthesis and Characterization of Oriented Polyacetylene Films," *Synthetic Metals*, 24, 1–5, 1988.

[13] M. Aldissi, "Molecular and Supramolecular Orientation in Polya cetylene," *Journal of Polymer Science Part C-Polymer Letters*, 27, 105–110, 1989.

[14] T. Schimmel, G. Denninger, W. Riess, J. Voit, M. Schwoerer, W. Schoepe, and H. Naarmann, "High-Sigma Polyacetylene – Dc Conductivity between 14-Mk and 300-K," *Synthetic Metals*, 28, D11–D18, 1989.

[15] J. Tsukamoto, A. Takahashi, and K. Kawasaki, "Structure and Electrical-Properties of Polyacetylene Yielding a Conductivity of 105 S/Cm," *Japanese Journal of Applied Physics Part 1-Regular Papers Short Notes & Review Papers*, 29, 125–130, 1990.

[16] E. Reichmanis, S. A. MacDonald, and T. Iwayanagi, Eds.,"Polymers in Microlithography: Materials and Processes," *ACS Symposium Series, American Chemical Society*, Washington, DC, 1989.

[17] J. M. Shaw, "*Imaging for Microfabrication, Imaging Processes and Materials*," J. Sturge, V. Walworth, and A. Shepp, Eds., Van Nostrand Reinhold Co., New York, pp. 567–586, 1989.

[18] B. Chapman, Ed., "Glow Discharge Processes," John Wiley & Sons, Inc., New York, 1980.

[19] J. M. Ryan, A. C. F. Hoole, and A. N. Broers, "A Study of the Effect of Ultrasonic Agitation during Development of Poly(methylmethacrylate) for Ultrahigh Resolution Electron-Beam Lithography," *Journal of Vacuum Science & Technology B*, 13, 3035–3039, 1995.

[20] H. C. Pfeiffer, R. S. Dhaliwal, S. D. Golladay, S. K. Doran, M. S. Gordon, T. R. Groves, R. A. Kendall, J. E. Lieberman, P. F. Petric, D. J. Pinckney, R. J. Quickle, C. F. Robinson, J. D. Rockrohr, J. J. Senesi, W. Stickel, E. V. Tressler, A. Tanimoto, T. Yamaguchi, K. Okamoto, K. Suzuki, T. Okino, S. Kawata, K. Morita, S. C. Suziki, H. Shimizu, S. Kojima, G. Varnell, W. T. Novak, D. P. Stumbo, and M. Sogard, "Projection Reduction Exposure with Variable Axis Immersion Lenses: Next Generation Lithography," *Journal of Vacuum Science & Technology B*, 17, 2840–2846, 1999.

[21] D. L. Laird, R. L. Engelstad, D. M. Puisto, R. E. Acosta, K. D. Cummings, and W. A. Johnson, "Predicting In-plane Distortion from Electron-Beam Lithography on X-ray Mask Membranes," *Journal of Vacuum Science & Technology B*, 14, 4308–4313, 1996.

[22] H. Todokoro, S. Fukuhara, and T. Komoda, "Electron-Beam Lsi Tester," *Japan Annual Reviews in Electronics Computers & Telecommunications*, 13, 373–382, 1984.

[23] Y. Todokoro, A. Kajiya, and H. Watanabe, "Conductive 2-Layer Resist System for Electron-Beam Lithography," *Journal of Vacuum Science & Technology B*, 6, 357–360, 1988.

[24] H. Watanabe, E. Sugiura, T. Imoriya, Y. Todokoro, and M. Inoue, "Repair Technique for Phase-Shifting Masks Using Silicon-Containing Resist," *IEEE Transactions on Electron Devices*, 40, 2211–2215, 1993.

[25] W. S. Huang, "Synthesizing and Processing Conducting Polythiophene Derivatives for Charge Dissipation in Electron-Beam Lithography," *Polymer*, 35, 4057–4064, 1994.

[26] A. G. Macdiarmid, J. C. Chiang, A. F. Richter, and A. J. Epstein, "Polyaniline – a New Concept in Conducting Polymers," *Synthetic Metals*, 18, 285–290, 1987.

[27] A. J. Epstein, J. M. Ginder, F. Zuo, R. W. Bigelow, H. S. Woo, D. B. Tanner, A. F. Richter, W. S. Huang, and A. G. Macdiarmid, "Insulator-to-Metal Transition in Polyaniline," *Synthetic Metals*, 18, 303–309, 1987.

[28] M. Angelopoulos, A. Ray, A. G. Macdiarmid, and A. J. Epstein, "Polyaniline – Processability from Aqueous-Solutions and Effect of Water-Vapor on Conductivity," *Synthetic Metals*, 21, 21–30, 1987.

[29] M. Angelopoulos, G. E. Asturias, S. P. Ermer, A. Ray, E. M. Scherr, A. G. Macdiarmid, M. Akhtar, Z. Kiss, and A. J. Epstein, "Polyaniline – Solutions, Films and Oxidation-State," *Molecular Crystals and Liquid Crystals*, 160, 151–163, 1988.

[30] L. W. Shacklette, "Dipole and Hydrogen-Bonding Interactions in Polyaniline – a Mechanism for Conductivity Enhancement," *Synthetic Metals*, 65, 123–130, 1994.

[31] L. W. Shacklette, "Electrical Applications of Conducting Polymers," *Abstracts of Papers of the American Chemical Society*, vol. 207, pp. 246-Poly, 1994.

[32] K. T. Tzou and R. V. Gregory, "Improved Solution Stability and Spinnability of Concentrated Polyaniline Solutions Using N,N'-Dimethyl Propylene Urea as the Spin Bath Solvent," *Synthetic Metals*, 69, 109–112, 1995.

[33] A. G. MacDiarmid, J. C. Chiang, A. F. Richter, N. L. D. Somasiri, and A. J. Epstein, "Polyaniline: Synthesis and Characterization of the Emeraldine Oxidation State by Element Analysis," in Conducting Polymers, L. Alcacer, Ed., Reidel, Dordrecht, pp. 105–120, 1987.

[34] J. Yue, Z. H. Wang, K. R. Cromack, A. J. Epstein, and A. G. Macdiarmid, "Effect of Sulfonic-Acid Group on Polyaniline Backbone," *Journal of the American Chemical Society*, 113, 2665–2671, 1991.

[35] J. Yue, A. J. Epstein, and A. G. Macdiarmid, "Sulfonic-Acid Ring-Substituted Polyaniline, a Self-Doped Conducting Polymer," *Molecular Crystals and Liquid Crystals*, 189, 255–261, 1990.

[36] C. Dearmitt, S. P. Armes, J. Winter, F. A. Uribe, S. Gottesfeld, and C. Mombourquette, "A Novel N-Substituted Polyaniline Derivative," *Polymer*, 34, 158–162, 1993.

[37] M. T. Nguyen, P. Kasai, J. L. Miller, and A. F. Diaz, "Synthesis and Properties of Novel Water-Soluble Conducting Polyaniline Copolymers," *Macromolecules*, 27, 3625–3631, 1994.

[38] Y. Wei, R. Hariharan, and S. A. Patel, "Chemical and Electrochemical Copolymerization of Aniline with Alkyl Ring-Substituted Anilines," *Macromolecules*, 23, 758–764, 1990.

[39] M. Leclerc, J. Guay, and L. H. Dao, "Synthesis and Characterization of Poly(Alkylanilines)," *Macromolecules*, 22, 649–653, 1989.

[40] Y. H. Liao, M. Angelopoulos, and K. Levon, "Ring-Substituted Polyaniline Copolymers Combining High Solubility with High-Conductivity," *Journal of Polymer Science Part A-Polymer Chemistry*, 33, 2725–2729, 1995.

[41] M. Angelopoulos, S. P. Ermer, S. K. Manohar, A. G. Macdiarmid, and A. J. Epstein, "Pseudo-Protonic Acid Doping of Polyaniline," *Molecular Crystals and Liquid Crystals*, 160, 223–223, 1988.

[42] Y. Cao, G. M. Treacy, P. Smith, and A. J. Heeger, "Solution-Cast Films of Polyaniline – Optical-Quality Transparent Electrodes," *Applied Physics Letters*, 60, 2711–2713, 1992.

[43] Y. Cao, P. Smith, and A. J. Heeger, "Counterion Induced Processibility of Conducting Polyaniline and of Conducting Polyblends of Polyaniline in Bulk Polymers," *Synthetic Metals*, 48, 91–97, 1992.

[44] M. Angelopoulos, N. Patel, and R. Saraf, "Amic Acid Doping of Polyaniline – Characterization and Resulting Blends," *Synthetic Metals*, 55, 1552–1557, 1993.

[45] E. W. Paul, A. J. Ricco, and M. S. Wrighton, "Resistance of Polyaniline Films as a Function of Electrochemical Potential and the Fabrication of Polyaniline-Based Microelectronic Devices," *Journal of Physical Chemistry*, 89, 1441–1447, 1985.

[46] W. S. Huang, B. D. Humphrey, and A. G. Macdiarmid, "Polyaniline, a Novel Conducting Polymer – Morphology and Chemistry of Its Oxidation and Reduction in Aqueous-Electrolytes," *Journal of the Chemical Society-Faraday Transactions I*, 82, 2385–2400, 1986.

[47] M. Angelopoulos and J. M. Shaw, "Polyanilines – In situ Induced Conductivity and Applications Thereof," *Synthetic Metals*, 41, 1109–1109, 1991.

[48] M. Angelopoulos, J. M. Shaw, R. D. Kaplan, and S. Perreault, "Conducting Polyanilines – Discharge Layers for Electron-Beam Lithography," *Journal of Vacuum Science & Technology B*, 7, 1519–1523, 1989.

[49] M. Angelopoulos, J. M. Shaw, M. A. Lecorre, and M. Tissier, "Conducting Polyaniline – Removable Sem Discharge Layer," *Microelectronic Engineering*, 13, 515–518, 1991.

[50] S. A. Chen and G. W. Hwang, "Synthesis of Water-Soluble Self-Acid-Doped Polyaniline," *Journal of the American Chemical Society*, 116, 7939–7940, 1994.

[51] S. A. Chen and G. W. Hwang, "Water-Soluble Self-Acid-Doped Conducting Polyaniline – Structure and Properties," *Journal of the American Chemical Society*, 117, 10055–10062, 1995.

[52] A. O. Patil, Y. Ikenoue, F. Wudl, and A. J. Heeger, "Water-Soluble Conducting Polymers," *Journal of the American Chemical Society*, 109, 1858–1859, 1987.

[53] Y. Ikenoue, N. Uotani, A. O. Patil, F. Wudl, and A. J. Heeger, "Electrochemical Studies of Self-Doped Conducting Polymers – Verification of the Cation-Popping Doping Mechanism," *Synthetic Metals*, 30, 305–319, 1989.

[54] S. A. Chen and M. Y. Hua, "Structure and Doping Level of the Self-Acid-Doped Conjugated Conducting Polymers – Poly[N-(3'-Thienyl)Alkanesulfonic Acid]S," *Macromolecules*, 26, 7108–7110, 1993.

[55] S. X. Cai, J. F. W. Keana, J. C. Nabity, and M. N. Wybourne, "Conducting Polymers as Deep-UV and Electron-Beam Resists – Direct Production of Micrometer Scale Conducting Structures from Poly(3-Octylthiophene)," *Journal of Molecular Electronics*, 7, 63–68, 1991.

[56] S. X. Cai, M. Kanskar, J. C. Nabity, J. F. W. Keana, and M. N. Wybourne, "Fabrication of Submicron Conducting and Chemically Functionalized Structures from Poly(3-Octylthiophene) by an Electron-Beam," *Journal of Vacuum Science & Technology B*, 10, 2589–2592, 1992.

[57] J. Lowe and S. Holdcroft, "Synthesis and Photolithography of Polymers and Copolymers Based on Poly(3-(2-(Methacryloyloxy) Ethyl)Thiophene)," *Macromolecules*, 28, 4608–4616, 1995.

[58] W. S. Huang, M. Angelopoulos, J. R. White, and J. M. Park, "Metallization of Printed-Circuit Boards Using Conducting Polyaniline," *Molecular Crystals and Liquid Crystals*, 189, 227–235, 1990.

[59] S. Gottesfeld, F. A. Uribe, and S. P. Armes, "The Application of a Polypyrrole Precoat for the Metallization of Printed-Circuit Boards," *Journal of the Electrochemical Society*, 139, L14–L15, 1992.

[60] J. Fjelstad, Printed Wiring Board Technology: Current Capabilities and Limitations, in Electronics Materials Handbook, C. A. Dostal, Ed., ASM International, Materials Park, OH, pp. 507–512, 1989.

[61] L. Lynch and R. A. Nesbitt, Rigid Printed Wiring Board Fabrication Techniques, in Electronics Materials Handbook, C. A. Dostal, Ed., ASM International, Materials Park, OH, pp. 538–555, 1989.

[62] D. P. Seraphim, D. E. Barr, W. T. Chen, G. P. Schmitt, and R. R. Tummala, Printed Circuit Board Packaging, in Microelectronics Packaging Handbook, R. R. Tummala and E. J. Rymaszewski, Eds., Van Nostrand Reinhold, New York, pp. 853–922, 1989.

[63] J. J. Steppan, J. A. Roth, L. C. Hall, D. A. Jeannotte, and S. P. Carbone, "A Review of Corrosion Failure Mechanisms During Accelerated Tests – Electrolytic Metal Migration," *Journal of the Electrochemical Society*, 134, 175–190, 1987.

[64] V. Brusic, M. A. Frisch, B. N. Eldridge, F. P. Novak, F. B. Kaufman, B. M. Rush, and G. S. Frankel, "Copper Corrosion with and Without Inhibitors," *Journal of the Electrochemical Society*, 138, 2253–2259, 1991.

[65] V. Brusic, G. S. Frankel, J. Roldan, and R. Saraf, "Corrosion and Protection of a Conductive Silver Paste," *Journal of the Electrochemical Society*, 142, 2591–2594, 1995.

[66] G. S. Frankel, C. V. Jahnes, V. Brusic, and A. J. Davenport, "Repassivation Transients Measured with the Breaking-Electrode Technique on Aluminum Thin-Film Samples," *Journal of the Electrochemical Society*, 142, 2290–2295, 1995.

[67] V. Brusic, M. Angelopoulos, and T. Graham, "Use of Polyaniline and its Derivatives in Corrosion Protection of Copper and Silver," *Journal of the Electrochemical Society*, 144, 436–442, 1997.

[68] D. W. Deberry, "Modification of the Electrochemical and Corrosion Behavior of Stainless-Steels with an Electroactive Coating," *Journal of the Electrochemical Society*, 132, 1022–1026, 1985.

[69] D. A. Wrobleski, B. C. Benicewicz, K. G. Thompson, and C. J. Byran, "Corrosion-Resistant Coatings from Conducting Polymers," *Polymer Preprint, (Am. Chem. Soc, Div. Polym. Chem.)*, 35, 265–266, 1994.

[70] S. Sathiyanarayanan, S. K. Dhawan, D. C. Trivedi, and K. Balakrishnan, "Soluble Conducting Polyethoxy Aniline as an Inhibitor for Iron in Hcl," *Corrosion Science*, 33, 1831–1841, 1992.

[71] B. Wessling, "Passivation of Metals by Coating with Polyaniline – Corrosion Potential Shift and Morphological-Changes," *Advanced Materials*, 6, 226–228, 1994.

[72] W. K. Lu, R. L. Elsenbaumer, and B. Wessling, "Corrosion Protection of Mild-Steel by Coatings Containing Polyaniline," *Synthetic Metals*, 71, 2163–2166, 1995.

[73] S. Jasty and A. J. Epstein, "Corrosion Prevention Capability of Polyaniline (Emeraldine Base and Salt) – an XPS Study," *Polymeric Material Science & Engineering*, 72, 565–566, 1995.

[74] C. Duvvury and A. Amerasekera, "ESD – a Pervasive Reliability Concern for IC Technologies," *Proceedings of the IEEE*, vol. 81, pp. 690–702, 1993.

[75] R. V. Gregory, W. C. Kimbrell, and H. H. Kuhn, "Conductive Textiles," *Synthetic Metals*, 28, C823–C835, 1989.

[76] H. H. Kuhn, *Characterization and Application of Polypyrrole-Coated Textiles, Intrinsically Conducting Polymers: An Emerging Technology*, M. Aldissi, Ed., Kluwer Academic Publishers, Dordrecht, p. 25, 1993.

[77] N. F. Colaneri and L. W. Shacklette, "EMI Shielding Measurements of Conductive Polymer Blends," *IEEE Transactions on Instrumentation and Measurement*, 41, 291–297, 1992.

[78] L. W. Shacklette, C. C. Han, and M. H. Luly, "Polyaniline Blends in Thermoplastics," *Synthetic Metals*, 57, 3532–3537, 1993.

[79] V. G. Kulkarni, J. C. Campbell, and W. R. Mathew, "Transparent Conductive Coatings," *Synthetic Metals*, 57, 3780–3785, 1993.

[80] V. G. Kulkarni, Processing of Polyanilines, in Intrinsically Conducting Polymers: An Emerging Technology, M. Aldissi, Ed., Kluwer Academic Publishers, Dordrecht, p. 45, 1993.

[81] C. Y. Yang, Y. Cao, P. Smith, and A. J. Heeger, "Morphology of Conductive, Solution-Processed Blends of Polyaniline and Poly(Methyl Methacrylate)," *Synthetic Metals*, 53, 293–301, 1993.

[82] O. T. Ikkala, J. Laakso, K. Väkiparta, E. Virtanen, H. Ruohonen, H. Järvinen, T. Taka, P. Passiniemi, J. -E. Österholm, Y. Cao, A. Andreatta, P. Smith and A. J. Heeger, "Counter-ion Induced Processibility of Polyaniline: Conducting Melt Processible Polymer Blends," *Synthetic Metals*, 69, 97–100, 1995.

[83] F. Xue, Y. Su, and K. Varahramyan, "Conducting Polypyrrole-based Field Effect Transistors Fabricated by Spin Coating and Inkjet Printing," *Spring MRS Conference Symposium I*, 2004.

[84] J. A. Covington, J. W. Gardner, P. N. Bartlett, and C. S. Toh, "Conductive Polymer Gate FET Devices for Vapour Sensing," *IEE Proceedings-Circuits Devices and Systems*, vol. 151, pp. 326–334, 2004.

[85] S. Ashizawa, Y. Shinohara, H. Shindo, Y. Watanabe, and H. Okuzaki, "Polymer FET with a Conducting Channel," *Synthetic Metals*, 153, 41–44, 2005.

[86] Y. Liu, K. Varahramyan, and T. H. Cui, "Low-Voltage All-Polymer Field-Effect Transistor Fabricated using an Inkjet Printing Technique," *Macromolecular Rapid Communications*, 26, 1955–1959, 2005.

[87] V. C. Nguyen and K. Potje-Kamloth, "Electrical and Chemical Sensing Properties of Doped Polypyrrole/Gold Schottky Barrier Diodes," *Thin Solid Films*, 338, 142–148, 1999.

[88] C. N. Van and K. Potje-Kamloth, "Electrical and NOx Gas Sensing Properties of Metallophthalocyanine-doped Polypyrrole/Silicon Heterojunctions," *Thin Solid Films*, 392, 113–121, 2001.

[89] D. Xie, Y. D. Jiang, W. Pan, D. Li, Z. M. Wu, and Y. R. Li, "Fabrication and Characterization of Polyaniline-Based Gas Sensor by Ultra-Thin Film Technology," *Sensors and Actuators B-Chemical*, 81, 158–164, 2002.

[90] S. V. Mello, P. Dynarowicz-Latka, A. Dhanabalan, R. F. Bianchi, R. Onmori, R. A. J. Janssen, and O. N. Oliveira, "Langmuir and Langmuir-Blodgett Films from the N-hexyl-pyrrole-thiophene (AB) Semi-Amphiphilic Copolymer," *Colloids and Surfaces a-Physicochemical and Engineering Aspects*, 198, 45–51, 2002.

[91] N. V. Bhat, A. P. Gadre, and V. A. Bambole, "Investigation of Electropolymerized Polypyrrole Composite Film: Characterization and Application to Gas Sensors," *Journal of Applied Polymer Science*, 88, 22–29, 2003.

[92] K. H. An, S. Y. Jeong, H. R. Hwang, and Y. H. Lee, "Enhanced Sensitivity of a Gas Sensor Incorporating Single-walled Carbon Nanotube-Polypyrrole Nanocomposites," *Advanced Materials*, 16, 1005–1009, 2004.

[93] G. F. Li, M. Josowicz, J. Janata, and S. Semancik, "Effect of Thermal Excitation on Intermolecular Charge Transfer Efficiency in Conducting Polyaniline," *Applied Physics Letters*, 85, 1187–1189, 2004.

[94] J. Elizalde-Torres, H. L. Hu, and A. Garcia-Valenzuela, "NO2-Induced Optical Absorbance Changes in Semiconductor Polyaniline Thin Films," *Sensors and Actuators B-Chemical*, 98, 218–226, 2004.

[95] M. K. Ram, O. Yavuz, and M. Aldissi, "NO2 Gas Sensing Based on Ordered Ultrathin Films of Conducting Polymer and its Nanocomposite," *Synthetic Metals*, 151, 77–84, 2005.

[96] D. Blackwood and M. Josowicz, "Work Function and Spectroscopic Studies of Interactions Between Conducting Polymers and Organic Vapors," *Journal of Physical Chemistry*, 95, 493–502, 1991.

[97] A. A. Athawale, S. V. Bhagwat, and P. P. Katre, "Nanocomposite of Pd-Polyaniline as a Selective Methanol Sensor," *Sensors and Actuators B-Chemical*, 114, 263–267, 2006.

[98] J. Janata and M. Josowicz, "Conducting Polymers in Electronic Chemical Sensors," *Nature Materials*, 2, 19–24, 2003.

[99] H. Chen, M. Josowicz, and J. Janatax, "Chemical Effects in Organic Electronics," *Chemistry of Materials*, 16, 4728–4735, 2004.

[100] A. G. Shrivas, R. G. Bavane, and A. M. Mahajan, "Electronic Nose: A Toxic Gas Sensor by Polyaniline Thin Film Conducting Polymer," *International Workshop on Physics of Semiconductor Devices*, pp. 621–623, 2007.

[101] E. Pringsheim, D. Zimin, and O. S. Wolfbeis, "Fluorescent Beads Coated with Polyaniline: A Novel Nanomaterial for Optical Sensing of pH," *Advanced Materials*, 13, 819–822, 2001.

[102] A. Bossi, S. A. Piletsky, E. V. Piletska, P. G. Righetti, and A. P. F. Turner, "An Assay for Ascorbic Acid Based on Polyaniline-Coated Microplates," *Analytical Chemistry*, 72, 4296–4300, 2000.

[103] S. Sukeerthi and A. Q. Contractor, "Molecular Sensors and Sensor Arrays Based on Polyaniline Microtubules," *Analytical Chemistry*, 71, 2231–2236, 1999.

[104] Z. X. Wei, Z. M. Zhang, and M. X. Wan, "Formation Mechanism of Self-Assembled Polyaniline Micro/Nanotubes," *Langmuir*, 18, 917–921, 2002.

[105] X. Y. Zhang, W. J. Goux, and S. K. Manohar, "Synthesis of Polyaniline Nanofibers by "Nanofiber Seeding"," *Journal of the American Chemical Society*, 126, 4502–4503, 2004.

[106] N. R. Chiou and A. J. Epstein, "Polyaniline Nanofibers Prepared by Dilute Polymerization," *Advanced Materials*, 17, 1679–1683, 2005.

[107] J. X. Huang, S. Virji, B. H. Weiller, and R. B. Kaner, "Polyaniline Nanofibers: Facile Synthesis and Chemical Sensors," *Journal of the American Chemical Society*, 125, 314–315, 2003.

[108] J. X. Huang, "Syntheses and Applications of Conducting Polymer Polyaniline Nanofibers," *Pure and Applied Chemistry*, 78, 15–27, 2006.

[109] J. Huang, S. Virji, B. H. Weiller, and R. B. Kaner, "Nanostructured Polyaniline Sensors," *Chemistry-A European Journal*, 10, 1315–1319, 2004.

[110] S. Virji, J. X. Huang, R. B. Kaner, and B. H. Weiller, "Polyaniline Nanofiber Gas Sensors: Examination of Response Mechanisms," *Nano Letters*, 4, 491–496, 2004.

[111] J. X. Huang and R. B. Kaner, "Nanofiber Formation in the Chemical Polymerization of Aniline: A Mechanistic Study," *Angewandte Chemie-International Edition*, 43, 5817–5821, 2004.

[112] L. Cai, A. Kovalev, and T. S. Mayer, "Conducting Polymer Nanofibers for Gas Sensor," *Proceedings of the 5th International Conference on Information Technology and Application in Biomedicine*, pp. 196–198, 2008.

[113] K. Krishnamoorthy, R. S. Gokhale, A. Q. Contractor, and A. Kumar, "Novel Label-Free DNA Sensors Based on Poly(3,4-ethylenedioxythiophene)," *Chemical Communications*, 7, 820–821, 2004.

[114] J. Wang, Y. L. Bunimovich, G. D. Sui, S. Savvas, J. Y. Wang, Y. Y. Guo, J. R. Heath, and H. R. Tseng, "Electrochemical Fabrication of Conducting Polymer Nanowires in an Integrated Microfluidic System," *Chemical Communications*, 29, 3075–3077, 2006.

[115] K. Ramanathan, M. A. Bangar, M. Yun, W. Chen, N. V. Myung, and A. Mulchandani, "Bioaffinity Sensing using Biologically Functionalized Conducting-Polymer Nanowire," *Journal of the American Chemical Society*, 127, 496–497, 2005.

[116] E. S. Forzani, H. Q. Zhang, L. A. Nagahara, I. Amlani, R. Tsui, and N. J. Tao, "A Conducting Polymer Nanojunction Sensor for Glucose Detection," *Nano Letters*, 4, 1785–1788, 2004.

[117] E. Komarova, M. Aldissi, and A. Bogomolova, "Direct Electrochemical Sensor for Fast Reagent-Free DNA Detection," *Biosensors & Bioelectronics*, 21, 182–189, 2005.

[118] H. Peng, C. Soeller, M. B. Cannell, G. A. Bowmaker, R. P. Cooney, and J. Travas-Sejdic, "Electrochemical Detection of DNA Hybridization Amplified by Nanoparticles," *Biosensors & Bioelectronics*, 21, 1727–1736, 2006.

[119] T. Livache, A. Roget, E. Dejean, C. Barthet, G. Bidan, and R. Teoule, "Preparation of a DNA Matrix Via an Electrochemically Directed Copolymerization of Pyrrole and Oligonucleotides Bearing a Pyrrole Group," *Nucleic Acids Research*, 22, 2915–2921, 1994.

[120] N. Lassalle, P. Mailley, E. Vieil, T. Livache, A. Roget, J. P. Correia, and L. M. Abrantes, "Electronically Conductive Polymer Grafted with Oligonucleotides as Electrosensors of DNA – Preliminary Study of Real Time Monitoring by in situ Techniques," *Journal of Electroanalytical Chemistry*, 509, 48–57, 2001.

[121] H. Peng, C. Soeller, N. Vigar, P. A. Kilmartin, M. B. Cannell, G. A. Bowmaker, R. P. Cooney, and J. Travas-Sejdic, "Label-Free Electrochemical DNA Sensor Based on Functionalised Conducting Copolymer," *Biosensors & Bioelectronics*, 20, 1821–1828, 2005.

[122] P. Godillot, H. KorriYoussoufi, P. Srivastava, A. ElKassmi, and F. Garnier, "Direct Chemical Functionalization of as-grown Electroactive Polypyrrole Film Containing Leaving Groups," *Synthetic Metals*, 83, 117–123, 1996.

[123] G. Bidan, M. Billon, K. Galasso, T. Livache, C. Mathis, A. Roget, L. M. Torres-Rodriguez, and E. Vieil, "Electropolymerization as a Versatile Route for Immobilizing Biological Species onto Surfaces – Application to DNA Biochips," *Applied Biochemistry and Biotechnology*, 89, 183–193, 2000.

[124] F. Garnier, H. Korri-Youssoufi, P. Srivastava, B. Mandrand, and T. Delair, "Toward Intelligent Polymers: DNA Sensors Based on Oligonucleotide-Functionalized Polypyrroles," *Synthetic Metals*, 100, 89–94, 1999.

[125] S. K. Kang, J. H. Kim, J. H. An, E. K. Lee, J. H. Cha, G. B. Lim, Y. S. Park, and D. J. Chung, "Synthesis of Polythiophene Derivatives and their Application for Electrochemical DNA Sensor," *Polymer Journal*, 36, 937–942, 2004.

[126] H. Peng, C. Soeller, and T.-S. Jadranka, "DNA Sensors based on Conducting Polymers Functionalized with Conjugated Side Chain," *IEEE SENSORS Conference*, pp. 1124–1127, 2007.

[127] B. Li, S. Santhanam, L. Schultz, M. Jeffries-EL, M. C. Iovu, G. Sauve, J. Cooper, R. Zhang, J. C. Revelli, A. G. Kusne, J. L. Snyder, T. Kowalewski, L. E. Weiss, R. D. McCullough, G. K. Fedder, and D. N. Lambeth, "Inkjet Printed Chemical Sensor Array Based on Polythiophene Conductive Polymers," *Sensors and Actuators B-Chemical*, 123, 651–660, 2007.

[128] P. Woias, "Micropumps – Past, Progress and Future prospects," *Sensors and Actuators B-Chemical*, 105, 28–38, 2005.

[129] D. J. Laser and J. G. Santiago, "A Review of Micropumps," *Journal of Micromechanics and Microengineering*, 14, R35–R64, 2004.

[130] M. Koch, A. G. R. Evans, and A. Brunnschweiler, "The Dynamic Micropump Driven with a Screen Printed PZT Actuator," *Journal of Micromechanics and Microengineering*, 8, 119–122, 1998.

[131] A. Wego and L. Pagel, "A Self-Filling Micropump Based on PCB Technology," *Sensors and Actuators A-Physical*, 88, 220–226, 2001.

[132] T. Bourouina, A. Bosseboeuf, and J. P. Grandchamp, "Design and Simulation of an Electrostatic Micropump for Drug-Delivery Applications," *Journal of Micromechanics and Microengineering*, 7, 186–188, 1997.

[133] S. Bohm, W. Olthuis, and P. Bergveld, "A Plastic Micropump Constructed with Conventional Techniques and Materials," *Sensors and Actuators A-Physical*, 77, 223–228, 1999.

[134] J. H. Park, K. Yoshida, and S. Yokota, "Resonantly Driven Piezoelectric Micropump – Fabrication of a Micropump Having High Power Density," *Mechatronics*, 9, 687–702, 1999.

[135] J. Darabi, M. Rada, M. Ohadi, and J. Lawler, "Design, Fabrication, and Testing of an Electrohydrodynamic Ion-Drag Micropump," *Journal of Microelectromechanical Systems*, 11, 684–690, 2002.

[136] J. W. Munyan, H. V. Fuentes, M. Draper, R. T. Kelly, and A. T. Woolley, "Electrically Actuated, Pressure-Driven Microfluidic Pumps," *Lab on a Chip*, 3, 217–220, 2003.

[137] T. S. Hansen, K. West, O. Hassager, and N. B. Larsen, "An All-Polymer Micropump Based on the Conductive Polymer Poly(3,4-ethylenedioxythiophene) and a Polyurethane Channel System," *Journal of Micromechanics and Microengineering*, 17, 860–866, 2007.

[138] K. Yamato and K. Kaneto, "Tubular Linear Actuators Using Conducting Polymer, Polypyrrole," *Analytica Chimica Acta*, 568, 133–137, 2006.

[139] J. H. Kim, K. T. Lau, and D. Diamond, "Fabrication of Microfluidic Pump Using Conducting Polymer Actuator," *IEEE International*

Conference on Sensor Networks, Ubiquitous, and Trustworthy Computing, pp. 457–463, 2008.

[140] Y. Wu, D. Zhou, G. M. Spinks, P. C. Innis, W. M. Megill, and G. G. Wallace, "TITAN: a Conducting Polymer Based Microfluidic Pump," *Smart Materials & Structures*, 14, 1511–1516, 2005.

[141] T. A. Ezquerra, F. Kremer, M. Mohammadi, J. Ruhe, G. Wegner, and B. Wessling, "Ac Conductivity Measurements in Polymeric Insulator Conductor Systems," *Synthetic Metals*, 28, C83–C88, 1989.

[142] T. Taka, "EMI-Shielding Measurements on Poly(3-Octyl Thiophene) Blends," *Synthetic Metals*, 41, 1177–1180, 1991.

[143] S. K. Dhawan, N. Singh, and S. Venkatachalam, "Shielding Effectiveness of Conducting Polyaniline Coated Fabrics at 101 GHz," *Synthetic Metals*, 125, 389–393, 2001.

[144] C. Y. Lee, H. G. Song, K. S. Jang, E. J. Oh, A. J. Epstein, and J. Joo, "Electromagnetic Interference Shielding Efficiency of Polyaniline Mixtures and Multilayer Films," *Synthetic Metals*, 102, 1346–1349, 1999.

[145] S. Koul, R. Chandra, and S. K. Dhawan, "Conducting Polyaniline Composite for ESD and EMI at 101 GHz," *Polymer*, 41, 9305–9310, 2000.

[146] H. K. Kim, M. S. Kim, K. Song, Y. H. Park, S. H. Kim, J. Joo, and J. Y. Lee, "EMI Shielding Intrinsically Conducting Polymer/PET Textile Composites," *ICSM International Conference on Science and Technology of Synthetic Metals, Shanghai , CHINE*, vol. 135, no. 36, p. 881, 2002.

[147] Y. Y. Wang and X. L. Jing, "Intrinsically Conducting Polymers for Electromagnetic Interference Shielding," *Polymers for Advanced Technologies*, 16, 344–351, 2005.

[148] J. H. Burroughes, D. D. C. Bradley, A. R. Brown, R. N. Marks, K. Mackay, R. H. Friend, P. L. Burns, and A. B. Holmes, "Light-Emitting-Diodes Based on Conjugated Polymers," *Nature*, 347, 539–541, 1990.

[149] C. W. Tang and S. A. Vanslyke, "Organic Electroluminescent Diodes," *Applied Physics Letters*, 51, 913–915, 1987.

[150] R. H. Friend, R. W. Gymer, A. B. Holmes, J. H. Burroughes, R. N. Marks, C. Taliani, D. D. C. Bradley, D. A. Dos Santos, J. L. Bredas, M. Logdlund, and W. R. Salaneck, "Electroluminescence in Conjugated Polymers," *Nature*, 397, 121–128, 1999.

[151] A. W. Grice, D. D. C. Bradley, M. T. Bernius, M. Inbasekaran, W. W. Wu, and E. P. Woo, "High Brightness and Efficiency Blue Light-Emitting Polymer Diodes," *Applied Physics Letters*, 73, 629–631, 1998.

[152] N. C. Greenham, S. C. Moratti, D. D. C. Bradley, R. H. Friend, and A. B. Holmes, "Efficient Light-Emitting-Diodes Based on Polymers with High Electron-Affinities," *Nature*, 365, 628–630, 1993.

[153] P. K. H. Ho, J. S. Kim, J. H. Burroughes, H. Becker, S. F. Y. Li, T. M. Brown, F. Cacialli, and R. H. Friend, "Molecular-Scale Interface Engineering for Polymer Light-Emitting Diodes," *Nature*, 404, 481–484, 2000.

[154] Y. Cao, I. D. Parker, G. Yu, C. Zhang, and A. J. Heeger, "Improved Quantum Efficiency for Electroluminescence in Semiconducting Polymers," *Nature*, 397, 414–417, 1999.

[155] Z. Shuai, D. Beljonne, R. J. Silbey, and J. L. Bredas, "Singlet and Triplet Exciton Formation Rates in Conjugated Polymer Light-Emitting Diodes," *Physical Review Letters*, 84, 131–134, 2000.

[156] J. S. Kim, P. K. H. Ho, N. C. Greenham, and R. H. Friend, "Electroluminescence Emission Pattern of Organic Light-Emitting Diodes: Implications for Device Efficiency Calculations," *Journal of Applied Physics*, 88, 1073–1081, 2000.

[157] R. Friend, J. Burroughes, and T. Shimoda, "Polymer Diodes," *Physics World*, 12, 35–40, 1999.

[158] J. J. M. Halls, J. Cornil, D. A. dos Santos, R. Silbey, D. H. Hwang, A. B. Holmes, J. L. Bredas, and R. H. Friend, "Charge- and Energy-Transfer Processes at Polymer/Polymer Interfaces: A Joint Experimental and Theoretical Study," *Physical Review B*, 60, 5721–5727, 1999.

[159] J. J. M. Halls, C. A. Walsh, N. C. Greenham, E. A. Marseglia, R. H. Friend, S. C. Moratti, and A. B. Holmes, "Efficient Photodiodes from Interpenetrating Polymer Networks," *Nature*, 376, 498–500, 1995.

[160] G. Yu, J. Gao, J. C. Hummelen, F. Wudl, and A. J. Heeger, "Polymer Photovoltaic Cells – Enhanced Efficiencies via a Network of Internal Donor-Acceptor Heterojunctions," *Science*, 270, 1789–1791, 1995.

[161] M. Granstrom, K. Petritsch, A. C. Arias, A. Lux, M. R. Andersson, and R. H. Friend, "Laminated Fabrication of Polymeric Photovoltaic Diodes," *Nature*, 395, 257–260, 1998.

[162] K. Shankar, X. Feng, and C. A. Grimes, "Enhanced Harvesting of Red Photons in Nanowire Solar Cells: Evidence of Resonance Energy Transfer," *ACS NANO*, 3, 788–794, 2009.

[163] R. H. Baughman, "Conducting Polymer Artificial Muscles," *Synthetic Metals*, 78, 339–353, 1996.

[164] Q. B. Pei and O. Inganas, "Electrochemical Applications of the Bending Beam Method, a Novel Way to Study Ion-Transport in Electroactive Polymers," *Solid State Ionics*, 60, 161–166, 1993.

[165] Q. B. Pei and O. Inganas, "Conjugated Polymers as Smart Materials, Gas Sensors and Actuators Using Bending Beams," *Synthetic Metals*, 57, 3730–3735, 1993.

[166] T. E. Herod and J. B. Schlenoff, "Doping-Induced Strain in Polyaniline – Stretch Electrochemistry," *Chemistry of Materials*, 5, 951–955, 1993.

[167] R. Pytel, E. Thomas, and I. Hunter, "Anisotropy of Electroactive Strain in Highly Stretched Polypyrrole Actuators," *Chemistry of Materials*, 18, 861–863, 2006.

[168] M. R. Warren and J. D. Madden, "Electrochemical Switching of Conducting Polymers: A Variable Resistance Transmission Line Model," *Journal of Electroanalytical Chemistry*, 590, 76–81, 2006.

[169] J. D. Madden, R. A. Cush, T. S. Kanigan, and I. W. Hunter, "Fast Contracting Polypyrrole Actuators," *Synthetic Metals*, 113, 185–192, 2000.

[170] S. Hara, T. Zama, W. Takashima, and K. Kaneto, "Free-Standing Polypyrrole Actuators with Response Rate of 10.8% s(–1)," *Synthetic Metals*, 149, 199–201, 2005.

[171] J. Ding, L. Liu, G. M. Spinks, D. Z. Zhou, G. G. Wallace, and J. Gillespie, "High Performance Conducting Polymer Actuators Utilising a Tubular Geometry and Helical Wire Interconnects," *Synthetic Metals*, 138, 391–398, 2003.

[172] G. M. Spinks, V. Mottaghitalab, M. Bahrami-Saniani, P. G. Whitten, and G. G. Wallace, "Carbon-Nanotube-Reinforced Polyaniline Fibers for High-Strength Artificial Muscles," *Advanced Materials*, 18, 637–640, 2006.

[173] G. M. Spinks and V. T. Truong, "Work-per-cycle Analysis for Electromechanical Actuators," *Sensors and Actuators A-Physical*, 119, 455–461, 2005.

[174] M. J. Marsella, R. J. Reid, S. Estassi, and L. S. Wang, "Tetra[2,3-thienylene]: A Building Block for Single-Molecule Electromechanical Actuators," *Journal of the American Chemical Society*, 124, 12507–12510, 2002.

[175] A. DellaSanta, A. Mazzoldi, and D. DeRossi, "Steerable Microcatheters Actuated by Embedded Conducting Polymer Structures," *Journal of Intelligent Material Systems and Structures*, 7, 292–300, 1996.

[176] Y. Z. Lam, J. Swingler, and J. W. McBride, "The Contact Resistance Force Relationship of an Intrinsically Conducting Polymer

Interface," *IEEE Transactions on Components and Packaging Technologies*, 29, 294–302, 2006.

[177] E. C. Cooper and B. Vincent, "Electrically Conducting Organic Films and Beads Based on Conducting Latex-Particles," *Journal of Physics D-Applied Physics*, 22, 1580–1585, 1989.

[178] E. Sancaktar and C. J. Liu, "Use of Polymeric Emeraldine Salt for Conductive Adhesive Applications," *Journal of Adhesion Science and Technology*, 17, 1265–1282, 2003.

[179] F. Corsat, C. Davoine, A. Gasse, M. Fendler, G. Feuillet, L. Mathieu, F. Marion, and A. Pron, "Imprint Technologies on Conductive Polymers and Metals for Interconnection and Bumping Purposes," *1st IEEE Electronics System Integration Technology Conference (ESTC)*, pp. 1336–1341, 2006.

[180] L. W. Chow, J. Li, and M. F. Yuen, "Development of Low Temperature Processing Thermoplastic Intrinsically Conductive Polymer," *8th International Symposium on Advanced Packaging Materials*, pp. 127–131, 2002.

[181] F. Kuechenmeister and E. Meusel, "Polypyrrole as an Interlayer for Bonding Conductive Adhesives to Activated Aluminum Bond Pads," *IEEE Transactions on Components Packaging and Manufacturing Technology Part A*, 20, 9–14, 1997.

[182] J. X. Lu, K. S. Moon, B. K. Kim, and C. P. Wong, "High Dielectric Constant Polyaniline/Epoxy Composites via In Situ Polymerization for Embedded Capacitor Applications," *Polymer*, 48, 1510–1516, 2007.

Chapter 9
Future Trend of Conductive Adhesive Technology

9.1 Recent Advances in Conductive Adhesive Technology

As can be seen from previous chapters, tremendous progress has been made to improve the conductive adhesive technology for ICAs, ACA, and NCA.

Significant progress has been made in the last few years to address various issues of ICA technology. Conductivity mechanism was studied and different effective approaches such as adding silver flake lubricant removers and increasing resin curing shrinkage to enhance the conductivity of ICAs were demonstrated. The mechanism underlying the unstable contact resistance of ICAs was clearly elucidated. Based on this understanding, various ways to stabilize contact resistance of ICAs, such as utilizing pure resin with low moisture pick-up, adding oxygen scavengers, adding corrosion inhibitors, and incorporating low melting alloy filler, were studied. An effective corrosion inhibitor was identified and its mechanism was elucidated too. Finally, an epoxy-terminated polyurethane resin was demonstrated to be an effective resin to dramatically enhance the mechanical impact performance of an ICA.

Ag nanowires were shown to be able to provide ICAs with similar conductivity as traditional Ag flakes at a much lower filler loading and thus provide ICAs with better mechanical performance. Adding Ag nanoparticles into an ICA filled with Ag flakes generally showed a negative effect on electrical conductivity. However, some factors such as high-temperature annealing and adding certain surfactants on the surfaces of nanoparticles can enhance the inter-diffusion of Ag atoms among nanoparticles and thus improve the conductivity. Incorporating CNTs into ICAs filled with Ag flakes enhanced the conductivity greatly only when the Ag filler loading was still below the percolation threshold. Functionalizing

Y. Li et al., *Electrical Conductive Adhesives with Nanotechnologies*,
DOI 10.1007/978-0-387-88783-8_9, © Springer Science+Business Media, LLC 2010

CNT surfaces to improve the interaction between the CNTs and the matrix significantly improved the mechanical performance of CNT-filled ICAs.

ACAs/ACFs filled with Ag nanoparticles showed low resistance due to the sintering of the nanoparticles at relatively low temperatures, and lower resistance was observed for ACAs/ACFs sintered at a higher temperature. By introducing self-assembled monolayers (SAMs) into the interfaces between the metal fillers and metal contact pads, lower joint resistance and higher maximum allowable current were observed for low-temperature curable ACAs (curing temperature <100°C). By chelating silver fillers with an organic compound, such as a carboxylic acid, the silver migration was greatly reduced. ACAs filled with Ag/Co nanowires were developed with acceptable electrical performance. In situ formation of Ag nanoparticles during ACA curing was demonstrated, and better filler dispersion was achieved.

9.2 Challenges and Opportunities of ICAs

9.2.1 Electrical Performance Improvement

For applications which do not require high power and high current density, conductive adhesives have been shown to have similar electrical performance to solders. However, the electrical conductivity must be improved in order to make ICA a viable option to replace solder for high power applications. Silver-filled ICAs achieve their electrical conductivity through physical contact among the Ag flaks. Due to the high particle–particle contact resistance, ICAs exhibit high bulk resistivity. Some preliminary work has been done to improve electrical conductivity by introducing low melting point alloys, which form metallurgical interconnetions with the Ag flakes. Also, more in-depth understanding of the behavior of ICA joints under high current or high power conditions and high temperature/humidity/bias is needed.

9.2.2 Silver Migration

Silver-filled ICAs have a potential for silver migration, which cause electrical shorts especially in fine-pitch applications. A palladium-treated silver filler exhibited much improved anti-migration characteristics compared to standard silver-filled ICAs. However, the preparation of the Pd-coated silver particles is expensive. Some low-cost approaches must be devel-

oped. More comprehensive understanding of the fatigue resistance of ICA joints is required.

9.2.3 Mechanical Property Improvement

In a conventional silver flake-filled ICAs, a high filler loading (70–80wt%) is generally utilized to achieve high conductivity. However, the high filler loading causes degradation of mechanical property (such as shear strength). Nano wire and aggregates of nano-sized Ag particles showed potential for improving mechanical strength of ICAs. The challenge is to improve both mechanical strength and conductivity of ICAs at the same time.

9.2.4 Manufacturability and Yields

Since most commercial ICAs are epoxy based, they are thermosetting materials and thus not reworkable. Reworkable ICAs may be needed for certain applications, for example, CSP applications. Reworkable ICAs can be developed by using thermoplastic or thermally degradable resins. Due to their high surface tension, SnPb solders have a self-alignment capability during solder reflow operations. However, conventional ICAs cannot self-align. Therefore, components that are bonded using ICAs require a high placement accuracy. Some preliminary research has been conducted to improve the self-alignment capability of ICAs [1, 2], but much more work needs to be done.

9.2.5 Cost Reduction

ICAs are several times more expensive than most solders. The high cost is primarily due to the use of high loading of Ag filler. There is a strong need to reduce the cost of ICAs in order to make them more attractive. Using conductive fillers with lower cost such as copper filler has been reported in the literature. However, copper-filled ICAs generally suffer from the oxidation of copper filler and the deterioration of the electrical properties as a result of the non-conductive nature of such oxide layers. Unlike aluminum, copper is readily oxidized at a low temperature and has no self-protective layer to prevent further oxidation. One of the key challenges is to keep the copper from oxidizing during aging especially during 85°C/85%RH aging. Coating the copper particles with silver is one way to keep them from oxidation. Silver-coated copper, nickel, and aluminum have been attempted in ICA formulations [3]. One of the potential issues is that the non-noble metal such as Cu from the interior may diffuse to the surface of silver-coated

powder and react with the oxygen in the air to form oxide, which will degrade the electrical conductivity of ICAs. Another possible solution for cost reduction is to use metal nanowires which could offer a much lower threshold (i.e., much lower filler loading required) for achieving electrical conductivity. This option becomes practical only when the cost of nanowire comes down significantly in the future.

9.2.6 ICAs Based on Intrinsically Conducting Polymers

There are two distinct types of stability for conducting polymers. Extrinsic stability is related to vulnerability to external environmental agent such as oxygen, water, peroxides. This is determined by the polymers' susceptibility of charged sites to attack by nucleophiles, electrophiles, and free radicals. If a conducting polymer is extrinsically unstable, then it must be protected by a stable coating. Many conducting polymers, however, degrade over time even in dry, oxygen-free environment. This intrinsic instability is thermodynamic in origin. It is likely to be caused by irreversible chemical reaction between charged sites of polymer and either the dopant counter ion or the *p*-system of an adjacent neutral chain, which produces an sp^3 carbon, breaking the conjugation. Intrinsic instability can also come from a thermally driven mechanism which causes the polymer to lose its dopant. This happens when the charge sites become unstable due to conformational changes in the polymer backbone. This has been observed in alkyl-substituted polythiophenes [4].

Another problem of conducting polymers stems from the conjugated backbone, which makes such polymers intractable, insoluble films, or powders that cannot melt. There are two main strategies to overcome these problems. They are to either modify the polymer so that it may be more easily processed or to manufacture the polymer in its desired shape and form.

Even though very high electrical conductivity (10^4 S/cm) has been demonstrated for conducting polymers, their environmental instability and lack of processability preclude its use. A dramatic enhancement of the conductivity of some of the more processable and environmentally stable polymers is required before they can be realistically considered as viable interconnection materials. Their chemical stability, environmental sensitivity, material ease of use (curing temperature, adhesion and flexibility, dry time, etc.) require further improvements. The cost of such polymers must also be substantially lowered.

9.2.7 ICAs for Printed Organic Electronics

Printed or plastic electronics is about the use of organic semiconductors (that is, conductive plastics, as opposed to traditional inorganic semiconductors such as silicon or gallium arsenide), their unique physical properties, and the new approach they entail to electronic and optoelectronic device fabrication. The use of inks and standard printing technology to produce electrics, electronics, and optoelectronics based on organic semiconductors has stimulated a massive commercial interest and a huge technical effort worldwide. The new technology has the potential to unlock new markets and introduce disruptive technologies across a wide range of fields. It is expected that, over the next 10 years, we will witness the introduction of a new generation of optoelectronic devices and components, which will be deployed in places where silicon and inorganic semiconductor electronics cannot be utilized because they are too costly, too brittle, too fragile, or because they require excessive time to market. Large-area device arrays for extended electronic backplanes, inexpensive and disposable single components, and flexible, lightweight devices will be manufactured at unprecedented low costs. Ultimate device customization and integration, including batteries, transistors, displays, sensors, and loudspeakers, will become not only technically feasible but also affordable.

Printed electronics will focus on addressing three major needs: a) small, low-cost, and disposable electronics (RFID tags, smart packaging, disposable sensors); (b) large, rugged, and inexpensive electronics (large signage displays, integrated photovoltaic panels, smart shelving, EMI/RF shields); (c) flexible optoelectronics (foldable e-papers, e-books, rollable displays).

ICAs are a suitable candidate for forming electrical traces/lines by inkjet printing or for electrical interconnection. The ICAs for this application need to have the following properties: low processing temperature and flexible (low modulus). Li et al. [5] have recently developed a novel flexible ICA. By introducing the flexible epoxy and tuning the ratios of rigid and flexible epoxies, the elastic moduli (G'-storage moduli and G"-loss moduli), glass transition temperatures, adhesion strength, electrical conductivity, and impact strength have been successfully modified. These flexible conductive adhesives provide a gateway for the flexible interconnect materials, especially under highly mechanical bending conditions of printed electronics.

Also, transparent conductive adhesive is needed for some applications such as organic LED (OLED) application. Ouyang et al. [6] have demonstrated a transparent conducting polymer glue and the feasibility of fabricating organic electronic devices through a lamination process by using the PEDOT:PSS electric glue. By combining this technology with the large-area

continuous coating process of organic films, it is possible to fabricate large-area organic electronic devices through a continuous roll-to-roll coating process. This electric glue made from a conducting polymer provides new applications for conducting polymers; it will revolutionize the fabrication process of flexible electronic devices.

9.3 Challenges and Opportunities for ACAs

9.3.1 Thermo-mechanical Reliability

Development of new ACA materials that have good adhesion, high T_g, fast curing, storage stability at ambient, and stable contact resistance after various conditions frequently encountered in the field such as thermal aging and cycling, thermal shock, high temperature/high humidity/bias are required. Also, ACAs with low CTE are required. Commercially available ACAs typically exhibit very high CTEs because of the low filler loading levels utilized. Some preliminary studies have shown that ACAs with a low CTE created by introducing non-conductive silica fillers have a lower shear strain and better contact resistance stability during thermal cycling test [7].

9.3.2 High-Frequency Compatibility

The number of high-frequency applications and utilizations is increasing rapidly, thus it is important to characterize the cross-talk between particles, coupling with semiconductor devices and other fundamental behavior of ACAs under high-frequency in excess of 40–100 GHz conditions. It is also necessary to maximize the current-carrying capability of ACAs at high-frequency range and after exposure to various environment tests.

9.3.3 Current–Carrying Capability

Conventional ACAs rely on the physical contact between conductive spheres and the contact metal pads on the components and substrates. Due to the high interfacial resistance, the currents-carrying capability of each electrical contact is relatively low, which limits ACAs only to low current applications. Recently much research has been conducted to improve the

current-carrying capability of ACAs by introducing self-assembled monolayer (SAM) of certain "molecular wire" – molecules with high mobile electron density (conjugated double or triple bonds). This approach seems to be able to enhance the current-carrying capability of ACA joints. However, much work must be done to understand the behavior of SAM in polymer matrix during curing, stability of this layer during reliability tests, during multiple reflow, etc.

9.3.4 Reliability

It is necessary to understand the effects of the chip carrier (or substrate) material and the matrix of the ACA on ACA join reliability. This is a key issue before ACA technology is widely utilized in manufacturing (i.e., in high-volume and low-cost applications). It is also necessary to establish failure rate prediction models for ACA joints for a wide variety of field conditions. It is essential to gain full understanding on effects of high current and high power on ACA joints, degradation and stress relaxation of polymeric matrices; and the effects of temperature, humidity, and other environments on matrix materials and the effects of fillers.

9.3.5 Manufacturability

With particle size of ACAs becoming smaller for nano-ACAs, there is serious implication from manufacturing process point of view. When ACAs are used to attach the metal pads on two mating surfaces, the warpage and coplanarity of these surfaces need to be carefully controlled to ensure that all the metal pads on the mating surfaces are making contact to the conductive spheres in the ACA simultaneously. Large and compliant (deformable) conductive particles will ease the manufacturing process because these particles can accommodate the warpage and non-coplanarity. With conductive particles becoming even smaller in nano-ACAs, the manufacturing will become more challenging.

9.4 Challenges and Opportunities for NCAs

Non-conductive adhesives, primarily dielectric liquids, have been used to mechanically mate flip chips to substrates. The components must have raised bumps so that there is some clearance under the die or package. The adhesive shrinks during curing to pull the component or bare die to the substrate. The electrical contact is directly through the package or die

terminations to the substrate lands. The adhesive serves a mechanical and protective function only. For future low cost fine pitch flip chip on flex applications, NCA technology might gain more momentum. However, NCAs without any filler generally have high CTE, which might affect the joint reliability under thermal cycle condition. The effects of NCA material properties to the reliability of the NCA joints need to be fully understood.

References

[1] J. Wu, K. Moon, and C. P. Wong, "Self-Alignment Feasibility Study and Contact Resistance Improvement of Electrically Conductive Adhesives (ECAs)," *Proceedings of 51st Electronic Components and Technology Conference*, Orlando, FL, pp. 571–575, 2001.

[2] K. Moon, J. Wu, and C. P. Wong, "Study on Self-Alignment Capability of Electrically Conductive Adhesives (ECAs) for Flip-Chip Application," *Proceedings of International Symposium on Advanced Packaging Materials: Processes, Properties and Interfaces*, Braselton, GA, pp. 341–346, 2001.

[3] Y. S. Lin and S. S. Chiu, "Effects of Oxidation and Particle Shape on Critical Volume Fractions of Silver-Coated Copper Powders in Conductive Adhesives for Microelectronic Applications," *Polymer Engineering and Science*, 44, 2075–2082, 2004.

[4] M. Angelopoulos, "Conducting Polymers in Microelectronics," *IBM Journal of Research and Development*, 45, 57–75, 2001.

[5] Y. Li, M. J. Yim, K. Moon, R. W. Zhang, and C. P. Wong, "Development of Novel, Flexible, Electrically Conductive Adhesives for Next-Generation Microelectronics Interconnect Applications," *Proceedings of 58th IEEE Electronic Components and Technology Conference*, pp. 1272–1276, 2008.

[6] H. Y. Ouyang and Y. Yang, "Conducting Polymer as Transparent Electric Glue," *Advanced Materials*, 18, 2141–2144, 2006.

[7] M. J. Yim and K. W. Paik, "Effect of Nonconducting Filler Additions on ACA Properties and the Reliability of ACA Flip-Chip on Organic Substrates," *IEEE Transactions on Components and Packaging Technologies*, 24, 24–32, 2001.

Index